

NASA
RP
1022
c.1

NASA Reference Publication 1022

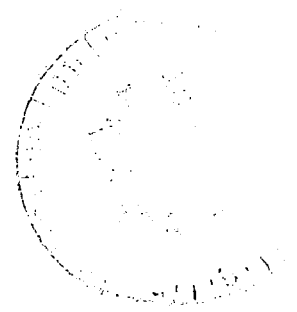
TECH LIBRARY KAFB, NM
0063278

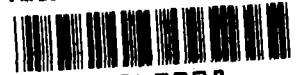
LOAN COPY: RETURN TO
AFWL TECHNICAL LIBRARY
KIRTLAND AFB, NM

Man's Impact on the Troposphere

Lectures in Tropospheric Chemistry

SEPTEMBER 1978





NASA Reference Publication 1022

Man's Impact on the Troposphere

Lectures in Tropospheric Chemistry

Joel S. Levine and David R. Schryer, *Editors*
Langley Research Center
Hampton, Virginia

NASA

National Aeronautics
and Space Administration

**Scientific and Technical
Information Office**

1978



PREFACE

About 85 percent of the total mass of the atmosphere is contained in the troposphere. Man lives in the troposphere and breathes its molecules; tropospheric species regulate climate, influence weather, and control levels of stratospheric ozone. The chemical composition of the troposphere is determined by complex geochemical cycles of carbon, nitrogen, sulfur, oxygen, and hydrogen species between the atmosphere, the oceans, the crust, and the biosphere.

Over the last few decades, anthropogenic activities have become a significant source of tropospheric species. For example, man's intervention in the carbon cycle affects the most abundant carbon-containing tropospheric species: carbon dioxide, methane, and carbon monoxide. The measured global increase in carbon dioxide over the last 25 years has been attributed to the burning of fossil fuel. In addition, combustion processes may account for more than half of the global production of carbon monoxide and may be responsible for the pronounced observed latitudinal gradient of carbon monoxide. Furthermore, on the basis of photochemical considerations, it has been hypothesized that enhanced levels of anthropogenic carbon monoxide will lead to enhanced levels of methane. Another example of man's intervention is perturbation of the nitrogen cycle affecting the most abundant nitrogen-containing tropospheric species other than molecular nitrogen: nitrous oxide, ammonia, nitric oxide, and nitrogen dioxide. Enhanced levels of nitrous oxide have been theorized to result from increased bacterial denitrification associated with increased nitrogen fixation in agricultural fertilizers. The volatilization of ammonia, again resulting from increased nitrogen fixation in agricultural fertilizers, may become an important anthropogenic source of ammonia. Combustion is an important source of nitric oxide and nitrogen dioxide. Man's activities directly result in a large portion of the total sulfur entering the atmosphere. Most of the sulfur enters the atmosphere in the form of sulfur dioxide resulting from fossil fuel combustion. The sulfur dioxide undergoes a number of oxidation reactions leading to the production of sulfate aerosols, especially ammonium sulfate aerosols. The anthropogenic contribution of sulfur dioxide and sulfates overwhelms the natural background on a regional scale.

Changes in the natural abundance of tropospheric species may alter other species via chemistry as well as produce perturbations in climate. For example, tropospheric ozone is strongly affected by tropospheric levels of nitrogen dioxide and methane, and stratospheric ozone is controlled by tropospheric nitrous oxide. Many of these anthropogenically produced species have absorption lines within the 8- to 12- μm "atmospheric window" which contribute to the "greenhouse" effect. These greenhouse absorbers include carbon dioxide, methane, nitrous oxide, ammonia, and ozone.

To assess the current state of knowledge of man's impact on the troposphere, on both a global and regional scale, the NASA Langley Research Center (LaRC) organized a series of invited lectures on tropospheric chemistry during the summer and early fall of 1977. The series was initiated and coordinated by the Atmospheric Environmental Sciences Division and the Marine and Applications

Technology Division of LaRC and sponsored by the Environmental Quality Program Office (EQPO) of the NASA Office of Space and Terrestrial Applications.

The lectures covered a broad spectrum of current research in tropospheric chemistry with particular emphasis on the interaction of measurements, modeling, and understanding of fundamental processes. As the series progressed, it became apparent that formal documentation of the material presented was desirable. All of the lecturers were, therefore, invited to submit written papers based on their talks. This publication presents these papers.

Use of trade names or names of manufacturers in this publication does not constitute official endorsement, either expressed or implied, by the National Aeronautics and Space Administration.

The editors wish to thank all of the lecturers for their efforts and to express their appreciation to John P. Mugler, Jr., and Wendell G. Ayers of EQPO for their support of both the lecture series and this publication.

Joel S. Levine

David R. Schryer

CONTENTS

PREFACE	iii
1. MECHANISMS, MODELS, AND MYTHS: FICTION AND FACT IN TROPOSPHERIC CHEMISTRY James N. Pitts, Jr., Statewide Air Pollution Research Center	1
2. THE NATURAL AND PERTURBED TROPOSPHERE Richard W. Stewart, NASA Goddard Space Flight Center, and Sultan Hameed and Joseph Pinto, State University of New York at Stony Brook	27
3. POSSIBLE NONURBAN ENVIRONMENTAL EFFECTS DUE TO CARBON MONOXIDE AND NITROGEN OXIDES EMISSIONS Shaw C. Liu, National Center for Atmospheric Research	65
4. THE EFFECTS OF INCREASED CO AND NO _x UPON TROPOSPHERIC OH, CH ₄ , AND RELATED SPECIES W. L. Chameides, University of Florida	81
5. THE TRANSPORT CYCLE OF ATMOSPHERIC OZONE AND ITS MEASUREMENTS FROM AIRCRAFT AND AT THE EARTH'S SURFACE Phillip D. Falconer, Robert Pratt, and Volker A. Mohnen, State University of New York at Albany	109
6. URBAN PRECURSORS AND THEIR PHOTOCHEMICAL PRODUCTS T. E. Graedel, Bell Laboratories	149
7. MATHEMATICAL MODELING OF THE POLLUTED TROPOSPHERE John H. Seinfeld, California Institute of Technology	203
8. THE ROLE OF COMPUTER MODELING OF PHOTOCHEMICAL SMOG IN DEFINING EXISTING MEASUREMENT NEEDS Alan C. Lloyd, Environmental Research & Technology, Inc.	255
9. ATMOSPHERIC SULFUR BEHAVIOR IN POWER PLANT AND REGIONAL PLUMES Rudolf B. Husar, Air Pollution Research Laboratory	319
10. SOOT-CATALYZED OXIDATION OF SULFUR DIOXIDE S. G. Chang and T. Novakov, Lawrence Berkeley Laboratory	349
CONTRIBUTORS	371

MECHANISMS, MODELS, AND MYTHS: FICTION AND FACT IN TROPOSPHERIC CHEMISTRY*

James N. Pitts, Jr.
Statewide Air Pollution Research Center
Riverside, California

INTRODUCTION

During the last 5 to 10 years, modeling of the chemistry of the lower and the upper atmosphere has become popular, not only from the viewpoint of basic science but also as a basis for pollution control strategies in both regions of the atmosphere. Thus, significant progress has been made in taking complex kinetic and mechanistic information and, by use of modern computers and associated mathematical methodologies, developing submodels of chemical transformations in the troposphere. These are then incorporated into a variety of overall airshed models.

Properly understood and utilized, that is, with a clear understanding of both their usefulness and their limitations, airshed models describing, for example, ozone formation from its precursors (hydrocarbons (HC) and oxides of nitrogen (NO_x)) during transport and transformation across an air basin, can be helpful tools to those responsible for the control of this secondary pollutant. Indeed, such models are currently being used by the U.S. Environmental Protection Agency (EPA) as a major element of their proposed revised oxidant control strategies.

While it is exciting for most scientists to see how fundamental data on reaction kinetics and mechanisms are now being put to use in solving real-world problems, it is also somewhat sobering to realize that billions of dollars ride on the results that are being derived from such models. Entire industries are seriously affected by the accuracy of model predictions; consider, for example, the aircraft and fluorocarbon industries in relationship to the ozonosphere question. Although less dramatic in public visibility, these increasingly stringent tropospheric oxidant controls being proposed and implemented for seriously polluted air basins also have significant economic ramifications, not only for automobile manufacturers but also for such stationary sources of reactive organics as coal-fired power plants, the paint industry, and so forth.

Thus, while acknowledging the importance and usefulness of such chemical kinetic computer models, it seems useful to pause and examine those factors that significantly affect their accuracy and precision. In so doing, remember

*This work was partially funded by the National Science Foundation - Research Applied to National Needs (Grant No. ENV73-02904-A04, R. Corrigan, project officer) and the U.S. Environmental Protection Agency (Grant No. EPA804546-02, Phil Hanst, project officer). The contents of this paper do not necessarily reflect the view and/or policies of the NSF-RANN and the EPA.

that a chemical model describing "Los Angeles smog," for example, really consists basically of a photochemical reaction mechanism plus a computer.

Historically, in the early days of gas-phase photochemistry and photooxidation, the validity of the kinetic-mechanistic "models" developed for even very simple systems was limited to a significant extent by mathematical capabilities. Thus, obtaining mathematical solutions describing the events occurring in even relatively uncomplicated chain reactions was at best very tedious; the generation of reliable time-concentration profiles for reactants and products in more complex systems was virtually impossible. Sometime around the late 1950's and early 1960's, the power of computer technology and the associated mathematics began to emerge, and during the last 15 years, the computational aspects of chemical models for multicomponent simulated atmospheres have generally not been the limiting factor in the final accuracy of the model's predictions. Present computers are, of course, highly sophisticated and capable of handling what to a photochemist of the 1950's would have been an incredible number of individual reactions, for example, well over 200 in the propylene-NO_x-air-hν system alone! Thus, today kinetic computer models are, in effect, chemistry limited; that is, the validity of these models describing reaction sequences in the natural or polluted troposphere depends far more on the accuracy and precision of the input chemical data than upon the mathematical subtleties and techniques presently used to translate such data into useful concentration-time profiles.

Experienced atmospheric chemists are usually aware of the deficiencies in the experimental data base for both the troposphere and the stratosphere and generally assign realistic probable errors to the predictions produced by their models of chemical transformations. This is important because only in this way can one who is not an expert in this specific field have some understanding of the degree of accuracy and precision of models used in control strategies. Unfortunately, some scientists who develop and utilize photochemical models for tropospheric pollution do not always clarify the degree to which the experimental data that they are using in their models are reliable, both in accuracy and precision. Thus a nonchemist modeler could unknowingly generate an overall airshed model quite sound in one component, for example, in the submodel dealing with meteorology, but seriously in error in the package describing the chemical and physical transformations of pollutants during transport in the real atmosphere.

This paper will illustrate some aspects of this general problem, that is, the dangers inherent in being overconfident about the reliability (especially the absolute accuracy) of the atmospheric chemistry input into current models for tropospheric air pollution. First, a review is presented of the criteria that must be met before even a simple homogeneous gas-phase photochemical reaction carried out under laboratory conditions can be considered proof of a mechanism. Then, the paper will discuss specific examples of "fiction and fact" in the enormously complex heterogeneous systems that characterize ambient polluted atmospheres.

In so doing, the author will express his personal ideas on the subject. Thus, no attempt will be made to review or reference the literature; this has been done elsewhere (refs. 1 to 3). Furthermore, the examples cited will be

taken largely from current work, much as yet unpublished, in the laboratories of the University of California Statewide Air Pollution Research Center and Departments of Chemistry and Biology.¹

CRITERIA FOR ESTABLISHING THE VALIDITY OF A MECHANISM FOR

A GAS-PHASE PHOTOCHEMICAL REACTION

Some of the more important types of experiments that should be carried out in the laboratory to develop and validate a mechanism for a gas-phase photochemical process are summarized below; they are discussed in detail elsewhere (ref. 4):

- (1) Measurement of the primary (ϕ) and overall (Φ) photochemical quantum yields for the loss of reactants
- (2) Identification and determination of ϕ and Φ for the formation of major and minor products
- (3) Identification and quantification of trace, but mechanistically important, product molecules
- (4) Identification and measurement of the concentration-time profiles of key intermediate species, for example, methyl or hydroxyl radicals, singlet molecular oxygen ($O_2^1\Delta$), triplet states of photoexcited organic compounds, and unstable isomeric forms
- (5) Determination of the quantum yields of the photophysical processes associated with the absorption of light, for example, internal conversion, intersystem crossing, fluorescence, and phosphorescence

In the laboratory, insofar as possible, all of these experiments should be conducted as a function of temperature, wavelength and intensity of absorbed radiation, pressures and/or concentrations of reactants, physical and chemical quenching by added gases, surface/volume ratio, other parameters that involve the homogeneous versus heterogeneous nature of the reaction, and when appropriate, pressures of gaseous free radical traps (e.g., I_2 , NO, and olefins). Additionally, isotopic labeling experiments may be required for confirmation. Finally, a reasonably good material balance (number of atoms in reactant molecules equal to number of atoms in product molecules) should be sought.

Considering the number and complexity of such experiments required to elucidate with confidence the mechanism of the gas-phase photooxidation of

¹The author's colleagues have tackled a variety of difficult research problems in tropospheric chemistry with zeal and competence to produce the results discussed herein. They include W. L. Belser, Jr., R. Atkinson, K. R. Darnall, R. A. Graham, D. Grosjean, G. B. Knudson, R. Perry, J. P. Schmid, J. P. Smith, E. C. Tuazon, K. A. Van Cauwenberghe, A. M. Winer, F. R. Burleson, D. R. Fitz, P. M. Hynds, K. Pettus, and T. M. Mischke.

only a single compound, say formaldehyde or methyl ethyl ketone, one might despair at the thought of ever understanding with some degree of assurance the mechanism of photochemical smog formation in urban atmospheres. The urban atmosphere may contain literally hundreds of hydrocarbons - alkanes, alkenes, and aromatics - and other organics such as aldehydes, ketones, and halogenated species, as well as inorganics, including NO, NO₂, HONO, and HNO₃.

Actually, much progress has been made in dealing with this admittedly difficult situation, partly by studying the reactions of model hydrocarbons in simulated atmospheres contained in smog chambers. On the basis of such studies and by utilizing fundamental kinetic and mechanistic data, both highly detailed complex mechanisms (ref. 1) and simplified lumped parameter models (ref. 5) have been developed. These predict values in quite good agreement with experiments for such parameters as rates of loss of hydrocarbons, rates of formation of O₃ and peroxyacetyl nitrate (PAN), NO to NO₂ conversion, and maximum O₃ levels. However, as implied earlier in a more general context, it is the author's personal feeling that a sense of false security has developed in some quarters as to the actual ability of such models to reflect accurately the events occurring in real ambient air over wide ranges of temperature, relative humidity, intensity and wavelength of solar irradiation, and number, nature and concentration of reactants - all in a heterogeneous system where gas-to-particle conversion and associated surface reactions play a major role in determining air quality.

Therefore, over the last few years the research team at the Statewide Air Pollution Research Center (SAPRC) and the Chemistry Department at the University of California, Riverside, has developed several facilities and experimental techniques that permit exploration of the effects of changing these variables on the rates and mechanisms of formation of major, minor, and trace pollutants over a wide range of concentrations, approximately 10 ppm to 10 ppb. The following sections illustrate how these facilities have been used to test several recently expressed ideas important to modeling tropospheric reactions and how these ideas were found to be significantly in error.

SMOG CHAMBER STUDIES OF PHOTOCHEMICAL SMOG FORMATION IN SIMULATED URBAN ATMOSPHERES

Spectroscopic Identification and Measurement of Minor and Trace Products

Having Mechanistic and Health Implications:

Establishment of a Material Balance

Two of the grave deficiencies of many of the earlier experiments on photochemical oxidant formation from HC-NO_x mixtures in smog chambers are (1) the inability to detect by conventional methods (e.g., "wet chemistry") many of the highly labile molecules produced and (2) as a consequence, an inability to achieve good (e.g., 85 to 90 percent or greater) overall material balances for nitrogen and carbon, indicating that substantial quantities of products were not being identified. Obviously, at best this lack of crucial product information

frustrates those attempting to develop reliable mechanisms for the photooxidation of various HC-NO_x systems; in practice, the problem becomes critical when smog chamber results with such information gaps are used without considerable caution in developing computer kinetic models of photochemical smog.

The short scan times, large wave number range per scan, and high spectral resolution and sensitivity of long-path (50 to 1000 m) Fourier transform infrared (FT-IR) spectrometers make them highly useful tools for determining time-concentration profiles for a large number of reactive species that cannot be measured by conventional monitoring instruments. Furthermore, in situ FT-IR spectroscopy can contribute to improved nitrogen and carbon balance in chamber experiments. For example, an interferometer interfaced with a multiple-reflection cell in the SAPRC 5800-liter evacuable smog chamber (fig. 1) was used to measure spectra during an experiment in which a mixture of propylene, NO, and NO₂ (at concentrations in the ppm range) in air at 9.4° C was irradiated with a 24-kW solar simulator.

A high-resolution (0.125 cm⁻¹) spectrum from this run, shown in figure 2, contains quantitative information about four species not normally monitored in smog-chamber studies, nitric acid (HNO₃), peroxyxynitric acid (HOONO₂), formic acid (HCOOH), and N₂O₅, and a fifth, formaldehyde (HCHO), that is generally monitored by a notoriously unreliable wet-chemical method. The observation and quantitative determination (with a time resolution of several minutes during a multihour irradiation) of these species illustrate the increased amount of useful chemical information afforded by the FT-IR technique. In part, this has allowed much better mass balances, approaching 100 percent, to be obtained.

It is interesting that it was in similar FT-IR studies that the formation of peroxyxynitric acid was first discovered in 1976 by Niki and co-workers (ref. 6) and independently by Hanst and Gay (ref. 7). Until that time the generation of peroxyxynitric acid under atmospheric conditions generally had not been anticipated. Formation of HOONO₂ by reaction of HO₂ with NO₂ in photochemical smog (as well as in the stratosphere) is plausible both thermodynamically and kinetically. However, while the rate of formation of HOONO₂ in such systems could be as large as that of peroxyacetyl nitrate (PAN), it is less stable thermally. Thus, only low concentrations of HOONO₂, relative to PAN, should be expected under warm, ambient conditions. However, the discovery in the laboratory of HOONO₂ by FT-IR spectroscopy has spurred a search for it in ambient air, especially on cooler days in bright sunlight.

Effects of Temperature on Ozone Formation

One of the long-term myths about photochemical smog is based in part on statistical analysis of air quality data in the Los Angeles Air Basin. Essentially, the myth is that ozone formation is negligible at temperatures below 13° C; indeed this statement was made in a recent draft of the revised EPA document, "Air Quality Criteria for Photochemical Oxidants."

In order to examine the validity of this statement and to test current models of photochemical smog which are based to a large degree on smog chamber data taken at typical chamber operating temperatures (20° to 30° C), the SAPRC

research team recently initiated a series of experiments on HC-NO_x mixtures in air over a wide temperature range (5° to 50° C) in the thermostatted, evacuable chamber (fig. 1). Preliminary results are interesting and informative.

First, in a mixture of a HC surrogate (2.3 ppm of carbon) and NO_x (0.24 ppm) at 5° C, enough O₃ was generated to exceed the Federal ambient air quality standard for oxidant, 0.08 ppm for 1 hour. This seems to refute the statement cited at the beginning of this section, especially when taken with the recent observation that significant levels of O₃ can build up on bright and cold winter days in Denver.

Second, in a run at 49° C two especially interesting features of the O₃ time-concentration profiles were observed: not only did the ozone maximum occur after complete consumption of the NO_x initially present (and plateau at the peak for over 1 hour), but also there were two ozone maxima. To the author's knowledge, this is the first time that such phenomena have been observed in smog chamber studies. Thus, although in these runs the HC and NO_x concentrations were in the ppm range and it remains to be seen whether these phenomena also occur at concentration levels in the ambient range, it is abundantly clear that the atmospheric chemistry of the polluted troposphere is significantly dependent on temperature. Although this can be deduced from an examination of the temperature dependencies of certain key elementary reactions in current models, for example, the temperature coefficient of the rate of dissociation of PAN,



obviously a great deal of experimental work must be carried out in the future to obtain specific, accurate information on this important, real-world concern: What is the effect of temperature on photochemical oxidants?

AMBIENT AIR STUDIES OF PHOTOCHEMICAL SMOG

Identification of Trace Pollutants

In order to obtain a comprehensive understanding of chemical and physical transformations in the polluted troposphere so that one can validate kinetic computer models (and better estimate the possible impact of photochemical smog on health), conventional air monitoring instrumentation must be augmented by sensitive and specific analytical methods for trace species. For the past 25 years, long-path infrared (LP-IR) absorption spectroscopy has played an important role in the identification and quantitative determination of such trace pollutants, not only in chambers (vide supra) but also in ambient air. Two examples are the discovery and identification of PAN in photochemical smog some 20 years ago by Stephens and associates (ref. 8) and the FT-IR study of ambient smog by Hanst and associates of the EPA in Pasadena, California, in the summer of 1973 (ref. 9).

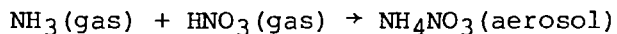
In collaboration with Hanst, who designed and furnished the basic instrument, another long-path Fourier transform infrared facility (in addition to that

associated with the evacuable chamber, vide supra) was established at SAPRC in the summer of 1976. The prime task was to employ this system to identify and measure trace species in the ppb to pphm (parts per hundred million) concentration range in ambient atmospheres. The design and operation of this FT-IR facility and some of the initial results obtained with it are summarized here and presented in more detail elsewhere (ref. 10).

In this system, a Fourier transform infrared spectrometer has been interfaced with a multiple-reflection cell consisting of eight gold-coated mirrors with a 22.5-m base path (fig. 3). This cell has been routinely operated at total path lengths of 1 km or greater, and detection limits of 2 to 10 ppb have been established for many species suspected or known to be present in photochemical smog. These include HCHO, HCOOH, HNO₃, HONO, NH₃, N₂O₅, PAN, and other peroxyacyl nitrates. Some of these are shown in table I (refs. 9 and 11 to 15), along with the useful measurement frequencies and the absorptivities (as well as the resolutions at which they were measured).

During the summer of 1976 the first spectroscopic detection of HNO₃ and HCHO in ambient smog was achieved and time-concentration profiles were obtained for these species as well as for formic acid, ammonia, ozone, and PAN (ref. 10). Concentrations of a number of these trace species detected during a smog episode in Riverside, California, on August 12, 1977, as determined with this FT-IR facility operating at a path length of 900 m, are shown in table II. Of particular interest is the fact that substantial levels of the basic NH₃ and the acidic HNO₃ can coexist in ambient smog, as seen from the spectra taken at 12:32 (fig. 4).

Clearly, much research lies ahead in order to understand better the obviously complex interactions in the heterogeneous system,



Indeed, such an understanding may well be essential in determining the extent and causes of a so-called nitrate filter artifact that has been reported recently by several laboratories. Thus, in the past, using conventional high volume samplers and glass fiber filters, particulate nitrate levels as high as 80 µg/m³ on some winter days have been reported at a number of monitoring stations throughout California's South Coast Air Basin. However, Spicer et al. have presented considerable evidence that much of this nitrate that has been assumed to be particulate in origin actually may result from gaseous nitric acid being neutralized on the glass filter (ref. 16). There seems to be a problem here, and current research is going on in a number of laboratories to define its nature and magnitude.

Another species of considerable interest in terms of its mechanistic importance is hydrogen peroxide. In photochemical smog, it is formed in a chain termination reaction and, indeed, is an index of hydroperoxyl (HO₂) radical concentrations. Thus, knowledge of the concentration of H₂O₂ in simulated atmospheric systems and actual urban smog is particularly interesting to atmospheric modelers. However, because of the analytical difficulties encountered in measurements of ppb concentrations of H₂O₂, there have been relatively few laboratory or smog chamber studies in which its levels were

monitored quantitatively, or even qualitatively. Furthermore, there has been only one set of atmospheric measurements, that of Gay and Bufalini (ref. 17). These workers reported H_2O_2 concentrations of up to 40 ppb in Hoboken, New Jersey, and of up to 180 ppb in Riverside, California, in 1970 during a very severe smog episode in which the oxidant concentration reached 0.65 ppm.

Recently SAPRC collaborated with Kok and co-workers at Harvey Mudd College and Gay from the EPA Research Triangle Park Laboratory in measurements of hydrogen peroxide concentrations at two locations (Claremont and Riverside) in California's South Coast Air Basin during the months of July and August 1977. Three different analytical methods were employed: a chemiluminescent method and two colorimetric procedures.

There was reasonable agreement among the three procedures, and typical midafternoon concentrations of H_2O_2 during moderate smog episodes (i.e., O_3 concentrations of ≈ 150 to 220 ppb) ranged from approximately 10 to 30 ppb. These values are much lower than the 180 ppb reported by Gay and Bufalini in the 1970 study in Riverside. Hopefully, predictions of ambient H_2O_2 levels generated from current chemical computer models will be consistent with these new, significantly lower values for hydrogen peroxide in ambient air.

Chemical Inhibition of Photochemical Smog

Recently, a proposal for controlling the products of photochemical smog such as O_3 , PAN, and secondary aerosols by adding to urban air 100 ppb of an inhibitor, diethylhydroxylamine (DEHA), $(C_2H_5)_2NOH$, has been strongly advocated in some quarters (ref. 18). This chemical approach, Heicklen has stated, would eliminate the need for exhaust control devices on motor vehicles and save billions of dollars. Indeed, actual field trials involving introduction of DEHA into the air of several major cities in the world suffering from photochemical smog have been suggested (ref. 19).

Heicklen's research on which his proposal was originally based was carried out on $HC-NO_x$ systems containing DEHA at concentration levels greater than 1 ppm and was generally conducted under laboratory, not simulated ambient, conditions. Thus the researchers at SAPRC, among others, were concerned not only with the possible health effects of photooxidation products of $DEHA-NO_x-HC$ mixtures generated in ambient photochemical smog but also with the atmospheric uncertainties involved in this extrapolation (ref. 19).

To test the idea under realistic conditions, the reactions of 100 ppb and 500 ppb of DEHA in ambient air or in hydrocarbon surrogate mixtures simulating 6 to 9 a.m. Los Angeles air were studied in a large outdoor environmental chamber constructed from 2-mil Teflon² (FEP) fluorocarbon film (ref. 20), similar to the chamber shown in figure 5.

Typically, the chamber was first covered with a black plastic light shield and filled with ambient air to a volume of about 50 m³. It was then divided

²Teflon: Registered trademark of E. I. du Pont de Nemours & Co., Inc.

into two compartments of equal volume and a known amount of DEHA in high-purity N₂ was added to one of the compartments. The black cover was then removed exposing both compartments to sunlight for at least 6 hours. Since identical samples of polluted air, one with and one without DEHA, were subjected simultaneously to the same environmental conditions (i.e., solar irradiation, temperature, and humidity), differences in the time-concentration profiles of the smog parameters measured in the two compartments could unambiguously be attributed to the DEHA in one compartment.

The results for an experiment in which 100 ppb of DEHA was added to Riverside ambient air were quite revealing. The DEHA did not inhibit formation of photochemical smog; in fact, it substantially accelerated the conversion of NO to NO₂ as well as the production of O₃, PAN, and light-scattering secondary aerosols.

With 0.5 ppm of DEHA added to ambient air doped with the hydrocarbon surrogate mixture, an "intermediate" behavior was observed. Inhibition was predominant during the first hour of irradiation, but at that point a marked acceleration of smog formation took place.

In short, DEHA is indeed an inhibitor of certain symptoms of photochemical smog for several hours when present at ppm concentrations. However, it is an accelerator of O₃, PAN, and aerosol formation and NO to NO₂ conversion when present at the 100 ppb level recommended. Furthermore, even if high ppm levels of DEHA (odor threshold 0.5 ppm) could be added to ambient air (not considering the health implications, which could be serious), its dilution as the air mass was being transported would soon lead to increased photochemical smog in suburban, and even rural areas, downwind.

Clearly, proposals for the control of photochemical smog by chemical additives cannot be based only on extrapolations from experiments conducted in the laboratory at torr pressure and ppb concentration ranges. They must be experimentally validated at realistic pollutant levels in ambient air.

CHEMICAL MUTAGENS AND/OR CARCINOGENS IN REAL AND SIMULATED ATMOSPHERES

Historically, researchers and control officials have focused their attention on the criteria air pollutants - sulfur dioxide, carbon monoxide, nitrogen dioxide, photochemical oxidants (including ozone), and total suspended particulates. Recently, however, as discussed previously, considerable interest has developed in better understanding the sources, transport, and associated chemical and physical transformations and sinks of several types of "noncriteria" pollutants, including those cited in table II. Certain of these species, though present in urban atmospheres at much lower concentrations than the criteria pollutants, are known to produce disproportionately severe health effects in experimental animals, and possibly in man. A classic example is the well-known carcinogenic polycyclic aromatic hydrocarbon (PAH) benzo(a)pyrene (BaP). It is formed during the combustion of fossil fuels and in 1952 was identified and measured in ambient particulate soot particles collected at 10 stations throughout Great Britain by Waller (ref. 21). Today it is known to be distributed globally.

A second class of noncriteria pollutants of current concern are the N-nitrosamines, very potent carcinogens having the general formula R_2NNO . Recently, they have been identified in a variety of systems including pesticides, synthetic cutting and grinding fluids, and drinking water. However, in contrast to the ubiquitous nature of BaP, they have been identified as air pollutants only in a limited number of locations, including those in or near industrial plants in East Germany (ref. 22) and the United States (refs. 23 to 27). The Germany industry employed dimethylamine (DMA) and the United States plant dimethylnitrosamine (DMN) in organic syntheses.

Pronounced societal interest in such real or potential atmospheric carcinogens is illustrated by the amendments to the U.S. Clean Air Act passed by Congress and signed into law by President Carter in August 1977. Thus, Section 104(b) requires the Administrator of the U.S. Environmental Protection Agency to review and critique all available information on "nitric and nitrous acids, nitrites, nitrates, nitrosamines, and other carcinogenic and potentially carcinogenic derivatives of oxides of nitrogen." Similarly in Section 122(a), the Administrator is required to "determine whether or not emissions of polycyclic organic matter (POM) into the ambient air will cause, or contribute to air pollution which may reasonably be anticipated to endanger public health."

Clearly, these mandates reflect growing concern over possible health effects of increasing emissions of NO_x and organic particulates associated with proposed major shifts to a far greater use of coal, shale oil, diesel-powered motor vehicles, and so forth, to relieve, in part, the energy crisis facing the United States.

In terms of the thrust of this paper, fiction and fact in atmospheric chemistry, clouding the issue with respect to particulate polycyclic aromatic hydrocarbons as air pollutants are statements such as "They are chemically inert and thus are removed from the air only by rain or the slow sedimentation of the particulate." (See refs. 28 and 29.) Actually, although the evidence to date is meager, chemically speaking many PAH, including BaP, are reactive compounds in the laboratory. Thus, they might well undergo a variety of thermal and photochemical reactions in urban air with a number of copollutants; these include both molecular and radical species. (For detailed reviews, see refs. 30 and 31.)

With respect to nitrosamines, a 1976 EPA review and critique (ref. 32) states that in solution, "Unlike the secondary amines which can form nitrosamines . . . only a few tertiary amines form nitrosamines." This is clearly not the case; tertiary amines do in fact react readily in solution with aqueous nitrous acid to form N-nitrosamines (refs. 33 to 35). A key question is, "Can tertiary and secondary aliphatic amines at sub-ppm concentrations react in air with ambient levels of NO_x (containing small traces of nitrous acid)?" Thus, Hanst et al. recently showed that dimethylamine (DMA) reacts readily with HONO in air to produce dimethylnitrosamine (DMN) when both are in the ppm concentration range (ref. 36).

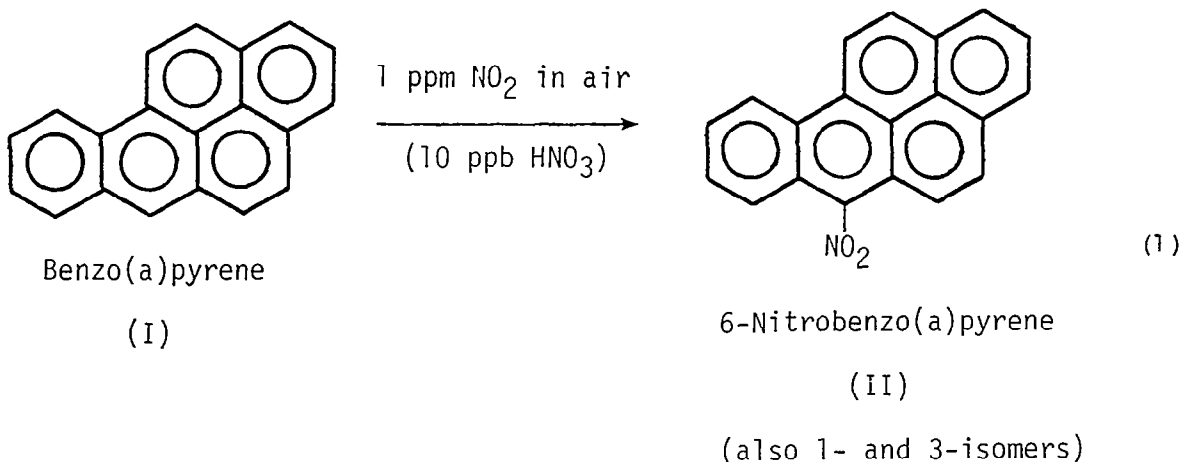
To resolve such issues involving known and potential atmospheric carcinogens, researchers at SAPRC have been studying (1) reactions in simulated and

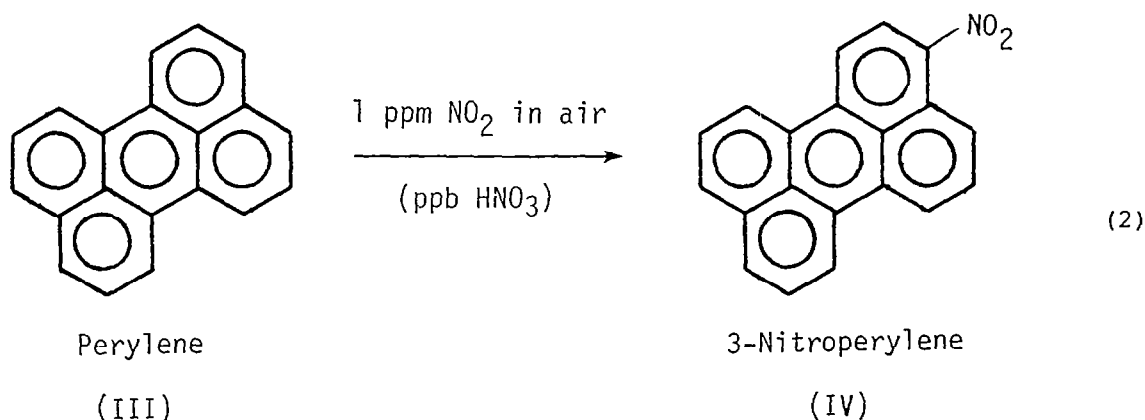
real urban atmospheres of the carcinogen BaP and of its noncarcinogenic isomer perylene and (2) reactions of mixtures of simple aliphatic amines and NO_x in air containing traces of HONO. Although at first glance the two systems, particulate PAH and gaseous nitrosamines, may seem quite unrelated, they both participate in chemical transformations in which OH and HO_2 radicals and NO_x play major roles, just as these species do in tropospheric photochemical smog and in determining the stratospheric ozone balance. For detailed considerations, the following SAPRC papers should be consulted: references 37 and 38, on the mutagenic activity of ambient organic particulates; reference 39, a recent review and discussion of the reactions of PAH and nitrosamines in simulated atmospheres which will be appearing in the Philosophical Transactions of the Royal Society; and references 40 to 41, two detailed papers on thermal and photochemical reactions in amine- NO_x -HONO-air systems.

Polycyclic Aromatic Hydrocarbons

SAPRC recently discovered direct mutagenic activity, as determined by the Ames' Salmonella typhimurium reversion microbiological assay (refs. 42 to 44) in the organic fractions of all ambient urban aerosols collected throughout southern California. This discovery led to an investigation of the reactions of BaP deposited on washed glass fiber filters with ambient photochemical smog, as well as with approximately ppm levels of O_3 , NO_2 , and PAN in simulated atmospheres. In direct contrast to the statements cited previously (refs. 28 and 29), a variety of derivatives of BaP are readily formed, including phenols, diphenols, dihydrodiols, and quinones (ref. 39).

Furthermore, in contrast to BaP which is an activatable mutagen (a promutagen) requiring microsomal activation to produce mutagenic activity, it was found that directly mutagenic nitroderivatives of BaP are readily formed upon exposure of the coated filters to 1 ppm of NO_2 in air. Additionally, it was recently found that directly mutagenic nitroderivatives are formed in a facile reaction not only from the known carcinogen BaP but also from perylene and pyrene. Both of these PAH are noncarcinogens and, along with BaP, are widely distributed in organic particulate pollutants from a variety of sources. The acid catalyzed reactions with NO_2 of BaP and perylene (deposited on filters) are as follows:





If such reactions actually occur in urban atmospheres, they may account in part for the formation of the presently unknown species responsible for the "excess" carcinogenicity (over that which could be ascribed to other known carcinogenic polycyclic aromatic compounds measured in the samples) that has been observed in animals treated with organic extracts of the particulates collected from smog and exhausts of gasoline engines (ref. 31). However, complicating matters is the fact that such gas-solid interface processes as those observed for NO₂ and the three PAH may also have occurred on the filters used to collect the particulates which were then extracted and administered to the experimental animals. Thus, the possibility of such filter artifacts must be recognized when using existing air quality data on particulate PAH to develop and validate models predicting their atmospheric levels and possible health effects (e.g., dose-response curves). Finally, there is a distinct possibility that BaP, perylene, and other PAH may react differently depending upon the physical and chemical nature of the surfaces on which they are deposited. All of these points seem relevant to atmospheric modeling of these heterogeneous processes.

Atmospheric Chemistry of Amine-NO_x Mixtures

The SAPRC research group recently studied the reactions in air of the possible atmospheric precursors to diethylnitrosamine, (C₂H₅)₂NNO, that is, mixtures of secondary or tertiary amines with NO_x and some HONO. Experiments were conducted both at sub-ppm levels in air in the 50 m³ outdoor chamber shown in figure 5 (ref. 40) and at ppm levels in the long-path (720 m) FT-IR facility described earlier (fig. 3 (ref. 41)).

At sub-ppm concentrations, both diethylamine (DEA) and triethylamine (TEA) in the presence of ambient levels of NO_x (~300 ppb) readily form photochemical oxidants (e.g., O₃, PAN, and aerosols). This is seen in figure 6(a) which shows the time-concentration profiles for the loss of TEA and the formation of certain oxidant-type products. Additionally, small but significant amounts of (C₂H₅)₂NNO are formed in the dark from DEA (~3 percent yield) but are destroyed in sunlight. In contrast, (C₂H₅)₂NNO is initially formed on irradiation of TEA-NO_x mixtures containing some HONO, reaches a maximum (~1.8 percent yield), and then subsequently photodecomposes (fig. 6(b)). Thus,

in contrast to the recent EPA statement cited previously (ref. 32), under the appropriate circumstances, tertiary amines can in fact react in sunlight with air containing NO_x and HONO to form nitrosamines.

Other significant nitrogenous compounds formed in sunlight from both DEA- NO_x and TEA- NO_x mixtures include dialkyl nitramines (R_2NNO_2), which are a major product of all amines, and a number of substituted amides (fig. 6(b)). As a spin-off, dimethyl nitramine (CH_3) $_2\text{NNO}_2$ was in fact shown to be the "unknown major product" found by Hanst et al. when they irradiated dimethyl nitrosamine in air (ref. 36). Finally, small amounts of acetamide (CH_3CONH_2) are present in the particulate phase from irradiation of both DEA- NO_x and TEA- NO_x mixtures.

In terms of the biological and environmental implications of these results, it is somewhat sobering to note that both (CH_3) $_2\text{NNO}_2$ and CH_3CONH_2 are carcinogens in animals, though less potent than nitrosamines; the activity of dimethyl nitramine (C_2H_5) $_2\text{NNO}_2$ is not known. Furthermore, amines are emitted into industrial atmospheres as a result of a wide variety of activities; some of these are secondary and tertiary aliphatic amines or related compounds such as ethanolamines. However, although little is known about their concentrations in ambient air, they are probably usually very low. Thus, the risk of forming significant amounts of nitrosamines or nitramines in urban air from their precursors seems correspondingly small.

However, in industrial situations in which sub-ppm concentrations of amines may be released into urban atmospheres containing NO_x and HONO, within and immediately downwind from the facility, formation of significant amounts of nitrosamines in the dark and nitramines and amides in sunlight seems possible. Clearly, in such cases, measurement of the actual ambient levels of amines, NO_x , nitrosamines, nitramines, and, if possible, HONO would be useful to modelers and control officials alike.

CONCLUSION

While the science of atmospheric chemistry is advancing rapidly, the several examples of results from current research cited in this paper may serve to demonstrate that there is more to air pollution, and its modeling, than meets the eye.

REFERENCES

1. Demerjian, Kenneth L.; Kerr, J. Alistair; and Calvert, Jack G.: The Mechanism of Photochemical Smog Formation. *Advances in Environmental Science and Technology*, Volume 4, James N. Pitts, Jr., and Robert L. Metcalf, eds., John Wiley & Sons, c.1974, pp. 1-262.
2. Finlayson, Barbara J.; and Pitts, James N., Jr.: Photochemistry of the Polluted Troposphere. *Science*, vol. 192, no. 4235, Apr. 9, 1976, pp. 111-119.
3. Finlayson-Pitts, Barbara J.; and Pitts, James N., Jr.: The Chemical Basis of Air Quality: Kinetics and Mechanisms of Photochemical Air Pollution and Application to Control Strategies. *Advances in Environmental Science and Technology*, Volume 7, James N. Pitts, Jr., and Robert L. Metcalf, eds., John Wiley & Sons, c.1977, pp. 75-162.
4. Calvert, J. G.; and Pitts, J. N.: *Photochemistry*. John Wiley & Sons, Inc., 1966.
5. Hecht, Thomas A.; Seinfeld, John H.; and Dodge, Marcia C.: Further Development of Generalized Kinetic Mechanism for Photochemical Smog. *Environ. Sci. & Technol.*, vol. 8, no. 4, Apr. 1974, pp. 327-339.
6. Niki, H.; Maker, P. D.; Savage, C. M.; and Breitenbach, L. P.: Fourier Transform IR Spectroscopic Observation of Pernitric Acid Formed Via $\text{HO}_2 + \text{NO}_2 \rightarrow \text{HOONO}_2$. *Chem. Phys. Lett.*, vol. 45, no. 3, Feb. 1, 1977, pp. 564-566.
7. Hanst, Philip L.; and Gay, Bruce W., Jr.: Photochemical Reactions Among Formaldehyde, Chlorine, and Nitrogen Dioxide in Air. *Environ. Sci. & Technol.*, vol. 11, no. 12, Nov. 1977, pp. 1105-1109.
8. Stephens, Edgar R.; Hanst, Philip L.; Doerr, Robert C.; and Scott, William E.: Reactions of Nitrogen Dioxide and Organic Compounds in Air. *Ind. & Eng. Chem.*, vol. 48, no. 9, Sept. 1956, pp. 1498-1504.
9. Hanst, Philip L.; Wilson, William E.; Patterson, Ronald K.; Gay, Bruce W., Jr.; Chaney, Lucian W.; and Burton, Charles S.: A Spectroscopic Study of California Smog. EPA-650/4-75-006, U.S. Environ. Prot. Agency, Feb. 1975. (Available from NTIS as PB 241 022.)
10. Tuazon, E. C.; Graham, R. A.; Winer, A. M.; Easton, R. R.; Pitts, J. N., Jr.; and Hanst, P. L.: A Kilometer Pathlength Fourier-Transform Infrared System for the Study of Trace Pollutants in Ambient and Synthetic Atmospheres. *Atmos. Environ.*, vol. 12, no. 4, 1978, pp. 865-875.

11. Pitts, James N., Jr.; McAfee, John M.; Long, William D.; and Winer, Arthur M.: Long-Path Infrared Spectroscopic Investigation at Ambient Concentrations of the 2% Neutral Buffered Potassium Iodide Method for Determination of Ozone. *Environ. Sci. & Technol.*, vol. 10, no. 8, Aug. 1976, pp. 787-793.
12. McAfee, John M.; Stephens, Edgar R.; Fitz, Dennis R.; and Pitts, James N., Jr.: Infrared Absorptivity of the 9.6 μm Ozone Band as a Function of Spectral Resolution and Abundance. *J. Quant. Spectros. & Radiat. Transfer*, vol. 16, no. 10, Oct. 1976, pp. 829-837.
13. Stephens, Edgar R.: Absorptivities for Infrared Determination of Peroxyacyl Nitrates. *Anal. Chem.*, vol. 36, no. 4, Apr. 1964, pp. 928-929.
14. Chan, Walter H.; Nordstrom, Robert J.; Calvert, Jack G.; and Shaw, John H.: Kinetic Study of HONO Formation and Decay Reactions in Gaseous Mixtures of HONO, NO, NO₂, H₂O, and N₂. *Environ. Sci. & Technol.*, vol. 10, no. 7, July 1976, pp. 674-682.
15. Graham, Richard A.; Winer, Arthur M.; and Pitts, James N., Jr.: Temperature Dependence of the Unimolecular Decomposition of Pernitric Acid and Its Atmospheric Implications. *Chem. Phys. Lett.*, vol. 51, no. 2, Oct. 15, 1977, pp. 215-220.
16. Spicer, Chester W.; Schumacher, Philip M.; Kouyoumjian, John A.; and Joseph, Darrell W.: Sampling and Analytical Methodology for Atmospheric Particulate Nitrates - Final Report. EPA Contract No. 68-02-2213, Battelle Columbus Lab.
17. Gay, Bruce W., Jr.; and Bufalini, Joseph J.: Hydrogen Peroxide in the Urban Atmosphere. *Adv. Chem. Ser. No. 113*, 1972, pp. 255-263.
18. Heicklen, J.: The DEHA Method of Photochemical Smog Control. Proceedings of Specialty Conference on Ozone/Oxidants - Interaction With the Total Environment, Air Pollut. Control Assoc., 1976, pp. 146-156.
19. Maugh, Thomas H., II: Photochemical Smog: Is It Safe To Treat the Air? *Science*, vol. 193, no. 4256, Sept. 3, 1976, pp. 871-873.
20. Pitts, James N., Jr.; Smith, Jerome P.; Fitz, Dennis R.; and Grosjean, Daniel: Enhancement of Photochemical Smog by N,N'-Diethylhydroxylamine in Polluted Ambient Air. *Science*, vol. 197, no. 4300, July 15, 1977, pp. 255-257.
21. Waller, R. E.: The Benzopyrene Content of Town Air. *British J. Cancer*, vol. 6, 1952, pp. 8-21.
22. Bretschneider, K.; and Matz, J.: Nitrosamines in the Atmospheric Air and in the Air at the Places of Employment. *Arch. Geschwulstforsch.*, vol. 43, no. 1, 1974, pp. 36-41.

23. Fine, D. H.; Rounbehler, D. P.; Belcher, N. M.; and Epstein, S. S.: N-Nitroso Compounds: Detection in Ambient Air. *Science*, vol. 192, no. 4246, June 25, 1976, pp. 1328-1330.
24. Fine, D.; Edwards, G.; Krull, I.; and Wolf, M.: N-Nitroso Compounds in the Air Environment. Paper Presented at 175th American Chem. Soc. Natl. Meeting (Anaheim, California), Mar. 1978.
25. Fine, David H.; Rounbehler, David P.; Rounbehler, Anna; Silvergleid, Arlene; Sawicki, Eugene; Krost, Ken; and DeMarrais, Gerard A.: Determination of Dimethylnitrosamine in Air, Water, and Soil by Thermal Energy Analysis: Measurements in Baltimore, Md. *Environ. Sci. & Technol.*, vol. 11, no. 6, June 1977, pp. 581-584.
26. Pellizzari, Edo D.: The Measurement of Carcinogenic Vapors in Ambient Atmospheres. EPA-600/7-77-055, U.S. Environ. Prot. Agency, June 1977. (Available from NTIS as PB 269 582.)
27. Reconnaissance of Environmental Levels of Nitrosamines in the Central United States. EPA-330/1-77-001, U.S. Environ. Prot. Agency, Feb. 1977.
28. Berry, R. Stephen; and Lehman, Peter A.: Aerochemistry of Air Pollution. Annual Review of Physical Chemistry, Volume 22, H. Eyring, C. J. Christensen, and H. S. Hohnston, eds., Annu. Rev., Inc., 1971, pp. 47-84.
29. Fishbein, Lawrence: Atmospheric Mutagens. Chemical Mutagens - Principles and Methods for Their Detection, Volume 4, Alexander Hollaender, ed., Plenum Press, c.1976, pp. 219-319.
30. Committee on Biologic Effects of Atmospheric Pollutants, Div. Medical Sci.: Particulate Polycyclic Organic Matter. Natl. Acad. Sci., 1972.
31. Hoffmann, Dietrich; and Wynder, Ernst L.: Organic Particulate Pollutants - Chemical Analysis and Bioassays for Carcinogenicity. Air Pollution - Third Edition. Volume II - The Effects of Air Pollution, Arthur C. Stern, ed., Academic Press, Inc., 1977, pp. 361-455.
32. Scientific and Technical Assessment Report on Nitrosamines. EPA-600/6-77-001, U.S. Environ. Prot. Agency, Nov. 1976.
33. Geuther, A.: Ueber die Einwirkung von salpetrigsaurem Kali auf Salzsaures Triethylamin. *Arch. Pharm. (Weinheim, Ger.)*, vol. 123, second series, 1865, pp. 200-202.
34. Smith, Peter A. S.; and Loeppky, Richard N.: Nitrosative Cleavage of Tertiary Amines. *J. American Chem. Soc.*, vol. 89, no. 5, Mar. 1, 1967, pp. 1147-1157.
35. Walters, C. L.: Nitrosamines - Environmental Carcinogens? *Chem. Britain*, vol. 13, no. 4, Apr. 1977, pp. 140-145.

36. Hanst, Philip L.; Spence, John W.; and Miller, Matthew: Atmospheric Chemistry of N-Nitroso Dimethylamine. *Environ. Sci. & Technol.*, vol. 11, no. 4, Apr. 1977, pp. 403-405.
37. Pitts, James N., Jr.; Grosjean, Daniel; Mischke, Thomas M.; Simmon, Vincent F.; and Poole, Denis: Mutagenic Activity of Airborne Particulate Organic Pollutants. *Toxicol. Lett.*, vol. 1, 1977, pp. 65-70.
38. Pitts, James N., Jr.; Grosjean, Daniel; Mischke, Thomas M.; Simmon, Vincent F.; and Poole, Dennis: Mutagenic Activity of Airborne Particulate Organic Pollutants. Paper Presented at the 174th American Chemical Society Meeting, Symposium on Biological Effects of Environmental Pollutants (Chicago, Illinois), Aug. 1977.
39. Pitts, J. N., Jr.: Photochemical and Biological Implications of the Atmospheric Reactions of Amines and Benzo(a)pyrene. Paper presented at the Royal Society meeting on Pathways of Pollutants in the Atmosphere (London), Nov. 1977.
40. Pitts, James N., Jr.; Grosjean, Daniel; Van Cauwenberghe, Karel; Schmid, Joachim P.; and Fitz, Dennis R.: Photooxidation of Aliphatic Amines Under Simulated Atmospheric Conditions: Formation of Nitrosamines, Nitramines, Amides, and Photochemical Oxidant. *Environ. Sci. & Technol.*, vol. 12, no. 8, Aug. 1978.
41. Tuazon, Ernesto C.; Winer, Arthur M.; Graham, Richard A.; Schmid, Joachim P.; and Pitts, James N., Jr.: Fourier Transform Infrared Detection of Nitramines in Irradiated Amine-NO_x Systems. *Environ. Sci. & Technol.*, vol. 12, no. 8, Aug. 1978.
42. Ames, Bruce N.; Durston, William E.; Yamasaki, Edith; and Lee, Frank D.: Carcinogens Are Mutagens: A Simple Test System Combining Liver Homogenates for Activation and Bacteria for Detection. *Proc. Natl. Acad. Sci. USA*, vol. 70, no. 8, Aug. 1973, pp. 2281-2285.
43. Ames, Bruce N.; and McCann, Joyce: Carcinogens are Mutagens: A Simple Test System. *Screening Tests in Chemical Carcinogenesis*, R. Montesano, H. Bartsch, and L. Tomatis, eds., IARC Sci. Publ. No. 12, 1976, pp. 493-504.
44. Ames, Bruce N.; McCann, Joyce; and Yamasaki, Edith: Methods for Detecting Carcinogens and Mutagens With the Salmonella/Mammalian-Microsome Mutagenicity Test. *Mutat. Res.*, vol. 31, 1975, pp. 347-364.

TABLE I.- CALCULATED LIMITS FOR DETECTION BY LP-IR SPECTROSCOPY OF SEVERAL
IMPORTANT SPECIES IN PHOTOCHEMICAL SMOG

Compound	Measurement frequency, cm^{-1}	Absorptivity, ^a α , at 23° C and 760 torr, $\text{cm}^{-1}\text{-atm}^{-1}$	Resolution, cm^{-1}	Reference	Approximate detection limit at 1-km path, ppb
O ₃	1055	9.7	1 to 2	11 and 12	10
PAN	1162	32	2 to 4	13	3
NH ₃	931	27	0.5	Unpublished	4
	967.5	35	0.5		3
	993	21	0.5		4
HNO ₃	896	^b 12	0.5	Unpublished	6
HCHO	2779	^b 16	0.5	Unpublished	6
	2781.5				
HCOOH	1105	^b 70	0.5	Unpublished	2
HONO	791 (trans)	≈30	0.5	14	10 (cis + trans)
	853 (cis)	71	0.5		
H ₂ O ₂	1251	9 ± 3	2	9	40
HOONO ₂	803	^b 27	0.5 to 1	15	8

^a $\alpha = \ln(I_0/I)/pl$ where I_0 is incident intensity, I is transmitted intensity, l is path length (cm), and p is pressure (atm).

^bMeasured from the intensity of the Q branch only.

TABLE II.- POLLUTANT CONCENTRATIONS IN RIVERSIDE AIR, AUGUST 12, 1977, AS
 DETERMINED WITH THE FT-IR FACILITY OPERATING AT A PATH LENGTH OF 900 m

Time	Concentration, ppb, of -					
	O ₃	PAN	NH ₃	HNO ₃	HCOOH	HCHO
12:00	171	6	---	14	11	20
12:32	181	7	15	16	10	19
13:02	177	7	33	11	8	16
13:30	195	8	38	9	8	18
14:00	229	7	46	9	9	17
14:30	241	8	32	---	8	25
15:00	247	11	29	9	6	25
15:30	249	11	32	9	7	22
15:59	211	10	22	9	9	25
16:29	182	4	20	10	5	9
17:03	178	5	13	11	5	
17:12	182	6	9	10	7	
17:21						18
17:31						20
17:40	156	4	6	8	5	
17:49	156	7	7	9	6	
18:01						21
18:10						20

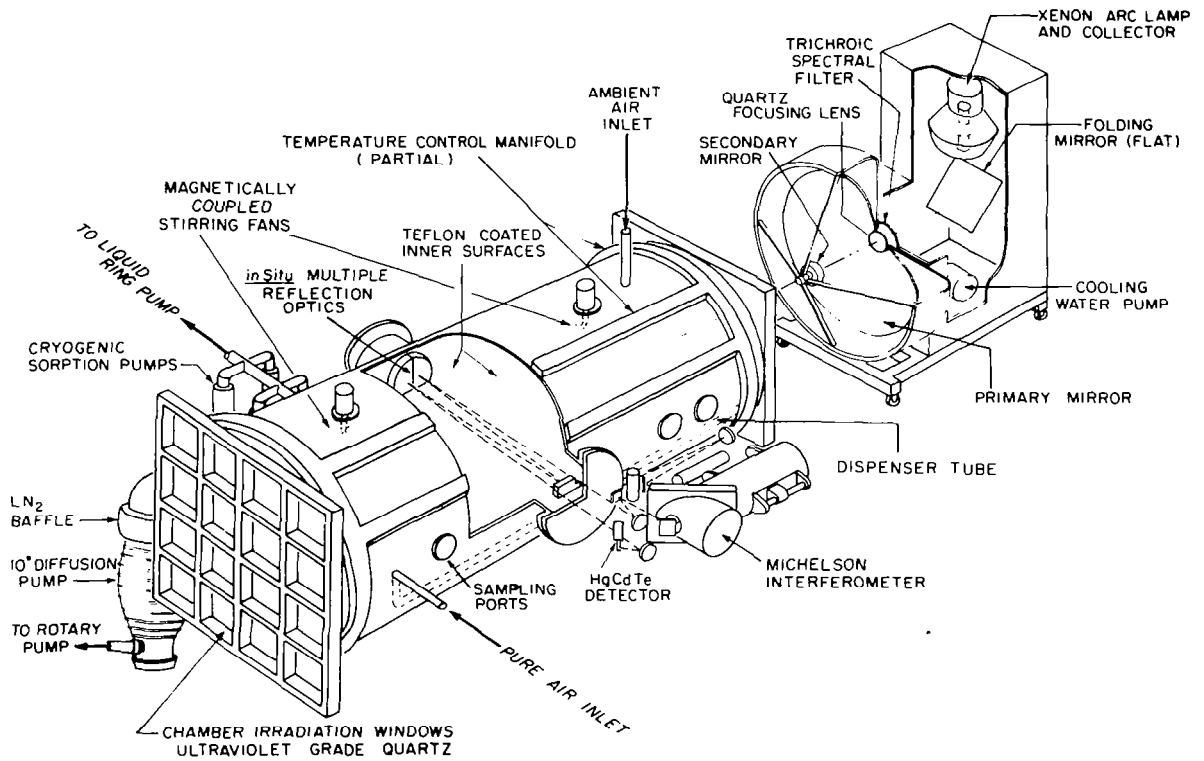


Figure 1.- SAPRC 5800-liter evacuable smog chamber, temperature controlled from -35°C to 100°C , and associated 24-kW solar simulator and Fourier interferometer with long-path infrared optical system.

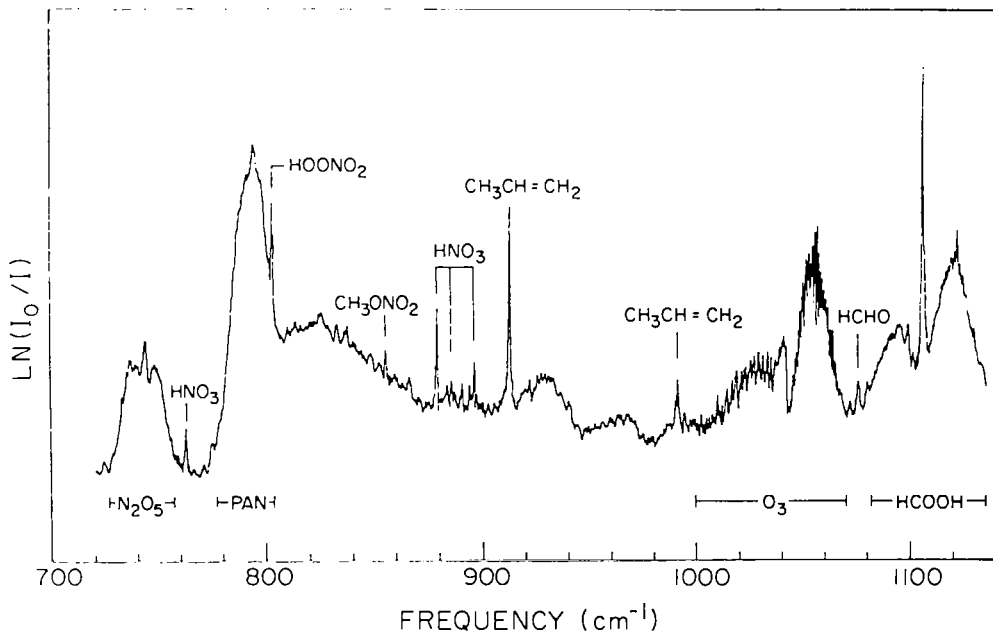


Figure 2.- FT-IR spectrum (absorbance $\text{LN}(I_0/I)$ versus frequency) of products from irradiation of a propylene- NO_x mixture in air at 9.4°C and 85-m path length.

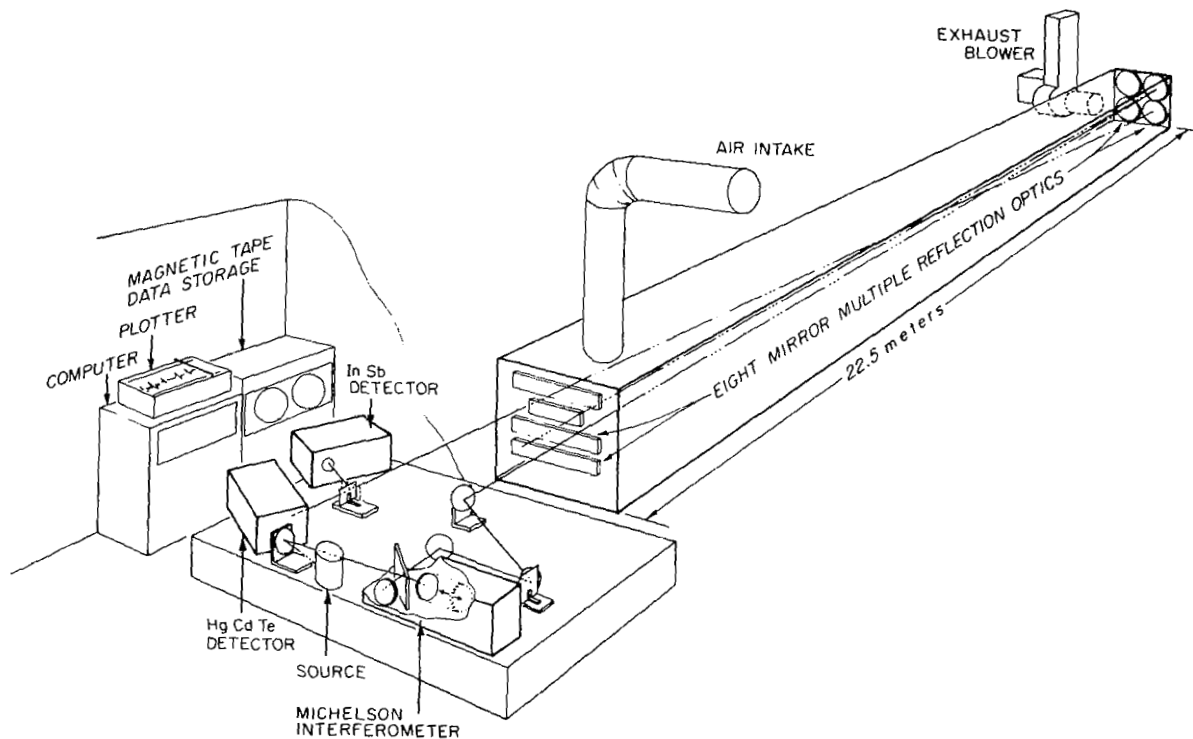


Figure 3.- FT-IR spectrometer and kilometer-path-length multiple-reflection cell used in identifying and measuring trace pollutants in ambient photochemical smog.

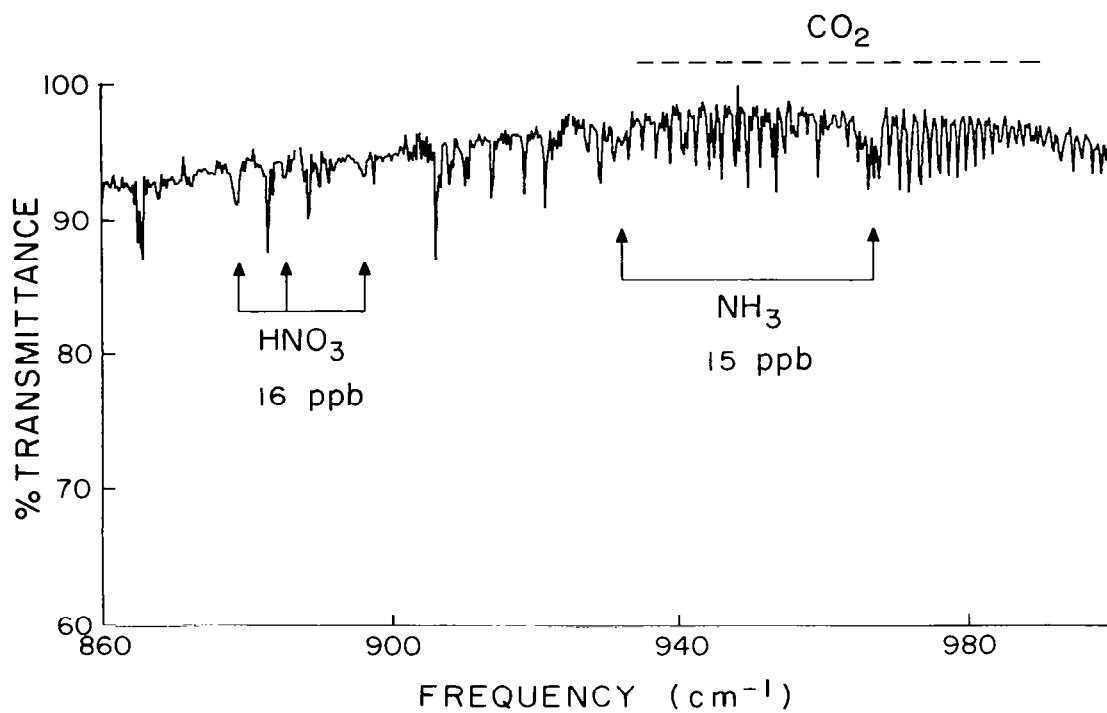


Figure 4.- Riverside ambient air spectrum (August 12, 1977, at 12:32) with 0.5-cm⁻¹ spectral resolution, 900-m path length, HgCdTe detector. Note simultaneous presence of nitric acid and ammonia.

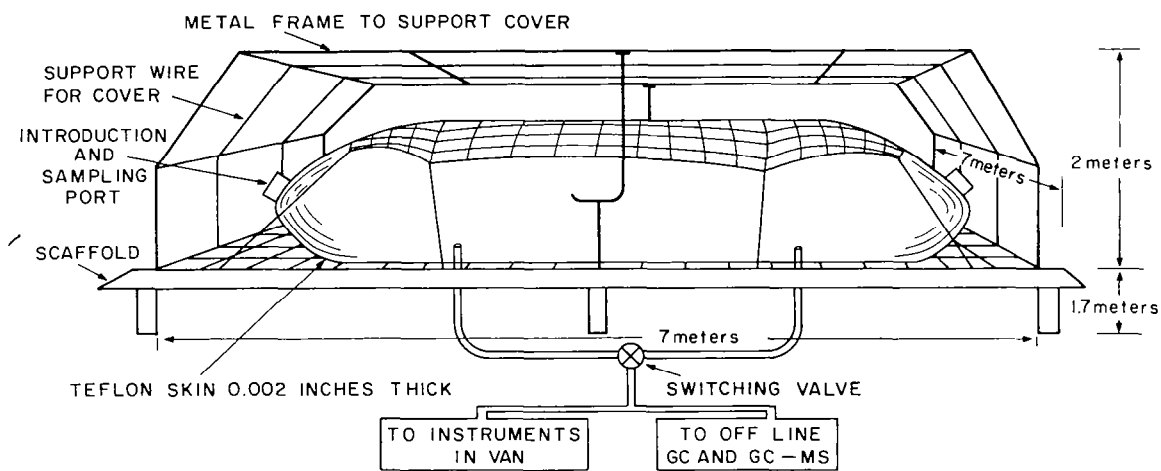
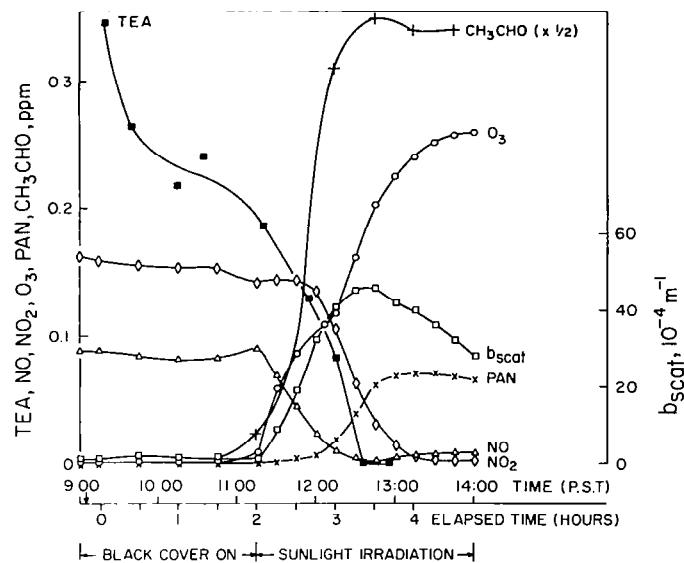
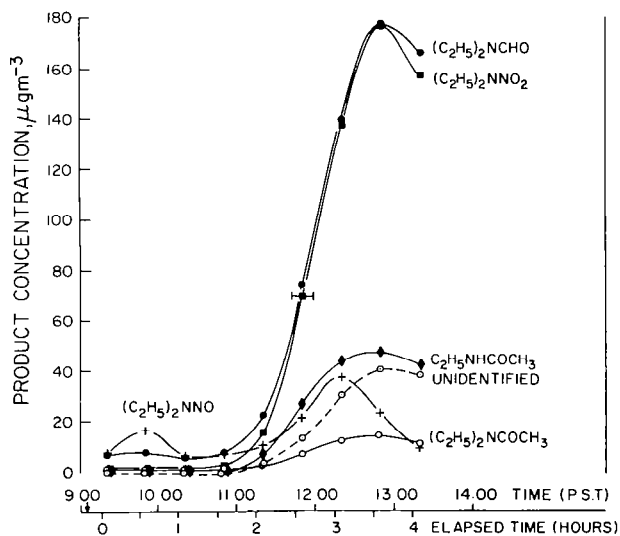


Figure 5.- Outdoor environmental chamber (50 m^3) for the study of the atmospheric reactions of amine- NO_x mixtures in the ppb to ppm concentration range.



(a) Concentrations of TEA, NO, NO₂, O₃, acetaldehyde, and PAN and light scattering coefficient b_{scat} .



(b) Concentrations of diethylformamide, diethylnitramine, ethylacetamide, diethylacetamide, and diethylnitrosamine. Concentration of unidentified compound with molecular weight of 87 was estimated by assuming the same mass spectrometer response factor as diethylacetamide.

Figure 6.- Concentration-time profiles in mixture of triethylamine (TEA) and NO_x on June 23, 1977.



THE NATURAL AND PERTURBED TROPOSPHERE

Richard W. Stewart
NASA Goddard Space Flight Center
Greenbelt, Maryland

Sultan Hameed and Joseph Pinto
State University of New York at Stony Brook
Stony Brook, New York

SUMMARY

The troposphere is a region of great chemical complexity, and many human activities may alter the chemical structure of the region. Any realistic assessment of human impacts on pollution and climate requires an understanding of the natural budgets of atmospheric gases. This understanding, in turn, requires a detailed knowledge of physical, chemical, and biological processes within the various reservoirs which are involved in the cycles of these gases. This paper first reviews the processes important in establishing the concentrations of a number of tropospheric species and discusses gaps in current understanding of these processes. The points at which man may intervene in the major cycles of atmospheric gases are identified and the possible consequences of such interventions are described. Pollutants released into the troposphere may adversely affect the environment by virtue of their chemical interactions with other atmospheric species, their radiative properties, or both. Problems discussed in this review include the growth of atmospheric carbon dioxide (CO₂) resulting from the burning of fossil fuels and its possible climatic effects, the consequences of increased levels of carbon monoxide (CO) emission on the self-cleansing ability of the troposphere and on the radiation budget, and possible changes in the stratospheric odd nitrogen and ozone amounts due to increased use of fertilizers in agriculture. The magnitude of the perturbations predicted by various model studies are reviewed with particular attention to uncertainties which may affect the results.

INTRODUCTION

Although problems of urban pollution have been studied for many years, the fact that the global-scale troposphere is an extremely complex chemical system subject to a variety of anthropogenic perturbations is only now being appreciated. Various aspects of the photochemistry of the natural troposphere have been described by several authors (refs. 1 to 3). An understanding of the chemical, biological, and physical processes affecting the concentrations of trace species in clean tropospheric air is clearly a prerequisite to any realistic assessment of the effects of human activities on the state of the atmosphere. Although major problems remain in identifying sources, sinks, and chemical reaction paths for some species, it does appear that tropospheric models can be constructed which are consistent with much of the present knowl-

edge of the concentrations of trace species and their chemical reaction rates. At least a qualitative understanding of the impact of industrial activities on the global-scale troposphere may be attempted.

Changes in the natural abundance of trace species are of concern for one or both of two reasons. A particular gas may absorb infrared (IR) radiation emitted by the Earth's surface and contribute to the greenhouse effect and the climatic state. Changes in the concentration of such a gas would thus have a direct influence on climate. The spectral region from about 8 to 12 μm is of particular importance since it includes the central portion of the Planck spectrum radiated by the Earth and is also a relatively clear "window" in which few natural constituents absorb strongly. Other species have undesirable chemical properties; for example, they may be toxic substances. Still other gases may possess both thermal and toxic properties. It is also possible that a species which is innocuous in itself may, through chemical interactions, alter the concentrations of harmful species. The problems involved in studying the impact of anthropogenic emissions can be quite complex and have many ramifications.

The study of the chemical and climatic effects of industrial emissions into the atmosphere is just beginning, and a quantitative assessment of these effects requires an understanding of the complex interactions of species within the atmosphere and of the atmosphere with other physical systems such as the oceans, lithosphere, and biosphere. In this paper, current knowledge of the budgets of various species in the natural troposphere is reviewed, and man's intervention in these budgets and possible consequences of such intervention are discussed.

ABUNDANCES OF TROPOSPHERIC GASES

The concentration of a particular species is determined by competition between various production and loss processes. These processes may consist of physical, biological, or chemical interactions between the atmosphere and other geological systems or they may consist of chemical and physical interactions within the atmosphere itself. With the exception of the noble gases, all elements in the atmosphere undergo exchange processes between the atmosphere and other reservoirs. The sum of these exchange processes constitutes a cycle for the element (or species) in question, and the average time an atom or molecule spends in a particular reservoir is its lifetime or residence time in that reservoir.

A convenient way of considering the multitude of trace species of importance in the troposphere is to organize them into certain elemental groups as shown in table I. The first two columns of this table give the name and chemical symbol of various tropospheric species. The third column gives the mixing ratio, which for most species must be calculated since their abundances are too small to measure. Those species concentrations which have been measured are indicated by a footnote; calculated values were derived by the present authors and represent daytime-averaged mid-latitude values. The lifetime of a species (fourth column) is related to its mixing ratio in that those which are highly reactive and have short lifetimes will generally not be abundant. Absorption bands in the thermal IR region are indicated in the fifth column. The sixth and seventh columns of table I indicate whether the sources and sinks for a

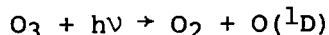
particular species are primarily anthropogenic (A), biological or microbiological (B), chemical reactions in the atmosphere (C), or physical (P). Some of the information in the table was taken from references 4 to 20; these sources are given in the eighth column.

OXYGEN GROUP

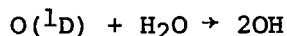
The most abundant member of this group, molecular oxygen (O_2), is a major constituent comprising about 20 percent of the atmosphere. The oxygen cycle has been reviewed by Walker (ref. 21) and by several others (refs. 22 to 24) in the context of discussions of the carbon cycle. To address the question of intervention by human activities in the oxygen cycle, it must be noted that there are two different time scales in which oxygen is exchanged between the atmosphere and terrestrial reservoirs. The shorter of these time scales involves the exchange of about 3×10^5 million metric tons per year (3×10^5 Mt/yr) of oxygen between the atmosphere and biosphere via processes of photosynthesis and respiration and decay. The reservoir of atmospheric oxygen involved in this exchange ($\approx 10^9$ Mt) is much larger than the reservoir of biospheric carbon ($\approx 3.5 \times 10^6$ Mt) or of available fossil fuels ($\approx 7 \times 10^6$ Mt). Since 2.67 Mt of O_2 will oxidize 1 Mt of carbon, human intervention in the carbon cycle, either through nearly complete combustion of available fossil fuels or through substantial alterations in the populations of photosynthesizing organisms, will have small (less than 4 percent) impact on the atmospheric O_2 abundance over times of the order of hundreds of years.

The longer time scale involves the exchange of O_2 between the atmosphere and crustal sediments. The source of oxygen on this scale is due to about 300 Mt/yr of O_2 produced by photosynthesis which is not utilized in the oxidation of dead organic carbon. The stoichiometric equivalent amount of carbon is sequestered in ocean sediments. A corresponding sink of 300 Mt/yr for O_2 results from erosion and weathering of these sediments as they are again exposed to the atmosphere. The reservoir of sedimentary carbon contains about 5.5×10^{10} Mt and could readily absorb all the O_2 presently in the atmosphere if the O_2 source were extinguished. The time over which this would occur is about 10^9 Mt/(300 Mt/yr) or ≈ 3 million years. Because of the long time scale involved in potential human impacts on the oxygen cycle, it will not be discussed in detail; instead, some problems of more immediate concern involving other members of the oxygen group are discussed in the following paragraphs.

Ozone (O_3) is the next most abundant member of the oxygen group and is a chemically important tropospheric constituent. Almost all tropospheric photochemistry is initiated by the photolysis of ozone in the 300 to 310 nm region of the ultraviolet (UV) spectrum. The reaction is

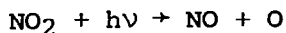


The $O(^1D)$ thus formed may then react with water vapor



to give two, highly reactive hydroxyl radicals (OH) which initiate several com-

plex reaction chains. Another potential precursor of tropospheric photochemistry is nitrogen dioxide (NO₂) which can dissociate over the UV wavelength range from 300 to 400 nm:

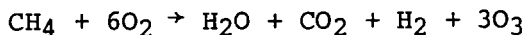


Both O and NO are involved in subsequent chemical reactions.

The oxygen budget of the troposphere is represented schematically in figure 1. This figure indicates that NO₂ photolysis and downward transport from the stratosphere are primary sources of tropospheric ozone. Photolysis of this ozone results in O(¹D) and, after reaction of O(¹D) with H₂O, in OH radicals. These in turn oxidize methane and other hydrocarbons to produce more ozone. Ozone is lost via reactions with NO_x (NO and NO₂) and HO_x (OH and HO₂) radicals. The lesser sink due to reaction at the ground is not indicated in figure 1.

A problem that has generated much recent debate is that of the sources and sinks of tropospheric ozone. The "classical" view has been that ozone, created as a result of O₂ dissociation by UV radiation with wavelengths less than 240 nm, is transported downward and destroyed at the ground (ref. 25). The observed ground-level background ozone concentration is about 3 pphm (parts per hundred million), and if downward transport and ground-level destruction are in fact the major source and sink mechanisms for tropospheric ozone, its lifetime is of the order of 1 month. Chameides and Walker (refs. 26 and 27) proposed an alternative view, that ozone in the lower troposphere is photochemically created, especially as a consequence of the methane oxidation chain. The role of reactive hydrocarbons in ozone production in polluted urban air is well known (refs. 3 and 28), and the possible importance of the much less reactive but more abundant methane in the global-scale production of ozone was noted by Crutzen (ref. 29).

The reaction scheme by which methane (CH₄) oxidation results in ozone production is discussed by Fishman and Crutzen (ref. 30). The net effect, which is the sum of 15 individual reactions, is



This reaction sequence essentially extracts O₂ molecules from the ambient reservoir and makes their component atoms available for ozone formation. It thus provides an alternative to the direct splitting of O₂ by UV radiation, which does not occur in the troposphere.

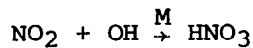
The importance of transport in establishing the tropospheric ozone abundance is supported by observational evidence on the latitudinal distributions of this constituent. The tropospheric ozone burden (total amount of ozone in a column) shows maxima in regions of enhanced troposphere-stratosphere exchange, 30°, 45°, and 60° latitude (refs. 5 and 31). Photochemical models have not addressed the problem of the observed latitudinal distribution of ozone, but there is no obvious photochemical argument which might account for it.

The sharp disagreement between the conclusions of the photochemical models of Chameides and Walker (refs. 26 and 27) and the arguments supporting a purely

dynamic source for tropospheric ozone has motivated additional model studies (refs. 32 and 33). The results of these more recent calculations indicate that photochemical production alone cannot account for observed levels of tropospheric ozone and that, in fact, the troposphere acts as a net chemical sink. In the calculation of Chameides and Stedman (ref. 32), 70 percent of the ozone in a typical mid-latitude tropospheric column is produced by downward transport from the stratosphere and 30 percent is photochemically produced. In this typical column, 70 percent of the ozone is chemically destroyed and 30 percent destroyed by reaction at the ground. Calculations made with the box model of Stewart et al. (ref. 33) lead to similar conclusions regarding the relative importance of transport and photochemistry in establishing the tropospheric ozone distribution.

The divergent conclusions of the newer and older photochemical models illuminate the principal problem in state-of-the-art models of tropospheric composition, which is their sensitivity to the data base used in the calculations. The most important component of this data base is the large number (usually ≥ 60) of chemical reactions used in the calculations. Rates for these reactions are constantly being revised as new experimental data become available. The most generally accepted chemical data base is provided by the compilation of Hampson and Garvin (ref. 34) in which these authors, and others cited in their publication, review the available experimental data and provide preferred values for a large body of chemical reaction rates. This review process is by its nature always somewhat dated, and there are usually more recent data of interest which must be considered in model calculations.

The different conclusions reached by the older (refs. 26 and 27) and newer (refs. 32 and 33) models of tropospheric ozone may be traced for the most part to the faster rates adopted for certain important reactions in which odd hydrogen and odd nitrogen radicals combine; for example,

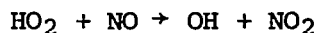


These rates were revised between publication of the older and newer models. Such reactions reduce the concentration of OH in the troposphere and thus render the methane oxidation mechanism less effective.

Another factor leading to differing conclusions in these models is the different NO_2 background adopted. The earlier models used 3 ppb NO_2 , a value suggested by Robinson and Robbins (ref. 35) based on their analysis of the nitrogen budget and the sparse data then available. As additional data have become available, it has become clear that 3 ppb is too high to be representative of global background NO_2 values. The spectroscopic measurements of Noxon (ref. 11) in particular suggest that $[\text{NO}_2] \lesssim 0.1$ ppb. The use of lower NO_2 concentrations ($\lesssim 0.5$ ppb) in the more recent photochemical models reduces ozone production resulting from NO_2 photolysis.

The newer photochemical models (refs. 32 and 33) discussed previously represent a synthesis of the arguments concerning photochemical and dynamic sources for tropospheric ozone. They establish the importance of photochemical interactions in contributing to the overall ozone abundance but are consistent with the view that transport plays the major role in establishing the global

ozone distribution. Unfortunately, this consensus has proved to be short-lived. A recent measurement by Howard and Evenson (ref. 36) of the rate of the reaction,



is 8 to 20 times faster than the previously accepted values. This has extremely important consequences for the problem of production and loss of tropospheric ozone, and for tropospheric chemistry generally, since this reaction produces NO_2 , an ozone precursor, and OH , which initiates the methane oxidation chain and again produces ozone.

In the model of Stewart et al. (ref. 33) the troposphere must import 1480 Mt/yr of ozone from the stratosphere to maintain the average observed midtropospheric background value of 4.5 pphm O_3 . This transport value is consistent with that quoted in the meteorological literature (refs. 5 and 37). However, if the Howard and Evenson value for the reaction given previously is used in the Stewart et al. model, the troposphere switches from being a strong chemical sink to a strong chemical source; it must export 2000 Mt/yr of ozone. This is an unacceptable result because it is inconsistent with the observed tropospheric distribution explained previously and because the observed troposphere-stratosphere ozone gradient implies downward rather than upward transport.

Thus, the problem of the sources and sinks of tropospheric ozone remains. Even if revision of other reaction rates is found to provide a chemical sink which compensates for the chemical source given by the rate for reaction of HO_2 and NO , ozone may be found to have too short a residence time to be consistent with the indicated importance of transport in establishing its distribution.

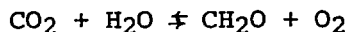
CARBON GROUP

Natural Carbon Cycle

The principal carbon-containing species in the atmosphere are carbon dioxide, methane, and carbon monoxide, which have mean concentrations of about 330 ppm, 1.4 ppm, and 0.12 ppm, respectively. Other hydrocarbons such as aldehydes, olefins, alkanes, and terpenes are generally present in much smaller amounts. Study of the global-scale effects of the carbon group on pollution and climate has centered on the three species noted. Hydrocarbons with higher molecular weights and carbon monoxide are important also in urban-scale pollution problems (refs. 28, 38, and 39). Carbon dioxide (CO_2) and methane (CH_4) are climatologically significant gases since they absorb in the thermal IR region. The contribution of CO_2 to the greenhouse effect is well known, but CH_4 has a band at 7.7 μm and changes in its abundance are also potentially important. Carbon monoxide (CO) is not active in the thermal IR region but is of concern because of its chemical properties. In high concentrations, CO is toxic; but on the global scale, concern is with its possible chemical interaction with and impact on species such as OH and CH_4 (refs. 40 and 41).

The abundance of carbon dioxide is regulated by interaction between the troposphere and biosphere (ref. 42) via the process of photosynthesis which may

be written schematically as



The forward reaction represents the utilization of CO_2 by plants in the synthesis of organic compounds represented here by formaldehyde (CH_2O). The reverse reaction represents the return of CO_2 to the atmosphere by oxidation of dead organic matter. The flow of carbon between the atmosphere and other reservoirs is shown in figure 2. Several quantitative models of the carbon cycle have been developed (refs. 22, 23, and 43 to 45) which may differ from one another and from figure 2 in the details of the adopted reservoirs and fluxes.

In figure 2, the consumption of CO_2 by the biosphere has been given as 1.5×10^5 Mt/yr, 1.1×10^5 by the land biomass and 4×10^4 by the ocean biomass. These numbers, like most of the flux and reservoir values of figure 2, are meant to be representative, but widely varying values can be found in the literature. The exchange of CO_2 between the atmosphere and biomass by photosynthesis is balanced to within 1 part in a thousand. The slight imbalance between consumption and release of CO_2 , represented by the sedimentation flux in figure 2, has resulted in the deposit over geologic time of a reservoir of fossil organic carbon of perhaps 1.2×10^7 Mt (ref. 46), of which about 7.3×10^6 Mt is available for exploitation.

Methane (CH_4) and carbon monoxide (CO) are less abundant, but important, members of the carbon group. Methane distribution is approximately uniform in the troposphere with a concentration of 1.4 ppm (ref. 6). At least 80 percent of tropospheric methane is produced by the anaerobic decomposition of organic matter in such places as swamps and paddy fields, and its sources are thus biological and microbiological. The remainder of the CH_4 comes from natural gas wells. A present estimate of the total source strength of CH_4 is about 10^3 Mt/yr (ref. 46) and is included in the soil respiration flux in figure 2. There are 4×10^3 Mt of CH_4 in the atmosphere which, combined with the source strength, implies an atmospheric residence time of 4 years. It is now generally believed that oxidation of methane via the reaction



provides the major sink. The effectiveness of this sink depends on the abundance of tropospheric OH radicals and on the rate of this reaction. The mean tropospheric abundance of OH is not well established. Measurements (refs. 14, 15, and 47) show it to be quite variable and theoretical arguments support OH concentrations ranging from 2×10^5 to 3×10^6 cm^{-3} (refs. 18 and 48). Adopting a rate of $k = 4.6 \times 10^{-15}$ cm^3/sec for the $\text{CH}_4 + \text{OH}$ reaction (ref. 34) gives a lifetime $\tau_{\text{CH}_4} = (k[\text{OH}])^{-1}$ ranging from 2.3 to 35 years. There is thus at

least a factor-of-10 uncertainty in the parameters determining the methane abundance.

Carbon monoxide distribution is approximately uniform vertically in the troposphere but shows a strong latitudinal gradient. The globally averaged concentration of CO is about 0.12 ppm, but there is a factor of 4 difference in mean concentrations between the Northern (0.20 ppm) and Southern (0.05 ppm)

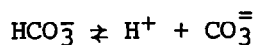
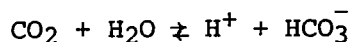
Hemispheres (ref. 8). (See fig. 3 adopted from ref. 8.) This interhemispheric concentration difference indicates the importance of Northern Hemisphere anthropogenic sources, mainly automobile and space heating, in determining the global CO abundance, but the oxidation of methane provides a strong natural source. The relative importance of these two mechanisms is still a matter of debate (refs. 49 to 51).

Perturbations to the Carbon Cycle

The long-term increase of CO₂ is the best documented of the global-scale changes in the atmospheric environment that have occurred as a result of human activities (refs. 9 and 52). Figure 4 shows monthly average values of CO₂ concentrations measured at Mauna Loa Observatory, Hawaii. The long-term increase is quite apparent. Seasonal variations in photosynthesis produce the annual cycle. Carbon dioxide absorbs in the thermal IR region, and it has been suggested by several theoretical studies that substantial increase (e.g., doubling) of CO₂ will lead to climatologically significant temperature increases in the lower atmosphere. There are two parts to a quantitative evaluation of the environmental impact of enhanced CO₂ levels: the first is to project future CO₂ concentrations as a function of time; the second is to calculate the change in surface temperature ΔT_s due to these concentrations. Each part of this problem has been addressed by several investigators, but with no consensus on either point.

The long-term increase of CO₂ has been modeled in several studies (refs. 43, 44, 53, and 54), and the results of three of these are shown in figure 5. Projections of future CO₂ levels in these model studies are obtained by solving the continuity equation for CO₂ which equates the rate of change of CO₂ in a specified reservoir to the difference between sources and sinks for that reservoir. The models shown in figure 5 use comparable source functions for the anthropogenic emission (fossil fuel burning). Hoffert (ref. 44), for example, fits a Gaussian source function to historical emission data over the 1950 to 1970 period. This source function results in consumption of about 70 percent of available fossil fuels in the 100-year period centered about the year 2069. The anthropogenic source functions used in the other two models of figure 5 differ in some details but are essentially similar in magnitude and functional form.

The two central issues in current research on this problem involve the roles of the oceans and the biomass as sources and sinks of CO₂. The substantial difference in the long-range projections of the authors cited in figure 5 is due to the differing treatments of the oceanic sink in their models. Hoffert (ref. 44) has discussed the differences between his model and that of Cramer and Myers (ref. 43) as being primarily due to treatment of the deep-ocean CO₂. In Hoffert's model, deep-ocean CO₂ is determined from the carbonic acid equilibrium,



which constrains the deep-ocean CO₂ to smaller values than in the Cramer and

Myers model in which this CO₂ is determined by exchange with the mixed layer and the ocean floor. The ability of the oceans for CO₂ uptake is smaller in Hoffert's model and thus a greater amount of CO₂ accumulates in the atmosphere. In the Keeling and Bacastow model (ref. 54), the thermal stability of the main oceanic thermocline (70 to 1000 m deep) prevents the complete mixing of CO₂ between the deep ocean and the warm surface layer, thus rendering the oceans a still less effective sink than in the Hoffert model.

Another issue which has recently been raised (refs. 55 and 56) concerns the effect of human alterations of the land biosphere, such as deforestation and agricultural expansion, on atmospheric CO₂ changes. Bolin (ref. 56) suggests that such changes in the land biota constitute a source of CO₂ equal to about 10 to 35 percent of the emission due to fossil fuel combustion. He also concludes that since this auxiliary source of CO₂ has previously gone unrecognized, the oceans must provide a more effective sink than hitherto realized. The results of Adams et al. (ref. 55) and Bolin (ref. 56) imply that the oceans are capable of absorbing 58 to 83 percent of the fossil fuel CO₂ emitted into the atmosphere. This conclusion is in sharp contrast to the trend of recent model development in which the oceans play a diminished role from that of earlier models. Broecker (ref. 57), for example, estimates that of the CO₂ emitted into the atmosphere, 52 percent remains in the atmosphere, 38 percent dissolves in the oceans, and 10 percent is assimilated by the biosphere. There is thus no current consensus as to the magnitude of the ocean sink or whether the land biota constitute a source or a sink of CO₂.

Part of the difficulty in assessing the role of the biosphere in the carbon cycle stems from the fact that relatively small changes in the biomass would substantially alter the CO₂ flux between atmosphere and biosphere. The deforestation flux of 1000 Mt/yr shown in figure 2 corresponds to a decrease in the land biosphere of less than 0.2 percent. A similarly small increase would provide a sink of the same magnitude. As discussed subsequently in the nitrogen cycle, the ocean biomass is controlled by nutrients other than carbon.

The thermal effects of a given CO₂ increase have been studied by several authors (refs. 58 to 61), and a review of these efforts through 1975 has been published by Schneider (ref. 62). Differences in predicted surface-temperature increase ΔT_s among various one-dimensional radiative-convective models are fairly well understood in terms of differing assumptions and computational procedures. The most detailed radiative transfer calculation appears to be that of Augustsson and Ramanathan (ref. 63) who included the temperature dependence of the band absorptance in the 15- μ m bands as well as the contribution to the greenhouse effect of the weak bands in the 12 to 18 μ m, 9 to 10 μ m, and 7 to 8 μ m regions. Their result for a doubling of CO₂ concentration is a ΔT_s of 1.98 K. Manabe and Wetherald (ref. 59) have utilized a general circulation model to calculate a ΔT_s of 2.9 K (globally averaged), about 46 percent larger than the value of Augustsson and Ramanathan. In the Manabe and Wetherald model, the surface-temperature increase is greater at high latitudes because of greater thermal stability of the troposphere and decreased albedo resulting from recession of the snow boundary. This relatively large surface-temperature increase at high latitudes results in a larger globally averaged ΔT_s than is obtained with radiative-convective models.

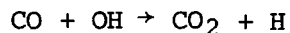
The greatest uncertainty in model calculations of surface-temperature response to increased CO₂ abundance is in the treatment of other meteorological parameters such as relative humidity and cloud amount, which may also respond to temperature changes and feedback into the CO₂ perturbation. Augustsson and Ramanathan (ref. 63), for example, show differences of up to 62 percent in ΔT_s between models with constant cloud-top altitude and others with constant cloud-top temperature.

According to Schneider (ref. 62), a present estimate of ΔT_s resulting from a doubling of atmospheric CO₂ abundance would be $1.5 \text{ K} < \Delta T_s < 3 \text{ K}$, but, as Schneider cautions, this estimate could be considerably modified by the effects of important feedback mechanisms not included in current models.

Considering the combined uncertainties of projecting future CO₂ levels and of computing ΔT_s for a given CO₂ increase, it does not seem reasonable at present to attempt a quantitative prediction of temperature increases resulting from CO₂ emissions at any specified future time. The uncertainties in the CO₂ and ΔT_s projections are indicated in figure 6 (after Baes et al. (ref. 46)). The higher of the two inner solid lines represents an assumed 4.3-percent annual growth rate in fossil fuel burning reduced in proportion to the fraction of the net supply that has been used; the lower of the two inner solid lines represents an assumed 2-percent growth rate until 2025 followed by a symmetrical decrease. The inner band in each of these cases represents the effect of a $\pm 2000 \text{ Mt/yr}$ variation in the net flux to the land, while the outer band represents the effect of varying the assumed ocean uptake from 40 to 60 percent. The right vertical axis shows the range of uncertainty in ΔT_s (as estimated by Baes et al.) for each value of CO₂ increase.

Another perturbation to the carbon group which has been discussed recently involves possible alteration of the CH₄ concentration as a result of changes in the anthropogenic CO flux into the atmosphere (refs. 40 and 41). According to calculations by Sze (ref. 40), a CO emissions increase of 4 percent per year from 1940 to 1971 followed by a 1.33 percent per year increase thereafter will result in a doubling of CH₄ concentration over its 1950 value by the year 2035. Chameides et al. (ref. 41) consider a 4.5-percent increase in CO emissions from 1976 and find an increase of CH₄ from present levels to about 2.45 ppm by the year 2010 (a 75-percent increase).

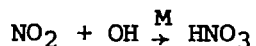
These projected CH₄ increases occur because CO is an effective scavenger of the hydroxyl radical (OH) through the reaction,



and OH is the major species capable of initiating the methane oxidation sequence. Thus, more CO results in less OH, and this in turn causes an increase in CH₄ amount.

Hameed et al. (ref. 64) have pointed out that the magnitude of the CH₄ perturbation resulting from a given CO flux increase is extremely sensitive to the NO_x background assumed in the model, and since this is presently only poorly known, quantitative statements concerning the magnitude of the CO-CH₄ perturbation are not yet feasible. According to the calculations of Hameed et al., a

doubling of the present level of CO emissions would result in an increase of CH₄ to 1.9 ppm for [NO_x] = 0.1 ppb. The reason for this sensitivity is that NO_x compounds are also effective scavengers of OH through reactions such as



The hydroxyl radical concentration is thus much more sensitive to the CO flux for low values of NO_x than for higher values.

According to Wang et al. (ref. 65), a doubling of CH₄ concentration would result in an incremental surface temperature ΔT_s of 0.28 K or 0.40 K for a fixed-cloud-top-temperature model, depending on whose absorption data are used. It is important to establish more firmly the possible magnitudes of methane increases and to study in greater detail the more general changes which would result from lowered hydroxyl radical concentrations.

NITROGEN GROUP

Natural Nitrogen Cycle

Molecular nitrogen (N₂) is the most abundant gas in the atmosphere, but it is relatively inert chemically and therefore has little direct interaction with other tropospheric species. Other forms of tropospheric nitrogen such as ammonia (NH₃), nitric oxide (NO), and nitrogen dioxide (NO₂) result from various microbiological and industrial processes which break the N₂ bond. Such processes are said to fix nitrogen in a biologically useful form. These fixation processes occur naturally in various soil and marine organisms and to a much lesser extent by the reaction of N₂ and O₂ in lightning discharges. Industrial production of fertilizer is the principal source of artificial fixation, and a debate is in progress over the degree to which this process may upset the natural cycling of nitrogen through the ecosystem. The current status of this problem will be described in this section.

After N₂, nitrous oxide (N₂O) is the most abundant form of nitrogen in the troposphere. Its spatial distribution appears to be relatively uniform, but temporal fluctuations have been interpreted as implying an atmospheric residence time of from 4 to 70 years for this gas (refs. 10 and 66). Chemical destruction in the stratosphere alone would result in a longer lifetime of 118 to 160 years (ref. 67). With an atmospheric abundance of 0.25 to 0.30 ppm (1800 to 2160 Mt as N₂O), this range of lifetime implies source and sink strengths ranging from 11.3 Mt/yr to 540 Mt/yr. Although the source of atmospheric N₂O is clearly denitrifying bacteria, there is still a problem in identifying a sink of the appropriate magnitude. The role of the oceans in this regard is a subject of debate. Hahn (ref. 68) identified the oceans as a possible net source of N₂O, whereas McElroy et al. (ref. 69) believe that a flux of N₂O into the oceans may exist and provide the necessary sink. More data are required to assess accurately the role of the oceans in the nitrogen cycle.

Nitrous oxide is of importance because of its fundamental role in controlling the abundance of stratospheric ozone. In the stratosphere, N₂O dissociates by reaction with O(¹D) to form nitric oxide which catalytically reduces the

ambient ozone. N_2O also has an absorption band at $7.78 \mu m$, and it has been estimated that a doubling of its concentration could result in a global mean increase in surface temperature of $0.68 K$ (ref. 65). Because of the strength and position of the N_2O $7.78\text{-}\mu m$ band, it is the second most important absorber of thermal IR radiation (after CO_2 and neglecting the highly variable water vapor). The gas is of potential climatological significance due to both its thermal IR and chemical properties.

Ammonia (NH_3), the next most abundant form of atmospheric nitrogen, exhibits strong spatial and temporal variabilities (ref. 70). There is a strong decrease of NH_3 with altitude, the concentration above $2 km$ being about one-third of the ground-level value. Seasonally, mean ground-level NH_3 concentrations may vary from about $6 ppb$ in summer to $2 ppb$ in winter over land areas, but over the oceans there is a sharp decrease to about 0.2 to $1.0 ppb$. The natural source of atmospheric NH_3 is bacterial decomposition of biologically fixed nitrogen found in plant tissues. The magnitude of this production depends on soil type, temperature, pH, and moisture content. Dawson (ref. 12) has recently calculated a soil source of $47 Mt/yr$ of NH_3 from unperturbed land on a global basis. This source would be balanced by corresponding rainout and dry deposition. The atmospheric residence time of NH_3 is about a week before it is removed by precipitation.

An anthropogenic source of ammonia results from the volatilization of ammonium contained in nitrogenous fertilizers applied to agricultural soils. The remainder of the fertilizer nitrogen is assimilated by the biomass or undergoes transfer from the inorganic nitrogen soil to other reservoirs by processes noted subsequently. The quantitative relationship between these processes is not established, though it likely depends on the same soil variables described previously (ref. 12). Ammonia is thus strongly coupled with the processes affecting the cycling of nitrogen through the ecosystem via its interactions in the biosphere.

The oxides of nitrogen, NO and NO_2 , are the least abundant tropospheric nitrogen species. Their global distribution and background concentration are poorly known in the troposphere. Recent measurements by Noxon (ref. 11) indicate values of the order of $0.1 ppb$ or less. Tropospheric sources for NO_x are combustion processes and lightning (10 to $40 Mt/yr$ (refs. 71 and 72)) and denitrification of soil nitrogen. NO_x plays an important role in tropospheric chemistry involving the production and loss of ozone (ref. 33) and the effect of CO emissions on CH_4 abundances (ref. 64). Its global mean background concentration must be much better established.

The nitrogen cycle is schematically represented in figure 7. The reservoir values are similar to those stated in published reviews (refs. 24 and 73) but have been adjusted to be consistent with observed C/N ratios of $80/1$ for the living terrestrial biomass and $10/1$ for other biospheric reservoirs.

Perturbations to the Nitrogen Cycle

Man's intervention in the nitrogen cycle is largely through the production of nitrogen oxides in combustion and the manufacture and use of nitrogen fertil-

izers. As seen in figure 7, fertilizers add fixed nitrogen to the inorganic soil reservoir from which it begins cycling through the ecosystem. In 1959 the use of fertilizers was responsible for the fixation of 3.5 Mt/yr of N. This had grown to 40 Mt/yr by 1974 (ref. 74) and could reach 200 Mt/yr by 2000. Biological fixation rates are uncertain, particularly for the oceans. The fixation rate due to the land biomass has been put at 44 Mt/yr of N by Delwiche (ref. 73) and at 175 Mt/yr by Hardy and Havelka (ref. 75). The marine fixation rate has been estimated to be 10 Mt/yr of N (ref. 69). Thus, if the lower biological fixation rates are correct, man's contribution to nitrogen fixation is already equal to the natural source, or, if the higher biological fixation rates are accepted, it will become so by the year 2000. The consequences of this potentially large anthropogenic source of fixed nitrogen have been the subject of several papers (refs. 76 to 79).

Figure 7 indicates four major reservoirs which contain the nitrogen cycling through the ecosystem: atmosphere, land, ocean, and biosphere. The atmosphere contains 4×10^9 Mt of nitrogen mostly as N_2 , but there is a subreservoir (not shown explicitly in fig. 7) of fixed atmospheric nitrogen which contains about 1 Mt of N and consists primarily of NO_x and NH_3 . The flow of nitrogen into this atmospheric subreservoir from the atmosphere results from lightning discharges (10 to 40 Mt/yr (refs. 71 and 72)) and combustion (20.7 Mt/yr (ref. 74)). Interest in perturbations to the nitrogen cycle centers on the interactions of the biosphere with the other reservoirs and on the flow of nitrogen within the subreservoirs of the biosphere itself. The fixation flux, both natural and fertilizer, into the biosphere refers to processes of conversion of nitrogen from the biologically unutilizable N_2 to forms in which it can be used as nutrients, ammonium (NH_4^+), nitrate (NO_3^-), and nitrite (NO_2^-). The reverse process is denitrification which produces either N_2 or N_2O .

Within the land biosphere, three reservoirs are indicated: the living biomass, which contains about 7500 Mt of N; dead organic matter, called humus on land, which contains about 10^5 Mt of N; and the inorganic nitrogen pool, smallest of the three subreservoirs, containing about 5000 Mt of N. The flow of nitrogen into the biomass by natural fixation results from the activities of a multitude of microorganisms, either free-living or living in association with plants, that are able to utilize the energy stored in the products of photosynthesis to break the N_2 bond and fix nitrogen into forms which may be used for the synthesis of protein, amino acids, and other organic compounds. This process essentially represents a flow of nitrogen directly from the atmosphere to the biomass subreservoir. Fertilizer, by contrast, adds fixed nitrogen to the inorganic soil reservoir which consists of soluble nitrate and nitrite. From the inorganic nitrogen pool, the nitrogen may be assimilated by the biomass, which is the goal of fertilization; it may be immobilized, which means transferred to the organic nitrogen reservoir by bacterial assimilation or by sequestering of ammonia in clay particles; it may be lost by leaching from the soil, which may lead to problems such as the eutrophication of lakes; or it may be denitrified by denitrifying bacteria. The present debate on the impact of fertilizer nitrogen centers on the relative efficiencies and characteristic times for these loss processes.

The denitrification flux from the inorganic soil reservoir to the atmosphere is shown with a question mark in figure 7 since estimates published in

the literature vary substantially (e.g., 43 Mt/yr (ref. 73) and 210 Mt/yr (ref. 24)). Even if the flux is large, it is of possible importance only if a significant part of it consists of N_2O rather than N_2 . Significance, in this context, must be judged relative to the magnitude of other sources and sinks of atmospheric N_2O and these, as noted previously, are themselves a subject of debate. Finally, if these N_2O parameters were firmly established, there is still the uncertainty of the effect of a given N_2O increase on stratospheric ozone.

Johnston (ref. 67) has recently published a review of this subject in which he sought to place limits on the values of the variables described in the previous paragraph. The fraction of nitrogen fertilizer that is rapidly denitrified, β in Johnston's analysis, is highly uncertain. For a worst-case analysis of ozone reduction, β may be taken to be 1. The fraction of N_2O in denitrified gases α is taken to be in the range $0.025 < \alpha < 0.4$ by Johnston based on his review of the available data. As Johnston notes, these are estimates, not rigorous bounds. The importance of denitrified N_2O relative to other sources and sinks is discussed by Johnston in terms of the equivalent problem of the atmospheric residence time of N_2O . Large natural sources and sinks, which would minimize the impact of a given nitrous oxide flux in denitrified gases, correspond to shorter values of the residence time τ . From consideration of observed temporal and spatial variabilities of N_2O on the one hand (implying a short residence time and giving a lower bound to τ (ref. 66)) and the rate of stratospheric destruction on the other (giving the upper bound), the range of N_2O residence time given by Johnston is $5 \text{ years} < \tau < 160 \text{ years}$. Johnston seeks to place limits on the combinations of α and τ consistent with identified nitrogen fixation sources, and he concludes that for reasonable values of these variables, the maximum ozone reduction due to added 100 Mt/yr of N from fertilizer will lie between 0.4 and 12 percent and will occur within a few decades for 1- to 2-percent reduction or over hundreds of years for larger (≈ 10 -percent) reductions.

This analysis is based on estimates of the uncertainties involved in the parameters of the biospheric portion of the nitrogen cycle and does not discuss the possible impact of the uncertainties in the many chemical rate constants involved in the stratospheric modeling of ozone reductions (refs. 80 and 81), as Johnston clearly states. However, as noted in the discussion of tropospheric ozone, the revision of a single chemical rate constant involved in a complex system can substantially alter the model conclusions. It is not possible to be even order-of-magnitude quantitative regarding the impact of nitrogenous fertilizers on stratospheric ozone and even Johnston's wide limits may be overly restrictive.

The nitrogen and carbon cycles are strongly coupled through the biosphere, but potential consequences of this fact have yet to be quantitatively explored. One aspect of this coupling was noted previously in describing the constancy of the ocean biomass in the face of increased CO_2 input to the oceans. This presumed constancy results from the fact that nitrogen, rather than carbon, is a limiting nutrient in the oceans. For example, the 5000 Mt/yr of carbon currently entering the atmosphere because of fossil fuel burning (fig. 2) could be assimilated entirely by the ocean biomass if an increased nitrogen input of 400 Mt/yr to the oceans occurred, assuming a C/N ratio of 12 for the ocean bio-

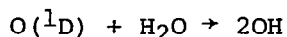
mass. This nitrogen input is 10 times the 1974 nitrogen fertilizer use and twice the projected use for the year 2000 (ref. 74). The assimilation of this amount of nitrogen and carbon would require a yearly increase of 4 percent in the ocean biomass. There are yet insufficient data to determine the actual runoff of nitrate into the oceans, but the data discussed by Commoner (ref. 82) on nitrates in U.S. river systems show that this runoff has increased by a factor of 3 to 5 in the past 20 years.

Phosphorous, another limiting nutrient for the ocean biomass, is also being discharged into the oceans from land areas. The SCEP report (ref. 83) gives the 1968 U.S. mean phosphorous content of runoff as 0.44 Mt.

In view of the increasing anthropogenic supply of limiting nutrients to the ocean biomass, it is conceivable that the increase in atmospheric CO₂ could be moderated in future years, but the amounts of these nutrients required to reverse the effect are relatively large compared with projected usage. This problem deserves quantitative study with attention to the role of phosphorous as a limiting oceanic nutrient and to the fraction of fertilizer nitrogen which finds its way to the oceans.

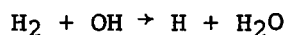
HYDROGEN GROUP

The most abundant member of this group is water vapor (H₂O) which is present in the atmosphere as a consequence of evaporation of liquid water at the Earth's surface. Water vapor is chiefly responsible for the greenhouse effect through its strong absorption of infrared radiation, and it is an essential precursor for the OH radical produced through the reaction



The amount of H₂O in the atmosphere is highly variable and little influenced by human activities, and its properties, therefore, will not be described in further detail.

Molecular hydrogen (H₂) is the next most abundant member of this group, having a concentration of about 0.5 ppm. The prevailing view (ref. 13) is that H₂ is formed mainly by bacterial fermentation in soils and from the photodissociation of formaldehyde, one of the intermediate products in the photooxidation of methane, but the relative importance of these two paths is uncertain. The sink for H₂ is reaction with OH:



The most important member of this group in influencing the concentrations of many trace tropospheric species is the hydroxyl radical (OH). Reaction with OH is the dominant removal mechanism for constituents which are shielded from dissociation and are not removed via interaction with the hydrologic cycle. This is the case for many of the gases released into the atmosphere as a result of human activities, such as CO, NO₂, various halogenated methane compounds (CHCl₂F, CHClF₂, CHCl₃, CH₃Cl), halogenated ethylenes, and CH₃CCl₃. In many cases, reaction of the halogenated hydrocarbons with tropospheric OH removes a

large potential source of stratospheric chlorine and thus reduces a potential harmful impact on the ozone layer. Recent measurements (refs. 14, 15, and 47) show tropospheric mean OH concentrations of the order of 10^6 cm^{-3} . Reaction with OH is also the dominant removal mechanism for reduced gases of biological origin such as CH_4 and H_2S .

Hydroperoxyl radicals (HO_2) are formed mainly by the reaction of CO and H_2 with OH. Because anthropogenic emissions of CO are now considered to represent a large fraction of the total atmospheric CO source, the potential exists for man's intervention in determining the background abundances of OH and HO_2 radicals in the troposphere. HO_2 radicals are not as reactive toward many species as are OH radicals, and a shift in the odd hydrogen balance ($\text{OH} + \text{HO}_2$) could have consequences in determining the abundances of compounds mainly lost by reaction with OH, as was pointed out recently by Sze (ref. 40), Chameides et al. (ref. 41), and Hameed et al. (ref. 64).

SULFUR GROUP

The abundances, sources and sinks, and photochemistry of atmospheric sulfur compounds are all poorly understood relative to oxygen, carbon, or nitrogen compounds. Various sulfur species are important components of air pollution in many parts of the world. The anthropogenic input to the sulfur cycle is clearly significant and likely to increase in magnitude, but the consequences of these facts have been relatively little explored. The details of the sulfur cycle have been reviewed by Friend (ref. 16), Kellogg et al. (ref. 84), Robinson and Robbins (ref. 35), and Junge (ref. 25).

The importance of sulfur as a pollutant derives mainly from the properties of sulfur dioxide (SO_2). This gas is toxic to plants and animals and is oxidized in the atmosphere to sulfuric acid (H_2SO_4). It thus acts as an aerosol precursor, may have an effect on cloud formation, and is therefore of potential climatological significance. The H_2SO_4 may lower the pH of rainwater with deleterious consequences. Toxicity of SO_2 and acid rain are likely to be confined to local- and regional-scale effects because of the short (≈ 1 week) residence time of atmospheric sulfur, but changes in aerosol or cloud properties are global-scale phenomena.

The chemistry of the atmospheric portion of the sulfur cycle over land is shown in figure 8. Volcanic activity is a modest source of natural SO_2 (2 Mt/yr of S) compared with industrial output (65 Mt/yr of S). The largest natural source of atmospheric sulfur is decay of organic material in the biosphere (58 Mt/yr of S over land). This input is in the form of reduced sulfur such as hydrogen sulfide (H_2S) and organic sulfides (dimethyl sulfide (DMS), dymethyl disulfide (DMDS)) and is rapidly oxidized to SO_2 by reactions with atmospheric trace constituents (ref. 85). The oxidation mechanism is as yet unclear. The lifetime of reduced sulfur in the atmosphere is of the order of hours, but reaction of H_2S with O_3 results in a lifetime of a month or more. Reaction of H_2S with OH is faster but still results in a lifetime of a few days. It may be that oxidation of reduced sulfur in the atmosphere results from reaction of organic sulfides with NO_x , but this mechanism is uncertain.

Sulfur dioxide is itself oxidized in the atmosphere with a lifetime of hours. This may occur by gas-phase reaction with OH and HO₂ radicals to form SO₃ which is then rapidly absorbed in water vapor to form sulfuric acid, or the SO₂ may undergo heterogeneous removal by reaction with dissolved O₂ in water droplets. The relative importance of these mechanisms is uncertain, but it is difficult to account for the short SO₂ lifetime solely by gas-phase chemistry.

A schematic diagram of the sulfur cycle is shown in figure 9. The magnitudes of the sulfur reservoirs and fluxes are based on the model of Friend (ref. 16) but have been adjusted where necessary to maintain the observed N/S ratio of 7 (ref. 86). The large impact which human activity has on the sulfur budget is obvious. The 65 Mt/yr of sulfur emitted to the atmosphere has a substantial influence on pollution on the urban and regional scale, but whether there are global effects associated with this input or with potentially larger SO₂ inputs is a largely unexplored problem. The 26 Mt/yr of sulfur added to the soil in fertilizers is a significant and growing fraction of the total soil input of 147 Mt/yr. Possible ecological consequences of this addition have not been addressed.

HALOGEN GROUP

The concentration of halogen compounds in the atmosphere is much less than that of the other groups thus far discussed, being generally of the order of parts per billion or less. Recent research interest in this group derives from the fact that the anthropogenic contribution to atmospheric halogens is a clearly significant source and that these species are believed to efficiently reduce stratospheric ozone and in some cases to possess radiative properties of possible climatic significance (ref. 87).

The most abundant, naturally occurring halogens are the marine organic halogens, methyl chloride (CH₃Cl), methyl bromide (CH₃Br), and methyl iodide (CH₃I) (ref. 18) which are present in abundances of about 780 ppt, 10 ppt, and 1.2 ppt, respectively.

Anthropogenic contributions to the halogen budget consist primarily of the chlorofluoromethanes (CCl₃F and CCl₂F₂) and carbon tetrachloride (CCl₄) (ref. 88). In the early 1970's, the tropospheric concentrations of CCl₃F, CCl₂F₂, and CCl₄ were about 90 ppt, 100 ppt, and 120 ppt, respectively (ref. 89).

Most of the concern over atmospheric halogens centers on the ability of the long-lived industrial compounds CCl₃F and CCl₂F₂ to diffuse into the stratosphere where they will dissociate and release chlorine, leading to a postulated reduction of ozone. A review of the extensive literature on this subject is not within the scope of this paper. (See refs. 17 and 90.)

The accumulation of chlorofluorocarbons and CCl₄ in the troposphere could have climatic consequences; however, Ramanathan (ref. 87) states that a surface-temperature increase of 0.8 K could occur if the concentrations of CCl₃F and CCl₂F₂ were each increased to 2 ppb, about a twentyfold increase over present levels. Wang et al. (ref. 65) derive a maximum surface-temperature increase of

0.54 K for the same assumed increase in CCl_3F and CCl_2F_2 concentrations. The difference in these two results is to some extent due to the fact that Wang et al. use more recently measured band intensities for the ν_1 (9.13 μm) and ν_8 (10.93 μm) bands of CCl_2F_2 and the ν_1 (9.22 μm) and ν_4 (11.82 μm) bands of CCl_3F . These recent measurements are roughly half the older values used by Ramanathan.

CONCLUDING REMARKS

Man's intervention in the geochemical cycles which control the composition of the atmosphere has only recently been appreciated. Attempts to predict the consequences of such interventions now occupy the efforts of a growing number of researchers in many fields. These efforts are necessarily of a broadly interdisciplinary character involving biologists, chemists, geologists, oceanographers, meteorologists, aeronomers, and others seeking answers to the many questions of environmental concern which have been raised by man's activities.

Interest in the oxygen group, from the point of view of its influence on pollution and climate, centers on the role of ozone and atomic oxygen in tropospheric photochemistry. Ozone is the precursor of all global-scale tropospheric photochemistry, and understanding of the processes which produce and destroy ozone in the troposphere is thus of fundamental importance to the understanding of the atmospheric phase of other geochemical cycles. This problem is currently an active area of research, but the major questions regarding the relative importance of transport and photochemistry in establishing the ozone distribution remain unanswered.

Man's intervention in the carbon cycle results chiefly from the burning of fossil fuels and is mainly manifested in the increasing atmospheric concentration of carbon dioxide (CO_2). The general problem is to predict future atmospheric levels of CO_2 and the climatic consequences of such levels. The major issues involved in predicting these levels presently include the role of deforestation as a CO_2 source and the present and future effectiveness of the oceans as a CO_2 sink. The major difficulties in predicting the climatic consequences of increased CO_2 abundances are with properly including climate feedback mechanisms, such as albedo and cloud cover changes, and ocean coupling in mathematical models.

A perturbation to the nitrogen cycle is occurring as a result of the increasing use of fertilizers in agriculture. The annual industrially fixed nitrogen resulting from this use is either already or by the end of the century will be equal to the amount of nitrogen fixed naturally. It has been suggested that one consequence of this intervention in the nitrogen cycle will be an increase in the abundance of nitrous oxide (N_2O) as the denitrification rate adjusts to the increased fixation rate. Additional N_2O could result in a decrease in the amount of stratospheric ozone and might also make a contribution to the greenhouse effect. Uncertainties abound in this problem. Among those that have been discussed in the literature are the atmospheric residence time of N_2O (5 to 160 years), the fraction of denitrified fertilizer nitrogen that enters the atmosphere as N_2O (0.025 to 0.4), the fraction of fertilizer nitrogen that is rapidly denitrified (highly uncertain), and the effect of a

given N₂O increase on stratospheric ozone and the greenhouse effect (perhaps a factor-of-2 uncertainty).

The hydrogen group is chemically active in the atmosphere and is thus subject to perturbations. Changes in the abundances of the components of this group would not (excepting water vapor) have a direct influence on pollution or climate. The extremely active hydroxyl radical, however, reacts strongly with every other major atmospheric group, and changes in its mean abundance could have far-reaching consequences.

Man is also intervening in the sulfur cycle, but global-scale consequences of this influence have yet to be identified. Most of the sulfur dioxide that enters the atmosphere is of industrial origin and can potentially alter such things as the atmospheric aerosol loading and the acidity of rainfall over at least mesoscale regions. The 26 Mt/yr of sulfur added to the soil in fertilizers is relatively large compared with natural sources. If substantially increased coal burning occurs in the future in response to shortages of alternate fuels, the magnitude of the industrial sulfur source will increase still further. It is essential that some attempts to understand the potential impact of this fact be made in future research.

The halogens are relatively inactive chemically in the troposphere, and recent research interest has centered on the reduction of stratospheric ozone which might be a consequence of their release into the atmosphere. Some of the components of this group do, however, have absorption bands in the thermal IR region, and it has been suggested that their continued buildup in the troposphere might contribute more than 0.5 K to the greenhouse effect.

It must be borne in mind that the elemental cycles of oxygen, carbon, nitrogen, hydrogen, and sulfur which have been discussed individually are strongly coupled with one another through the biosphere and atmosphere. The carbon and oxygen cycles are coupled over time scales up to $\sim 10^3$ years by the biological processes of photosynthesis, respiration, and decay and over longer time scales by geochemical interactions. The carbon, nitrogen, and sulfur cycles are coupled by the nutrient needs of the biosphere and to a lesser extent by chemical interactions in the atmosphere. The increasing abundance of carbon dioxide resulting from human intervention in the carbon cycle may not in itself permit an expansion of the biomass since other nutrients such as nitrogen and phosphorus are the limiting factors. On a small ecological scale, the eutrophication of lakes and streams provides examples of the extent to which natural cycles may be perturbed when limiting nutrients are supplied by man. With the possible exception of the interactions of the carbon-oxygen cycle, the interactions between the elemental cycles have not yet been explored in adequate quantitative detail. It is likely that as understanding increases, interrelationships among the various geochemical cycles will emerge and that the interdisciplinary nature of this research will be enhanced.

REFERENCES

1. Levy, Hiram, II: Photochemistry of the Lower Troposphere. *Planet. & Space Sci.*, vol. 20, no. 6, June 1972, pp. 919-935.
2. Levy, H., II: Photochemistry of Minor Constituents in the Troposphere. *Planet. & Space Sci.*, vol. 21, no. 4, Apr. 1973, pp. 575-591.
3. Heicklen, Julian: *Atmospheric Chemistry*. Academic Press, Inc., 1976.
4. Cauer, H.: Some Problems of Atmospheric Chemistry. *Compendium of Meteorology*, Thomas F. Malone, ed., American Meteorol. Soc., 1951, pp. 1126-1136.
5. Fabian, P.; and Pruchniewicz, P. G.: Meridional Distribution of Ozone in the Troposphere and Its Seasonal Variations. *J. Geophys. Res.*, vol. 82, no. 15, May 20, 1977, pp. 2063-2073.
6. Ehhalt, D. H.: The Atmospheric Cycle of Methane. *Tellus*, vol. 26, nos. 1-2, 1974, pp. 58-70.
7. Robinson, E.; Rasmussen, R. A.; Westberg, H. H.; and Holdren, M. W.: Non-urban Nonmethane Low Molecular Weight Hydrocarbon Concentrations Related to Air Mass Identification. *J. Geophys. Res.*, vol. 78, no. 24, Aug. 20, 1973, pp. 5345-5351.
8. Seiler, Wolfgang: The Cycle of Atmospheric CO. *Tellus*, vol. 26, nos. 1-2, 1974, pp. 116-135.
9. Bolin, Bert; and Bischof, Walter: Variations of the Carbon Dioxide Content of the Atmosphere in the Northern Hemisphere. *Tellus*, vol. 22, no. 4, 1970, pp. 431-442.
10. Schütz, K.; Junge, C.; Beck, R.; and Albrecht, B.: Studies of Atmospheric N₂O. *J. Geophys. Res.*, vol. 75, no. 12, Apr. 20, 1970, pp. 2230-2246.
11. Noxon, J. F.: Nitrogen Dioxide in Stratosphere and Troposphere Measured by Ground-Based Absorption Spectroscopy. *Science*, vol. 189, no. 4202, Aug. 1975, pp. 547-549.
12. Dawson, G. A.: Atmospheric Ammonia From Undisturbed Land. *J. Geophys. Res.*, vol. 82, no. 21, July 20, 1977, pp. 3125-3133.
13. Schmidt, Ulrich: Molecular Hydrogen in the Atmosphere. *Tellus*, vol. 26, nos. 1-2, 1974, pp. 78-90.
14. Davis, D. D.; Heaps, W.; and McGee, T.: Direct Measurements of Natural Tropospheric Levels of OH Via an Aircraft Borne Tunable Dye Laser. *Geophys. Res. Lett.*, vol. 3, no. 6, June 1976, pp. 331-333.

15. Perner, D.; Ehhalt, D. H.; Pätz, H. W.; Platt, U.; Röth, E. P.; and Volz, A.: OH-Radicals in the Lower Troposphere. *Geophys. Res. Lett.*, vol. 3, no. 8, Aug. 1976, pp. 466-468.
16. Friend, James P.: The Global Sulfur Cycle. *Chemistry of the Lower Atmosphere*, S. I. Rasool, ed., Plenum Press, 1973, pp. 177-201.
17. Halocarbons: Effects on Stratospheric Ozone. *Natl. Acad. Sci.*, 1976.
18. Singh, Hanwant B.: Atmospheric Halocarbons: Evidence in Favor of Reduced Average Hydroxyl Radical Concentration in the Troposphere. *Geophys. Res. Lett.*, vol. 4, no. 3, Mar. 1977, pp. 101-104.
19. Farmer, C. B.; Raper, O. F.; and Norton, R. H.: Spectroscopic Detection and Vertical Distribution of HCl in the Troposphere and Stratosphere. *Geophys. Res. Lett.*, vol. 3, no. 1, Jan. 1976, pp. 13-16.
20. Junge, C.: The Cycle of Atmospheric Gases - Natural and Man Made. *Q. J. R. Meteorol. Soc.*, vol. 98, no. 418, Oct. 1972, pp. 711-729.
21. Walker, James C. G.: Stability of Atmospheric Oxygen. *American J. Sci.*, vol. 274, no. 3, Mar. 1974, pp. 193-214.
22. Garrels, Robert M.; Lerman, Abraham; and Mackenzie, Fred T.: Controls of Atmospheric O₂ and CO₂: Past, Present, and Future. *American Sci.*, vol. 64, no. 3, May-June 1976, pp. 306-315.
23. Junge, C. E.; Schidlowski, M.; Eichmann, R.; and Pietrek, H.: Model Calculations for the Terrestrial Carbon Cycle: Carbon Isotope Geochemistry and Evolution of Photosynthetic Oxygen. *J. Geophys. Res.*, vol. 80, no. 33, Nov. 20, 1975, pp. 4542-4552.
24. McElroy, M. B.: Chemical Processes in the Solar System: A Kinetic Perspective. *Physical Chemistry Series Two. Volume 9 - Chemical Kinetics*, D. R. Herschbach, ed., Butterworth & Co. (Publishers) Ltd., c.1976, pp. 127-211.
25. Junge, Christian E.: *Air Chemistry and Radioactivity*. Academic Press, Inc., 1963.
26. Chameides, William; and Walker, James C. G.: A Photochemical Theory of Tropospheric Ozone. *J. Geophys. Res.*, vol. 78, no. 36, Dec. 20, 1973, pp. 8751-8760.
27. Chameides, William L.; and Walker, James C. G.: A Time-Dependent Photochemical Model for Ozone Near the Ground. *J. Geophys. Res.*, vol. 81, no. 3, Jan. 20, 1976, pp. 413-420.
28. Leighton, Philip A.: *Photochemistry of Air Pollution*. Academic Press, Inc., 1961.

29. Crutzen, Paul J.: Gas-Phase Nitrogen and Methane Chemistry in the Atmosphere. *Physics and Chemistry of Upper Atmospheres*, B. M. McCormac, ed., D. Reidel Publishing Co., c.1973, pp. 110-124.
30. Fishman, Jack; and Crutzen, Paul J.: A Numerical Study of Tropospheric Photochemistry Using a One-Dimensional Model. *J. Geophys. Res.*, vol. 82, no. 37, Dec. 20, 1977, pp. 5897-5906.
31. Fabian, Peter: Comments on 'A Photochemical Theory of Tropospheric Ozone' by W. Chameides and J. C. G. Walker. *J. Geophys. Res.*, vol. 79, no. 27, Sept. 20, 1974, pp. 4124-4125.
32. Chameides, W. L.; and Stedman, D. H.: Tropospheric Ozone: Coupling Transport and Photochemistry. *J. Geophys. Res.*, vol. 82, no. 12, Apr. 20, 1977, pp. 1787-1794.
33. Stewart, Richard W.; Hameed, Sultan; and Pinto, Joseph P.: Photochemistry of Tropospheric Ozone. *J. Geophys. Res.*, vol. 82, no. 21, July 20, 1977, pp. 3134-3140.
34. Hampson, Robert F., Jr.; and Garvin, David, eds.: *Chemical Kinetic and Photochemical Data for Modelling Atmospheric Chemistry*. NBS Tech. Note 866, U.S. Dep. Commer., June 1975.
35. Robinson, E.; and Robbins, R. C.: Sources, Abundance, and Fate of Gaseous Atmospheric Pollutants. SRI Project PR-6755, Stanford Res. Inst., Feb. 1968.
36. Howard, C. J.; and Evenson, K. M.: Laser Magnetic Resonance Study of HO₂ Chemistry. *EOS Trans., American Geophys. Union*, vol. 58, no. 6, June 1977, p. 464.
37. Danielsen, Edwin F.; and Mohnen, Volker A.: Project DUSTORM Report: Ozone Measurements and Meteorological Analyses of Tropopause Folding. ASRC-SUNY-PUB-394 (Contract N00014-76-C-0283), State Univ. of New York at Albany, May 1976. (Available from DDC as AD A032 555.)
38. Westberg, Karl; Cohen, Norman; and Wilson, K. W.: Carbon Monoxide: Its Role in Photochemical Smog Formation. *Science*, vol. 171, no. 3975, March 12, 1971, pp. 1013-1015.
39. Glasson, William A.: Effect of Carbon Monoxide on Atmospheric Photooxidation of Nitric Oxide - Hydrocarbon Mixtures. *Environ. Sci. & Technol.*, vol. 9, no. 4, Apr. 1975, pp. 343-347.
40. Sze, N. D.: Anthropogenic CO Emissions: Implications for the Atmospheric CO-OH-CH₄ Cycle. *Science*, vol. 195, no. 4279, Feb. 18, 1977, pp. 673-675.
41. Chameides, W. L.; Liu, S. C.; and Cicerone, R. J.: Possible Variations in Atmospheric Methane. *J. Geophys. Res.*, vol. 82, no. 12, Apr. 20, 1977, pp. 1795-1798.

42. Bolin, Bert: The Carbon Cycle. *Sci. American*, vol. 223, no. 3, Sept. 1970, pp. 124-132.
43. Cramer, J.; and Myers, A. L.: Rate of Increase of Atmospheric Carbon Dioxide. *Atmos. Environ.*, vol. 6, no. 8, Aug. 1972, pp. 563-573.
44. Hoffert, Martin I.: Global Distributions of Atmospheric Carbon Dioxide in the Fossil-Fuel Era: A Projection. *Atmos. Environ.*, vol. 8, no. 12, Dec. 1974, pp. 1225-1249.
45. Keeling, Charles D.: The Carbon Dioxide Cycle: Reservoir Models to Depict the Exchange of Atmospheric Carbon Dioxide With the Oceans and Land Plants. *Chemistry of the Lower Atmosphere*, S. I. Rasool, ed., Plenum Press, 1973, pp. 251-329.
46. Baes, C. F., Jr.; Goeller, H. E.; Olson, J. S.; and Rotty, R. M.: Carbon Dioxide and Climate: The Uncontrolled Experiment. *American Sci.*, vol. 65, no. 3, May-June 1977, pp. 310-320.
47. Wang, Charles C.; Davis, L. I., Jr.; Wu, C. H.; Japar, S.; Niki, H.; and Weinstock, B.: Hydroxyl Radical Concentrations Measured in Ambient Air. *Science*, vol. 189, no. 4205, Sept. 5, 1975, pp. 797-800.
48. Crutzen, Paul J.: Photochemical Reactions Initiated by and Influencing Ozone in Unpolluted Tropospheric Air. *Tellus*, vol. 26, nos. 1-2, 1974, pp. 47-57.
49. Wofsy, Steven C.: Interactions of CH₄ and CO in the Earth's Atmosphere. *Annual Review of Earth and Planetary Sciences*, Fred A. Donath, Francis G. Stehli, and George W. Wetherill, eds., Volume 4, Annual Reviews Inc., 1976, pp. 441-469.
50. Warneck, Peter: Role of Hydroxyl and Hydroperoxyl Radical in the Troposphere. *Tellus*, vol. 26, nos. 1-2, 1974, pp. 39-46.
51. Newell, Reginald E.: One-Dimensional Models: A Critical Comment, and Their Application to Carbon Monoxide. *J. Geophys. Res.*, vol. 82, no. 9, Mar. 20, 1977, pp. 1449-1450.
52. Bischof, Walter; and Bolin, Bert: Space and Time Variations of the CO₂ Content of the Troposphere and Lower Stratosphere. *Tellus*, vol. 18, nos. 2-3, 1966, pp. 155-159.
53. Machta, Lester: The Role of the Oceans and Biosphere in the Carbon Dioxide Cycle. *The Changing Chemistry of the Oceans*, David Dyrssen and Daniel Jagner, eds., John Wiley & Sons, Inc., c.1972, pp. 121-145.
54. Keeling, Charles D.; and Bacastow, Robert B.: Impact of Industrial Gases on Climate. *Energy and Climate*, *Natl. Acad. Sci.*, 1977, p. 72.

55. Adams, J. A. S.; Mantovani, M. S. M.; and Lundell, L. L.: Wood Versus Fossil Fuel as a Source of Excess Carbon Dioxide in the Atmosphere: A Preliminary Report. *Science*, vol. 196, no. 4285, April 1, 1977, pp. 54-56.
56. Bolin, Bert: Changes of Land Biota and Their Importance for the Carbon Cycle. *Science*, vol. 196, no. 4290, May 6, 1977, pp. 613-615.
57. Broecker, W. S.: The Climate Consequences of a Coal Economy. Paper presented at the 1977 Spring Meeting of the American Geophysical Union (Washington, D.C.), May-June 1977. (Abstract - *EOS Trans.*, American Geophys. Union, vol. 58, no. 10, Oct. 1977, p. 989.)
58. Rasool, S. I.; and Schneider, S. H.: Atmospheric Carbon Dioxide and Aerosols: Effects of Large Increases on Global Climate. *Science*, vol. 173, no. 3992, July 9, 1971, pp. 138-141.
59. Manabe, Syukuro; and Wetherald, Richard T.: The Effects of Doubling the CO₂ Concentration on the Climate of a General Circulation Model. *J. Atmos. Sci.*, vol. 32, no. 1, Jan. 1975, pp. 3-15.
60. Möller, F.: On the Influence of Changes in the CO₂ Concentration in Air on the Radiation Balance of the Earth's Surface and on the Climate. *J. Geophys. Res.*, vol. 68, no. 13, July 1, 1963, pp. 3877-3886.
61. Manabe, Syukuro: Estimates of Future Change of Climate Due to the Increase of Carbon Dioxide Concentration in the Air. *Man's Impact on the Climate*, William H. Matthews, William W. Kellogg, and G. D. Robinson, eds., The MIT Press, c.1971, pp. 249-264.
62. Schneider, Stephen H.: On the Carbon Dioxide-Climate Confusion. *J. Atmos. Sci.*, vol. 32, no. 11, Nov. 1975, pp. 2060-2066.
63. Augustsson, T.; and Ramanathan, V.: A Radiative-Convective Model Study of the CO₂ Climate Problem. *J. Atmos. Sci.*, vol. 34, no. 3, Mar. 1977, pp. 448-451.
64. Hameed, S.; Pinto, J. P.; and Stewart, R. W.: Carbon Monoxide Emissions: Modification of the CO-OH₄ Perturbation by NO_x. *EOS Trans.*, American Geophys. Union, vol. 58, no. 6, June 1977, p. 396.
65. Wang, W. C.; Yung, Y. L.; Lacis, A. A.; Mo, T.; and Hansen, J. E.: Greenhouse Effects Due to Man-Made Perturbations of Trace Gases. *Science*, vol. 194, no. 4266, Nov. 12, 1976, pp. 685-690.
66. Junge, C. E.: Residence Time and Variability of Tropospheric Trace Gases. *Tellus*, vol. 26, no. 4, 1974, pp. 477-488.
67. Johnston, Harold S.: Analysis of the Independent Variables in the Perturbation of Stratospheric Ozone by Nitrogen Fertilizers. *J. Geophys. Res.*, vol. 82, no. 12, Apr. 20, 1977, pp. 1767-1772.

68. Hahn, Juergen: The North Atlantic Ocean as a Source of Atmospheric N₂O. *Tellus*, vol. 26, nos. 1-2, 1974, pp. 160-168.
69. McElroy, Michael B.; Elkins, James W.; Wofsy, Steven C.; and Yung, Yuk Ling: Sources and Sinks for Atmospheric N₂O. *Rev. Geophys. & Space Phys.*, vol. 14, no. 2, May 1976, pp. 143-150.
70. Hales, J. M.; Wilkes, J. O.; and York, J. L.: Recent Measurements of Hydrogen Sulfide Oxidation Rates and Their Implications to Atmospheric Chemistry. *Tellus*, vol. 26, nos. 1-2, 1974, pp. 277-283.
71. Noxon, J. F.: Atmospheric Nitrogen Fixation by Lightning. *Geophys. Res. Lett.*, vol. 3, no. 8, Aug. 1976, pp. 463-465.
72. Chameides, W. L.; Stedman, D. H.; Dickerson, R. R.; Rusch, D. W.; and Cicerone, R. J.: NO_x Production in Lightning. *J. Atmos. Sci.*, vol. 34, no. 1, Jan. 1977, pp. 143-149.
73. Delwiche, C. C.: The Nitrogen Cycle. *Sci. American*, vol. 223, no. 3, Sept. 1970, pp. 136-146.
74. Effect of Increased Nitrogen Fixation on Stratospheric Ozone. Rep. No. 53, Counc. Agric. Sci. & Technol., Jan. 19, 1976.
75. Hardy, R. W. F.; and Havelka, U. D.: Nitrogen Fixation Research: A Key to World Food? *Science*, vol. 188, no. 4188, May 9, 1975, pp. 633-643.
76. Liu, S. C.; Cicerone, R. J.; Donahue, T. M.; and Chameides, W. L.: Limitation of Fertilizer Induced Ozone Reduction by the Long Lifetime of the Reservoir of Fixed Nitrogen. *Geophys. Res. Lett.*, vol. 3, no. 3, Mar. 1976, pp. 157-160.
77. Crutzen, Paul J.: Upper Limits on Atmospheric Ozone Reductions Following Increased Application of Fixed Nitrogen to the Soil. *Geophys. Res. Lett.*, vol. 3, no. 3, Mar. 1976, pp. 169-172.
78. Sze, Nien Dak; and Rice, Harbert: Nitrogen Cycle Factors Contributing to N₂O Production From Fertilizers. *Geophys. Res. Lett.*, vol. 3, no. 6, June 1976, pp. 343-346.
79. Liu, S. C.; Cicerone, R. J.; Donahue, T. M.; and Chameides, W. L.: Sources and Sinks of Atmospheric N₂O and the Possible Ozone Reduction Due to Industrial Fixed Nitrogen Fertilizers. *Tellus*, vol. 29, no. 3, June 1977, pp. 251-263.
80. Duewer, William H.; Wuebbles, Donald J.; Ellsaesser, Hugh W.; and Chang, Julius S.: NO_x Catalytic Ozone Destruction: Sensitivity to Rate Coefficients. *J. Geophys. Res.*, vol. 82, no. 6, Feb. 20, 1977, pp. 935-942.

81. Johnston, Harold S.; and Nelson, Herbert: Comment on 'NO_x Catalytic Ozone Destruction: Sensitivity to Rate Coefficients' by W. H. Duewer, D. J. Wuebbles, H. W. Ellsaesser, and J. S. Chang. *J. Geophys. Res.*, vol. 82, no. 18, June 20, 1977, pp. 2593-2598.
82. Commoner, Barry: Threats to the Integrity of the Nitrogen Cycle: Nitrogen Compounds in Soil, Water, Atmosphere and Precipitation. *The Changing Global Environment*, S. Fred Singer, ed., D. Reidel Publishing Co., c.1975, pp. 341-366.
83. Man's Impact on the Global Environment. Report of the Study of Critical Environmental Problems (SCEP). The MIT Press, c.1970.
84. Kellogg, W. W.; Cadle, R. D.; Allen, E. R.; Lazrus, A. L.; and Martell, E. A.: The Sulfur Cycle. *Science*, vol. 175, no. 4022, Feb. 11, 1972, pp. 587-596.
85. Rasmussen, R. A.: Emission of Biogenic Hydrogen Sulfide. *Tellus*, vol. 26, nos. 1-2, 1974, pp. 254-260.
86. Anderson, G.: Sulfur in Soil Organic Substances. *Soil Components - Volume 1*, John E. Gieseking, ed., Springer Verlag, 1975, pp. 333-341.
87. Ramanathan, V.: Greenhouse Effect Due to Chlorofluorocarbons: Climatic Implications. *Science*, vol. 190, no. 4209, Oct. 3, 1975, pp. 50-52.
88. Rowland, F. S.; and Molina, Mario J.: Chlorofluoromethanes in the Environment. *Rev. Geophys. & Space Phys.*, vol. 13, no. 1, Feb. 1975, pp. 1-35.
89. Lovelock, J. E.: Atmospheric Halocarbons and Stratospheric Ozone. *Nature*, vol. 252, no. 5481, Nov. 22, 1974, pp. 292-294.
90. Grobecker, A. J.; Coroniti, S. C.; and Cannon, R. H., Jr.: The Effects of Stratospheric Pollution by Aircraft. DOT-TST-75-50, U.S. Dep. Transp., Dec. 1974. (Available from DDC as AD A005 458.)

TABLE I.- TROPOSPHERIC COMPOSITION

Species	Chemical symbol	Fractional abundance	Lifetime	Thermal IR band, μm	Sources (a)	Sinks (a)	References
Oxygen group:							
Oxygen (molecular)	O_2	$b_{0.2}$	10^6 yr		B	B, P	4
	$\text{O}_2(^1\Delta_g)$	10^{-13}	0.26 s		C	C	
Oxygen (atomic)	O	10^{-16}	10^{-5} s				
	$\text{O}(^1D)$	10^{-23}	10^{-9} s		C	C	
Ozone	O_3	$b_3 \times 10^{-8}$	2 mo	9.6	P, C	P, C	5
Carbon group:							
Methane	CH_4	$b_{1.4} \times 10^{-6}$	4 yr	7.7	B	C	6
Non-methane hydrocarbons		$\sim 10^{-9}$					7
Methyl radical	CH_3	10^{-21}	10^{-10} s		C	C	
Methoxy radical	CH_3O	10^{-15}	0.1 s		C	C	
Methylperoxy radical	CH_3O_2	10^{-11}	10^3 s		C	C	
Methylhydroperoxy radical	CH_3OOH	10^{-11}	2 d		C	P, C	
Formyl radical	HCO	10^{-22}	10^{-8} s		C	C	
Formaldehyde	H_2CO	$b_4 \times 10^{-10}$	0.4 d		C, A	C	4
Acetaldehyde	CH_3CHO				C	C	
Carbon monoxide	CO	$b_{1.2} \times 10^{-7}$	4 mo		C, A	C, P	8
Carbon dioxide	CO_2	$b_{3.3} \times 10^{-4}$	5 yr	15	B, A	B, P	9
Nitrogen group:							
Nitrogen	N_2	$b_{0.8}$	10^6 yr		B, P	B, P	4
Nitrous oxide	N_2O	$b_{3.3} \times 10^{-7}$	20 yr?	7.8, 17	B, P	C	10
Nitric oxide	NO	10^{-11}			A, B	C	
Nitrogen dioxide	NO_2	$b_{10^{-10}}$		7.6	A, B, C	C	11
Nitrogen trioxide	NO_3	10^{-14}	15 s		C	C	
Dinitrogen pentoxide	N_2O_5	10^{-14}	15 s		C	C	

^aKey to entries in sixth and seventh columns: A - anthropogenic, B - biological or microbiological, C - chemical, and P - physical.

^bMeasured value. Other entries in third column were calculated.

TABLE I.- Continued

Species	Chemical symbol	Fractional abundance	Lifetime	Thermal IR band, μm	Sources (a)	Sinks (a)	References		
Nitrous acid	HNO_2	10^{-12}	10^3 s	5.9, 7.5, 11.3, 21.8 10.53	C	C	12		
Nitric acid	HNO_3	10^{-9}	1 week		C	P, C			
Ammonia	NH_3	$^{b}10^{-9}$	1 week		B, A	C, P			
Amino radical	NH_2	10^{-21}	10^{-5} s		C	C			
Aminoxy radical	NH_2O	10^{-16}	1 s		C	C			
Aminoperoxy radical	NH_2O_2	10^{-12}	1 min		C	C			
Nitroxyl radical	HNO	10^{-14}	10 s		C	C			
Ammonium nitrate	NH_4NO_3	10^{-10}	1 week		C	P			
Hydrogen group:									
Hydrogen (molecular)	H_2	$^{b}5 \times 10^{-7}$	10 yr		6.25, 10.0, 20.0	C, B, A		C	13
Hydrogen (atomic)	H	10^{-21}	10^{-7} s	C		C			
Water	H_2O	$^{b}0.014$	1 week	P		P	4		
Hydroxyl radical	OH	$^{b}10^{-14}$	1 s	C	C	14, 15			
Hydroperoxyl radical	HO_2	10^{-11}	4 min	C	C				
Hydrogen peroxide	H_2O_2	10^{-9}	2 d	C	C				
Sulfur group:									
Hydrogen sulfide	H_2S	$^{b}2 \times 10^{-10}$	3 d	8.7, 7.3	B, A	C	16		
Dimethyl sulfide	$(\text{CH}_3)_2\text{S}$				B	C			
Dimethyl disulfide	$(\text{CH}_3)_2\text{S}_2$				B	C			
Sulfur dioxide	SO_2	$^{b}2 \times 10^{-10}$	hours		B, A	C, P	16		
Carbonyl sulfide	COS	5×10^{-10}			B	C			
Thiyl radicals	HS	10^{-21}	10^{-6} s		C	C			
Sulfoxy	SO	10^{-18}	10^{-3} s		C	C			
Sulfur trioxide	SO_3	10^{-22}	10^{-6} s		C	C			
Sulfurous acid	H_2SO_3	10^{-10}	1 week		C	P			
Sulfuric acid	H_2SO_4	10^{-10}	1 week		C	P			

^aKey to entries in sixth and seventh columns: A - anthropogenic, B - biological or micro-biological, C - chemical, and P - physical.

^bMeasured value. Other entries in third column were calculated.

TABLE I.- Concluded

Species	Chemical symbol	Fractional abundance	Lifetime	Thermal IR band, μm	Sources (a)	Sinks (a)	References
Halogen group:							
Trichlorofluoromethane (Freon 11)	CCl_3F	$b_{10^{-10}}$	50 yr	9.22, 11.82	A	C	17
Dichlorodifluoromethane (Freon 12)	CCl_2F_2	$b_2 \times 10^{-10}$	100 yr		A	C	17
Dichlorofluoromethane (Freon 21)	CHCl_2F	$b_{1.4} \times 10^{-11}$	2 yr		A	C	18
Chlorodifluoromethane (Freon 22)	CHF_2Cl		16 yr		A	C	
Carbon tetrachloride	CCl_4	$b_{10^{-10}}$	60 yr	12.99	A, B	C	17
Methyl bromide	CH_3Br	$b_{4.7} \times 10^{-12}$	1.5 yr	16.4, 10.5, 7.66, 6.92	A, B	C	18
Methyl chloride	CH_3Cl	$b_7 \times 10^{-10}$	1.4 yr	13.66, 9.85, 7.14	A, B	C	17
Methyl iodide	CH_3I	$b_{10^{-11}}$		18.76, 11.36, 7.99, 6.94	A, B	C	
Hydrogen chloride	HCl	10^{-9}	1 week		A, P	C	19
Chloroform	CHCl_3	$b_{9.4} \times 10^{-12}$	7 mo		A, B	C	18
Trichloroethylene	C_2HCl_3	$b_{8.2} \times 10^{-11}$	6 d		A	C	18
Tetrachloroethylene	C_2Cl_4	$b_{3.1} \times 10^{-11}$	5 mo		A	C	18
1,1,1 trichloroethane (methyl chloroform)	CH_3Cl_3	$b_7 \times 10^{-11}$	2.3 yr		A, B	C	18
Vinyl chloride	$\text{C}_2\text{H}_3\text{Cl}$		2 mo		A	C	
Phosgene	COCl_2	$b_2 \times 10^{-11}$			A	C	18
Noble gases:							
Argon	A	$b_{9.3} \times 10^{-3}$			P		20
Neon	Ne	$b_{1.8} \times 10^{-5}$			P		20
Krypton	Kr	$b_{1.1} \times 10^{-6}$			P		20
Xenon	Xe	$b_{9.0} \times 10^{-8}$			P		20
Helium	He	$b_{5.2} \times 10^{-6}$			P	P	20
Radon	Rn		3 d		P	P	

^aKey to entries in sixth and seventh columns: A - anthropogenic, B - biological or microbiological, C - chemical, and P - physical.

^bMeasured value. Other entries in third column were calculated.

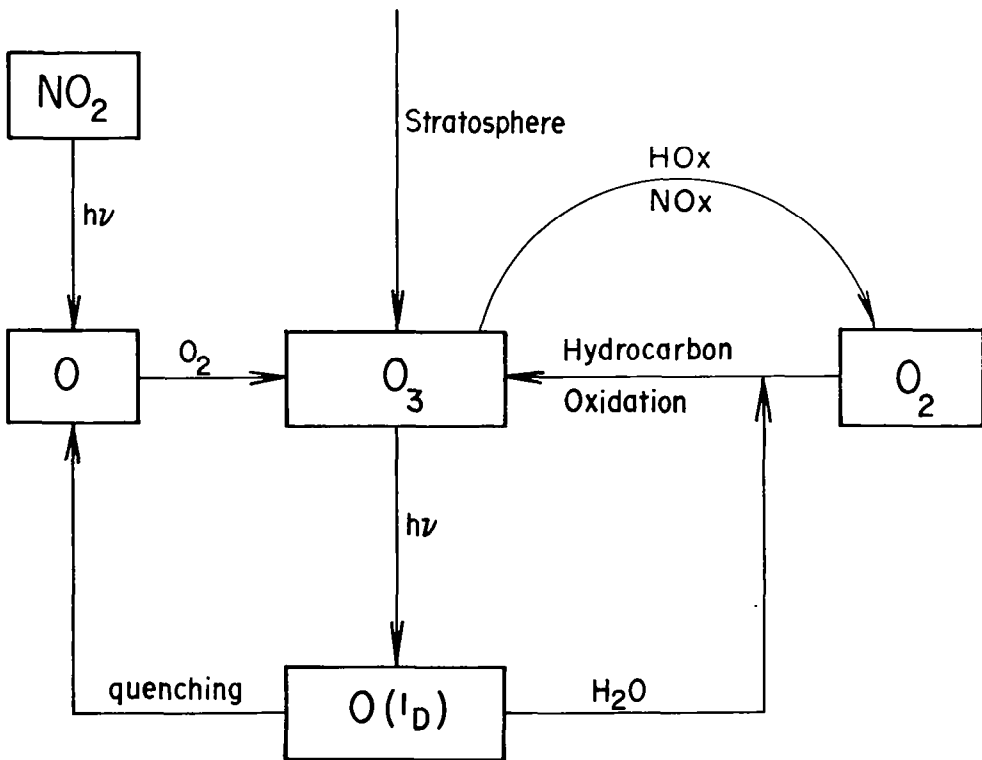


Figure 1.- Oxygen budget of troposphere.

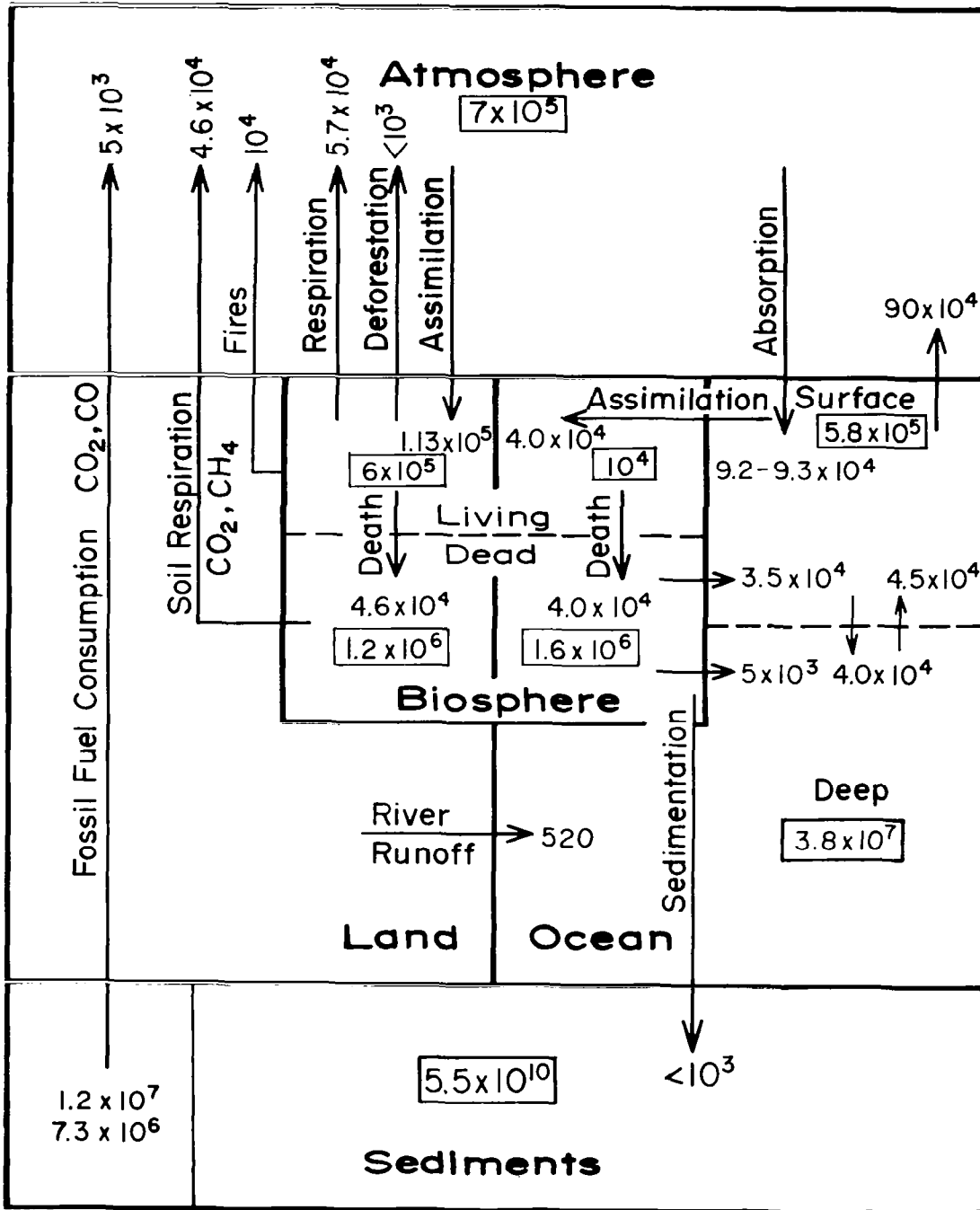


Figure 2.- Carbon cycle. The number of megatons of carbon (C) in indicated reservoirs is shown in boxes. Total fossil fuel carbon (1.2×10^7 Mt) and amount available for use (7.3×10^6 Mt) are shown at left of sediment reservoir. Fluxes between reservoirs are shown by arrows and given in Mt/yr of C.

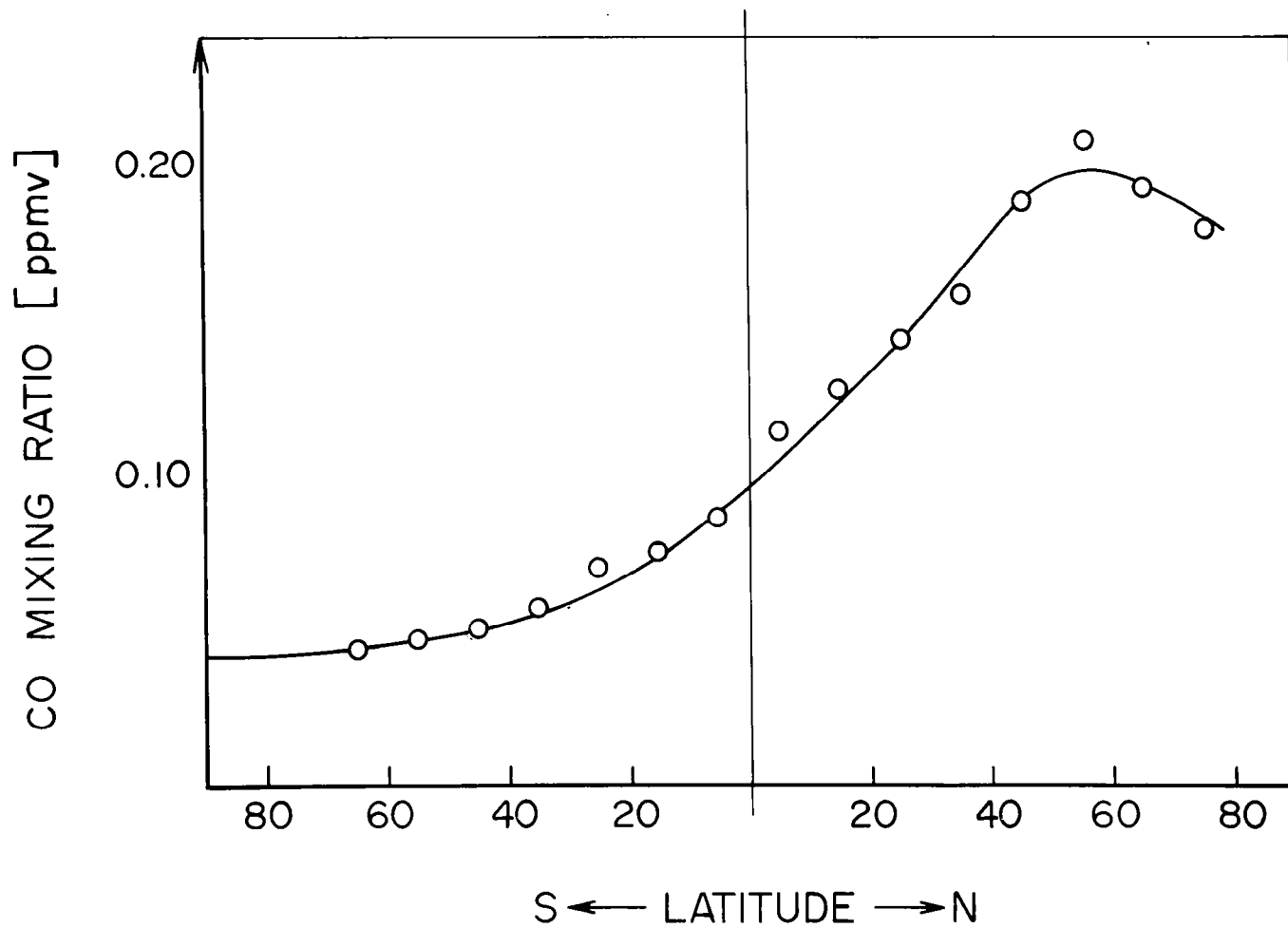


Figure 3.- Latitudinal variation of CO in troposphere. (From Seiler (ref. 8) with permission of publisher.)

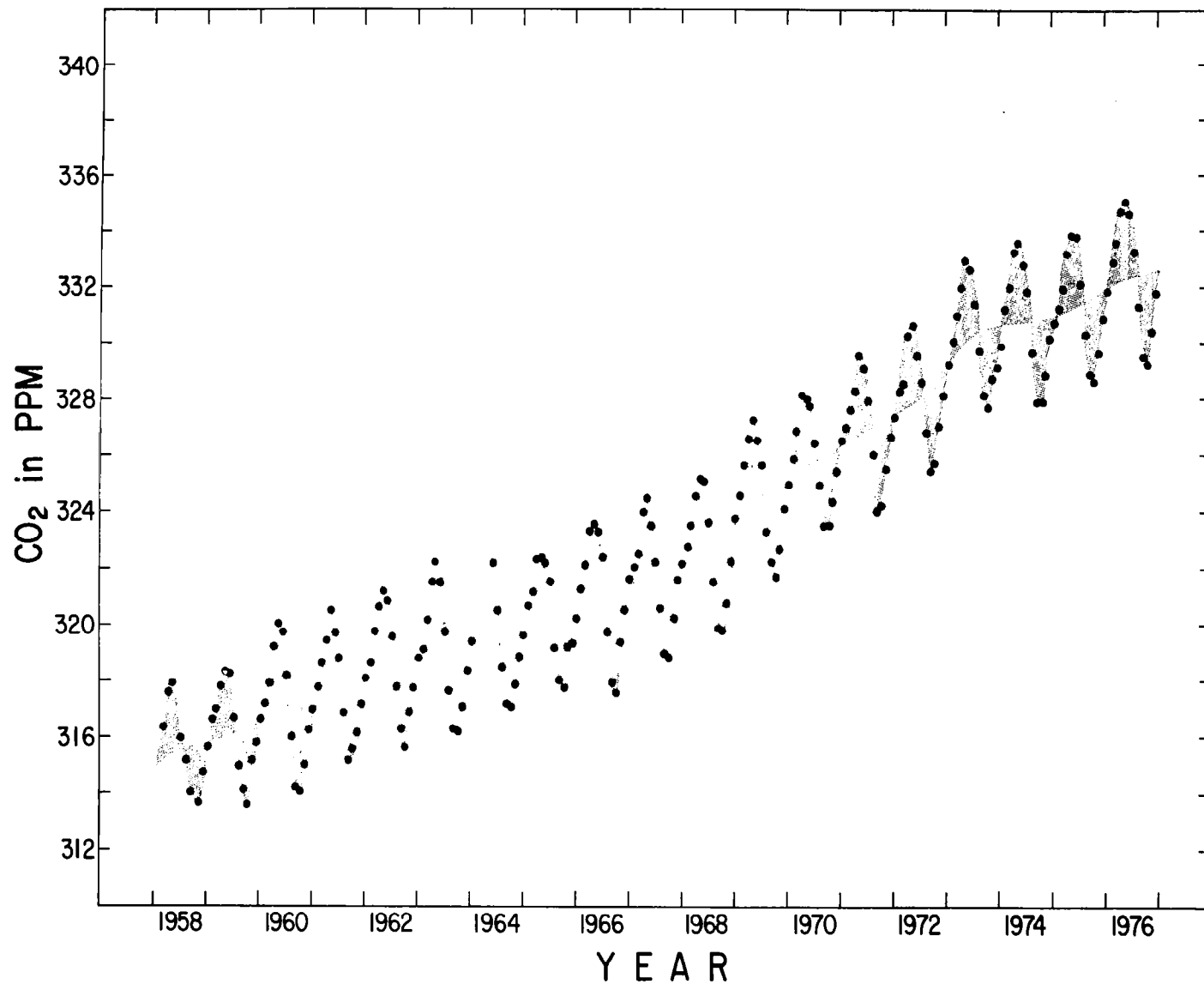


Figure 4.- Monthly average concentration of CO₂ in atmosphere at Mauna Loa Observatory, Hawaii, since beginning of monitoring in 1958. Seasonally adjusted long-term rising trend is indicated approximately by wavy line defined by shaded triangles. (Furnished by C. D. Keeling.)

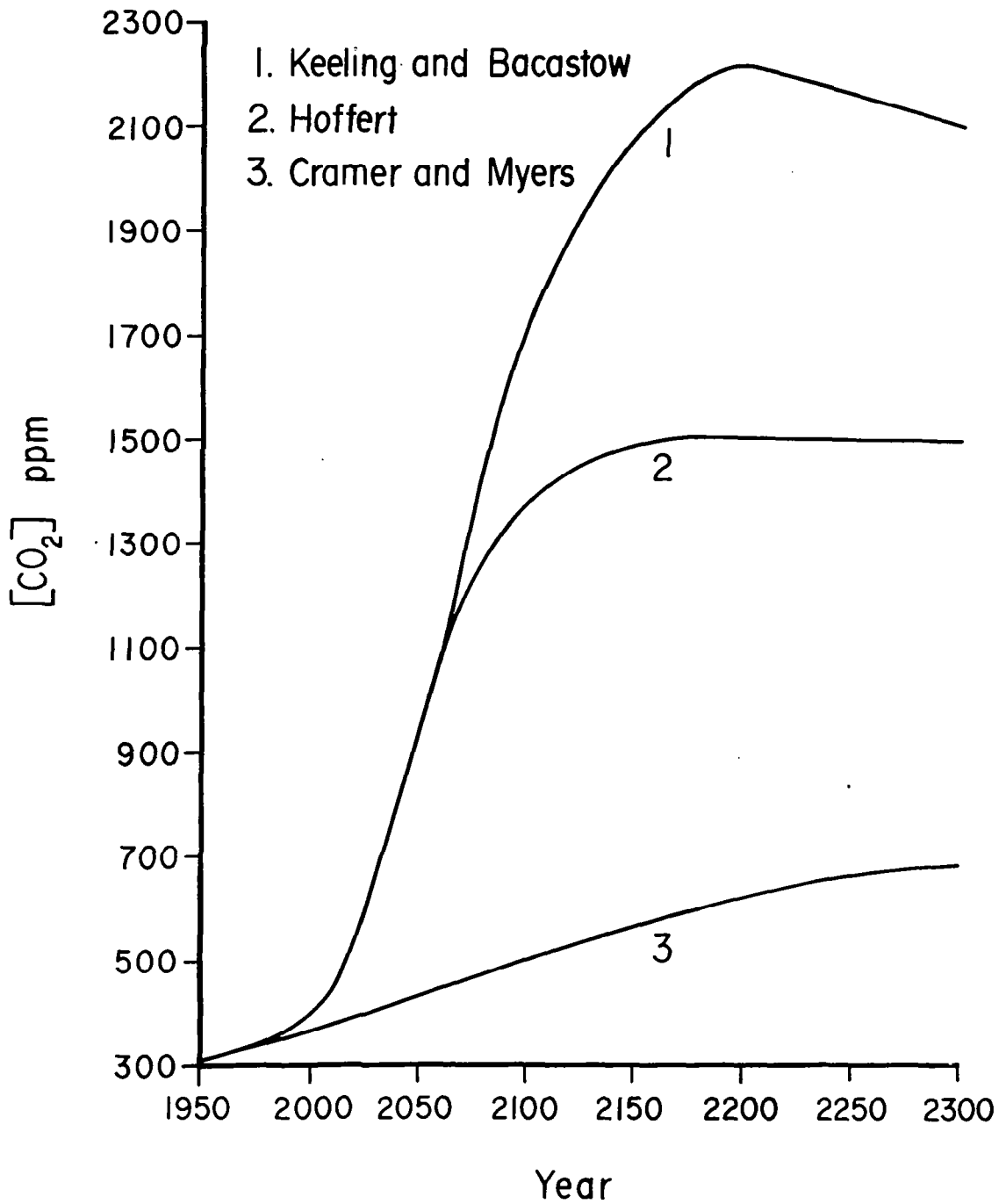


Figure 5.- Projected atmospheric CO₂ increases due to fossil fuel burning from three model studies.

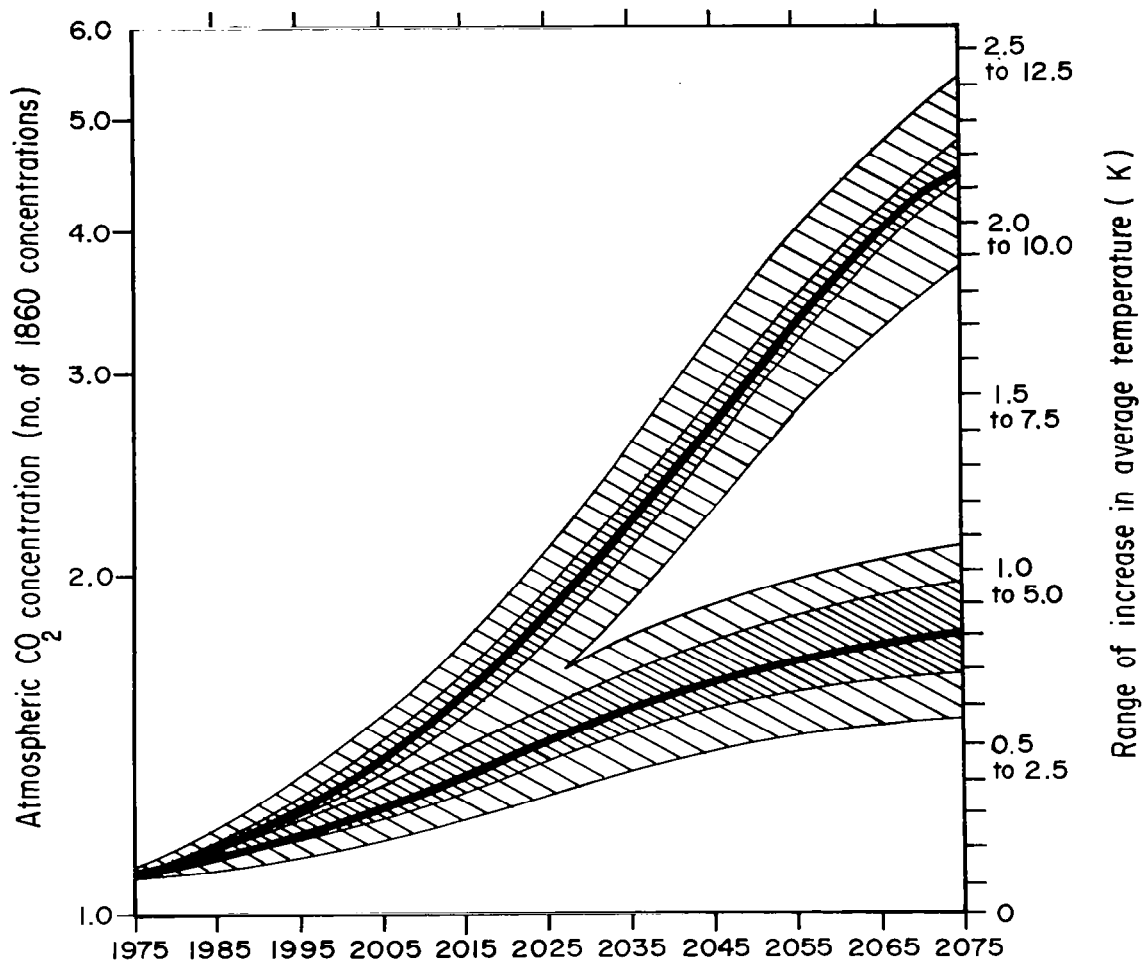


Figure 6.- Projected growth in atmospheric CO₂ and associated range of ΔT_s values for two scenarios of fossil fuel utilization. These curves show sensitivity of model to high and low use production scenarios (inner solid lines), assimilation of CO₂ by land biota (inner band), and oceanic uptake (outer band). The right vertical axis shows the range of uncertainty in ΔT_s for each value of CO₂ increase. (From Baes et al. (ref. 46) with permission of publisher.)

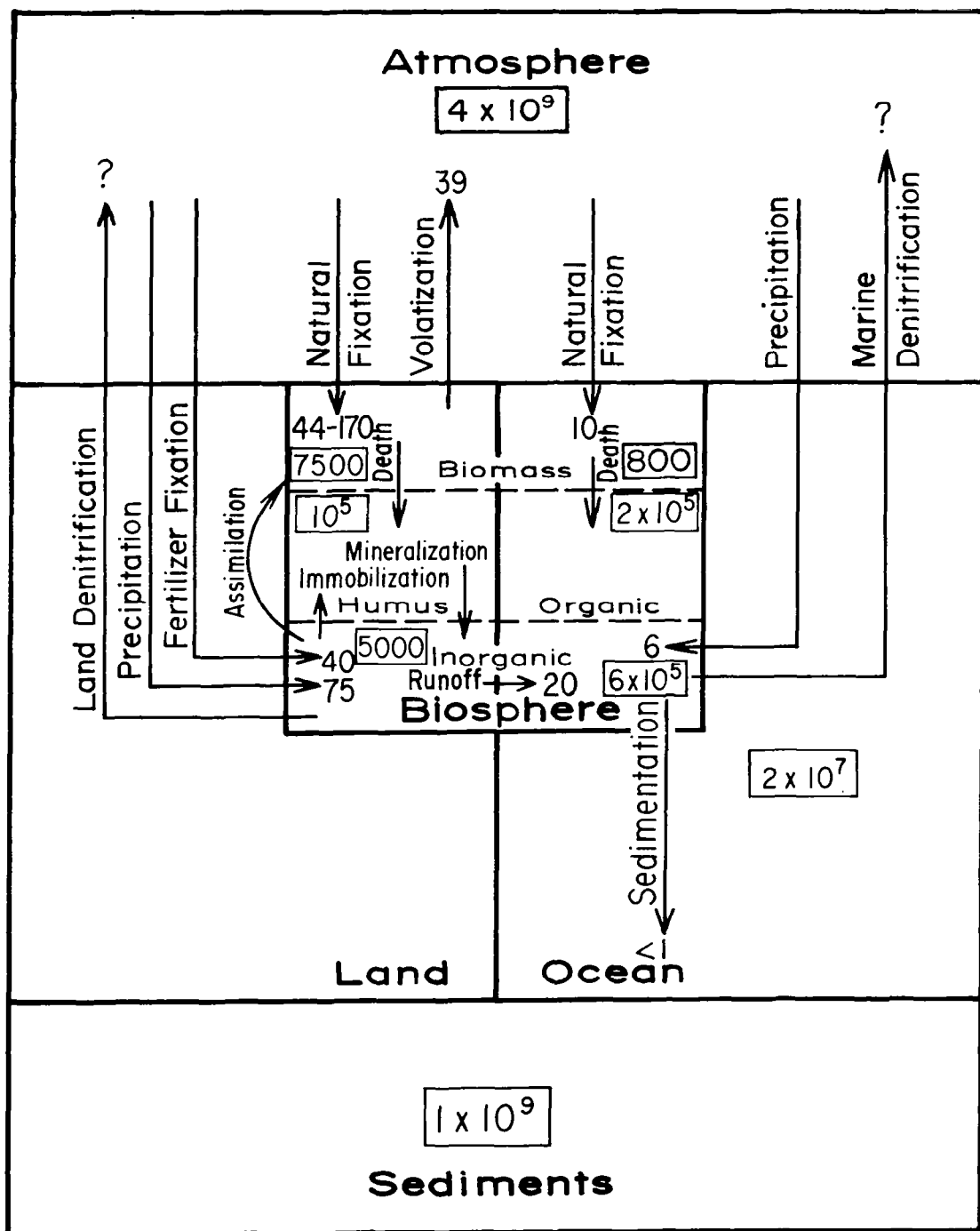


Figure 7.- Nitrogen cycle. The number of megatons of nitrogen (N) in indicated reservoirs is shown in boxes. Fluxes between reservoirs are shown by arrows and given in Mt/yr of N.

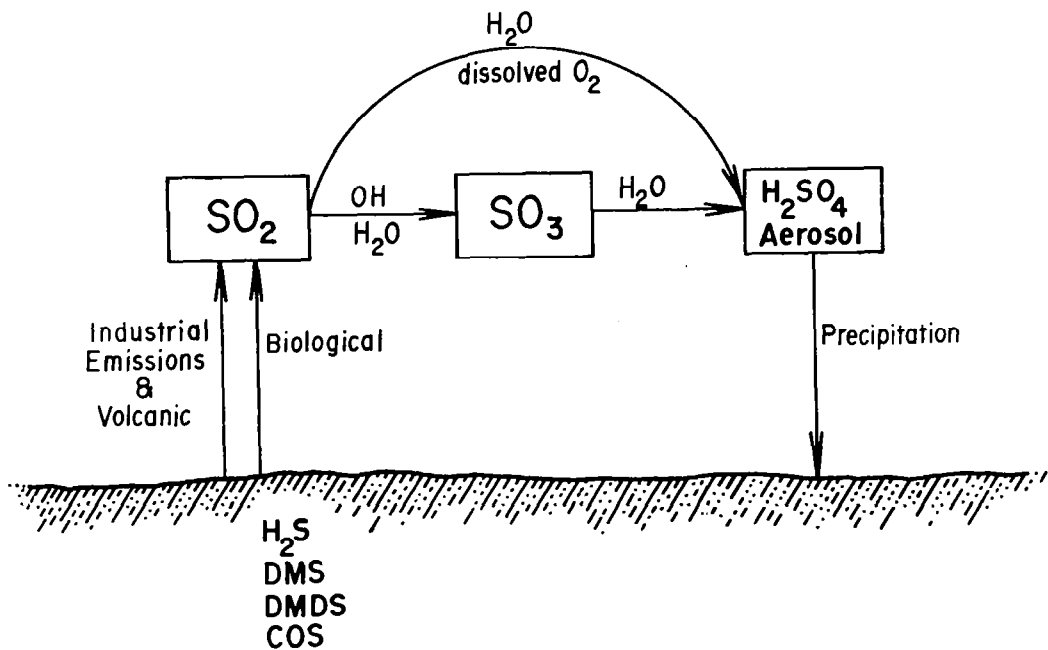


Figure 8.- Tropospheric sulfur chemistry over land. Biological sources emit reduced sulfides H_2S , DMS (dimethylsulfide), DMDS (dimethyldisulfide), and COS (carbonyl sulfide). Industrial and volcanic sources emit SO_2 directly.

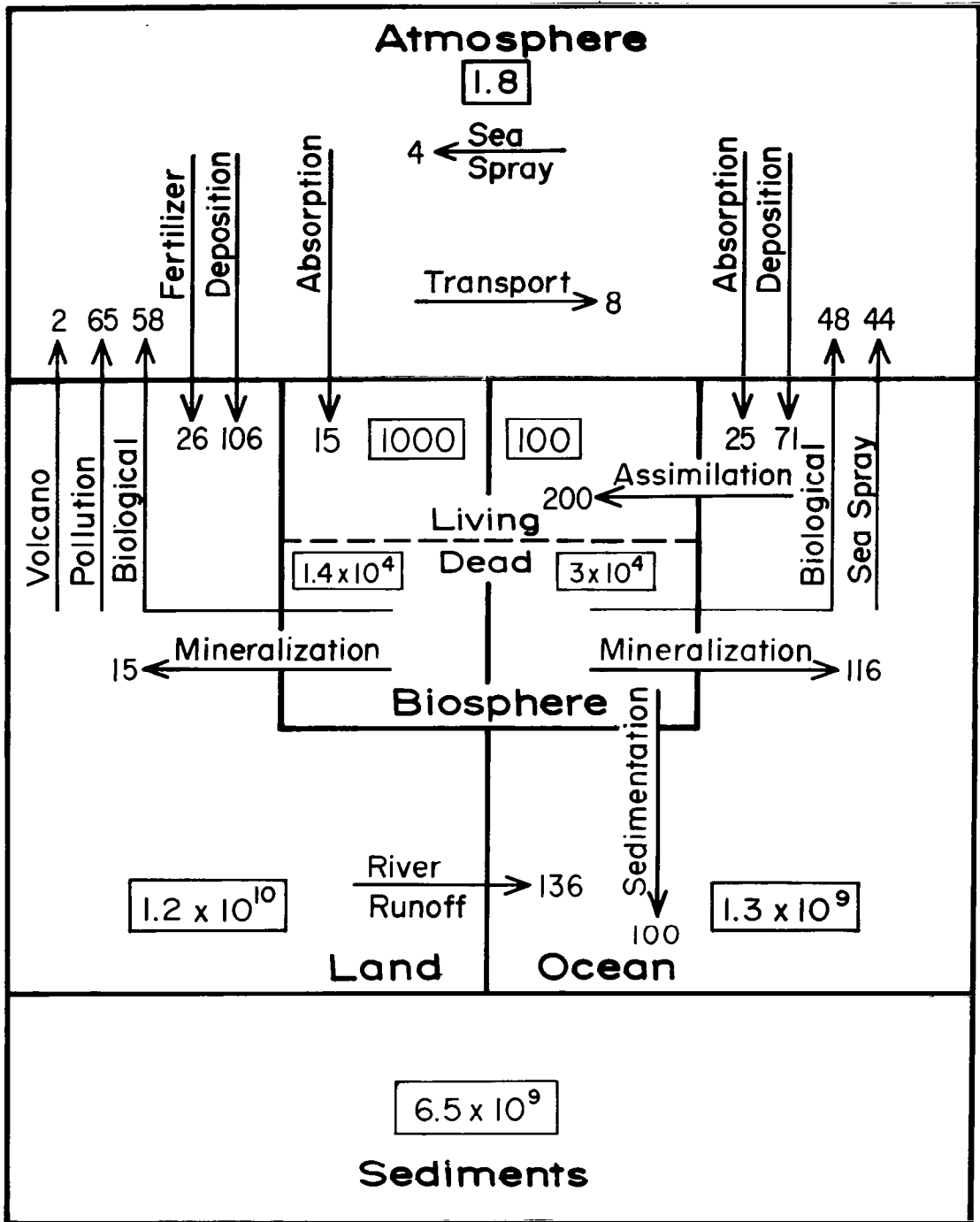


Figure 9.- Sulfur cycle. The number of megatons of sulfur (S) in indicated reservoirs is shown in boxes. Fluxes between reservoirs are shown by arrows and given in Mt/yr of S.

POSSIBLE NONURBAN ENVIRONMENTAL EFFECTS DUE TO CARBON MONOXIDE

AND NITROGEN OXIDES EMISSIONS

Shaw C. Liu[†]
National Center for Atmospheric Research*
Boulder, Colorado

INTRODUCTION

During the last few years, the nonurban environmental effects of carbon monoxide (CO) and nitrogen oxides (i.e., $\text{NO}_x = \text{NO} + \text{NO}_2$) emissions have been investigated by an increasing number of people (e.g., Crutzen (ref. 1), Sze (ref. 2), Chameides et al. (ref. 3), Stewart et al. (ref. 4), and Liu (ref. 5)). In this paper, these environmental effects which have been investigated will be reviewed and some new effects explored. Also, the sources and sinks of NO_x and its concentrations in the troposphere will be discussed in detail. Only a brief discussion of the sources and sinks of CO will be given here since there are already excellent discussions on this subject (Seiler (ref. 6), Jaffe (ref. 7), and Crutzen and Fishman (ref. 8)).

SOURCES, SINKS, AND CONCENTRATIONS OF NO_x

Nitric oxide (NO) is usually produced during high-temperature combustion. When NO is released into the atmosphere, it is quickly converted to NO_2 through the reaction,



This conversion gives NO a lifetime of about 100 seconds in the clean troposphere. Most of the NO_2 produced is photolyzed back to NO, but some recombines with OH to give HNO_3 , which is scavenged by rain. The sources and sinks of NO_x are very uncertain. Table I lists the possible sources and sinks. The anthropogenic source, the only well-known one, contributes about 10 million metric tons of nitrogen per year (10 Mt(N)/yr) from automobiles and another 10 Mt(N)/yr from industrial sources, mainly power plants. The stratospheric downward flux of NO_x is calculated from a one-dimensional model. Its source is oxidation of N_2O by $\text{O}(^1\text{D})$ in the stratosphere. Production of NO_x from the reaction of NH_3 with OH is very uncertain because the average concentration of NH_3 is not known. Measurements in the clean rural area are scarce (Georgii and Muller (ref. 9) and Lodge et al. (ref. 10)). However, the average concentration of NH_3 in the troposphere can be estimated if its source and

*The National Center for Atmospheric Research is sponsored by the National Science Foundation.

[†]Visiting scientist from University of Michigan, Ann Arbor, Michigan.

lifetime are known. Dawson (ref. 11) estimated the source of NH_3 to be about 50 Mt(N)/yr. Since NH_3 is easily scavenged by rain droplets and absorbed by plants and soil, its lifetime can be assumed to be less than 5 days. If the average OH concentration is assumed to be $4 \times 10^5 \text{ cm}^{-3}$ (Singh (ref. 12)), then the lifetime for NH_3 oxidation by OH is about 180 days. Therefore, less than 3 percent of the NH_3 will be oxidized by OH; that is, the upper limit of this source of NO_x is 2 Mt(N)/yr. The most important natural source of NO_x is probably lightning. Noxon (ref. 13) measured enhancements of NO_2 during a number of storms and gave an order-of-magnitude estimate of a global source of NO_2 from lightning of about $10^{10} \text{ cm}^{-2}\text{-sec}^{-1}$ or 40 Mt(N)/yr. Recent theoretical calculations (Griffing (ref. 14)) have arrived at somewhat the same order of magnitude for production of NO_2 in lightning. Since there is probably as much NO produced in lightning (Griffing (ref. 14), Chameides et al. (ref. 15), and Tuck (ref. 16)), the total NO_x source due to lightning is about 80 Mt(N)/yr. This value is probably too high because the ultimate sink of NO_x is the soil and ocean, where it is converted to nitrate. This source strength implies that a substantial amount of fixed nitrogen nutrient is input into the soil and ocean. The natural nitrogen fixation rate is only about 175 Mt(N)/yr on the land (Hardy and Havelka (ref. 17)) and only about 10 Mt(N)/yr in the ocean (Delwiche (ref. 18)). How much NO_x is produced from forest fires and agricultural burning is uncertain; however, if it is assumed that the emission efficiency is the same as for coal burning, this source can be estimated to be less than 10 Mt(N)/yr.

The sinks of NO_x are very uncertain except for the photochemical sink,



The averaged tropospheric OH concentrations, $2 \times 10^5 \text{ cm}^{-3}$ in the Northern Hemisphere (N.H.) and $6 \times 10^5 \text{ cm}^{-3}$ in the Southern Hemisphere (S.H.), have been deduced by Singh (ref. 12) by examining the global budget and measured distribution of methyl chloroform (CH_3CCl_3). By adopting his values, the average lifetime for NO_x due to this reaction is calculated to be 2 days in the S.H. and 6 days in the N.H. Since NO_2 is soluble in water and must therefore be subject to rain scavenging, the lifetime of NO_2 against rain scavenging can be assumed to be 6 days, the same as the lifetime of water vapor. This implies that the lifetime of NO_x is about 10 days since the NO_2 to NO_x ratio is about 2 to 3. The dry deposition lifetime for NO_x is calculated from an arbitrarily assumed deposition velocity of 0.1 cm-sec^{-1} for NO_2 .

Until recently, there were very few measurements of NO_x in the nonurban areas. Table II was adopted from the summaries of NO and NO_2 measurements by Drummond (ref. 19) and Noxon (ref. 20) who cite references 10 and 21 to 31. Most of these measurements were taken at one location for a short period of time with the exceptions of Noxon (ref. 20) and Lodge et al. (ref. 10). Since the lifetime of NO_x is only about 4 days, the standard deviation of its mixing ratio in the troposphere should be about 10, according to Junge (ref. 32), and even larger near the Earth's surface which is closer to the sources and sinks. Therefore, a large amount of data spread over a wide range of areas is needed to establish the average NO_x content in the troposphere. Nevertheless, in table II, one can see that very low concentrations ($\lesssim 0.1$ ppb) of NO and NO_2

have been indicated by recent measurements. Noxon, in particular, has monitored NO₂ at the National Oceanographic and Atmospheric Administration's Fritz Peak Observatory in Colorado since fall 1974 (ref. 30) and has made numerous observations over North America and Peru (ref. 20). His data have convincingly shown that in the Western Hemisphere (W.H.), the clean air tropospheric column density of NO₂ is below 5×10^{14} cm⁻². If the scale height of NO₂ is assumed to be about 2 km, as suggested in some recent models (Chameides (ref. 33), Crutzen et al. (ref. 34), and Liu (ref. 5)), this column density of NO₂ corresponds to a mixing ratio of only 0.1 ppb at the Earth's surface.

However, if 95 percent of the industrial NO_x and 50 percent of the NO_x from lightning are assumed to be emitted into the Northern Hemisphere, a simple one-dimensional model (e.g., Fishman and Crutzen (ref. 35), Liu (ref. 5), or Chameides (ref. 36)) would give a mixing ratio of 0.5 ppb for NO₂ and 0.2 ppb for NO at the surface. These values are 5 times higher than the upper limit set by Noxon's NO₂ observations and about 10 times higher than Drummond's NO measurements. Crutzen (private communication, 1977) suggested that there might be some as yet unknown mechanisms for removal of NO_x that is more than 5 times as efficient as the sink of reaction (2). On the other hand, Chameides (ref. 36) suggested that for a rural area which is far away from NO_x sources, the NO_x observed is probably due to the photolysis of HNO₃ because HNO₃ has a longer lifetime than NO_x. Therefore, one can assume that HNO₃ is emitted into the atmosphere instead of NO_x. The NO_x mixing ratio evaluated in this way does fall below the observed upper limit. However, more realistic multi-dimensional models are needed to verify this concept, and more measurements of NO_x, especially of the height profiles, are needed to establish the NO_x content in the troposphere.

SOURCES, SINKS, AND CONCENTRATIONS OF CO

A detailed discussion on this subject was given by Seiler (ref. 6). More detailed discussion on the anthropogenic sources of CO and its concentrations in the urban area was given by Jaffe (ref. 7). In table III, their values are given with modifications only to the photochemical source of CO from methane (CH₄) oxidation and the sink of CO due to oxidation by OH. These were calculated by using the averaged OH densities given by Singh (ref. 12) for the two hemispheres and the CO distributions given by Seiler (ref. 6). These estimates agree with an earlier study by Crutzen and Fishman (ref. 8). The sink of CO due to oxidation by OH is much larger because of the reaction,



for which the pressure-dependent rate has been recently measured by Cox et al. (ref. 37), Sie et al. (ref. 38), Chan et al. (ref. 39), and Perry et al. (ref. 40). In the troposphere, this rate is about twice that previously accepted (Hampson and Garvin (ref. 41)). The imbalance of the source and the sink of CO is so large that there has to be an important unknown source of CO, as suggested by Crutzen and Fishman (ref. 8).

The average concentration of CO in the N.H. (0.2 ppm) is about a factor of 4 higher than in the S.H. (0.05 ppm), as shown by Seiler (ref. 6). Most

of this difference can probably be attributed to the fact that 95 percent of the anthropogenic sources of CO emitted are in the N.H.

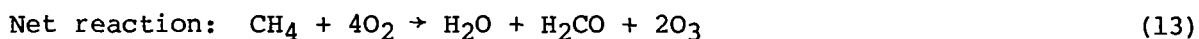
POSSIBLE EFFECTS DUE TO CO AND NO_x EMISSIONS

Increase in Tropospheric Ozone

This problem has been studied by many investigators (e.g., Chameides and Stedman (ref. 42), Stewart et al. (ref. 4), Fishman and Crutzen (ref. 35), and Liu (ref. 5)). The mechanism of production of ozone is a catalytic cycle:



This is a very efficient catalytic cycle. The only weak link before was reaction (5), for which the reaction rate was accepted to be $4 \times 10^{-13} \text{ cm}^3\text{-sec}^{-1}$ (Hampson and Garvin (ref. 41)) but has since been measured accurately to be $8 \times 10^{-12} \text{ cm}^3\text{-sec}^{-1}$ (Howard and Evenson (ref. 43)). Reactions (3) and (4) can be replaced with a methane oxidation chain:



Further reactions of H_2CO will produce CO . Without the anthropogenic emissions, the CO mixing ratio was probably less than 0.03 ppm, since most of the CO was produced from methane oxidation. The catalytic ozone production should have been dominated by the methane oxidation chain, reaction (13). With the present averaged CO concentration, reaction (8) now dominates the catalytic ozone production.

Anthropogenic NO_x emissions will speed up reaction (5) and thus increase ozone production rate. As discussed before, the natural NO_x source is very uncertain. Nevertheless, if the values in table I are adopted and NO_x distributions are assumed to be consistent with Noxon's upper limit on NO_2 , an upper limit for ozone increase is about 40 percent in the N.H. and negligible in the S.H. These estimates can only be regarded as qualitative because of the neglect of some important nonlinear effects, such as the large deviations in water vapor and NO_x distributions. The ozone production rate has been found to increase less than linearly with NO_x , especially when NO_x concentration is higher than 1 ppb.

There are some experimental data (Fishman and Crutzen (ref. 44)) which indicate that the ozone concentration in the N.H. is about 50 percent higher than in the S.H. Of course, this could just be coincidental and the different ozone concentrations in the N.H. and S.H. could be due to other mechanisms, such as dynamics.

Stratospheric Ozone Increase

Mechanism (8) may increase the lower stratospheric ozone when tropospheric CO is transported above the tropopause. In the stratosphere, the NO_x is produced from oxidation of N_2O by $\text{O}(^1\text{D})$. Tropospheric NO_x does not penetrate into the stratosphere because of its small scale height, as discussed before. One-dimensional model calculation shows that the northern stratospheric ozone column density is increased by about 1 to 2 percent because of CO emission. Locally, the increase in ozone can be as high as 15 percent near the tropopause. However, Seiler's (ref. 6) CO measurements just above the tropopause seem to indicate very little penetration of tropospheric CO into the stratosphere. More measurements and multidimensional calculations are needed to resolve this problem.

Effects on Tropospheric OH

The important role that the OH radical plays in the tropospheric self-cleansing processes of gases such as NO_2 , SO_2 , H_2S , CO , CH_4 , RH , and $\text{CH}_x\text{Cl}_y\text{F}_z$ has long been appreciated (Levy (ref. 45) and McConnell et al. (ref. 46)). Wofsy (ref. 47) noted that an increase in the global CO concentration may decrease the tropospheric OH concentration since CO and CH_4 are major sinks of OH . Sze (ref. 2) and Chameides et al. (ref. 3) have shown that CH_4 may increase by as much as 40 percent by the year 2000 if the anthropogenic emissions of CO keep increasing. In fact, Sze (ref. 2) has shown that CH_4 may be already increased by 20 percent since 1950. If the OH concentrations (6×10^5 and $2 \times 10^5 \text{ cm}^{-3}$) in the S.H. and N.H. deduced by Singh (ref. 12) are assumed

to represent unperturbed and perturbed conditions, respectively, they imply a 33-percent decrease in globally averaged OH concentration. This corresponds to a 33-percent increase in CH₄ concentration, slightly higher than Sze's calculation. These calculations assumed a constant CH₄ source which may have increased because of human activities, according to Crutzen (ref. 48).

Emissions of NO_x can increase the tropospheric OH concentrations through reaction (5) (Liu (ref. 5)). Like the tropospheric ozone increase problem, a quantitative estimate depends on the knowledge of the background NO_x abundance and natural NO_x source. Using the values in table I and assuming NO_x to be consistent with the upper limit of Noxon's measurement, an upper limit is estimated to be a 25-percent increase in tropospheric OH concentration due to NO_x emissions. Here again, note that the nonlinear effect of large spatial deviations in NO_x concentrations is not included. This effect tends to diminish the increase of OH due to NO_x emissions.

Increases in CH₄, CH₃Cl, CH₃CCl₃, and other hydrocarbons due to decrease in OH not only could perturb the stratospheric photochemistry of odd hydrogen but also could increase the amount of odd chlorine released in the stratosphere by these species and thus further reduce stratospheric ozone (McConnell and Schiff (ref. 49)). Furthermore, the greenhouse effect of these species will be enhanced and result in a perturbation of the climate.

Acid Rain

Likens (ref. 50) has shown that the pH of precipitation in the United States and Western Europe has been dropping significantly during the last 30 years. Sulfuric and nitric acids are major sources of acidity in precipitation. The Hubbard Brook Experimental Forest in the White Mountains of New Hampshire provides the longest known record for pH of precipitation in the United States. Likens found that, although sulfuric acid had been the dominant acid in precipitation there, the increased deposition of hydrogen ions has been due primarily to the increased amounts of nitric acid in the rain and snow. It is reasonable to believe that the increase in nitric acid in the precipitation is the result of anthropogenic NO_x emissions. In Scandinavia, it has been shown that, as the acidity of precipitation increased, the number of barren lakes increased sharply. In addition, the increased acidity enhances the weathering and erosion of buildings and materials.

Fertilizer

As mentioned before, the NO_x emissions will eventually be rained out and deposited in the land and ocean as nitrate. The industrial nitrogen fertilizer production is only about 40 Mt(N)/yr (Hardy and Havelka (ref. 17)), about twice as much as NO_x emissions. Therefore, the NO_x emissions represent an important amount of fixed nitrogen fertilizer. Since nitrogen is one of the limiting nutrients in the land and ocean, it should help increase the productivity of plants. In this respect, NO_x emissions may play a positive role. However, increased fixed nitrogen input into the soil may increase the denitrification

rate and thus increase the N₂O flux into the atmosphere (Crutzen (ref. 51), Crutzen (ref. 52), McElroy et al. (ref. 53), Liu et al. (ref. 54), and Sze and Rice (ref. 55)). Increase in N₂O not only could perturb the ozone layer but also could have an increased greenhouse effect on the climate. Furthermore, increased nitrogen nutrient input into aquatic systems may speed up the rate of eutrophication of rivers and lakes.

REFERENCES

1. Crutzen, Paul J.: Photochemical Reactions Initiated by and Influencing Ozone in Unpolluted Tropospheric Air. *Tellus*, vol. 26, nos. 1-2, 1974, pp. 47-57.
2. Sze, N. D.: Anthropogenic CO Emissions: Implications for the Atmospheric CO-OH-CH₄ Cycle. *Science*, vol. 195, no. 4279, Feb. 18, 1977, pp. 673-675.
3. Chameides, W. L.; Liu, S. C.; and Cicerone, R. J.: Possible Variations in Atmospheric Methane. *J. Geophys. Res.*, vol. 82, no. 12, Apr. 20, 1977, pp. 1795-1798.
4. Stewart, Richard W.; Hameed, Sultan; and Pinto, Joseph P.: Photochemistry of Tropospheric Ozone. *J. Geophys. Res.*, vol. 82, no. 21, July 20, 1977, pp. 3134-3140.
5. Liu, Shaw Chen: Possible Effects on Tropospheric O₃ and OH Due to NO Emissions. *Geophys. Res. Lett.*, vol. 4, no. 8, Aug. 1977, pp. 325-328.
6. Seiler, Wolfgang: The Cycle of Atmospheric CO. *Tellus*, vol. 26, nos. 1-2, 1974, pp. 116-135.
7. Jaffe, Louis S.: Carbon Monoxide in the Biosphere: Sources, Distribution, and Concentrations. *J. Geophys. Res.*, vol. 78, no. 24, Aug. 20, 1973, pp. 5293-5305.
8. Crutzen, Paul J.; and Fishman, Jack: Average Concentrations of OH in the Troposphere, and the Budgets of CH₄, CO, H₂ and CH₃CCl₃. *Geophys. Res. Lett.*, vol. 4, no. 8, Aug. 1977, pp. 321-324.
9. Georgii, H. W.; and Muller, W. J.: Distribution of Ammonia in the Middle and Lower Troposphere. *Tellus*, vol. 26, nos. 1-2, 1974, pp. 180-184.
10. Lodge, James P., Jr.; Machado, P. A.; Pate, J. B.; Sheesly, D. C.; and Wartburg, A. F.: Atmospheric Trace Chemistry in the American Humid Tropics. *Tellus*, vol. 26, nos. 1-2, 1974, pp. 250-253.
11. Dawson, G. A.: Atmospheric Ammonia From Undisturbed Land. *J. Geophys. Res.*, vol. 82, no. 21, July 20, 1977, pp. 3125-3133.
12. Singh, Hanwant B.: Preliminary Estimation of Average Tropospheric HO Concentrations in the Northern and Southern Hemispheres. *Geophys. Res. Lett.*, vol. 4, no. 10, Oct. 1977, pp. 453-456.
13. Noxon, J. F.: Atmospheric Nitrogen Fixation by Lightning. *Geophys. Res. Lett.*, vol. 3, no. 8, Aug. 1977, pp. 463-465.
14. Griffing, George W.: Ozone and Oxides of Nitrogen Production During Thunderstorms. *J. Geophys. Res.*, vol. 82, no. 6, Feb. 20, 1977, pp. 943-950.

15. Chameides, W. L.; Stedman, D. H.; Dickerson, R. R.; Rusch, D. W.; and Cicerone, R. J.: NO_x Production in Lightning. *J. Atmos. Sci.*, vol. 34, no. 1, Jan. 1977, pp. 143-149.
16. Tuck, A. F.: Production of Nitrogen Oxides by Lightning Discharges. *Q. J. R. Meteorol. Soc.*, vol. 102, no. 434, Oct. 1976, pp. 749-755.
17. Hardy, R. W. F.; and Havelka, U. D.: Nitrogen Fixation Research: A Key to World Food? *Science*, vol. 188, no. 4188, May 9, 1975, pp. 633-643.
18. Delwiche, C. C.: The Nitrogen Cycle. *Sci. American*, vol. 223, no. 3, Sept. 1970, pp. 136-146.
19. Drummond, John Wendell: Atmospheric Measurements of Nitric Oxide Using a Chemiluminescent Detector. Ph.D. Diss., Univ. of Wyoming, 1977.
20. Noxon, John F.: Tropospheric NO₂. *J. Geophys. Res.*, vol. 83, no. C5, May 1978.
21. Atmospheric Condensation Nuclei and Trace Gases. Contract DA-91-591-EUC-2126, Dep. Phys., Univ. College (Galway, Ireland), 1962. (Available from DDC as AD 420 435.)
22. Junge, Christian E.: Air Chemistry and Radioactivity. Academic Press, Inc., 1963.
23. Lodge, James P., Jr.; and Pate, John B.: Atmospheric Gases and Particulates in Panama. *Science*, vol. 153, no. 3734, July 22, 1966, pp. 408-410.
24. Ripperton, Lyman A.; Worth, James J. B.; and Kornreich, Lawrence: Nitrogen Dioxide and Nitric Oxide in Non-Urban Air. Paper presented at the 61st Annual Meeting of the Air Pollution Control Association, June 1968.
25. Hamilton, Harry L., Jr.; Worth, James J. B.; and Ripperton, Lyman A.: An Atmospheric Physics and Chemistry Study on Pikes Peak in Support of Pulmonary Edema Research. Contract DAHCl9-67-C-0029, Research Triangle Inst., May 1968. (Available from DDC as AD 670 989.)
26. Hidy, G. M.: Removal Processes of Gaseous and Particulate Pollutants. *Chemistry of the Lower Atmosphere*, S. I. Rasool, ed., Plenum Press, 1973, pp. 121-176.
27. Breeding, R. J.; Lodge, J. P., Jr.; Pate, J. B.; Sheesley, D. C.; Klonis, H. B.; Fogle, B.; Anderson, J. A.; Englert, T. R.; Haagenson, P. L.; McBeth, R. B.; Morris, A. L.; Pogue, R.; and Wartburg, A. F.: Background Trace Gas Concentrations in the Central United States. *J. Geophys. Res.*, vol. 78, no. 30, Oct. 20, 1973, pp. 7057-7064.
28. Nash, T.: Nitrous Acid in the Atmosphere and Laboratory Experiments on Its Photolysis. *Tellus*, vol. 26, nos. 1-2, 1974, pp. 175-179.

29. Moore, Howard: Isotopic Measurement of Atmospheric Nitrogen Compounds. *Tellus*, vol. 26, nos. 1-2, 1974, pp. 169-174.
30. Noxon, J. F.: Nitrogen Dioxide in the Stratosphere and Troposphere Measured by Ground-Based Absorption Spectroscopy. *Science*, vol. 189, no. 4202, Aug. 1975, pp. 547-549.
31. Briehl, D. C.; Hilsenrath, E.; Ridley, B. A.; and Schiff, H. I.: In Situ Measurements of Nitric Oxide, Water Vapour and Ozone From an Aircraft. Second International Conference on the Environmental Impact of Aerospace Operations in the High Atmosphere - Preprints, American Meteorol. Soc., July 1974, pp. 11-15.
32. Junge, C. E.: Residence Time and Variability of Tropospheric Trace Gases. *Tellus*, vol. 26, no. 4, 1974, pp. 477-488.
33. Chameides, William: Tropospheric Odd Nitrogen and the Atmospheric Water Vapor Cycle. *J. Geophys. Res.*, vol. 80, no. 36, Dec. 20, 1975, pp. 4989-4996.
34. Crutzen, Paul J.; Isaksen, Ivar S. A.; and McAfee, John R.: The Impact of the Chlorocarbon Industry on the Ozone Layer. *J. Geophys. Res.*, vol. 83, no. C1, Jan. 20, 1978, pp. 345-363.
35. Fishman, Jack; and Crutzen, Paul J.: A Numerical Study of Tropospheric Photochemistry Using a One-Dimensional Model. *J. Geophys. Res.*, vol. 82, no. 37, Dec. 20, 1977, pp. 5897-5906.
36. Chameides, W. L.: The Photochemical Role of Tropospheric Nitrogen Oxides. *Geophys. Res. Lett.*, vol. 5, no. 1, Jan. 1978, pp. 17-20.
37. Cox, Richard A.; Derwent, Richard G.; and Holt, Pauline M.: Relative Rate Constants for the Reactions of OH Radicals With H₂, CH₄, CO, NO and HONO at Atmospheric Pressure and 296 K. *J. Chem. Soc., Faraday Trans. I*, vol. 72, pt. 9, 1976, pp. 2031-2043.
38. Sie, B. K. T.; Simonaitis, R.; and Heicklen, J.: The Reaction of OH With CO. *Int. J. Chem. Kinet.*, vol. 8, no. 1, 1976, pp. 85-98.
39. Chan, Walter H.; Uselman, William M.; Calvert, Jack G.; and Shaw, John H.: The Pressure Dependence of the Rate Constant for the Reaction: HO + CO → H + CO₂. *Chem. Phys. Lett.*, vol. 45, no. 2, Jan. 15, 1977, pp. 240-243.
40. Perry, R. A.; Atkinson, R.; and Pitts, J. N., Jr.: Kinetics of the Reactions of OH Radicals With C₂H₂ and CO. *J. Chem. Phys.*, vol. 67, no. 12, Dec. 15, 1977, pp. 5577-5584.
41. Hampson, Robert F., Jr.; and Garvin, David, eds.: Chemical Kinetic and Photochemical Data for Modelling Atmospheric Chemistry. NBS Tech. Note 866, U.S. Dep. Commer., June 1975.

42. Chameides, William L.; and Stedman, Donald H.: Ozone Formation From NO_x in "Clean Air." Environ. Sci. & Technol., vol. 10, no. 2, Feb. 1976, pp. 150-153.
43. Howard, Carleton J.; and Evenson, K. M.: Kinetics of the Reaction of HO₂ With NO. Geophys. Res. Lett., vol. 4, no. 10, Oct. 1977, pp. 437-440.
44. Fishman, J.; and Crutzen, P. J.: Computed and Observed Differences Between the Northern and Southern Hemisphere Distribution of Various Trace Constituents in the Troposphere. Paper presented at the 1977 Fall Meeting of the American Geophysical Union (San Francisco, California), Dec. 1977. (Abstract - EOS Trans., American Geophys. Union, vol. 58, no. 12, Dec. 1977, p. 1148.)
45. Levy, H., II: Normal Atmosphere: Large Radical and Formaldehyde Concentrations Predicted. Science, vol. 173, no. 3992, July 9, 1971, pp. 141-143.
46. McConnell, J. C.; McElroy, M. B.; and Wofsy, S. C.: Natural Sources of Atmospheric CO. Nature, vol. 233, no. 5316, Sept. 17, 1971, pp. 187-188.
47. Wofsy, Steven C.: Interactions of CH₄ and CO in the Earth's Atmosphere. Annual Review of Earth and Planetary Sciences, Fred A. Donath, Francis G. Stehli, and George W. Wetherill, eds., Volume 4, Annual Reviews Inc., 1976, pp. 441-469.
48. Crutzen, Paul J.: An Attempt To Reconstruct the Composition of the Pre-Industrial Atmosphere. Paper presented at the Third General Scientific Assembly of the International Association of Geomagnetism and Aeronomy and the Second Special Assembly of the International Association of Meteorology and Atmospheric Physics (Seattle, Washington), Aug.-Sept. 1977. (Abstract - EOS Trans., American Geophys. Union, vol. 58, no. 8, Aug. 1977, p. 689.)
49. McConnell, J. C.; and Schiff, H. I.: Methyl Chloroform: Impact on Stratospheric Ozone. Science, vol. 199, no. 4325, Jan. 1978, pp. 174-176.
50. Likens, Gene E.: Acid Precipitation. Chem. & Eng. News, vol. 54, no. 48, 1976, pp. 29-31.
51. Crutzen, Paul J.: SST's. Threat to the Earth's Ozone Shield. Ambio, vol. 1, no. 2, 1972, pp. 41-51.
52. Crutzen, Paul J.: Upper Limits on Atmospheric Ozone Reductions Following Increased Application of Fixed Nitrogen to the Soil. Geophys. Res. Lett., vol. 3, no. 3, Mar. 1976, pp. 169-172.
53. McElroy, Michael B.; Elkins, James W.; Wofsy, Steven C.; and Yung, Yuk Ling: Sources and Sinks for Atmospheric N₂O. Rev. Geophys. & Space Phys., vol. 14, no. 2, May 1976, pp. 143-150.

54. Liu, S. C.; Cicerone, R. J.; Donahue, T. M.; and Chameides, W. L.: Sources and Sinks of Atmospheric N_2O and the Possible Ozone Reduction Due to Industrial Fixed Nitrogen Fertilizers. *Tellus*, vol. 29, no. 3, June 1977, pp. 251-263.
55. Sze, Nien Dak; and Rice, Harbert: Nitrogen Cycle Factors Contributing to N_2O Production From Fertilizers. *Geophys. Res. Lett.*, vol. 3, no. 6, June 1976, pp. 343-346.

TABLE I.- SOURCES AND SINKS OF TROPOSPHERIC NO_x

Sources, Mt(N)/yr:	
Anthropogenic	20
Stratospheric downward flux	0.5
NH ₃ + OH	<2
Lightning	≈80
Forest fires	<10
Sinks, lifetime against sink:	
NO ₂ + OH	^a 2 to 6 days
Rain out	10 days
Dry deposition	30 days

^aThe lifetime was calculated to be 2 days in the Southern Hemisphere and 6 days in the Northern Hemisphere. See the discussion in text.

TABLE II.- SUMMARY OF NO AND NO₂ MEASUREMENTS

[Adopted from Drummond (ref. 19) and Noxon (ref. 20)]

Gas	Amount, ppb	Location	Reference
NO ₂	0.02 to 0.3	Ireland	Reference 21
NO ₂	1 to 2	Florida; Hawaii	Junge (ref. 22)
NO ₂	0.9 to 3.6	Panama	Lodge and Pate (ref. 23)
NO ₂	4.6	North Carolina	Kronreich et al. (ref. 24)
NO ₂	4.1	Pikes Peak, Colorado	Hamilton et al. (ref. 25)
NO	2.7	Pikes Peak, Colorado	Hamilton et al. (ref. 25)
NO ₂	0.5 to 4		Hidy (ref. 26)
NO	0.2 to 2		Hidy (ref. 26)
NO ₂	1 to 3	Central United States	Breeding et al. (ref. 27)
NO ₂	4 to 21	Southern England	Nash (ref. 28)
NO ₂	0.2 to 0.7	Tropics	Lodge et al. (ref. 10)
NO	0.1 to 0.7	Tropics	Lodge et al. (ref. 10)
NO ₂	0.1 to 0.3	Boulder, Colorado	Moore (ref. 29)
NO ₂	<0.1	Fritz Peak, Colorado	Noxon (ref. 30)
NO	≤0.05	8 to 12 km over Pacific Ocean	Briehl et al. (ref. 31)
NO	0.01 to 0.05	Laramie, Wyoming	Drummond (ref. 19)
NO _x	0.1 to 0.4	Laramie, Wyoming	Drummond (ref. 19)
NO ₂	≤0.1	North America; Peru	Noxon (ref. 20)

TABLE III.- SOURCES AND SINKS OF TROPOSPHERIC CO

[Mostly adopted from Seiler (ref. 6) and Jaffe (ref. 7)]

	Northern Hemisphere	Southern Hemisphere	Global
Sources, Mt(N)/yr:			
Anthropogenic	450	50	500
Ocean	40	60	100
Forest fires	40	20	60
Oxidation of hydrocarbon	40	20	60
Oxidation of CH ₄	<u>80</u>	<u>240</u>	<u>320</u>
Total	650	390	1040
Sinks, Mt(N)/yr:			
Upward flux into stratosphere	90	20	110
Uptake by soil	300	150	450
Oxidation by OH	<u>600</u>	<u>600</u>	<u>1200</u>
Total	990	770	1760

THE EFFECTS OF INCREASED CO AND NO_x UPON TROPOSPHERIC OH, CH₄,
AND RELATED SPECIES

W. L. Chameides
University of Florida
Gainesville, Florida

SUMMARY

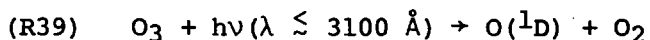
The tropospheric OH density is shown to be sensitive to the atmospheric abundance of CO and NO_x (NO + NO₂). The anthropogenic production of CO and NO_x is significant when compared with natural sources of these compounds, and thus the abundances of CO and NO_x may increase in the coming decades if present trends continue. Model calculations are presented to indicate the possible magnitude of future perturbations in OH and related compounds such as CH₄, due to increased CO and NO_x emissions.

INTRODUCTION

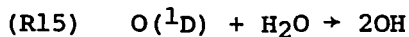
With the exception of CO₂ and halocarbons, chemical pollution of the troposphere has been largely limited to local regions of intense anthropogenic activity such as urban centers. However, recent studies of the CO and NO_x (NO + NO₂) budgets indicate that anthropogenic emissions of these compounds are presently comparable with natural sources (cf. Seiler (ref. 1), Newell (ref. 2), Chameides et al. (ref. 3), and Galbally (ref. 4)) and may even surpass natural sources in the coming decades if present trends continue. Present understanding of the tropospheric photochemistry implies, however, that a perturbation in the levels of CO or NO_x will result in changes in the OH abundance of the troposphere (Sze (ref. 5), Chameides et al. (ref. 6), and Liu (ref. 7)) and thereby perturb the densities of CH₄, CH₃Cl, CH₃CCl₃, and other related compounds. These perturbations could have a serious impact upon the atmospheric environment, affecting stratospheric O₃ and the atmosphere's thermal equilibrium. In this work, a discussion of the effects of increased emissions of CO and NO_x upon the global photochemistry is presented.

TROPOSPHERIC OH

The presence of the free radical OH in the background troposphere was first proposed by Weinstock (ref. 8) to explain the residence time of atmospheric CO. Levy (ref. 9) noted that the production of metastable oxygen atoms via

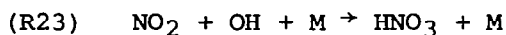


followed by

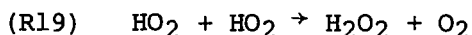


could lead to significant OH abundances in the background, or unpolluted, troposphere with O₃ densities of about 20 to 40 ppb and relative humidities of about 50 percent. Present-day photochemical models yield tropospheric OH number densities of 10⁵ to 10⁶ cm⁻³, although the OH abundance is uncertain because of uncertainties in key reaction rates (e.g., the quantum yield of O(¹D) in the photolysis of O₃). Nevertheless, the predicted OH abundance is in qualitative agreement with recent measurements (Davis et al. (ref. 10), Wang et al. (ref. 11), and Perner et al. (ref. 12)) and with average OH densities inferred from halocarbon abundances (Singh (ref. 13)). For instance, the calculated OH profiles shown in figure 1 imply a CH₃CCl₃ lifetime due to reaction with OH of about 7 years as compared with Singh's (ref. 13) estimate of (7.2 ± 1.2) years. More measurements are needed however before a detailed comparison between observation and theory is possible.

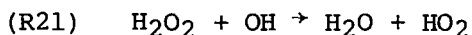
Since Levy's pioneering work, much research has been carried out to determine the role of free radicals in tropospheric photochemistry (cf. McConnell et al. (ref. 14), Wofsy et al. (ref. 15), Crutzen (refs. 16 and 17), Chameides and Walker (refs. 18 and 19), Chameides (ref. 20), Wofsy (ref. 21), Chameides and Stedman (ref. 22), Fishman and Crutzen (ref. 23), and Stewart et al. (ref. 24)). It is now believed that the production of OH leads to a long series of reactions involving free radicals that help determine the tropospheric abundances of many trace gases of interest; these free radicals are removed from the system by chain-terminating reactions such as



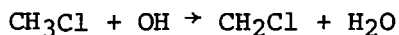
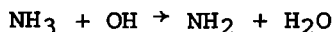
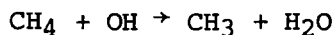
followed by heterogeneous removal and

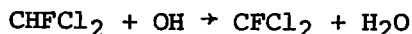


followed by



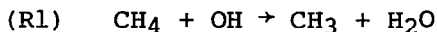
Of particular importance is the role of OH as a scavenger of trace gases produced in the troposphere by natural and anthropogenic processes. Reactions such as





are believed to play a major role in controlling the tropospheric abundances of the trace species included in these reactions. Thus, a perturbation in OH could lead to variations in the densities of gases such as CH₄, CO, NH₃, SO₂, CH₃Cl, etc.

For example, CH₄ is produced at the Earth's surface primarily by biological fermentation in anaerobic environments such as swamps, tropical rain forests, and paddy fields (Koyama (ref. 25)). Tropospheric CH₄ is characterized by a well-mixed profile with a vertically constant mixing ratio of 1.4 ppm (Ehhalt et al. (ref. 26)). Studies of the flux of CH₄ from various soil types imply a global production rate of CH₄ molecules of the order of 10¹¹ cm⁻²-s⁻¹ (Koyama (ref. 25) and Baker-Blocker et al. (ref. 27)) and thus a CH₄ atmospheric residence time of about 10 years. The major sink of CH₄ is photochemical destruction via oxidation by OH (Levy (ref. 9)),



Thus, the tropospheric CH₄ abundance is determined by a balance between biological production, transport upward, and destruction by (R1). The CH₄ continuity equation may be written as

$$\frac{dn(\text{CH}_4)}{dt} = - \frac{dF(\text{CH}_4)}{dz} - n(\text{OH}) n(\text{CH}_4) K_1 \quad (1)$$

where F is vertical flux, n is number density, K_i is the rate constant for the ith reaction (K₁ corresponds to (R1)), z is vertical distance, t is time and no net horizontal transport is assumed. Since CH₄ has a constant mixing ratio X(CH₄), equation (1) can be integrated over the troposphere to yield

$$N_m \frac{dX(\text{CH}_4)}{dt} = \left[F(\text{CH}_4)_{z=0} - F(\text{CH}_4)_{z=z_{tp}} \right] - X(\text{CH}_4) D \quad (2)$$

where

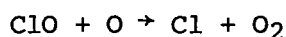
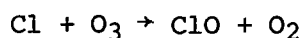
$$N_m = \int_0^{z_{tp}} n_M dz$$

$$D = \int_0^{z_{tp}} n(\text{OH}) n_M dz$$

and where n_M is the ambient number density and z_{tp} is the height of the tropopause. The equilibrium CH₄ mixing ratio X(CH₄)⁰ is given by

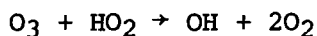
$$X(\text{CH}_4)^0 = \frac{F(\text{CH}_4)_{z=0} - F(\text{CH}_4)_{z=z_{\text{tp}}}}{D} \approx \frac{F(\text{CH}_4)_{z=0}}{D} \quad (3)$$

since $F(\text{CH}_4)_{z=z_{\text{tp}}} \ll F(\text{CH}_4)_{z=0}$. Thus, the CH_4 abundance is inversely proportional to the OH density and a perturbation in OH will result in a variation in CH_4 . Similar expressions can be derived for species such as CH_3Cl , CH_3CCl_3 , CHF_2Cl , and CHFCl_2 . However, variations in the densities of these gases could lead to deleterious effects. Increases in the tropospheric abundances of chlorocarbons could result in a greater input of free chlorine to the stratosphere and thus a decrease in stratospheric O_3 due to the catalytic cycle of

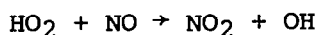


Similarly, CH_4 plays a key role in the stratospheric photochemistry, and a perturbation in its tropospheric abundance could lead to variations in stratospheric O_3 . Furthermore, Wang et al. (ref. 28) have shown that CH_4 , NH_3 , and HNO_3 play a significant role in the atmosphere's radiative thermal equilibrium, and perturbations in these densities could possibly lead to climatic variations.

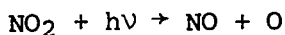
It is also believed that the conversion of OH to HO_2 can play a role in controlling the abundance of tropospheric ozone with



destroying O_3 and



followed by



and



producing O_3 . Recent calculations indicate that these photochemical processes may produce and destroy tropospheric O_3 at rates comparable with the injection of stratospheric O_3 into the troposphere and the loss of ozone due to reaction with the Earth's surface (cf. Chameides and Stedman (ref. 22), Fishman and Crutzen (ref. 23), and Stewart et al. (ref. 24)).

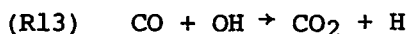
In view of the sensitivity of the tropospheric photochemical system to OH, a potential perturbation in tropospheric OH on a global scale is of concern. Since the photochemical lifetime of OH is short (~ 1 second), OH may be considered to be in photochemical equilibrium, and a global perturbation in tropospheric OH must involve a change in the local volume OH production and/or destruction rates throughout the troposphere. Table I based on model calcula-

tions discussed in the next section lists the rates of production and destruction of OH near the ground for equinoctial conditions in mid-latitudes. Note that CO and NO_x play important roles in the OH photochemistry and lead to significant loss and production of OH, respectively. The calculated rate of production of OH due to NO_x has been significantly increased over past estimates as a result of recent measurements which indicated an increase in the (NO + HO₂) rate constant by a factor of 20 (Howard and Evenson (ref. 29)). Similarly, recent measurements of the (CO + OH) reaction, which led to a doubling of that rate constant in the lower troposphere (Sie et al. (ref. 30), Cox et al. (ref. 31), and Chan et al. (ref. 32)), increased the calculated rate of OH destruction by CO. As a result, the sensitivity of calculated OH densities to NO_x, and to a lesser extent CO, has been significantly enhanced. While an increase in CO would lead to a decrease in OH, a NO_x increase would result in an increase in OH. In addition to the dependence on these two rate coefficients, the extent to which the CO effect on OH dominates over the NO_x effect, or vice versa, depends on the relative magnitudes of the increases in CO and NO_x over present-day levels. In this work, the variation in tropospheric OH is examined for a variety of assumed future CO and NO_x emission rate patterns. The magnitude of the OH perturbation is calculated with a one-dimensional model, as described in the next section. In view of the many uncertainties in the tropospheric photochemical system, the predictions presented here should be taken as rough estimates of possible future trends.

It should be noted that the column abundance of stratospheric ozone also influences the OH level in the troposphere (Chameides and Walker (ref. 18) and Chameides et al. (ref. 6)). In table I, note that the reaction of O(¹D) with H₂O constitutes the major source of OH. Since the O(¹D) density can be altered either by changing the flux of near-ultraviolet radiation or by changing the local O₃ density, a perturbation to stratospheric O₃ can affect tropospheric OH in two ways: by changing the flux of near-ultraviolet radiation penetrating the tropopause and by changing the O₃ density in the lower stratosphere and thus the injection rate of stratospheric O₃ into the troposphere. The coupling between tropospheric OH and stratospheric O₃ has been discussed by Chameides et al. (ref. 6) and is not addressed in this work.

MODEL CALCULATIONS

Calculations are based on the one-dimensional steady-state model (specifically the "LoNo_x Model 3") of Chameides (ref. 33), which couples vertical transport and photochemistry. Vertical transport is parameterized with a constant eddy diffusion coefficient K of $1 \times 10^5 \text{ cm}^2\text{-s}^{-1}$. The reactions and rate coefficients included in the model are listed in table II. Most of the rate coefficients were taken from Chameides and Stedman (ref. 22) or Hudson (ref. 34). Note that the fast rate coefficients for



recently measured by Sie et al. (ref. 30), Cox et al. (ref. 31), and Chan et al. (ref. 32) and the fast rate coefficient for



measured by Howard and Evenson (ref. 29) have been adopted. The effect of varying these rate constants has been discussed in detail by Chameides (ref. 33). The adoption of a heterogeneous loss term for CH₃OOH (i.e., (R4b)) leads to an efficiency of only 70 percent for the conversion of CH₄ to CO via the CH₄ oxidation chain.

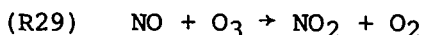
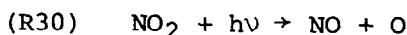
The treatment of the nitrogen oxide and ozone system follows that of Chameides (ref. 33). The NO_x (NO + NO₂) density profile is obtained by solving the steady-state NO_x continuity equation

$$\frac{dn(\text{NO}_x)}{dt} = 0 = n(\text{HNO}_3) [n(\text{OH}) K_{25b} + J_{25a}] - 2 n(\text{N}_2\text{O}_5) n(\text{H}_2\text{O}) K_{35} - n(\text{NO}_2) n(\text{OH}) K_{23} + \frac{\partial}{\partial z} (K n_M) \frac{\partial}{\partial z} \left[\frac{n(\text{NO}_x)}{n_M} \right] \quad (4)$$

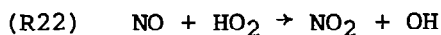
where J_i is the photodissociation rate for the i th reaction (J_{25a} corresponds to (R25a)) and photochemical equilibrium for NO₃, N₂O₅, and HNO₂ is assumed. Boundary conditions for equation (4) include a ground-level emission term $F(\text{NO}_x)$, a deposition velocity of 0.1 cm-s⁻¹, and zero flux at 10 km. The HNO₃ profile shape is prescribed by the water vapor control equation (Chameides (ref. 20) and Stedman et al. (ref. 35)):

$$n(\text{HNO}_3) = X n(\text{H}_2\text{O}) \quad (5)$$

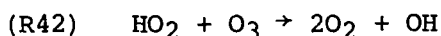
where the constant X is determined by balancing source and loss terms for HNO₃. Note that the HNO₃ source terms can include photochemical sources (i.e., via (R23)) or direct injections $F(N)$, as discussed subsequently. The calculation of the O₃ profile is complicated by the existence of the rapid cycle of reactions



which does not produce or destroy O₃ but tends numerically to obscure slower reactions, such as



followed by (R30) and



which do result in the net production or loss of O₃. To eliminate the rapid reaction cycle from the ozone continuity equation, the NO continuity equation is subtracted from the O₃ equation to yield in the steady state

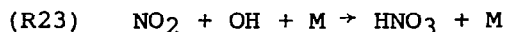
$$\begin{aligned}
\frac{d}{dt}[n(\text{O}_3) - n(\text{NO})] = 0 = & n(\text{NO}) [n(\text{HO}_2) K_{22} + n(\text{CH}_3\text{O}_2) K_6 + n(\text{NO}_3) K_{32}] \\
& - n(\text{O}_3) [n(\text{NO}_2) K_{28} + n(\text{HO}_2) K_{42} + n(\text{OH}) K_{41}] \\
& - n(\text{O}({}^1\text{D})) [n(\text{H}_2\text{O}) K_{15} + n(\text{H}_2) K_{16}] \\
& - n(\text{NO}_3) (J_{33b} - J_{33a}) \\
& + \frac{\partial}{\partial z} (K n_M) \frac{\partial}{\partial z} \left[\frac{n(\text{O}_3) - n(\text{NO})}{n_M} \right]
\end{aligned} \tag{6}$$

where photochemical equilibrium for O, O(¹D), and HNO₂ is assumed. Boundary conditions for equation (6) include a fixed density condition of $1 \times 10^{12} \text{ cm}^{-3}$ at 11 km (Krueger and Minzner (ref. 36)) and a ground-level deposition velocity of 0.08 cm-s^{-1} . Equations (4), (5), and (6) along with the photostationary state equation (Leighton (ref. 37)),

$$\frac{n(\text{NO})}{n(\text{NO}_2)} = \frac{J_{30}}{n(\text{O}_3) K_{29}} \tag{7}$$

and the appropriate photochemical equilibrium equations for the short-lived species yield a closed system which can be solved.

The average source strength of atmospheric odd nitrogen compounds is believed to be about $(2 \text{ to } 3) \times 10^{10} \text{ cm}^{-2}\text{-s}^{-1}$ (cf. Burns and Hardy (ref. 38) and Chameides et al. (ref. 3)) in the form of NO_x. However, since the characteristic time to convert NO_x to HNO₃ via



is only about 1 day, the NO_x injected into an air mass by an odd nitrogen source is rapidly converted to HNO₃, the most abundant form of tropospheric odd nitrogen. Thus to simulate clean, remote locations removed from direct NO_x sources, it is assumed that odd nitrogen production at a rate of $2.4 \times 10^{10} \text{ cm}^{-2}\text{-s}^{-1}$ is effectively in the form of HNO₃ (cf. Chameides (ref. 33)). The resulting NO_x and O₃ profiles are illustrated in figures 2 and 3. Table III lists some of the key parameters obtained in the model calculation. The model also yields $X = 4 \times 10^{-7}$. Experimental data from Danielsen and Mohnen (ref. 39), Nastrom and Belmont (ref. 40), Fabian and Pruchniewicz (ref. 41), Seiler (ref. 1), Chameides and Cicerone (ref. 42), and Singh (ref. 13) are presented in table III for comparison with the calculations.

The NO_x profile with less than 0.1 ppb in the lower troposphere is consistent with Noxon's (ref. 43) measurements. However, even at these low NO_x densities, the photochemical production of O₃ is significant when compared with the injection of ozone from the stratosphere (see table III). The large photochemical production of O₃ results from the fast rate coefficient for (R22) measured by Howard and Evenson (ref. 29). The O₃ profile is in qualitative

agreement with averaged O₃ observations of Krueger and Minzner (ref. 36) and Chatfield and Harrison (ref. 44); a better fit to the data could be obtained by lowering the eddy diffusion coefficient in the upper troposphere and increasing it in the lower troposphere. The results listed in table III indicate that both photochemistry and transport are important in the tropospheric O₃ budget. More detailed studies of trace gas densities, relevant reaction rates, and vertical transport in the troposphere are needed to further define the relative roles of transport and photochemistry in controlling the abundance of tropospheric O₃.

Important input parameters to the calculation of future OH perturbations are the anthropogenic source strengths of CO and NO_x. In the next sections, the budgets of CO and NO_x are discussed.

CARBON MONOXIDE BUDGET

Carbon monoxide has an average tropospheric mixing ratio of about 0.12 ppm; however, about 3 times as much CO resides in the Northern Hemisphere where anthropogenic activities are most intense than in the Southern Hemisphere (Seiler (ref. 1)). This hemispheric asymmetry, with the maximum CO abundance occurring in the lower troposphere of northern mid-latitudes, indicates that anthropogenic processes are an important source of CO. A CO budget which includes source rates taken from Seiler (ref. 1), Chameides and Cicerone (ref. 42), and Seiler and Giehl (ref. 45) is presented in table IV. A study of this CO budget implies that anthropogenic sources are responsible for at least 30 percent of the atmosphere's CO. The large sink of CO, brought about by the faster rate constant for (R13) coupled with the smaller calculated source of CO from CH₄ due to lower OH densities and rainout of CH₃OOH, implies the existence of another significant source of CO. This source could be a natural process or related to anthropogenic activities which were not taken into account by Seiler (ref. 1). In this work, the unknown CO source is assumed to be from natural processes. The anthropogenic source of 10¹¹ cm⁻²-s⁻¹ in table IV is due primarily to emissions from the internal combustion engine. While the global anthropogenic CO source strength probably increased annually by about 4.5 percent before 1968 (U.S. Department of Health Education and Welfare (ref. 46) and Broecker et al. (ref. 47)), the introduction of pollution control devices on automobiles produced in the United States after 1968 should have caused a slowing in the rate of anthropogenic CO emissions in the United States. Nevertheless, globally the CO emission rate is probably still on the rise, although at a slower rate of increase (Jaffe (ref. 48)). In order to bracket the future effects of CO emissions, calculations are presented in the section "Future Perturbations" for anthropogenic sources increasing at annual rates ranging from 0 to 4.5 percent; the actual rate of increase probably lies somewhere between these two limits. In other words if it is assumed that at time $t = 1975$ (in years), the anthropogenic CO source strength was 10¹¹ cm⁻²-s⁻¹, the total non-CH₄, CO source $F(\text{CO})$ may be represented by (in units of cm⁻²-s⁻¹)

$$F(\text{CO}) = 1.6 \times 10^{11} + (1.0 \times 10^{11})(1.0 + a)^{t-1975} \quad (8)$$

where $0 \leq a \leq 0.045$.

NITROGEN OXIDE BUDGET

NO_x ($\text{NO} + \text{NO}_2$) concentrations in the troposphere are highly variable (Ackerman (ref. 49)) but are believed to be present at a background concentration of 0.1 ppb or less (see Noxon (ref. 43) and fig. 2). However, HNO_3 produced in the oxidation of NO_2 via (R23) is thought to have a concentration approaching 1 ppb in the lower troposphere (Chameides (ref. 20)), making it the most abundant form of tropospheric odd nitrogen. Unfortunately HNO_3 has as yet not been measured in the ambient troposphere and thus understanding of tropospheric nitrogen oxides is uncertain. The major sink of atmospheric odd nitrogen is believed to be rainout of HNO_3 (Chameides (ref. 20)); assuming a 10-day residence time for HNO_3 , calculations yield a rainout rate for HNO_3 of $2.4 \times 10^{10} \text{ cm}^{-2}\text{-s}^{-1}$ in rough agreement with measurements of NO_3^- in rainwater (Eriksson (ref. 50), Robinson and Robbins (ref. 51), and Burns and Hardy (ref. 38)).

To balance the loss of atmospheric nitrogen oxides, there must be sources of equal strength. Estimates of these sources from Robinson and Robbins (ref. 51) and Chameides et al. (ref. 3) are listed in table V. Note that the anthropogenic processes comprise a significant fraction of the total source strength. The anthropogenic source is largely due to combustion in mobile and stationary sources. While anthropogenic NO_x emissions increased globally at a rate of about 5 percent per year before the introduction of pollution control in the United States (U.S. Environmental Protection Agency (ref. 52)), the future global rate of increase is uncertain. As in the case of CO, the limits of the possible impact of future NO_x emissions are determined by varying the annual rate of increase from 0 to 5 percent. Thus, the total odd nitrogen source strength $F(N)$ assumed to have been converted to HNO_3 , is represented by (in units of $\text{cm}^{-2}\text{-s}^{-1}$)

$$F(N) = 1.7 \times 10^{10} + (7 \times 10^9)(1 + b)t^{-1975} \quad (9)$$

where $0 \leq b \leq 0.05$. Note that the assumption that all anthropogenic nitrogen oxide is mixed into the ambient atmosphere may lead to an overestimate of the NO_x impact. Unlike CO with a photochemical lifetime of about 30 days, NO_x is rapidly converted to HNO_3 which may then be removed in precipitation. Thus, nitrogen oxides produced in urban areas may be significantly depleted before being mixed into the ambient atmosphere. These second-order effects need to be investigated further.

FUTURE PERTURBATIONS

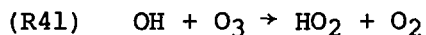
To illustrate the possible magnitude of future perturbations, the CO and NO_x source strengths were varied as functions of time t according to equations (8) and (9); the values of a and b are listed in table VI. For each case, equation (2) was integrated to yield $X(\text{CH}_4)$ as a function of $F(\text{CO})$ and $F(N)$ and appropriate densities of the other species. Shorter lived species, such as O_3 , CO, and NO_x , were assumed to be in equilibrium with transport and photochemical processes, while very short-lived species, such as OH, were taken to be in photochemical equilibrium. Initially, at $t = 1975$, present-day con-

ditions were adopted. The present-day CH₄ abundance of 1.4 ppb was assumed to be in equilibrium with a ground-level flux of $5.4 \times 10^{10} \text{ cm}^{-2}\text{-s}^{-1}$ prescribed by equation (3). However, as Sze (ref. 5) pointed out, the high levels of CO in the Northern Hemisphere may indicate that CH₄ is already perturbed and on the rise globally. Alternately, drainage of swamplands may have decreased the global CH₄ production rate and thus CH₄ may be presently decreasing globally.

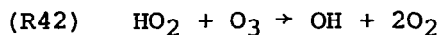
The calculated ground-level OH densities and CH₄ mixing ratios are shown in figures 4 and 5, respectively. Also illustrated in figure 5 is a calculation of $X(\text{CH}_4)^0$ indicating that the actual CH₄ mixing ratio lags behind the equilibrium value. At any given time, should the emission rates suddenly level off and remain constant, $X(\text{CH}_4)$ would continue to change until it reached its equilibrium value. On the other hand, since the atmosphere is able to rapidly scavenge CO and NO_x, if at some point, CO and NO_x emissions returned to their 1975 values, $X(\text{CH}_4)$ would quickly begin to return to its initial value (with an e-folding time of about 10 years).

The calculations indicate that significant increases or decreases in OH, CH₄, and related compounds may occur in the coming decades depending on the rates of increase of CO and NO_x. Perturbations of as much as 50 to 60 percent in OH and CH₄ may occur. If CO and NO_x emissions increase at equivalent rates, calculations indicate that the CO effect on OH will dominate over the NO_x effect and thus CH₄ will increase, although at a slower rate than for constant NO_x emissions. However, it is also possible that CO and NO_x will increase at rates which will lead to a cancellation of effects and a negligible perturbation in OH and CH₄.

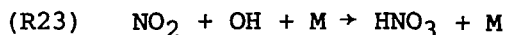
It is interesting to note that other long-lived species, such as CH₃Cl, CH₃CCl₃, CHFCl₂, CHF₂Cl, NH₃, and H₂, which are attacked by OH in the troposphere, should undergo variations similar to those for CH₄. These variations are particularly significant in the case of chlorocarbons since they may directly affect stratospheric O₃. Since stratospheric ozone affects the abundance of tropospheric OH and tropospheric OH affects the level of stratospheric O₃, by regulating the abundance of CH₄ and several halocarbons, the possibility for tropospheric-stratospheric feedback effects exists. In the case of chlorocarbons, which act to destroy stratospheric O₃, the feedback is negative, tending to reduce an initial perturbation in either tropospheric OH or stratospheric O₃. CH₄, as a source of stratospheric odd hydrogen, may act to increase or decrease stratospheric O₃ (Crutzen (ref. 53), McElroy et al. (ref. 54), Rao-Vupputuri (ref. 55), and Liu et al. (ref. 56)). While reactions



and



act as an O₃ sink,



tends to enhance O₃ by removing an odd nitrogen molecule from the catalytic chain which destroys O₃. Similarly, in a stratosphere with chlorine, CH₄ can enhance O₃ by removing Cl from its catalytic O₃-destroying chain:



Whether CH₄ acts to decrease or increase stratospheric O₃ and thus whether the system described will stabilize or destabilize stratospheric O₃ depend upon the relative importance of these reactions. Further study, both in the laboratory and with numerical models, is needed to help clarify this point.

CONCLUDING REMARKS

Calculations indicate that significant perturbations in tropospheric OH, CH₄, and related compounds may occur in the coming decades because of increased anthropogenic emissions of CO and NO_x. The magnitude and direction of the perturbation depend upon future emission rates of CO and NO_x (and also the efficiency with which urban NO_x is transported to the ambient atmosphere). The effects of a variation in tropospheric OH and its resultant change in CH₄, halocarbons, and other compounds include perturbations to stratospheric ozone and to the atmosphere's thermal equilibrium. The possibility of stabilizing or destabilizing feedback effects needs to be investigated further.

To further understanding of the CO-NO_x-OH interaction, long-term monitoring programs are needed to determine the global distribution of CO and NO_x, as well as OH, CH₄, and halocarbons. The 30-day photochemical lifetime of CO indicates that its global distribution may be most efficiently monitored from a satellite platform. In the case of nitrogen oxides, the development of techniques for measuring HNO₃ as well as NO and NO₂ is essential. Continued laboratory experiments are also needed to characterize thoroughly the tropospheric photochemical system. Finally, the further development and implementation of pollution control for combustion systems, as well as the use of alternate power sources, may alleviate future perturbations to the tropospheric photochemistry.

REFERENCES

1. Seiler, Wolfgang: The Cycle of Atmospheric CO. *Tellus*, vol. 26, nos. 1-2, 1974, pp. 116-135.
2. Newell, Reginald E.: One-Dimensional Models: A Critical Comment, and Their Application to Carbon Monoxide. *J. Geophys. Res.*, vol. 82, no. 9, Mar. 20, 1977, pp. 1449-1450.
3. Chameides, W. L.; Stedman, D. H.; Dickerson, R. R.; Rusch, D. W.; and Cicerone, R. J.: NO_x Production in Lightning. *J. Atmos. Sci.*, vol. 34, no. 1, Jan. 1977, pp. 143-149.
4. Galbally, I. E.: Emission of Oxides of Nitrogen (NO_x) and Ammonia From the Earth's Surface. *Tellus*, vol. 27, no. 1, 1975, pp. 67-70.
5. Sze, N. D.: Anthropogenic CO Emissions: Implications for the Atmospheric CO-OH-CH₄ Cycle. *Science*, vol. 195, no. 4279, Feb. 18, 1977, pp. 673-675.
6. Chameides, W. L.; Liu, S. C.; and Cicerone, R. J.: Possible Variations in Atmospheric Methane. *J. Geophys. Res.*, vol. 82, no. 12, Apr. 20, 1977, pp. 1795-1798.
7. Liu, Shaw Chen: Possible Effects on Tropospheric O₃ and OH Due to NO Emissions. *Geophys. Res. Lett.*, vol. 4, no. 8, Aug. 1977, pp. 325-328.
8. Weinstock, Bernard: Carbon Monoxide: Residence Time in the Atmosphere. *Science*, vol. 166, no. 3902, Oct. 1969, pp. 224-225.
9. Levy, H., II: Normal Atmosphere: Large Radical and Formaldehyde Concentrations Predicted. *Science*, vol. 173, no. 3992, July 9, 1971, pp. 141-143.
10. Davis, D. D.; Heaps, W.; and McGee, T.: Direct Measurements of Natural Tropospheric Levels of OH Via an Aircraft Borne Tunable Dye Laser. *Geophys. Res. Lett.*, vol. 3, no. 6, June 1976, pp. 331-333.
11. Wang, Charles C.; Davis, L. I., Jr.; Wu, C. H.; Japar, S.; Niki, H.; and Weinstock, B.: Hydroxyl Radical Concentrations Measured in Ambient Air. *Science*, vol. 189, no. 4205, Sept. 5, 1975, pp. 797-800.
12. Perner, D.; Ehhalt, D. H.; Pätz, H. W.; Platt, U.; Röth, E. P.; and Volz, A.: OH-Radicals in the Lower Troposphere. *Geophys. Res. Lett.*, vol. 3, no. 8, Aug. 1976, pp. 466-468.
13. Singh, Hanwant B.: Atmospheric Halocarbons: Evidence in Favor of Reduced Average Hydroxyl Radical Concentration in the Troposphere. *Geophys. Res. Lett.*, vol. 4, no. 3, Mar. 1977, pp. 101-104.
14. McConnell, J. C.; McElroy, M. B.; and Wofsy, S. C.: Natural Sources of Atmospheric CO. *Nature*, vol. 233, no. 5316, Sept. 17, 1971, pp. 187-188.

15. Wofsy, Steven C.; McConnell, John C.; and McElroy, Michael B.: Atmospheric CH₄, CO, and CO₂. *J. Geophys. Res.*, vol. 77, no. 24, Aug. 20, 1972, pp. 4477-4493.
16. Crutzen, Paul J.: Gas-Phase Nitrogen and Methane Chemistry in the Atmosphere. *Physics and Chemistry of Upper Atmospheres*, B. M. McCormac, ed., D. Reidel Publishing Co., c.1973, pp. 110-124.
17. Crutzen, Paul J.: Photochemical Reactions Initiated by and Influencing Ozone in Unpolluted Tropospheric Air. *Tellus*, vol. 26, nos. 1-2, 1974, pp. 47-57.
18. Chameides, William; and Walker, James C. G.: A Photochemical Theory of Tropospheric Ozone. *J. Geophys. Res.*, vol. 78, no. 36, Dec. 20, 1973, pp. 8751-8760.
19. Chameides, William L.; and Walker, James C. G.: A Time-Dependent Photochemical Model for Ozone Near the Ground. *J. Geophys. Res.*, vol. 81, no. 3, Jan. 20, 1976, pp. 413-420.
20. Chameides, William: Tropospheric Odd Nitrogen and the Atmospheric Water Vapor Cycle. *J. Geophys. Res.*, vol. 80, no. 36, Dec. 20, 1975, pp. 4989-4996.
21. Wofsy, Steven C.: Interactions of CH₄ and CO in the Earth's Atmosphere. *Annual Review of Earth and Planetary Sciences*, Fred A. Donath, Francis G. Stehli, and George W. Wetherill, eds., Volume 4, Annual Reviews Inc., 1976, pp. 441-469.
22. Chameides, W. L.; and Stedman, D. H.: Tropospheric Ozone: Coupling Transport and Photochemistry. *J. Geophys. Res.*, vol. 82, no. 12, Apr. 20, 1977, pp. 1787-1794.
23. Fishman, Jack; and Crutzen, Paul J.: A Numerical Study of Tropospheric Photochemistry Using a One-Dimensional Model. *J. Geophys. Res.*, vol. 82, no. 37, Dec. 20, 1977, pp. 5897-5906.
24. Stewart, Richard W.; Hameed, Sultan; and Pinto, Joseph P.: Photochemistry of Tropospheric Ozone. *J. Geophys. Res.*, vol. 82, no. 21, July 20, 1977, pp. 3134-3140.
25. Koyama, Tadashi: Gaseous Metabolism in Lake Sediments and Paddy Soils and the Production of Atmospheric Methane and Hydrogen. *J. Geophys. Res.*, vol. 68, no. 13, July 1, 1963, pp. 3971-3973.
26. Ehhalt, D. H.; Heidt, L. E.; Lueb, R. H.; and Roper N.: Vertical Profiles of CH₄, H₂, CO, N₂O, and CO₂ in the Stratosphere. *Proceedings of the Third Conference on the Climatic Impact Assessment Program*, Anthony J. Broderick and Thomas M. Hard, eds., DOT-TSC-OST-74-15, U.S. Dep. Transp., Nov. 1974, pp. 153-160. (Available from DDC as AD A003 846.)

27. Baker-Blocker, Anita; Donahue, Thomas M.; and Mancy, Khalil H.: Methane Flux From Wetlands Areas. *Tellus*, vol. 29, no. 3, June 1977, pp. 245-250.
28. Wang, W. C.; Yung, Y. L.; Lacis, A. A.; Mo, T.; and Hansen, J. E.: Greenhouse Effects Due to Man-Made Perturbations of Trace Gases. *Science*, vol. 194, no. 4266, Nov. 12, 1976, pp. 685-690.
29. Howard, Carleton J.; and Evenson, K. M.: Kinetics of the Reaction of HO₂ With NO. *Geophys. Res. Lett.*, vol. 4, no. 10, Oct. 1977, pp. 437-440.
30. Sie, B. K. T.; Simonaitis, R.; and Heicklen, J.: The Reaction of OH With CO. *Int. J. Chem. Kinet.*, vol. 8, no. 1, 1976, pp. 85-98.
31. Cox, Richard A.; Derwent, Richard G.; and Holt, Pauline M.: Relative Rate Constants for the Reactions of OH Radicals With H₂, CH₄, CO, NO and HONO at Atmospheric Pressure and 296 K. *J. Chem. Soc., Faraday Trans. I*, vol. 72, pt. 9, 1976, pp. 2031-2043.
32. Chan, Walter H.; Uselman, William M.; Calvert, Jack G.; and Shaw, John H.: The Pressure Dependence of the Rate Constant for the Reaction: HO + CO → H + CO₂. *Chem. Phys. Lett.*, vol. 45, no. 2, Jan. 15, 1977, pp. 240-243.
33. Chameides, W. L.: The Photochemical Role of Tropospheric Nitrogen Oxides. *Geophys. Res. Lett.*, vol. 5, no. 1, Jan. 1978, pp. 17-20.
34. Hudson, Robert D., ed.: Chlorofluoromethanes and the Stratosphere. NASA RP-1010, 1977.
35. Stedman, D. H.; Chameides, W. L.; and Cicerone, R. J.: The Vertical Distribution of Soluble Gases in the Troposphere. *Geophys. Res. Lett.*, vol. 2, no. 8, Aug. 1975, pp. 333-336.
36. Krueger, Arlin J.; and Minzner, Raymond A.: A Mid-Latitude Ozone Model for the 1976 U.S. Standard Atmosphere. *J. Geophys. Res.*, vol. 81, no. 24, Aug. 20, 1976, pp. 4477-4481.
37. Leighton, Philip A.: Photochemistry of Air Pollution. Academic Press, Inc., 1961.
38. Burns, R. C.; and Hardy, R. W.: Nitrogen Fixation in Bacteria & Higher Plants. Volume 21 of *Molecular Biology, Biochemistry, & Biophysics*, Springer Verlag, 1975.
39. Danielsen, Edwin F.; and Mohnen, Volker A.: Project DUSTORM Report: Ozone Measurements and Meteorological Analyses of Tropopause Folding. ASRC-SUNY-PUB-394 (Contract N00014-76-C-0283), State Univ. of New York at Albany, May 1976. (Available from DDC as AD A032 555.)

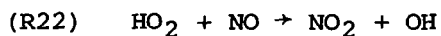
40. Nastrom, G. D.; and Belmont, A. D.: The Variability and Transport of Ozone Near the Tropopause. *EOS Trans.*, American Geophys. Union, vol. 58, no. 6, June 1977, p. 461.
41. Fabian, P.; and Pruchniewicz, P. G.: Final Report on Project "Tropospherisches Ozon." MPAE-W-100-76-21, Max-Planck-Institut Aeron., May 1976.
42. Chameides, W. L.; and Cicerone, R. J.: Effects of Nonmethane Hydrocarbons in the Atmosphere. *J. Geophys. Res.*, vol. 83, no. C2, Feb. 20, 1978, pp. 947-952.
43. Noxon, J. F.: Nitrogen Dioxide in the Stratosphere and Troposphere Measured by Ground-Based Absorption Spectroscopy. *Science*, vol. 189, no. 4202, Aug. 1975, pp. 547-549.
44. Chatfield, Robert; and Harrison, Halstead: Tropospheric Ozone. 2. Variations Along a Meridional Band. *J. Geophys. Res.*, vol. 82, no. 37, Dec. 20, 1977, pp. 5969-5976.
45. Seiler, W.; and Giehl, H.: Influence of Plants on the Atmospheric Carbon Monoxide. *Geophys. Res. Lett.*, vol. 4, no. 8, Aug. 1977, pp. 329-332.
46. Air Quality Criteria for Carbon Monoxide. NAPCA Publ. No. AP-62, U.S. Dep. Health, Educ., & Welfare, Mar. 1970. (Available from NTIS as PB 190 261.)
47. Broecker, Wallace S.; Li, Yuan-Hui; and Peng, Tsung-Hung: Carbon Dioxide - Man's Unseen Artifact. Impingement of Man on the Oceans, Donald W. Hood, ed., Wiley-Interscience, c.1971, pp. 287-324.
48. Jaffe, Louis S.: Carbon Monoxide in the Biosphere: Sources, Distribution, and Concentrations. *J. Geophys. Res.*, vol. 78, no. 24, Aug. 20, 1973, pp. 5293-5305.
49. Ackerman, Marcel: NO, NO₂, and HNO₃ Below 35 km in the Atmosphere. *J. Atmos. Sci.*, vol. 32, no. 9, Sept. 1975, pp. 1649-1657.
50. Eriksson, Erik: Composition of Atmospheric Precipitation. I. Nitrogen Compounds. *Tellus*, vol. 4, 1952, pp. 215-232.
51. Robinson, Elmer; and Robbins, Robert C.: Gaseous Nitrogen Compound Pollutants From Urban and Natural Sources. *J. Air Pollut. Control Assoc.*, vol. 20, no. 5, May 1970, pp. 303-306.
52. Air Quality Criteria for Nitrogen Oxides. NAPCA-Publ. No. AP-84, U.S. Environ. Prot. Agency, Jan. 1971. (Available from NTIS as PB 197 333.)
53. Crutzen, P. J.: Ozone Production Rates in an Oxygen-Hydrogen-Nitrogen Oxide Atmosphere. *J. Geophys. Res.*, vol. 76, no. 30, Oct. 20, 1971, pp. 7311-7327.

54. McElroy, Michael B.; Wofsy, Steven C.; Penner, Joyce E.; and McConnell, John C.: Atmospheric Ozone: Possible Impact of Stratospheric Aviation. *J. Atmos. Sci.*, vol. 31, no. 1, Jan. 1974, pp. 287-303.
55. Rao-Vupputuri, R. K.: A Zonally Averaged Circulation Model of the Stratosphere Incorporating Radiative Heating and Ozone Photochemistry in an Oxygen-Hydrogen-Nitrogen Atmosphere. *Proceedings of the Third Conference on the Climatic Impact Assessment Program*, Anthony J. Broderick and Thomas M. Hard, eds., DOT-TSC-OST-74-15, U.S. Dep. Transp., Nov. 1974, pp. 390-402. (Available from DDC as AD A003 846.)
56. Liu, S. C.; Donahue, T. M.; Cicerone, R. J.; and Chameides, W. L.: Effect of Water Vapor on the Destruction of Ozone in the Stratosphere Perturbed by ClX or NO_x Pollutants. *J. Geophys. Res.*, vol. 81, no. 18, June 20, 1976, pp. 3111-3118.

TABLE I.- CALCULATED RATES OF OH PRODUCTION AND DESTRUCTION NEAR THE GROUND
FOR EQUINOCTIAL CONDITIONS AT MID-LATITUDES

OH source		Rate, $\text{cm}^{-3}\text{-s}^{-1}$	OH sink		Rate, $\text{cm}^{-3}\text{-s}^{-1}$
(R15)	$\text{O}(^1\text{D}) + \text{H}_2\text{O}$	6.2×10^5	(R13)	$\text{CO} + \text{OH}$	9.1×10^5
(R22)	$\text{HO}_2 + \text{NO}^a$	4.5×10^5	(R1)	$\text{CH}_4 + \text{OH}$	2.2×10^5
(R42)	$\text{HO}_2 + \text{O}_3$	2.5×10^5	(R21)	$\text{H}_2\text{O}_2 + \text{OH}$	1.0×10^5
(R20a)	$\text{H}_2\text{O}_2 + h\nu$	1.6×10^5	(R14)	$\text{H}_2 + \text{OH}$	$.8 \times 10^5$
(R5)	$\text{CH}_3\text{OOH} + h\nu$	$.6 \times 10^5$	(R4a)	$\text{CH}_3\text{OOH} + \text{OH}$	$.8 \times 10^5$
			(R8)	$\text{H}_2\text{CO} + \text{OH}$	$.4 \times 10^5$
			(R23)	$\text{NO}_2 + \text{OH}$	$.2 \times 10^5$
			(R17)	$\text{HO}_2 + \text{OH}$	$.1 \times 10^5$
Total		15×10^5	Total		15×10^5

^aActually involves a catalytic cycle of



followed by



TABLE II.- REACTIONS AND RATE COEFFICIENTS

Reaction		Coefficient (a)	References
(R1)	$\text{CH}_4 + \text{OH} \rightarrow \text{CH}_3 + \text{H}_2\text{O}$	$K_1 = 2.35 \times 10^{-12} \exp(-1710/T)$	Hudson (ref. 34)
(R2)	$\text{CH}_3 + \text{M} + \text{O}_2 \rightarrow \text{CH}_3\text{O}_2 + \text{M}$	$K_2 = 3 \times 10^{-32}$	Chameides & Stedman (ref. 22)
(R3a)	$\text{CH}_3\text{O}_2 + \text{HO}_2 \rightarrow \text{CH}_3\text{OOH} + \text{O}_2$	$K_{3a} = K_{19}$	Chameides & Stedman (ref. 22)
(R3b)	$2\text{CH}_3\text{O}_2 \rightarrow 2\text{CH}_3\text{O} + \text{O}_2$	$K_{3b} = 2.6 \times 10^{-13}$	Chameides & Stedman (ref. 22)
(R4a)	$\text{CH}_3\text{OOH} + \text{OH} \rightarrow \text{CH}_3\text{O}_2 + \text{H}_2\text{O}$	$K_{4a} = K_{21}$	Chameides & Stedman (ref. 22)
(R4b)	$\text{CH}_3\text{OOH} \rightarrow \text{Rainout}$	$K_{4b} = 1 \times 10^{-6}$	Assumed
(R5)	$\text{CH}_3\text{OOH} + h\nu \rightarrow \text{CH}_3\text{O} + \text{OH}$	$K_5 = K_{20}$	Chameides & Stedman (ref. 22)
(R6)	$\text{CH}_3\text{O}_2 + \text{NO} \rightarrow \text{CH}_3\text{O} + \text{NO}_2$	$K_6 = 3.3 \times 10^{-12} \exp(-500/T)$	Chameides & Stedman (ref. 22)
(R7)	$\text{CH}_3\text{O} + \text{O}_2 \rightarrow \text{H}_2\text{CO} + \text{HO}_2$	$K_7 = 1.6 \times 10^{-13} \exp(-3300/T)$	Hudson (ref. 34)
(R8)	$\text{H}_2\text{CO} + \text{OH} \rightarrow \text{HCO} + \text{H}_2\text{O}$	$K_8 = 3 \times 10^{-11} \exp(-250/T)$	Hudson (ref. 34)
(R9)	$\text{H}_2\text{CO} + h\nu \rightarrow \text{HCO} + \text{H}$	${}^b\text{J}_9(z=0) = 7.1 \times 10^{-6}$	Chameides & Stedman (ref. 22)
(R10)	$\text{H}_2\text{CO} + h\nu \rightarrow \text{CO} + \text{HO}_2$	${}^b\text{J}_{10}(z=0) = 2.2 \times 10^{-5}$	Chameides & Stedman (ref. 22)
(R11)	$\text{H} + \text{O}_2 + \text{M} \rightarrow \text{HO}_2 + \text{M}$	$K_{11} = 3 \times 10^{-32} (273/T)^{1.3}$	Chameides & Stedman (ref. 22)
(R12)	$\text{HCO} + \text{O}_2 \rightarrow \text{CO} + \text{HO}_2$	$K_{12} = 1 \times 10^{-13}$	Chameides & Stedman (ref. 22)
(R13)	$\text{CO} + \text{OH} \rightarrow \text{CO}_2 + \text{H}$	$K_{13} = 2.1 \times 10^{-13} \exp(-115/T) + 7.3 \times 10^{-33} n_M$	Sie et al. (ref. 30) Cox et al. (ref. 31) Chan et al. (ref. 32)

^aThe rate coefficient units are s^{-1} for one-body reactions, $\text{cm}^3\text{-s}^{-1}$ for two-body reactions, and $\text{cm}^6\text{-s}^{-1}$ for three-body reactions, and T is temperature (K).

^bQuantities shown are the daily averaged photodissociation frequencies for equinoctial conditions at 45°N .

TABLE II.- Continued

Reaction	Coefficient (a)	References
(R14) $\text{H}_2 + \text{OH} \rightarrow \text{H} + \text{H}_2\text{O}$	$K_{14} = 6.8 \times 10^{-12} \exp(-2020/T)$	Chameides & Stedman (ref. 22)
(R15) $\text{O}(^1\text{D}) + \text{H}_2\text{O} \rightarrow 2\text{OH}$	$K_{15} = 2.3 \times 10^{-10}$	Chameides & Stedman (ref. 22)
(R16) $\text{O}(^1\text{D}) + \text{H}_2 \rightarrow \text{H} + \text{OH}$	$K_{16} = 1.3 \times 10^{-10}$	Chameides & Stedman (ref. 22)
(R17) $\text{HO}_2 + \text{OH} \rightarrow \text{H}_2\text{O} + \text{O}_2$	$K_{17} = 3 \times 10^{-11}$	Hudson (ref. 34)
(R18) $\text{OH} + \text{OH} \rightarrow \text{H}_2\text{O} + \text{O}$	$K_{18} = 1 \times 10^{-11} \exp(-550/T)$	Chameides & Stedman (ref. 22)
(R19) $\text{HO}_2 + \text{HO}_2 \rightarrow \text{H}_2\text{O}_2 + \text{O}_2$	$K_{19} = 3 \times 10^{-11} \exp(-500/T)$	Chameides & Stedman (ref. 22)
(R20a) $\text{H}_2\text{O}_2 + h\nu \rightarrow 2\text{OH}$	${}^b\text{J}_{20a}(z=0) = 6.2 \times 10^{-7}$	Chameides & Stedman (ref. 22)
(R20b) $\text{H}_2\text{O}_2 \rightarrow \text{Rainout}$	$K_{20b} = 1 \times 10^{-6}$	Assumed
(R21) $\text{H}_2\text{O}_2 + \text{OH} \rightarrow \text{HO}_2 + \text{H}_2\text{O}$	$K_{21} = 1 \times 10^{-11} \exp(-750/T)$	Hudson (ref. 34)
(R22) $\text{HO}_2 + \text{NO} \rightarrow \text{OH} + \text{NO}_2$	$K_{22} = 8 \times 10^{-12}$	Howard & Evenson (ref. 29)
(R23) $\text{OH} + \text{NO}_2 + \text{M} \rightarrow \text{HNO}_3 + \text{M}$	$K_{23} = (1.25 \times 10^{-11})/n_{\text{M}}$	Hudson (ref. 34)
(R24) $\text{OH} + \text{NO} + \text{M} \rightarrow \text{HNO}_2 + \text{M}$	$K_{24} = (2 \times 10^{-12})/n_{\text{M}}$	Chameides & Stedman (ref. 22)
(R25a) $\text{HNO}_3 + h\nu \rightarrow \text{OH} + \text{NO}_2$	${}^b\text{J}_{25a}(z=0) = 1.1 \times 10^{-7}$	Chameides & Stedman (ref. 22)
(R25b) $\text{HNO}_3 + \text{OH} \rightarrow \text{NO}_3 + \text{H}_2\text{O}$	$K_{25b} = 8 \times 10^{-14}$	Hudson (ref. 34)
(R26) $\text{HNO}_3 \rightarrow \text{Rainout}$	$K_{26} = 1 \times 10^{-6}$	Assumed
(R27) $\text{HNO}_2 + h\nu \rightarrow \text{NO} + \text{OH}$	${}^b\text{J}_{27}(z=0) = 1.5 \times 10^{-4}$	Chameides & Stedman (ref. 22)

^aThe rate coefficient units are s^{-1} for one-body reactions, $\text{cm}^3\text{-s}^{-1}$ for two-body reactions, and $\text{cm}^6\text{-s}^{-1}$ for three-body reactions, and T is temperature (K).

^bQuantities shown are the daily averaged photodissociation frequencies for equinoctial conditions at 45°N .

TABLE II.- Concluded

Reaction		Coefficient (a)	References
(R28)	$\text{NO}_2 + \text{O}_3 \rightarrow \text{NO}_3 + \text{O}_2$	$K_{28} = 1.1 \times 10^{-13} \exp(-2450/T)$	Chameides & Stedman (ref. 22)
(R29)	$\text{NO} + \text{O}_3 \rightarrow \text{NO}_2 + \text{O}_2$	$K_{29} = 2.1 \times 10^{-12} \exp(-1450/T)$	Hudson (ref. 34)
(R30)	$\text{NO}_2 + h\nu \rightarrow \text{NO} + \text{O}$	${}^b J_{30}(z=0) = 2.6 \times 10^{-3}$	Chameides & Stedman (ref. 22)
(R31)	$\text{NO}_3 + \text{NO}_2 + \text{M} \rightarrow \text{N}_2\text{O}_5 + \text{M}$	$K_{31} = (3.8 \times 10^{-12})/n_M$	Chameides & Stedman (ref. 22)
(R32)	$\text{NO}_3 + \text{NO} \rightarrow 2\text{NO}_2$	$K_{32} = 8.7 \times 10^{-12}$	Chameides & Stedman (ref. 22)
(R33a)	$\text{NO}_3 + h\nu \rightarrow \text{NO}_2 + \text{O}$	${}^b J_{33a}(z=0) = 2.3 \times 10^{-3}$	Chameides & Stedman (ref. 22)
(R33b)	$\text{NO}_3 + h\nu \rightarrow \text{NO} + \text{O}_2$	$J_{33b}(z=0) = 2.3 \times 10^{-3}$	Chameides & Stedman (ref. 22)
(R34)	$\text{NO} + \text{NO}_2 + \text{H}_2\text{O} \rightarrow 2\text{HNO}_2$	$K_{34} = 6 \times 10^{-37}$	Chameides & Stedman (ref. 22)
(R35)	$\text{N}_2\text{O}_5 + \text{H}_2\text{O} \rightarrow 2\text{HNO}_3$	$K_{35} = 1 \times 10^{-20}$	Chameides & Stedman (ref. 22)
(R36)	$\text{N}_2\text{O}_5 \rightarrow \text{NO}_3 + \text{NO}_2$	$K_{36} = 5.7 \times 10^{14} \exp(-10600/T)$	Chameides & Stedman (ref. 22)
(R37)	$\text{O}_3 + h\nu(\text{visible}) \rightarrow \text{O}_2 + \text{O}$	${}^b J_{37}(z=0) = 1.3 \times 10^{-4}$	Chameides & Stedman (ref. 22)
(R38)	$\text{O} + \text{O}_2 + \text{M} \rightarrow \text{O}_3 + \text{M}$	$K_{38} = 1.1 \times 10^{-34} \exp(510/T)$	Chameides & Stedman (ref. 22)
(R39)	$\text{O}_3 + h\nu(\text{ultraviolet}) \rightarrow \text{O}({}^1\text{D}) + \text{O}_2$	${}^b J_{39}(z=0) = 3.8 \times 10^{-6}$	Chameides & Stedman (ref. 22)
(R40)	$\text{O}({}^1\text{D}) + \text{M} \rightarrow \text{O} + \text{M}$	$K_{40} = 3.2 \times 10^{-11}$	Chameides & Stedman (ref. 22)
(R41)	$\text{OH} + \text{O}_3 \rightarrow \text{HO}_2 + \text{O}_2$	$K_{41} = 1.5 \times 10^{-12} \exp(-1000/T)$	Hudson (ref. 34)
(R42)	$\text{HO}_2 + \text{O}_3 \rightarrow \text{OH} + 2\text{O}_2$	$K_{42} = 1 \times 10^{-13} \exp(-1250/T)$	Chameides & Stedman (ref. 22)

^aThe rate coefficient units are s^{-1} for one-body reactions, $\text{cm}^3\text{-s}^{-1}$ for two-body reactions, and $\text{cm}^6\text{-s}^{-1}$ for three-body reactions, and T is temperature (K).

^bQuantities shown are the daily averaged photodissociation frequencies for equinoctial conditions at 45°N .

TABLE III.- KEY PARAMETERS CALCULATED IN MODEL

Column-integrated photochemical production rate of O ₃ , cm ⁻² -s ⁻¹	1.2 × 10 ¹¹
Column-integrated photochemical loss rate of O ₃ , cm ⁻² -s ⁻¹	1.8 × 10 ¹¹
Downward O ₃ flux at 10.5 km, ^a cm ⁻² -s ⁻¹	1.4 × 10 ¹¹
Downward O ₃ flux at 0 km, ^b cm ⁻² -s ⁻¹	0.8 × 10 ¹¹
Column-integrated CO production rate from CH ₄ oxidation, ^c cm ⁻² -s ⁻¹	3.3 × 10 ¹⁰
Column-integrated CO loss rate from (R13), ^d cm ⁻² -s ⁻¹	2.6 × 10 ¹¹
Tropospheric lifetime of CH ₃ CCl ₃ against reaction with OH, ^e years	7.0

^aObservations indicate a flux of about 0.7 × 10¹¹ cm⁻²-s⁻¹ (Danielsen and Mohnen (ref. 39) and Nastrom and Belmont (ref. 40)).

^bFabian and Pruchniewicz (ref. 41) recommend a flux of (5.8 ± 1.8) × 10¹⁰ cm⁻²-s⁻¹.

^cOther sources of CO include an anthropogenic source of 1 × 10¹¹ cm⁻²-s⁻¹ (Seiler (ref. 1)) and possibly a source from the oxidation of non-methane hydrocarbons of as much as 3 × 10¹⁰ cm⁻²-s⁻¹ (Chameides and Cicerone (ref. 42)).

^dAlso included in the model is a ground deposition rate of about 3 × 10¹⁰ cm⁻²-s⁻¹.

^eSingh (ref. 13) has inferred a CH₃CCl₃ lifetime of (7.2 ± 1.2) years.

TABLE IV.- ESTIMATED GLOBAL SOURCES AND SINKS OF CO

	Rate, $\text{a cm}^{-2}\text{-s}^{-1}$	Reference
Known sources:		
Anthropogenic	10×10^{10}	Seiler (ref. 1)
CH ₄ oxidation	3	This work
Non-CH ₄ hydrocarbon oxidation . . .	1	Extrapolated from Chameides and Cicerone (ref. 42)
Oceans	1	Seiler (ref. 1)
Plants	1	Seiler and Giehl (ref. 45)
Fires	1	Seiler (ref. 1)
Total	17×10^{10}	
Sinks:		
CO + OH	26×10^{10}	This work
Uptake by soil	3	This work
Total	29×10^{10}	

^aA production or loss rate of CO molecules of $10^{10} \text{ cm}^{-2}\text{-s}^{-1}$ equals $70 \times 10^{12} \text{ g CO/yr}$.

^bAn extra, unknown source of $12 \times 10^{10} \text{ cm}^{-2}\text{-s}^{-1}$ is needed to balance CO budget; thus, the total non-CH₄, CO source strength F(CO) would be $26 \times 10^{10} \text{ cm}^{-2}\text{-s}^{-1}$.

TABLE V.- ESTIMATED GLOBAL SOURCES AND SINKS OF NO_x

	Rate, a _{cm⁻²-s⁻¹}	Reference
Sources:		
Anthropogenic (in 1975)	0.7 × 10 ¹⁰	Robinson and Robbins (ref. 51) ^b
Lightning	1	Chameides et al. (ref. 3)
NH ₃ oxidation	<1	Chameides et al. (ref. 3)
Soils	Uncertain	
Total	~2 × 10¹⁰	
Sinks:		
Heterogeneous removal of HNO ₃	2.4 × 10 ¹⁰	This work
Deposition of NO _x	~0.001	This work
Total	~2.4 × 10¹⁰	

^aA production or loss rate of NO_x molecules of 10¹⁰ cm⁻²-s⁻¹ equals 36 × 10¹² g N/yr.

^bExtrapolated from Robinson and Robbins estimate using data from 1965 and assuming a 5-percent annual rate of increase.

^cIn rough agreement with observations (Eriksson (ref. 50) and Burns and Hardy (ref. 38)).

TABLE VI.- VALUES OF a, THE ANNUAL RATE OF GROWTH OF ANTHROPOGENIC CO EMISSIONS, AND b, THE ANNUAL RATE OF GROWTH OF ANTHROPOGENIC NO_x EMISSIONS

Case	a	b
I	0.045	0
II	.025	0
III	.045	.05
IV	.025	.05
V	0	.05

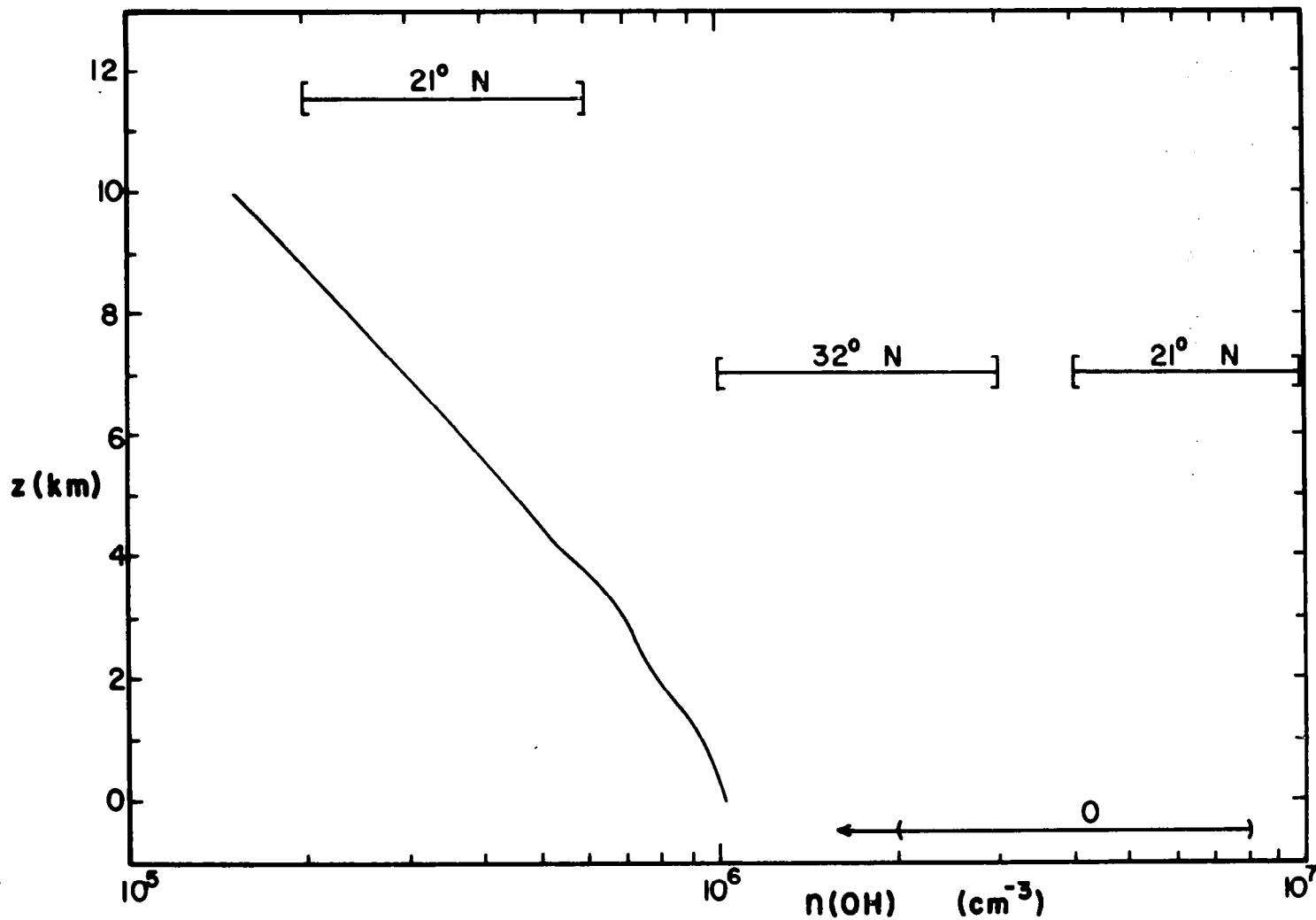


Figure 1.- Calculated diurnally averaged OH profile (solid line). Daytime observations of OH are indicated for Davis et al. (ref. 10) at 21° N and 32° N by the square bracketed lines; for Perner et al. (ref. 12), who obtained several measurements between 2×10^6 and $7 \times 10^6 \text{ cm}^{-3}$ and several below the limit of detectability of $2 \times 10^6 \text{ cm}^{-3}$, by the parentheses and arrow; and the recommended global daily average of Wang et al. (ref. 11) by the circle.

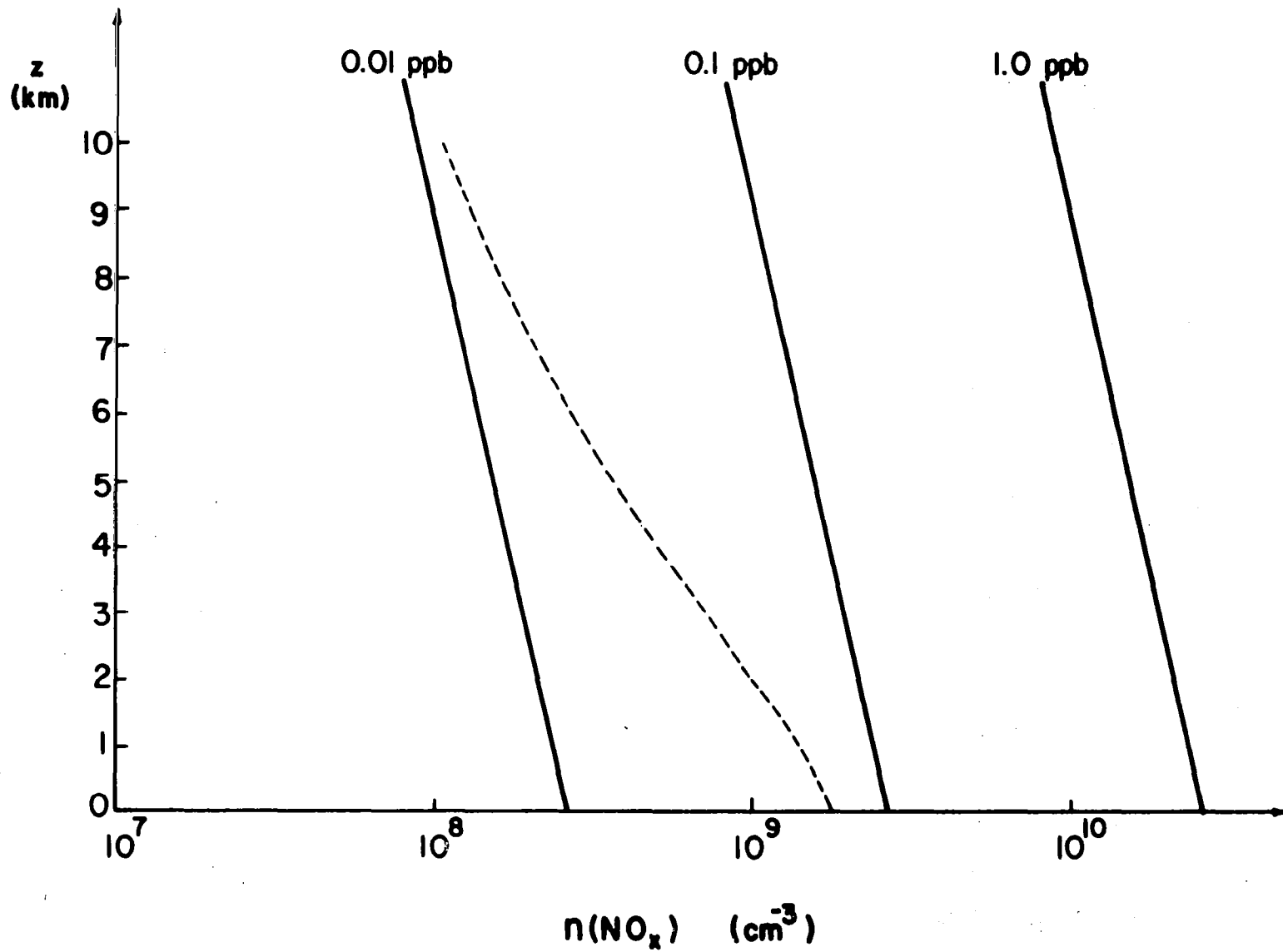


Figure 2.- Calculated NO_x density profile (dashed line). Heavy solid lines roughly indicate lines of constant mixing ratio.

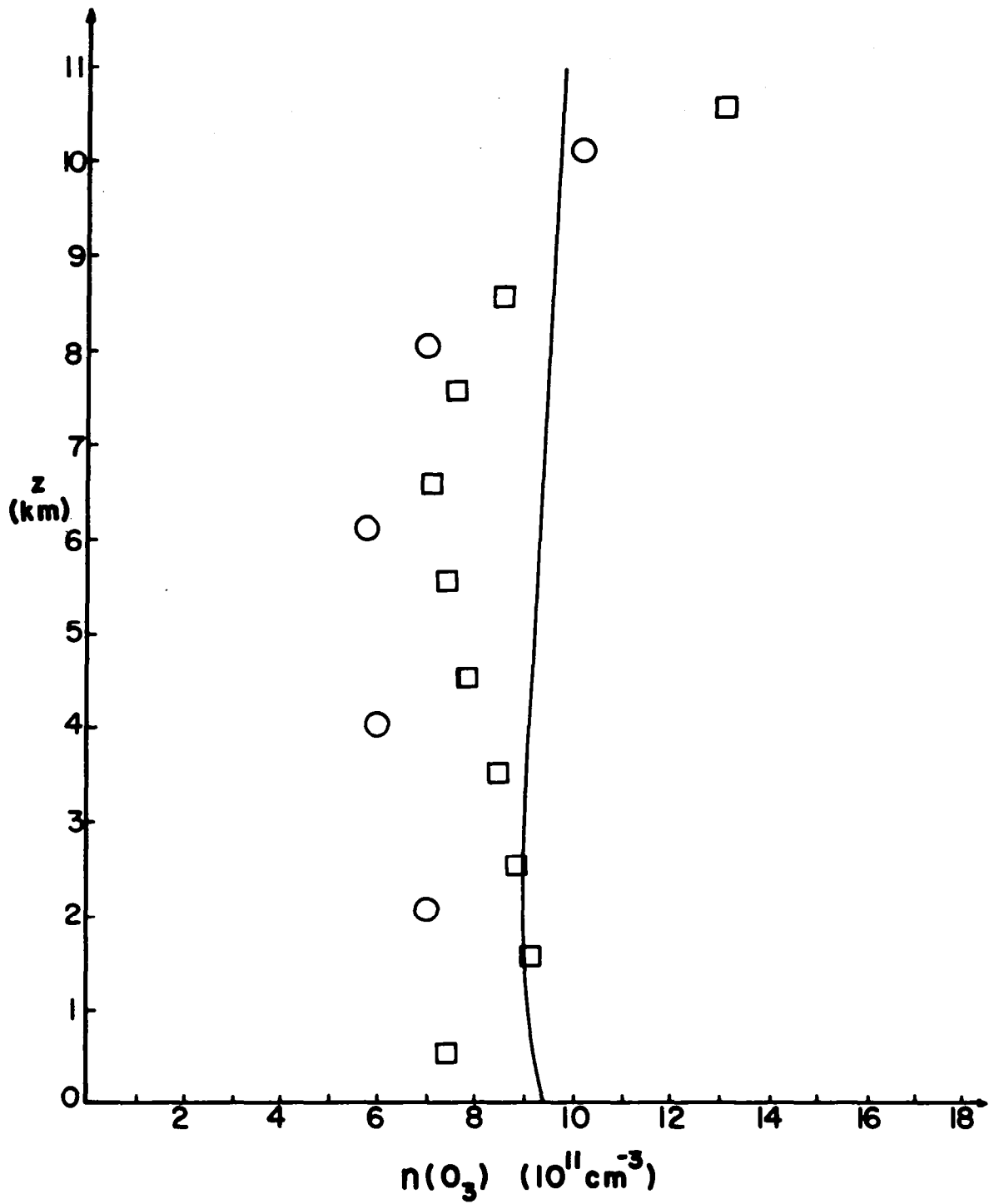


Figure 3.- Calculated O₃ profile (solid line). Circles represent measurements reported by Krueger and Minzner (ref. 36) and squares data reported by Chatfield and Harrison (ref. 44).

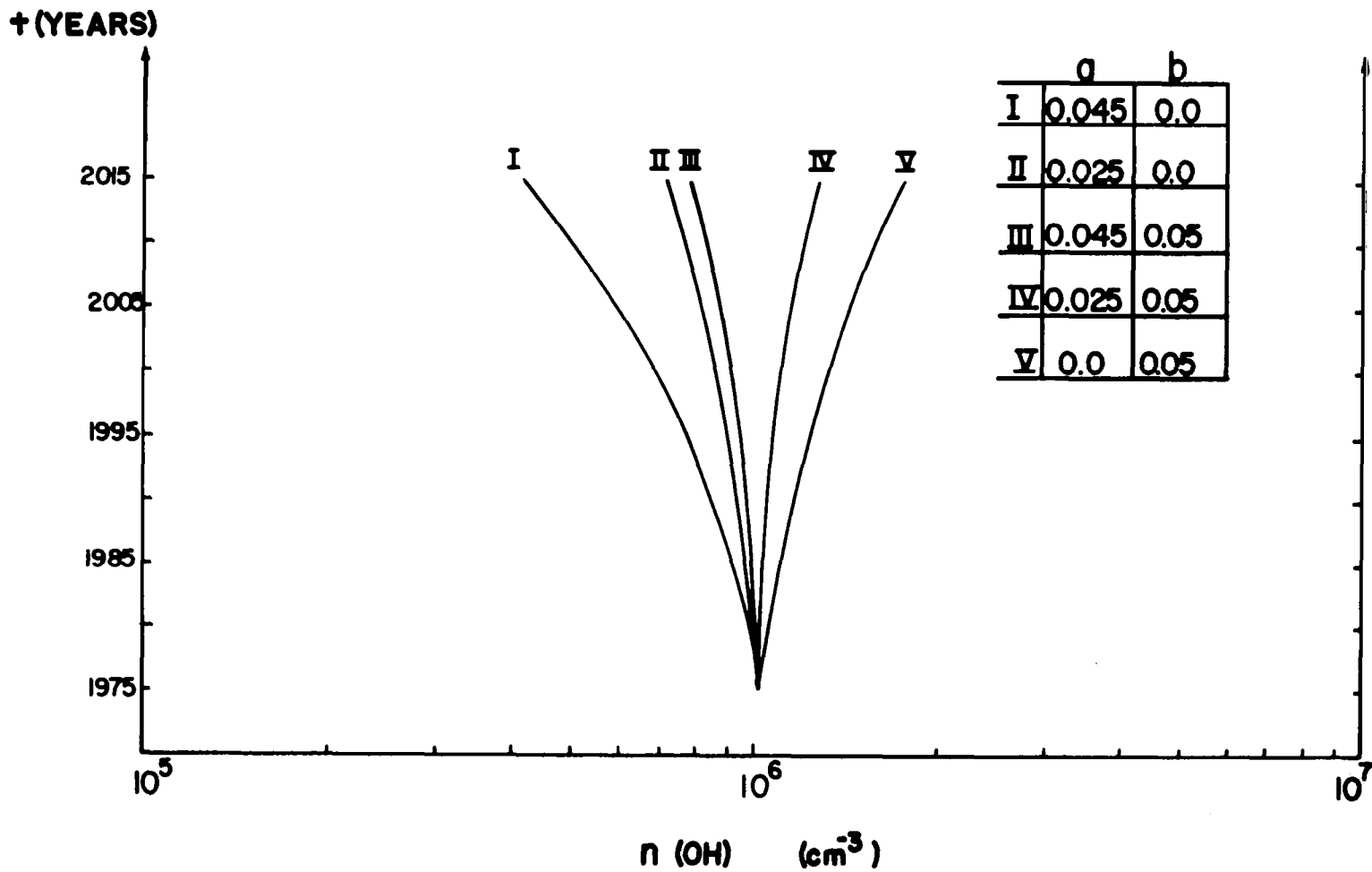


Figure 4.- Time variation in ground-level OH densities for various emission rate patterns.

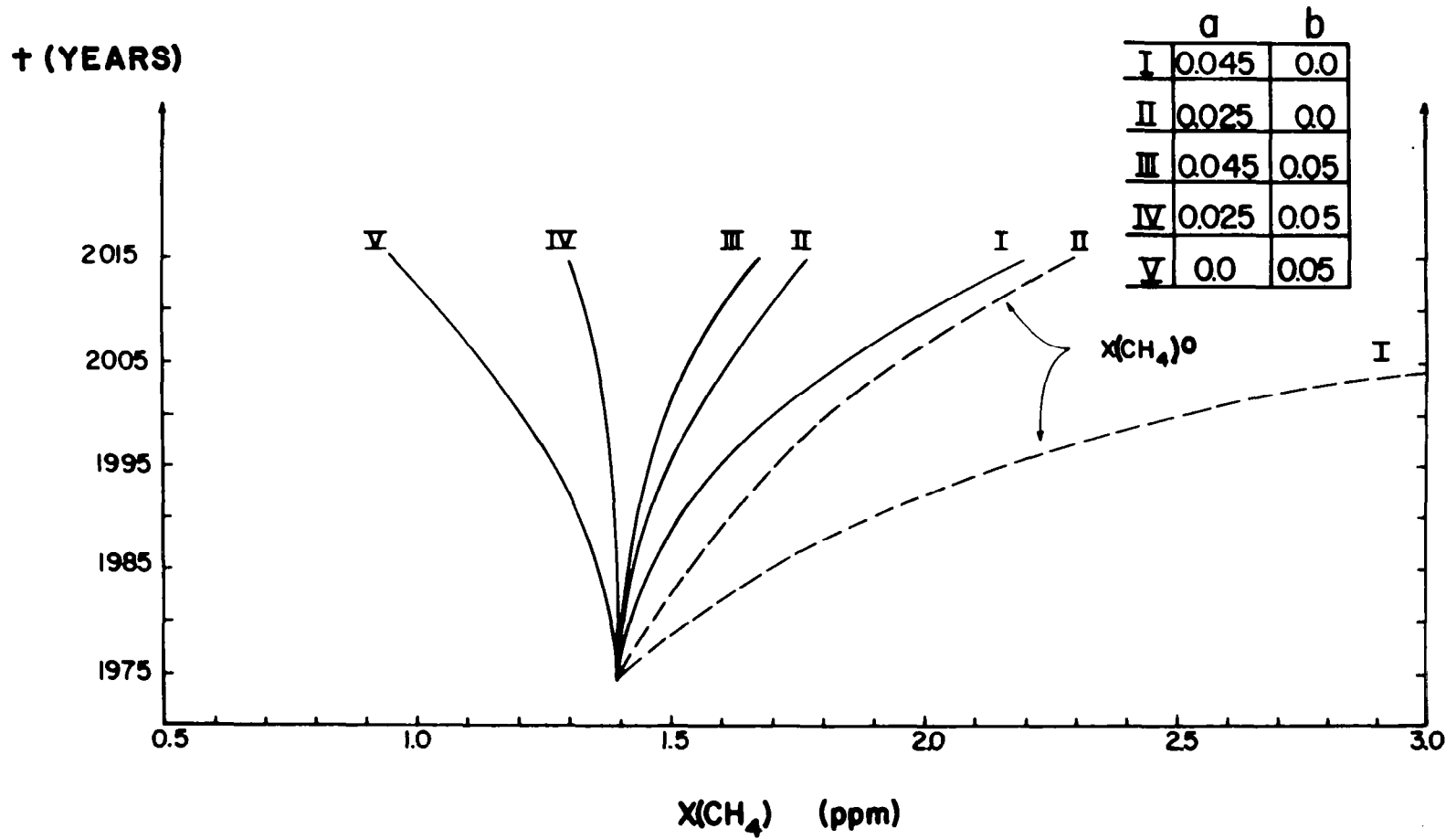


Figure 5.- Time variation of CH₄ mixing ratio (solid lines) and equilibrium CH₄ mixing ratio, X(CH₄)[°] (broken lines) for various emission rate patterns.

THE TRANSPORT CYCLE OF ATMOSPHERIC OZONE AND ITS MEASUREMENTS FROM
AIRCRAFT AND AT THE EARTH'S SURFACE

Phillip D. Falconer, Robert Pratt,
and Volker A. Mohnen
State University of New York at Albany
Albany, New York

CLASSICAL CONCEPTS OF THE TRANSPORT-DOMINATED OZONE CYCLE

The fundamental aspects of the ozone cycle, for which there appears to be solid observational documentation, may be summarized as follows:

- Process 1: Photochemical production within the equatorial stratosphere
- Process 2: Poleward flux of ozone through the general circulation patterns of the stratosphere
- Process 3: Intrusion of ozone into the troposphere through various transport and mixing processes
- Process 4: Ozone mixing within the troposphere
- Process 5: Ozone destruction within the planetary boundary layer or at the Earth's surface

These mechanisms are illustrated (fig. 1) in a tentative model for large-scale ozone fluxes as suggested by Dütsch (ref. 1). It is clear that both atmospheric dynamics and photochemistry play important roles in the distribution of ozone in the atmosphere; however, this paper concentrates upon the last four phases of this cycle where recent, sometimes conflicting theories of ozone transport pathways to the troposphere have been proposed.

Process 2: Poleward Flux of Ozone in the Stratosphere

The photochemical theory of ozone predicts maximum ozone concentrations at altitudes between 20 and 30 km with the total ozone burdens in a vertical column decreasing from equator to pole and from summer to winter. However, long-term observations of total ozone indicate a distinct departure from theory with the vertical column burdens increasing toward higher latitudes and during late winter and early spring. Numerous investigators have attributed this discrepancy to atmospheric circulation patterns since the photochemical relaxation times increase rapidly downward through the stratosphere. (See fig. 2 adapted from ref. 2.) This is equivalent to saying that ozone production (and destruction) by photochemical reactions becomes so slow in the lower stratosphere that the concentration of ozone there must be largely determined by its redistribution by air currents. This also suggests that the ozone-air mixing ratio is a

quasi-conservative property of an air parcel and that ozone may therefore be used as a tracer for various scales of motion in this region. However, this general description does not indicate what types of circulations produce the ozone flux. Brewer (ref. 3) has attributed this transport exclusively to mean meridional circulations between equator and higher latitudes, but this solution is difficult to resolve with the requirement of conservation of angular momentum. Alternatively, large-scale mixing via eddy motions in the lower stratosphere would also account for the observed distribution of ozone above the tropopause, providing that poleward motion is positively correlated with sinking motion. Recent evidence from numerical simulations of ozone transport (refs. 4 and 5) shows quite clearly that the actual transport represents a strong interaction between these two modes. The task of decomposing the total (combined stratospheric and tropospheric) observed poleward ozone flux into its constituent mean and eddy (standing and transient) components has been attempted by several investigators (refs. 6 to 11) for various seasons and across various latitude circles within the stratosphere. The reader should refer to these papers for a more complete discussion of the mathematical methodologies and data bases used. Transport within the stratosphere exclusively, however, has not been widely discussed; but, where such studies have been reported, two points may be made:

(1) The effect of mean and eddy motions exists at all latitudes. However, the net poleward ozone flux is dominated by mean meridional motions in low latitudes and by eddies in middle and high latitudes. Available evidence suggests that this lower stratospheric, transient eddy flux in middle latitudes is roughly 3 times greater during the cold season ($0.6-1.6 \times 10^7$ g-sec⁻¹) than in the warmer season ($0.2-0.6 \times 10^7$ g-sec⁻¹). (See refs. 5, 7, 8, and 12.) Mean meridional fluxes in middle latitudes are generally directed equatorward, although the magnitudes and directions have not yet been clearly established.

(2) The mid-latitude northward transport by eddies reaches a maximum in the lower stratosphere at the 10 to 14 km level. Also, observations indicate that the mean isolines of ozone mixing ratio, radioactivity, and potential vorticity have nearly the same slope in this region (refs. 13 and 7) even though each of these quantities has different source and sink regions. Because eddy motions are expected to conserve potential vorticity, they are efficient in mixing and transporting tracer materials in the stratosphere along surfaces of constant potential vorticity. The fact that these surfaces slope downward and poleward implies that ozone is carried by eddies from its equatorial source region at high altitudes to the photochemically inert lower stratosphere at high latitudes. Although the mixing ratio of ozone increases at a fixed level from equator to pole, the slope of the eddy transport pathways in the meridional direction is still consistent with the down-gradient transport of ozone (ref. 14). The details of this phenomenon are, however, still unclear. Part of the confusion lies with the interpretation of Eulerian quantities (fluxes or correlations at a fixed point or latitude); a different perspective of the transport may be gained from Lagrangian analyses from which the air motion trajectories are derived. Experiments with numerical general circulation tracer models should prove helpful in this respect (ref. 15).

Process 3: Stratospheric-Tropospheric Exchange

Although the gross aspects of this step are fairly well established, the details are relatively poorly understood, especially from a quantitative standpoint. The important property of the tropopause in the context of the ozone cycle is that it represents a nonmaterial boundary which separates well-mixed tropospheric air from the more stable air of the stratosphere. Thus, air (or ozone) which enters the troposphere is likely to experience contact with the ground within a short time. Since ozone acts as an inert tracer at tropopause levels, it is necessary to consider all processes which may result in the transfer of air from the stratosphere to the troposphere. This transfer has usually been viewed within the following categories, which generally follow those outlined by Mahlman (private communication, 1976):

(1) Intensifying upper tropospheric cyclones: Deepening upper tropospheric cyclones in the mid-latitudes are often associated with a large extrusion of stratospheric air which passes beneath the frontal jet stream and mixes with tropospheric air (refs. 16 and 17). Often the frontal zone beneath the jet stream can be considered an extension of or "fold" in the local tropopause; contained within this fold is air largely of stratospheric origin. It has been suggested that a more diffuse flow of tropospheric air into the stratosphere exists in areas adjacent to the jet stream as well.

(2) Vertical motions associated with jets and waves: Even in the absence of cyclogenetic development described in item (1), significant vertical components of motion can be associated with the upper tropospheric flow. Mahlman (ref. 18) has reviewed much of the literature on this phenomenon and has analyzed a typical case of transverse flow around a nearly straight segment of the polar front jet observed over the continental United States. Waves in the upper-level flow are also accompanied by vertical motions near the tropopause, which is a dynamically complicated region since synoptic-scale tropospheric waves are damped as they penetrate into stable stratospheric air. Such vertical motions can be important in transporting tracer substances to, if not actually through, the tropopause (ref. 19).

(3) Tropopause lifting: This process might better be described as a re-formation of the tropopause at a different level, which leads to a change in the amount of air above and below the boundary (ref. 20). Although this type of process is undoubtedly associated with seasonal variations in the radiation balance, it is difficult to include this process in a precise budget of stratospheric-tropospheric mass exchange, since the source of air which resides under the newly formed tropopause is not obvious.

(4) Mesoscale and smaller scale motions: Evidence based on radioactivity deposition indicates that severe cumulus convection can penetrate the tropopause and extract some stratospheric air (ref. 21). Gravity wave activity, either associated with this process or related to clear air turbulence situations (ref. 22), may also produce irreversible mixing across the tropopause.

(5) Mean meridional circulation: Although well-defined mathematically as the zonal mean of the meridional and vertical components of motion, the mean meridional circulation can physically represent statistical contributions from

any of the phenomena in items (1) to (4), especially in the mid-latitudes. It therefore cannot be considered as independent from the other mechanisms.

The most striking and widely accepted mechanism of ozone input to the troposphere is through cyclogenetic events (item (1)), which correlate well with the day-to-day and annual variations observed in mid-latitude surface ozone and radioactivity. However, a quantitative estimate of the annual ozone flux by this mechanism, and the others previously listed, is difficult to establish. The observational problems are the small magnitude of vertical velocities in the atmosphere, the wide range of space scales involved, and the time variability of all the mechanisms. Therefore, any estimate of the ozone flux based on meteorological data necessarily involves considerable subjectivity in order to extrapolate the annual hemispheric flux from the very limited data available.

Although estimates of ozone exchange due to large-scale eddy exchange are relatively scarce, Danielsen and Mohnen (ref. 23) and Mohnen (ref. 24) have attempted to quantify this flux by using meteorological data and representative ozone mixing ratios in the lower stratosphere. In order to establish this quantity, the authors make reference to earlier works by Danielsen¹ in which the cross-tropopause exchange of stratospheric air had been investigated. The yearly outflow rate based upon strontium-90 distributions was given as 3.6×10^{20} g(air)-yr⁻¹ while, in a later study, a value of 4.3×10^{20} g(air)-yr⁻¹ (e.g., 4.0×10^{17} g(air) per cyclogenetic event times a representative number of events per year) was determined. The annual ozone flux due to this process was estimated in both cases by assuming an ozone mixing ratio of 1.3×10^{-6} g-g⁻¹; this results in roughly 470×10^{12} and 560×10^{12} g-yr⁻¹, respectively (see details in ref. 23).

These various injection fluxes may be compared with estimates of the last step in the ozone cycle, destruction at the ground. The stratospheric-tropospheric exchange and destruction fluxes should agree in the classical transport cycle if the former represents the total net ozone input to the troposphere. The hemispheric ozone fluxes in the previous paragraph (multiplied by 2 for global conditions) are close to the upper limit of the latest global sink estimate in table I derived by Fabian and Pruchniewicz (ref. 25). Obviously, the meteorological estimate entails considerable subjectivity, such as the value of mean ozone mixing ratio. However, the fact remains that crude estimates based on limited meteorological data are roughly consistent with those based on the present understanding of surface destruction.

For comparison, Reiter (ref. 26) estimates the total annual mass (not specifically ozone) flux from cyclogenetic events to be only about 25 percent of Danielsen's estimate. However, the discrepancy between these authors' estimates arises from the number of cyclogenetic events per year rather than from the mass transfer per event. Reiter also estimates that the mean meridional circulation (item (5)) transfers air from stratosphere to troposphere at twice

¹Although the estimates discussed in these references are based on works described in Danielsen's earlier publications, details of the estimates themselves, beyond those discussed in references 23 and 24, apparently remain unpublished.

the annual rate as cyclogenetic events (item (1)). However, his estimate of the mean circulation does not seem to account for the possibility that part of the mean flow may be contributed by cyclogenetic events in mid-latitudes, as discussed previously. Therefore, it is not at all clear that the estimates of even total mass flow by Danielsen and Reiter are in agreement.

Another type of estimate has been done by Nastrom (ref. 12) from Global Atmospheric Sampling Program data. Instead of extrapolating from case studies, he computed the average ozone concentration from a large number of aircraft measurements near the tropopause, when the large-scale flow indicated either positive or negative vertical motion. By assuming a typical large-scale vertical velocity magnitude (0.5 cm-sec^{-1}), he arrived at a mean ozone flux of $7.8 \times 10^{10} \text{ molecules-cm}^{-2}\text{-sec}^{-1}$ for latitudes poleward of 30° N . A reasonable conversion of this mid-latitude figure to the hemisphere yields an annual hemispheric flow a little lower than that deduced from Danielsen's detailed analysis of a single cyclogenetic event and hence well in the range of global sink estimates. Physically, Nastrom's estimate represents a very different approach in that it is based on large-scale properties rather than on the subsynoptic-scale details which are important in a folding event.

Three meteorological estimates of the cross-tropopause ozone flux have been reviewed here and all three agree roughly with surface destruction estimates. In view of the considerable simplifications necessary for these estimates and the limited understanding of the transport of air across the tropopause, it may seem fortuitous that such agreement does exist. It appears that current estimates may look right for the wrong reasons and a complete understanding of cross-tropopause transfer has yet to be achieved.

Process 4: Ozone Mixing and Transport Within the Troposphere

Ozone ingested into the troposphere from the stratosphere or any fraction which may have been produced (or destroyed) by photochemical reactions (refs. 27 and 28) is frequently assumed to be well mixed at all latitudes down to, or near the Earth's surface. The mixing efficiencies associated with the free troposphere are sufficiently large, on the average, to produce vertical ozone mixing ratio gradients perhaps an order of magnitude smaller than those found in the lower stratosphere (0 to 10 ppbv-km^{-1} versus 25 to 50 ppbv-km^{-1}). However, on a day-to-day basis, observations show that the troposphere is not as well stirred as mean vertical ozone profiles would suggest. Ozone layers fluctuate in height or may disappear altogether on successive days, depending upon stability and circulation patterns in the lowest 10 to 12 km of the atmosphere. Pruchniewicz (ref. 29) has illustrated these interdiurnal mixing variations in the middle troposphere (400 to 500 hPa) by using extensive ozone sounding records obtained at Boulder, Colorado (see also Dütsch et al. (ref. 30)). By comparing the ozone mixing ratios at these levels on a certain day T with the corresponding values for day $T - 1$ or $T - 2$, Pruchniewicz demonstrated the great variability of midtropospheric ozone away from the major injection and sink regions (figs. 3 and 4). The results, of course, suggest the importance of either quasi-horizontal ozone transport through the troposphere, photochemical production and destruction, or an uncertain combination of both

mechanisms. These findings therefore embody the central issues of the tropospheric ozone controversy (ref. 31).

Process 5: The Ozone Sink Near the Earth's Surface

The flux of ozone into the planetary boundary layer and to the Earth's surface is, according to classical theory, the main sink for tropospheric ozone. The rate of ozone destruction through chemical contact and reaction with various surface features, for instance, ice, water, deserts, grasslands, and forests, has been experimentally and theoretically determined (refs. 25, 32, and 33). (See table I.)

There are two points here which should be considered in connection with table I. First, the flux estimates given by various authors are generally applicable to unpolluted surface atmospheres where the effects of ozone-destructive precursors are generally eliminated. Second, according to the classical transport-dominated ozone theory, the value quoted for the mean annual ozone loss at the surface must be nearly equal to the mean annual ozone input to the troposphere. The range of estimates provided in table I is unfortunately large enough to permit a variety of interpretations on the amount of ozone exchanged across the tropopause.

AIRCRAFT OBSERVATIONS OF OZONE

Historically, aircraft measurements of atmospheric ozone may be divided into two categories: (1) those obtained from dedicated research aircraft deployed on short missions during preselected weather conditions or observing periods (refs. 23 and 34 to 37) and (2) those obtained from commercial aircraft in routine service where a variety of weather conditions along differing air routes may be encountered (refs. 38 to 40). Clearly, different analytical procedures are appropriate for each of the data sets. One common objective of aircraft ozone measurements, however, is to describe adequately the three-dimensional (latitude-longitude-height) and time variations near the injection regions and, where possible, to determine the relative importance of various ozone exchange mechanisms (cf. the section "Process 3: Stratospheric-Tropospheric Exchange").

Dedicated Research Aircraft Programs

It is safe to say that the atmospheric science community is most familiar with upper air ozone measurements obtained from dedicated aircraft missions. By and large, the information which has been recovered from these research platforms includes the details of microscale and mesoscale ozone fluctuations associated with atmospheric (e.g., temperature and wind) structure, estimates of the background tropospheric ozone content through repetitive vertical profiling, and estimates of the relative abundance of ozone-specific precursor or destruction gases (e.g., oxides of nitrogen, hydroxyl radicals) in the upper troposphere and lower stratosphere.

Perhaps one of the most interesting points of discussion in this regard involves the verification of the existence of tropopause folds beneath the jet stream core through carefully planned aircraft monitoring experiments. Although radioactive fission products were originally used as the tracers in these studies (refs. 41 and 42), ozone has proved to be an ideal species to complement these other measurements because of its quasi-conservative behavior (refs. 23, 34, and 43). From these unique sets of measurements, an important means has been isolated by which the troposphere is replenished quickly and directly with ozone from the stratosphere whenever tropopause folds develop. Danielsen and Mohnen have succinctly illustrated the structure of ozone embedded within these features (fig. 5), pointing out that the dilution of stratospheric ozone within the fold through mixing with tropospheric air is relatively slow and that ozone may occasionally reach the Earth's surface at values exceeding the current federal standards.²

Aircraft data have also been used to assess the average background ozone concentration between the boundary layer and the tropopause. Singh et al. (ref. 44) indicate that the average ozone mixing ratios obtained along the east coast during the summer months range between 43 and 56 ppbv (table II). Similar results have been obtained by Mohnen from measurements which he obtained aboard commercial aircraft during ascents and descents into various international airports (fig. 6). Interestingly, these records, as well as those from recent ozonesonde profiles, point to background tropospheric concentrations roughly 50 percent higher than previously reported during the 1960's by Hering and Borden (refs. 45 to 48). Clearly, a more rigorous reevaluation of the tropospheric ozone budget in light of such aircraft measurements will be increasingly called upon.

Mention should also be made of the most recent attempts in monitoring various ozone-producing or ozone-destroying trace species from aircraft platforms well above the planetary boundary layer.³ The highly sensitive instruments required for measuring these minor constituents have been modified for flight operations in recent years, in large measure because of the cooperation of scientists around the world who participated in the federally sponsored Climatic Impact Assessment Program during the years 1972 to 1974 (ref. 49). Various spin-off monitoring programs have focused attention upon the upper troposphere as well. A brief summary of recent trace gas measurements (refs. 50 to 53) in the mid-to-upper troposphere has been compiled in table III; the reader is however encouraged to refer to the paper by Stewart, Hameed, and Pinto of this compilation for more detailed information.

²In 1970, Congress requested the U.S. Environmental Protection Agency to establish ambient air quality standards for ozone and other photochemical oxidants. The maximum ozone level, not to be exceeded for more than 1 hr, was set at 80 ppbv.

³Historically, most measurements of this sort have been, and continue to be, acquired from ground-based monitoring networks. This is largely due to the ultimate need within state and federal governments for establishing a sound scientific basis for oxidant control strategies.

Commercial Aircraft Measurements

Only recently has the concept of utilizing commercial aircraft in routine national or international service been tested. Depending upon the application of a particular project, experiments have been conducted either with scientific personnel on board the aircraft (refs. 23, 39, and 54) or as fully automated, unattended (refs. 55 and 56) missions. In either case, in situ measurements are, except in rare instances, a strict function of airlines' routing procedures, and therefore, many aspects of true case study research are restricted. For instance, flights into and out of the stratosphere as well as cruise altitude changes are never fully anticipated but must be accounted for in post-flight data evaluation. However, the wide and repetitive coverage offered by commercial aircraft provides a unique data base for examining ozone climate along various flight routes.

As part of an extensive ozone monitoring program supported by the Deutsche Forschungsgemeinschaft (German Science Foundation) and the Max-Planck-Institute for Chemistry, German investigators utilized numerous airliners in order to obtain upper tropospheric (10 to 12 km) ozone records (ref. 39). A flight corridor between longitudes 20° W and 35° E and extending from Norway to South Africa was established with continuous ozone registrations being acquired periodically from September 1970 through July 1973. An illustration of the tropical measurements (25° N to 25° S) has been extracted from one of their reports (figs. 7 and 8). For each season, the distribution of ozone in the tropics appears to be uniform with no systematic latitudinal variation (fig. 7). The mid-latitude data show greater variability and higher magnitudes, presumably related to the mechanisms described in the section "Process 3: Stratospheric-Tropospheric Exchange." On the other hand, there is a marked annual variation in the tropics of each hemisphere (fig. 8) with an ozone maximum in the spring months of the northern hemisphere. No detectable influence of the mean sun position upon ozone is apparent.

The Global Atmospheric Sampling Program (GASP) conceived by NASA Lewis Research Center (ref. 57) in the early 1970's is currently obtaining ozone measurements at altitudes of 6 to 13 km and latitudes 40° S to 70° N (fig. 9 taken from ref. 58). Data from these altitudes have been analyzed in a variety of fashions; the salient points of these analyses are as follows:

(1) Ozone observations obtained in the tropical upper troposphere (0° to 30° N and 50 to 100 hPa below the tropopause) are qualitatively consistent with those presented by Pruchniewicz et al. (ref. 39); that is to say that, on the average, no significant meridional gradient has been observed during the period from March 1975 to September 1976 (Falconer, unpublished data). However, an annual cycle also appears at all latitudes, which shall be discussed in the following sections. Similar conclusions may also be extracted from an analysis of the ozone distribution at 11 to 12 km by month and latitude presented by Nastrom (ref. 12). Ozone variability and its mean abundance poleward of 30° N increase sharply in the altitude range from 6 to 13 km.

(2) Zonally averaged ozone concentrations in the layer 50 to 100 hPa below the tropopause between 10° N and 60° N exhibit an annual cycle during 1975 and 1976 which shows a late fall minimum and two maxima during the spring and summer

months (ref. 38). (See fig. 10.) The cycle appears to be explained in terms of meteorological processes. The initial maximum during April begins with concomitant increases in the stratospheric ozone reservoir over mid-latitudes and in the vigor of cyclone disturbances which may transport ozone out of this reservoir. Alternatively, the prominent fall minimum arises not so much because of the weakening of cyclone exchange processes but rather because of reduced ozone content within the stratosphere. To this extent, the GASP aircraft results confirm the basic structure of the classical ozone cycle. The secondary ozone maximum during the summer probably is in part due to the rapid upward adjustment of the tropopause in late spring; ozone previously embedded within the lower stratosphere is suddenly introduced into the upper troposphere as the lifting accelerates.

(3) The space scale variability of ozone in the lower stratosphere is comparable with typical length scales for synoptic disturbances. Nastrom (ref. 12) performed lagged autocorrelation analyses upon 5-minute ozone records obtained just above the tropopause from a set of 33 carefully selected (east-west) flights. His evaluations indicated that the distance lagged correlation coefficients are crudely approximated as the product of exponential decay and a cosine variation whose half-wavelength is near 950 km. This implies a wavelength of 1900 km, typical of the east-west distance across intense ridges or troughs. He points out that the resolution of these features by ground-based or satellite measurements is unlikely.

OZONE MEASUREMENTS AT THE EARTH'S SURFACE IN REMOTE LOCATIONS

In their study of ozone variations in clean remote atmospheres, Singh et al. (ref. 44) have chosen monitoring stations which (1) were located away from urban pollution centers (at least 400 km in the case of "remote" sites) and (2) had at least a 2-year record of ozone measurements. Five stations from this work have been selected which are believed to represent ozone behavior at either mountainous or flat terrain locations.

Seasonal Variations of Surface Ozone in Rural Environments

Monthly averages of the daily ozone maxima at the Earth's surface are probably representative of the seasonal behavior of free tropospheric ozone (refs. 44, 59, and 60). These values generally occur around noon, or shortly thereafter, when vertical mixing is greatest and when the influence of the surface destruction layer is minimized. Although there appears to be a regular annual oscillation in many data records of this type, it is equally striking that many other surface ozone records in rural environments exhibit an additional, shorter term fluctuation as well. The rhythmic nature of surface ozone variations may be approximated in most instances through the application of harmonic analysis; the authors have found that the sum of the first two harmonics (e.g., annual and semiannual waves) usually accounts for at least 90 percent of the variance.

In figure 11, the annual behavior of ozone is illustrated at four remote observatories - Mauna Loa, Hawaii (19.5° N); White River, Utah (39.9° N);

Rio Blanco, Colorado (39.8° N); and Quillayute, Washington (47.9° N). All stations exhibit a rapid ozone increase (10 ppbv-month⁻¹) in spring, reaching a local maximum which ranges from March at White River to June at Rio Blanco, based on the first two harmonics. At White River and Quillayute, a second maximum occurs later in the year leading to a bimodal behavior, while Mauna Loa and Rio Blanco have more nearly a simple annual cycle.

It is instructive to examine the data in figure 11 in the context of existing models of the tropospheric ozone budget. Junge (ref. 59), Fabian (ref. 61), and Pruchniewicz (ref. 62) have developed such hemispheric or zonally averaged models based on the classical ozone cycle. The important ingredients of this type of model are stratospheric injection, surface destruction, and tropospheric ozone content, each of which is represented simply by the amplitude and phase of an annual harmonic. They also allow for a phase delay between time of maximum injection and the appearance of maximum ozone at the Earth's surface.

There is no problem with interpreting the data at Mauna Loa and Rio Blanco in terms of such a model. Each data set shows a simple annual cycle. The time of maximum ozone is different, but this could be accounted for by a latitudinal variation in the time of maximum injection and of the phase delay. Maximum injection would be expected in mid-latitudes in the late winter or spring, when the stratospheric burden of ozone is largest and cyclonic disturbances are still active. In the case of Mauna Loa, located in the subtropics, the phase delay might be considered an average time for ozone to be transported southward from the areas of strong injection in mid-latitudes.

The timing of the first ozone maximum at White River and Rio Blanco, however, is difficult to resolve in the context of a zonally averaged model. These stations are only 160 km apart. The 3-month difference in their times of maximum ozone is unlikely related to a corresponding difference in the time of maximum injection or in phase delay of the maximum, since these are intended to be large-scale properties representative of at least an entire latitude band. The bimodal nature of the White River and Quillayute records is also clearly at odds with the annual harmonic representation of simple budget models; important details of ozone variations at individual stations are unfortunately missed in these cruder mathematical approaches. Figure 12, obtained from a publication by Chatfield and Harrison (ref. 63), seems to express the inadequacies of the simple annual wave solution. The actual station records presented are, however, not necessarily inconsistent with the classical ozone transport cycle, which allows for ozone mixing and transport on various scales before it is ultimately destroyed at the Earth's surface or within the boundary layer. It is conceivable, for instance, that the secondary ozone maxima at White River and Quillayute could be attributed to late summer variations in local meteorology.

There is, however, evidence that the data presented in figures 11 and 12 could support the effects of photochemistry. Fortunately, the nitrogen oxides and hydrocarbon species records for White River and Quillayute are available for evaluating this point. At White River, where naturally occurring, non-methane hydrocarbons are always present at concentrations of at least 100 $\mu\text{g}\cdot\text{m}^{-3}$, nitrogen oxides concentrations rapidly increase nearly fivefold during midsummer (to approximately 50 $\mu\text{g}\cdot\text{m}^{-3}$) and gradually decline to roughly 10 $\mu\text{g}\cdot\text{m}^{-3}$ by the end of the year. The source for the nitrogen oxides during

the summer was not identified by Singh and his co-workers (ref. 44), but they believe that the second ozone maximum here may be indicative more of photochemical synthesis than of meteorological factors.

A similar conclusion for the secondary ozone maximum at Quillayute was not supported by the ozone precursor data records; the abundances of nitrogen oxides and hydrocarbons were found to be nonmeasurably low during this period. In the case studies of the Quillayute data, Singh et al. attribute the second warm-season maximum to long-range ozone transport from distant urban centers, such as Portland, Oregon, based upon their trajectory analyses.

Figure 13 illustrates schematically a possible explanation of how a double warm-season maximum might arise at remote mid-latitude observatories. Long-range transport of ozone from distant urban centers, or ozone synthesis in the presence of nitrogen oxides and naturally occurring, reactive hydrocarbon species, may be important (refs. 44 and 64) at stations such as White River. Dimitriadis and Altshuller (ref. 65) have recently discussed the problems of quantifying the relative effects of photochemistry and transport. If the timing of the first and second peaks suggested in figure 13 is close, the resulting profile may exhibit a single delayed maximum, as does Rio Blanco (fig. 11). However, it is difficult to discriminate between photochemistry and mixing based upon the ozone records alone. If the challenge of understanding the yearly ozone cycle in clean environments is to be successfully met, a more thorough documentation of both the local meteorology and the ozone precursor behavior must be undertaken.

Diurnal Ozone Variations in Rural Environments

The daily ozone variations in clean environments depend upon the topographic setting of the monitoring station. The diurnal ozone waves which are reported at mountain locations often show small amplitude (refs. 44, 66, and 67). Also, most such records suggest that the ozone maxima are least likely to occur at noon, or shortly thereafter. On the other hand, ozone data obtained either on flat terrain or at hilltop sites generally exhibit an afternoon maximum and an early morning minimum. The diurnal ozone variations for the mountain observatories at Mauna Loa, Hawaii (19.5° N, 3400 m above mean sea level (MSL) and Whiteface Mountain, New York (44.3° N, 1510 m above MSL) will be compared with those from two nonmountain stations at Quillayute, Washington (47.9° N, 62 M above MSL) and White River, Utah (39.9° N, 1625 m above MSL).

The average daily variations at Mauna Loa and Whiteface Mountain (fig. 14) for the years indicated suggest that, in fact, the ozone maximum is almost equally probable at any time of the day, although it appears least likely in the hours surrounding noon. It is believed that these records may be interpreted in terms of the unique wind circulation characteristics of mountainous terrain (refs. 67 and 68). The limited likelihood of observing the daily ozone maximum during midday is consistent with the timing of the most vigorous upslope flow when ozone-depleted air from the rural surroundings below is brought upward along the side of the mountain. Conversely, during the evening and early morning hours when downslope flow prevails, air relatively richer in ozone is imported from above. However, a more detailed documentation of ozone in

relation to other local and larger scale wind systems in mountain areas is necessary to understand mountain data completely. There is probably considerable variation in flow characteristics among individual mountain sites.

At nonmountain stations such as Quillayute and White River (fig. 15), the daily ozone maximum generally occurs in midafternoon and the ozone minimum during the early morning hours. These characteristics agree with the well-known diurnal variation of meteorological mixing in the boundary layer. During stable conditions, vertical exchange at the top of the rural boundary layer is minimal. Ozone is isolated from its free tropospheric source aloft and is rapidly destroyed through surface contact or by chemical reactions within the shallow boundary layer. The greatest depletion of ozone appears just prior to sunrise. During the day, surface heating tends to destabilize the boundary layer, which promotes mixing of ozone from the free troposphere above down through the lower layers. This effect would, in theory, result in a midafternoon ozone maximum since the turbulent mixing would be at its peak strength at this time.

Finally, a by no means comprehensive comment is made on the prospects for interpreting ozone records obtained at clean ground-level stations and those obtained in urban-suburban locations (which have not been dealt with here). The behavior of the diurnal ozone cycle is the most likely candidate for these brief remarks since there is evidence that the afternoon ozone maximum, which may well be largely due to meteorological factors in rural settings, can also be quite plausibly related to photochemistry in urban surroundings. Conversely, boundary-layer mixing in urban environments and photochemistry (including both natural and anthropogenic precursor gases) in rural environments cannot be dismissed as important factors in the diurnal behavior at individual stations. The situation is no less complicated if the effects of ozone transport during the course of the day are considered.

The classical concept of tropospheric ozone needs no basic revision when compared with experimental findings. However, tropospheric photochemical activity involving, or producing, ozone from naturally occurring trace gases, cannot be excluded in the ozone cycle. The net destruction or production of ozone in the troposphere cannot exceed the error limits associated with the experimentally determined net flow of ozone across the tropopause and into the boundary layer. These two fluxes have been shown to be roughly comparable.

REFERENCES

1. Dütsch, H. U.: Atmospheric Ozone - A Short Review. *J. Geophys. Res.*, vol. 75, no. 9, Mar. 20, 1970, pp. 1707-1712.
2. Grobecker, Alan J.: Progress Report on the Climatic Impact Assessment Program. Proceedings of the Third Conference on the Climatic Impact Assessment Program, Anthony J. Broderick and Thomas M. Hard, eds., DOT-TSC-OST-74-15, U.S. Dep. Transp., Nov. 1974, pp. 1-15. (Available from DDC as AD A003 846.)
3. Brewer, A. W.: The Measurement of the Vertical Distribution of Ozone and Its Meteorological Significance. *Les Problèmes Météorologiques de la Stratosphère et de la Mésosphère*, Presses Universitaires de France (Paris), 1966, pp. 369-382.
4. Mintz, Yale; and Schlesinger, Michael: Ozone Production and Transport With the UCLA General-Circulation Model. Proceedings of the Fourth Conference on the Climatic Impact Assessment Program, Thomas M. Hard and Anthony J. Broderick, eds., DOT-TSC-OST-75-38, U.S. Dep. Transp., Feb. 1975, pp. 201-223.
5. Cunnold, D.; Alyea, F.; Phillips, N.; and Prinn, R.: A Three-Dimensional Dynamical-Chemical Model of Atmospheric Ozone. *J. Atmos. Sci.*, vol. 32, no. 1, Jan. 1975, pp. 170-194.
6. Newell, Reginald E.; Boer, George J.; and Dopplick, Thomas G.: Influence of the Vertical Motion Field on Ozone Concentration in the Stratosphere. *Pure & Appl. Geophys.*, vol. 106-108, 1973, pp. 1531-1543.
7. Hering, Wayne S.: Ozone and Atmospheric Transport Processes. *Tellus*, vol. 18, nos. 2-3, 1966, pp. 329-336.
8. Dutsch, H. U.; and Favarger, D.: Meridional Ozone Transport by Transient Eddies Over Boulder, Colorado. *Ann. Géophys.*, t. 25, nr. 1, 1969, pp. 219-221.
9. Hutchings, J. W.; and Farkas, Edith: The Vertical Distribution of Atmospheric Ozone Over Christchurch, New Zealand. *Q. J. R. Meteorol. Soc.*, vol. 97, no. 412, Apr. 1971, pp. 249-254.
10. London, Julius; and Park, Jae H.: The Interaction of Ozone Photochemistry and Dynamics in the Stratosphere. A Three-Dimensional Atmospheric Model. *Canadian J. Chem.*, vol. 52, no. 8 (pt. 2), Apr. 15, 1974, pp. 1599-1609.
11. Mahlman, J. D.: Dynamic Mechanisms Producing Large-Scale Transport of Atmospheric Trace Substances. NPS-51MZ70101A, U.S. Naval Postgraduate School, Oct. 1970. (Available from DDC as AD 719 895.)
12. Nastrom, G. D.: Vertical and Horizontal Fluxes of Ozone at the Tropopause From the First Year of GASP Data. *J. Appl. Meteorol.*, vol. 16, no. 7, July 1977, pp. 740-744.

13. Dobson, G. M. D.: Atmospheric Ozone and the Movement of the Air in the Stratosphere. *Pure & Appl. Geophys.*, vol. 106-108, no. 5-7, 1973, pp. 1520-1530.
14. Newell, R. E.: Transfer Through the Tropopause and Within the Stratosphere. *Q. J. R. Meteorol. Soc.*, vol. 89, no. 380, Apr. 1963, pp. 167-204.
15. Kida, Hideji: A Numerical Investigation of the Atmospheric General Circulation and Stratospheric-Tropospheric Mass Exchange: II Lagrangian Motion of the Atmosphere. *J. Meteorol. Soc. Japan*, vol. 55, no. 1, Feb. 1977, pp. 71-88.
16. Danielsen, Edwin F.: Stratospheric-Tropospheric Exchange Based on Radioactivity, Ozone and Potential Vorticity. *J. Atmos. Sci.*, vol. 25, no. 3, May 1968, pp. 502-518.
17. Reiter, Elmar R.; and Mahlman, J. D.: Heavy Radioactive Fallout Over the Southern United States, November 1962. *J. Geophys. Res.*, vol. 70, no. 18, Sept. 15, 1965, pp. 4501-4520.
18. Mahlman, J. D.: On the Maintenance of the Polar Front Jet Stream. *J. Atmos. Sci.*, vol. 30, no. 4, May 1973, pp. 544-557.
19. Wallace, John M.: Trajectory Slopes, Countergradient Heat Fluxes, and Mixing by Lower Stratospheric Waves. *J. Atmos. Sci.*, vol. 35, no. 3, Mar. 1978, pp. 554-558.
20. Staley, D. O.: On the Mechanism of Mass and Radioactivity Transport From Stratosphere to Troposphere. *J. Atmos. Sci.*, vol. 19, no. 6, Nov. 1962, pp. 450-467.
21. Reiter, E. R.; and Mahlman, J. D.: Heavy Iodine-131 Fallout Over the Midwestern United States, May 1962. Further Studies on Radioactive Fallout, Tech. Paper No. 70 (Contract AT (11-1) - 1340), Dep. Atmos. Sci., Colorado State Univ., Sept. 1965, pp. 1-53.
22. Lilly, D. K.; Waco, D. E.; and Adelfang, S. I.: Stratospheric Mixing Estimated From High-Altitude Turbulence Measurements. *J. Appl. Meteorol.*, vol. 13, no. 4, June 1974, pp. 488-493.
23. Danielsen, Edwin F.; and Mohnen, Volker A.: Project DUSTORM Report: Ozone Measurements and Meteorological Analyses of Tropopause Folding. ASRC-SUNY-PUB-394 (Contract N00014-76-C-0283), State Univ. of New York at Albany, May 1976. (Available from DDC as AD A032 555.)
24. Mohnen, V. A.; and Reiter, E. R.: International Conference on Oxidants, 1976 - Analysis of Evidence and Viewpoints. Part III. The Issue of Stratospheric Ozone Intrusion. EPA-600/3-77-115, U.S. Environ. Prot. Agency, Dec. 1977.
25. Fabian, P.; and Pruchniewicz, P. G.: Final Report on Project "Tropospherisches Ozon." MPAE-W-100-76-21, Max-Planck-Institut Aeron., May 1976.

26. Reiter, Elmar R.: Stratospheric-Tropospheric Exchange Processes. Rev. Geophys. & Space Phys., vol. 13, no. 4, Aug. 1975, pp. 459-474.
27. Crutzen, Paul J.: Photochemical Reactions Initiated by and Influencing Ozone in Unpolluted Tropospheric Air. Tellus, vol. 26, nos. 1-2, 1974, pp. 47-57.
28. Stewart, Richard W.; Hameed, Sultan; and Pinto, Joseph P.: Photochemistry of Tropospheric Ozone. J. Geophys. Res., vol. 82, no. 21, July 20, 1977, pp. 3134-3140.
29. Pruchniewicz, Paul Gerd: Über ein Ozon-Registriergerät und Untersuchung der zeitlichen und räumlichen Variationen des Troposphärischen Ozons auf der Nordhalbkugel der Erde. Nr. 42, Max-Planck-Institut Aeron., 1970.
30. Dütsch, H. U.; Züllig, W.; and Ling, Ch.: Regular Ozone Observation at Thalwil, Switzerland and at Boulder, Colorado. LAPETH-1, Lab. Atmos. Phys., ETH, Jan. 1970.
31. Chatfield, Robert; and Harrison, Halstead: Ozone in the Remote Troposphere: Mixing Versus Photochemistry. J. Geophys. Res., vol. 81, no. 3, Jan. 20, 1976, pp. 421-423; Reply by William L. Chameides and James C. G. Walker, p. 424.
32. Aldaz, Luis: Flux Measurements of Atmospheric Ozone Over Land and Water. J. Geophys. Res., vol. 74, no. 28, Dec. 20, 1969, pp. 6943-6946.
33. Fabian, Peter; and Junge, Christian E.: Global Rate of Ozone Destruction at the Earth's Surface. Arch. Meteorol., Geophys. & Bioklimatol, Ser. A, vol. 19, no. 2, 1970, pp. 161-172.
34. Briggs, J.; and Roach, W. T.: Aircraft Observations Near Jet Streams. Q. J. R. Meteorol. Soc., vol. 89, no. 380, Apr. 1963, pp. 225-247.
35. Penn, Samuel: Temperature and Ozone Variations Near Tropopause Level Over Hurricane Isbell October 1964. J. Appl. Meteorol., vol. 5, no. 4, Aug. 1966, pp. 407-410.
36. Kuhn, Peter M.; Komhyr, Walter D.; Harris, Thomas B.; Allee, Paul A.; and Marlatt, W. E.: Observations of the Vertical Transport of Water Vapor, Ozone, and Aerosols by Thunderstorms. NOAA Tech. Rep. ERL 253-APCL 25, U.S. Dep. Commer., Feb. 1973.
37. Interhemispheric Survey of Minor Upper Atmospheric Constituents During October-November 1976. NASA TM X-73630, 1977.
38. Falconer, Phillip D.: The Global Atmospheric Sampling Program: The Prospects for Establishing a Tropospheric Ozone Budget From Commercial Aircraft Data. ASRC Publ. No. 655, State Univ. of New York at Albany, Aug. 1977.

39. Pruchniewicz, P. G.; Tiefenau, H.; Fabian, P.; Wilbrandt, P.; and Jessen, W.: The Distribution of Tropospheric Ozone From Worldwide Surface and Aircraft Observations. Proceedings of International Conference on Structure, Composition and General Circulation of the Upper and Lower Atmospheres and Possible Anthropogenic Perturbations. Volume I, Int. Assoc. of Meteorol. & Atmos. Phys., 1974, pp. 439-451.
40. Osechkin, V. V.: Possibility of Investigating the Spatial Distribution of Atmospheric Ozone With the Aid of an Ozonometer Installed in the Cockpit of an Aircraft. Meteorol. & Hidrol., no. 2, Feb. 1974, pp. 103-107.
41. Danielsen, Edwin F.: Project Springfield Report. Contract DA-49-146-XZ-079, Isotopes, Inc., July 15, 1964. (Available from DDC as AD 607 980.)
42. Danielsen, E. F.; Bergman, K. H.; and Paulson, C. A.: Radioisotopes, Potential Temperature and Potential Vorticity - A Study of Stratospheric-Tropospheric Exchange Processes. Dep. Meteorol. & Climatol., Univ. of Washington, 1962.
43. Danielsen, E.; Bleck, R.; Shedlovsky, J.; Wartburg, A.; Haagenson, P.; and Pollock, W.: Observed Distribution of Radioactivity, Ozone, and Potential Vorticity Associated With Tropopause Folding. J. Geophys. Res., vol. 75, no. 12, Apr. 20, 1970, pp. 2353-2361.
44. Singh, Hanwant B.; Ludwig, Francis L.; and Johnson, Warren B.: Ozone in Clean Remote Atmospheres: Concentrations and Variabilities. CRC-APRAC CAPA-15-76, Coord. Res. Council, Inc., June 1977. (Available from NTIS as PB 272 290.)
45. Hering, Wayne S., ed.: Ozonesonde Observations Over North America. Vol. I. AFCRL-64-30(1), U.S. Air Force, Jan. 1964. (Available from DDC as AD 435 873.)
46. Hering, Wayne S.; and Borden, Thomas R., Jr., eds.: Ozonesonde Observations Over North America. Vol. 2. AFCRL-64-30(II), U.S. Air Force, July 1964. (Available from DDC as AD 604 880.)
47. Hering, Wayne S.; and Borden, Thomas R., Jr.: Ozonesonde Observations Over North America. Vol. 3. AFCRL-64-30(III), U.S. Air Force, Aug. 1965. (Available from DDC as AD 623 018.)
48. Hering, Wayne S.; and Borden, Thomas R., Jr.: Ozonesonde Observations Over North America. Vol. 4. AFCRL-64-30(IV), U.S. Air Force, Dec. 1967. (Available from DDC as AD 666 436.)
49. The Natural Stratosphere of 1974. CIAP Monograph 1. DOT-TST-75-51, U.S. Dep. Transp., Sept. 1975. (Available from NTIS as PB 246 318.)
50. Goldan, P. D.; Bush, Y. A.; Fehsenfeld, F. C.; Albritton, D. L.; Crutzen, P. J.; Schmeltekopf, A. L.; and Ferguson, E. E.: Tropospheric N₂O Mixing Ratio Measurements. J. Geophys. Res., vol. 83, no. C2, Feb. 20, 1978, pp. 935-939.

51. Inn, Edward C. Y.; Tyson, Bennett J.; and Arvesen, John C.: Atmospheric Halocarbon Experiment. Interhemispheric Survey of Minor Upper Atmospheric Constituents During October–November 1976. NASA TM X-73630, 1977, pp. 79–93.
52. Davis, D. D.; Heaps, W.; and McGee, T.: Direct Measurements of Natural Tropospheric Levels of OH Via an Aircraft Borne Tunable Dye Laser. Geophys. Res. Lett., vol. 3, no. 6, June 1976, pp. 331–333.
53. Stedman, D. H.; Ritter, J.; and Kelly, T.: Measurements of Background Levels of Tropospheric NO_x. Univ. of Michigan paper presented before the Division of Environmental Chemistry, American Chemical Society (Anaheim, California), Mar. 1978.
54. Bischof, Walter: Ozone Measurements in Jet Airliner Cabin Air. Water, Air, & Soil Pollut., vol. 2, no. 1, Mar. 1973, pp. 3–14.
55. Perkins, Porter J.: Global Measurements of Gaseous and Aerosol Trace Species in the Upper Troposphere and Lower Stratosphere From Daily Flights of 747 Airliners. NASA TM X-73544, 1976.
56. Holdeman, James D.; and Falconer, Phillip D.: Analysis of Atmospheric Ozone Measurements Made From a B-747 Airliner During March 1975. NASA TN D-8311, 1976.
57. Steinberg, Robert: Role of Commercial Aircraft in Global Monitoring Systems. Science, vol. 180, no. 4084, Apr. 27, 1973, pp. 375–380.
58. Holdeman, J. D.; Nastrom, G. D.; and Falconer, P. D.: An Analysis of the First Two Years of GASP Data. NASA TM-73817, 1977.
59. Junge, Christian E.: Global Ozone Budget and Exchange Between Stratosphere and Troposphere. Tellus, vol. 14, no. 4, Nov. 1962, pp. 363–377.
60. Fabian, P.; and Pruchniewicz, P. G.: Meridional Distribution of Ozone in the Troposphere and Its Seasonal Variations. J. Geophys. Res., vol. 82, no. 15, May 20, 1977, pp. 2063–2073.
61. Fabian, P.: A Theoretical Investigation of Tropospheric Ozone and Stratospheric-Tropospheric Exchange Processes. Pure & Appl. Geophys., vol. 106–108, no. 5–7, 1973, pp. 1044–1057.
62. Pruchniewicz, P. G.: The Average Tropospheric Ozone Content and Its Variation With Season and Latitude as a Result of the Global Ozone Circulation. Pure & Appl. Geophys., vol. 106–108, no. 5–7, 1973, pp. 1058–1073.
63. Chatfield, Robert; and Harrison, Halstead: Tropospheric Ozone. 2. Variations Along a Meridional Band. J. Geophys. Res., vol. 82, no. 37, Dec. 20, 1977, pp. 5969–5976.

64. Chatfield, R.; and Rasmussen, R. A.: An Assessment of the Continental Lower Tropospheric Ozone Budget. International Conference on Photochemical Oxidant Pollution and Its Control. Proceedings: Volume I, Basil Dimitriades, ed., EPA-600/3-77-001a, U.S. Environ. Prot. Agency, Jan. 1977, pp. 121-136. (Available from NTIS as PB-264 232.)
65. Dimitriades, Basil; and Altshuller, A. Paul: International Conference on Oxidant Problems: Analysis of the Evidence/Viewpoints Presented. Part I. Definition of Key Issues. J. Air Pollut. Control Assoc., vol. 27, no. 4, Apr. 1977, pp. 299-307.
66. Lovill, James E.: Note on the Variability of Ozone at a High Mountain Location. Arch. Meteorol., Geophys. & Bioklimatol, Ser. A, vol. 19, no. 4, 1970, pp. 439-442.
67. Mohnen, V. A.; Hogan, A.; Whitby, R.; and Coffey, P.: Ozone Measurements in Rural Areas. State Univ. of New York at Albany paper presented at Symposium on the Non-Urban Tropospheric Composition (Hollywood, Florida), Nov. 1976. (Available from DDC as AD A037 360.)
68. Mendonca, Bernard G.: Local Wind Circulation on the Slopes of Mauna Loa. J. Appl. Meteorol., vol. 8, no. 4, Aug. 1969, pp. 533-541.

TABLE I.- ESTIMATES OF THE GLOBAL SINK FOR ATMOSPHERIC OZONE
BY VARIOUS AUTHORS

Author	Data base	Global sink estimate, 10^{12} g-yr ⁻¹
Lettau (1951) ^a	Not specified	51
Paetzold (1955) ^a	Not specified	320 to 640
Kroening & Ney (1962) ^a	Vertical profiles near the Earth's surface	770
Junge (1962) ^a	From theoretical model prediction	470
Brewer & Wilson (1968) ^a	Photochemical calculations	750
Aldaz (1969) ^a	Experimental	1300 to 2100
Fabian & Junge (1970) (ref. 33)	From theoretical model prediction	400 to 710
Fabian & Pruchniewicz (1976) (ref. 25)	From theoretical model prediction	479 to 931

^aDestruction flux rates quoted have been adapted from data compilation by Fabian and Junge (ref. 33).

TABLE II.- AIRCRAFT MEASUREMENTS OF OZONE IN THE FREE TROPOSPHERE (ABOVE THE PLANETARY BOUNDARY LAYER)

[From Singh et al. (ref. 44)]

Locations	Dates	Sources	Average O ₃ concentrations (free troposphere), ppbv	Number of flights considered
Canton, Ohio	July 2-22, 1976	Washington State University at Pullman	51 ± 13	10
Groton, Conn.	July 15-30, 1975	Washington State University at Pullman	43 ± 10	21
	August 6-19, 1975	Washington State University at Pullman	51 ± 14	16
Boston, Mass.	August 12-27, 1975	U.S. Environmental Protection Agency	56 ± 8	30
New Brunswick, N.J. (and vicinity)	August 10-20, 1975	Interstate Sanitation Commission of New York	53 ± 14	62
Bridgford, Conn. (and vicinity)	July 20-27, 1975	Battelle Columbus Lab.	56 ± 8	5
	August 5-20, 1975	Battelle Columbus Lab.	56 ± 9	5

TABLE III.- RECENT TROPOSPHERIC MEASUREMENTS OF OZONE-REACTIVE SPECIES
FROM DEDICATED RESEARCH PLATFORMS

Compound	Reaction chain	Data base	Abundance in free troposphere, ppbv	Reference
N ₂ O	$\text{N}_2\text{O} + \text{O}(^1\text{D}) \rightarrow 2\text{NO}$ $\text{NO} + \text{O}_3 \rightarrow \text{NO}_2 + \text{O}_2$	Interhemispheric survey at 7 to 17 km; six parachute descent profiles	318 ± 2 (Approximate)	50
			306 ± 21 (Northern Hemisphere)	51
			314 ± 39 (Southern Hemisphere)	51
OH	$\text{OH} + \text{O}_3 \rightarrow \text{O}_2 + \text{HO}_2$	Several aircraft flights during October 1975 at 21° N and 32° N	0.28 to 0.70 (Approximate)	52
NO	$\text{NO} + \text{O}_3 \rightarrow \text{NO}_2 + \text{O}_2$	Measurements obtained at Fritz Peak, Colo.	0.1 to 0.3	53
	$\text{NO} + \dot{\text{R}}\text{O}_2 \rightarrow \text{NO}_2 + \dot{\text{R}}\text{O}$			

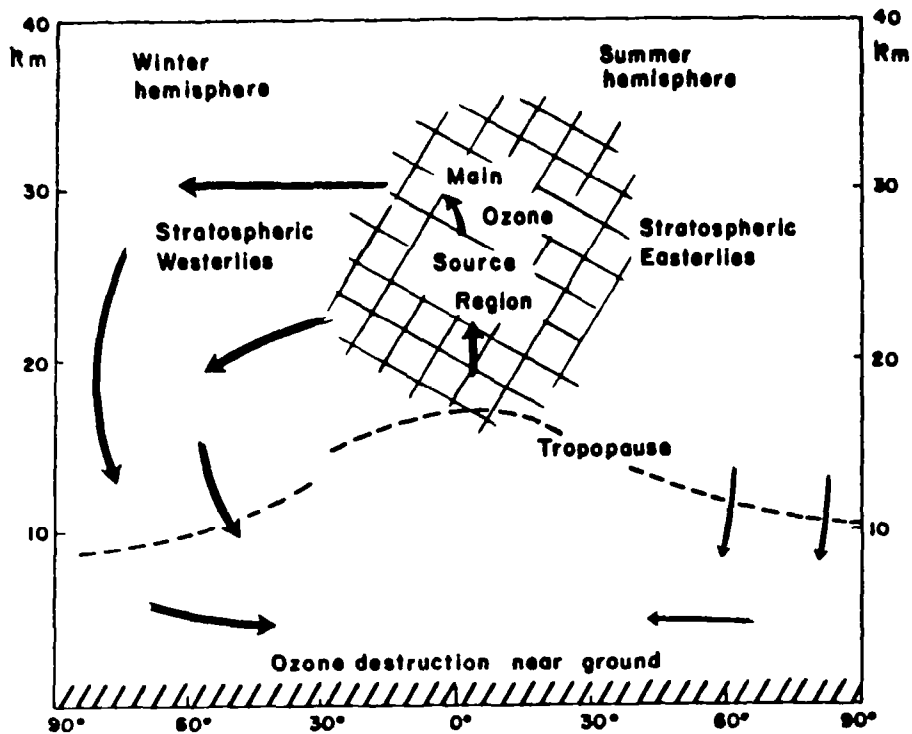


Figure 1.- Tentative model of large-scale ozone fluxes and of seasonal ozone cycle. (From Dütsch (ref. 1), copyrighted by American Geophysical Union; reproduced with permission.)

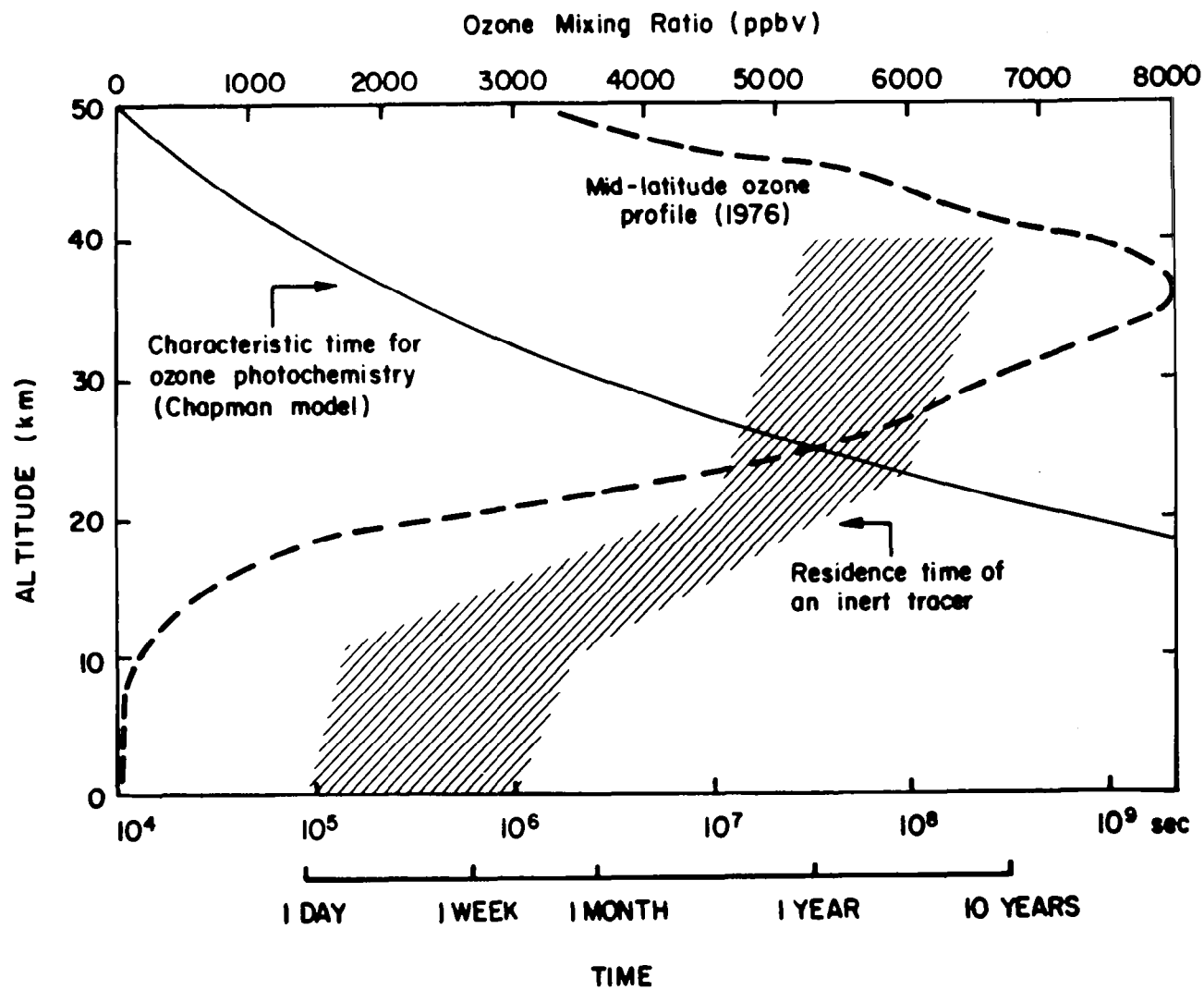


Figure 2.- Characteristic time scales for chemistry and motions in the atmosphere. (Adapted from ref. 2.)

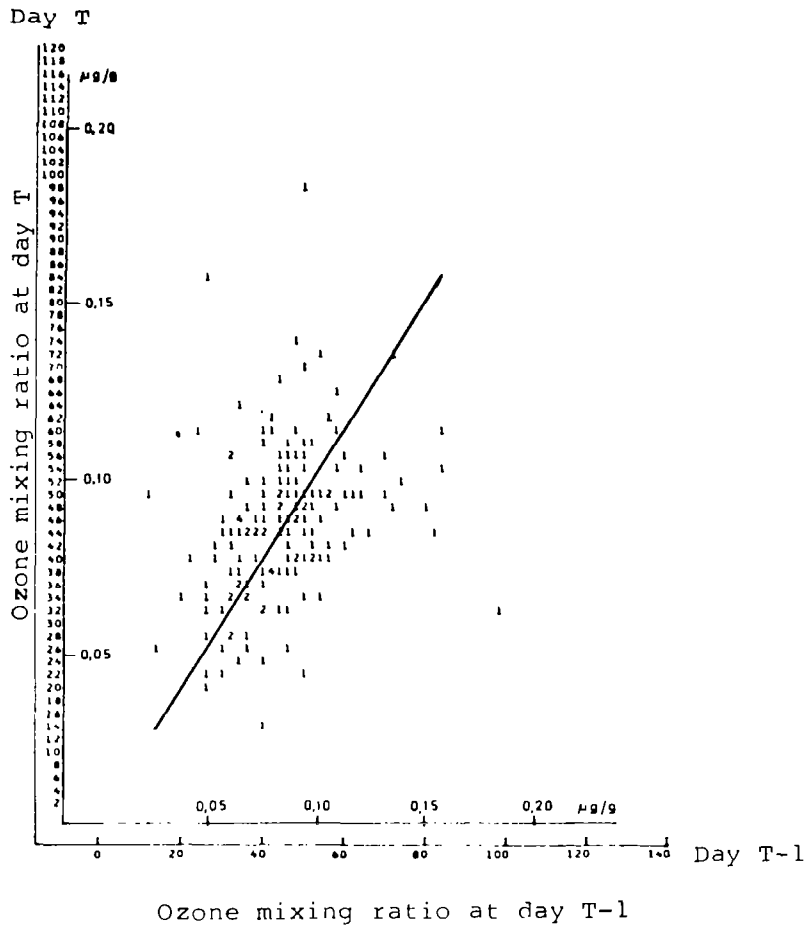


Figure 3.- Correlation between ozone mixing ratio on day T with that on day T - 1 at 400 hPa and 500 hPa levels over Boulder, Colorado. Each of 161 data points consists of a pair of values for days T and T - 1. (From Pruchniewicz (ref. 29) with permission of publisher.)

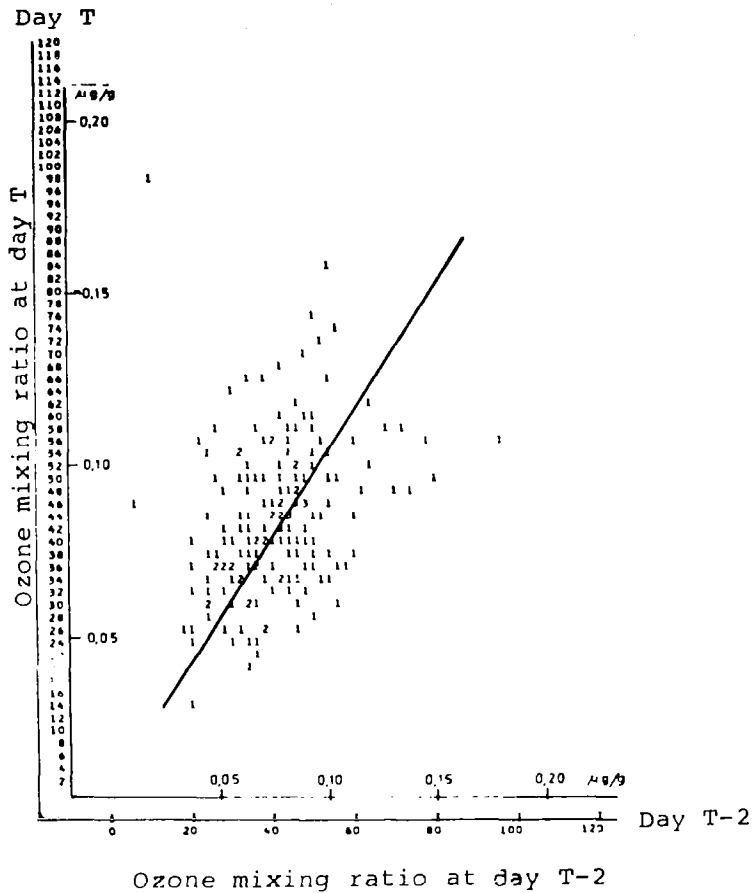
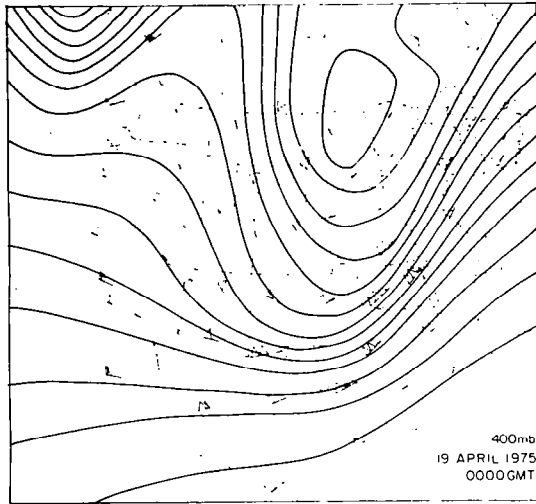
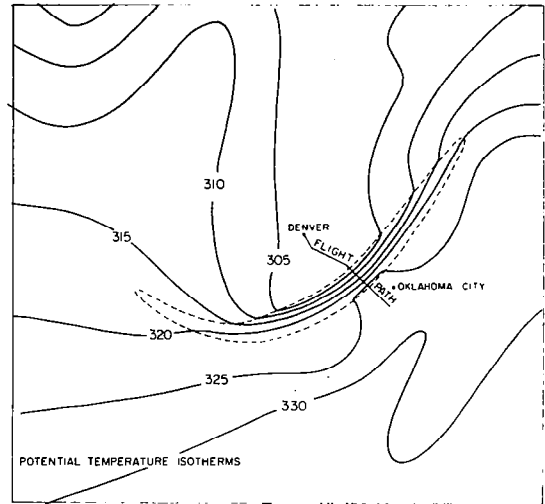


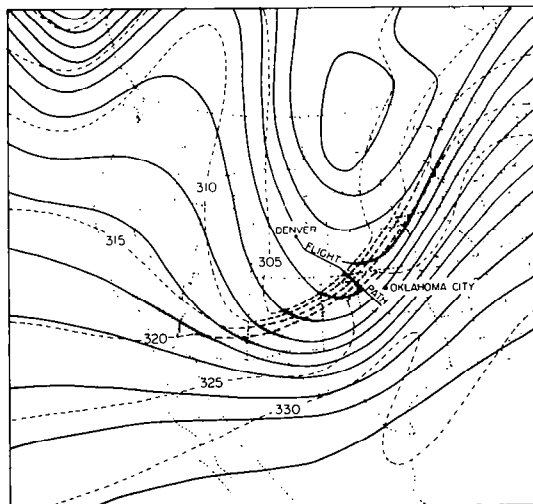
Figure 4.- Correlation between ozone mixing ratio on day T with that on day T - 2 at 400 hPa and 500 hPa levels over Boulder, Colorado. Each of 174 data points consists of a pair of values for days T and T - 2. (From Pruchniewicz (ref. 29) with permission of publisher.)



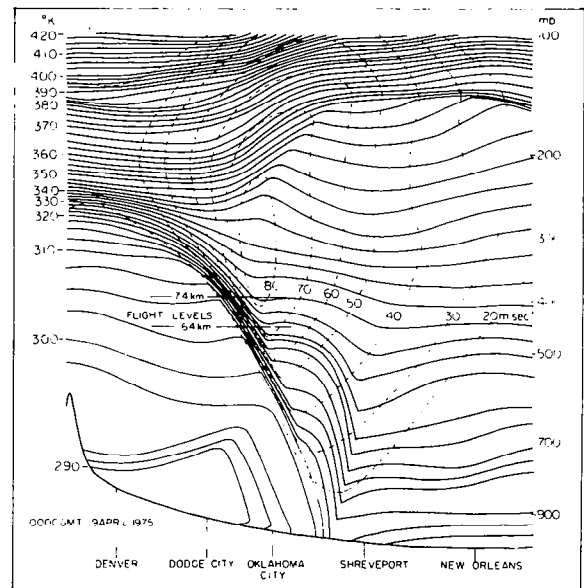
(a) 400 hPa (mb) height field.



(b) Potential temperature isotherms in K at 400 hPa.

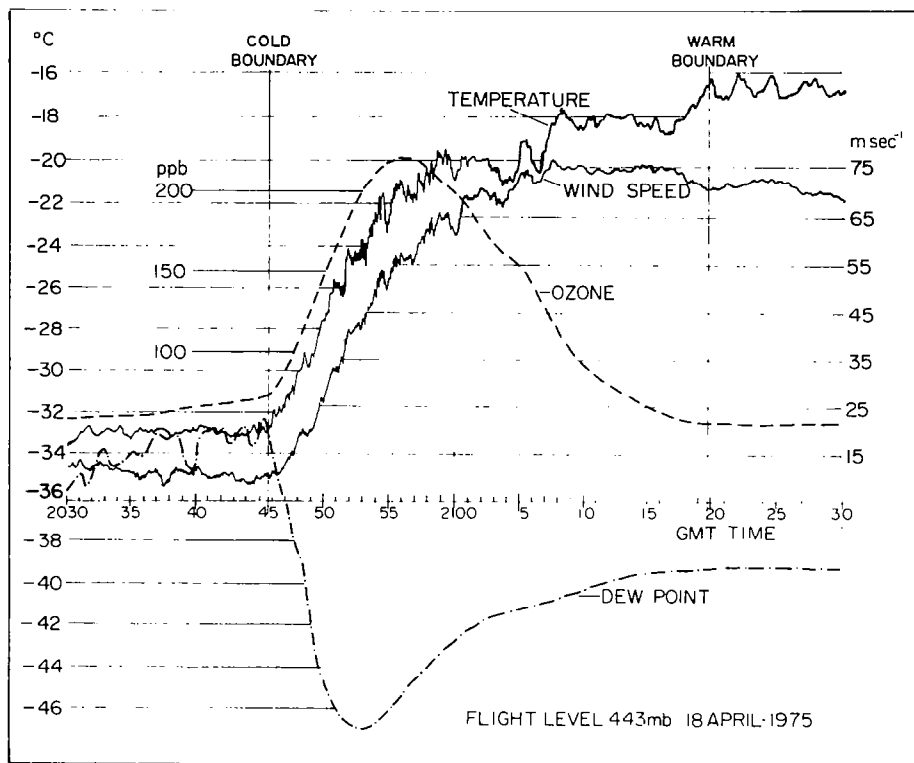


(c) Intersection of folded tropopause with 400 hPa surface.



(d) Vertical cross section of potential temperature (solid lines) and wind speed (dotted lines).

Figure 5.- Meteorological conditions at 00:00 GMT, April 19, 1975, in the upper troposphere associated with tropopause foldings. (From Danielsen and Mohnen (ref. 23).)



(e) Measurements of ozone and other meteorological variables across folded tropopause at flight level of 443 hPa from the National Center for Atmospheric Research Electra aircraft.

Figure 5.- Concluded.

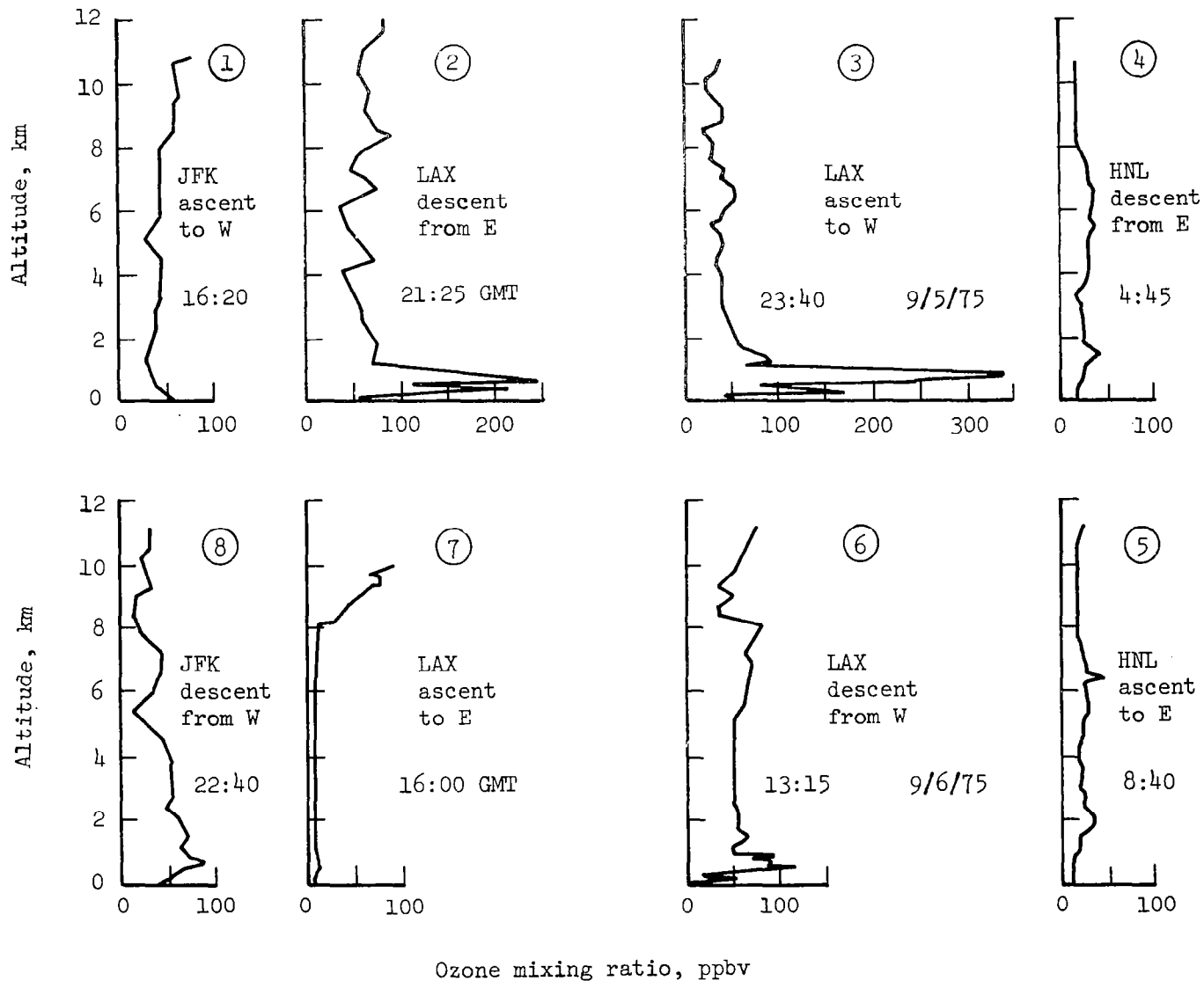


Figure 6.- Vertical ozone mixing ratio profiles obtained on September 5 and 6, 1975, aboard commercial aircraft during ascent from or descent into New York City (JFK), Los Angeles (LAX), and Honolulu (HNL). (From V. Mohnen, unpublished data.)

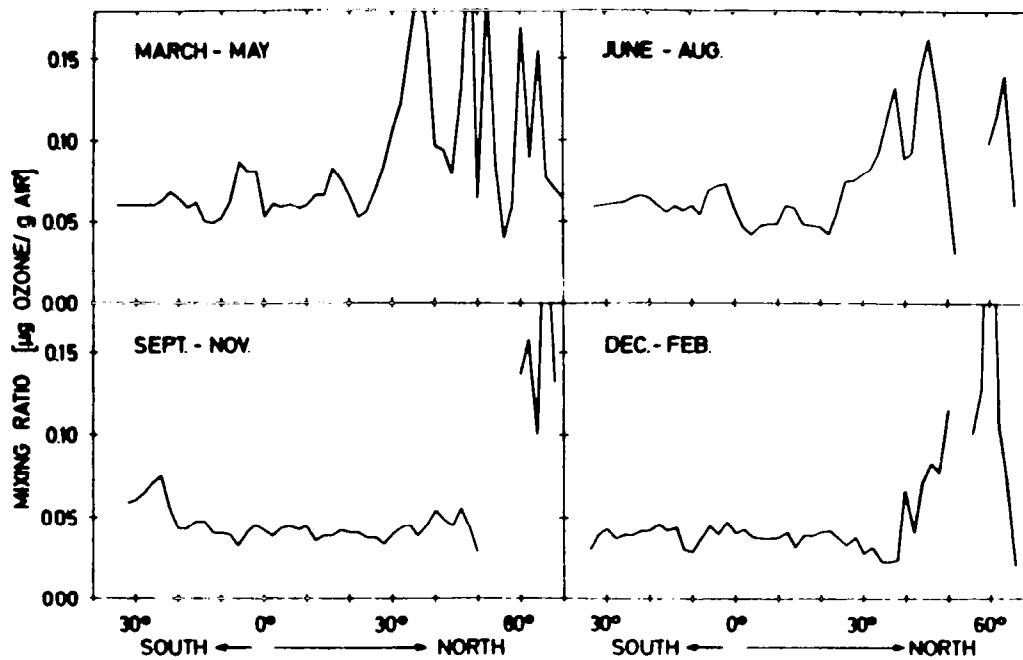


Figure 7.- Latitudinal profiles of mean ozone mixing ratio in four 3-month intervals from aircraft measurements over Europe and Africa. (From Pruchniewicz et al. (ref. 39).)

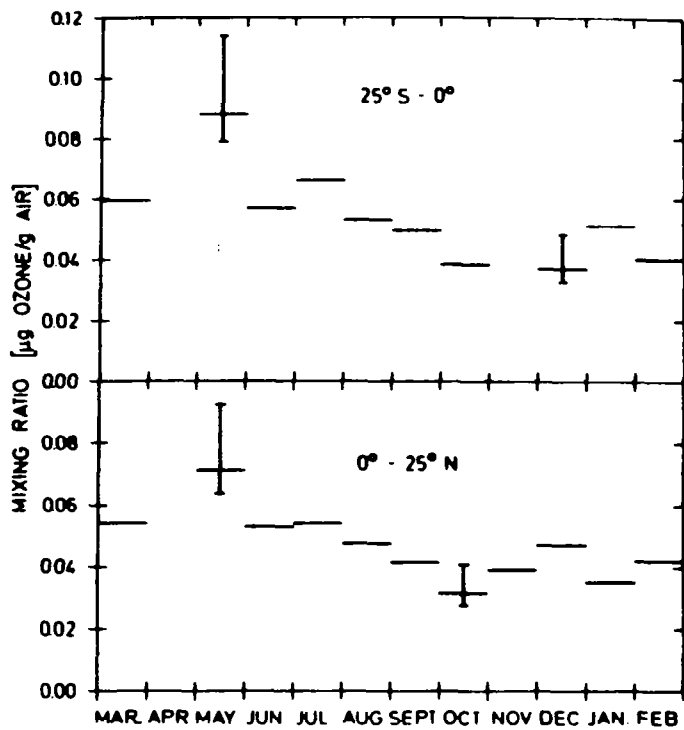


Figure 8.- Seasonal variation of monthly mean tropospheric ozone from aircraft measurements between 25° N and 25° S. (From Pruchniewicz et al. (ref. 39).)

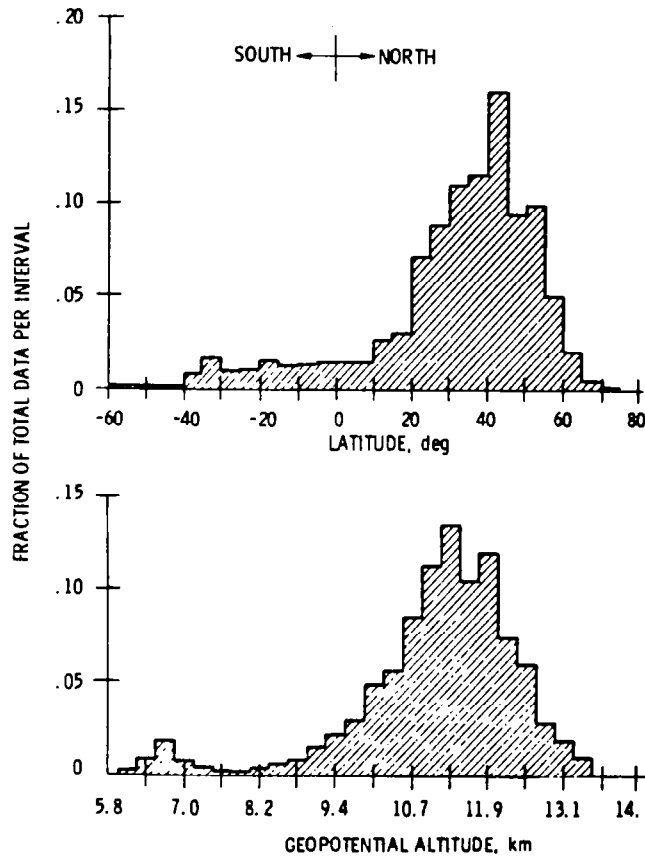
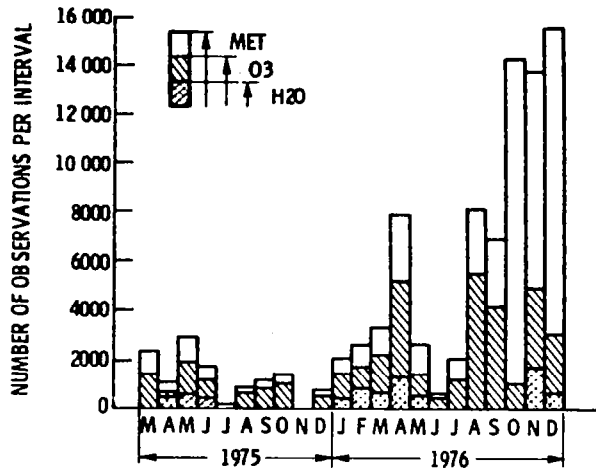
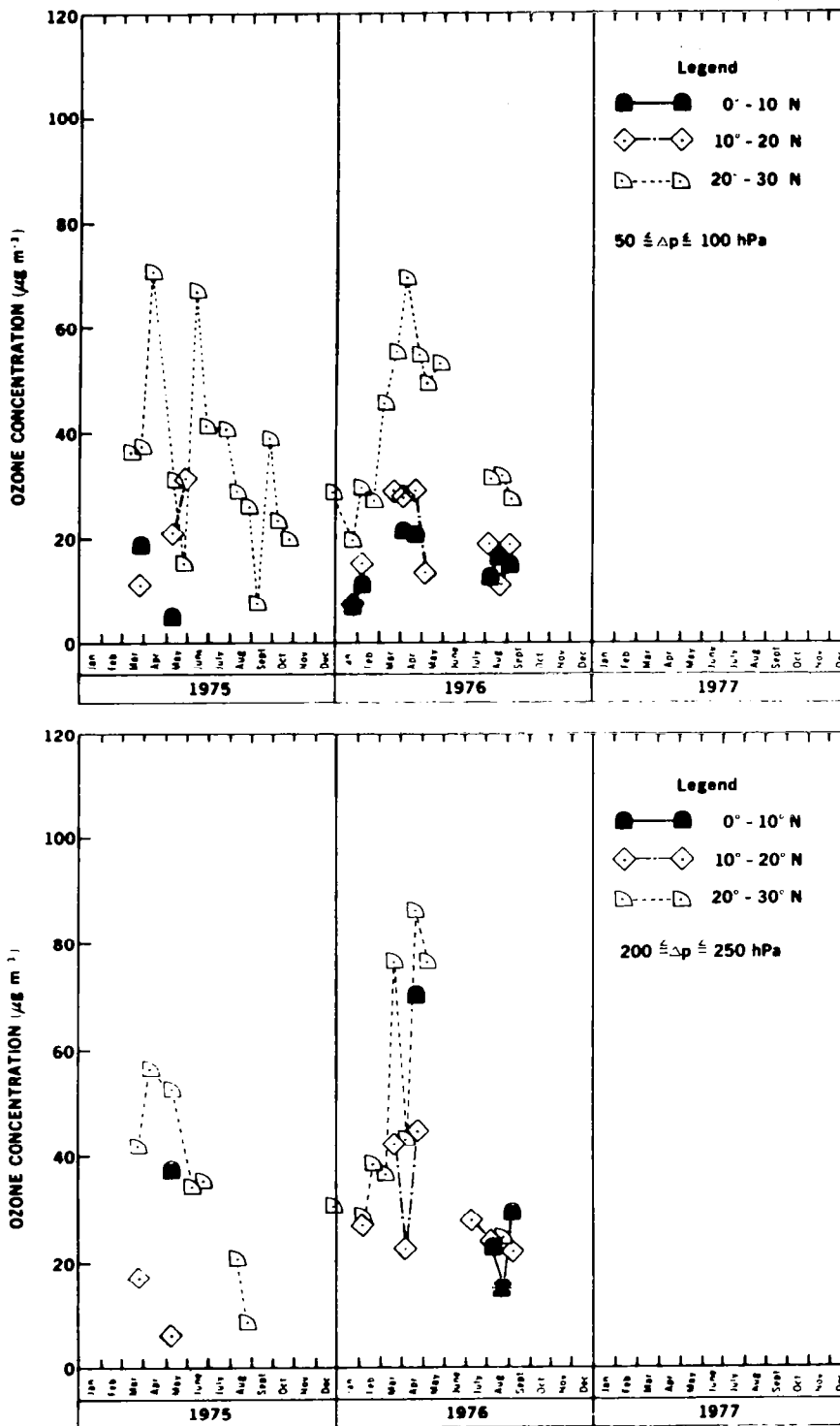
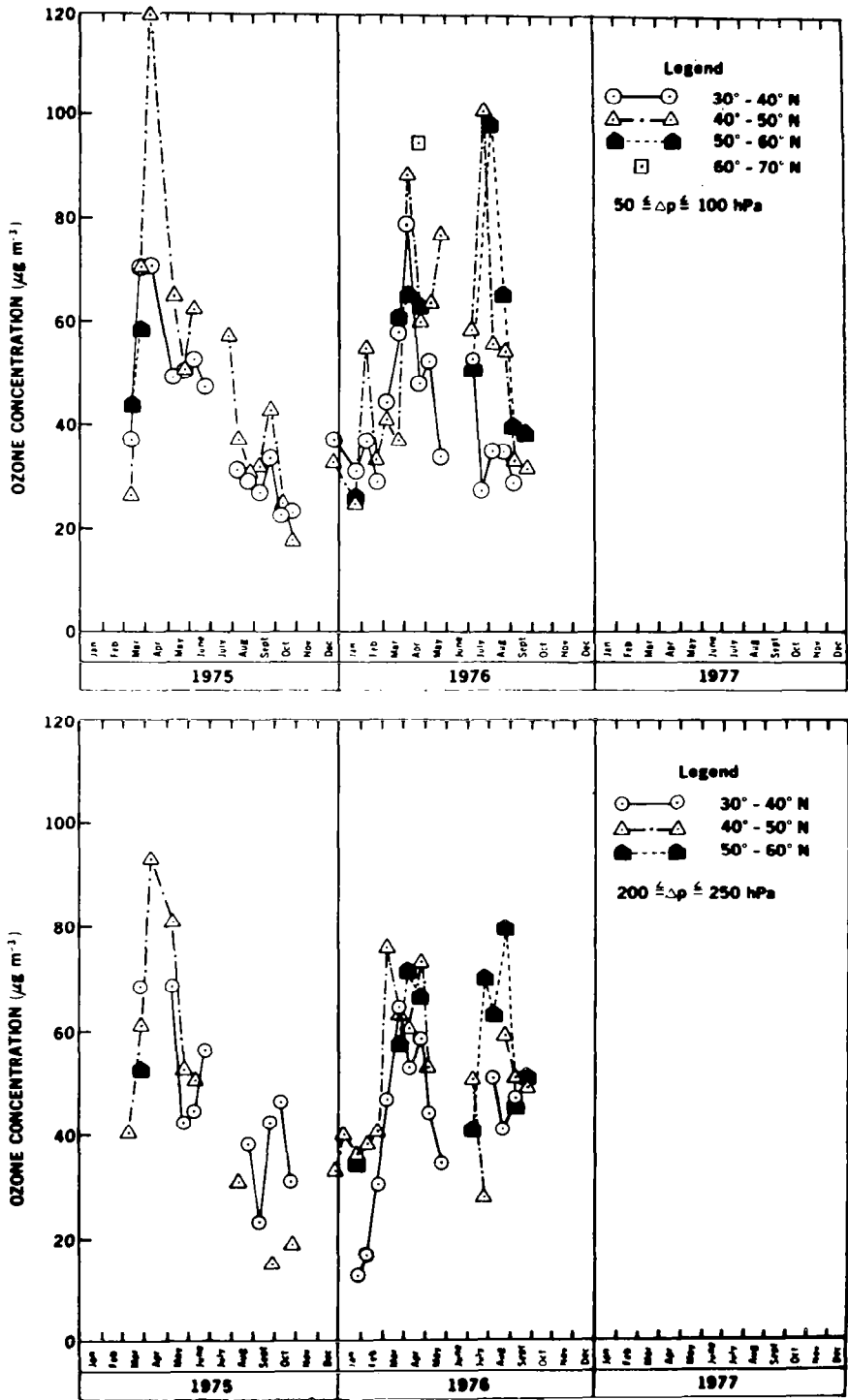


Figure 9.- Distribution of flight and meteorological (MET), ozone (O3), and water vapor (H2O) data by month, latitude, and altitude from commercial B-747 airliners participating in the Global Atmospheric Sampling Program. (From ref. 58.)



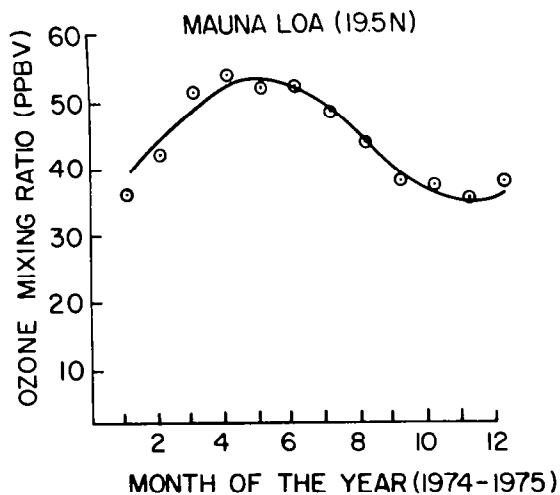
(a) Between 0° N and 30° N.

Figure 10.- Biweekly ozone concentrations ($\mu\text{g}\cdot\text{m}^{-3}$) obtained aboard participating GASP airliners for two pressure intervals, 50 to 100 hPa below tropopause and 200 to 250 hPa below tropopause.

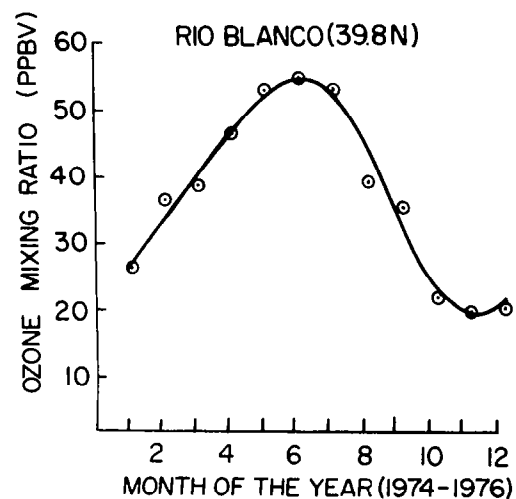


(b) Between 30° N and 70° N.

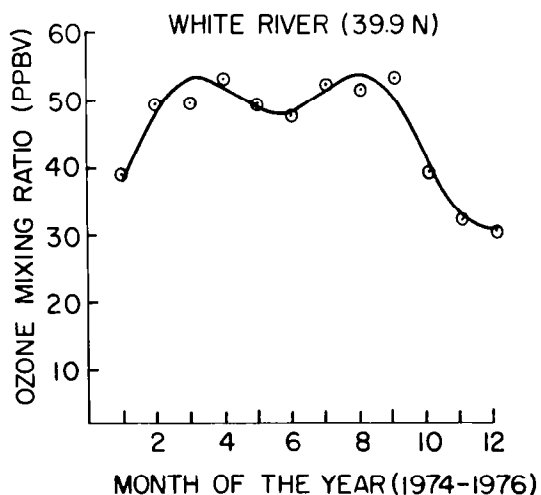
Figure 10.- Concluded.



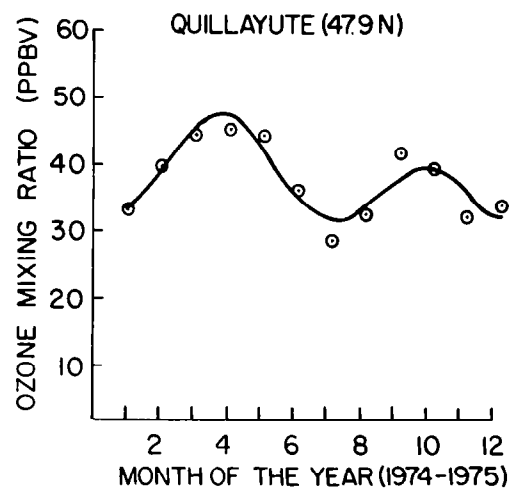
(a) At Mauna Loa, Hawaii.



(b) At Rio Blanco, Colorado.



(c) At White River, Utah.



(d) At Quillayute, Washington.

Figure 11.- Variations of monthly averages of daily 1-hour ozone maxima for the years 1974 and 1976. Individual data points have been interpolated from Singh et al. (ref. 44) and fitted by a smoothed harmonic function representing sum of annual and semiannual waves.

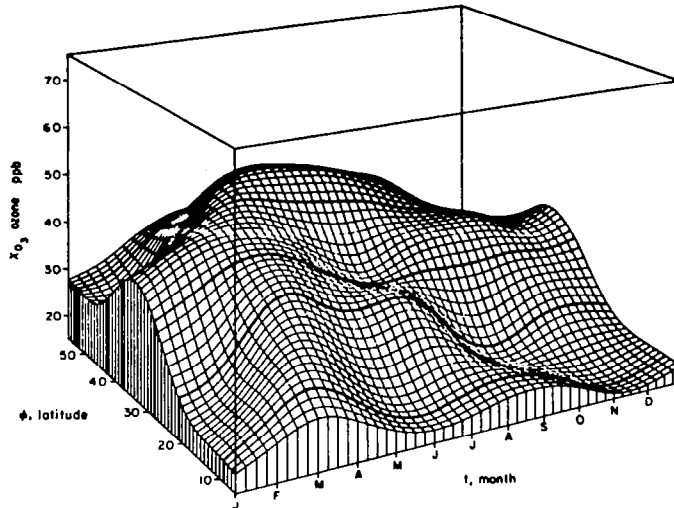


Figure 12.- Latitude-season perspective of ozone mixing ratios at 2 to 3 km above six stations near 75° W longitude. (From Chatfield and Harrison (ref. 63), copyrighted by American Geophysical Union; reproduced with permission.)

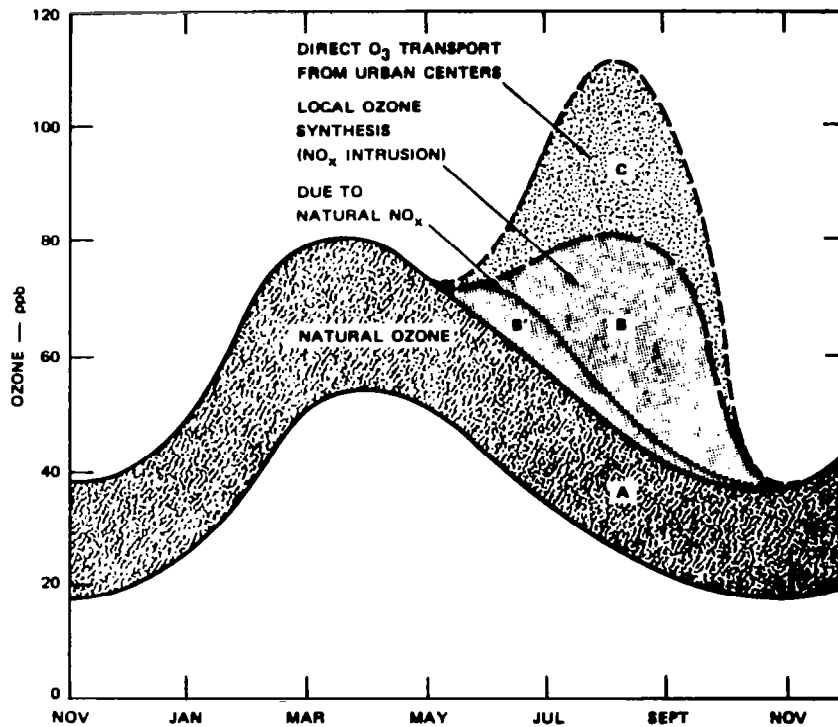


Figure 13.- Idealized sketch of ozone variations at remote observatories. (From Singh et al. (ref. 44).)

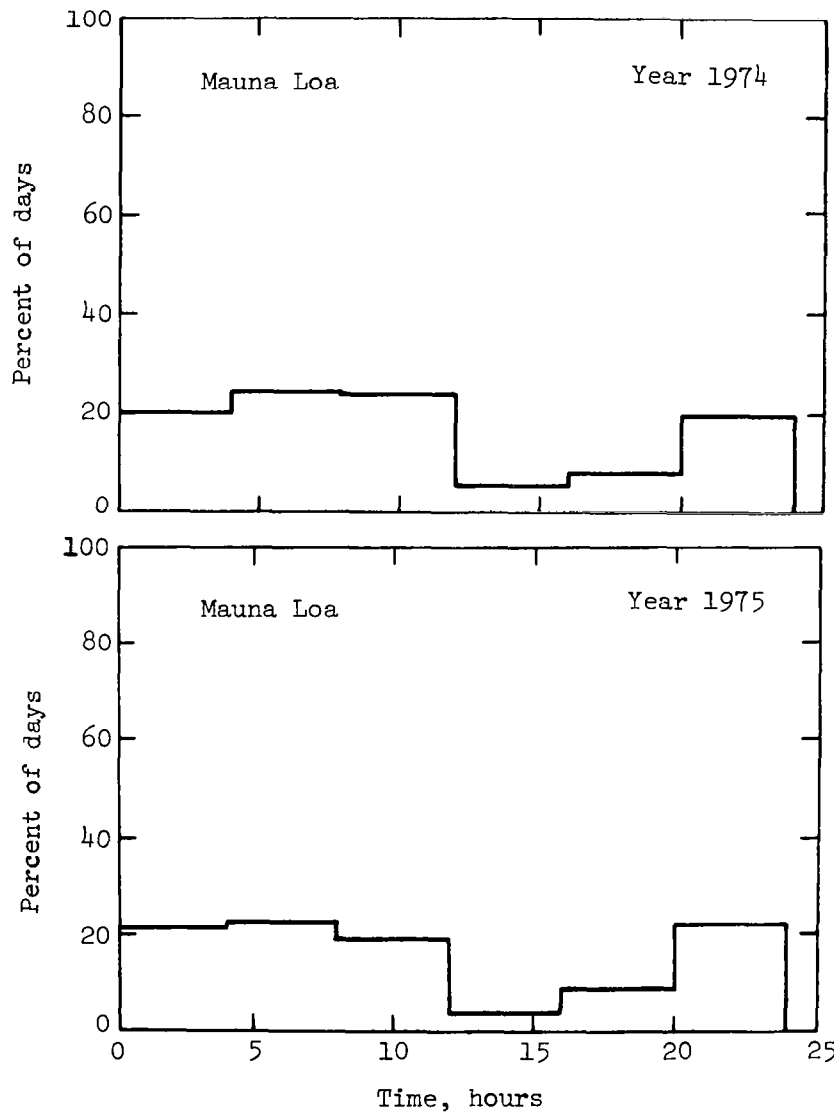
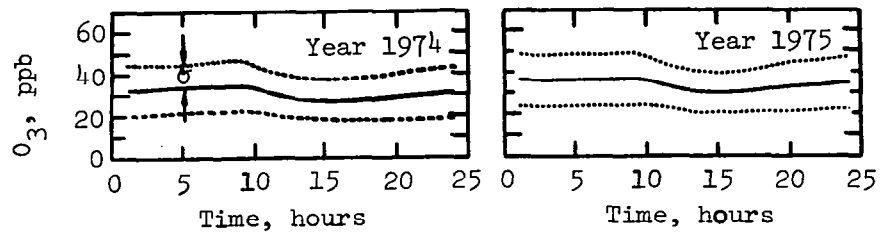


Figure 14.- Yearly average diurnal ozone variations and frequency distributions of daily 1-hour ozone maxima at Mauna Loa, Hawaii, and Whiteface Mountain, New York. Both stations are representative of mountain ozone behavior in rural environments. (From Singh et al. (ref. 44).)

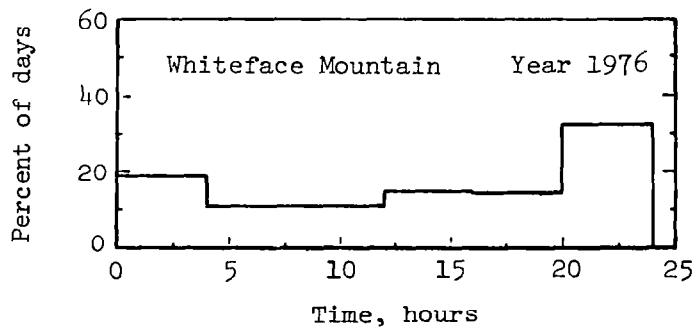
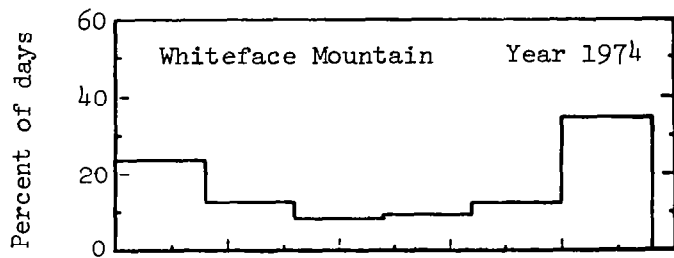
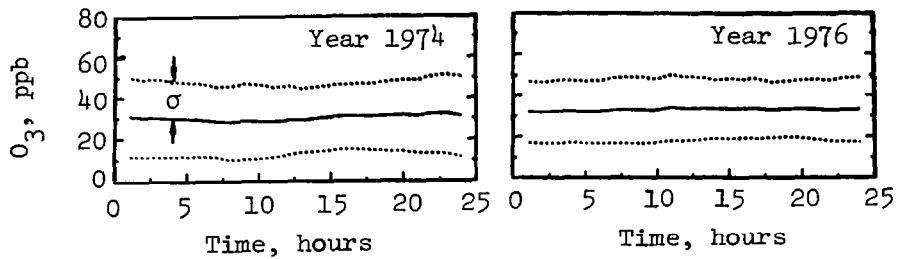


Figure 14.- Concluded.

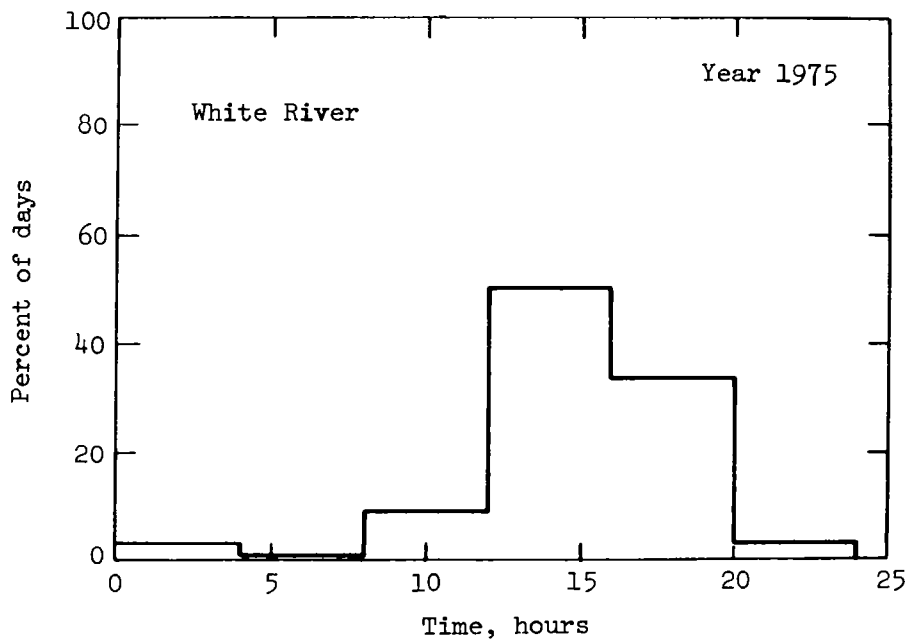
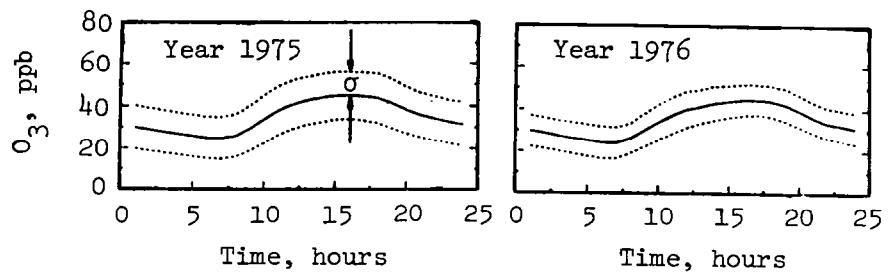


Figure 15.- Yearly average diurnal ozone variations and frequency distributions of daily 1-hour ozone maxima at Quillayute, Washington, and White River, Utah. Both stations are representative of ground-level ozone behavior in rural environments. (From Singh et al. (ref. 44).)

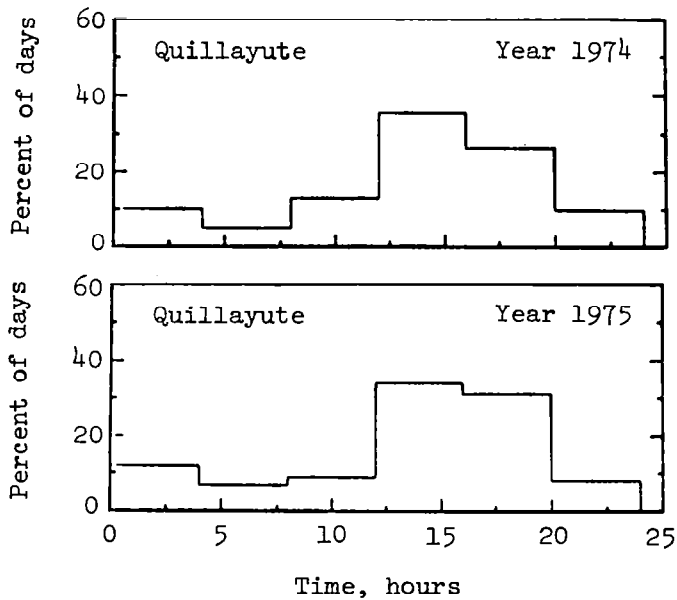
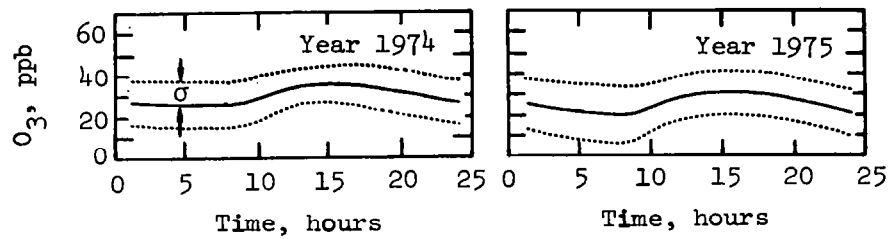


Figure 15.- Concluded.

URBAN PRECURSORS AND THEIR PHOTOCHEMICAL PRODUCTS

T. E. Graedel
Bell Laboratories
Murray Hill, New Jersey

SUMMARY

Many aspects of the photochemical processes in the troposphere near and within urban areas have recently been explored by kinetic computer modeling. Comparison with the results of data analyses indicates that features of and patterns in air quality data can be semiquantitatively reproduced for a variety of geographical and chemical situations. Results are presented for calculations representing urban workdays, urban Sundays, transport and chemistry upwind of, within, and downwind of urban areas, and overwater transport. The effects of incomplete or insufficiently accurate information on the results of photochemical calculations are described. A current limitation in the detailed validation of these theoretical chemical studies is a sparseness of data on reactive free radicals, on inorganic photochemical products, on organic reactants and products, and on certain of the applicable meteorological processes. Appropriate chemical and meteorological measurements needed to alleviate these interpretive limitations on the understanding of urban tropospheric processes are discussed.

INTRODUCTION

An initial determination of air quality in urban atmospheres is provided by measurements of emitted trace species known to be undesirable: carbon monoxide, sulfur dioxide, benzene, and so forth. A more detailed assessment includes evaluations of the presence and concentrations of the chemical products of these precursors. Although the product compounds are crucial constituents of many atmospheric processes, little information is presently available concerning their concentrations, reactions, or lifetimes in ambient air.

A variety of approaches promises to ameliorate this situation. Laboratory studies of individual reactions provide vital information on reaction rates and products. Another technique that has been useful over the years has been the monitoring of products in smog chamber experiments. More recently, improvements in computer codes for kinetic simulations of large chemical systems have resulted in the development of models of the chemistry of the urban atmosphere. The results produced by all these techniques, together with confirmatory field measurements, are necessary for an improved chemical understanding of the atmosphere. Of particular interest from a chemical standpoint are the interrelationships between the precursors and their atmospheric products.

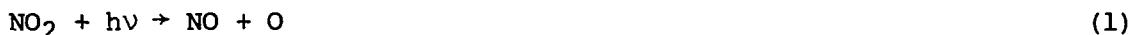
This paper¹ attempts to define the most significant of the precursor-product combinations in the urban atmosphere, together with the chemical intermediates that link them. A survey of recent results of kinetic computer modeling of the northern New Jersey atmosphere is then presented, and the accomplishments and limitations of such approaches are discussed. Finally, suggestions for field measurements of particular interest to the atmospheric chemist are made.

The discussion herein is restricted to the gas phase, despite substantial evidence that certain effects, particularly the removal of oxygenated photochemical products, may be controlled by gas-surface interactions and subsequent aerosol chemistry. Among the important processes are the formation of sulfate and nitrate aerosols, the loss of ammonia to form ammonium salts in aerosols, and the oxidation of alcohols, aldehydes, and ketones to carboxylic acids on aerosol surfaces. A recent review of these topics has been given by the Subcommittee on Ozone and Other Photochemical Oxidants (ref. 1). Further information and the incorporation of aerosol chemistry into kinetic models will doubtless be topics of active research interest within the coming years.

CHEMICAL REACTION CHAINS IN URBAN ATMOSPHERES

The chemical processes in urban atmospheres utilize anthropogenically emitted compounds as precursors for the formation of a variety of more highly oxygenated products. Solar radiation is an important constituent in these chemical reaction chains, since photodissociation of several common emittants produces the reactive free radicals that control most of the chemistry.

A simple schematic overview of a central reaction chain in urban atmospheres is shown in figure 1. The chain utilizes the aldehyde (RCHO), nitric oxide (NO), and hydrocarbon (HC) species that are common anthropogenic emittants to produce large numbers of free radicals and oxygenated products. The complete cycle shown requires only three molecules of the types RCHO, NO, HC and two solar photons ($h\nu_1$ and $h\nu_2$). Perhaps the most interesting species of figure 1 from a chemical standpoint is ozone (O_3). Ozone is not directly emitted from sources but is produced and destroyed by a very complicated series of chemical reactions among and with its precursors. As a result of this complexity, the precursor-product relationships for ozone and other chemicals involved in atmospheric oxidation cycles are not straightforward, although many of the individual reactions have now been studied. The basic equations involved in tropospheric creation and destruction are



¹Much of the work discussed herein was done in collaboration with the author's colleagues at Bell Laboratories: W. S. Cleveland, D. Edelson, L. A. Farrow, R. S. Freund, B. Kleiner, K. B. McAfee, and T. A. Weber.



where M signifies a third body which acts to stabilize the reaction. The first equation demonstrates that solar radiation ($h\nu$) is required for ozone formation; the third that ozone destruction by NO is a direct process. Since NO is the principal oxide of nitrogen emitted by combustion sources, ozone is preferentially removed near strong combustion sources and preferentially formed by oxidized products when away from those sources. In addition to the effects of NO and NO₂, it has been surmised that hydrocarbon emissions could affect ozone concentrations, since peroxy radicals (RO₂·) of the hydrocarbons provide a means for oxidizing NO to NO₂ without the ozone loss involved in reaction (3):



Calculational results pertaining to this topic will be discussed later in this paper.

Most of the products of urban photochemistry do not appear to be subject to the cyclic oxidation-reduction sequences characteristic of ozone. Rather, their reactions proceed unremittingly in the direction of further oxidation, forming low-vapor-pressure compounds whose fate is likely to be deposition on aerosols or on boundary-layer surfaces. Some of these chains are shown in figure 2. Emission of the precursors SO₂, NO, and hydrocarbons (HC) is followed by initial oxidation, largely through free-radical reactions. (The reactions shown are specific in the cases of SO₂ and NO but merely representative of typical processes for the chemically diverse hydrocarbon compounds.) A second oxidation step, which may also be through a free-radical process, produces inorganic acids from the inorganic precursors. For the organic species, the reaction chains are longer and the products more numerous; acrolein and peroxyacetyl nitrate (PAN), as shown in figure 2, are among the products. More detailed discussions of organic chemical chains in urban atmospheres are given by Demerjian et al. (ref. 2), the Panel on Vapor-Phase Organic Pollutants (ref. 3), Graedel et al. (ref. 4), and Heicklen (ref. 5).

The four subdivisions of figure 2 provide a useful insight into the present status of atmospheric measurement capabilities. Many of the emittants have been extensively measured at a variety of tropospheric locations; thus, information on their emission fluxes and ambient lifetimes is available. For relatively unreactive species, of which carbon monoxide is perhaps the prime example, the measurements serve in addition as tracers of meteorological transport and diffusion processes.

The initial oxidation products of figure 2 have a diverse measurement status. Nitrogen dioxide (NO₂) is widely monitored; the remainder have been seldom or never detected (in part because of their high reactivity and short lifetimes). The final oxidation products have been measured infrequently. The same is true of the chemical constituents of aerosols.

Thus, it is possible to categorize the species of figure 2 (and other similar species not shown) as potentially providing insight into (1) emission and dispersion of trace atmospheric constituents, (2) initial chemical reactions, (3) final products of gas-phase chemical chains, and (4) products of gas-aerosol

interactions. The successful description of each of these processes is required for a comprehensive understanding of the chemistry of the urban troposphere.

KINETIC PHOTOCHEMICAL MODELS

The details of urban photochemistry involve the complex and time-varying interplay of chemical kinetics, contaminant emissions, and bulk airflow. Modeling of these processes thus requires appropriate descriptions of both chemistry and meteorology and of the nonchemical source and sink processes that are involved. The calculations to be described in this paper are primarily intended to study the chemical details. For this reason, a large reaction set has been constructed which can yield information about many minor constituents as well as provide calculated curves for comparison with data on those species for which measurements have been made. This set consists of 143 reactions in 76 species and has been presented by Graedel et al. (ref. 4). It includes extensive descriptions of O-H-N and sulfur chemistry, together with a representation of the chemistry of atmospheric hydrocarbons and their products. The organic compounds that are specifically treated are methane, ethane, propylene, and the aliphatic aldehydes. In addition to the commonly measured emittants and products, the chemical set treats specifically a number of photochemical products of relatively low vapor pressure: the inorganic acids HNO_3 and H_2SO_4 , the organic acids HCOOH and CH_3COOH , the alcohols CH_3OH and $\text{CH}_3\text{CH}_2\text{OH}$, a number of organic nitrates, and a variety of other species.

The interactions of aerosols and gases in the atmosphere are imperfectly understood yet are vital to a complete description of urban photochemistry. Although the techniques for including an assessment of these interactions in a computational representation of the troposphere are not well developed, a key to inclusion of heterogeneous atmospheric chemistry is the realization that pure inert solid particles may be a rarity in the atmosphere and that the chemically inert particle core is in most or all cases surrounded by a hygroscopic layer (Winkler (ref. 6)). This layer, upon contact with water vapor, will form a solution with an equilibrium vapor pressure suitably depressed from that of pure water so that the aqueous layer is stable. Thus, atmospheric aerosols may be accurately represented as solid core particles with water shells (perhaps only a few monolayers thick during low humidity) rather than as particles with solid surfaces. The functional result of this deduction is that the aerosol-gas interaction may be treated by gas-liquid, as opposed to gas-solid, interface techniques. Graedel et al. (ref. 7) have established that the amounts of stable atmospheric gases absorbed in the aerosol are negligible fractions of the total gas-phase concentrations and can thus be neglected for atmospheric chemical purposes (but not necessarily for considerations of the chemistry within the aerosols themselves). The interactions between radicals and water-covered aerosols are likely to be substantially more efficient than the interactions between free radicals and stable gases. It appears certain that the inorganic radicals, such as $\text{HO}_2\cdot$ and $\text{HO}\cdot$, will be instantly absorbed on impact; this is also extremely likely for other radicals. In this initial formulation, therefore, it has been assumed that all radicals will be absorbed into aerosols on impact, a conclusion that has been reached independently by Warneck (ref. 8). The resulting concept for aerosol-gas interaction is indicated in figure 3.

The computational architecture that is utilized to represent northern New Jersey is based on a matrix of geographical areas in which each matrix element is a rectangularized transformation of the dimensions of a county. The flow of gases from one matrix element to the next is controlled by the local wind velocity and direction. In the computations discussed here, an average diurnal wind flow pattern derived from measurements at Newark Airport (Essex County) on summer days of normal convective mixing has been used. The variations in mixing height are specified by a function derived from lidar measurements of the atmospheric aerosol. The chemical species within each reaction volume are assumed to be fully mixed.

Inventories for emission of trace contaminants have been compiled on a countywide basis. Each of the counties is thus treated as a "reaction volume" with source terms corresponding to the emission data. Emissions attributable to mobile sources are varied in accordance with local traffic density functions, and those for power plants in accordance with energy generation patterns. Other emissions are regarded as constant with time.

The elements utilized in the computations are (from west to east, in the typical direction of the summer wind flow and that used in the calculations) Morris County (a semirural county with low anthropogenic emissions), Essex County (a suburban county with moderate anthropogenic emissions), and Hudson County (an urban county with high anthropogenic emissions). A schematic diagram of this meteorological and geographical approach is shown in figure 4.

URBAN PHOTOCHEMISTRY

Workdays

Computations representing the chemistry of the troposphere on sunny summer workdays with westerly wind flow have been carried out for Morris, Essex, and Hudson Counties and the results for Hudson County compared with an extensive set of air quality data from a monitoring site in Bayonne (Hudson County). The data values that result for O_3 , NO, NO_2 , and SO_2 are plotted in figure 5, together with the diurnal concentration patterns resulting from the calculations. The computed diurnal curve for NO demonstrates good time coincidence with the measured peak and therefore indicates the general appropriateness of the emission terms in the computation and the NO removal reactions in the chemical set. NO_2 decreases at sunrise as the volume of the mixed layer rapidly increases. The principal NO removal paths involve oxidation to NO_2 , and it is therefore satisfying to find a 9 a.m. NO_2 peak with temporal agreement between computations and measurements. The computations also reproduce the NO_2 increase following sunset, which reflects both the lowered depth of the mixed layer and the absence of NO_2 photodissociation. The results of the model for the hours following sunset appear to be too low for both NO and NO_2 . This occurs because of the gradual termination of the vigorous mixing conditions that were prevalent in the sunlit hours. The ground-level measurements thus reflect the ground-level concentrations to a greater degree than the altitude-averaged concentrations of the model.

The best evidence for the general correctness of the extensive chemical model is provided by the diurnal curves for ozone. Although the patterns differ slightly, both show the afternoon peak typical of measured ozone values, and their integrated diurnal concentrations (i.e., the total amount of ozone that is created) are similar.

One of the characteristic daily patterns of the photochemical smog sequence is the existence of sequential concentration peaks of NO, NO₂, and O₃ (e.g., U.S. Environmental Protection Agency (ref. 9)). This pattern has recently been confirmed for data from northern New Jersey (Cleveland et al. (ref. 10)). Figure 5 demonstrates that such a pattern is also a feature of the computational results.

The computed diurnal variation for the SO₂ concentration follows the observed concentration pattern closely and exceeds the observed mean values by about a factor of 2. Conversion of SO₂ to sulfate in the atmosphere is fairly rapid, however, and a large portion of this conversion may be catalyzed by aerosols from the SO₂ dissolved in them. In the absence of sufficient experimental data to permit kinetic studies of interior aerosol chemistry, it is impossible to calculate the magnitude of such an effect. In lieu of such an approach, however, the "sticking coefficient" between SO₂ and aerosol surfaces that would be required for the diurnal calculations to reproduce the observed SO₂ concentration data has been calculated. Since additional gas-phase removal mechanisms for SO₂ may, of course, be important, the resulting sticking coefficient is appropriately regarded as an upper limit to the true number. The required value is 0.05; that is, 5 of every 100 gas kinetic collisions between SO₂ molecules and aerosol surfaces result in SO₂ incorporation into the liquid surface layer of the aerosol.

Computational results are available not only for the total diurnal behavior of the major species shown in figure 5 but also for a spectrum of secondary species. In several cases, their concentrations can be compared with measurements in northern New Jersey or elsewhere (refs. 11 to 14). These comparisons, shown in table I, confirm in more detail the basic validity of the model, although for species measured outside New Jersey the comparison must be regarded as an order-of-magnitude confirmation. Nonetheless, the good agreement between the computed and measured concentrations and diurnal patterns for both primary and secondary trace species indicates that the model formulation contains the essence of the chemical and meteorological processes that occur in the urban atmosphere of northern New Jersey.

The results of the urban workday computation have been discussed in detail by Graedel et al. (ref. 4); the discussion need not be repeated here. It is appropriate, however, to list some of the most important conclusions of the work:

- (1) Free-radical reactions are of vital importance for many chemical processes in the urban atmosphere. The oxidation of olefins, for example, is controlled by initial reactions with the hydroxyl radical. The computed peak concentrations of important free radicals have been predicted: HO₂•, 6×10^8 molecules-cm⁻³; CH₃O₂•, 1×10^8 molecules-cm⁻³; HO•, 1×10^6 molecules-cm⁻³.

(2) The aliphatic aldehydes occupy central positions in many chemical chains. They provide the primary urban source for the reactive free radicals and are precursors to such important toxic products as PAN.

(3) The effects of sulfur chemistry on the overall gas-phase chemistry of the urban troposphere do not appear to be of major importance (see also Graedel (ref. 15)). The major influence is the scavenging of odd hydrogen radicals ($\text{HO}\cdot$ and $\text{HO}_2\cdot$) by SO_2 . The importance of oxidized sulfur compounds to aerosol chemistry has not been adequately assessed; however, they may be much more important in that chemical regime.

Sundays

Recent statistical investigations of air quality data have clearly disclosed a tendency for similar average ozone levels on summer Sundays and workdays, despite markedly different traffic patterns (Bruntz et al. (ref. 16) and Cleveland et al. (ref. 17)). The complex relationships among ozone, a photochemical product, and NO , NO_2 , and hydrocarbons, its supposed precursors, have thus been demonstrated to be highly nonlinear. To investigate this situation, the urban workday computation just described is modified to allow a simulation of urban atmospheric chemistry on Sundays. The most important change is the marked difference in motor vehicle emission and power generation functions. Atmospheric aerosol concentrations are lower on Sundays and, perhaps as a result, the solar radiation at ground level is somewhat higher (Cleveland et al. (ref. 17)). In addition to its meteorological effects, the change in aerosol concentration reduces the heterogeneous interactions which affect tropospheric chemistry (Farrow et al. (ref. 18) and Graedel et al. (ref. 7)). The increased solar radiation increases the rate of the photosensitive reactions included in the chemical set.

The diurnal concentration patterns for O_3 , NO , and NO_2 for the workday and Sunday calculations are shown in figure 6. The Sunday calculation reproduces two important characteristics of the Sunday ozone data illustrated by Bruntz et al. (ref. 16): the virtual equivalence of the afternoon ozone peak and the higher ozone values on Sunday morning. The calculation demonstrates higher Sunday evening values not reflected in the data; this discrepancy may be a result of inadequate representation of the heavy traffic flow from New Jersey shore points into the metropolitan area that occurs on summer Sunday evenings.

The rather complex analytical techniques used to interpret the urban Sunday calculations have been presented elsewhere (Graedel (ref. 19) and Graedel et al. (ref. 20)). Their use demonstrates that the near equivalence in urban ozone concentrations on workdays and Sundays results from the near workday-Sunday equivalence of the following factors: tight balance between ozone production through NO_2 photodissociation and ozone scavenging by NO (reactions (1) and (3)), the advection of ozone from less urban areas, and the incorporation of similar quantities of ozone preexisting above the morning mixed layer. The higher levels of NO_2 on workdays increase the rates of the $\text{NO-NO}_2\text{-O}_3$ shuttle reactions but do not significantly alter the similar behavior of odd oxygen on workdays and Sundays. The increased levels of oxides of nitrogen on workdays have other consequences, however. The advective transport of NO_x is somewhat enhanced relative

to Sundays, with a concomitant expansion of the downwind impact of the urban area. In addition, the rates of secondary reactions are higher on workdays, resulting in higher concentrations of organic and inorganic nitrates and concomitant increases in the potential of the atmosphere to cause lachrymation.

AIR TRANSPORT AND AIR QUALITY

The transport of urban air over long distances and its subsequent influence on downwind air quality have been deduced for several years in data from the Los Angeles basin (Altshuller (ref. 21)). More recent investigations have demonstrated that urban plume effects are seen in other geographical areas as well. An example of such work by Cleveland et al. (ref. 22) is shown in figure 7, which illustrates ozone concentrations at different times of day for air monitoring sites throughout the Northeastern United States. The prevailing wind on the day in question was from the southwest (i.e., from Washington, D.C., to Boston). The high ozone concentrations demonstrate the transport of urban air across this region, the peak levels in northern Massachusetts actually occurring after sunset when photochemical ozone production has ceased.

Other trace constituents in the air are also subject to transport effects. The dependence of total particulate matter in Greenwich, Connecticut, on prevailing wind direction is illustrated in figure 8 taken from Bruckman (ref. 23). This particulate matter almost certainly contains both physically and chemically produced components (Cunningham et al. (ref. 24) and Grosjean and Friedlander (ref. 25)) and is thus directly related to studies of chemical precursors and products. Similar results for sulfate aerosol throughout the Northeastern United States have been presented by Lloy et al. (ref. 26).

Photochemical calculations investigating the interesting and important effects of transport on air quality on subcontinental size scales have yet to be performed. On a less ambitious scale, however, the air quality upwind of, within, and downwind of urban areas in northern New Jersey has been modeled by expanding the geographical regime of figure 4. The size of the computational matrix was increased to 6×1 by adding three representative but fictitious counties downwind of the three to which the previous results apply. This procedure was followed because the actual counties downwind of Hudson County (New York City and Long Island and adjacent waters) are associated with certain meteorologically complicating factors, such as the Manhattan "heat island" and the land-sea interfaces with Long Island Sound and the Atlantic Ocean. Such manifestations would interfere with any straightforward examination of the chemical processes and have been avoided. The resulting computational sequence is shown in figure 9. The three added counties are given descriptive names for convenience in referencing: Shopview (emissions flux equal to Essex County without power plants), Deerfield (emissions flux set to estimated natural rates), and Farmland (emissions flux set to estimated natural rates).

The computed peak concentrations of NO , NO_2 , and O_3 for normal emission fluxes are presented in figure 10 for the six-county sequence. As in previous work, the results apply to sunny summer days with west winds of average speed. Two features are immediately apparent: the ozone decrease as the urban area is approached from upwind and the subsequent increase downwind of the urban area.

The effects of advection are also seen, since the flow of oxides of nitrogen from Hudson County results in the highest NO and NO₂ peaks and the lowest O₃ peak occurring in Shopview County, an area of lower emission rates. Further downwind, the effects of dilution and decreased emissions outweigh those of advection. This is consistent with the observation that ozone concentrations in regions of high emission rates are lower than in surrounding, less urban areas (e.g., Spicer (ref. 27)).

For photochemical products other than ozone, it seems appropriate to examine the concentrations at 7 p.m., by which time the bulk of the precursor emissions and product reactions have occurred. Figure 11 shows the concentration behavior of C₃H₆, NO₂, SO₂, and four photochemical products - acrolein, nitric acid, PAN, and SO_x⁻². SO_x⁻² is defined as H₂SO₄ + HSO₃[·], since the present computational formulation does not treat the ultimate fate of the HSO₃[·] radical. (SO_x⁻² is regarded as essentially equal to gas-phase sulfate.) The progression of SO₂ oxidation with downwind distance is readily apparent, the SO_x⁻² concentration increasing from 0.4 ppb in Morris County to 1.5 ppb, 125 km downwind. Similar but somewhat less dramatic behavior is shown by nitric acid, PAN (CH₃C(O)O₂NO₂), and acrolein. The impact of these photochemical products is thus felt not principally in the urban area from which the precursors originate but in the downwind areas within the urban plume. Additional results and chemical analyses are presented by Graedel et al. (ref. 28).

OVERWATER TRANSPORT OF URBAN AIR

Recent observations at shoreline sites downwind and overwater from urban areas have shown enhanced ozone concentrations when the predominant wind direction is from the urban area to the site (Graedel and Farrow (ref. 29)). This result suggests a further manifestation of the interplay between atmospheric chemistry and meteorology, since ozone undoubtedly represents in some sense the family of photochemically produced species. To investigate the overwater transport situation computationally, the six-county sequence of figure 9 is modified by replacing the fourth region (Shopview County) in the overland downwind case by a traverse overwater (Aqua County) during which no emissions of hydrocarbons or nitric oxides occur (fig. 12). The resulting concentrations and rates are then analyzed for Shopview and Aqua Counties and for the counties further downwind. The peak ozone concentrations calculated for both the overland and the overwater traverses are shown in figure 13. It is readily apparent that the enhanced ozone levels observed in air quality data following overwater transport are reproduced by the calculations. The computed enhancements are 7 percent in Aqua County (in comparison with Shopview County), 3 percent in Deerfield County, and 1 percent in Farmland County.

The presence of enhanced photochemical activity during the overwater traverse suggests that chemical product formation as well as ozone concentrations may be enhanced in comparison with those of the overland case. To investigate this hypothesis, three pairs of precursors and products have been examined: NO₂ and HNO₃, SO₂ and gaseous sulfate (H₂SO₄ + HSO₃[·]), and C₃H₆ and PAN. In figure 14, the ratios of products to precursors at 7 p.m. are plotted for six-county overland and overwater traverses. The results indeed indicate increased photochemical processing during overwater transport. The largest change occurs

in the sulfate conversion ratio, which is 51 percent higher in Aqua County than in Shopview County. Further downwind, however, the influence of the overwater transport diminishes to ≤ 10 percent of the conversion ratios. The overwater transport has thus caused local but not enduring changes in the conversion ratios of the photochemical products.

As air that has been involved in an overwater traverse again encounters land areas with significant anthropogenic emissions, the NO_2/NO concentration ratio adjusts to a balance between the overland sources and sinks of oxides of nitrogen. This adjustment is reflected in a gradual approach of the concentrations of the chemical species to the conditions obtained under overland traverses. In these calculations, the recovery of the air parcel from overwater transport is much less rapid than is its response to the initial perturbation, because the emission density of Shopview County is much higher than that of Deerfield County. Reestablishment of the unperturbed chemistry of the overland traverse is hence not specified completely in the overwater calculations, which are able to follow the air parcels only limited distances downwind. It appears, however, that the long-range effects of brief overwater traverses in a chiefly overland trajectory will be small and that the total integrated emissions inventory will be the dominant influence on the atmospheric chemical product concentrations in locations far downwind of urban areas.

EMISSION VARIATIONS IN THE URBAN ENVIRONMENT

The success of model calculations in reproducing a wide variety of field data suggests that calculations may also be used to predict the effects of significant changes in the emission rates of selected gaseous species. This approach has been used in the northern New Jersey calculations to study the potential effects of large changes in NO and hydrocarbon (HC) emission rates. Calculations with altered source strengths are accomplished as follows. In each county, the normal summer rates for the emission of trace contaminants are established. Variations in source strength are then treated as fractional changes to the basic rates; diurnal emission patterns are retained. The calculations are thus equivalent to source alterations applied on a uniform percentage basis. All calculations utilize the meteorological conditions that have been described previously.

Two sets of computational experiments have been performed for the six-county sequence of figure 9. One set examines the air quality resulting from different NO emission fluxes at constant HC emission flux. The second utilizes different HC emission fluxes at constant NO emission flux. The differences are readily demonstrated by plotting the diurnal peak ozone values for different computations as a function of downwind distance (fig. 15).

The "ozone shield" set up by dense urban areas is illustrated by the Hudson County values, where increases in NO emission rates are seen to decrease peak ozone values by as much as 15 percent, for the cases studied here. Increases in HC emissions cause increases in the ozone maxima but the magnitudes are very small (≤ 3 percent for a threefold emissions increase). These effects are consistent with predictions by Dimitriadis (ref. 30) based on smog chamber experiments and with the smog chamber modeling results of Hecht (ref. 31) and Lawrence

Livermore Laboratory (ref. 32) for non-methane hydrocarbon/NO_x ratios typical of urban conditions.

The interrelationships between precursors and products may be studied by examining the product concentrations in a single location as the precursor emission rates are varied. The left side of figure 16 shows the resulting product concentrations in Hudson County at 7 p.m. for computations in which the HC emission rates in the several counties were varied relative to the best current source estimate (1.0 on the abscissa); NO emission rates were held constant. In addition to the gas-phase species, the heterogeneous aerosol mass gain resulting from accretion of low-vapor-pressure compounds (TPM) is included. The effects of HC emission variation on all species, even for those products that are primarily organic in nature, are seen to be no larger than 2 percent for changes in HC emission as large as a factor-of-2 decrease or a factor-of-1.5 increase.

Photochemical product concentrations for computations in which the NO emission rates were varied and the HC rates held constant are shown on the right side of figure 16. Here the concentration changes of the photochemical products are substantial. Although the magnitudes of the effects differ, in every case a reduction in NO emissions produces a concomitant decrease in the photochemical product. The concentration variations of other photochemical product species included in the computations are similar.

The trends of O₃, NO, and NO₂ concentrations discussed in this paper suggest that the increase in ozone concentrations in the downwind suburban and rural counties is coincident with an increase in the ratio of the peak values of NO₂ and NO. This "photostationary state" condition (Stedman and Jackson (ref. 33)) is seen in all of the computed results. This is shown in figure 17 where the ozone maxima for all of the six-county overland calculations are plotted as a function of the NO₂/NO concentration ratio at noon. The relationship is nearly linear over the very wide range of urban density and emission flux utilized in the calculations. This suggests that the effects of changes in emission fluxes on ozone concentrations, at least in the northern New Jersey region and for the conditions represented by the calculations, can be assessed by answering the question, "How will the change perturb the NO₂/NO ratio?" For example, an increase in the NO emission flux will decrease the ratio locally but may allow for increased NO oxidation and an increased ratio downwind. The ozone maxima will follow these changes.

For many of the photochemical products discussed herein, the interactions of the hydroxyl radical turn out to be quite important (e.g., Davis et al. (ref. 34) and fig. 2 of this work). This circumstance renders the reaction



doubly significant, since it is the principal source of hydroxyl radicals in the urban atmosphere (Graedel et al. (ref. 4)). This dependence is demonstrated by figure 18, in which the relationship between NO₂ and HO· (Farrow and Graedel (ref. 35)) for all of the six-county computations is shown. The very slight dependence of any of the photochemical products on hydrocarbon emission appears to be due to the natural background of hydrocarbons throughout the region (and most of the continental United States) and to the central position of reac-

tion (5) as a rate-limiting step for much of the free-radical chemistry of the atmosphere. In a qualitative sense, these results may be generally applicable to urban atmospheres in which incoming air has encountered predominantly overland traverses. Regardless of the particular spectrum of urban hydrocarbons, each hydrocarbon compound will react predominantly with HO· (e.g., Gorse and Volman (ref. 36) and Hansen et al. (ref. 37)). Since the formation of oxygenated products in all currently proposed atmospheric sequences involves oxygen abstraction and/or NO_x addition and since NO_x is the principal oxygen abstractor in the troposphere, it appears that virtually all atmospheric photochemical products will be responsive to ambient concentrations of NO_x, at least in the urban atmospheres where the radical sources and sinks are dominated by NO_x reactions.

The implications of these results are substantial ones for tropospheric chemistry and it is thus important that the limits to their generality be firmly stated. First, it is cautioned that, although the computational results are in reasonable agreement with air quality data for workdays and Sundays and for the case of overwater transport, the comparisons apply to the specific conditions of full sun, westerly wind flow, and simplified treatment of the applicable meteorology. A further limitation is the accuracy of the hydrocarbon emissions inventory, which is probably no better than ±25 percent. The minimal response of photochemical product formation to large hydrocarbon emission variations ameliorates that problem to a great extent, however. While the conclusions appear to reflect a basic understanding of the atmospheric processes that occur, the results cannot be quantitatively applied to arbitrary geographical areas with arbitrary meteorological situations. In particular, the treatment of urban meteorology is insufficient to predict in detail the behavior of atmospheric chemistry during "episode" periods, when winds are low or calm and when mixing is much reduced.

SOURCES OF ERROR IN URBAN PHOTOCHEMICAL COMPUTATIONS

The complex and extensive data required to formulate an atmospheric model are inherently limited in precision and accuracy. It is therefore of substantial interest to assess the effects of inaccurate specification of the various parameters on the computational results. Although it is possible in principle to study the maximum perturbation of an individual computational output produced by variation of all the input parameters within their estimated error limits (e.g., Cukier et al. (ref. 38)), such techniques are not tractable for computations of the complexity dealt with here. One can perform computational experiments, however, in which selected individual parameters or groups of parameters are varied within their error limits. While the results cannot be said to define the "sensitivity" of the computation in a mathematically precise way, they provide approximate bounds to the accuracy of the computation if the variational experiments are carefully chosen (Dewer et al. (ref. 39)). In this section, a variety of such experiments with the Bell Laboratories model are described and the results assessed.

Incomplete Chemical Formulation

The spectrum of compounds in urban air is so large that a complete formulation of the chemical reaction chains would involve thousands of reactions, the majority of which would have undefined rate constants, products, or both. A drastic condensation of this "ultimate" reaction set is thus necessary if models are to be constructed. The condensation inevitably involves personal judgments as to the degree of complexity required for effective simulation of the real system and the degree to which unmeasured reaction parameters can be estimated.

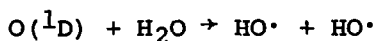
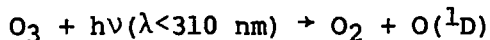
The major condensation in most tropospheric models is made with the organic chemical reactions. Although scores of hydrocarbons are commonly measured in urban air (e.g., Altshuller et al. (ref. 40) and Grob and Grob (ref. 41)), most of the carbon atoms present are contained in perhaps a dozen compounds. The tendency of hydrocarbon chains to produce identical fragment products suggests that careful treatment of these principal species may suffice for all practical purposes. Even this restricted goal seems intractable at present, however, because of the deficiencies in laboratory and field data (particularly for the aromatic compounds). A further consideration is that emission inventories for urban areas do not generally subdivide hydrocarbon emissions by species; thus, there is the danger that a complete chemical treatment will be coupled with a totally insufficient set of boundary conditions.

The choice made in the Bell Laboratories model for representation of organic chemistry has been to restrict the treatment of hydrocarbons to methane, ethane, propylene, formaldehyde, acetaldehyde, and their reaction products. Source emissions are subdivided according to experimental species determinations from representative emission sources. Methane and, to a lesser extent, ethane are moderately reactive species and have important global chemical roles in addition to their participation in urban chemistry. The use of propylene to represent the spectrum of reactive compounds provides access to the singly bonded two-carbon group and the one-carbon fragment necessary for the production of many of the compounds and radicals (e.g., CH_3CHO , $\text{HO}_2\cdot$, $\text{CH}_3\text{C}(\text{O})\cdot$) thought to be chemically important (Leighton (ref. 42), Demerjian et al. (ref. 2), and Morris and Niki (ref. 43)). Nonetheless, the limitation of hydrocarbon chemistry in this way prevents the computation from providing information on many organic atmospheric products of interest, and thus, the computation cannot be regarded as a total representation of atmospheric chemical processes. Perhaps the best assessment that can be made of its general utility is the comparison of measured and computed concentrations of selected products of the organic chemistry. This comparison (table I) suggests that the current organic formulation is a reasonable one.

The chemistry of atmospheric sulfur is poorly defined at present (Davis and Klauber (ref. 44) and Graedel (ref. 45)). The initial loss reactions are well known, however, so that the effects of SO_2 on $\text{HO}\cdot$ and $\text{HO}_2\cdot$ (the principal scavenging species) can be calculated. The effects of the optional chemical paths for the oxidized sulfur products on the overall chemistry have been explored in a series of sensitivity studies (Graedel (ref. 15)). It was concluded that while a full and accurate treatment of urban gas-phase sulfur chemistry is doubtless required for assessments of the atmospheric sulfur cycle,

such a treatment is not crucial to the accurate representation of the chemistry of non-sulfur compounds.

In nonurban atmospheres, the primary source of the important hydroxyl radicals is thought to be (Crutzen (ref. 46))



In urban atmospheres, however, the principal source is (Graedel et al. (ref. 4))



where the $\text{HO}_2\cdot$ comes from aldehyde photolysis. The importance of including $\text{O}({}^1\text{D})$ chemistry in urban calculations has been assessed by a calculation omitting its sources and sinks (Graedel et al. (ref. 4)). The results demonstrated that the $\text{O}({}^1\text{D})$ chemistry was indeed of significance, primarily because it represents a pure source of odd hydrogen radicals rather than a reshuffling of existing ones.

Heterogeneous processes (i.e., the interaction of gas-phase molecules with atmospheric aerosols and with ground surfaces) are not well understood. The treatment adopted herein has been discussed in the section "Kinetic Photochemical Models;" it is clearly a preliminary formulation. The inclusion of such effects in the urban kinetic computations has been investigated at some length (Farrow et al. (ref. 18) and Graedel et al. (refs. 4 and 7)), and it has been concluded that the processes are significant but not dominant for substances (e.g., $\text{HO}\cdot$ and $\text{HO}_2\cdot$) with very short chemical lifetimes. For more stable species, particularly photochemical products of low vapor pressure such as HNO_3 , H_2SO_4 , and $\text{CH}_3\text{C}(\text{O})\text{O}_2\text{NO}_2$, surface removal is the principal loss mechanism. The inclusion of surface effects in a chemically consistent manner is thus an important goal for studies of the cycles of these product species. It appears that the reactions of compounds containing only oxygen, hydrogen, and nitrogen are treated with sufficient comprehensiveness in the present formulation of the urban model. An exception that might be noted is that the chemistry of ammonia is not included. Ammonia's gas-phase processes are not rapid, however (Graedel (ref. 47)), and it appears that the atmospheric chemical cycles of ammonia are principally heterogeneous (Charlson et al. (ref. 48)). Therefore, its omission has little potential effect on gas-phase processes.

A variety of organic (Glasson and Heuss (ref. 49)) and sulfoxy (Calvert (ref. 50)) nitrates are likely to be formed in urban atmospheres. The present information about such compounds is sketchy. If present, they will be chemical end products rather than reactive intermediates; this property makes it unlikely that their omission will significantly perturb other aspects of urban photochemistry. The work described here treats PAN and other organic nitrogen-containing compounds whose chemistry appears to be reasonably well specified.

As has been discussed by Duewer et al. (ref. 39) for the case of stratospheric models, one cannot exclude the possibility of an important chemical

process being omitted from these chemical calculations. It is possible, however, to justify the inclusion of specific processes (as has been done in this paper in several cases). There appears to be good evidence that the current treatment includes the reaction paths of major tropospheric significance. Nonetheless, knowledge of the chemistry of specific organic groups (such as the aromatic compounds) and of heterogeneous processes is inadequate or nonexistent at present. For products or processes where these deficiencies are important, much additional information is obviously needed.

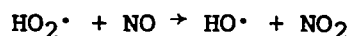
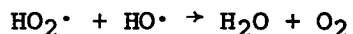
Inaccurate Rate Parameters and Incorrect Products

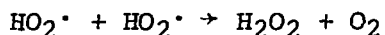
Four types of processes occur in tropospheric gas-phase chemistry: molecule-molecule reactions, molecule-radical reactions, radical-radical reactions, and unimolecular processes (of which photodissociation is the most important example). In the first case, laboratory techniques are relatively straightforward and rate parameters and product determinations appear to be satisfactory. Molecule-radical reactions receive a mixed assessment. The two most important tropospheric radicals are HO· and HO₂·. The former can be satisfactorily handled in the laboratory and most of its molecular reaction parameters appear to be sufficiently well determined. HO₂·, on the other hand, is difficult to generate and measure in analytically tractable laboratory systems. Fortunately, the number of tropospheric reactions in which HO₂· enters is much smaller than for HO·, and good progress is being made on laboratory techniques for HO₂· kinetics.

Radical-radical reactions are very hard to study in laboratory systems. Further, they have been shown to be of great importance in stratospheric chemical cycles. The situation is much less severe in the urban troposphere, because the presence of relatively high concentrations of reactive molecules and aerosols and the proximity of ground surfaces increase alternate loss processes greatly.

Some uncertainties exist in the specification of quantum yields and products for photodissociation reactions. The quantum yield results must be obtained in such a way that collisional quenching at 1 atmosphere of pressure is appropriately included; this is sometimes a difficult requirement. Consideration of the variations in quantum yield with temperature, which is important for models with wide altitude ranges, is not of consequence in urban calculations.

The specific reactions in which inaccuracies in the rate parameters may be reflected strongly in the computational output are thought to be

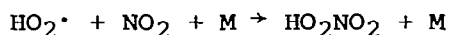




As may be seen at once, $\text{HO}_2\cdot$ is involved as a reactant in each. The effects of a change of 1 order of magnitude in the rate constant for the first reaction have been specifically assessed (Graedel et al. (ref. 4)); they were minimal because of the predominance of competing reactions for both species. The last reaction, for which the error limits in the rate constant are much tighter (Hampson and Garvin (ref. 51)), is expected to behave similarly. The rate constant for $\text{HO}_2\cdot + \text{NO}$ has recently been remeasured (Howard and Evenson (ref. 52)) to be about a factor of 40 larger than the previously accepted value (Hampson and Garvin (ref. 51)). Sensitivity studies of the effect of this change are in progress.

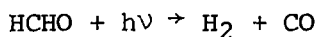
Any uncertainties in the rate parameter for $\text{HO}_2\cdot + \text{O}_3$ appear unlikely to influence urban chemistry very much. The effect of the reaction is twofold: it reduces $\text{HO}_2\cdot$ to $\text{HO}\cdot$ and it provides an ozone sink. The first process is also accomplished by $\text{HO}_2\cdot + \text{NO}$, a reaction which has a rate 35 times as great as $\text{HO}_2\cdot + \text{O}_3$, even at 1975 rate constant values. The latter process is much less important as an ozone sink than many competing reactions, such as the scavenging of ozone by the olefins.

The formation of pernitric acid by the reaction



has recently been confirmed (Levine et al. (ref. 53) and Niki et al. (ref. 54)). It appears that thermal dissociation of the product is rapid enough so that this process should be unimportant (Pitts, private communication, 1977); nonetheless, a calculational assessment of its influence is underway.

Of the photodissociation reactions in the urban atmosphere, those of formaldehyde are perhaps of the greatest present concern:



Some complexities in measured values (Calvert et al. (ref. 55), Houston and Moore (ref. 56), and Lewis et al. (ref. 57)) make specification of both the total quantum yields and the branching ratios for these processes uncertain. A related problem is the specification of the chemical rates of the $\text{CHO}\cdot$ radical (Osif and Heicklen (ref. 58) and Niki et al. (ref. 59)). The effects of these uncertainties are being studied in calculations now underway.

Since the rate of any bimolecular reaction



is given by the product of the concentrations of its reactants and its rate constant

$$R = k[A][B]$$

the effects on a chemical system of a factor-of-2 uncertainty in the rate constant can be assessed either by changing k or by changing the concentrations of one of the reactants. From this standpoint, the emission variation studies described in the section "Emission Variations in the Urban Environment" can be looked upon as sensitivity studies of groups of reactions. Since changes of a factor of 2 in the spectrum of hydrocarbon compound emissions perturbed the basic chemical system to only a small degree, the sensitivity of the urban model to rate parameter inaccuracies affecting the hydrocarbons may be inferred to be small. This is not true for nitric oxide, for which emission variations resulted in substantial differences in the computed results. The uncertainty in the rate parameters for the oxides of nitrogen is of the same order of magnitude as for hydrocarbons (Hampson and Garvin (ref. 51)). Thus, the emission variation calculations provide no sensitivity analysis for the NO_x chemistry, which is best assessed by the individual reaction studies already discussed.

Solar Insolation Values

Many of the important reactions in urban chemistry involve solar photons; thus, an imprecise specification of the photon flux is of potential concern. Solar insolation is location and time dependent, unlike the chemical formulation and specification of reaction parameters. One must therefore interpret solar insolation accuracy as a function of the goals of the model. If one wishes to simulate a particular day in a given location, insolation measurements for that situation must be provided. If an average air quality for selected days or seasons is desired, the measurements must be appropriate to those goals. In principle, solar insolation can be measured with accuracies better than 1 percent (Marchgraber (ref. 60)), and a significant error in the computational results can thus be avoided with careful attention to field data.

Although computational errors due to poor insolation specification can be avoided, it is of interest to assess the sensitivity of the photochemistry to changes in insolation resulting from variations in solar zenith angle, clouds, aerosols, and so forth. In the case of photosensitive species such as ozone, model calculations have shown that the imposition of full cloud cover on a summer workday in New Jersey can cause concentration decreases of greater than a factor of 10 (Graedel et al. (ref. 61)). Similar results have been presented by Peterson and Demerjian (ref. 62). It is apparent that modeling of air quality processes at a specific time and place will require accurate photon flux information. Modeling efforts with didactic or prognostic goals, however, can be adequately achieved with specification of average or typical solar flux values.

Background Concentrations

The concentrations of trace species in the air entering an urban region are quite significant to the subsequent chemistry. For most species, these background concentrations are lower than those within the urban area and the advected air tends to cleanse the urban atmosphere. For ozone the situation is often reversed; advection is thus a net source.

The background concentrations are, in general, poorly established. The exception again is ozone, for which extensive data are now available for the Northeastern United States. For other species, it is necessary to rely on less detailed measurements. In modeling specific days, one is thus often presented with boundary conditions that are not defined by field observations. Calculations representing typical conditions, however, are less likely to be strongly influenced by boundary factors. This is particularly true if qualitative interpretations rather than quantitative predictions are desired. In the former case, it is perhaps sufficient that the sign of species concentration change due to advection is specified, as was discussed in the previous paragraphs. Since urban emissions are greater than advective sources for most molecules, the effects of improper choices for background concentrations are less severe than if the relative source strengths were reversed.

No specific sensitivity studies of background concentration effects have been carried out for the Bell Laboratories model, but other urban model studies (Duewer et al. (ref. 63)) have demonstrated that the effects can be important in some circumstances. It thus appears that the accurate specification of background concentrations is an important consideration if results pertaining to specific days are to be procured from modeling efforts.

Entrainment

As solar heating warms the morning air, the depth of the mixed layer increases, reaching a maximum in the mid-to-late afternoon. The air entrained into the mixed layer brings trace species with it. Two simultaneous processes occur: the increase in the volume of the mixed boundary layer tends to decrease the concentrations of the trace species, while the presence of certain species in the entrained air tends to modulate that decrease. If the entrained air contains higher concentrations of a species than the air into which entrainment occurs, a net increase in concentration may result.

Molecules present in entrained air will generally be those with reasonably long atmospheric lifetimes such as CH_4 , CO , CO_2 , H_2 , and N_2O . Of the species with intermediate lifetimes, NO_2 , O_3 , and certain of the non-methane hydrocarbons have been measured above the predawn inversion (Lea (ref. 64), Blumenthal and White (ref. 65), Siddiqi and Worley (ref. 66), and Tesche et al. (ref. 67)). It is thus required that incorporation of these species into the mixed layer be reflected in model simulations.

A number of sensitivity studies have been performed with the Bell Laboratories model to investigate the effects of entrained species. The initial conclusion (Graedel et al. (ref. 4)) was that entrainment of trace species was not

only intuitively required but produced computational results in better agreement with data than were computations performed with entrainment of pure air. More extensive work (as yet unpublished) indicates that such inclusion is critical only for species whose entrained concentrations are of the same order as, or of greater order than, concentrations in the air into which entrainment occurs. This condition appears to be often present for ozone and for the long-lifetime species mentioned previously, but not (in urban areas) for oxides of nitrogen or reactive hydrocarbons.

A parameter affecting not only the number of molecules added by entrainment but also the volume of the mixed layer is the mixed layer depth. This quantity is not always capable of being measured with precision and is seldom determined at several different times throughout a given day. A full description is required, however, for calculations attempting to simulate air quality at a specific time and place. For didactic purposes, it appears sufficient to specify mixed layer depth by joining typical morning and afternoon mixing height measurements by a theoretical curve such as those of Tennekes (ref. 68).

Emission Inventory

Emission inventories are never up to date, never complete, and of varying accuracy. Their compilation is tedious and mundane, as pointed out by Roth et al. (ref. 69), yet such work is necessary in order to derive good quantitative results from calculations. Deficiencies in the emissions inventory for a given region are generally difficult to estimate but may be the principal limitation to the accuracy of model results if other potential sources of error are carefully addressed.

Incomplete emission inventories affect calculational results differently for different species. The emission variations studies discussed in the section "Emission Variations in the Urban Environment" function also as sensitivity studies for the emission inventory. The results of those calculations showed that for the northern New Jersey urban area, the production of a variety of photochemical products was influenced markedly by changes in NO emission flux but minimally by changes in hydrocarbon emission flux. Separate studies for CO and SO₂ were not performed, but the minimal involvement of these species in urban atmospheric chemistry suggests that inaccuracies in their emission rates would not perturb the chemical system to any marked degree. The emission sources and rates for these species are also rather well defined: CO is emitted almost entirely from motor vehicles, and SO₂ largely from power generation facilities. The relative insensitivity of urban photochemistry to hydrocarbon emission fluxes is fortuitous, since hydrocarbon emissions, both anthropogenic and natural, are the least well defined of the major source terms. Nitric oxide is a product of combustion processes and its emission rates, while generally less well determined than those for CO and SO₂, will probably be more accurate than those for hydrocarbons.

To summarize, model results are reasonably sensitive to the emission rates of certain species. If the air quality on specific days is to be modeled, intensive effort will be needed to ensure a good emission inventory. Useful semi-quantitative results representing certain average conditions can generally be

derived with a less detailed picture of emissions, however, particularly if accuracy for NO emission fluxes is emphasized.

The Full Mixing Assumption

Chemical kinetic calculations require that a uniformly mixed volume at some scale size be assumed. In the urban atmosphere such an assumption is obviously inappropriate for length scales of the order of a hundred meters (the dimension of influence of a multilane highway, for example). Models generally utilize length and width scales of the order of 1 to 30 km, with the vertical dimension being equal to the mixing height (perhaps 0.3 to 2.0 km). Spatial profiles for a variety of species often show reasonable homogeneity on such scales if strong convective mixing conditions are present (Tennekes (ref. 70), Cleveland et al. (ref. 17), and Siddiqi and Worley (ref. 66)); such behavior is common on many summer days but uncommon at night.

The absence of uniform mixed conditions has been shown by Donaldson and Hilst (ref. 71) to have potentially significant effects on chemical results. It is therefore important that models be applied only to situations that can be simulated accurately by their meteorological formulation and data. This requirement currently limits the applicability of most models to days with normal mixing rather than to the inversion-stagnation periods of perhaps greatest concern from an air quality standpoint.

Summary

Potential sources of error are present in nearly every aspect of urban photochemical computations and limit the accuracy and usefulness of the results. Many of these limitations can be alleviated by suitable data-gathering efforts: solar insolation, background concentrations, entrainment considerations, and emission inventories. Difficulties with mixing and advection can be reduced by careful selection of the types of conditions to which the calculations apply. Uncertainties in the chemical formulation are the most difficult factors to assess, but it currently appears unlikely that major inaccuracies are present in the understanding of the principal processes of urban photochemistry. Those areas that seem of most concern have been the subject of sensitivity analyses or are under active investigation.

From a practical point of view, it seems unlikely that the necessary information will be available in the near future to allow urban calculations to simulate specific days and times with good accuracy. (A possible exception is the Regional Air Pollution Study for St. Louis, for which data are now being prepared for dissemination.) In the interim, it appears that model calculations can be regarded as instructive in an average semiquantitative sense and that the relative effects of selected perturbations on urban photochemistry can be assessed with a moderate degree of confidence.

DESIRABLE FIELD STUDIES

The meteorology and chemistry of the atmosphere in and near urban areas are incompletely specified, and many theoretical studies now rest on inadequate data bases. Some of the simplifications and assumptions that have been made in modeling studies have already been described. In other cases, models have not been formulated because insufficient information is available. In this section, these inadequacies are described more completely and their relative importance is assessed.

Meteorological Parameters

Perhaps the most critical need in this category is for a good specification of horizontal mixing of tropospheric air. This is particularly true for the mesoscale (20 to 200 km), although smaller scales are also imperfectly specified. Accurate statistical descriptions of mesoscale mixing are needed to determine how rapidly and completely urban air is mixed with nonurban air and thus the time scales over which the full interactive smog chemistry occurs. The variation of this mixing under differing solar insolation conditions also needs to be studied. It is knowledge in these areas that will be important in determining the fraction of precursor molecules which is converted to oxygenated products and drops out (perhaps literally) of the chemistry and the fraction which is added to the global background.

Nearly as important as horizontal mixing information is a statistical description of vertical mixing, especially under extreme meteorological conditions. Such information is crucial to determining the dilution of the urban air mass by background air. Both horizontal and vertical mixing could be studied by using relatively unreactive molecules as tracers; meteorological parameters (e.g., temperature and wind profiles) might also be appropriate.

The interplay of meteorology and chemistry is demonstrated by vertical profiles of reactive molecules. Very few measurements of this type are available; many are needed. If vertical mixing were well specified, for example, simultaneous vertical profiles of propylene and ozone would provide an indirect but reliable determination of the concentration of the hydroxyl radical, since it and ozone are the major reactants for propylene. For SO_2 , generally emitted at moderate heights from stacks, vertical diffusion both up and down is of interest, as is conversion in transit to sulfate species. Additional examples of the uses of height profiles of reactive compounds abound.

Chemical Parameters

From the standpoint of the chemist, the history of chemical species measurements in the troposphere has been one of emphasis on precursors rather than on products. An obvious reason for this preference is that precursors are generally easier to measure and their concentrations are higher. The products, however, are often the more toxic. The product source and sink mechanisms for many systems are poorly specified but are important considerations in assessing the global atmospheric cycles of chemical elements. The measurement of a wide vari-

ety of precursor-product pairs is thus to be encouraged, as is the measurement of the free radicals that so often control the transition from precursor to product.

The only free-radical intermediate thus far measured in the troposphere is HO·. The limited number of measurements suggests a typical diurnal ground-level peak of the order of $2-3 \times 10^6$ molecules-cm⁻³ (Wang et al. (ref. 72), Davis et al. (ref. 34), and Perner et al. (ref. 73)); the variations of the hydroxyl concentrations with such factors as latitude, time of year, amount of cloud cover, time of day, and concentrations of other atmospheric species remain to be determined. Other atmospherically important radicals that have not been detected in situ but have been measured under laboratory conditions are HO₂· (Radford et al. (ref. 74) and Becker et al. (ref. 75)), CH₃O₂· (Parkes et al. (ref. 76)), and NO₃· (Graham and Johnston (ref. 77)). The estimated atmospheric diurnal peak concentrations of these radicals in urban atmospheres (as predicted by the Bell Laboratories kinetic photochemical model) are given in table II.

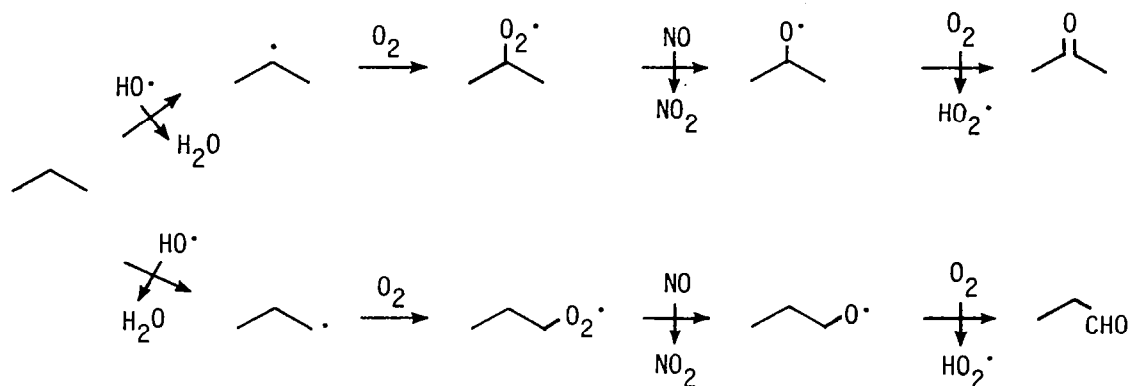
Several precursor-product pairs involving odd nitrogen compounds are of atmospheric interest. All involve the formation of acids. The production reactions are



Of these compounds, NO and NO₂ are readily measured and HNO₃ is measurable with some difficulty. HNO₂ has been detected only once in the atmosphere (Nash (ref. 13)). Pernitric acid (HO₂NO₂) has not been measured in ambient air but has been detected in the laboratory (Niki et al. (ref. 54)). Approximate urban atmospheric concentrations for these compounds, based on a combination of data and model studies, are given in table III. The most chemically instructive measurements would be simultaneous determinations of the concentrations of both members of a precursor-product pair. Determinations at different times of day and under different meteorological conditions are desirable. The concurrent measurement of the concentration of the linking species would be of great value.

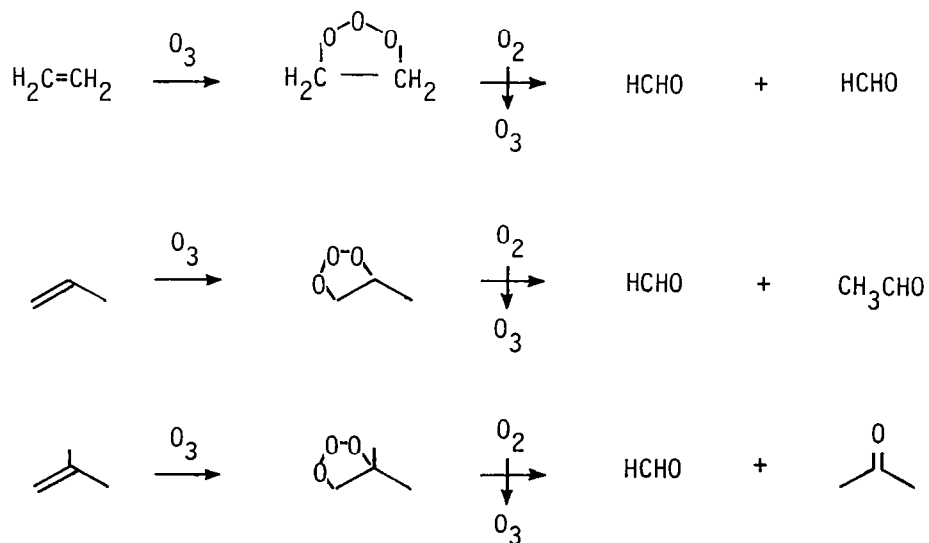
Measurements of individual organic compounds in the atmosphere are sparse, despite the knowledge that such compounds play important roles in atmospheric chemical processes. The situation is compounded by the diversity of compounds and by the tendency for the same product to result from several precursors and by several chemical paths. Most common organic emittants are hydrocarbon compounds, however, and their oxidation products are aldehydes, ketones, alcohols,

and acids. The chain-initiating reaction is usually with the hydroxyl radical, although sometimes with ozone. A sample sequence is the twin-route reaction of propane with hydroxyl:

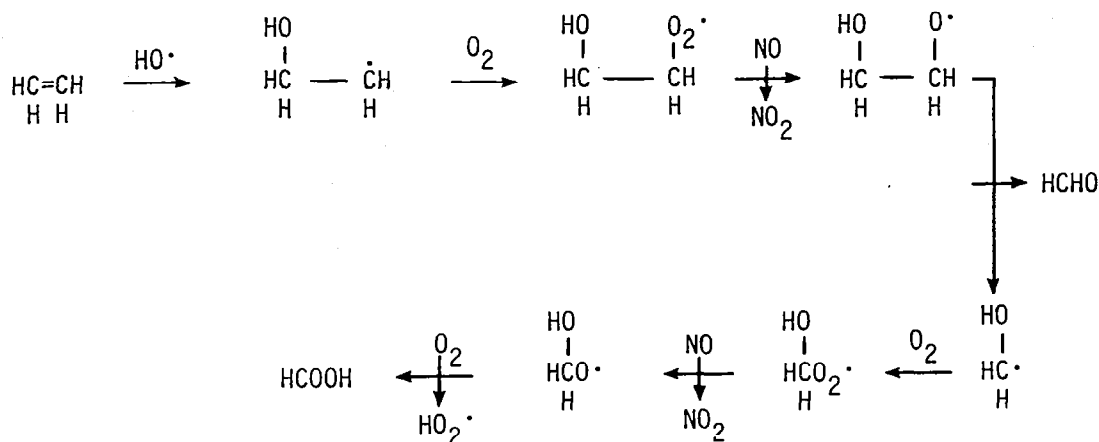


(The short orthogonal arrows indicate the progression of the attacking molecule from reactant to product.) In this sequence, the product is acetone or propional, depending on the hydrogen abstraction site. Both products are subject to photodissociation at tropospheric wavelengths, and both have sources other than this sequence.

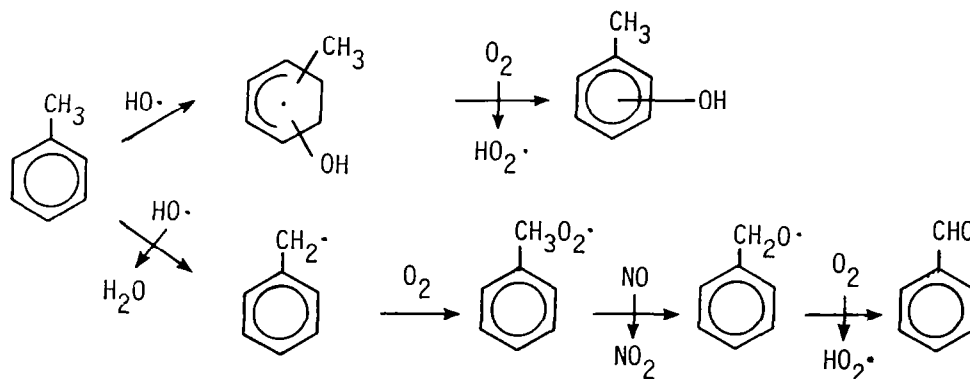
More diverse chemistry results with the alkenes. The reaction of ozone with 1-alkenes produces formaldehyde (HCHO), a second carbonyl product, and perhaps other oxygenated species (Herron and Huie (ref. 78)):



Many of the same products result from hydroxyl attack on alkenes. Such reactions are capable of forming acids as well as carbonyl compounds, as demonstrated for ethene, as follows:



The atmospheric fates of aromatic compounds have received little attention, but the most plausible sequences appear to involve hydroxyl initiation. For toluene, these include:



Because of the multiplicity of these chains, precursor-product pairs are defined less precisely than is the case with the odd nitrogen compounds. For some products, however, the principal precursor or precursors can be deduced from information concerning relative concentrations of possible precursors and their rate constants for hydroxyl radical or ozone reaction. A selected list of precursors and products developed by this technique is given in table IV. As with the odd nitrogen compounds of table III, concurrent measurement of precursor-product pairs, and if possible of the linking species, is most useful, as are measurements for a variety of temporal and meteorological conditions.

CONCLUDING REMARKS

The ability to model satisfactorily the processes of urban atmospheres is presently restricted to selected chemical processes, a handful of geographical regions, and stringently stratified meteorological conditions. Nonetheless, much has been learned. Such distinct situations as urban workdays, urban Sundays, transport and chemistry upwind of, within, and downwind of urban areas, and overwater transport have been qualitatively simulated by computer techniques. The agreement with ambient data appears to be reasonably good, sug-

gesting that at least the principal processes of urban photochemistry and meteorology are fairly well understood.

Simulations of urban photochemistry with altered source conditions have also been completed. Although the generality of the results remains to be established, the results suggest that, at least in northern New Jersey, nitric oxide is the rate-limiting reactant for many of the principal photochemical smog processes. Decreases in its emission flux thus appear likely to result in decreases in the concentrations of a variety of photochemical products, both within the urban area and downwind of it.

Many of the details of atmospheric chemical processes are poorly determined. To this end, concurrent measurements of a variety of precursors, linking species, and products are desirable. Suggestions for and chemical justification of such groups have been given. The availability of such data will markedly enhance understanding of the chemistry of the urban atmosphere.

REFERENCES

1. Subcommittee on Ozone and Other Photochemical Oxidants: Ozone and Other Photochemical Oxidants - Volume I, EPA-600/1-76-027a, U.S. Environ. Prot. Agency, Aug. 1976, pp. 45-125. (Available from NTIS as PB-260 570.)
2. Demerjian, Kenneth L.; Kerr, J. Alistair; and Calvert, Jack G.: The Mechanism of Photochemical Smog Formation. Advances in Environmental Science and Technology, Volume 4, James N. Pitts, Jr., and Robert L. Metcalf, eds., John Wiley & Sons, c.1974, pp. 1-262.
3. Panel on Vapor-Phase Organic Pollutants: Vapor-Phase Organic Pollutants Volatile Hydrocarbons and Oxidation Products. EPA-600/1-75-005, U.S. Environ. Prot. Agency, Oct. 1975. (Available from NTIS as PB-249 357.)
4. Graedel, T. E.; Farrow, L. A.; and Weber, T. A.: Kinetic Studies of the Photochemistry of the Urban Troposphere. Atmos. Environ., vol. 10, no. 12, 1976, pp. 1095-1116.
5. Heicklen, Julian: Atmospheric Chemistry. Academic Press, Inc., 1976.
6. Winkler, Peter: The Growth of Atmospheric Aerosol Particles as a Function of the Relative Humidity - II. An Improved Concept of Mixed Nuclei. J. Aerosol Sci., vol. 4, no. 5, Sept. 1973, pp. 373-387.
7. Graedel, T. E.; Farrow, L. A.; and Weber, T. A.: The Influence of Aerosols on the Chemistry of the Troposphere. Chemical Kinetics Data for the Upper and Lower Atmosphere, Int. J. Chem. Kinet., Symp. No. 1, 1975, pp. 581-594.
8. Warneck, Peter: Role of Hydroxyl and Hydroperoxyl Radical in the Troposphere. Tellus, vol. 26, nos. 1-2, 1974, pp. 39-46.
9. Air Quality Criteria for Photochemical Oxidants. NAPCA Publ. No. AP-63, U.S. Environ. Prot. Agency, [1970].
10. Cleveland, William S.; Kleiner, Beat; and Warner, Jack L.: Robust Statistical Methods and Photochemical Air Pollution Data. J. Air Pollut. Control Assoc., vol. 26, no. 1, Jan. 1976, pp. 36-38.
11. Altshuller, A. P.; and McPherson, S. P.: Spectrophotometric Analysis of Aldehydes in the Los Angeles Atmosphere. J. Air Pollut. Control Assoc., vol. 13, no. 3, 1963, pp. 109-111.
12. Gay, Bruce W., Jr.; and Bufalini, Joseph J.: Hydrogen Peroxide in the Urban Atmosphere. Adv. Chem. Ser. No. 113, 1972, pp. 255-263.
13. Nash, T.: Nitrous Acid in the Atmosphere and Laboratory Experiments on Its Photolysis. Tellus, vol. 26, nos. 1-2, 1974, pp. 175-179.
14. Spicer, Chester W.: Nonregulated Photochemical Pollutants Derived From Nitrogen Oxides. Scientific Seminar on Automotive Pollutants, EPA-600/9-75-003, U.S. Environ. Prot. Agency, Feb. 1975.

15. Graedel, T. E.: Sulfur Dioxide, Sulfate Aerosol, and Urban Ozone. *Geophys. Res. Lett.*, vol. 3, no. 3, Mar. 1976, pp. 181-184.
16. Bruntz, S. M.; Cleveland, W. S.; Graedel, T. E.; Kleiner, B.; and Warner, J. L.: Ozone Concentrations in New Jersey and New York: Statistical Association With Related Variables. *Science*, vol. 186, no. 4160, Oct. 18, 1974, pp. 257-259.
17. Cleveland, W. S.; Graedel, T. E.; Kleiner, B.; and Warner, J. L.: Sunday and Workday Variations in Photochemical Air Pollutants in New Jersey and New York. *Science*, vol. 186, no. 4168, Dec. 13, 1974, pp. 1037-1038.
18. Farrow, L. A.; Graedel, T. E.; and Weber, T. A.: Heterogeneous Removal of Free Radicals by Aerosols in the Urban Troposphere. *ACS Symp. Ser.*, vol. 17, 1975, pp. 17-27.
19. Graedel, T. E.: Functional Group Analysis of Large Chemical Kinetic Systems. *J. Phys. Chem.*, vol. 81, no. 25, 1977, pp. 2372-2374.
20. Graedel, Thomas E.; Farrow, Leonilda A.; and Weber, Thomas A.: Photochemistry of the "Sunday Effect." *Environ. Sci. & Technol.*, vol. 11, no. 7, July 1977, pp. 690-694.
21. Altshuller, A. P.: Evaluation of Oxidant Results at CAMP Sites in the United States. *J. Air Pollut. Control Assoc.*, vol. 25, no. 1, Jan. 1975, pp. 19-24.
22. Cleveland, W. S.; Kleiner, B.; McRae, J. E.; and Warner, J. L.: Photochemical Air Pollution: Transport From the New York City Area Into Connecticut and Massachusetts. *Science*, vol. 191, no. 4223, Jan. 16, 1976, pp. 179-181.
23. Bruckman, Leonard: Suspended Particulate Transport in Connecticut: An Investigation Into the Relationship Between TSP Concentrations and Wind Direction in Connecticut. *Connecticut Dep. Environ. Prot.*, Dec. 24, 1976.
24. Cunningham, Paul T.; Johnson, Stanley A.; and Yang, Ralph T.: Variations in Chemistry of Airborne Particulate Material With Particle Size and Time. *Environ. Sci. & Technol.*, vol. 8, no. 2, 1974, pp. 131-135.
25. Grosjean, Daniel; and Friedlander, Sheldon K.: Gas-Particle Distribution Factors for Organic and Other Pollutants in the Los Angeles Atmosphere. *J. Air Pollut. Control Assoc.*, vol. 25, no. 10, Oct. 1975, pp. 1038-1044.
26. Lioy, Paul J.; Wolff, George T.; Czachor, Joseph S.; Coffey, Peter E.; Stasiuk, William N.; and Romano, David: Evidence of High Atmosphere Concentrations of Sulfates Detected at Rural Sites in the Northeast. *J. Environ. Sci. & Health*, vol. A12, nos. 1 & 2, 1977, pp. 1-14.
27. Spicer, C. W.: Formation and Transport of Ozone in the Troposphere. *Proceedings of Specialty Conference on Ozone/Oxidants - Interaction With the Total Environment*, *Air Pollut. Control Assoc.*, 1976, pp. 207-220.

28. Graedel, T. E.; Farrow, L. A.; and Weber, T. A.: Urban Kinetic Chemical Calculations With Altered Source Conditions. *Atmos. Environ.*, vol. 12, 1978.
29. Graedel, T. E.; Farrow, L. A.: Kinetic Photochemistry Downwind Over Water From Urban Areas. *J. Geophys. Res.*, vol. 82, no. 31, Oct. 20, 1977, pp. 4943-4946.
30. Dimitriadis, B.: The Role of NO_x in the Ambient NO_2 and Oxidant Problems. Smog Chamber Studies. Scientific Seminar on Automotive Pollutants, EPA-600/9-75-003, U.S. Environ. Prot. Agency, Feb. 1975.
31. Hecht, Thomas A.: Smog Simulation Models and Their Use in Evaluating Air Quality Control Strategies. Scientific Seminar on Automotive Pollutants, EPA-600/9-75-003, U.S. Environ. Prot. Agency, Feb. 1975.
32. Appendix 9-3. Photochemical Rates, Hydrocarbon Reactivities, Validation With Data, and Sensitivity Studies. Development of an Air Pollution Model for the San Francisco Bay Area - Final Report to the National Science Foundation. Volume 2, M. C. MacCracken and G. D. Sauter, eds., UCRL-51920 Vol. 2, Lawrence Livermore Lab., Oct. 1, 1975.
33. Stedman, D. H.; and Jackson, J. O.: The Photostationary State in Photochemical Smog. Chemical Kinetics Data for the Upper and Lower Atmosphere, *Int. J. Chem. Kinet.*, Symp. No. 1, 1975, pp. 493-501.
34. Davis, D. D.; Heaps, W.; and McGee, T.: Direct Measurements of Natural Tropospheric Levels of OH Via an Aircraft Borne Tunable Dye Laser. *Geophys. Res. Lett.*, vol. 3, no. 6, June 1976, pp. 331-333.
35. Farrow, L. A.; and Graedel, T. E.: Steady State Approximations and Urban Atmospheric Chemistry. *J. Phys. Chem.*, vol. 81, no. 25, 1977, pp. 2480-2483.
36. Gorse, R. A.; and Volman, D. H.: Photochemistry of the Gaseous Hydrogen Peroxide-Carbon Monoxide System. II. Rate Constants for Hydroxyl Radical Reactions With Hydrocarbons and for Hydrogen Atom Reactions With Hydrogen Peroxide. *J. Photochem.*, vol. 3, nos. 2-3, 1974, pp. 115-122.
37. Hansen, D. A.; Atkinson, R.; and Pitts, J. N., Jr.: Rate Constants for the Reaction of OH Radicals With a Series of Aromatic Hydrocarbons. *J. Phys. Chem.*, vol. 79, no. 17, Aug. 14, 1975, pp. 1763-1766.
38. Cukier, R. I.; Levine, H. B.; and Shuler, K. E.: Nonlinear Sensitivity Analysis of Multiparameter Model Systems. *J. Phys. Chem.*, vol. 81, no. 25, 1977, pp. 2365-2366.
39. Duewer, William H.; Wuebbles, Donald J.; Ellsaesser, Hugh W.; and Chang, Julius S.: NO_x Catalytic Ozone Destruction: Sensitivity to Rate Coefficients. *J. Geophys. Res.*, vol. 82, no. 6, Feb. 20, 1977, pp. 935-942.

40. Altshuller, Aubrey P.; Lonneman, William A.; Sutterfield, Frank D.; and Kopczynski, Stanley L.: Hydrocarbon Composition of the Atmosphere of the Los Angeles Basin - 1967. *Environ. Sci. & Technol.*, vol. 5, no. 10, 1971, pp. 1009-1016.
41. Grob, K.; and Grob, G.: Gas-Liquid Chromatographic-Mass Spectrometric Investigation of C₆-C₂₀ Organic Compounds in an Urban Atmosphere. *J. Chromatog.*, vol. 62, no. 1, Oct. 18, 1971, pp. 1-13.
42. Leighton, Philip A.: *Photochemistry of Air Pollution*. Academic Press, Inc., 1961.
43. Morris, E. D., Jr.; and Niki, H.: Reaction of the Nitrate Radical With Acetaldehyde and Propylene. *J. Phys. Chem.*, vol. 78, no. 13, June 20, 1974, pp. 1337-1338.
44. Davis, D. D.; and Klauber, Gary: Atmospheric Gas Phase Oxidation Mechanisms for the Molecule SO₂. *Chemical Kinetics Data for the Upper and Lower Atmosphere*, *Int. J. Chem. Kinet.*, Symp. No. 1, 1975, pp. 543-556.
45. Graedel, T. E.: The Homogeneous Chemistry of Atmospheric Sulfur. *Rev. Geophys. & Space Phys.*, vol. 15, no. 4, Nov. 1977, pp. 421-428.
46. Crutzen, Paul J.: Gas-Phase Nitrogen and Methane Chemistry in the Atmosphere. *Physics and Chemistry of Upper Atmospheres*, B. M. McCormac, ed., D. Reidel Publishing Co., c.1973, pp. 110-124.
47. Graedel, T. E.: The Oxidation of Ammonia, Hydrogen Sulfide, and Methane in Nonurban Tropospheres. *J. Geophys. Res.*, vol. 82, no. 37, Dec. 20, 1977, pp. 5917-5922.
48. Charlson, R. J.; Porch, W. M.; Waggoner, A. P.; and Ahlquist, N. C.: Background Aerosol Light Scattering Characteristics: Nephelometric Observations at Mauna Loa Observatory Compared With Results at Other Locations. *Tellus*, vol. 26, no. 3, 1974, pp. 345-360.
49. Glasson, William A.; and Heuss, Jon M.: Synthesis and Evaluation of Potential Atmospheric Eye Irritants. *Environ. Sci. & Technol.*, vol. 11, no. 4, Apr. 1977, pp. 395-398.
50. Calvert, Jack G.: Interactions of Air Pollutants. *Proceedings of the Conference on Health Effects of Air Pollutants*, *Natl. Acad. Sci.*, 1973, pp. 19-101.
51. Hampson, Robert F., Jr.; and Garvin, David, eds.: *Chemical Kinetic and Photochemical Data for Modelling Atmosphere Chemistry*. NBS Tech. Note 866, U.S. Dep. Commer., June 1975.
52. Howard, C. J.; and Evenson, K. M.: Laser Magnetic Resonance Study of HO₂ Chemistry. *EOS Trans., American Geophys. Union*, vol. 58, no. 6, June 1977, p. 464.

53. Levine, Stuart Z.; Uselman, William M.; Chan, Walter H.; Calvert, Jack G.; and Shaw, John H.: The Kinetics and Mechanism of the HO₂-NO₂ Reactions; the Significance of Peroxynitric Acid Formation in Photochemical Smog. *Chem. Phys. Lett.*, vol. 48, no. 3, June 15, 1977, pp. 528-535.
54. Niki, H.; Maker, P. D.; Savage, C. M.; and Breitenbach, L. P.: Fourier Transform IR Spectroscopic Observation of Pernitric Acid Formed Via HOO + NO₂ → HOONO₂. *Chem. Phys. Lett.*, vol. 45, no. 3, Feb. 1, 1977, pp. 564-566.
55. Calvert, Jack G.; Kerr, J. Alistair; Demerjian, Kenneth L.; and McQuigg, Robert D.: Photolysis of Formaldehyde as a Hydrogen Atom Source in the Lower Atmosphere. *Science*, vol. 175, no. 4023, Feb. 18, 1972, pp. 751-752.
56. Houston, Paul L.; and Moore, C. Bradley: Formaldehyde Photochemistry: Appearance Rate, Vibrational Relaxation, and Energy Distribution of the CO Product. *J. Chem. Phys.*, vol. 65, no. 2, July 15, 1976, pp. 757-770.
57. Lewis, Roger S.; Tang, Kenneth Y.; and Lee, Edward K. C.: Photoexcited Chemiluminescence Spectroscopy: Detection of Hydrogen Atoms Produced From Single Vibronic Level Photolysis of Formaldehyde (A¹A₂). *J. Chem. Phys.*, vol. 65, no. 7, Oct. 1, 1976, pp. 2910-2911.
58. Osif, T. L.; and Heicklen, Julian: Oxidation of HCO Radicals. *J. Phys. Chem.*, vol. 80, no. 14, July 1976, pp. 1526-1531.
59. Niki, H.; Maker, P.; Savage, C.; and Breitenbach, L.: IR Fourier-Transform Spectroscopic Studies of Atmospheric Reactions. The 12th Informal Conference on Photochemistry - Extended Abstracts, Natl. Bur. Stand., U.S. Dep. Commer., June-July 1976, pp. N2-1 - N2-4.
60. Marchgraber, Reinhold M.: Development of Standard Instruments for Radiation Measurements. *Meteorol. Monogr.*, vol. 11, no. 33, Oct. 1970, pp. 302-314.
61. Graedel, T. E.; Farrow, L. A.; and Weber, T. A.: The Effects of Variations in Bulk Meteorological Parameters on Ozone Concentrations. Symposium on Atmospheric Diffusion and Air Pollution - Preprints, American Meteorol. Soc., Sept. 1974, p. 115.
62. Peterson, J. T.; and Demerjian, K. L.: The Sensitivity of Computed Ozone Concentrations to U.V. Radiation in the Los Angeles Area. *Atmos. Environ.*, vol. 10, no. 6, 1976, pp. 459-468.
63. Duewer, W. H.; MacCracken, M. C.; and Walton, J. J.: The Livermore Regional Air Quality Model: II. Verification and Sample Application in the San Francisco Bay Area. Preprint UCRL-77475 Pt. 2, Lawrence Livermore Lab., Dec. 18, 1975.
64. Lea, Duane A.: Vertical Ozone Distribution in the Lower Troposphere Near an Urban Pollution Complex. *J. Appl. Meteorol.*, vol. 7, no. 2, Apr. 1968, pp. 252-267.

65. Blumenthal, D. L.; and White, W. H.: The Stability and Long Range Transport of Ozone or Ozone Precursors. Paper presented at the 68th Annual Meeting of the Air Pollution Control Association (Boston, Massachusetts), June 1975.
66. Siddiqi, Aziz A.; and Worley, Frank L., Jr.: Urban and Industrial Air Pollution in Houston, Texas - I. Hydrocarbons. *Atmos. Environ.*, vol. 11, no. 2, 1977, pp. 131-143.
67. Tesche, T. W.; Ogren, J. A.; and Blumenthal, D. L.: Ozone Concentrations in Power Plant Plumes: Comparison of Models and Sampling Data. International Conference on Photochemical Oxidant Pollution and Its Control - Proceedings: Volume I, EPA-600/3-77-001a, U.S. Environ. Prot. Agency, Jan. 1977, pp. 157-171. (Available from NTIS as PB-264 232.)
68. Tennekes, H.: A Model for the Dynamics of the Inversion Above a Convective Boundary Layer. *J. Atmos. Sci.*, vol. 30, no. 4, May 1973, pp. 558-567.
69. Roth, Philip M.; Roberts, Philip J. W.; Liu, Mei-Kao; Reynolds, Steven D.; and Seinfeld, John H.: Mathematical Modeling of Photochemical Air Pollution - II. A Model and Inventory of Pollutant Emissions. *Atmos. Environ.*, vol. 8, no. 1, Jan. 1974, pp. 97-130.
70. Tennekes, Hendrik: The Atmospheric Boundary Layer. *Phys. Today*, vol. 27, no. 1, Jan. 1974, pp. 52-63.
71. Donaldson, Coleman duP.; and Hilst, Glenn R.: Effect of Inhomogeneous Mixing on Atmospheric Photochemical Reactions. *Environ. Sci. & Technol.*, vol. 6, no. 9, Sept. 1972, pp. 812-821.
72. Wang, Charles C.; Davis, L. I., Jr.; Wu, C. H.; Japar, S.; Niki, H.; and Weinstock, B.: Hydroxyl Radical Concentrations Measured in Ambient Air. *Science*, vol. 189, no. 4205, Sept. 5, 1975, pp. 797-800.
73. Perner, D.; Ehhalt, D. H.; Pätz, H. W.; Platt, U.; Röth, E. P.; and Volz, A.: OH-Radicals in the Lower Troposphere. *Geophys. Res. Lett.*, vol. 3, no. 8, Aug. 1976, pp. 466-468.
74. Radford, H. E.; Evenson, K. M.; and Howard, Carleton J.: HO₂ Detected by Laser Magnetic Resonance. *J. Chem. Phys.*, vol. 60, no. 8, Apr. 15, 1974, pp. 3178-3183.
75. Becker, K. H.; Fink, E. H.; Langen, P.; and Schurath, U.: Near Infrared Emission Bands of the HO₂ Radical. *J. Chem. Phys.*, vol. 60, no. 11, June 1, 1974, pp. 4623-4625.
76. Parkes, D. A.; Paul, D. M.; Quinn, C. P.; and Robson, R. C.: The Ultraviolet Absorption by Alkylperoxy Radicals and Their Mutual Reactions. *Chem. Phys. Lett.*, vol. 23, no. 3, Dec. 1, 1973, pp. 425-429.

77. Graham, Richard A.; and Johnston, Harold S.: The Photochemistry of NO_3 and the Kinetics of the $\text{N}_2\text{O}_5\text{-O}_3$ System. J. Phys. Chem., vol. 82, no. 3, Feb. 1978, pp. 254-268.
78. Herron, John T.; and Huie, Robert E.: Stopped-Flow Studies of the Mechanisms of Ozone-Alkene Reactions in the Gas Phase. Ethylene. J. American Chem. Soc., vol. 99, no. 16, Aug. 3, 1977, pp. 5430-5435.

TABLE I.- PEAK CONCENTRATIONS FOR MINOR ATMOSPHERIC COMPOUNDS

Compound	Computed peak concentration, ppm	Observed peak concentration, ppm	Location	Reference
CH ₂ =CHCHO	1.3×10^{-2}	1.4×10^{-2}	Los Angeles, Calif.	Altshuller and McPherson (ref. 11)
CH ₃ CHO	7.7×10^{-3}	1.2×10^{-2}	Bayonne, N.J.	(a)
CH ₃ C(O)O ₂ NO ₂	2.9×10^{-3}	3.7×10^{-3}	Hoboken, N.J.	Lonneman (Private communication, 1974)
HCHO	6.5×10^{-3}	8×10^{-3}	Bayonne, N.J.	Cleveland and Kleiner (Private communication, 1974)
H ₂ O ₂	6.1×10^{-2}	4×10^{-2}	Hoboken, N.J.	Gay and Bufalini (ref. 12)
HNO ₂	3.4×10^{-4}	3.2×10^{-3}	South England	Nash (ref. 13)
HNO ₃	3.9×10^{-3}	6×10^{-3}	St. Louis, Mo.	Spicer (ref. 14)

^aThe observed Bayonne concentration of CH₃CHO is based on the Bayonne observation of HCHO and the assumptions that the total aldehyde/formaldehyde ratio of Altshuller and McPherson (ref. 11) holds in northern New Jersey and that the total aldehydes concentration minus the formaldehyde concentration is essentially equal to the CH₃CHO concentration.



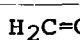
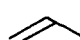

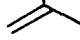
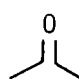
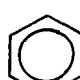
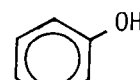
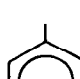
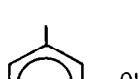
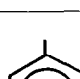
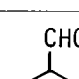
TABLE II.- MEASUREMENT NEEDS: FREE RADICALS

Species	Approximate concentration, molecules-cm ⁻³
HO [•]	1 × 10 ⁶
HO ₂ [•]	6 × 10 ⁸
NO ₃ [•]	5 × 10 ⁸
CH ₃ O ₂ [•]	1 × 10 ⁸

TABLE III.- MEASUREMENT NEEDS: ODD NITROGEN PRECURSORS AND PRODUCTS

Precursor	Approximate concentration, ppb	Linking species	Product	Approximate concentration, ppb
NO	10	HO [•]	HNO ₂	0.4
NO ₂	15	HO [•]	HNO ₃	4
NO ₂	15	HO ₂ [•]	HO ₂ NO ₂	?

TABLE IV.- MEASUREMENT NEEDS: ORGANIC PRECURSORS AND PRODUCTS

Precursor	Approximate concentration, ppb	Linking species	Product	Approximate concentration, ppb
H ₂ C=CH ₂ 	20	O ₃ , HO·	^a HCHO	10
	10			
	5	O ₃	^a CH ₃ CHO	4
H ₂ C=CH ₂ 	20	HO·	HCOOH	10
	10			
	5	O ₃		3
	25	HO·		?
	50	HO·		?
	50	HO·		?

^aAlso directly emitted by sources.

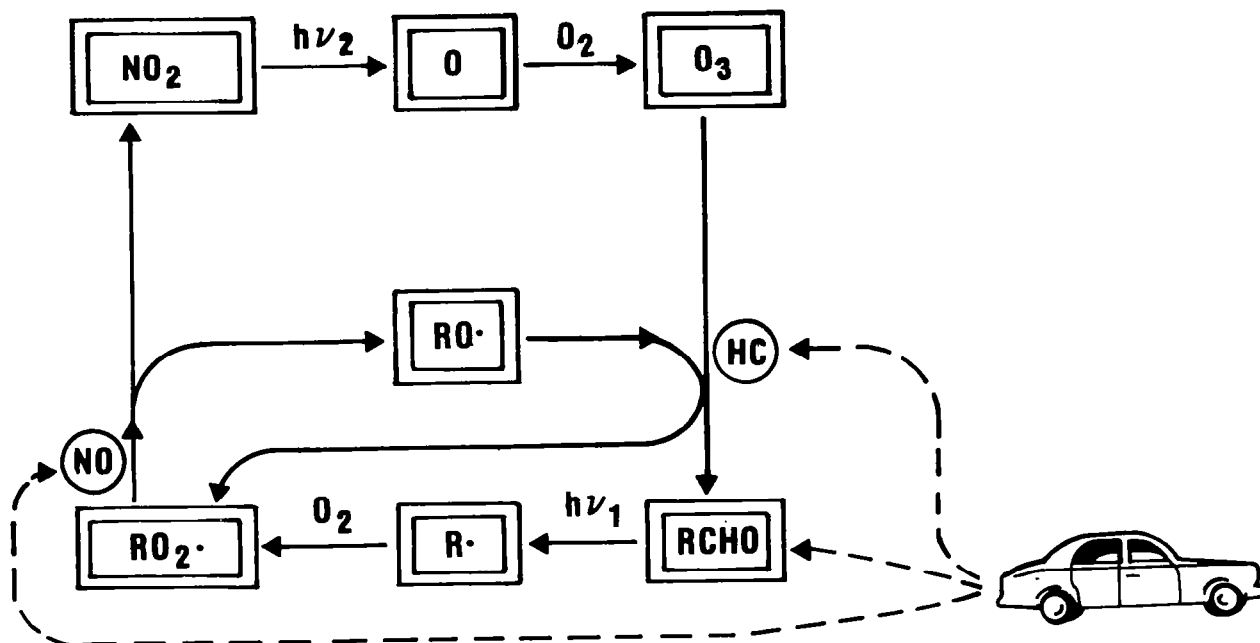


Figure 1.- Initiation and propagation of free-radical chemical chains in urban atmosphere. Sequence is initiated by photodissociation of aldehyde molecule, followed by oxidation of NO and hydrocarbon (HC) emittants.

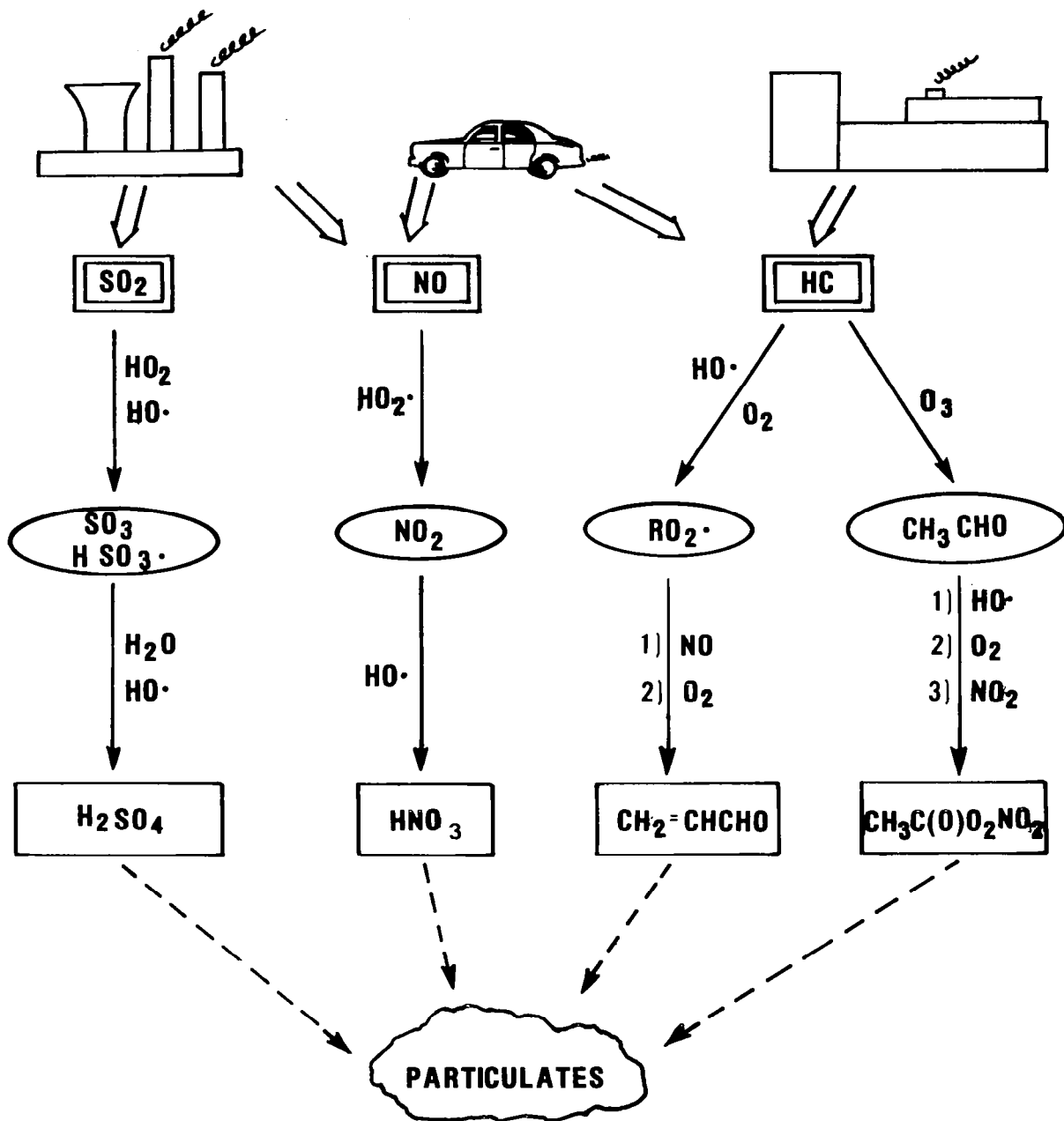


Figure 2.- Reaction sequences for formation of oxidized chemical products from urban precursors.

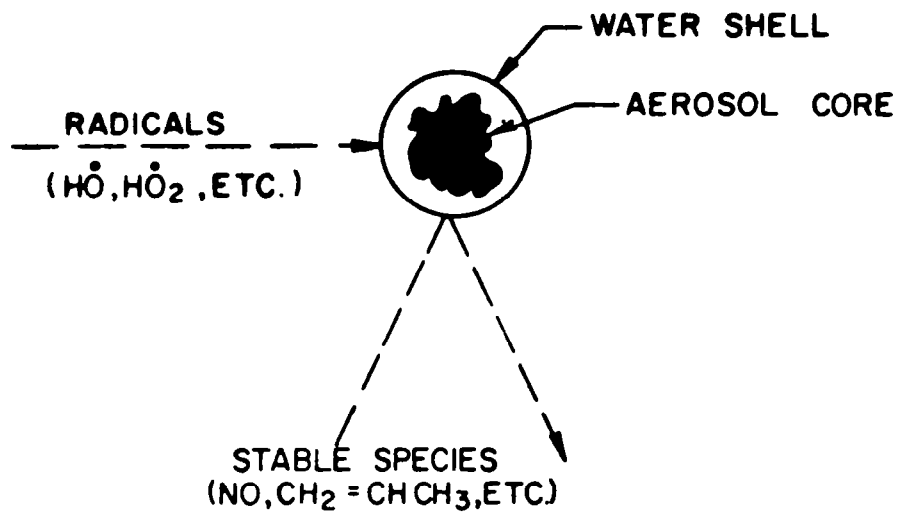


Figure 3.- Schematic representation of water-shell aerosol model for impact removal of radicals.

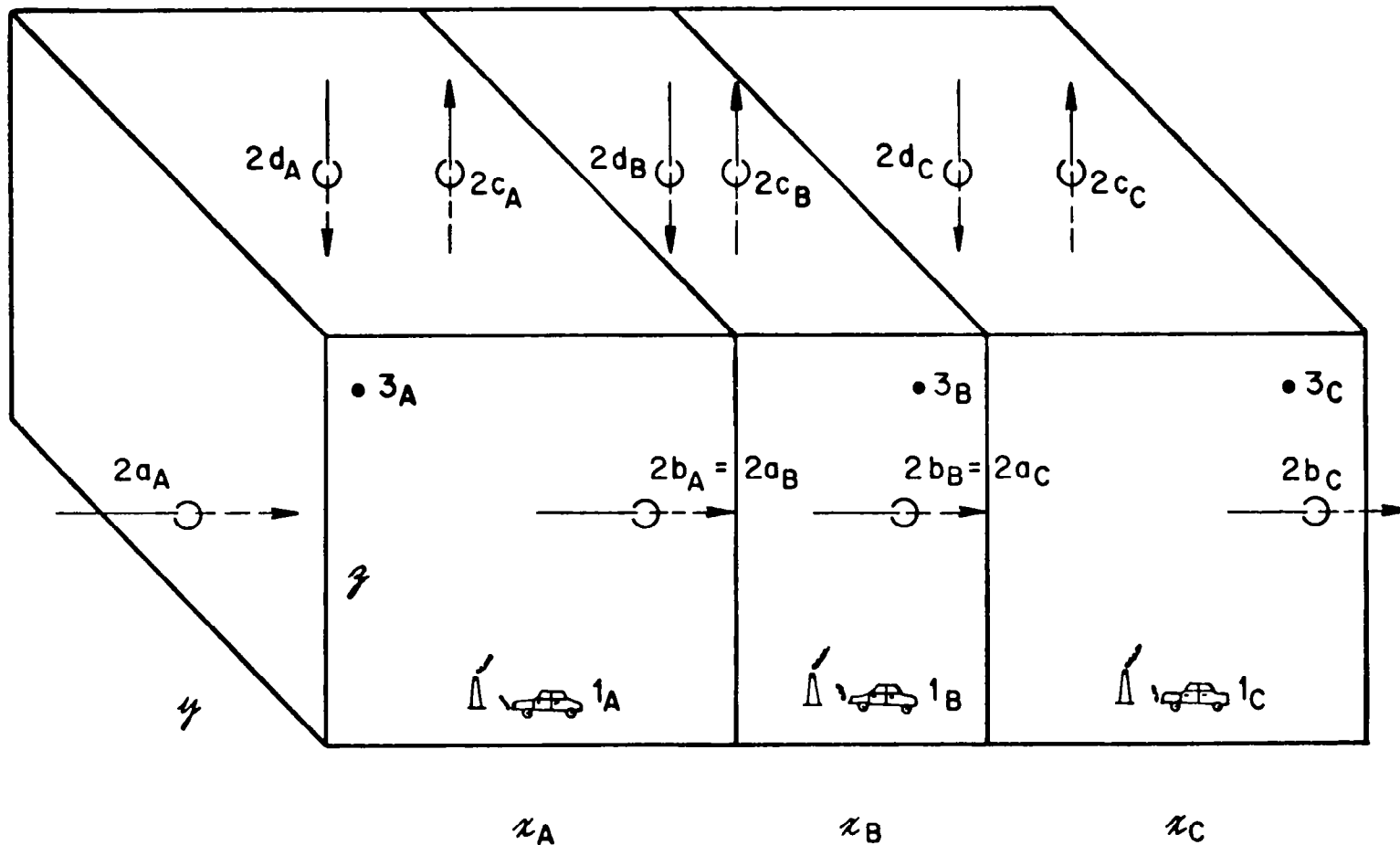


Figure 4.- Schematic representation of 3×1 reactant volume sequence. Symbols 1 refer to concentration changes resulting from source injection, symbols 2 to concentration changes resulting from meteorological processes, and symbols 3 to concentration changes resulting from chemical processes.

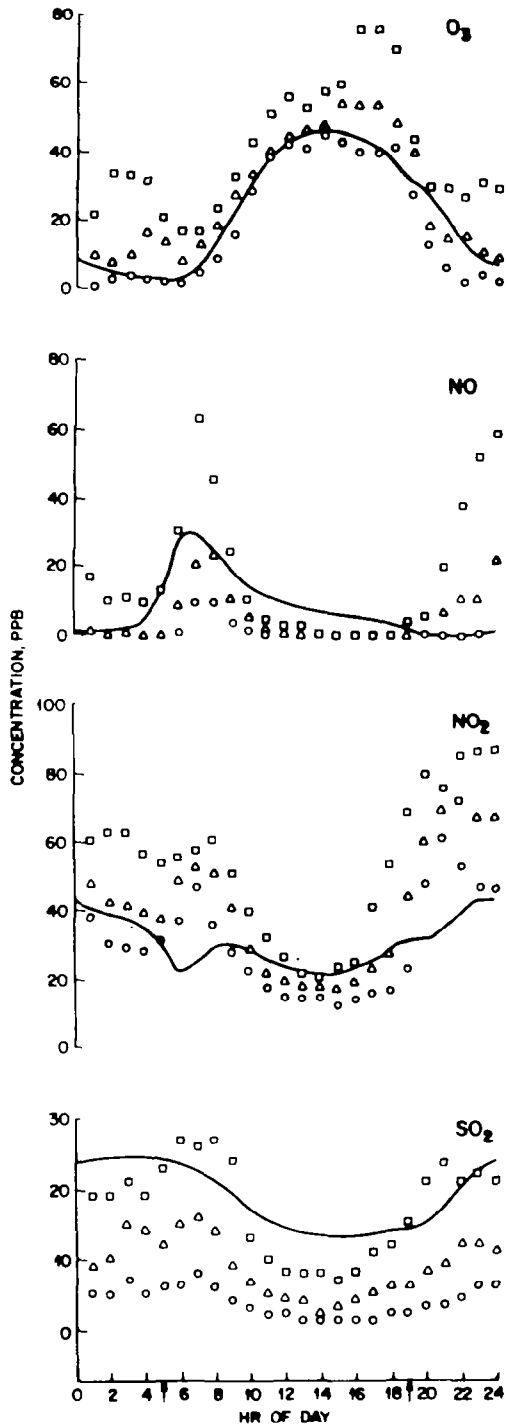


Figure 5.- Computed diurnal concentration patterns (solid lines) for Hudson County, N.J., compared with measured concentration distribution parameters: squares indicate upper quartile; triangles, median; and circles, lower quartile. Arrows on abscissa indicate times of sunrise and sunset.

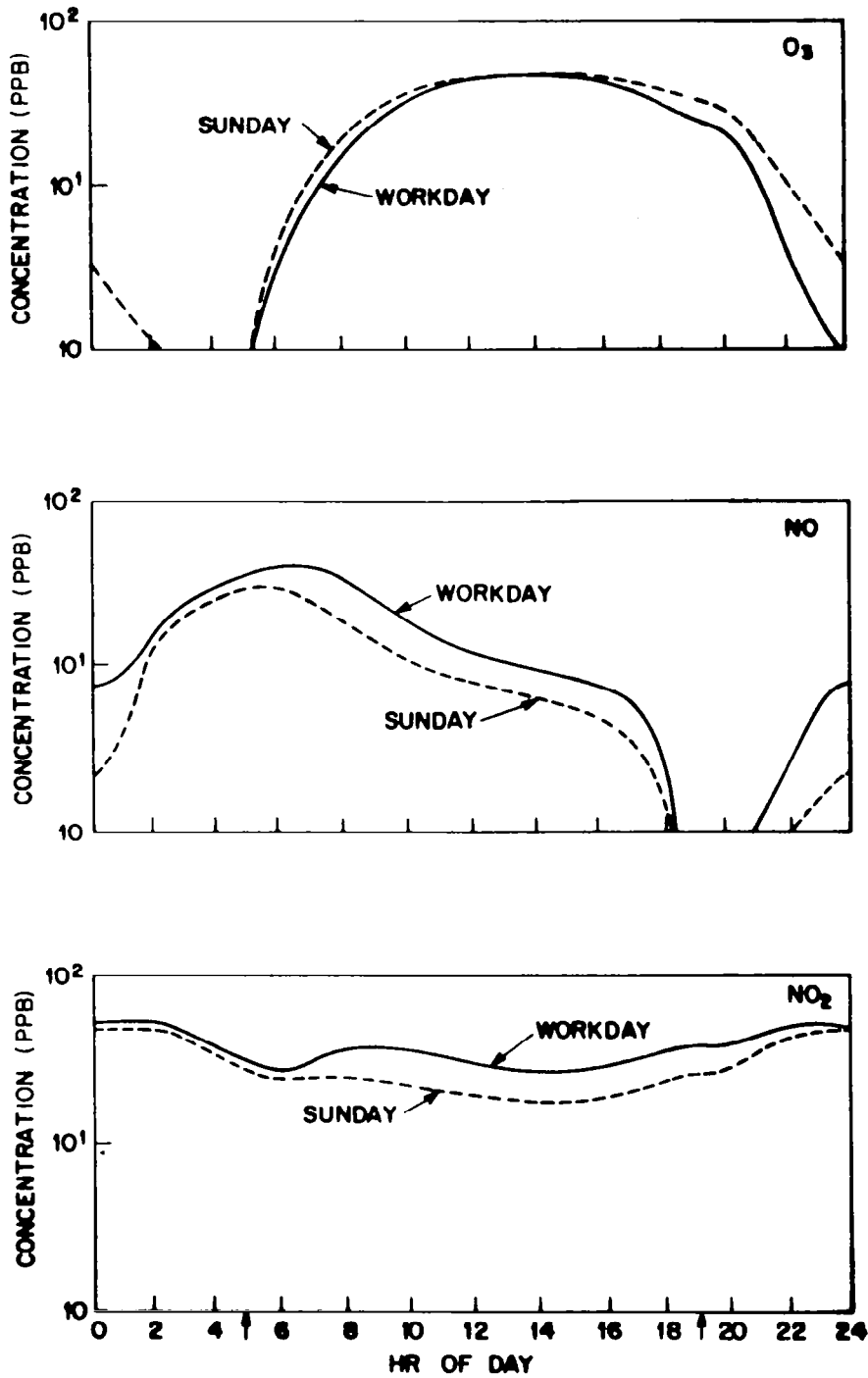


Figure 6.- Computed diurnal concentration patterns for workdays and Sundays in Hudson County, N.J. Arrows on abscissa indicate times of sunrise and sunset.

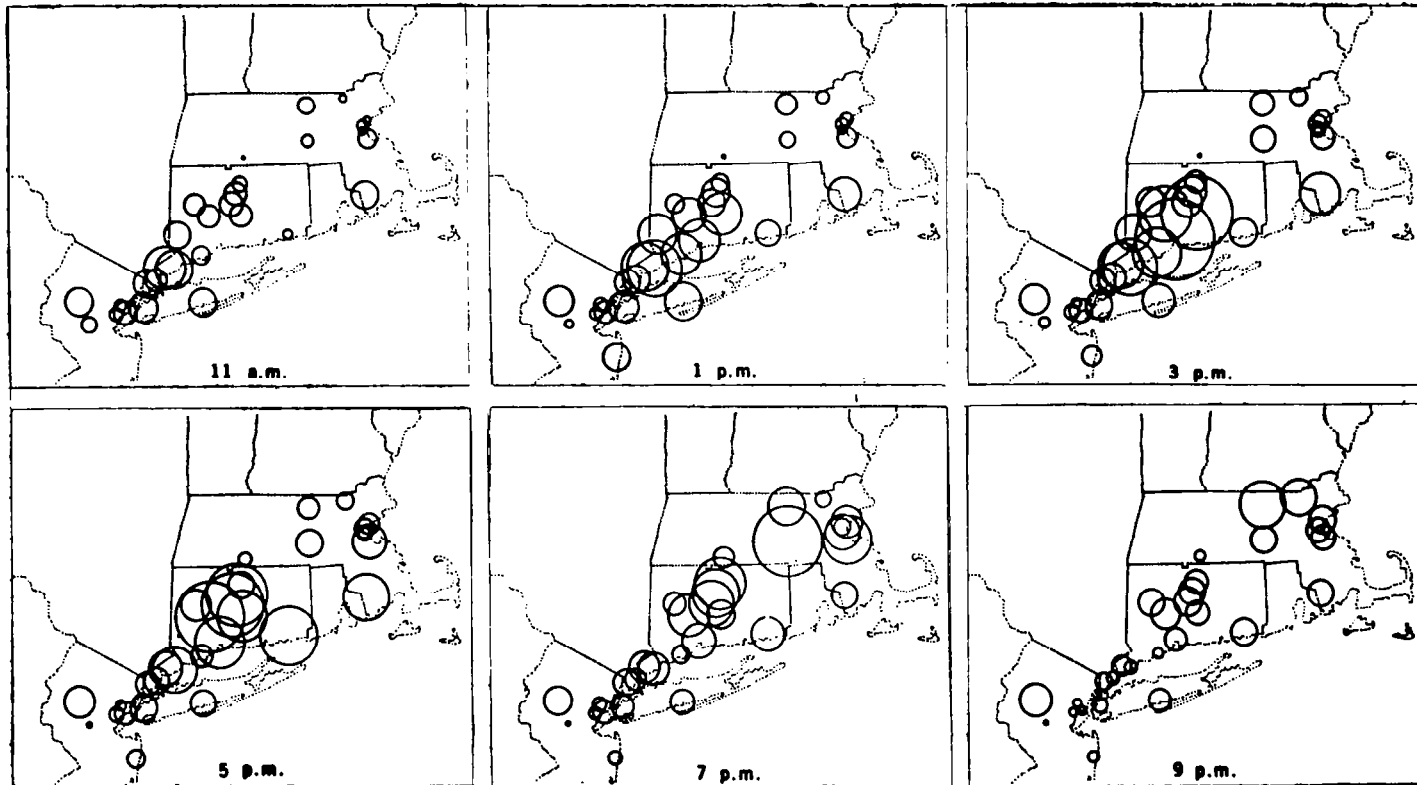


Figure 7.- Ozone concentrations at air monitoring sites in Northeastern United States measured at six different times during July 2, 1974, are coded by circle sizes. (From Cleveland et al. (ref. 22), copyright 1976 by the American Association for the Advancement of Science; reproduced with permission.)

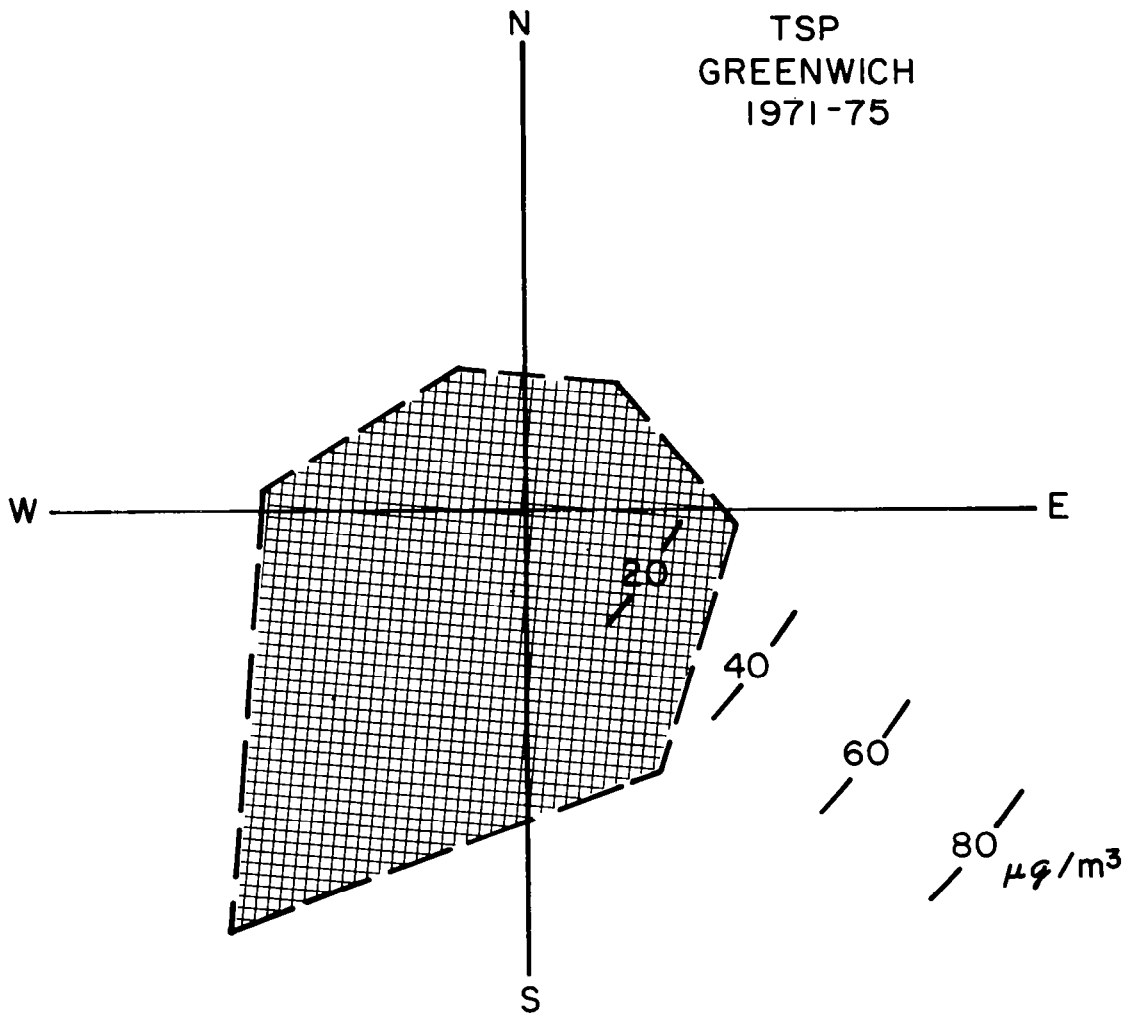


Figure 8.- Total particulate matter as a function of wind direction in Greenwich, Conn., from 1971 to 1975. New York-New Jersey metropolitan area is southwest of this monitoring site (Bruckman (ref. 23)).

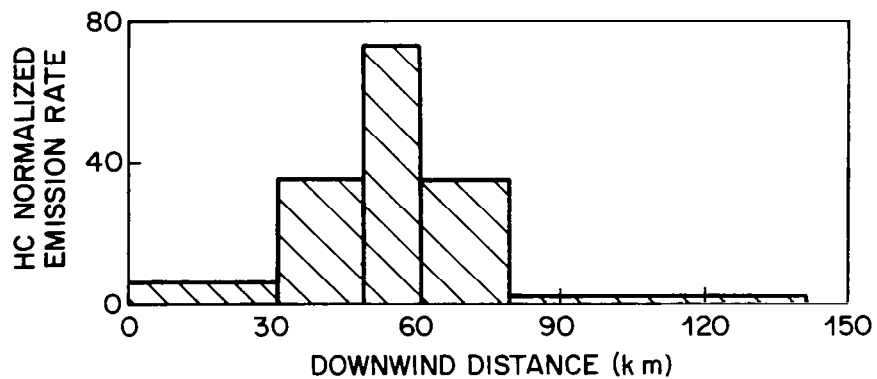
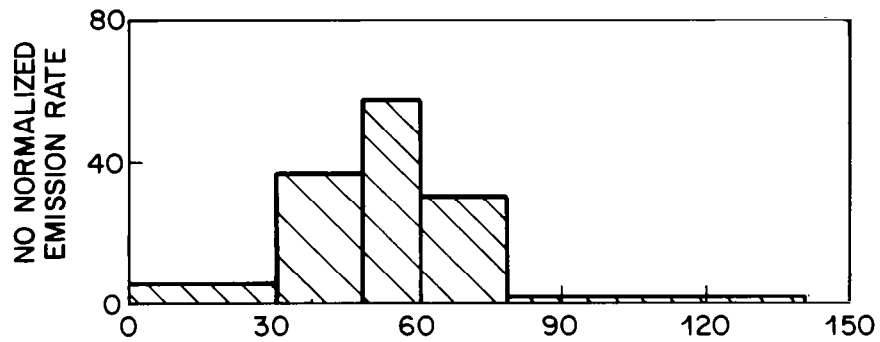
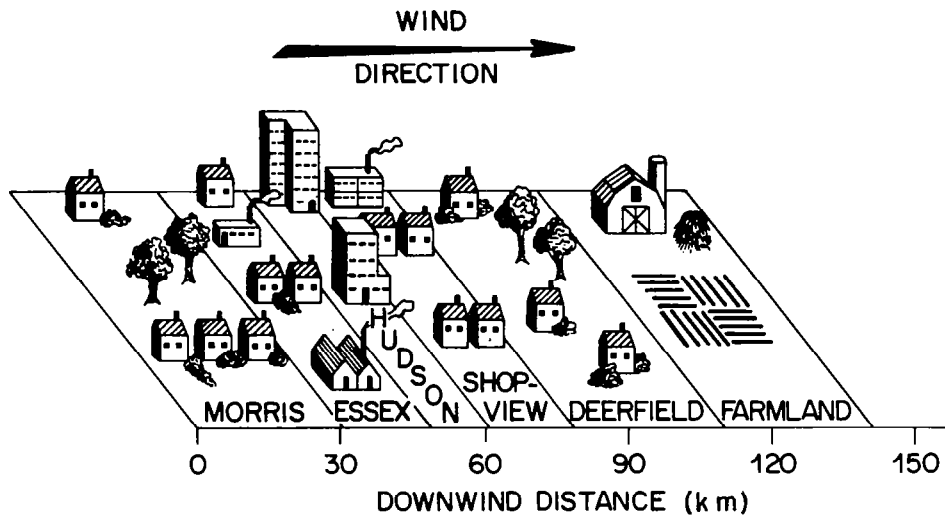


Figure 9.- Six-county computational sequence showing respective downwind distances (referenced to western edge of Morris County) and relative NO and hydrocarbon (HC) emission rates (for relative rate purposes, Deerfield and Farmland Counties' emission rates have unity values).

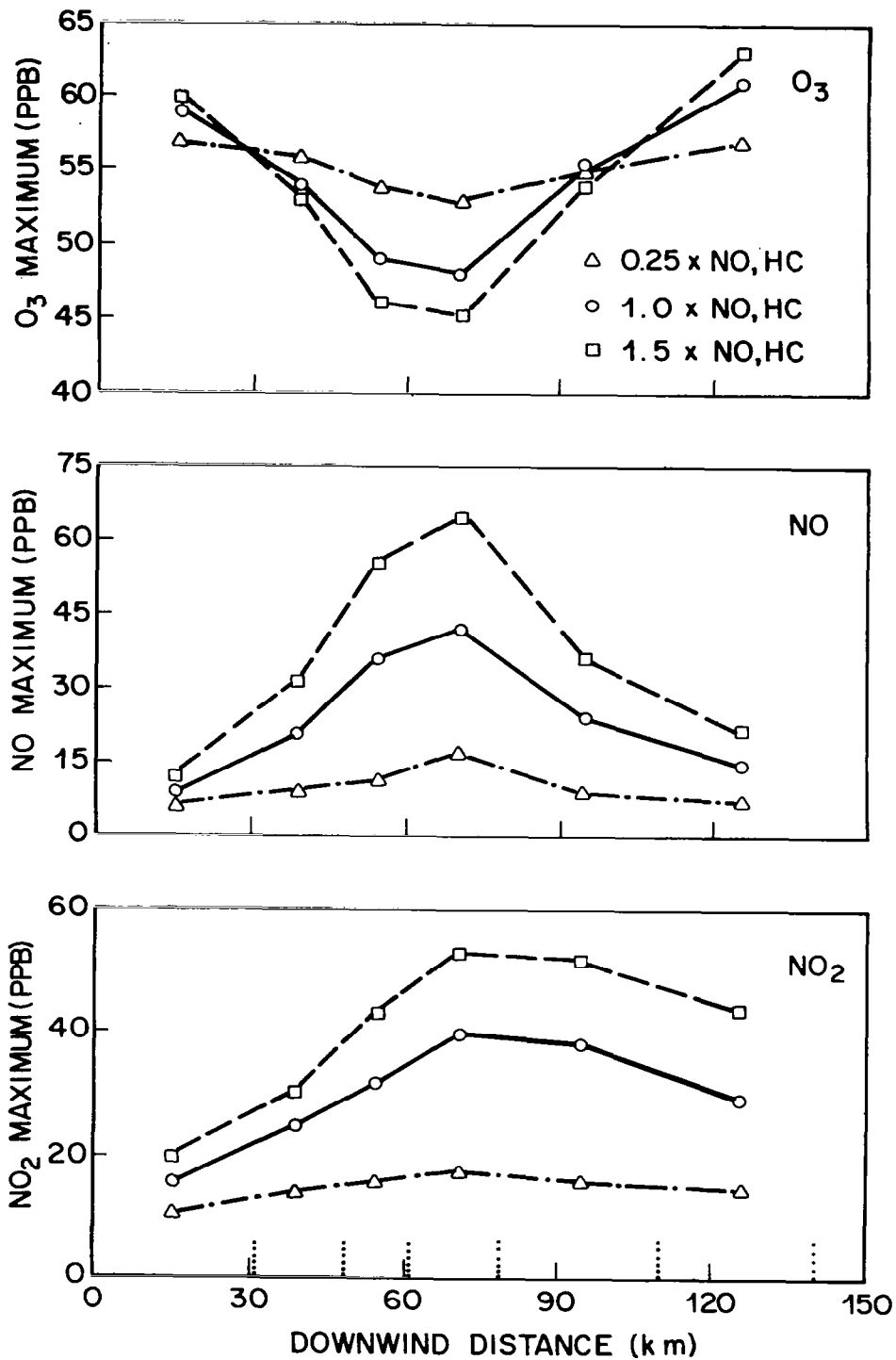


Figure 10.- Computed diurnal maximum concentrations of NO, NO₂, and O₃ in the six counties. Dotted lines on abscissa indicate county boundaries.

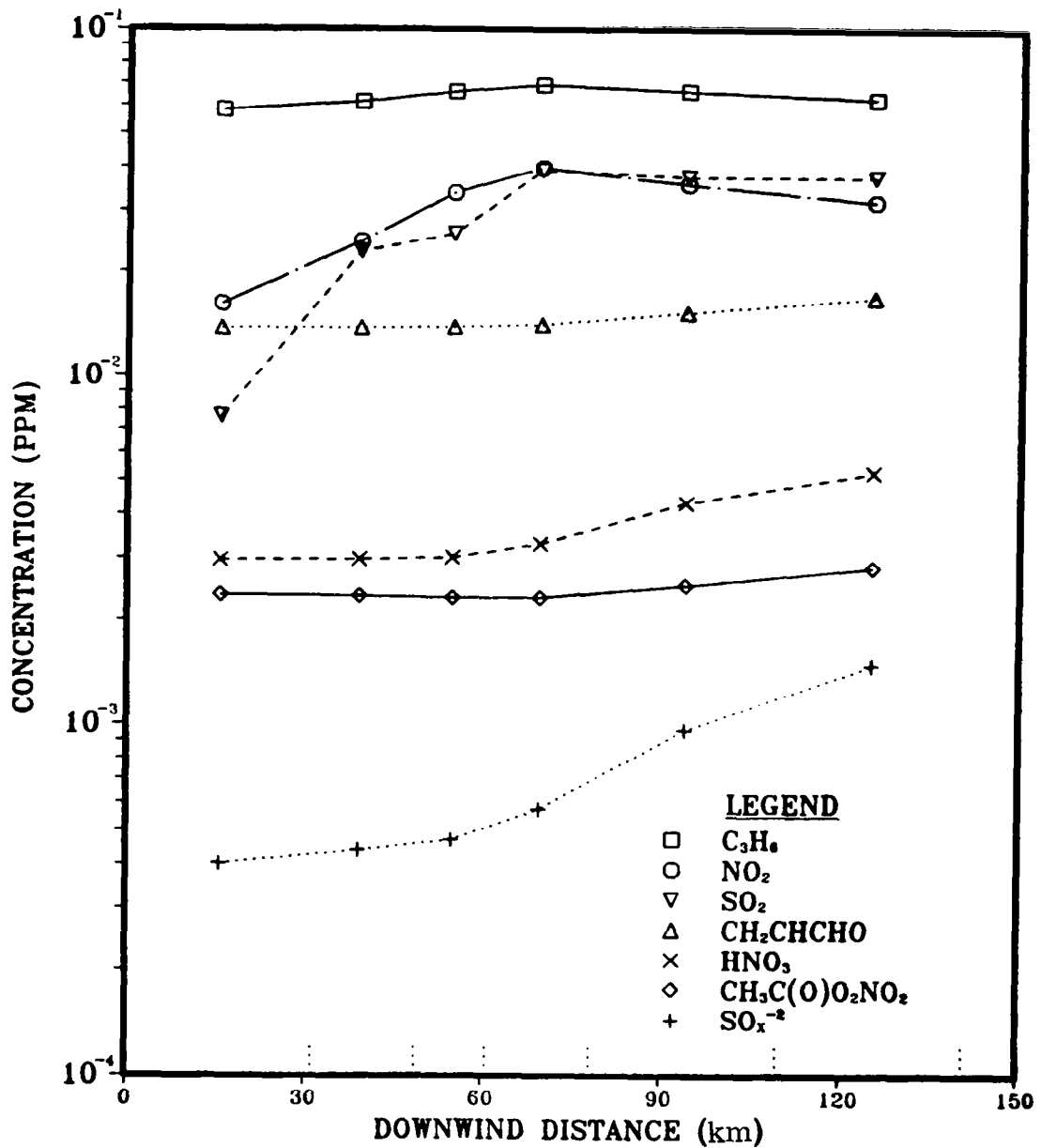


Figure 11.- Computed concentrations of precursors (NO₂, C₃H₆, and SO₂) and photochemical products (SO_x⁻², HNO₃, CH₃C(O)O₂NO₂, and CH₂CHCHO) in the six counties at 7 p.m. for days with normal emissions, sun, and wind. Dotted lines on abscissa indicate county boundaries.

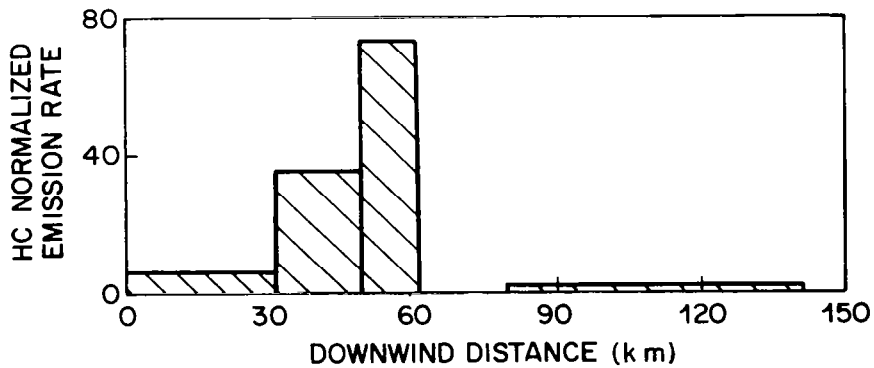
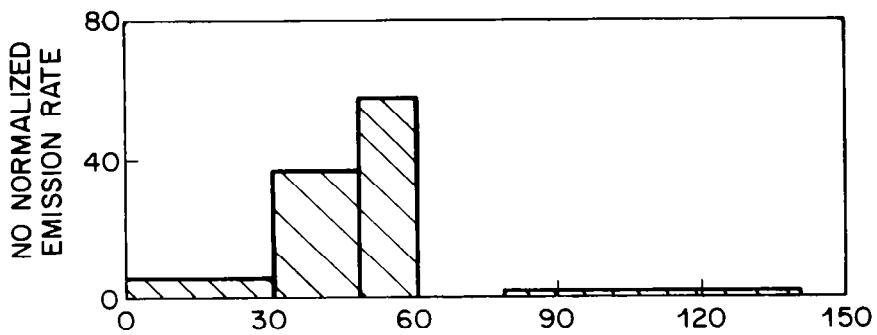
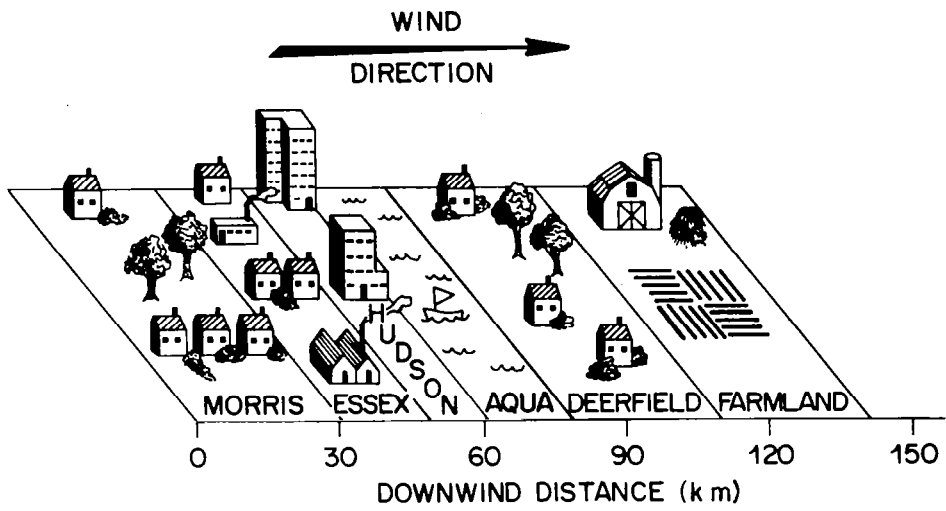


Figure 12.- Six-county computational sequence for overwater traverse together with normalized NO and hydrocarbon (HC) emission rates.

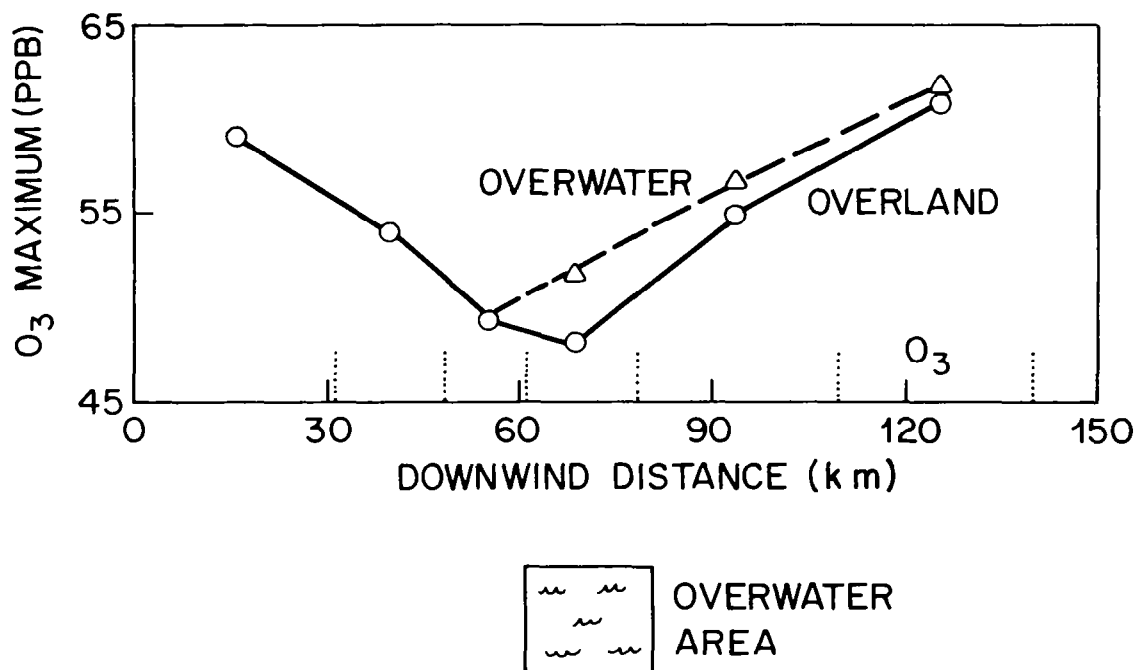


Figure 13.- Maximum computed ozone concentrations for overland and overwater traverses. Plotted points are averages over individual counties. Dotted lines on abscissa indicate county boundaries.

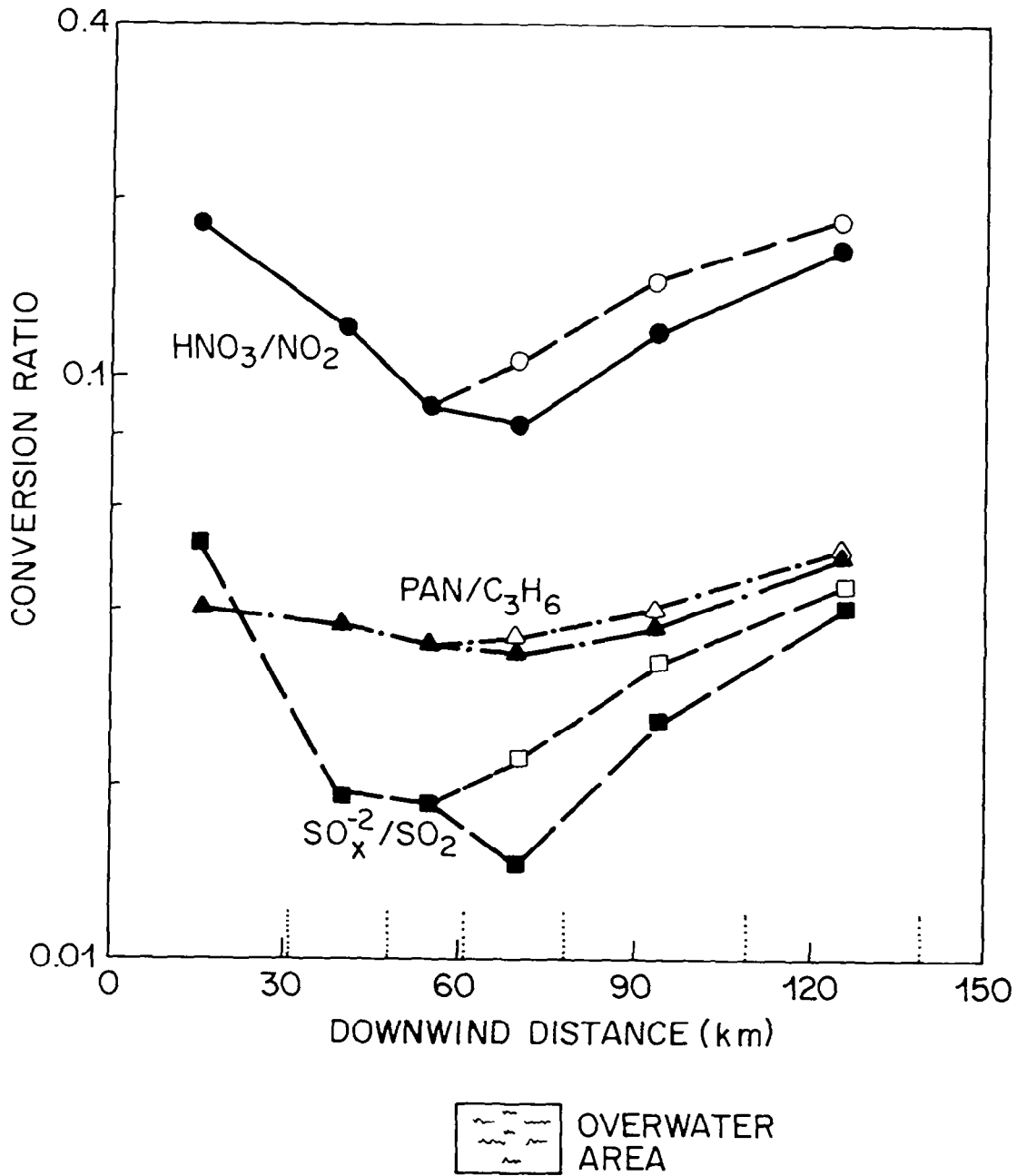
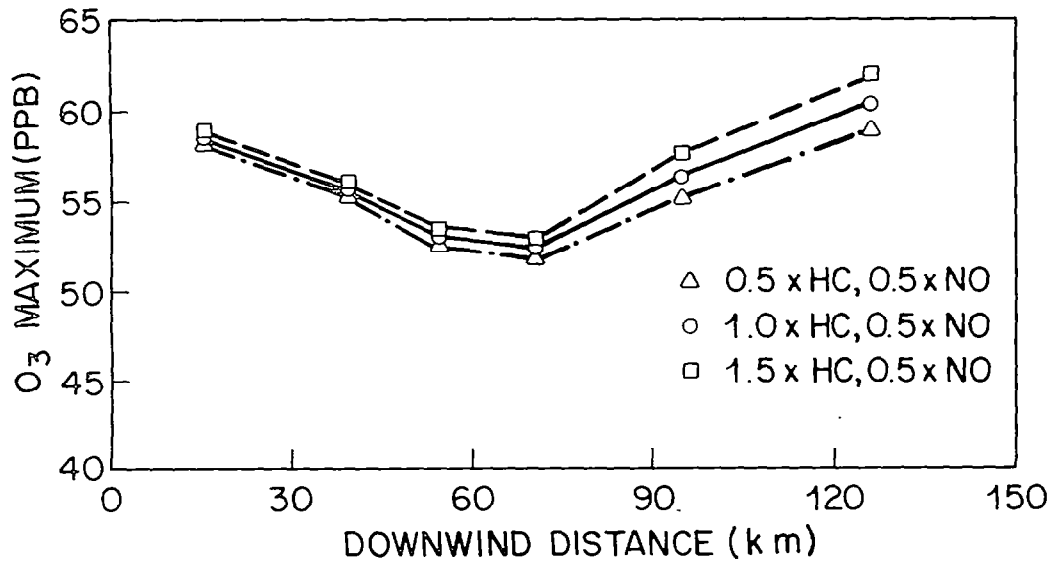
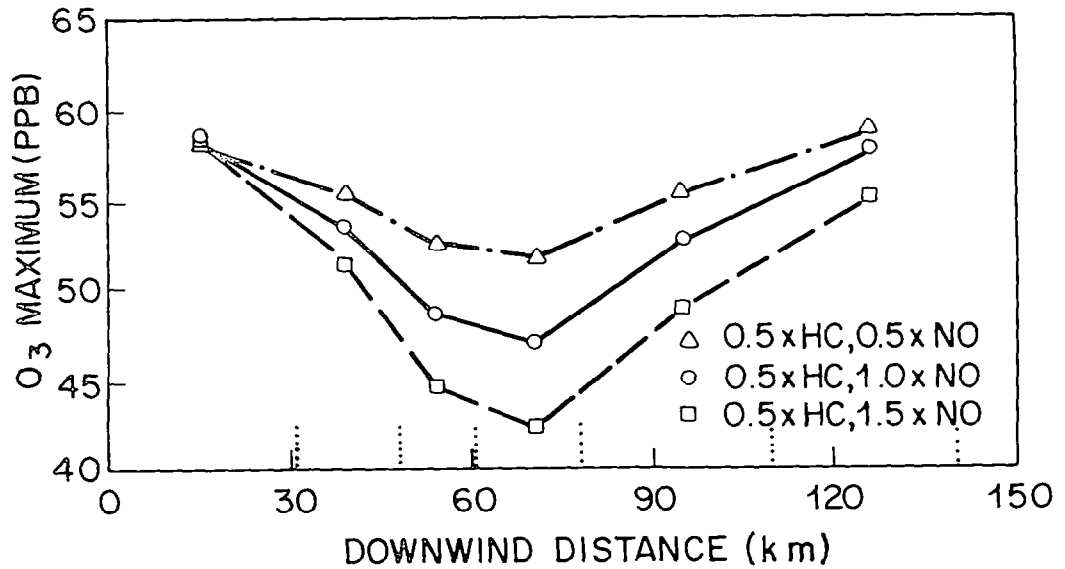


Figure 14.- Conversion ratios for nitrate (circles), sulfate (squares), and PAN (triangles) as functions of downwind distance at 7 p.m. Solid symbols refer to overland traverse and open symbols to overwater traverse. Dotted lines on abscissa indicate county boundaries.



(a) Variation of hydrocarbon emissions only.



(b) Variation of NO emissions only.

Figure 15.- Computed diurnal ozone maxima for the six counties in NO-HC anthropogenic emission plane. Dotted lines on abscissa indicate county boundaries.

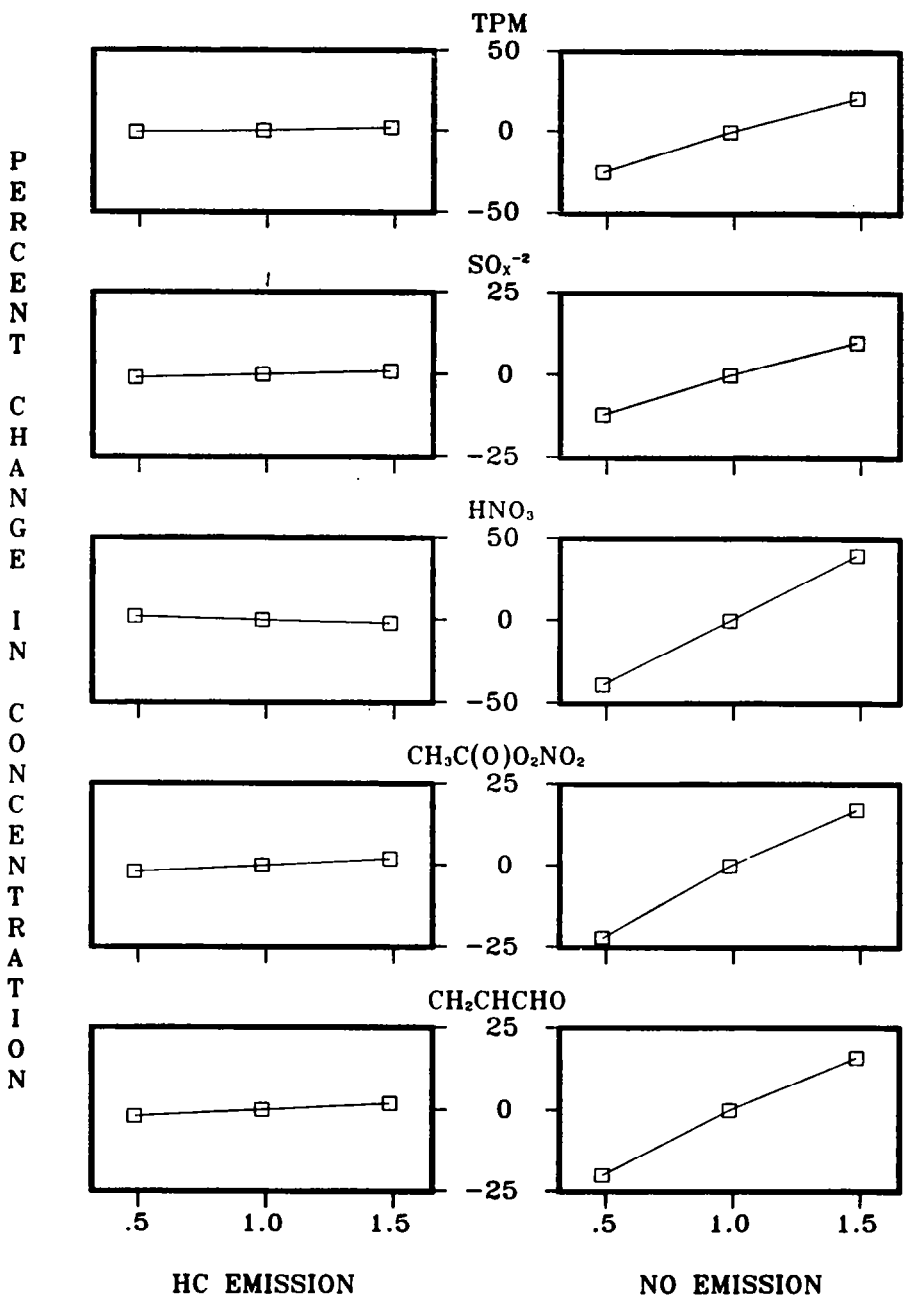


Figure 16.- Percent change in concentration of various photochemical products at 7 p.m. in Hudson County for different emission rates. Plots on the left are for variation in hydrocarbon (HC) emission normalized to current source estimate (Abcissa = 1.0); NO emissions are kept constant at current estimate for these computations. Plots on the right are for variation in NO emission with HC emission kept constant. TPM indicates total particulate matter.

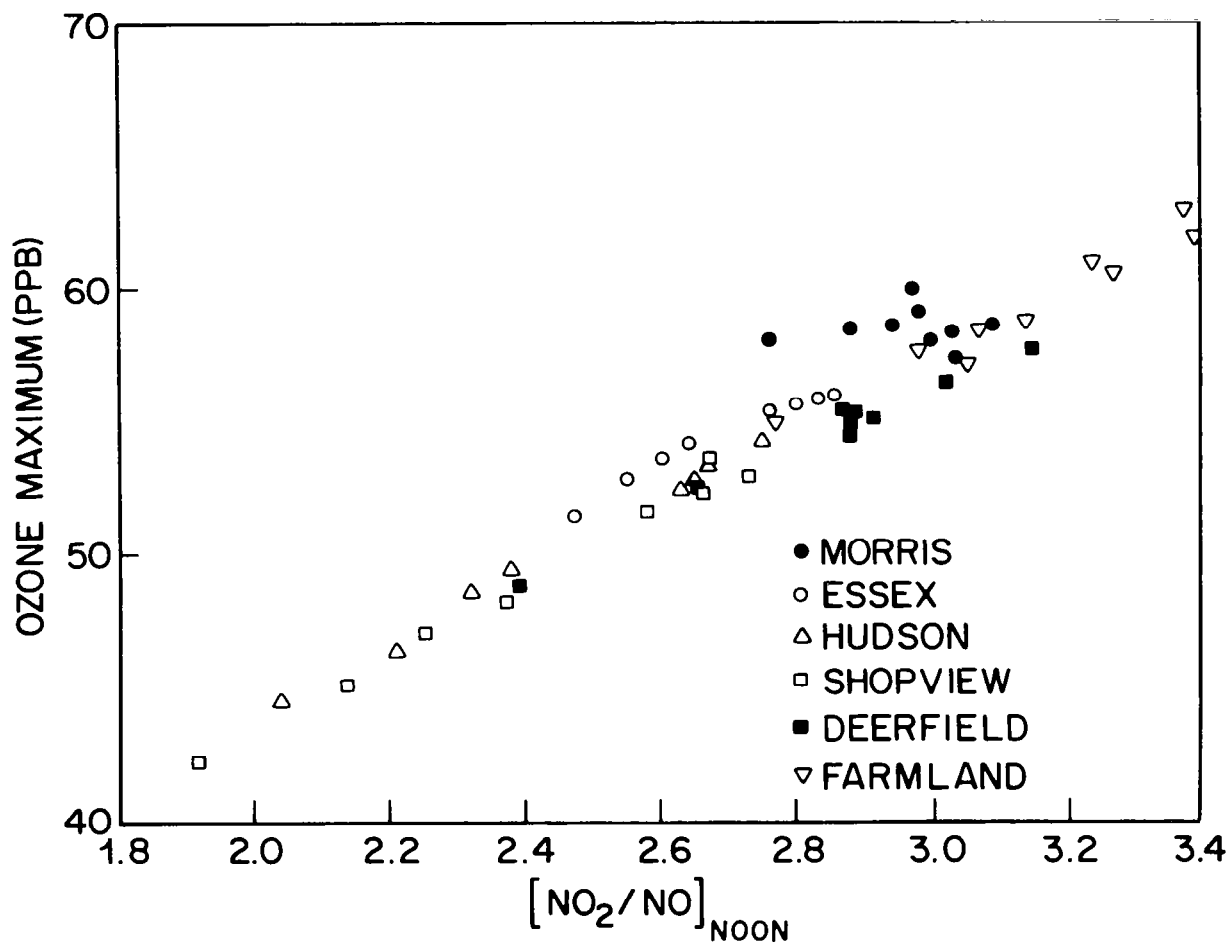


Figure 17.- Computed diurnal ozone maxima in the six counties as a function of noontime NO_2/NO concentration ratio.

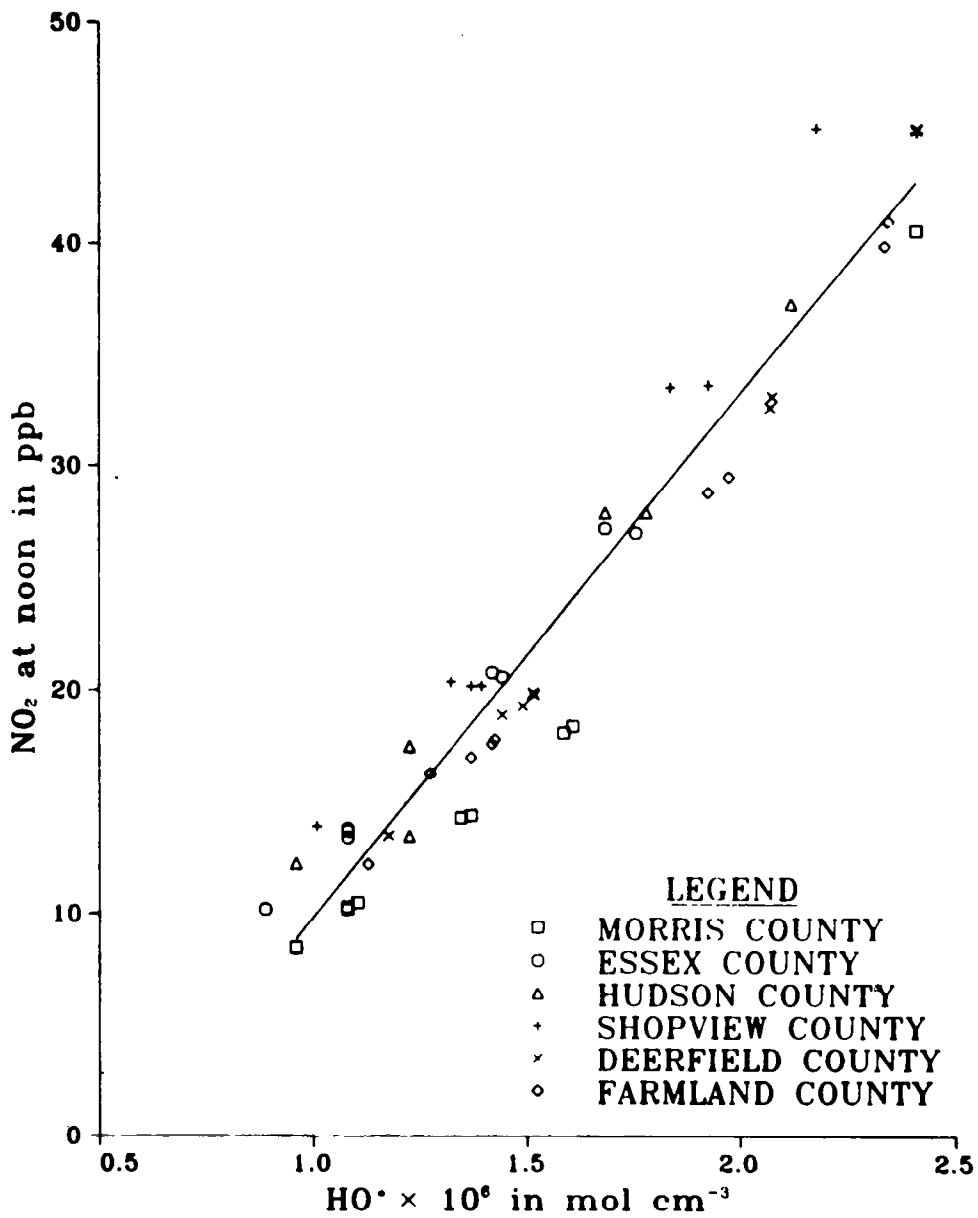
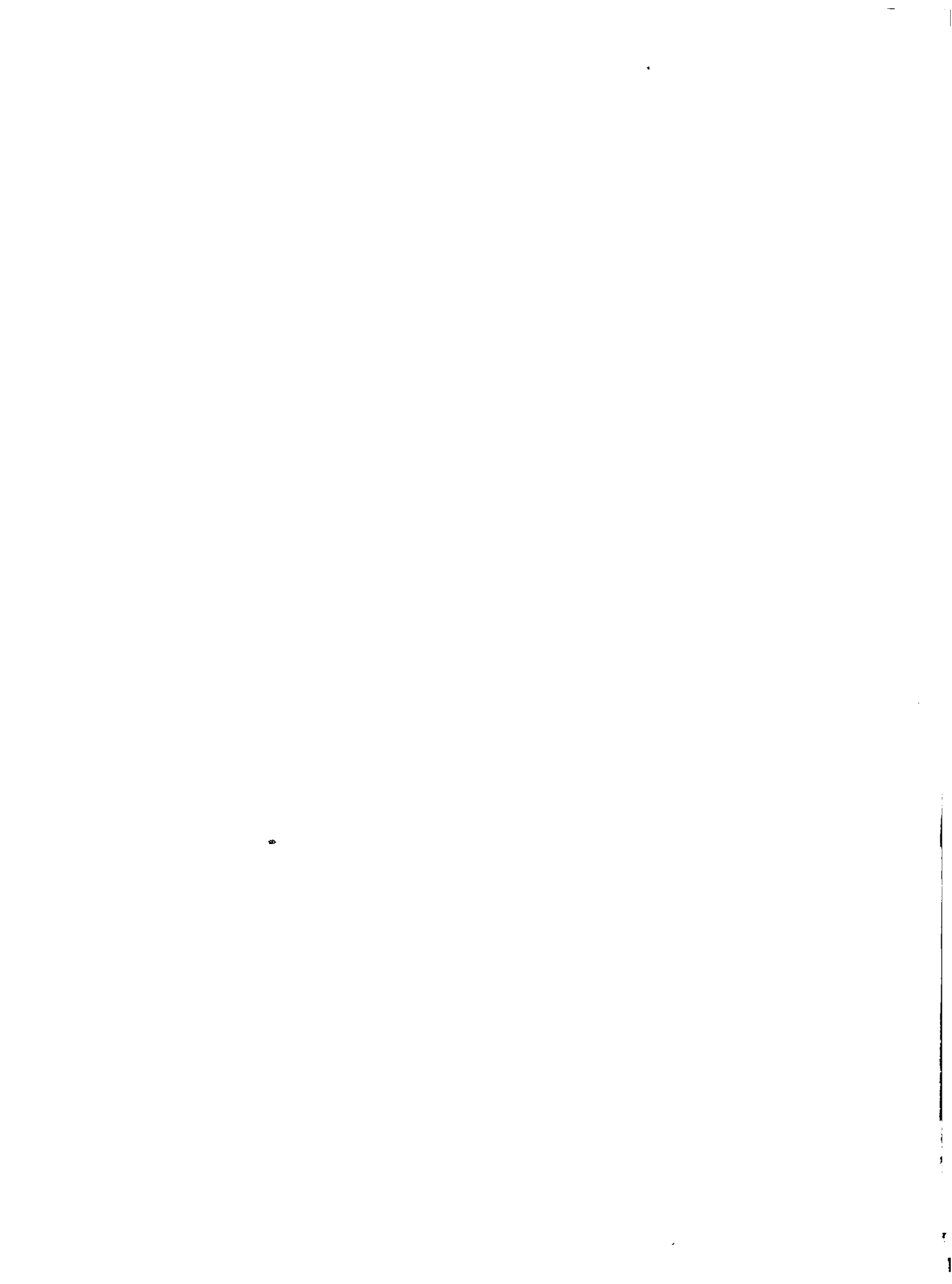


Figure 18.- Relationship between HO· maxima (molecules-cm⁻³) and NO₂ noontime concentrations (ppb) for all counties and emission fluxes included in this series of computations.



MATHEMATICAL MODELING OF THE POLLUTED TROPOSPHERE

John H. Seinfeld
California Institute of Technology
Pasadena, California

INTRODUCTION

The purpose of this paper is to provide an overview of the general problems involved in mathematical modeling of the polluted troposphere (principally the urban atmosphere). The paper is divided into two basic sections:

- (1) Fundamentals of air quality models
- (2) Aerosol processes in the polluted troposphere

The first section is essentially a review of the major elements of mathematical models. The second section consists of a development of a model capable of predicting the transformation of gaseous material to particulate material in the urban atmosphere and urban plume.

FUNDAMENTALS OF AIR QUALITY MODELS

All conventional atmospheric diffusion models are based on the equation of conservation of mass:

$$\frac{\partial c_i}{\partial t} + u \frac{\partial c_i}{\partial x} + v \frac{\partial c_i}{\partial y} + w \frac{\partial c_i}{\partial z} = D_i \left(\frac{\partial^2 c_i}{\partial x^2} + \frac{\partial^2 c_i}{\partial y^2} + \frac{\partial^2 c_i}{\partial z^2} \right) + R_i(c_1, \dots, c_N, T) + S_i(x, y, z, t) \quad (1)$$

where t is time; c_i is the concentration of species i ; u , v , and w are the fluid velocities in the three coordinate directions x , y , and z ; D_i is the molecular diffusivity of species i in air; R_i is the rate of generation (or the negative of the rate of disappearance) of species i by chemical reactions at temperature T ; and S_i is the rate of injection of species i into the fluid from sources.

Substituting the usual mean and fluctuating terms into equation (1) and averaging the resulting equation over the ensemble of flows result in the equa-

tion governing the ensemble average concentration \bar{c}_i . In atmospheric applications, the molecular diffusion term is negligible when compared with that representing advective transport. Thus, by neglecting the contribution of molecular diffusion, the equation for \bar{c}_i becomes

$$\frac{\partial \bar{c}_i}{\partial t} + \bar{u} \frac{\partial \bar{c}_i}{\partial x} + \bar{v} \frac{\partial \bar{c}_i}{\partial y} + \bar{w} \frac{\partial \bar{c}_i}{\partial z} + \frac{\partial}{\partial x} \overline{u'c_i'} + \frac{\partial}{\partial y} \overline{v'c_i'} + \frac{\partial}{\partial z} \overline{w'c_i'} = \overline{R_i(c_1, \dots, c_N, T)} + \bar{S}_i(x, y, z, t) \quad (2)$$

Equation (2) is a rigorously valid equation for \bar{c}_i (neglecting, of course, molecular diffusion); and, if the variables $u'c_i'$, $v'c_i'$, $w'c_i'$, and any of those arising from R_i are known as functions of space and time, it can be solved in principle to yield \bar{c}_i . Unfortunately, $u'c_i'$ and so on cannot be measured at all points in an atmospheric flow and cannot be predicted exactly because of the closure problem of turbulent flow. Thus, models must be used for these terms. The model employed in virtually all cases in which atmospheric flows are involved is that based on the concept of eddy diffusivities:

$$\overline{u'c_i'} = -K_H \frac{\partial \bar{c}_i}{\partial x} \quad \overline{v'c_i'} = -K_H \frac{\partial \bar{c}_i}{\partial y} \quad \overline{w'c_i'} = -K_V \frac{\partial \bar{c}_i}{\partial z} \quad (3)$$

The eddy diffusivities K_H and K_V are postulated to be functions of space and time (and not of \bar{c}_i or any of its gradients).

Although there has been some study of the nature of terms of the form $\overline{c_i'^2}$ arising from turbulent chemical reactions, no atmospheric diffusion models for chemically reactive pollutants currently include expressions for these terms. All models neglect the contribution of turbulent concentration fluctuations to the mean reaction rate and employ the approximation,

$$\overline{R_i(c_1, \dots, c_N, T)} \approx R_i(\bar{c}_1, \dots, \bar{c}_N, T) \quad (4)$$

The result of using equations (3) and (4) in equation (2) is the so-called atmospheric diffusion equation (ADE):

$$\frac{\partial \bar{c}_i}{\partial t} + \bar{u} \frac{\partial \bar{c}_i}{\partial x} + \bar{v} \frac{\partial \bar{c}_i}{\partial y} + \bar{w} \frac{\partial \bar{c}_i}{\partial z} = \frac{\partial}{\partial x} \left(K_H \frac{\partial \bar{c}_i}{\partial x} \right) + \frac{\partial}{\partial y} \left(K_H \frac{\partial \bar{c}_i}{\partial y} \right) + \frac{\partial}{\partial z} \left(K_V \frac{\partial \bar{c}_i}{\partial z} \right) + R_i(\bar{c}_1, \dots, \bar{c}_N, T) + \bar{S}_i(x, y, z, t) \quad (5)$$

Because the governing equations are nonlinear, they must be solved numerically. Furthermore, the use of numerical techniques generally requires that the modeling region be subdivided into an array of grid cells, where each cell may have horizontal and vertical dimensions on the order of a few kilometers and several tens of meters, respectively. Before the general mass continuity equation can be solved, it must be "filtered" to remove all small-scale variations that the grid cannot resolve, both in the concentration field and in the independent parameters, such as the wind velocities and the eddy diffusivities. The necessary filtering can be accomplished by averaging equation (5) at each point over a volume equivalent to that of a grid cell. This spatial averaging will be denoted by the symbol $\langle \rangle$. In addition, equation (5) has been time averaged over an interval equivalent to that used in each step of the numerical solution procedure. Thus, the concentration predictions obtained from equation (5) represent spatially and temporally averaged quantities.

Spatial averaging of equation (5) results in¹

$$\frac{\partial \langle \bar{c}_i \rangle}{\partial t} + \bar{u} \frac{\partial \langle \bar{c}_i \rangle}{\partial x} + \bar{v} \frac{\partial \langle \bar{c}_i \rangle}{\partial y} + \bar{w} \frac{\partial \langle \bar{c}_i \rangle}{\partial z} = \frac{\partial}{\partial x} \left(K_H \frac{\partial \langle \bar{c}_i \rangle}{\partial x} \right) + \frac{\partial}{\partial y} \left(K_H \frac{\partial \langle \bar{c}_i \rangle}{\partial y} \right) + \frac{\partial}{\partial z} \left(K_V \frac{\partial \langle \bar{c}_i \rangle}{\partial z} \right) + \langle R_i(\bar{c}_i, \dots, \bar{c}_N, T) \rangle + \langle \bar{S}_i \rangle \quad (6)$$

As in the case of equation (4), all models employ the approximation,

$$\langle R_i(\bar{c}_i, \dots, \bar{c}_N, T) \rangle \approx R_i(\langle \bar{c}_i \rangle, \dots, \langle \bar{c}_N \rangle, T) \quad (7)$$

Thus, the contribution of subgrid-scale concentration variations to the mean reaction rate are neglected.

The equation that is the basis of all air quality models is obtained by employing equation (7) in equation (6):

$$\frac{\partial \langle \bar{c}_i \rangle}{\partial t} + \bar{u} \frac{\partial \langle \bar{c}_i \rangle}{\partial x} + \bar{v} \frac{\partial \langle \bar{c}_i \rangle}{\partial y} + \bar{w} \frac{\partial \langle \bar{c}_i \rangle}{\partial z} = \frac{\partial}{\partial x} \left(K_H \frac{\partial \langle \bar{c}_i \rangle}{\partial x} \right) + \frac{\partial}{\partial y} \left(K_H \frac{\partial \langle \bar{c}_i \rangle}{\partial y} \right) + \frac{\partial}{\partial z} \left(K_V \frac{\partial \langle \bar{c}_i \rangle}{\partial z} \right) + R_i(\langle \bar{c}_i \rangle, \dots, \langle \bar{c}_N \rangle, T) + \langle \bar{S}_i \rangle \quad (8)$$

The validity of the atmospheric diffusion equation relates to how closely the predicted mean concentration $\langle \bar{c}_i \rangle$ corresponds to the true ensemble mean concentration. If the mean velocities \bar{u} , \bar{v} , and \bar{w} and the source emission

¹By virtue of the manner in which they are determined, \bar{u} , \bar{v} , and \bar{w} are assumed to represent spatially averaged quantities.

rate S_i are known precisely at all points as a function of time, then, for an inert species, the only source of a discrepancy between the predicted and true mean concentrations is the eddy diffusivity model for the turbulent fluxes. If the true ensemble mean velocities and concentrations are known for an atmospheric flow, then it is relatively straightforward to assess the validity of equation (8) for specified forms of K_H and K_V . Unfortunately, for any atmospheric flow, the ensemble mean velocities and concentrations can never be computed since the atmosphere presents only one realization of the flow at any time. (Of course, for a statistically stationary flow, ensemble averages can be replaced by time averages. The atmosphere is, however, seldom in a stationary condition for any appreciable period of time.) Because the true mean velocities and source emission rates that are required to solve equation (8) and the true mean concentration with which the solution of equation (8) is to be compared are not available in general, an unambiguous measure of the validity of equation (8) for any particular flow cannot be obtained.

Accuracy evaluation refers to the agreement between model predictions and observations for a model based on a perfectly sound principle; thus, accuracy evaluation is an assessment of the error introduced by inaccuracies of the input information.² Whereas an assessment of model validity is very difficult to obtain, accuracy evaluations can be made from estimates of the errors associated with the input information and from numerical sensitivity tests to determine the impacts of such errors on model predictions. Unlike verification and accuracy evaluation, direct determination of the validity of a model is extremely difficult to accomplish because the requisite exact data on emissions, meteorological variables, and air quality are neither available nor easy to obtain. It is therefore necessary to rely on combinations of verification and accuracy-evaluation studies in order to judge the adequacy of a model. By necessity, this approach is adopted here.

Table I summarizes the sources of invalidity and inaccuracy of equation (8). The sources of invalidity cannot be directly assessed for the reasons just stated. The sources of inaccuracy, on the other hand, can be assessed through verification and accuracy-evaluation studies.

The inputs needed to solve the atmospheric diffusion equation together with possible sources of error in those inputs are given in table I. In each instance unless the actual value of the input is known, the level of error in that input can only be estimated. From the standpoint of the effect of errors on the predictions of the equation, joint consideration must be given to the level of uncertainty in each input parameter and the sensitivity of the predicted concentration to the parameter. Uncertainty relates to the possible error in the parameter from its true value, and sensitivity refers to the effect that this variation in the parameter has on the solution of the equation. A parameter

²Another term often used in connection with model evaluation is "verification," referring to the agreement between predictions and observations for the specific case in which the observations used for verification were taken from the same pool of data used to develop the input information for the model. Verification contains elements, therefore, of both validation and accuracy evaluation. Henceforth, verification studies will be referred to as validation studies in keeping with the prevailing usage.

may have a large uncertainty associated with it but have little influence on the solution. In such a case, effort at reducing the uncertainty in the parameter value may be unwarranted. On the other hand, small uncertainties in a parameter to which the solution is quite sensitive may have a large impact on uncertainties in the predicted concentrations. Thus, both uncertainty and sensitivity must be considered when the accuracy of the atmospheric diffusion equation is evaluated.

Finally, note that discrepancies between predicted and measured concentrations may arise not only because of inaccuracies in input variables but also because concentrations are measured at a point, whereas the model predicts spatially averaged concentrations. Measurement errors may also, of course, contribute to discrepancies between model predictions and data.

Although the validity of the atmospheric diffusion equation cannot be established without question, it is generally accepted that the equation is essentially a valid description of atmospheric transport, mixing, and chemical reaction processes. The major source of invalidity is the eddy diffusivity representation of the turbulent fluxes. However, as long as the eddy diffusivity functions used have been determined empirically under conditions similar to those to which the equation is applied, the equation should be considered valid. The principal problem, therefore, lies with the question of accuracy, namely the effect of uncertain specification of input parameters on the predictions of the model.

Initial and Boundary Conditions

The initial condition for the atmospheric diffusion equation is that the concentration field at the time corresponding to the beginning of the simulation $\langle \bar{c}_i(x, y, z, 0) \rangle = \langle \bar{c}_i \rangle_0$. Simulations are normally begun at night or at sunrise, and the $\langle \bar{c}_i \rangle_0$ field at that time is constructed from the station readings. A ground-level interpolation routine and assumptions regarding the vertical variation of the concentrations are required to generate the full $\langle \bar{c}_i \rangle_0$ field from the station data. Because only surface readings are generally available from which to construct a $\langle \bar{c}_i \rangle_0$ field, the most uncertainty is expected in the initial conditions aloft.

The boundary conditions for equation (8) consist of the concentrations upwind of the region, the pollutant fluxes at the ground (the source emissions), and the flux condition at the upper vertical boundary of the region. Concentrations upwind of the modeling region can be estimated if monitoring stations exist at the upwind edge of the airshed. In such a case, uncertainties in these concentrations will be low when a previous time is simulated. The major source of uncertainty in boundary conditions generally arises at the upper vertical boundary. First, the temperature structure, for example, the height of the base of an elevated inversion layer, is not known precisely. Second, the pollutant flux condition at the boundary is also not known precisely. Thus, the major uncertainty in boundary conditions lies in specifying the upper vertical boundary conditions, both the location of the boundary and the species flux condition at the boundary.

Most models depend for their initial and boundary conditions (I.C. and B.C.) on routine air monitoring data. These data are typically interpolated to a fine mesh to provide the surface-level I.C. and the B.C. for the edges of the region. There are obvious problems with this approach:

(1) The monitoring data are often not representative of the concentration levels surrounding a monitoring station (see, for example, Ott and Eliassen (ref. 1)). The nature of this problem is site specific and must be evaluated for each monitoring site within the modeling region.

(2) The monitoring data represent surface-level measurements. All models require the concentration levels above the inversion base as an upper-level B.C. This problem with B.C. can to a certain extent be eliminated by extending the vertical coordinate of the model domain above the inversion so that background levels can be used. If this is not feasible, and depending on the atmospheric condition, a factor of 3 should be considered as the minimal level of uncertainty associated with upper-level boundary conditions. These uncertainty levels can be reduced if upper-level measurements are available. The problem with upper-level I.C. can to a certain extent be eliminated by starting the model well before the time period of interest.

(3) The most serious problem associated with I.C. and B.C. may be uncertainties associated with the monitoring methods themselves. J. Trijonis (personal communication, 1977) has performed a critical review and statistical analysis of the quality of monitoring methods. Based on this work, the precision of the data corrected for interference effects is recommended to be: O_x/O_3 - excellent, NO_x - good (10-percent error), total hydrocarbons - fair, and non-methane hydrocarbons - poor. Of these data, the largest uncertainty is in the non-methane hydrocarbon data which must be further split for validation according to the requirements of the particular chemical mechanism. A minimum of 50-percent uncertainty should be associated with these measurements unless more refined results are available.

In summary, for most models the major uncertainties are associated with the upper-level data (factor of 3) and with the hydrocarbon measurement (≈ 50 percent). The problem with horizontal boundary conditions can largely be removed by choice of the model boundaries away from strong gradients and pollutant sources. Uncertainties in initial conditions can be minimized by starting the calculation well before the time period of interest.

Meteorology

There are three basic meteorological variables of interest: wind field, mixing depth, and solar insolation. A problem, common to all models, is that sparse and often unrepresentative measurements are used to derive continuous fields over the region. The key question is, "How representative are the interpolated fields of the actual physical processes in the atmosphere?" Roth et al. (ref. 2) in their study of wind measuring stations in the Los Angeles region found that a substantial proportion of the data, taken at identical or adjacent sites at the same time, differed markedly. A 20-percent error in any of the measurements is not uncommon, the uncertainty in the vertical velocity field

being somewhat greater. The basic effect of small perturbations in the wind field is to introduce an artificial diffusion or smoothing process. Larger errors can affect the time-phasing and magnitudes of pollutant peaks at particular locations. Mass-consistent wind fields, derived by objective analysis procedures and appropriate weighting of station data, can substantially reduce the effects of uncertainties. The artificial creation of convergence and divergence zones can be minimized. Some problems still remain however in creating three-dimensional wind fields from very limited amounts of upper-level data. To some extent, errors in these measurements can often mask physically meaningful calculations of vertical velocities.

All models require specification of the mixing depth. In most regions it is only measured, or calculated from temperature profiles, at a very limited number of locations. A 20- to 30-percent error is typical; however, in regions of convergence or strong heating on surface slopes, the accuracy can be much worse. (In view of the fact that concentration predictions are very sensitive to mixing depth, it is vital to use objective analysis procedures that simultaneously couple the calculation of the wind field and inversion base location.)

The accurate specification of the wind field for use by an air quality model is of critical importance. Since numerical solution of the full Navier-Stokes equations has not yet been proven feasible, the common approach for computing a grid of wind vectors is to use the scattered measured values, generally available at hourly intervals.

The calculation of a continuous surface from discrete data points is a problem common to many fields of science. In general, for a given set of discrete data points, a unique solution does not exist, and, therefore, analysis of a given data set by different techniques often results in different fields.

Interpolation of a surface velocity field.- Much has been written on the subject of objective surface field generation from discrete data values. In an early paper, Panofsky (ref. 3) used third-degree polynomials to fit wind and pressure fields for use in weather map construction. The technique was later modified to handle areas with sparse data by Gilchrist and Cressman (ref. 4). Cressman (ref. 5) reported on a procedure for use in pressure-surface height analysis in which each station value was weighted according to its distance r from the grid point in question. Endlich and Mancuso (ref. 6) combined both polynomial fitting and distance weighting in their technique. A least-squares fit to a plane was performed by using the five nearest station values. Shepard (ref. 7) discussed an interpolation technique in which the value at grid point (i, j) was computed from

$$C_{ij} = \frac{\sum_{k=1}^n C_k W_k(r)}{\sum_{k=1}^n W_k(r)} \quad (9)$$

where C_k is the measured value at the k th measuring station and $W_k(r)$ is the weighting function. A direction factor was also included which accounted for shadowing of the influence of one data point by a nearer one in the same direction. The method also included the effect of barriers. If a "detour" of length $b(r)$, perpendicular to the line between the point (i,j) and the k th measuring station, was required to travel around the barrier between the two points, then $b(r)$ was considered to be the strength of the barrier. An effective distance r' was defined by

$$r' = [r^2 + b(r)^2]^{1/2} \quad (10)$$

If no barrier separated the two points, then $b(r) = 0$. Shenfeld and Boyer (ref. 8) presented a technique similar to that proposed by Endlich and Mancuso. In an attempt to produce reasonable values in regions of sparse data, Fritsch (ref. 9) used a cubic spline technique. He first fit spherical surfaces to the data to obtain an initial field, and then using the splines, he iteratively adjusted these values until convergence was obtained. He compared his technique with that of Cressman by using an idealized data set with a known solution, and the mean error (≈ 3 percent) was approximately half that of Cressman's. MacCracken and Sauter (ref. 10) used a weighting scheme based on distance r in the computation of the wind fields for use in the air quality simulation model LIRAQ. The weighting scheme chosen was

$$W(r) = \exp(-0.1r^2) \quad (11)$$

This Gaussian weighting scheme was chosen over r^{-2} weighting in order to eliminate the complete dominance of a measuring station located near a grid point.

In summary, interpolation of sparse data on a grid can be accomplished by weighting each data value according to its distance from the point in question or performing a least-squares fit of the data by a polynomial. In the first approach, stations within a "radius of influence" of the grid point are expected to influence that grid point. The grid point value may be influenced by shadowing, barriers, and/or upwind versus crosswind distance. The second method requires minimization of χ^2 , the goodness of fit to the data. For a second-degree polynomial, for example,

$$\chi^2 \equiv \sum_{k=1}^n (\Delta C_k)^2 = \sum_{k=1}^n (C_k - a_1 - a_2 x_k - a_3 y_k - a_4 x_k y_k - a_5 x_k^2 - a_6 y_k^2)^2 \quad (12)$$

must be a minimum, where C_k is the measured concentration (or wind speed) at point (x_k, y_k) . The minimum value of χ^2 can be determined by setting the derivatives of χ^2 with respect to each of the coefficients a_i equal to zero.

Effect of terrain on surface wind field.— The influence of gross terrain features (e.g., mountain ranges) is accounted for by the use of barriers to flow during the wind component interpolation procedure. However, this does not account for local terrain features on the scale of 1 grid length. Each measured wind vector obviously reflects the local terrain surrounding that station. However, the interpolated vector at a nonmeasuring station grid point is the weighted average of several measured vectors and is only partially indicative of its own local terrain. Therefore, following the aforementioned interpolation procedure, a terrain adjustment technique, which is similar to that of Anderson (refs. 11 and 12) except that surface heating is not included, can be used in the wind field calculation.

Within a layer of constant thickness, the flow can be assumed to be approximately two-dimensional. The scale of vertical variability is so much smaller than the horizontal scale that the flow may be considered as a horizontal flow perturbed by vertical disturbances. Therefore, the continuity equation can be written as

$$\int_h^H \nabla \cdot \underline{v}_H dz = - \int_h^H \frac{\partial w}{\partial z} dz \quad (13)$$

where \underline{v}_H is the terrain-adjusted surface wind vector, h is the height of terrain, and H is the top of the disturbed layer. If it is assumed that

$$w_H \approx 0$$

since the topographic influence is no longer felt at this altitude and that

$$w_h \approx \underline{v}_0 \cdot \nabla h$$

where \underline{v} is the velocity resulting from the interpolation procedure, equation (13) can be integrated to

$$(H - h) \nabla \cdot \underline{v}_H = \underline{v}_0 \cdot \nabla h \quad (14)$$

If it is assumed that the horizontal velocity can be represented by a velocity potential ϕ such that

$$U = \frac{\partial \phi}{\partial x} \quad V = \frac{\partial \phi}{\partial y} \quad (15)$$

then equation (14) becomes Poisson's equation,

$$\nabla^2\phi = \frac{y_0 \cdot \nabla h}{H - h} \quad (16)$$

The resulting field of ϕ values is used to adjust the initial interpolated surface velocity field to reflect the effect of the terrain as follows:

$$\left. \begin{aligned} u &= U_0 + \frac{\partial\phi}{\partial x} \\ v &= V_0 + \frac{\partial\phi}{\partial y} \end{aligned} \right\} \quad (17)$$

Determination of a mass-consistent three-dimensional wind field.- During recent years only a limited number of divergence reduction procedures have appeared in the literature. Endlich (ref. 13) used a point-iterative method to reduce the two-dimensional divergence in a wind field while retaining the vorticity in the original field. His method involved simple adjustment of the velocity components contributing to the divergence at a given point in order to make the divergence zero at that point. An adjustment was made simultaneously to the vorticity equation. The grid was scanned iteratively point by point until the divergence was reduced to a desired level.

Frankhauser (ref. 14) approached the three-dimensional divergence reduction problem from the point of view of measured data errors. On the basis of the assumption that errors in measured horizontal velocity increase with altitude (O'Brien (ref. 15)), he adjusted initial estimates of vertical velocity to account for this. The horizontal velocity at each vertical level was then adjusted by solving for a velocity potential ϕ from

$$\nabla^2\phi = D_R(x,y) \quad (18)$$

where $D_R(x,y)$ is the residual divergence at point (x,y) . He computed the new velocity components from equation (17).

More recently, Sherman (ref. 16) devised a procedure for construction of a three-dimensional mass-consistent wind field (MATHEW) by using the variational calculus approach of Sasaki (refs. 17 and 18). The approach involved solution of the following equation:

$$\frac{\partial^2 \lambda}{\partial x^2} + \frac{\partial^2 \lambda}{\partial y^2} + \frac{\alpha_1^2}{\alpha_2^2} \frac{\partial^2 \lambda}{\partial z^2} = -2\alpha_1^2 \left(\frac{\partial u_0}{\partial x} + \frac{\partial v_0}{\partial y} + \frac{\partial w_0}{\partial z} \right) \quad (19)$$

where $\lambda(x,y,z)$ is a Lagrange multiplier (or alternatively a velocity potential); u_0 , v_0 , and w_0 are the observed velocity values; α_1 and α_2 are Gauss' precision moduli defined by $\alpha^2 = 1/2\sigma^2$ where σ^2 is the error variance of the observed field. The adjusted velocity components are then calculated from

$$\left. \begin{aligned} 2\alpha_1^2(u - u_0) + \frac{\partial \lambda}{\partial x} &= 0 \\ 2\alpha_1^2(v - v_0) + \frac{\partial \lambda}{\partial y} &= 0 \\ 2\alpha_2^2(w - w_0) + \frac{\partial \lambda}{\partial z} &= 0 \end{aligned} \right\} \quad (20)$$

The technique requires different boundary conditions depending on the terrain; $\lambda = 0$ is appropriate for open, or "flow-through," boundaries, while $\partial\lambda/\partial n$ is used for closed, or "non-flow-through," boundaries. The procedure was tested on a grid of 24 000 grid points by using data from a canyon near Idaho Falls, Idaho. The precision module α_1^2 and α_2^2 were set to 0.5 and 5000, respectively, apparently from empirical tests. The divergence was reduced 12 orders of magnitude, but the execution time, which is dependent upon terrain complexity, was 2 to 5 minutes on a Control Data 7600 computer.

A two-dimensional vertically integrated version of MATHEW was incorporated into the LIRAQ model developed at Lawrence Livermore Laboratory (MacCracken and Sauter (ref. 10)). The model area extended up to the top of the mixed layer. The appropriate equation of continuity used in the model was

$$\frac{\partial h}{\partial t} + \frac{\partial (uh)}{\partial x} + \frac{\partial (vh)}{\partial y} + w = 0 \quad (21)$$

where h is the depth of the mixed layer and w is the vertical velocity which can be thought of as the relative motion between the vertical movement of the top of the mixed layer and the air through the top of the mixed layer. The variational approach yields the following equation which was solved to adjust the divergence:

$$\frac{\partial^2 \lambda}{\partial x^2} + \frac{\partial^2 \lambda}{\partial y^2} - \left(\frac{\alpha_1^2}{\alpha_2^2} \right) \lambda = -2\alpha_1^2 \left[\frac{\partial h}{\partial t} + \frac{\partial (u_0 h)}{\partial x} + \frac{\partial (v_0 h)}{\partial y} + w_0 \right] \quad (22)$$

When this procedure was tested with wind data from the San Francisco Bay area from July 26, 1973, the divergence was reduced from 10^{-1} to approximately 10^{-6} . A value of 10^{-9} was assumed for α_1^2/α_2^2 .

Liu and Goodin (ref. 19) adapted the technique of Endlich to a two-dimensional mesoscale wind field. The flow field below the mixed layer was assumed to be vertically integrated. The divergence was adjusted point by point with the capability of holding wind station values fixed. Since vorticity is not important on the mesoscale, this portion of Endlich's procedure was not implemented. The procedure was tested on wind data from Los Angeles on a 40×25 grid. The divergence in the field was reduced by about 3 orders of magnitude after 100 iterations while the measured station values were held fixed.

Emission Inventories

The assessment of the level of uncertainty in a particular emission inventory is obviously a substantial undertaking and, most properly, should be carried out when the inventory itself is compiled.³

Emissions from each class of source can be characterized according to

- (1) Level of spatial resolution
- (2) Level of temporal resolution
- (3) Source activity or emission factor

The level of spatial resolution achievable is in principle as fine as one desires since the locations of all sources can presumably be specified (although traffic count data may not be available on a street-by-street basis). Temporal emission rates will fluctuate somewhat from day to day. Emissions from some stationary sources may vary with ambient temperature, but these variations are generally known as a function of temperature. The major problem in properly specifying source emissions is uncertainty in emission quantities arising from uncertainties in source activities and emission factors.

Two basic factors are involved in emission specification, the quantity emitted and its composition. Emission compositions are typically estimated

³Typical levels of uncertainties in mobile and fixed source activities (e.g., vehicle distance traveled and units of fuel consumed) should be identified. Then, the typical uncertainties in emission factors (e.g., grams of pollutant emitted per vehicle distance traveled and gram of pollutant per unit of fuel consumed) should be combined with the uncertainties in activities to produce net uncertainties in emissions.

from handbooks such as AP-42 (ref. 20). Each table in AP-42 includes a qualitative estimate of the accuracy of the material on a scale that varies from A (excellent) to E (poor). Recent studies aimed at establishing NO_x and SO₂ emission inventories for stationary sources in the South Coast Air Basin have presented estimates of the level of accuracy of the overall inventories (Bartz et al. (ref. 21) and Hunter and Helgeson (ref. 22)). These reports estimate that a ±20-percent uncertainty in the total emissions is reasonable, whereas uncertainties in individual source emissions can range as high as ±300 percent. A compensating factor is that generally the large uncertainties are associated with small absolute emission levels. Mobile source emission estimates depend to a large extent on the quality of the traffic data. The level of uncertainty in the South Coast Air Basin mobile source emissions of NO_x, CO, and SO₂ is probably of the order of ±15 percent.

Probably the most serious emission inventory problems are those associated with hydrocarbon emissions. The level of uncertainty in the stationary source hydrocarbon emissions in the South Coast Air Basin is probably of the order of ±30 percent. Within individual source classes, the uncertainties can be as high as ±100 percent. Mobile source hydrocarbon emission uncertainties have been estimated in the range from 15 to 50 percent. Generally, insufficient information is available concerning the hydrocarbon composition of major hydrocarbon sources. It is necessary to estimate a hydrocarbon breakdown into the four classes. (Aldehydes constitute an important class of reacting species, and virtually nothing is known about aldehyde emissions.) It is difficult to estimate the uncertainty associated with estimated hydrocarbon speciation. From the point of view of predictions, errors in absolute hydrocarbon levels will be more influential on oxidant predictions than will errors in class assignments, because reactivities do not vary enormously for the classes. Thus, uncertainties in hydrocarbon emissions by class, while definitely leading to uncertainties in oxidant predictions, are not deemed as detrimental to accurate oxidant predictions as are uncertainties in hydrocarbon emissions by total level.

Chemical Kinetics

There are essentially two approaches that have been followed in developing kinetic mechanisms for photochemical smog:

(1) Lumped mechanisms: mechanisms in which organic species are grouped according to a common basis such as structure or reactivity. Examples include the mechanisms of Hecht and Seinfeld (ref. 23), Eschenroeder and Martinez (ref. 24), Hecht et al. (ref. 25), MacCracken and Sauter (ref. 10), and Whitten and Hogo (ref. 26).

(2) Surrogate mechanisms: mechanisms in which organic species in a particular class (e.g., olefins) are represented by a single member of that class (e.g., propylene). Examples include the mechanisms of Niki et al. (ref. 27), Demerjian et al. (ref. 28), Dodge (ref. 29), and Graedel et al. (ref. 30).

In general, the surrogate mechanisms tend to be more lengthy than lumped mechanisms because within a surrogate mechanism each individual species is treated as a separate chemical entity. For this reason surrogate mechanisms

have not found wide utility in models that have substantial meteorological treatments because of the computational requirements associated with calculating simultaneous chemistry and transport.

Table II presents a comparison of two lumped mechanisms that are currently employed in air quality models. The SAI and LIRAQ mechanisms, modified versions of the Hecht et al. (ref. 25) mechanism, are included in large-scale urban air quality models. Table II lists all the reactions and associated rate constants that are included in the two mechanisms. The issue of most interest here is which reactions are included in which mechanisms and not the particular rate constant value adopted. (The rate constant values in all mechanisms continually undergo revision as new measurements become available, and several of the constants given in table II have recently been reevaluated.)

From table II, it is clear that, aside from rate constant differences, the two mechanisms are quite similar, even though the interpretation of the lumped organic species varies somewhat between the mechanisms. Differences in rate constants are the result of choices from among available rate constant values and more recent determinations as well as the result of different lumping schemes.

The critical question, of course, in the development of a kinetic mechanism is its accuracy. The assessment of the accuracy of chemical kinetic mechanisms for photochemical smog has received a considerable amount of attention (Hecht and Seinfeld (ref. 23), Niki et al. (ref. 27), Hecht et al. (ref. 25), Demerjian et al. (ref. 28), Dodge and Hecht (ref. 31), Dodge (ref. 29), and Whitten and Hogo (ref. 26)). There are essentially two issues involved in assessing the accuracy of a kinetic mechanism: (1) identification of the major sources of uncertainty, such as inaccurately known rate constants or mechanisms of individual reactions, and (2) evaluation of so-called chamber effects, phenomena peculiar to the laboratory system in which the data are generated for testing of a mechanism.

Predicted concentrations are extremely sensitive to the values of several reaction rate constants. Reactions that are particularly important are those governing the conversion of NO to NO₂ and those that initiate the oxidation of hydrocarbons. Dodge and Hecht (ref. 31) performed a systematic sensitivity analysis of the reactions in the original Hecht-Seinfeld-Dodge kinetic mechanism. The conclusions of the study were compiled in the form of a ranking of the reactions by their "sensitivity-uncertainty" index. This index is an indicator of the combined sensitivity of the mechanism to variations in the reaction rate constant and the experimental uncertainty of the rate constant. Since this study was performed, several rate constant determinations have been significantly improved.

The overall smog formation process as simulated by present mechanisms can be described in terms of two radical pools. One of these pools is the oxygen radical pool; it is associated with NO₂ photolysis and the production of ozone. The other radical pool can be referred to as the peroxy-oxyl radical pool. In this pool, radical transfer reactions convert peroxy radicals to oxyl radicals and vice versa, with the concomitant conversion of NO to NO₂ and oxidation of hydrocarbons. Oxyl radicals are formed when peroxy radicals convert NO to NO₂.

Peroxy radicals are formed when hydroxyl radicals react with hydrocarbons, and hydroperoxy radicals are formed when alkoxy radicals react with molecular oxygen.

A major problem with simulating experimental smog chamber data is that it is difficult to reproduce the initial rate of hydrocarbon disappearance and the initial rate of conversion of NO to NO₂. This difficulty is often resolved by assuming an initial source of peroxy or oxyl radicals in addition to those formed by the reactions of oxygen atoms with hydrocarbons, for example, by assuming an initial concentration of nitrous acid, which photolyzes and supplies the initial radicals. Whether nitrous acid is initially present in the smog chambers in the amounts assumed is unknown.⁴

Once the pool of peroxy-oxyl radicals is established in a simulation, the radical pool must be maintained, because radical sinks, such as the reaction of hydroxyl radicals with NO₂ or peroxy-peroxy combination reactions, tend to consume more radicals than are produced by NO₂ photolysis and the subsequent reactions of oxygen atoms. The radical concentration is maintained in the mechanism by the photolysis of carbonyl compounds (and, in olefin systems by the ozone-olefin reactions). In some cases it is obvious that too many radicals are present initially and that the maintenance source of radicals in the mechanism is inadequate. It has been speculated that the walls of chambers in some way supply radicals to the peroxy-oxyl radical pool. The effect of such a process would be greatest when the concentration of normal radicals was the lowest - in a low activity and low hydrocarbon experiment. That the walls may be supplying radicals is supported by the similar need for a high initial HONO concentration (relative to equilibrium).

Kinetic mechanisms must be able to predict the photolysis rates of pollutants that absorb ultraviolet light. From Beer's law, in an optically thin medium the first-order rate constant governing the photolysis rate of a compound is given by

$$k = \frac{1}{(\lambda_2 - \lambda_1)} \int_{\lambda_1}^{\lambda_2} \phi(\lambda) I_0(\lambda) \epsilon(\lambda) d\lambda$$

where

$I_0(\lambda)$ incident light intensity distribution

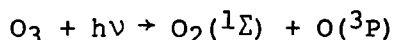
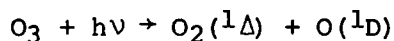
$\epsilon(\lambda)$ extinction coefficient

⁴There is evidence that nitrous acid is found during the loading of smog chambers (Chan et al. (ref. 32)). The amount required to simulate University of California, Riverside experiments was found by Whitten and Hogo (ref. 26) to be generally about one-third of the equilibrium concentration of nitrous acid that could form from the initial concentrations of NO, NO₂, and H₂O. Whether the walls of the smog chamber are an important source of initial radicals is unknown.

$\phi(\lambda)$ primary quantum yield

λ_1, λ_2 wavelength limits of the light reaching the urban atmosphere

In smog chamber simulations, the photolysis rate is usually expressed in terms of k_1 , the rate constant for NO_2 photolysis. From this, with information on $I_0(\lambda)$, $\epsilon(\lambda)$, and $\phi(\lambda)$, photolysis rates of other species can be predicted. Considerable uncertainty exists in the measurement of $\phi(\lambda)$ for certain species. For instance, the photolysis of ozone can be important in the formation of OH radicals. In the wavelength region of interest, the primary quantum yields for the processes



are still uncertain. While extinction coefficients are relatively easy to measure in the laboratory for most species, quantum yield measurements can be exceedingly difficult.

Another important photochemical process is the formation and subsequent reaction of excited states. The rates of thermal reactions can be enhanced by several orders of magnitude if one or more of the reactants are vibrationally or electronically excited. For instance, while ground-state $\text{O}(^3\text{P})$ atoms are unreactive toward such species as H_2 , H_2O , and N_2O , singlet oxygen, $\text{O}(^1\text{D})$, reacts rapidly. Similarly, the oxidation of SO_2 in clean air probably takes place by the reaction of triplet SO_2 ($^3\text{SO}_2$) formed by the absorption of ultraviolet light by ground-state SO_2 followed by internal energy transfer processes; $^3\text{SO}_2$ may also be considerably more reactive toward hydrocarbons than the ground-state SO_2 . Unfortunately, both the formation and the reaction mechanisms of most electronically excited species are highly uncertain.

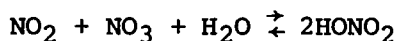
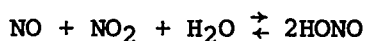
As noted previously, the characteristics of the chamber must be accounted for, since mechanisms must be validated with smog chamber data. Some of the specific effects or characteristics that must be considered are the spectral distribution and absolute intensity of the photolyzing lamps, the adsorption, desorption, and chemical reaction of species on the walls, the initial loading of impurity species in the chamber on the walls or in the gas, and the effects of leakage, sampling, and possible temperature variations during the run. Of these effects, probably the most important are the properties of the photolysis lamps. Photolysis rates of absorbing species cannot be predicted with accuracy if $I_0(\lambda)$, the incident light intensity distribution, is not known with accuracy. This information must be coupled with the absolute rate of photolysis of at least one species such as NO_2 to compute the appropriate photolysis rate constants.

Also important is the characterization of the initial contaminant loading in the chamber. When mechanisms overpredict the length of the induction period in which radical concentrations are initially building up, it may be due to the

presence of an absorbing species either in the gas phase or on the walls which photolyzes. Actual measurement of the species accounting for these effects is complicated by their low concentrations.

When these effects are not adequately characterized, one usually begins by parameterizing the NO_2 photolysis rate constant k_1 , the initial concentration of trace photolyzable species such as HONO, and the wall adsorption rate of ozone. If still less is known about the experimental situation, the value of simulating the data becomes questionable.

The third major set of unknowns in simulating laboratory systems concerns the reactions which take place heterogeneously, either on the walls or on aerosols. Many reactions are thought to take place heterogeneously. Among the most important are the reactions,



which produce nitrous acid and nitric acid. Evidence for the heterogeneous nature of these processes comes from the strong dependence of measured rate constants on the reactor surface-to-volume ratio. (The disappearance of SO_2 in smog chamber experiments also seems to have a strong heterogeneous component either as a result of reactions in droplets or the wall-catalyzed formation of polymeric sulfur-oxygen species which remain on the walls as films.) Recent work has shown that certain long-lived free radicals such as HO_2 can be lost to particles at appreciable rates. Diffusion and subsequent loss of radicals to reactor walls occur constantly, but these processes do not affect the homogeneous chemistry appreciably. Heterogeneous processes, in general, are difficult to account for in kinetic mechanisms and are usually ignored.

In summary, virtually every reaction occurring in an atmospheric system is subject to some degree of uncertainty, whether in the rate constant or the nature and quantity of the products. In evaluating a mechanism, the customary procedure is to compare the results of smog chamber experiments, usually in the form of concentration-time profiles, with simulations of the same experiment using the proposed mechanism. A sufficient number of experimental unknowns exist in all such mechanisms that the predicted concentration profiles can be varied somewhat by changing rate constants (and perhaps mechanisms) within accepted bounds. The inherent validity of a mechanism can be judged by evaluating how realistic the parameter values used are and how well the predictions match the data.

Numerical Analysis

A major area that must be considered is the numerical approximations required to solve the mathematical model. Complex numerical schemes are required to solve the three-dimensional, coupled, nonlinear, parabolic partial

differential equations that result from the atmospheric diffusion equation. The choice of numerical methods to be used in the approximated model are important factors that influence the accuracy and economy of the solution. In most cases, spatial and temporal discretization introduces additional averaging and a loss of characterization of subgrid-scale processes. This problem can be corrected, to some extent, by the use of subgrid-scale models, but they must be augmented by careful analysis of the influence of grid size and time step on the accuracy of the results.

A common source of inaccuracy in the solution of equation (8) is numerical truncation errors in the approximation of the advection terms. These should be minimized by using, for example, high-order schemes such as the zero average phase error technique of Fromm (ref. 33) or the sign preserving SHASTA method of Boris and Book (ref. 34). The requirements for high-order accuracy must be balanced with computer resource requirements.

The accuracy of numerical schemes can, in principle, be evaluated by performing numerical experiments with problems of known analytic solutions. Tests can be used to assess the effects of numerical diffusion and the influence of dispersion on phase errors. Numerical dissipation dominates in first-order difference schemes and tends to reduce the amplitude of concentration peaks, while in second-order approximations, dispersion at high wave numbers becomes the most serious problem. Dispersion is common to all methods but dissipation is absent from time-centered schemes. A common test is the Crowley (ref. 35) "color" problem in which a conical distribution of a scalar quantity is advected by a circular velocity field.

Special consideration must be given to the character of the chemical terms and their numerical properties. Solution of the stiff system of ordinary differential equations that often arises requires the use of Newton iteration or variable order methods like DIFSUB (Gear (ref. 36)). Stability requirements must be carefully evaluated with attention given to the disparity of the temporal scales of the processes being modeled.

Assessment of Accuracy of Models for Photochemical Oxidant

Inaccuracies in the predictions of models arise from two sources: (1) lack of complete understanding of atmospheric physics and chemistry and (2) inaccuracies in input data due to incomplete data bases.⁵ In terms of understanding of atmospheric physics and chemistry, the primary concerns are accurate treatment

⁵Liu and Seinfeld (ref. 37) showed that an important technical limitation of models is that the diffusion equation is difficult to solve accurately. In particular, conventional finite-difference techniques introduce a pseudodiffusion effect as a result of poor treatment of advective transport. For example, relative errors of as much as 50 percent could be generated by using the numerical method in the 1973 version of the SAI model. In general, the developers of all models have recognized this numerical problem and have implemented special techniques aimed at alleviating the undesired effect. Now, discrepancies between predictions and measurements are mainly attributable to errors introduced in the formulation of and inputs to the model.

of advection, turbulent diffusion, and chemistry. Although advection is a complicated process that has yet to be treated definitively, horizontal advection can be incorporated correctly. Turbulent diffusion (primarily in the vertical direction) may be treated inaccurately because of a lack of complete understanding of the process. Nevertheless, most parameterizations of the vertical eddy diffusivity provide an appropriate rate of vertical mixing. Inaccuracies in the understanding of turbulent diffusion, therefore, do not appear to pose a serious problem with respect to the accuracy of predictions. The greatest source of uncertainty is in the understanding of the chemical transformations that lead to ozone formation. These processes have been studied for many years in smog chambers, and several kinetic mechanisms have been proposed that provide concentration predictions that agree at least qualitatively with the experimental results. Yet, all the significant chemical reactions may not have been identified, and furthermore, the rate constants for many reactions believed to be important are not known very accurately. Finally, it has not been established conclusively that a mechanism validated with smog chamber data accurately represents actual atmospheric chemical processes. Initial and boundary conditions and source emissions lead to inaccuracies in predictions because of uncertainties due to an incomplete data base.

Few available studies present detailed analyses of the sensitivity of model predictions to changes in input parameters. The importance of sensitivity results cannot be overemphasized. Practically, they are of value in assessing the level of detail and accuracy required in model input parameters or the effects of uncertainties on predictions. The only extensive, published sensitivity study is that of Liu et al. (ref. 38) for the SAI model.⁶ Most of their findings are summarized in the following table:

RANKING OF THE RELATIVE IMPORTANCE OF THE INPUT PARAMETERS (SAI MODEL)

Variable	Importance ^a of variable to prediction of concentration of -			
	CO	NO	O ₃	NO ₂
Wind speed	A	A	A	A
K _H	D	D	D	D
K _y	C	C	C	C
Mixing depth	B	B	B	B
Radiation intensity	D	A	A	B
Emission rate	B	A	B	B

^aImportance is indicated by a scale from A (most important) to D (least important).

⁶For a description of the SAI model see Reynolds et al. (refs. 39 to 42) and Roth et al. (refs. 2 and 43).

The effect of varying boundary and initial conditions in the 1973-version of the SAI model was reported by Demerjian (ref. 44). Average ozone concentration maps for the Los Angeles basin between the hours of 1:00 and 2:00 p.m. were presented for the base case and the case of boundary conditions reduced by 50 percent. Only minor differences were found at the eastern and northern edges of the basin where the maxima occur, but significant differences were observed at the western and central portions of the basin. The initial conditions in addition to the boundary conditions were reduced by 50 percent. Reduction in the predicted ozone levels at the northern and eastern edges of the basin was found to be of the order of 20 to 30 percent corresponding to the reduced initial conditions.

AEROSOL PROCESSES IN THE POLLUTED TROPOSPHERE

Atmospheric pollutants in an urban airshed exist in both gaseous and particulate phases. In addition to direct emissions of both phases of pollutants (primary pollutants), there exist transformation processes from one gaseous pollutant to another and from gaseous to particulate pollutants (secondary pollutants). Considerable work has been done on the development of mathematical models describing the relationship between sources and ambient levels of gaseous pollutants, including the complex chemistry describing the formation of secondary gaseous pollutants. The development of models describing the evolution of atmospheric aerosols is the next step in the process of attempting to understand the physics and chemistry of the polluted atmosphere.

Dynamic Equation Governing Aerosol Behavior

Presented first are the dynamic equation governing aerosol behavior, with emphasis on application to an urban airshed, and a discussion of the mechanism that each term represents.

The derivation of the general dynamic equation has been presented elsewhere (Chu and Seinfeld (ref. 45)). The general dynamic equation governs the size-composition distribution function for the atmospheric aerosol. Since there exists no experimental means for measuring this distribution function, only the equation governing an integral moment of the general equation, the particle size distribution function, will be presented and discussed here.

If $n(D_p, \underline{r}, t)$ is the instantaneous distribution of particles by particle diameter (cm^3), then the general dynamic equation governing $\bar{n}(D_p, \underline{r}, t)$, the mean size distribution function, is⁷

⁷Stochastic coagulation and condensation terms have been neglected (see Seinfeld and Ramabhadran (ref. 46)).

$$\begin{aligned}
& \frac{\partial \bar{n}}{\partial t} + \sum_{i=1}^3 \frac{\partial}{\partial r_i} (\bar{u}_i \bar{n}) + \frac{\partial}{\partial D_p} (\bar{I}_0 \bar{n}) - u_s \frac{\partial \bar{n}}{\partial r_3} \\
& = \sum_{i=1}^3 \frac{\partial}{\partial r_i} \left(K_{ii} \frac{\partial \bar{n}}{\partial r_i} \right) + \int_0^{D_p/2^{1/3}} \beta \left[(D_p^3 - \tilde{D}_p^3)^{1/3}, \tilde{D}_p \right] \bar{n} \left[(D_p^3 - \tilde{D}_p^3)^{1/3}, \tilde{r}, t \right] \\
& \quad \times \bar{n}(\tilde{D}_p, \tilde{r}, t) \frac{D_p^2}{(D_p^3 - \tilde{D}_p^3)^{2/3}} d\tilde{D}_p - \int_0^\infty \beta(D_p, \tilde{D}_p) \bar{n}(D_p, \tilde{r}, t) \bar{n}(\tilde{D}_p, \tilde{r}, t) d\tilde{D}_p \\
& \quad + S_0(D_p, t) + S_1(D_p, \tilde{r}, t)
\end{aligned} \tag{23}$$

where

β	coagulation coefficient for particles of diameter D_p and \tilde{D}_p , $\text{cm}^3\text{-sec}^{-1}$
K_{ii}	turbulent diffusivity in i th direction, $\text{cm}^2\text{-sec}^{-1}$
I_0	rate of change of aerosol particle diameter from condensation, cm-sec^{-1}
r_i	spatial variable in i th direction, cm
S_0	rate of homogeneous nucleation, $\text{cm}^{-4}\text{-sec}^{-1}$
S_1	rate of particulate sources, $\text{cm}^{-4}\text{-sec}^{-1}$
\bar{u}_i	mean velocity in i th direction, cm-sec^{-1}
u_s	settling velocity, cm-sec^{-1}

The terms on the left-hand side of equation (23) represent accumulation, convection, and growth by condensation and settling. The terms on the right-hand side represent turbulent diffusion (Brownian diffusion has been neglected), coagulation, nucleation, and particulate sources. With appropriate boundary conditions, equation (23) represents the most general form of the dynamic equation for an aerosol the chemical composition of which is a unique function of its size, spatial position, and time.

If equation (23), with appropriate boundary conditions, could be solved numerically for conditions typifying a general urban airshed, the aerosol model would be complete. Understanding of many components of the model is inadequate, however, the most important components being primary particulate emissions inventories, the chemical mechanisms of gas-to-particle conversion, and rates of homogeneous nucleation. A preliminary step in proceeding toward a general urban aerosol model requires both a closer examination of the system as a whole and a more detailed look at the specific mechanisms present in equation (23).

Figure 1(a) is a diagram describing the interaction between gaseous and particulate pollutants. The additional complexity of the particulate system over the gaseous system becomes readily apparent. From primary emissions of gaseous pollutants, the chemical composition and size of an aerosol particle is altered by diffusion and condensation of vapor species and by absorption of primary gaseous pollutants. Once absorbed, dissolved vapors may participate in heterogeneous reactions. This process of condensation or absorption takes place on primary aerosols, background particles such as soil dust and marine aerosol, on stable nuclei formed by homogeneous nucleation, or on particles formed by coagulation of any of the above particulate species.

This dynamic process of chemical change, particle growth by condensation and coagulation, and removal and replenishment of particles takes place as the aerosol mass is transported through an urban airshed. Additional physical removal mechanisms (deposition, settling, washout, and rainout) affect the aerosol distribution.

The distribution of aerosols in an atmosphere or smog chamber is affected by different mechanisms, depending upon the aerosol number concentration, the gaseous compounds present, and whether the system of interest is open or closed. For example, the description of the evolution of an aerosol distribution in the immediate vicinity of a particulate source must generally include the coagulation mechanism, whereas the description of an "aged" aerosol far downwind from primary sources can usually neglect coagulation. Table III outlines various atmospheric aerosol-particulate systems and the important mechanisms for each system.

Before any system can be described in detail, the first and most important step is to close all mass and energy balances on the system. In the atmosphere, ambient conditions are such that the assumption of constant temperature, while strictly incorrect, can be made without introducing significant errors. Hence, the mass or material balance is the important equation to be considered first.

The next section is concerned with such a material balance of gas-phase and particulate pollutants. In that section, an attempt is made to answer the question, "By utilizing simple mechanisms for source, conversion, and removal rates in the general mass balance equation for particulate pollutants and gaseous precursors, can the ambient levels of these pollutants measured in urban airsheds be accounted for?"

Figure 1(b) outlines the relationship of the next section to the processes described in the general dynamic equation. The processes within the dashed line are replaced by a simple model of gas-to-particle conversion with no particle size dependence. As can be seen, the full system is considered, but certain detailed descriptions of the general equation are replaced with "black box" substitutes. These surrogate representations seek to describe the salient features of the mechanism involved while ignoring the detail of the mechanism. The mechanisms of gas-to-particle conversion are replaced by a simple first-order rate of conversion from gaseous pollutants to total particulate mass. By retaining the basic mechanisms of advection, diffusion, and removal of both gases and particulates, the question of accountability for reported ambient levels of pollutants can be answered.

Model for Predicting Gas-to-Particle Conversion

Most available mathematical models for the steady-state or dynamic behavior of air pollutants apply to gaseous pollutants (either chemically inert or reactive) or to particulate matter that may be considered chemically inert. One of the important atmosphere phenomena that requires elucidation is the conversion of air pollutants from gaseous form to particulate form. For example, of particular interest is the so-called urban plume, wherein sulfur dioxide is converted to particulate sulfate, nitrogen oxides to particulate nitrate, and hydrocarbons to particulate organic material. Several recent studies have been reported in which measurements (usually airborne) have been carried out downwind of large urban complexes in order to obtain material balances on gaseous and particulate pollutants (Haagenson and Morris (ref. 47), Stampfer and Anderson (ref. 48), and Breeding et al. (refs. 49 and 50)). A goal of these studies is to determine the relative roles of transport, conversion of gaseous pollutants to particulate pollutants, and removal on the overall pollutant material balance downwind of a major urban source.

In the analysis of urban plume data, it is desirable to have a mathematical model capable of describing the behavior of both gaseous and particulate pollutants and their interrelations. Eventually such a model would include both gaseous and particulate phases with detailed treatments of gas-phase and particulate-phase chemistry, as well as size distributions of the particles. However, before attempting to develop a model of full complexity, it is desirable to formulate a "first-order" model, one that contains all the major mechanisms influencing the airborne concentrations of gaseous and particulate pollutants but one that does not include the details of atmospheric chemistry and particle size distributions. The processes to be included are advection, turbulent diffusion, conversion of gaseous species to particulate material, settling, deposition, washout, and rainout. Such a first-order model is in essence a material balance, designed to provide estimates of the fraction of pollutants that still remain airborne at a certain distance downwind of a city and the fraction that has been removed by deposition and gas-to-particle conversion. The object of this study is to develop such a model. It is hoped that the model presented in this section will subsequently prove to be a convenient tool in the analysis of airborne urban plume pollutant flux measurements.

Although a dynamic model is desirable, a steady-state model will enable one to assess whether all the major mechanisms are accounted for in analyzing data on urban pollutant fluxes. The model will be restricted to scales of transport over which the atmospheric diffusion equation is applicable, that is, to problems on the mesoscale. "Long-range" transport is not considered because of the recognized inadequacy of the atmospheric diffusion equation in describing macroscale transport. (For consideration of long-range transport, the reader is referred to Bolin and Persson (ref. 51).) There exist a variety of numerical models (numerical solutions of the atmospheric diffusion equation) capable of simulating the transport and removal of air pollutants, for example, Belot et al. (ref. 52). However, there is considerable attractiveness in an analytical model that does not require numerical solution of the atmospheric diffusion equation. In previous work of this nature, Heines and Peters (ref. 53) have presented analytic steady-state solutions for gas-phase pollutants with no deposition or depletion due to reaction. Scriven and Fisher (ref. 54) have presented

a solution to the steady-state, two-dimensional atmospheric diffusion equation including deposition and first-order removal.

Presented in this paper is a new solution to the steady-state, three-dimensional atmospheric diffusion equation including settling, deposition, and first-order removal and conversion of gaseous pollutants to particulate pollutants. The main purpose of the model is to enable the carrying out of overall material balance calculations for the gaseous and particulate phases in the urban atmosphere and in the urban plume. The application of the model to the Los Angeles atmosphere and to the Los Angeles urban plume can be found in Peterson and Seinfeld (ref. 55). A study of that type not only provides estimates of the relative roles of transport and removal mechanisms but also is a necessary prerequisite to more detailed modeling studies involving gases and particles.

Formulation of the model.— The mean concentration $c(x,y,z)$ of a gaseous pollutant or of a primary particulate pollutant under conditions in which the mean wind is aligned with the x-axis and in which a first-order removal process exists can be described by the atmospheric diffusion equation. (Bars over c are omitted for convenience.)

$$\bar{u} \frac{\partial c}{\partial x} - w_s \frac{\partial c}{\partial z} = \frac{\partial}{\partial y} \left(K_H \frac{\partial c}{\partial y} \right) + \frac{\partial}{\partial z} \left(K_V \frac{\partial c}{\partial z} \right) - kc \quad (24)$$

where \bar{u} is the mean wind speed in the x-direction, w_s is the settling velocity (nonzero if c represents the concentration of particulate matter), K_H and K_V are the horizontal and vertical eddy diffusivities, and k is the first-order rate constant for removal of the species. The term kc may account for conversion of gaseous pollutants to particulate material (as long as the process may be represented approximately as first order) or for the removal of either gases or particles by rainout and washout.

The following boundary conditions to equation (24) are considered. The source is taken to be a point source of strength Q_1 ($g\text{-sec}^{-1}$) located at $x = 0, y = 0, z = z_s$. (From the solution for this elevated point source, solutions can be constructed for all other types of sources of interest.) Thus, the $x = 0$ boundary condition is

$$c(0,y,z) = \frac{Q_1}{\bar{u}} \delta(y) \delta(z-z_s) \quad (25)$$

where $\delta(\)$ is the Dirac delta function.

At infinite lateral distance, the concentration approaches zero:

$$c(x,y,z) = 0 \quad (y \rightarrow \pm\infty) \quad (26)$$

An elevated inversion base which inhibits vertical turbulent mixing is assumed to exist at $z = H_a$:

$$\frac{\partial c}{\partial z} = 0 \quad (z = H_a) \quad (27)$$

Finally, the pollutant may be removed across a layer at height $z = z_a$ through deposition with a deposition velocity v_d :

$$K_V \frac{\partial c}{\partial z} + w_s c = v_d c \quad (z = z_a) \quad (28)$$

Note that the lower boundary conditions was selected at z_a , the height corresponding to that at which a deposition velocity may have been measured. (A typical value of z_a is 1 meter.) For simplicity, K_H and K_V may be taken as constants. The problems associated with this assumption are well known (Monin and Yaglom (ref. 56)). Nevertheless, it is not deemed necessary to include the additional complication of spatially dependent K_H and/or K_V .

It is convenient to cast the problem in dimensionless form. To do so, the following dimensionless spatial variables are defined:

$$x = \frac{K_V x}{\bar{u} H^2} \quad y = \frac{y}{H} \quad z = \frac{z - z_a}{H} \quad (29)$$

where $H = H_a - z_a$. In addition, the dimensionless concentration is defined as

$$c = \frac{\bar{u} H^2 c}{Q_1} \quad (30)$$

With these definitions, equations (24) to (28) become

$$\frac{\partial c}{\partial x} - w \frac{\partial c}{\partial z} = \beta \frac{\partial^2 c}{\partial y^2} + \frac{\partial^2 c}{\partial z^2} - \alpha c \quad (31)$$

$$c(0, y, z) = \delta(y) \delta(z - z_s) \quad (32)$$

$$C(X, Y, Z) = 0 \quad (Y \rightarrow \pm\infty) \quad (33)$$

$$\frac{\partial C}{\partial Z} = 0 \quad (Z = 1) \quad (34)$$

$$\frac{\partial C}{\partial Z} = (N - W)C \quad (Z = 0) \quad (35)$$

where $W = w_g H / K_V$, $\beta = K_H / K_V$, $\alpha = k H^2 / K_V$, and $N = v_d H / K_V$ (N represents the dimensionless deposition velocity, or mass transfer coefficient).

The details of the solution are found in Peterson (ref. 57). The solution of equations (31) to (35) is

$$C(X, Y, Z) = \frac{1}{2\sqrt{\beta\pi X}} \exp(-\alpha X) \exp\left(-\frac{Y^2}{4\beta X}\right) \exp\left(-\frac{WZ}{2}\right) \left[\sum_{n=1}^{\infty} a_n \phi_n^{(1)}(Z) \exp(-\mu_n^{(1)} X) + \sum_{m=1}^M c_m \phi_m^{(2)}(Z) \exp(-\mu_m^{(2)} X) \right] \quad (36)$$

where

$$\phi_n^{(1)}(Z) = \cos(\gamma_n Z) + \delta_n \sin(\gamma_n Z) \quad (37)$$

$$\phi_m^{(2)}(Z) = \exp(\theta_m Z) - \tau_m \exp(-\theta_m Z) \quad (38)$$

$$\mu_n^{(1)} = \gamma_n^2 + \left(\frac{W}{2}\right)^2 \quad (39)$$

$$\mu_m^{(2)} = \left(\frac{W}{2}\right)^2 - \theta_m^2 \quad (40)$$

$$\delta_n = \frac{N - W/2}{\gamma_n} \quad (41)$$

$$\tau_m = \frac{N - W/2 - \theta_m}{N - W/2 + \theta_m} \quad (42)$$

$$a_n = \frac{\exp(WZ_S/2) [\cos(\gamma_n Z_S) + \delta_n \sin(\gamma_n Z_S)]}{\frac{1}{2}(1 + \delta_n^2) + (1 - \delta_n^2) \sin(2\gamma_n)/4\gamma_n + \delta_n \sin^2 \gamma_n / \gamma_n} \quad (43)$$

$$c_m = \frac{\exp(WZ_S/2) [\exp(\theta_m Z_S) - \tau_m \exp(-\theta_m Z_S)]}{\left\{ \exp(2\theta_m) - 1 + \tau_m^2 [1 - \exp(-2\theta_m)] \right\} / 2\theta_m - 2\tau_m} \quad (44)$$

and where the eigenvalue relations are

$$\frac{\tan \gamma_n}{\gamma_n} = \frac{N - W}{\gamma_n^2 + \frac{W}{2} \left(N - \frac{W}{2} \right)} \quad (n = 1, 2, \dots) \quad (45)$$

and

$$\exp(2\theta_m) = \left(\frac{N - W/2 - \theta_m}{N - W/2 + \theta_m} \right) \left(\frac{W/2 + \theta_m}{W/2 - \theta_m} \right) \quad (m = 1, 2, \dots, M) \quad (46)$$

The finite sum ($m = 1$ to M) in equation (36) arises from the finite number (M) of roots of equation (46), whereas the infinite sum in equation (36) arises from the infinite number of roots of equation (45). Whereas equations (43) and (44) are analytically exact, their inclusion in the solution (eq. (36)) does not yield a convergent expansion because the coefficients arise from the eigenfunction expansion of the delta function $\delta(Z - Z_S)$. For computational purposes, it is necessary to approximate the delta function by a more well-behaved function and then represent this function by an eigenfunction expansion. This procedure and the resultant equations for a_n and c_m are given in Peterson and Seinfeld (ref. 55).

Equation (36) can be extended to include L point sources, each of strength Q_i located at (X_i, Y_i, Z_S) for $i = 1, 2, \dots, L$:

$$\begin{aligned}
C(X, Y, Z) = & \frac{1}{2\sqrt{\beta\pi}} \exp\left(-\frac{WZ}{2}\right) \sum_{i=1}^L \hat{Q}_i U(X-X_i) \exp\left[-\frac{(Y-Y_i)^2}{4\beta(X-X_i)}\right] \frac{\exp[-\alpha(X-X_i)]}{\sqrt{X-X_i}} \\
& \times \left\{ \sum_{n=1}^{\infty} a_n \phi_n^{(1)}(Z) \exp[-\mu_n^{(1)}(X-X_i)] \right. \\
& \left. + \sum_{m=1}^M c_m \phi_m^{(2)}(Z) \exp[-\mu_m^{(2)}(X-X_i)] \right\} \quad (47)
\end{aligned}$$

where $\hat{Q}_i = Q_i/Q_1$, and $U(X-X_i)$ is the unit step function,

$$U(X-X_i) = \begin{cases} 0 & (X < X_i) \\ 1 & (X \geq X_i) \end{cases} \quad (48)$$

For L area sources, each of strength q_i ($g\text{-m}^{-2}\text{-sec}^{-1}$) located in the rectangular regions, $X_{ia} \leq X \leq X_{ib}$, $Y_{ia} \leq Y \leq Y_{ib}$, the mean concentration is given by

$$\begin{aligned}
C(X, Y, Z) = & \frac{1}{2} \exp\left(-\frac{WZ}{2}\right) \sum_{i=1}^L \hat{q}_i U(X-X_{ia}) \left[\sum_{n=1}^{\infty} a_n \phi_n^{(1)}(Z) \left(I_n^{(1)} - I_n^{(2)} \right) \right. \\
& \left. + \sum_{m=1}^M c_m \phi_m^{(2)}(Z) \left(I_m^{(3)} - I_m^{(4)} \right) \right] \quad (49)
\end{aligned}$$

where $\hat{q}_i = q_i/q_1$ and

$$I_n^{(1)} = I\left[\alpha + \mu_n^{(1)}, (Y-Y_{ia})/2\sqrt{\beta}\right] \quad (50)$$

$$I_n^{(2)} = I\left[\alpha + \mu_n^{(1)}, (Y-Y_{ib})/2\sqrt{\beta}\right] \quad (51)$$

$$I_m^{(3)} = I\left[\alpha + \mu_m^{(2)}, (Y-Y_{ia})/2\sqrt{\beta}\right] \quad (52)$$

$$I_m^{(4)} = I\left[\alpha + \mu_m^{(2)}, (Y - Y_{ib})/2\sqrt{\beta}\right] \quad (53)$$

and if $X_{ia} < X \leq X_{ib}$,

$$I(A, B) = \frac{1}{A} \left\{ \exp[-A(X - X_{ia})] \operatorname{erf}(B/\sqrt{X - X_{ia}}) \right\} - \frac{1}{2A} \left\{ \exp(2B\sqrt{A}) \operatorname{erfc}\left[\sqrt{A(X - X_{ia})} + B/\sqrt{X - X_{ia}}\right] + \exp(-2B\sqrt{A}) \operatorname{erfc}\left[-\sqrt{A(X - X_{ia})} + B/\sqrt{X - X_{ia}}\right] \right\} \quad (54)$$

whereas if $X > X_{ib}$,

$$I(A, B) = \frac{1}{A} \left\{ \exp[-A(X - X_{ib})] \operatorname{erf}(B/\sqrt{X - X_{ib}}) - \exp[-A(X - X_{ia})] \operatorname{erf}(B/\sqrt{X - X_{ia}}) \right\} + \frac{1}{2A} \left\{ \exp(2B\sqrt{A}) \left\{ \operatorname{erfc}\left[\sqrt{A(X - X_{ib})} + B/\sqrt{X - X_{ib}}\right] - \operatorname{erfc}\left[\sqrt{A(X - X_{ia})} + B/\sqrt{X - X_{ia}}\right] \right\} + \exp(-2B\sqrt{A}) \left\{ \operatorname{erfc}\left[-\sqrt{A(X - X_{ib})} + B/\sqrt{X - X_{ib}}\right] - \operatorname{erfc}\left[-\sqrt{A(X - X_{ia})} + B/\sqrt{X - X_{ia}}\right] \right\} \right\} \quad (55)$$

where $C(X, Y, Z)$ is the dimensionless concentration based on the area source strength q_1 , that is $C(X, Y, Z) = cK_V/q_1H$. If the area source is at ground level, Z_g is set equal to zero in equations (43) and (44).

Finally, of interest is the solution for an elevated vertical area source, wherein the flux of pollutant from an area in the $x = 0$ plane is specified. This problem may arise in the modeling of an urban plume, where the city is represented as an area source in the $x = 0$ plane that is situated at the downwind end of the area. If the pollutant flux Q_1 ($g\text{-sec}^{-1}$) through an area defined by $-b \leq y \leq b$ and $z_1 \leq z \leq z_2$ is specified, then the boundary condition analogous to equation (25) is

$$c(0, y, z) = \frac{Q_1 U(b+y) U(b-y) U(z-z_1) U(z_2-z)}{2\bar{u}b(z_2 - z_1)} \quad (56)$$

In dimensionless form, equation (56) becomes

$$C(0, Y, Z) = \frac{U(B+Y) U(B-Y) U(Z-Z_1) U(Z_2-Z)}{2B(Z_2 - Z_1)} \quad (57)$$

where $Z_1 = (z_1 - z_a)/H$, $Z_2 = (z_2 - z_a)/H$, and $B = b/H$.

The solution of equations (31), (33) to (35), and (57) is

$$C(X, Y, Z) = \frac{1}{4B} \exp(-\alpha X) \exp\left(-\frac{WZ}{2}\right) \left[\operatorname{erf}\left(\frac{B-Y}{2\sqrt{\beta X}}\right) + \operatorname{erf}\left(\frac{B+Y}{2\sqrt{\beta X}}\right) \right] \\ \times \left[\sum_{n=1}^{\infty} \bar{a}_n \phi_n^{(1)}(Z) \exp(-\mu_n^{(1)} X) + \sum_{m=1}^M \bar{c}_m \phi_m^{(2)}(Z) \exp(-\mu_m^{(2)} X) \right] \quad (58)$$

where $a_n = I_1/I_2$, $c_m = I_3/I_4$, and

$$I_1 = \frac{1}{\left[\left(\frac{W}{2}\right)^2 + \gamma_n^2\right] (Z_2 - Z_1)} \left(\exp\left(\frac{WZ_2}{2}\right) \left\{ \frac{W}{2} [\cos(\gamma_n Z_2) + \delta_n \sin(\gamma_n Z_2)] + \gamma_n [\sin(\gamma_n Z_2) - \delta_n \cos(\gamma_n Z_2)] \right\} - \exp\left(\frac{WZ_1}{2}\right) \left\{ \frac{W}{2} [\cos(\gamma_n Z_1) + \delta_n \sin(\gamma_n Z_1)] + \gamma_n [\sin(\gamma_n Z_1) - \delta_n \cos(\gamma_n Z_1)] \right\} \right) \quad (59)$$

$$I_2 = \frac{1}{2} (1 + \delta_n^2) + \frac{(1 - \delta_n^2)}{4\gamma_n} \sin(2\gamma_n) + \frac{\delta_n}{\gamma_n} \sin^2 \gamma_n \quad (60)$$

$$I_3 = \frac{1}{(z_2 - z_1)} \left(\frac{1}{\frac{W}{2} + \theta_m} \left\{ \exp \left[\left(\frac{W}{2} + \theta_m \right) z_2 \right] - \exp \left[\left(\frac{W}{2} + \theta_m \right) z_1 \right] \right\} - \frac{\tau_m}{\frac{W}{2} - \theta_m} \left\{ \exp \left[\left(\frac{W}{2} - \theta_m \right) z_2 \right] - \exp \left[\left(\frac{W}{2} - \theta_m \right) z_1 \right] \right\} \right) \quad (61)$$

$$I_4 = \frac{1}{2\theta_m} \left\{ \exp(2\theta_m) - 1 + \tau_m^2 [1 - \exp(-2\theta_m)] \right\} - 2\tau_m \quad (62)$$

Secondary particulate matter.— The model developed in the previous section is applicable to gaseous pollutants (with $W = 0$) and to primary particulate pollutants. Analyses of airborne particulate matter have established that a substantial fraction of the particulate matter often cannot be attributable to primary particulate sources but rather is the consequence of conversion of gaseous species to the particulate phase. Obviously sulfate represents one important example of the gas-to-particle conversion. Let us denote by c_p the airborne concentration of a secondary species (such as sulfate) in the particulate phase. Then, the steady-state material balance for this species, analogous to equation (24), is

$$\bar{u} \frac{\partial c_p}{\partial x} - w_s \frac{\partial c_p}{\partial z} = K_H \frac{\partial^2 c_p}{\partial y^2} + K_V \frac{\partial^2 c_p}{\partial z^2} + v_g k_c - k_p c_p \quad (63)$$

where v_g is the mass ratio of the secondary particulate species to the primary gaseous species which is being converted and k_p is the first-order rate constant for removal of particulate matter by washout and rainout. In writing equation (63) in this way, the rate constant k_p is taken to represent only the gas-to-particle conversion process and not other scavenging processes.

Since it is assumed that there are no direct sources of the secondary particulate matter, the boundary conditions for equation (63) are

$$c_p(0, y, z) = 0 \quad (64)$$

$$c_p(x, y, z) = 0 \quad (y \rightarrow \pm\infty) \quad (65)$$

$$\frac{\partial C_p}{\partial z} = 0 \quad (z = H_a) \quad (66)$$

$$K_V \frac{\partial C_p}{\partial z} + w_s C_p = v_{d,p} C_p \quad (z = z_a) \quad (67)$$

where $v_{d,p}$ is the deposition velocity of the particulate matter.

Equations (63) to (67) can be made dimensionless in the same manner as before, where the gaseous emission rate Q_1 is used in the definition of C_p (since there is no direct emission in this case). The result is

$$\frac{\partial C_p}{\partial X} - W \frac{\partial C_p}{\partial Z} = \beta \frac{\partial^2 C_p}{\partial Y^2} + \frac{\partial^2 C_p}{\partial Z^2} + v_g \alpha C - \alpha_p C_p \quad (68)$$

$$C_p(0, Y, Z) = 0 \quad (69)$$

$$C_p(X, Y, Z) = 0 \quad (Y \rightarrow \pm\infty) \quad (70)$$

$$\frac{\partial C_p}{\partial Z} = 0 \quad (Z = 1) \quad (71)$$

$$\frac{\partial C_p}{\partial Z} = (N_p - W) C_p \quad (Z = 0) \quad (72)$$

where $\alpha_p = k_p H^2 / K_V$ and $N_p = v_{d,p} H / K_V$.

It is not possible to obtain readily an analytic solution of equation (68) because of the presence of $C(X, Y, Z)$ accounting for the coupling between the gaseous and particulate phases. Therefore, in studying the behavior of C_p , it is necessary to resort to approximate techniques. Define

$$C_p'(X, Z) = \int_{-\infty}^{\infty} C_p(X, Y, Z) dY \quad (73)$$

$$\bar{C}_p(x) = \int_0^1 \int_{-\infty}^{\infty} C_p(x, y, z) dy dz \quad (74)$$

$$\bar{C}(x) = \int_0^1 \int_{-\infty}^{\infty} C(x, y, z) dy dz \quad (75)$$

The integrals C_p' , \bar{C}_p , and \bar{C} each have an important physical interpretation. The total flow G_g ($g\text{-sec}^{-1}$) of a gaseous pollutant through the plane at any x is given by

$$G_g = \int_{z_a}^{H_a} \int_{-\infty}^{\infty} \bar{u} c(x, y, z) dy dz \quad (76)$$

In dimensionless form (the concentration is based on the source strength Q_1), equation (76) becomes

$$\bar{C}(x) = \frac{G_g}{Q_1} = \int_0^1 \int_{-\infty}^{\infty} C(x, y, z) dy dz \quad (77)$$

Thus, $\bar{C}(x)$ is the ratio of the mass flow of pollutant at any x to the source strength; $\bar{C}_p(x)$ can be similarly interpreted. Integrals C_p' , \bar{C}_p , and \bar{C} are also related to the fraction of pollutant lost by deposition, reaction, or rain-out and washout. The total mass of pollutant removed by deposition between 0 and x is given by

$$M_d = \int_0^x \int_{-\infty}^{\infty} v_d c(x', y, 0) dy dx' \quad (78)$$

which in dimensionless form becomes

$$\frac{M_d}{Q_1} = N \int_0^x C'(x', 0) dx' \quad (79)$$

Similarly, the fraction of the pollutant removed by first-order reaction M_k/Q_1 is given by

$$\frac{M_k}{Q_1} = \alpha \int_0^X \bar{C}(x') dx' \quad (80)$$

Equivalent relationships can be written for the particulate matter.

If one assumes that $C_p^1(x,0)$ and $C_p^1(x,1)$ can be related to $\bar{C}_p(x)$ in the following approximate way,

$$C_p^1(x,0) = f_0 \bar{C}_p(x) \quad (81)$$

$$C_p^1(x,1) = f_1 \bar{C}_p(x) \quad (82)$$

then one obtains the following equation governing $\bar{C}_p(x)$,

$$\frac{d\bar{C}_p}{dx} + K\bar{C}_p = v_g \alpha \bar{C}(x) \quad (83)$$

$$\bar{C}_p(0) = 0 \quad (84)$$

where $K = N_p f_0 - W f_1 + \alpha_p$. The solution of equation (83) subject to equation (84) is

$$\bar{C}_p(x) = v_g \alpha \exp(-Kx) \int_0^x \exp(K\xi) \bar{C}(\xi) d\xi \quad (85)$$

For L point sources of gaseous pollutant, equation (85) becomes

$$\begin{aligned} \bar{C}_p(x) = v_g \alpha \sum_{i=1}^L \hat{Q}_i U(x-x_i) & \left(\sum_{n=1}^{\infty} \frac{a_n \Gamma_n^{(1)}}{K - (\alpha + \mu_n^{(1)})} \left\{ \exp\left[-(\alpha + \mu_n^{(1)})(x - x_i)\right] \right. \right. \\ & - \exp\left[-K(x - x_i)\right] \left. \right\} + \sum_{m=1}^M \frac{c_m \Gamma_m^{(2)}}{K - (\alpha + \mu_m^{(2)})} \left\{ \exp\left[-(\alpha + \mu_m^{(2)})(x - x_i)\right] \right. \\ & \left. \left. - \exp\left[-K(x - x_i)\right] \right\} \right) \end{aligned} \quad (86)$$

where

$$\Gamma_n^{(1)} = \frac{\exp\left(-\frac{W}{2}\right)\left[\gamma_n(\sin \gamma_n - \delta_n \cos \gamma_n) - \frac{W}{2}(\cos \gamma_n + \delta_n \sin \gamma_n)\right] + \frac{W}{2} + \delta_n \gamma_n}{\left(\frac{W}{2}\right)^2 + \gamma_n^2} \quad (87)$$

and

$$\Gamma_m^{(2)} = \frac{\exp\left(\theta_m - \frac{W}{2}\right) - 1}{\theta_m - \frac{W}{2}} - \frac{\tau_m \left\{ 1 - \exp\left[-\left(\theta_m + \frac{W}{2}\right)\right] \right\}}{\theta_m + \frac{W}{2}} \quad (88)$$

The assumptions of equations (81) and (82) are difficult or impossible to establish experimentally, and no direct means of estimating the values of f_0 and f_1 exist. However, the scaling of the solution and the values of the particulate deposition velocities cause the solution for $\bar{C}_p(x)$ to be quite insensitive to the values of f_0 and f_1 . If this were not the case, then it would be necessary to consider another means of obtaining a closed form solution for $\bar{C}_p(x)$.

For L area sources, equation (85) can also be evaluated. For $X_{ia} \leq x \leq X_{ib}$, the solution is

$$\begin{aligned} \bar{C}_p(x) = v_g \alpha \sum_{i=1}^L \hat{q}_i U(x-X_{ia}) (Y_{ib} - Y_{ia}) & \left(\frac{1 - \exp[-K(x - X_{ia})]}{K} \left(\sum_{n=1}^{\infty} \frac{a_n \Gamma_n^{(1)}}{\alpha + \mu_n^{(1)}} \right. \right. \\ & + \left. \left. \sum_{m=1}^M \frac{c_m \Gamma_m^{(2)}}{\alpha + \mu_m^{(2)}} \right) - \sum_{n=1}^{\infty} \frac{a_n \Gamma_n^{(1)}}{\alpha + \mu_n^{(1)}} \left\{ \frac{\exp[-(\alpha + \mu_n^{(1)})(x - X_{ia})] - \exp[-K(x - X_{ia})]}{K - (\alpha + \mu_n^{(1)})} \right\} \right. \\ & \left. - \sum_{m=1}^M \frac{c_m \Gamma_m^{(2)}}{\alpha + \mu_m^{(2)}} \left\{ \frac{\exp[-(\alpha + \mu_m^{(2)})(x - X_{ia})] - \exp[-K(x - X_{ia})]}{K - (\alpha + \mu_m^{(2)})} \right\} \right) \quad (89) \end{aligned}$$

and for $x \geq x_{ib}$, the solution is

$$\begin{aligned}
 \bar{c}_p(x) = & v_g \alpha \sum_{i=1}^L \hat{q}_i U(x-x_{ia}) (y_{ib} - y_{ia}) \left[\frac{1 - \exp[-K(x_{ib} - x_{ia})]}{K} \left(\sum_{n=1}^{\infty} \frac{a_n \Gamma_n^{(1)}}{\alpha + \mu_n^{(1)}} \right. \right. \\
 & + \left. \left. \sum_{m=1}^M \frac{c_m \Gamma_m^{(2)}}{\alpha + \mu_m^{(2)}} \right) + \sum_{n=1}^{\infty} \frac{a_n \Gamma_n^{(1)}}{\alpha + \mu_n^{(1)}} \frac{1}{K - (\alpha + \mu_n^{(1)})} \left(\left\{ 1 - \exp[-(\alpha + \mu_n^{(1)}) \right. \right. \right. \\
 & \times (x_{ib} - x_{ia}) \left. \left. \right\} \left\{ \exp[-(\alpha + \mu_n^{(1)}) (x - x_{ib})] - \exp[-K(x - x_{ib})] \right\} \right. \\
 & \left. \left. - \left\{ \exp[-(\alpha + \mu_n^{(1)}) (x_{ib} - x_{ia})] - \exp[-K(x_{ib} - x_{ia})] \right\} \right) \right) \\
 & + \sum_{m=1}^M \frac{c_m \Gamma_m^{(2)}}{\alpha + \mu_m^{(2)}} \frac{1}{K - (\alpha + \mu_m^{(2)})} \left(\left\{ 1 - \exp[-(\alpha + \mu_m^{(2)}) (x_{ib} - x_{ia})] \right\} \right. \\
 & \times \left\{ \exp[-(\alpha + \mu_m^{(2)}) (x - x_{ib})] - \exp[-K(x - x_{ib})] \right\} \\
 & \left. \left. - \left\{ \exp[-(\alpha + \mu_m^{(2)}) (x_{ib} - x_{ia})] - \exp[-K(x_{ib} - x_{ia})] \right\} \right) \right) \right] \quad (90)
 \end{aligned}$$

Finally, for the elevated area source in the $x = 0$ plane, $\bar{c}_p(x)$ is given by

$$\bar{C}_p(x) = v_g \alpha \left(\sum_{n=1}^{\infty} \frac{\bar{a}_n \Gamma_n^{(1)}}{K - (\alpha + \mu_n^{(1)})} \left\{ \exp \left[-(\alpha + \mu_n^{(1)}) x \right] - \exp(-Kx) \right\} \right. \\ \left. + \sum_{m=1}^M \frac{\bar{c}_m \Gamma_m^{(2)}}{K - (\alpha + \mu_m^{(2)})} \left\{ \exp \left[-(\alpha + \mu_m^{(2)}) x \right] - \exp(-Kx) \right\} \right) \quad (91)$$

Equation (91) is of the same form as equation (86) for a single point source at $X = 0$, with \bar{a}_n and \bar{c}_m replacing a_n and c_m in equation (86).

Figure 2 shows $\bar{C}(X)$ as a function of X for a hypothetical point source located at $X = 0.01$, and for $\alpha = N = 1$ (the parameters for SO_2 produce values of α and N of order 1). Figure 2 delineates the various contributions to the decay of the species. For these parameter values both deposition and conversion are important, with deposition more efficient near the source where ground-level concentrations are highest.

REFERENCES

1. Ott, Wayne; and Eliassen, Rolf: A Survey Technique for Determining the Representativeness of Urban Air Monitoring Stations With Respect to Carbon Monoxide. *J. Air Pollut. Control Assoc.*, vol. 23, no. 8, Aug. 1973, pp. 685-690.
2. Roth, P. M.; Reynolds, S. D.; Roberts, P. J. W.; and Seinfeld, J. H.: Development of a Simulation Model for Estimating Ground Level Concentrations of Photochemical Pollutants - Final Report. Rept-71SAI-21, Systems Applications, Inc., 1971. (Available from NTIS as PB 206 415.)
3. Panofsky, Hans Arnold: Objective Weather-Map Analysis. *J. Meteorol.*, vol. 6, no. 6, Dec. 1949, pp. 386-392.
4. Gilchrist, B.; and Cressman, G. P.: An Experiment in Objective Analysis. *Tellus*, vol. 6, no. 4, Nov. 1954, pp. 309-318.
5. Cressman, George P.: An Operational Objective Analysis System. *Mon. Weather Rev.*, vol. 87, no. 10, Oct. 1959, pp. 367-374.
6. Endlich, R. M.; and Mancuso, R. L.: Objective Analysis of Environmental Conditions Associated With Severe Thunderstorms and Tornadoes. *Mon. Weather Rev.*, vol. 96, no. 6, June 1968, pp. 342-350.
7. Shepard, D.: A Two-Dimensional Interpolation Function for Computer Mapping of Irregularly Spaced Data. TR-15 (Contract N00014-67A-029), Harvard Univ., Mar. 20, 1968. (Available from DDC as AD 668 707.)
8. Shenfeld, L.; and Boyer, A. E.: The Utilization of an Urban Air Pollution Model in Air Management. *Air Pollution - Proceedings of the Fifth Meeting of the Expert Panel on Air Pollution Modeling*, N. 35, NATO Comm. Challenges Mod. Soc., Aug. 1974, pp. 22-1 - 22-35.
9. Fritsch, J. Michael: Objective Analysis of a Two-Dimensional Data Field by the Cubic Spline Technique. *Mon. Weather Rev.*, vol. 99, no. 5, May 1971, pp. 379-386.
10. MacCracken, M. C.; and Sauter, G. D., eds.: Development of an Air Pollution Model for the San Francisco Bay Area - Final Report to the National Science Foundation, Volume 1. UCRL-51920 Vol. 1, Lawrence Livermore Lab., Oct. 1, 1975.
11. Anderson, Gerald E.: Mesoscale Influences on Wind Fields. *J. Appl. Meteorol.*, vol. 10, no. 3, June 1971, pp. 377-386.
12. Anderson, G. E.: A Mesoscale Windfield Analysis of the Los Angeles Basin. *Environmental Monitoring Series*. EPA-650/4-73-001, U.S. Environ. Prot. Agency, June 1973. (Available from NTIS as PB 231 832.)
13. Endlich, Roy M.: An Iterative Method for Altering the Kinematic Properties of Wind Fields. *J. Appl. Meteorol.*, vol. 6, no. 5, Oct. 1967, pp. 837-844.

14. Fankhauser, J. C.: The Derivation of Consistent Fields of Wind and Geopotential Height From Mesoscale Rawinsonde Data. *J. Appl. Meteorol.*, vol. 13, no. 6, Sept. 1974, pp. 637-646.
15. O'Brien, James J.: Alternative Solutions to the Classical Vertical Velocity Problem. *J. Appl. Meteorol.*, vol. 9, no. 2, Apr. 1970, pp. 197-203.
16. Sherman, Christine A.: A Mass-Consistent Model for Wind Fields Over Complex Terrain. UCRL Preprint 76171, Lawrence Livermore Lab., May 1975.
17. Sasaki, Y.: An Objective Analysis Based on the Variational Method. *J. Meteorol. Soc. Japan*, Ser. 2, vol. 36, no. 3, June 1958, pp. 77-88.
18. Sasaki, Yoshikazu: Some Basic Formalisms in Numerical Variational Analysis. *Mon. Weather Rev.*, Vol. 98, no. 12, Dec. 1970, pp. 875-883.
19. Liu, C. Y.; and Goodin, W. R.: An Iterative Algorithm for Objective Wind Field Analysis. *Mon. Weather Rev.*, vol. 104, no. 6, June 1976, pp. 784-792.
20. Compilation of Air Pollutant Emission Factors (Second Edition). Publ. No. AP-42, U.S. Environ. Prot. Agency, Apr. 1973. (Available from NTIS as PB 223 996.)
21. Bartz, D. R.; Arledge, K. W.; Gabrielson, J. E.; Hays, L. G.; and Hunter, S. C.: Control of Oxides of Nitrogen From Stationary Sources in the South Coast Air Basin of California. KVB 5800-179 (Contract No. ARB 2-1471), Sept. 1974.
22. Hunter, S. C.; and Helgeson, N. L.: Control of Oxides of Sulfur From Stationary Sources in the South Coast Air Basin of California. KVB 5802-432 (Contract No. ARB 4-421), Dec. 1975.
23. Hecht, Thomas A.; and Seinfeld, John H.: Development and Validation of a Generalized Mechanism for Photochemical Smog. *Environ. Sci. & Technol.*, vol. 6, no. 1, Jan. 1972, pp. 47-57.
24. Eschenroeder, Alan Q.; and Martinez, Jose R.: Concepts and Applications of Photochemical Smog Models. *Advan. Chem. Ser. No. 113*, 1972, pp. 101-168.
25. Hecht, Thomas A.; Seinfeld, John H.; and Dodge, Marcia C.: Further Development of Generalized Kinetic Mechanism for Photochemical Smog. *Environ. Sci. & Technol.*, vol. 8, no. 4, Apr. 1974, pp. 327-339.
26. Whitten, G. Z.; and Hogo, H.: Mathematical Modeling of Simulated Photochemical Smog - Final Report. EPA-600/3-77-011, U.S. Environ. Prot. Agency, June 1975/June 1976. (Available from NTIS as PB 263 348.)
27. Niki, H.; Daby, E. E.; and Weinstock, B.: Mechanisms of Smog Reactions. *Adv. Chem. Ser. No. 113*, 1972, pp. 16-57.

28. Demerjian, Kenneth L.; Kerr, J. Alistair; and Calvert, Jack G.: The Mechanism of Photochemical Smog Formation. *Advances in Environmental Science and Technology*, Volume 4, James N. Pitts, Jr., and Robert L. Metcalf, eds., John Wiley & Sons, c.1974, pp. 1-262.
29. Dodge, M. C.: Combined Use of Modeling Techniques and Smog Chamber Data To Derive Ozone-Precursor Relationships. *International Conference on Photochemical Oxidant Pollution and Its Control - Proceedings: Volume II*, EPA-600/3-77-001b, U.S. Environ. Prot. Agency, Jan. 1977, pp. 881-889. (Available from NTIS as PB 264 233.)
30. Graedel, T. E.; Farrow, L. A.; and Weber, T. A.: Kinetic Studies of the Photochemistry of the Urban Troposphere. *Atmos. Environ.*, vol. 10, no. 12, 1976, pp. 1095-1116.
31. Dodge, M. C.; and Hecht, T. A.: Rate Constant Measurements Needed To Improve a General Kinetic Mechanism for Photochemical Smog. *Chemical Kinetics Data for the Upper and Lower Atmosphere*, *Int. J. Chem. Kinet.*, Symp. No. 1, 1975, pp. 155-163.
32. Chan, Walter H.; Nordstrom, Robert J.; Calvert, Jack G.; and Shaw, John H.: Kinetic Study of HONO Formation and Decay Reactions in Gaseous Mixtures of HONO, NO, NO₂, H₂O, and N₂. *Environ. Sci. & Technol.*, vol. 10, no. 7, July 1976, pp. 674-682.
33. Fromm, Jacob E.: A Method for Reducing Dispersion in Convective Difference Schemes. *J. Comput. Phys.*, vol. 3, no. 2, Oct. 1968, pp. 176-189.
34. Boris, Jay P.; and Book, David L.: Flux-Corrected Transport. I. SHASTA, a Fluid Transport Algorithm That Works. *J. Comput. Phys.*, vol. 11, no. 1, Jan. 1973, pp. 38-69.
35. Crowley, W. P.: Numerical Advection Experiments. *Mon. Weather Rev.*, vol. 96, no. 1, Jan. 1968, pp. 1-11.
36. Gear, C. W.: Algorithm 407 - DIFSUB for Solution of Ordinary Differential Equations. *Commun. ACM*, vol. 14, no. 3, Mar. 1971, pp. 185-190.
37. Liu, Mei-Kao; and Seinfeld, John H.: On the Validity of Grid and Trajectory Models of Urban Air Pollution. *Atmos. Environ.*, vol. 9, no. 6/7, June/July 1975, pp. 555-574.
38. Liu, M. K.; Whitney, D. C.; Seinfeld, J. H.; and Roth, P. M.: Continued Research in Mesoscale Air Pollution Simulation Modeling: Volume I - Assessment of Prior Model Evaluation Studies and Analysis of Model Validity and Sensitivity. EPA 600/4-76-016 A, U.S. Environ. Prot. Agency, May 1976. (Available from NTIS as PB 257 526.)
39. Reynolds, Steven D.; Roth, Philip M.; and Seinfeld, John H.: Mathematical Modeling of Photochemical Air Pollution - I. Formulation of the Model. *Atmos. Environ.*, vol. 7, no. 11, Nov. 1973, pp. 1033-1061.

40. Reynolds, Steven D.; Liu, Mei-Kao; Hecht, Thomas A.; Roth, Philip M.; and Seinfeld, John H.: Mathematical Modeling of Photochemical Air Pollution - III. Evaluation of the Model. *Atmos. Environ.*, vol. 8, no. 6, June 1974, pp. 563-596.
41. Reynolds, S. D.; Ames, J.; Hecht, T. A.; Meyer, J. P.; Whitney, D. C.; and Yocke, M. A.: Continued Research in Mesoscale Air Pollution Simulation Modeling: Volume II - Refinements in the Treatment of Chemistry, Meteorology, and Numerical Integration Procedures. EPA 600/4-76-016 B, U.S. Environ. Prot. Agency, May 1976. (Available from NTIS as PB 257 527.)
42. Reynolds, S. D.: The Systems Applications, Incorporated Urban Airshed Model: An Overview of Recent Developmental Work. International Conference on Photochemical Oxidant Pollution and Its Control - Proceedings: Volume II, EPA-600/3-77-001b, U.S. Environ. Prot. Agency, Jan. 1977, pp. 795-802. (Available from NTIS as PB 264 233.)
43. Roth, Philip M.; Roberts, Philip J. W.; Liu, Mei-Kao; Reynolds, Steven D.; and Seinfeld, John H.: Mathematical Modeling of Photochemical Air Pollution - II. A Model and Inventory of Pollutant Emissions. *Atmos. Environ.*, vol. 8, no. 1, Jan. 1974, pp. 97-130.
44. Demerjian, K. L.: Photochemical Air Quality Simulation Modeling: Current Status and Future Prospects. International Conference on Photochemical Oxidant Pollution and Its Control - Proceedings: Volume II, EPA-600/3-77-001b, U.S. Environ. Prot. Agency, Jan. 1977, pp. 777-794. (Available from NTIS as PB 264 233.)
45. Chu, Kuang J.; and Seinfeld, John H.: Formulation and Initial Application of a Dynamic Model for Urban Aerosols. *Atmos. Environ.*, vol. 9, no. 4, Apr. 1975, pp. 375-402.
46. Seinfeld, J. H.; and Ramabhadran, T. E.: Atmospheric Aerosol Growth by Heterogeneous Condensation. *Atmos. Environ.*, vol. 9, no. 12, 1975, pp. 1091-1097.
47. Haagenson, Philip L.; and Morris, Alvin L.: Forecasting the Behavior of the St. Louis, Missouri, Pollutant Plume. *J. Appl. Meteorol.*, vol. 13, no. 8, Dec. 1974, pp. 901-909.
48. Stampfer, J. F., Jr.; and Anderson, J. A.: Locating the St. Louis Urban Plume at 80 and 120 km and Some of Its Characteristics. *Atmos. Environ.*, vol. 9, no. 3, Mar. 1975, pp. 301-313.
49. Breeding, R. J.; Haagenson, P. L.; Anderson, J. A.; and Lodge, J. P., Jr.: The Urban Plume as Seen at 80 and 120 km by Five Different Sensors. *J. Appl. Meteorol.*, vol. 14, no. 2, Mar. 1975, pp. 204-216.
50. Breeding, R. J.; Klonis, H. B.; Lodge, J. P., Jr.; Pate, J. B.; Sheesley, D. C.; Englert, T. R.; and Sears, D. R.: Measurements of Atmospheric Pollutants in the St. Louis Area. *Atmos. Environ.*, vol. 10, no. 4, 1976, pp. 181-194.

51. Bolin, Bert; and Persson, Christer: Regional Dispersion and Deposition of Atmospheric Pollutants With Particular Application to Sulfur Pollution Over Western Europe. *Tellus*, vol. 27, no. 3, 1975, pp. 281-310.
52. Belot, Y.; Baille, A.; and Delmas, J.-L.: Modele Numerique de Dispersion des Polluants Atmospheriques en Presence de Couverts Vegetaux. Application aux Couverts Forestiers. *Atmos. Environ.*, vol. 10, no. 2, 1976, pp. 89-98.
53. Heines, T. S.; and Peters, L. K.: The Effect of a Horizontal Impervious Layer Caused by a Temperature Inversion Aloft on the Dispersion of Pollutants in the Atmosphere. *Atmos. Environ.*, vol. 7, no. 1, Jan. 1973, pp. 39-48.
54. Scriven, R. A.; and Fisher, B. E. A.: The Long Range Transport of Airborne Material and Its Removal by Deposition and Washout - I. General Considerations. *Atmos. Environ.*, vol. 9, no. 1, Jan. 1975, pp. 49-58.
55. Peterson, Thomas W.; and Seinfeld, John H.: Mathematical Model for Transport, Interconversion, and Removal of Gaseous and Particulate Air Pollutants - Application to the Urban Plume. *Atmos. Environ.*, vol. 11, no. 12, 1977, pp. 1171-1184.
56. Monin, A. S.; and Yaglom, A. M.: *Statistical Fluid Mechanics: Mechanics of Turbulence. Volume I.* MIT Press, c.1971.
57. Peterson, Thomas William: *Aerosol Dynamics in an Urban Atmosphere.* Ph. D. Thesis, California Inst. Technol., 1978.

TABLE I.- SOURCES OF INVALIDITY AND INACCURACY IN AIR QUALITY MODELS

Source of error	Comment
Sources of invalidity	
<p>True form of the turbulent fluxes $u'c_i$, $v'c_i$, and $w'c_i$ is unknown.</p> <p>Turbulent fluctuating chemical reaction terms are neglected (e.g., eq. (4)).</p> <p>Effect of concentration fluctuations from spatial averaging on chemical reaction rate is neglected (e.g., eq. (7)).</p>	<p>Higher order closure models will offer improvement over eddy diffusivities in representing these terms. Such closure methods lead to large computational requirements.</p> <p>Closure models appropriate for turbulent chemistry can be developed, but large computational requirements may arise.</p> <p>Introduce "microscale model" in regions where strong point and line sources occur.</p>
Sources of Inaccuracy	
<p>Mean velocities \bar{u}, \bar{v}, and \bar{w} are not true ensemble means (usually \bar{u}, \bar{v}, and \bar{w} are calculated from data at a finite number of locations):</p> <ul style="list-style-type: none"> Uncertainties in the measurement of wind speed and direction Inadequate or nonrepresentative spatial measurements of wind speed and direction Uncertainties associated with wind field analysis techniques <p>Source emission function S_i is inaccurate:</p> <ul style="list-style-type: none"> Inaccurate or no specification of source location Uncertainties in emission factors Inaccurate or no temporal resolution of emission Inadequate or no verification of emission methodologies 	<p>There is no way to determine the true mean from the data; \bar{u}, \bar{v}, and \bar{w} can be calculated in principle from accurate fluid mechanical turbulence model.</p> <p>More detailed emission inventories are needed to reduce this source of inaccuracy.</p>

TABLE I.- Concluded

Source of error	Comment
Sources of inaccuracy	
<p>Chemical reaction mechanism does not accurately reflect those chemical processes occurring in the atmosphere: Uncertainties in experimental determinations of specific reaction rate constants Variations of rate constants with temperature either uncertain or unknown Inadequacies in lumping due to the nonrepresentativeness of lumped class reactions relative to specific species within the class, for example, reaction rates, products, and stoichiometric coefficients Inaccuracies in the mechanism due to insufficient verification studies</p>	<p>Continued study of chemical processes is needed to insure that R_i is accurate; elimination or quantification of the following smog chamber related errors is also needed: Inadequate or no control and measurement of levels of H_2O in the chamber Impurities in background chamber air Inadequate or no measurements of the spectral distribution and intensity of the chamber irradiation system Inaccurate or ambiguous analytical methods Nonhomogeneity due to inadequate stirring or poor chamber design Adsorption and desorption of reactants and products on chamber walls Chemical reactions occurring on chamber surfaces Inadequate control and measurement of chamber temperature</p>
<p>Boundary conditions are inaccurately specified: Concentrations Inversion height</p>	<p>There is no remedy except for more extensive data.</p>

TABLE II.- COMPARISON OF SAI AND LIRAQ KINETIC MECHANISMS

Reaction	Rate coefficient for -	
	SAI ^a	LIRAQ ^b
NO _x /H ₂ O chemistry:		
NO ₂ + hν → NO + O	Variable	Variable
O + O ₂ + M → O ₃ + M	2.08 × 10 ⁻⁵ ppm ⁻² min ⁻¹	2.16 × 10 ⁻⁵ ppm ⁻² min ⁻¹
O ₃ + NO → NO ₂ + O ₂	25.2	26.2
NO ₂ + O → NO + O ₂	1.34 × 10 ⁴	1.34 × 10 ⁴
NO ₂ + O ₃ → NO ₃ + O ₂	5.0 × 10 ⁻²	4.35 × 10 ⁻²
NO ₃ + NO → 2NO ₂	1.3 × 10 ⁴	1.28 × 10 ⁴
NO + NO ₂ + H ₂ O → 2HONO	2.2 × 10 ⁻⁹ ppm ⁻² min ⁻¹	-----
NO ₂ + NO ₃ + H ₂ O → 2HONO ₂	1.66 × 10 ⁻³ ppm ⁻² min ⁻¹	-----
O + NO + M → NO ₂ + M	-----	3.41 × 10 ⁻³ ppm ⁻² min ⁻¹
O + NO ₂ + M → NO ₃ + M	-----	3.49 × 10 ⁻³ ppm ⁻² min ⁻¹
NO ₃ + NO ₂ → N ₂ O ₅	-----	5.59 × 10 ³
N ₂ O ₅ → NO ₃ + NO ₂	-----	12.2 min ⁻¹
N ₂ O ₅ + H ₂ O → 2HNO ₃	-----	6.84 × 10 ⁻⁶
NO ₃ + hν → NO ₂ + O	-----	Variable
NO _x /HO _x chemistry:		
OH + NO → HONO	9 × 10 ³	8.82 × 10 ³
OH + NO ₂ → HONO ₂	9 × 10 ³	1.47 × 10 ⁴
HO ₂ + NO → OH + NO ₂	2 × 10 ³	4.54 × 10 ³
HO ₂ + NO ₂ → HONO + O ₂	20	-----
HO ₂ + NO ₂ → HO ₂ NO ₂	-----	26.2
HONO + hν → OH + NO	Variable	Variable
CO + OH → CO ₂ + HO ₂	2.06 × 10 ²	2.06 × 10 ²

^aA 31-step mechanism, called the carbon-bond mechanism, has been developed by SAI as a variation of the Hecht-Seinfeld-Dodge mechanism (Whitten and Hogo (ref. 26)). Because of the association of reactions and reactivities with carbon bonds, the range of reactions and the range of rate constants in a kinetic mechanism can be narrowed somewhat if each atom is treated according to its bond type. In this mechanism, hydrocarbons are divided into four groups: single-bonded carbon atoms, fast double bonds (i.e., relatively reactive double bonds), slow double bonds, and carbonyl bonds. Single-bonded carbon includes not only paraffin molecules, but also the single-bonded carbon atoms of olefins, aromatics, and aldehydes. Double bonds are treated as a pair of carbon atoms. An activated aromatic ring is considered as three double bonds in the present formulation of the mechanism, and because of a similarity in reactivities, aromatics are lumped with the slow (ethylene) double bonds rather than with the fast double bonds. In the mechanism HC1, HC2, HC3, and HC4 represent fast double bonds, slow double bonds, single-bonded carbon atoms, and carbonyl bonds, respectively.

^bIn the LIRAQ mechanism HC1 denotes olefins and highly reactive aromatics; HC2, paraffins, less reactive aromatics, and some oxygenates; HC4, aldehydes, some aromatics, and ketones.

TABLE II.- Continued

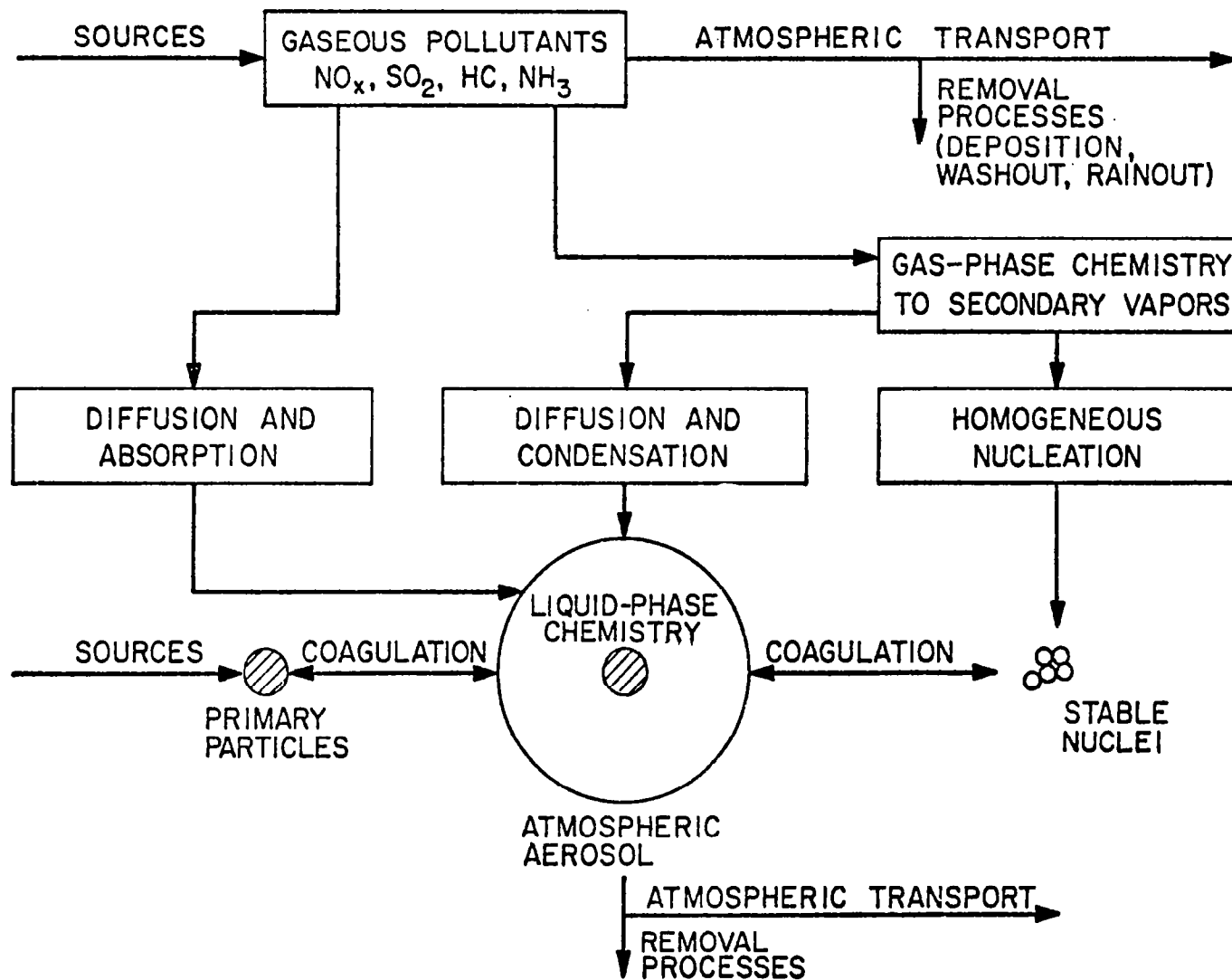
Reaction	Rate coefficient for -	
	SAI ^a	LIRAQ ^b
HO ₂ + O ₃ → OH + 2O ₂	-----	1.33
OH + HO ₂ → H ₂ O + O ₂	-----	2.94 × 10 ⁴
OH + O ₃ → HO ₂ + O ₂	-----	82.5
OH + HNO ₃ → H ₂ O + NO ₃	-----	1.32 × 10 ²
O ₃ + hν → O + O ₂	-----	Variable
O ₃ + hν + H ₂ O → O ₂ + 2OH	-----	Variable
HO ₂ + HO ₂ → H ₂ O ₂ + O ₂	4 × 10 ³	4.67 × 10 ³
H ₂ O ₂ + hν → 2OH	Variable	Variable
Hydrocarbon chemistry:		
HC1 + O → ROO + RCO ₃	5.3 × 10 ³	4.42 × 10 ⁻³
HC1 + OH → ROO + HC4	3.8 × 10 ⁴	3.93 × 10 ⁴
HC1 + OH → ROO + H ₂ O	-----	1.36 × 10 ⁴
HC1 + O ₃ → RCO ₃ + OH + HC4	1.0 × 10 ⁻²	-----
HC1 + O ₃ → OZONIDE	5.0 × 10 ⁻³	-----
HC1 + O ₃ → HO ₂ + RO + HC4	-----	1.75 × 10 ⁻²
HC1 + NO ₃ → HC ₂ + NO ₂	-----	6.70
HC2 + O → ROO + OH	-----	57.6
HC2 + OH → ROO + H ₂ O	-----	3.23 × 10 ³
HC2 + OH → HC4 + ROO	8.0 × 10 ³	-----
HC2 + O → RCO ₃ + ROO	37.0	-----
HC2 + O ₃ → RCO ₃ + HC4 + OH	2 × 10 ⁻³	-----
HC2 + NO ₃ → Products	50	-----
HC3 + O → ROO + OH	20	-----
HC3 + OH → ROO + H ₂ O	1.3 × 10 ³	-----
HC4 + hν → ROO + OH	Variable	-----
HC4 + hν → CO + H ₂	Variable	Variable
HC4 + OH → RCO ₃ + H ₂ O	1.0 × 10 ⁴	6.81 × 10 ³

TABLE II.- Concluded

Reaction	Rate coefficient for -	
	SAI ^a	LIRAQ ^b
HC4 + hν → RCO ₃ + HO ₂	-----	Variable
HC4 + O → OH + RCO ₃ + CO	-----	2.30 × 10 ²
HC4 + HO ₂ → H ₂ O ₂ + RCO ₃	-----	4.77 × 10 ⁻³
HC4 + RO ₂ → ROOH + RCO ₃	-----	4.03 × 10 ⁻³
HC4 + NO ₃ → RCO ₃ + HONO ₂	-----	0.215
HC4 + OH → CO + H ₂ O + HO ₂	-----	1.36 × 10 ⁴
Free radical chemistry:		
NO + ROO → RO + NO ₂	-----	2.15 × 10 ³
NO + ROO → NO ₂ + HC4 + HO ₂	2 × 10 ³	-----
NO ₂ + RO → RONO ₂	-----	2.94 × 10 ³
NO + RO → RONO	-----	2.94 × 10 ³
NO ₂ + RCO ₃ → PAN	150	397
PAN → RCO ₃ + NO ₂	0.02	-----
NO + RCO ₃ → ROO + NO ₂ + CO ₂	2 × 10 ³	1.07 × 10 ³
RO + O ₂ → HO ₂ + HC4	-----	0.92
ROO + HO ₂ → ROOH + O ₂	4 × 10 ³	3.97 × 10 ³
ROO + ROO → 2RO + O ₂	-----	3.97 × 10 ²
RCO ₃ + HO ₂ → R(O)OOH + O ₂	10 ⁴	-----
RCO ₃ + HO ₂ → ROOH	-----	6.6 × 10 ⁻²
RCO ₃ + RCO ₃ → HC4	-----	1.47 × 10 ³
Sulfur chemistry:		
OH + SO ₂ → OH + SO ₄ ⁻	-----	8.82 × 10 ²
RO + SO ₂ → HO ₂ + SO ₄ ⁻	-----	5.88 × 10 ²
ROO + SO ₂ → RO + SO ₄ ⁻	-----	2.94
HO ₂ + SO ₂ → OH + SO ₄ ⁻	-----	1.32

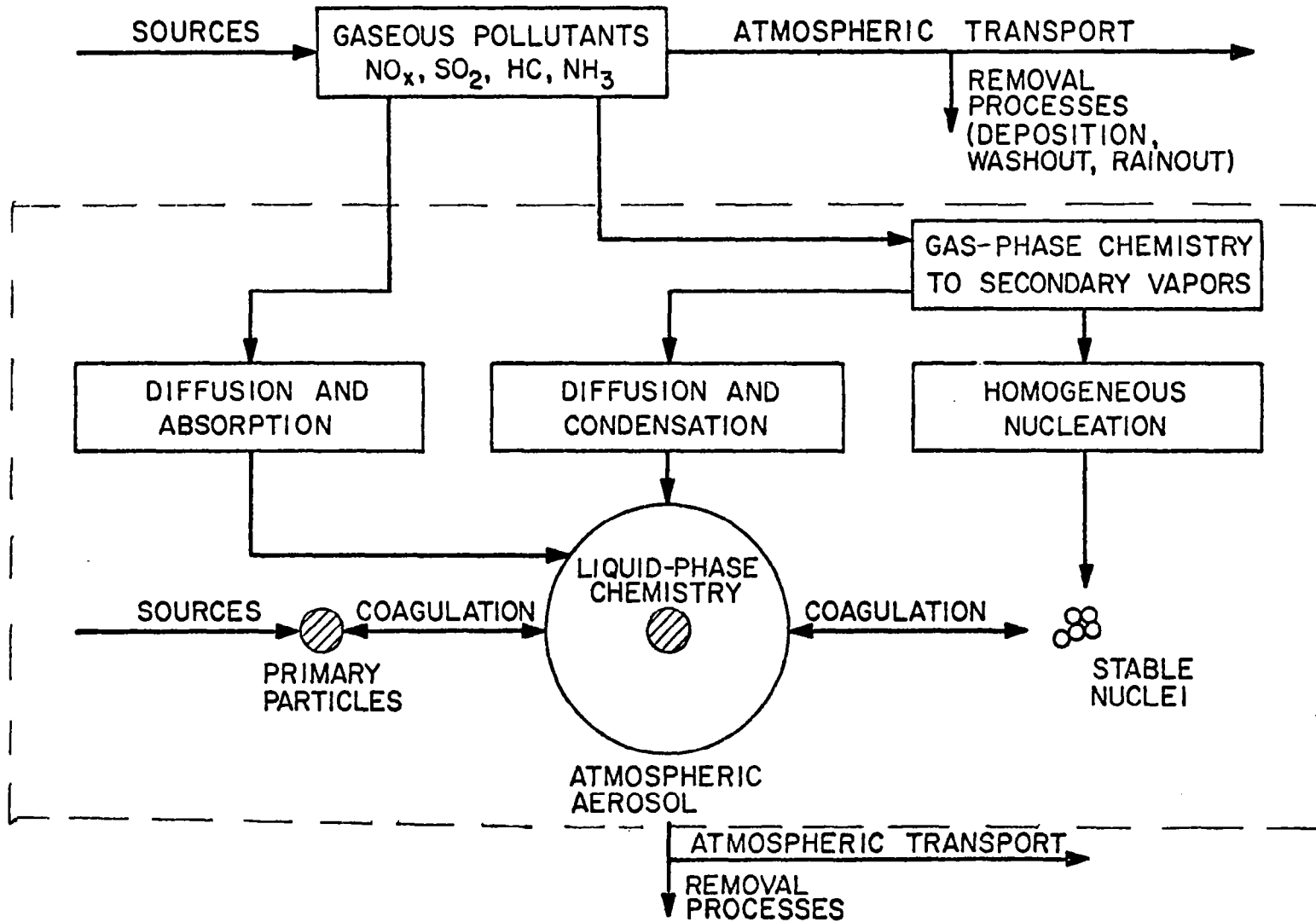
TABLE III.- ATMOSPHERIC AEROSOL SYSTEMS

System	Important mechanisms
Smog chamber	Condensation, coagulation, nucleation, and wall losses
Power plant plume	Convection, diffusion, condensation, coagulation, nucleation, sources, deposition and settling, and washout and rainout
Atmosphere Near particulate sources Far from particulate sources	Condensation, coagulation, nucleation, sources, and deposition and settling Convection, diffusion, condensation, sources, deposition and settling, and washout and rainout



(a) Schematic of complete process.

Figure 1.- Interaction between gaseous and particulate pollutants.



(b) Simple model replaces process within dashed lines.

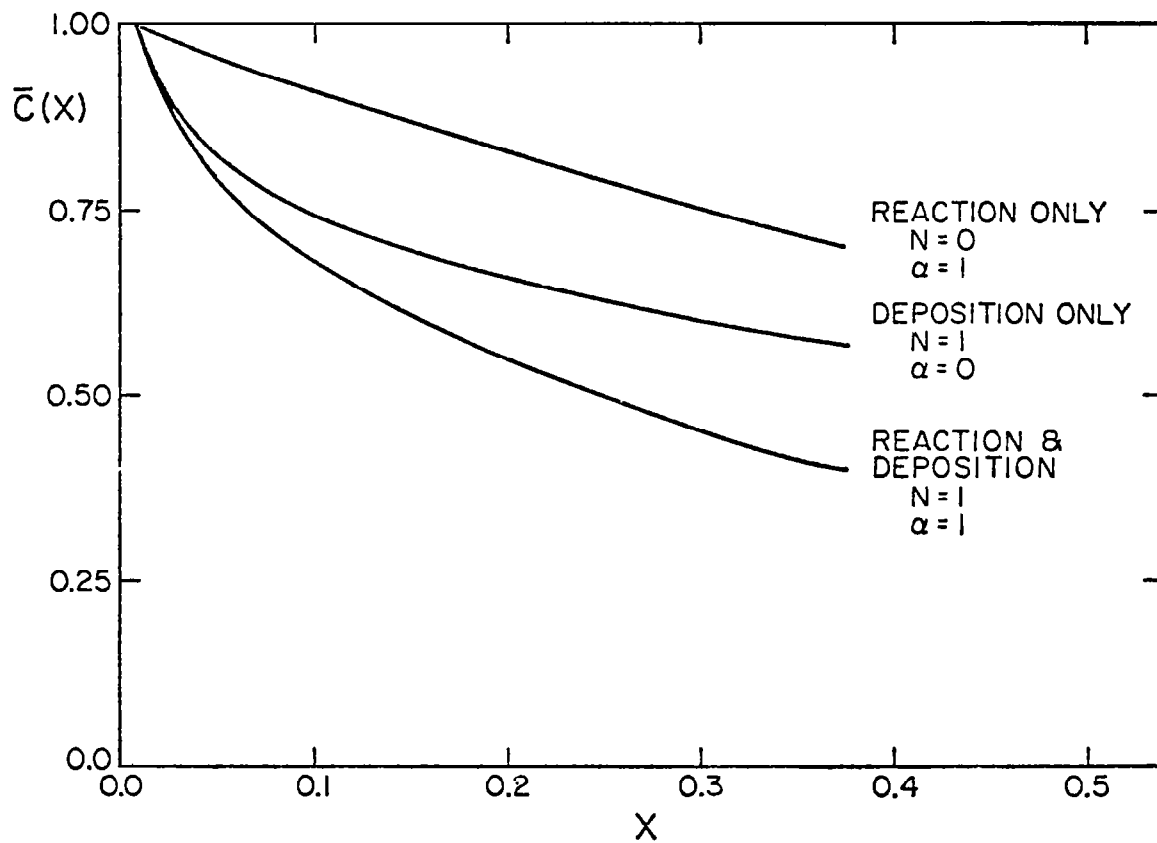


Figure 2.- Relative rates of removal of a gaseous pollutant by reaction and surface deposition.

THE ROLE OF COMPUTER MODELING OF PHOTOCHEMICAL SMOG IN DEFINING
EXISTING MEASUREMENT NEEDS*

Alan C. Lloyd
Environmental Research & Technology, Inc.
Santa Barbara, California

INTRODUCTION

One of the most useful applications of computer simulation of a complex chemical reaction system is in the elucidation of the key parameters in the system and in determining the sensitivity of the results to uncertainties in the rate constants or mechanisms of the individual reactions. This role of modeling will receive substantial emphasis in the following discussion on the computer simulation of photochemical smog formation in simulated and real atmospheres.

Photochemical smog was first identified in the Los Angeles Basin (Haagen-Smit (ref. 1)). This led to a major effort to understand and control the phenomenon with the result that a large base of atmospheric pollutant monitoring data has been accumulated. Consequently, where necessary, the Los Angeles area will be used to illustrate the various facets involved with understanding photochemical smog formation. Such an understanding is a necessary prerequisite to the design and implementation of effective control strategies. It should be recognized, however, that photochemical smog is now a worldwide phenomenon and is no longer confined to Los Angeles.

Following a brief history of photochemical smog formation and its effects in the Los Angeles Basin, the chemical mechanisms first suggested for photochemical smog formation will be discussed; this will be called the "pre-hydroxyl radical" or "pre-OH" era. Subsequently, the current ideas on photochemical smog formation in the "post-OH" era will be discussed in depth. This discussion will address the various kinetic and mechanistic inputs required to formulate a chemical mechanism to simulate photochemical smog formation. The computed and measured concentration-time profiles for a number of pollutants under various conditions will be presented. Finally, the role of measurements under laboratory and real atmospheric conditions in the further refinement of the chemical mechanism will conclude the discussion.

*Parts of the material presented in this paper are based upon research supported by the National Science Foundation (NSF) (Grant #ATM 75-18521) and by the Coordinating Research Council (CRC). Any opinions, findings, and conclusions or recommendations expressed in this paper are those of the author and do not necessarily reflect the views of the NSF or CRC.

HISTORICAL ASPECTS OF PHOTOCHEMICAL SMOG FORMATION

As early as 1542, the Los Angeles Basin was noted for its reduced visibility and for its potential to trap smoke or pollutants under a low-level inversion layer. Thus, in that year, Spanish explorer Juan Rodriguez Cabrillo, upon sailing into San Pedro Bay and spotting smoke rising from Indian fires, called the area La Bahia de Las Fummas, or The Bay of Smokes. He also noted in his diary that the smoke on shore was halted and spread out horizontally instead of continuing to ascend into the atmosphere.

It was in 1943 that the general public in Los Angeles and tourists to the area first began to realize that something serious was happening to the air they breathed. Complaints were initiated and the Los Angeles Times reported that ". . . thousands of eyes smarted. Many wept, sneezed, and coughed. Throughout the downtown area and into the foothills the fumes spread their irritation" At about the same time, a strange injury to vegetation was being observed. This was characterized by banding, silvering, and stippling of the leaves and was first investigated by Middleton et al. in 1944 in part of Los Angeles County. This type of injury soon spread throughout southern California, leading to economic losses for farmers and nurserymen (Middleton et al. (ref. 2)).

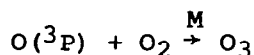
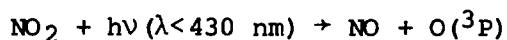
It was not until 1950 that the true cause of this air pollution and the associated plant damage was discovered. Thus, in November 1950, Arie J. Haagen-Smit, professor of bio-organic chemistry at the California Institute of Technology, announced that as a result of his extensive research, the major culprit in the air pollution formation was the unsaturated hydrocarbons from such sources as automobile exhausts and industrial plants. This discovery had quite an impact since, historically, the sulfur oxides had been the chief offenders in contaminating the air. Further research work by Haagen-Smit and co-workers (e.g., Haagen-Smit (ref. 1) and Haagen-Smit and Fox (ref. 3)) demonstrated conclusively that the new type of smog was formed photochemically by the action of sunlight on hydrocarbons and oxides of nitrogen (NO_x) to produce photochemical oxidants (mainly ozone) which were responsible for the plant damage.

In addition to ozone, Stephens et al. (ref. 4) found that a certain compound X nearly always seemed to be a product when a mixture of hydrocarbons and NO_x was irradiated. Compound X was eventually found to be peroxyacetyl nitrate (PAN) (Stephens (ref. 5)) and was shown to be an eye irritant and a powerful phytotoxicant. Once the idea of the participation of unsaturated hydrocarbons and nitrogen oxides became accepted, greater attention was given to the complex photochemistry and reactions occurring in the polluted atmosphere. Although the formation of identified components such as aldehydes, organic acids, and organic peroxides was attributed to atmospheric chemical transformations in the early 1950's (Chass and Feldman (ref. 6)), it was not until the publication in 1961 of the monumental treatise on photochemical smog formation by Leighton (ref. 7) that the subject was treated in a detailed and coordinated fashion. The mechanism suggested for its formation and that for ozone is discussed in the next section.

THE CHEMISTRY OF PHOTOCHEMICAL SMOG FORMATION

IN THE PRE-HYDROXYL RADICAL ERA

As discussed previously, Haagen-Smit and co-workers (refs. 1 and 3) demonstrated that Los Angeles' air pollution or photochemical smog was different from the London type smog, which is characterized by a chemically reducing atmosphere containing sulfur dioxide and particulates. Figure 1, taken from Haagen-Smit (ref. 1), shows the initial understanding of the interaction of the hydrocarbons, nitrogen oxides, sulfur oxides, and sunlight to produce the secondary pollutants such as ozone, acids, aldehydes, and peroxides. The key reaction in this system is the photolysis of nitrogen dioxide to produce ground-state oxygen atoms which in turn combine with atmospheric O₂ to produce O₃

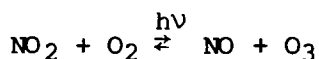


It was known that NO₂ absorbed actinic ultraviolet (UV) radiation and that the quantum yield of photodissociation was unity over most of the region of interest (λ ≈ 300 to 400 nm). Subsequently, it has been shown that the primary quantum yield is unity up to about 398 nm and then drops to zero at approximately 430 nm (Jones and Bayes (ref. 8)).

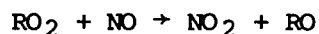
In the presence of NO, the O₃ concentration is decreased because of the rapid reaction,



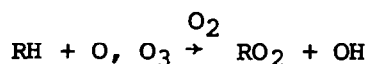
Thus, in the absence of hydrocarbons, a steady-state situation is reached which can be simplified to



Hence the levels of ozone, the chief protagonist in photochemical smog, are kept relatively low. However, it was discovered that significantly higher levels were produced when hydrocarbons were present (Haagen-Smit and Fox (ref. 3) and Darley et al. (ref. 9)). This was assumed to be due to the reaction,



where the alkyl peroxy radicals (RO₂) were assumed to be formed by the attack of O atoms and O₃ on the hydrocarbons (RH) particularly the olefins:



Leighton (ref. 7) indicated that other intermediates such as hydroperoxyl radicals (HO₂), hydroxyl radicals (OH), and alkoxy radicals (RO) were almost certainly participants in the hydrocarbon oxidation and conversion of NO to NO₂.

However, these were largely qualitative observations, and it was not until the late 1960's that the role of species other than O and O₃ was placed on a more quantitative basis.

Several investigators (see Leighton (ref. 7) and Niki, Daby, and Weinstock (ref. 10)) noted that the rate of disappearance of propylene or other olefins, in a simulated irradiated atmosphere containing NO and NO₂, could not be accounted for by attack on the olefin by O and O₃ alone. Thus, as the rate constant measurements for the reactions of O and O₃ with the olefins became more established, it was evident that one or more other species were reacting directly with the olefin and that there was a so-called excess rate at which the olefin was disappearing. This is illustrated in figure 2, taken from Niki, Daby, and Weinstock (ref. 10).

At about this time, some fundamental studies on the kinetics of the reaction of OH with several hydrocarbons around ambient temperature were being carried out by Greiner (ref. 11). The key role of OH in combustion systems had been recognized for years (Lewis and Von Elbe (ref. 12)), but the results of Greiner's studies indicated that OH could attack not only unsaturated hydrocarbons but also saturated hydrocarbons. These results prompted Greiner to state (ref. 11) that "these considerations suggest that OH could be important in the consumption, in polluted air, of saturated hydrocarbons which are relatively inert to other forms of chemical attack."

These and other studies provided the quantitative data to support the hypothesis that OH was the major intermediate responsible for the excess rate mentioned previously. This hypothesis was suggested at about the same time in 1969 and 1970 by two groups of workers - Niki, Daby, and Weinstock at the Ford Motor Company Research Laboratories and Heicklen, Cohen, and Westberg at the Aerospace Laboratories - who postulated the key role of OH in photochemical smog formation. The next section discusses the current understanding of the role of OH and its interaction with other intermediates, chiefly HO₂.

CURRENT MECHANISMS USED TO DESCRIBE PHOTOCHEMICAL SMOG FORMATION

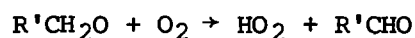
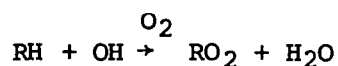
The mechanism currently considered to describe the general features of photochemical smog formation has been presented in detail in several recent articles (e.g., Altshuller and Bufalini (ref. 13), Niki, Daby, and Weinstock (ref. 10), Demerjian, Kerr, and Calvert (ref. 14), Pitts, Lloyd, and Sprung (ref. 15), and Finlayson-Pitts and Pitts (ref. 16)). Consequently, only the major aspects will be discussed briefly here. More mechanistic details are presented in the section "A Chemical Mechanism Used in an Atmospheric Model Development," which addresses the computer modeling of photochemical smog.

Role of Intermediates in O₃ Production

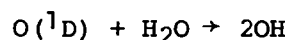
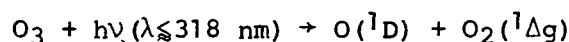
As indicated previously, rate constant determinations for the reaction of OH radicals with several classes of hydrocarbons at room temperature supported the idea that the OH radical is the key species in the initial attack on the hydrocarbons. Thus, the rate constants for OH radical attack on paraffins and

aromatics as well as on olefins are sufficiently large (Pitts et al. (ref. 17)) that these reactions are important in initiating chain oxidation of these hydrocarbons under atmospheric conditions. This is in sharp contrast to the other important intermediates such as O atoms and O₃ which only attack olefins sufficiently rapidly to be important in hydrocarbon oxidation.

Various peroxy radicals are formed subsequent to the initial attack by OH on the hydrocarbons. These species are responsible for the conversion of NO to NO₂. Examples of such reactions are

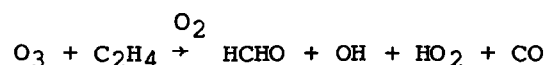


Sources of OH have been discussed by Demerjian, Kerr, and Calvert (ref. 14) and Calvert and McQuigg (ref. 18) and include the photolysis of nitrous acid (HONO) or hydrogen peroxide (H₂O₂), the photolysis of O₃ according to the reactions,



and indirect paths such as the photolysis of aldehydes (vide infra) and from the reaction of O₃ with olefins (Finlayson and Pitts (ref. 19)).

In addition to reactions of OH, O₃ and, to a much lesser extent, O(³P) are important in producing RO₂ and HO₂ radicals by reaction with olefins. Thus in the case of ethylene, the reaction mechanism is thought to be

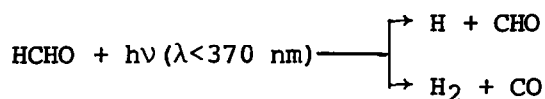


although Herron and Huie (ref. 20) have suggested an alternative route. They base this on results of their low-pressure studies in which they postulate another reaction pathway which produces fewer radicals. More recent work tends to confirm the fact that fewer radicals are formed in ozone-olefin reactions than older mechanisms predict (e.g., the mechanism given above for O₃ + C₂H₄).

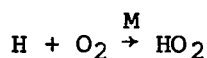
Species Other Than NO₂ Which Dissociate Under Atmospheric Conditions

Radical intermediates are produced by the absorption of radiation by various molecular species present in ambient air, which subsequently dissociate to give one or more radical or atomic species. The main compounds are listed in this section.

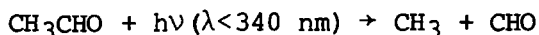
Aldehydes.- Aldehydes are emitted directly into the atmosphere from, for example, automobiles and certain stationary sources, and are also formed by chemical reactions such as those of O₃ with olefins. The photodecomposition of formaldehyde (HCHO) can proceed by a radical path and a molecular path (Calvert and Pitts (ref. 21)). The radical path yields H atoms and formyl (CHO) radicals; the molecular path yields molecular hydrogen and carbon monoxide:



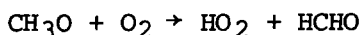
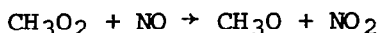
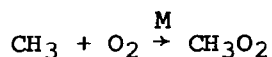
In air, both H atoms and formyl radicals react rapidly with molecular oxygen to form HO₂:



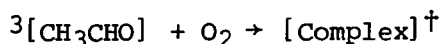
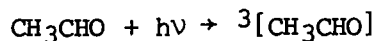
Aliphatic aldehydes other than formaldehyde also photodissociate to give formyl radicals. For example, the photodecomposition of acetaldehyde in the actinic UV region yields methyl and formyl radicals (Calvert and Pitts (ref. 21)):



The methyl radicals then initiate the following sequence of reactions which provides an additional path for the formation of HO₂:



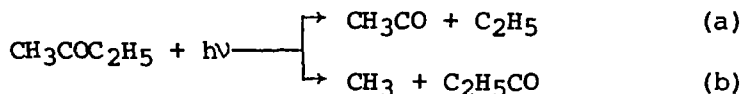
Recently, Weaver et al. (ref. 22) suggested that the photolytically excited triplet state of acetaldehyde undergoes a pressure-dependent reaction with O₂ forming radical products:



Their conclusion was based on a fit of their product data using a mechanism incorporating this reaction.

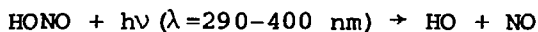
Aldehyde photolysis is an important process in photochemical smog formation (Dodge and Hecht (ref. 23)). Recent studies have provided improved quantum yield measurements for formaldehyde.

Ketones.— Ketones are major constituents of certain solvents and are used in dry-cleaning plants. Little is known about their ambient concentrations, but they can be sources of alkyl peroxy radicals since they photodissociate by the following paths in the actinic UV region (Calvert and Pitts (ref. 21)):

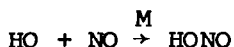
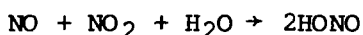


Little information is available on ketone photolysis under ambient conditions, and while Calvert and Pitts indicate that the relative quantum yields for paths (a) and (b) are about 27:1, it is uncertain whether this is true for atmospheric conditions in the presence of O₂.

Nitrous acid (HONO).— Nitrous acid photolyzes efficiently in the actinic UV region to give OH and NO



It can be formed either heterogeneously or homogeneously by the reactions,

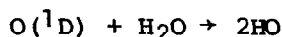
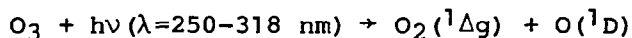


It has been suggested (Simonaitis and Heicklen (ref. 24)) that the reaction,

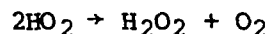


was also an important source, but recent work using Fourier transform infrared spectroscopy by several groups of workers (Niki, et al., Calvert, et al., and Pitts et al.) has shown that this reaction produces pernitric acid (HO₂NO₂) almost exclusively. This is discussed in a subsequent section.

O₃ and H₂O₂.— As mentioned earlier, both O₃ and H₂O₂ photolyze under ambient conditions and produce OH radicals. At short wavelengths in the actinic UV region, ozone undergoes photolysis to give O(¹D) atoms (Hampson and Garvin (ref. 25)) which yield OH upon reaction with water vapor:

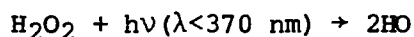


H₂O₂ formed by the reaction,



photodissociates (Calvert and Pitts (ref. 21)) to give OH directly, but the efficiency for smog pollution seems low because its absorption cross section

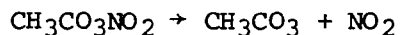
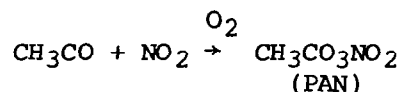
in the actinic UV region is small:



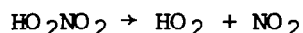
EFFECT OF TEMPERATURE ON PHOTOCHEMICAL SMOG MECHANISMS

It is well recognized that temperature plays a role in photochemical smog formation under atmospheric conditions (Schuck, Pitts, and Wan (ref. 26) and Stephens (ref. 27)), but the exact role is uncertain. While the reactions involved do depend on temperature, the variations in rate constants are probably not sufficiently large to effect the changes seen in ozone formation when temperatures get very high. Other meteorological parameters such as low wind speeds and low inversion heights which accompany high temperatures are probably far greater contributors to such high ozone levels.

However, two thermal reactions which have a strong temperature dependence have been elucidated recently: the thermal decomposition of peroxyacetyl nitrate (PAN) and pernitric acid,



with a rate constant of $1.95 \times 10^{16} \exp\left(-\frac{26910}{RT}\right) \text{ sec}^{-1}$ (Hendry and Kenley (ref. 28)), where R is the universal gas constant and T is absolute temperature, and



with a rate constant of $1.3 \times 10^{14} \exp\left(-\frac{20700}{RT}\right) \text{ sec}^{-1}$ (Graham et al. (ref. 29)).

Thus, a few degrees Celsius temperature change can affect the rate constants for these reactions; also since both reactions lead to the release of NO_2 , a change in rate constants can lead to a change in the final ozone levels.

In summary, the current understanding of photochemical smog formation can be simplified in terms of figure 3. This schematic shows the interactions of hydrocarbons, nitrogen oxides, and aldehydes with ultraviolet radiation to produce the major phenomenological features of smog.

The detailed listing of specific reactions has been presented by several authors and will not be repeated here (Demerjian, Kerr, and Calvert (ref. 14) and Graedel et al. (ref. 30)). However, the next section includes reactions used to describe chemical mechanisms for use in an urban airshed model; this mechanism is inherently less comprehensive than those used to validate detailed smog chamber data, since the costs involved in running an atmospheric model with

150 to 200 reactions would be prohibitive. Hence, approximations, such as the "lumping" of hydrocarbons and radical classes, are necessary in atmospheric model simulations.

A CHEMICAL MECHANISM USED IN AN ATMOSPHERIC MODEL DEVELOPMENT

This section describes the formulation and testing of a chemical mechanism developed by Environmental Research & Technology, Inc. (ERT) under funding from the Coordinating Research Council, Inc., the National Science Foundation, and ERT. This work is described in detail elsewhere (ref. 31) and is treated briefly here.

Extensive use has been made of previous and current modeling studies in developing the chemical module for the atmospheric model. These include studies by Niki et al. (ref. 10), Demerjian, et al. (ref. 14), Hecht et al. (ref. 32), Whitten and Hogo (ref. 33), and Graedel (ref. 34). However, in order for the chemical scheme to have practical applications in terms of airshed models, the number of species has to be carefully limited. Thus, inherently, the mechanism is an approximation adapted to the treatment of multicomponent mixtures of great complexity in contrast to the models developed by the majority of the above workers.

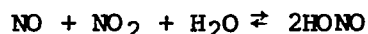
The chemical mechanism, shown in table I, has been significantly changed from that of Hecht, Seinfeld, and Dodge (ref. 32); however, the partitioning of the hydrocarbons into classes is very similar to that used by them with the exception that the aldehydes are split between formaldehyde and the higher aldehydes.

As indicated previously, the formulation of a chemical kinetic scheme for use in an atmospheric model requires a substantial reduction in the level of chemical detail to be treated. For example, the numerous individual hydrocarbons must be lumped into various representative categories. The type of lumping employed can vary. Thus, the hydrocarbons have been partitioned into five classes while other workers have used fewer classes (Hecht et al. (ref. 32)) or have treated the total reactive hydrocarbons in terms of propylene (Graedel et al. (ref. 35) and Wayne et al. (ref. 36)) or a mixture of propylene and n-butane (Dodge (ref. 37)), the latter two compounds representing the highly reactive and lesser reactive species, respectively, in the atmospheric mixture.

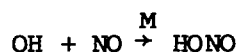
The reaction mechanism for the hydrocarbon/ NO_x system is presented in table I; the additional reactions necessary to describe the SO_2 oxidation are presented later in this paper. The rate constants shown in table I are operative at 305 K. In instances where M or O_2 occur in the reaction mechanism, their concentration has been included in the rate constant to give a pseudo first- or second-order rate constant. Many of these rate constants are taken from the National Bureau of Standards Technical Note #866 (Hampson and Garvin (ref. 25)). In some cases, particularly for the organic reactions, kinetic data are generally taken from the work of Carter, Lloyd, Sprung, and Pitts, while the remainder were derived in the model development program described previously. A detailed discussion of the basis for rate and mechanistic choices is not given here; only a few selected reactions are discussed.

Selected Features of the Mechanism

The chemistry of nitrous acid.- The formation of nitrous acid by the reaction,



has been investigated recently by several workers, including Chan et al. (refs. 38 and 39) and Cox (ref. 40). This reaction and



are presumed to be the major sources of nitrous acid formation in chamber studies, and probably in ambient air. The data obtained by Chan et al. (refs. 38 and 39) have been used for the formation and destruction of nitrous acid. In addition, the photolysis rate constant obtained recently by Cox and Derwent (ref. 41) has been used. Their value is a factor of about 2 greater than that formerly used.

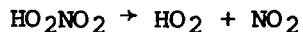
In order to account for the radical initiation in smog chamber studies (Whitten and Hogo (ref. 33), Dodge (ref. 37), and Wu et al. (ref. 42)) and to take into account chamber contamination (Bufalini et al. (ref. 43)), a portion of the equilibrium HONO concentration has been used to provide an initial radical source to initiate the smog reactions (Whitten and Hogo (ref. 33) and Jeffries et al. (ref. 44)). As discussed in the "Typical Results" section, the values used are usually one-quarter of the equilibrium HONO concentration. One problem in using this method to account for the radical initiation is that it tends to shorten the ozone initiation time but does not adequately account for any radical production later in the run. In essence, it affects the time to ozone maximum but not the value of the maximum. However, if no initial radical flux is used, then the reactivity of the system in terms of time to NO₂ maximum, rate of NO oxidation, and so forth is invariably underpredicted. As discussed subsequently, it may be unnecessary to use initial HONO as a radical initiator under ambient conditions, since there may be sufficient aldehydes present.

The reaction of HO₂ with NO.- There have been several studies (Hampson and Garvin (ref. 25)) of the reaction,



Many of these have been carried out at low pressures, and in view of the increasing number of instances in which rate constants have been found to be pressure dependent, the rate constants obtained under these conditions have not been used in this study. Cox (ref. 40) has studied the reaction under atmospheric conditions and obtained a value of about $3 \times 10^3 \text{ ppm}^{-1}\text{-min}^{-1}$ which is about a factor of 10 greater than the low-pressure studies, and this is the value the author used until recently. However the system is complex, and thus the rate constant is subject to some uncertainty. Recently, Howard (ref. 45) reported a value of about $1.2 \times 10^4 \text{ ppm}^{-1}\text{-min}^{-1}$ on the basis of a study using laser magnetic resonance detection of HO₂. This value has been used in the present version of the reaction mechanism.

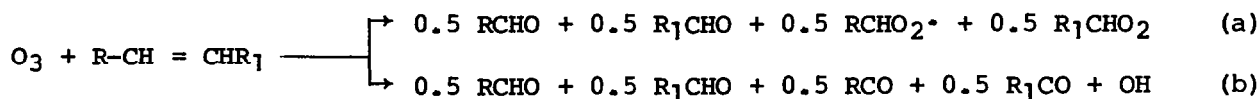
The formation of pernitric acid from the reaction of HO₂ with NO₂. Recently the importance of pernitric acid in photooxidation studies involving nitrogen oxides has become increasingly evident (Niki et al. (ref. 46) and Levine et al. (ref. 47)). While earlier studies (Simonaitis and Heicklen (refs. 24 and 48) and Cox and Derwent (ref. 49)) showed the formation of nitrous acid from this reaction, there now seems to be reasonable agreement that pernitric acid is the major if not the only product, although there is some uncertainty as to the subsequent fate of the pernitric acid. For example, Levine et al. (ref. 47) estimate that the pernitric acid, once formed, will tend to produce some nitrous acid either on the walls or in the gas phase. However, neither Niki et al. (refs. 46 and 50) nor Graham et al. (ref. 29) find evidence for the subsequent production of nitrous acid. In the present model, the production of a small amount of nitrous acid is shown by its inclusion in reaction (11) in table I. Experimental data obtained since the formulation of this mechanism do not support the formulation of nitrous acid in this reaction. Consequently, the current ERT model shows the production of HO₂NO₂ exclusively. The decomposition of the pernitric acid is treated in a manner similar to the peroxyacetyl nitrate:



The rate constant chosen for the pernitric acid decomposition is that suggested by J. G. Calvert (private communication, 1977), which is similar to that derived from the temperature study subsequently reported by Graham et al. (ref. 29)). The Arrhenius expression obtained by these workers was given earlier.

The value chosen for the HO₂NO₂ decomposition rate significantly affects the final O₃ peak, since HO₂NO₂ acts as a reservoir for NO₂. A short lifetime means that the net effect of reaction (11) in table I on O₃ production is not significant and vice versa.

Olefin reactions with O₃. The major role in photochemical oxidant formation played by the reactions of O₃ with olefin has been known for many years and is described in detail elsewhere (Niki et al. (ref. 10), Demerjian et al. (ref. 14), Hecht et al. (ref. 32), Whitten and Hogo (ref. 33), and Graedel et al. (ref. 35)). Recently (Niki et al. (ref. 51) and Walter et al. (ref. 52)), studies have shown that the reaction produces fewer radicals than previously thought. Thus, a major advance was made with the definitive identification of a stable secondary ozonide by Niki et al. which confirmed the earlier but less definitive work of Hanst et al. (ref. 53). Therefore, it appears that Criegee biradicals (RCHO₂•) are formed under atmospheric conditions and last sufficiently long to react bimolecularly. They are assumed to react rapidly with NO and NO₂. However, there is still significant uncertainty concerning the relative rates of molecular-forming (path (a)) compared with radical-forming (path (b)) routes in the overall reaction,



where $RCHO_2^*$ and $R_1CHO_2^*$ represent the Criegee intermediates. Most modeling studies have depicted the O_3 -olefin reaction in terms of path (b). The net reaction and overall rate constant is shown in table I. Until more definitive data become available for a variety of olefins, equal partitioning has been assumed between the two paths.

In a surrogate hydrocarbon model, the uncertainty of the mechanism of the O_3 -olefin reaction is compounded by the uncertainty inherent in choosing an appropriate olefin representative of the bulk olefin mixture. Such a choice has a bearing on both the rate constant and the mechanism. This is discussed later in more detail.

Olefin reactions with OH.- The consumption of olefins during the early stages of reaction before a significant buildup of ozone occurs is attributed to the reaction with the hydroxyl radical (Niki et al. (ref. 10) and Demerjian et al. (ref. 14)). Olefins react rapidly with OH and recent work by R. J. Cvetanovic has shown that the mechanism is largely one of addition with about 65 percent of reaction occurring by addition to the terminal carbon atom, while the other 35 percent occurs by addition to the internal carbon atom. The present mechanism ignores any hydrogen abstraction from the olefin.

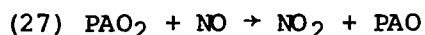
Following addition of OH and subsequently of O_2 to the radical so produced (reactions (19) to (21)), the mechanism shows the conversion of two molecules of NO to NO_2 which is the result of the findings of the work of Carter, Lloyd, Sprung, and Pitts. This is also generally consistent with the recent studies of Niki (1977). This mechanism differs from that used by Demerjian et al. (ref. 14) since the reaction of O_2 with the hydroxy-type radical (RCHOH) shown as reaction (21) in table I leads to the production of HO_2 and an oxygenated species rather than addition of O_2 to the RCHOH radical as follows:



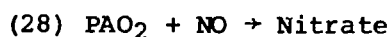
However, in spite of recent work elucidating the mechanism, there is still uncertainty regarding the reactions and products subsequent to the initial addition to a variety of olefins in the presence of NO_x .

The photooxidation of alkanes.- It is assumed in this study that the only mechanism for the consumption of alkanes under ambient conditions is reaction with OH. Since the C-H bond strengths in the paraffins are reasonably high (95 to 98 kcal-mol⁻¹), the only species for which hydrogen abstraction reactions are significantly fast is OH. The alkane photooxidation mechanism is probably the best understood of all the hydrocarbon species (Whitten and Hogo (ref. 33)) and is represented by reactions (26) to (33) in table I.

The mechanism is similar to that used in other investigations but has been updated to include two recent findings reported by Carter et al. (ref. 54) and Darnall et al. (ref. 55), namely, the formation of nitrates from the longer chain ($\geq C_4$) alkanes in the $RO_2 + NO$ reaction as shown subsequently, and also the isomerization of alkoxy radicals formed from C_4 and hydrocarbons. For example, the ratio of rate constant k_{27} for the reaction,



to the rate constant k_{28} for the reaction,



is about 11.2, as determined earlier by Darnall et al. (ref. 55) in a chamber study of n-butane/ NO_x /air mixtures.

The mechanism also takes into account nitrate formation from the normal reaction of alkoxy radicals with NO_2 (reaction (31)); in this case the alkoxy radical is denoted by PAO, which is the radical derived from the paraffins. Naturally, the choice of 11.2 for the ratio k_{27}/k_{28} may vary in going to ambient air when significant proportions of longer chain alkanes are present. Thus, the choice of this ratio in any model application has to be examined in light of any detailed hydrocarbon data available from urban airshed studies specific to the region under consideration.

Aromatic hydrocarbon photooxidation.- There is very little information on the photooxidation of aromatic compounds under photochemical smog conditions. The present mechanism is shown in figure 4; toluene is taken as a representative aromatic hydrocarbon. Thus the mechanism reflects the known addition (Davis et al. (ref. 56), Hansen et al. (ref. 57), Doyle et al. (ref. 58), and Lloyd et al. (ref. 59)) of OH to the aromatic compound followed by the subsequent reactions shown. In addition, it is assumed that abstraction of hydrogen atoms from the side chain occurs about 20 percent of the time (Perry et al. (ref. 60)), with the net result of the formation of an aldehyde; for example, from toluene, benzaldehyde would be produced as shown in figure 4.

The mechanism also considers the possibility of ring opening following addition of OH and O_2 to the cresol formed from the addition of OH to toluene. Likely products from ring opening would involve multifunctional oxygenated compounds, and the author has chosen to represent these compounds by an aldehyde (RCHO). This is done to conserve the number of species involved in the model, but also to take into account the possibility that the products resulting from ring opening will be photoreactive and create further radicals. This technique has been used previously (Pitts (ref. 61)).

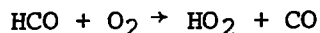
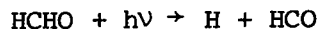
Although there is considerable uncertainty involved in the aromatic hydrocarbon oxidation mechanism, it was thought that aromatics should be included explicitly in the mechanism since they compose a significant fraction (≥ 30 percent) of gasoline (R. J. Campion, private communication, 1976). Indeed, since the phasing out of lead from gasoline, aromatics have been used by certain manufacturers to maintain the octane rating. Thus, ambient concentrations can be significant and their reactivity should be considered. The reaction mechanism will undoubtedly be refined as more data on the aromatic photooxidation steps become available; indeed, recent work by Niki et al. (ref. 62) suggests that the actual mechanism may be significantly different for reactions following initial OH attack than that presented here.

Aldehyde photolysis.- It has been known for some time that aldehydes are key radical initiators in the photooxidation systems present in ambient air and in smog chambers (Pitts et al. (ref. 63), Demerjian et al. (ref. 14), Dodge and Hecht (ref. 23), and Dodge and Whitten (ref. 64)). Quantum yields for radical

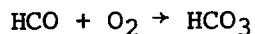
production for aldehydes in air are highly uncertain although it has been shown that the rate constants for aldehyde photolysis are very important in terms of photochemical smog modeling (Dodge and Hecht (ref. 23)).

The present mechanism differentiates between formaldehyde and the higher aldehydes. The author feels that this is important in view of the different radicals formed and the slightly different shape of the formaldehyde absorption curve compared with the higher aldehydes (Calvert and Pitts (ref. 21)). This is most manifested by absorption at longer wavelengths by formaldehyde compared with the other aldehydes and this is reflected in the urban airshed model by a difference in their photolysis rate constants with altitude. In addition, by differentiating the aldehydes in this way, more realistic predictions of PAN concentrations are possible since formaldehyde does not form PAN.

The model calculations are sensitive both to the initial concentrations used for aldehydes and to the rate constants used for photolysis. Radical production from aldehydes affects both the rate of ozone formation and the peak ozone attained. The chosen rate constants for aldehyde photolysis are based on measurements obtained in the glass chamber at the University of California, Riverside and the quantum yields of Lee et al. (ref. 65). The recent work of Weaver et al. (ref. 22) has been taken into account by combining the two possible photooxidation paths, one which is dependent on the oxygen concentration and the other which is independent. In addition, the formyl radical formed upon photolysis of formaldehyde is assumed to react with O₂ as follows:



This pathway appears to be the major one occurring under atmospheric conditions, rather than the alternative suggestion



(See Lloyd (ref. 66) who also describes recent studies which supersede that of Lee et al. (ref. 65).)

In view of the sensitivity of the model to both the rate constant and the initial conditions, it would be highly desirable for better data to be available on the photochemistry of the aldehydes both under ambient conditions and in ambient air under varying levels of photochemical smog intensity.

Testing of the Photochemical Model

The extensive body of smog chamber data obtained by the Statewide Air Pollution Research Center of the University of California, Riverside, in its studies for the California Air Resources Board (Pitts et al. (refs. 63 and 67) and for the U.S. Environmental Protection Agency (Pitts et al. (ref. 68)) has proved invaluable in checking the simulations against experimental observations under varying hydrocarbon/NO_x ratios and total concentrations of hydrocarbons and NO_x. The chamber facility is described in the above reports.

The following chamber data (Pitts et al. (refs. 17, 67, and 68)) have been utilized:

- (1) n-butane/NO_x mixtures
- (2) Propylene/NO_x mixtures
- (3) n-butane/propylene/NO_x mixtures
- (4) Surrogate hydrocarbon mixtures representative of the atmosphere and composed of four alkanes, four olefins, two aromatics, two aldehydes, CO, CH₄, and acetylene. The detailed composition is shown in table II (Pitts et al. (ref. 67)).

With the exception of the surrogate data, results were obtained in an evacuable, ¹Teflon-lined chamber (EC) irradiated by a solar simulator (Beauchene et al. (ref. 69)). The surrogate data were obtained in an all-glass chamber (AGC) operated under conditions of room temperature and pressure and irradiated externally by banks of black lights (Pitts et al. (refs. 17 and 67)).

The calculations, including those involving SO₂ described later, were performed on an IBM 360/75 computer and a Control Data 6400 computer with a chemical kinetics program written in FORTRAN IV. The list of species, reactions and rate constants, and stoichiometric coefficients were input to the program to form a set of kinetic differential equations. These equations were integrated with an ordinary differential equation integration package developed by Gear (ref. 70) for the variable-step-variable-order integration of coupled differential equations. Calculations were done in single precision with an error bound of 0.1 percent. Integrations ran smoothly with no problems encountered due to stiffness.

Typical Results

Figure 5 is included as being typical of the results obtained for the n-butane/propylene mixtures. This figure shows that the mechanism predicted the decay of both the paraffin and the olefin well, although in the late stages the model slightly overpredicted the decay. While the predicted ozone initiation time was slightly shorter than the experimental value, the overall agreement between the experimental and predicted values is good. The overprediction of the PAN concentration is reflected in the underprediction of the later NO₂ concentrations.

Six specific runs were chosen to test the mechanism against smog chamber data obtained for a surrogate mixture. These runs were chosen so that a variety of hydrocarbon/NO_x ratios were used to provide a stringent test for the model. A comparison of results of the model prediction with the experimental data for Statewide Air Pollution Research Center (SAPRC) run AGC 119, which has a molar

¹Teflon: Registered trademark of E. I. du Pont de Nemours & Co., Inc.

hydrocarbon/ NO_x ratio of 1.5, is presented in figure 6. The initial concentration of HONO used was one-quarter of its equilibrium value.

It can be seen that the mechanism does as well as might be expected from a lumped species mechanism although probably not as well as one with a larger number of reactions to account for all the different species involved. On the basis of the results of the six runs, the mechanism tends to underpredict the final O_3 concentration slightly but overpredicts the final NO_2 concentration. These deficiencies are being rectified.

Table III shows the percentage contribution of O, OH, and O_3 to the total rate of olefin oxidation after 15, 180, and 360 min of irradiation for run 119. As expected, OH is the major species responsible for attack on the olefin during the initial stages of irradiation. However, O_3 becomes the dominant species when it builds up to significant levels. Oxygen atoms play a small but significant role in the early stages but are not significant at later times. This chemical model has been incorporated into an atmospheric Lagrangian model developed by Environmental Research & Technology, Inc., and called Environmental Lagrangian Simulation of Transport and Atmospheric Reactions (ELSTAR). It is being tested by using data from the Los Angeles Reactive Pollutant Program (LARPP). Funding for ELSTAR development is being provided by the Coordinating Research Council, Inc.

While the chemical model predicts results which are in satisfactory agreement with available smog chamber data, there are many areas of uncertainty involved and assumptions made in its formulation necessitating continual refinement of the model. Significant and continuing improvements to such modeling efforts can only be effected through thorough and accurate measurement programs. Scientific areas in which these measurements are sorely needed are outlined in the concluding section on measurement needs.

FORMULATION OF A CHEMICAL MECHANISM FOR THE HOMOGENEOUS OXIDATION OF SO_2 UNDER ATMOSPHERIC CONDITIONS

Introduction and Background

Pollution of the air by sulfur oxides and particulates has been known for centuries. Until a few years ago, it was assumed that the chief adverse health effects were associated with SO_2 in conjunction with particulates and a synergism was attached to these pollutants when they occurred together. Thus, the well-known air pollution disasters of London in 1952 and 1962 and Donora in 1948 have been ascribed to this type of pollution (National Air Pollution Control Association (ref. 71)). However, in recent years, primarily as a result of the EPA CHES studies (U.S. Environmental Protection Agency (ref. 72)), it is hypothesized that adverse health effects are largely associated with sulfate rather than SO_2 or particulates. Examples of such sulfates are ammonium sulfate, zinc sulfate, or zinc ammonium sulfate. The gradation of adverse health effects is controlled both by the type of cation associated with the sulfate and also the particle size range in which the sulfate exists. To date, it is not known which are the most harmful sulfates. But evidence of suspected

adverse health effects of sulfates has led the California Air Resources Board to formulate an ambient air quality standard for sulfate (ref. 73). This standard is 25 $\mu\text{g}/\text{m}^3$ of sulfate as a 24-hour average.

Sulfates are emitted directly from automobiles equipped with catalytic converters (U.S. House of Representatives (ref. 74)) and are formed in ambient air from SO_2 precursors (e.g., Hidy and Burton (ref. 75)). Thus, power plants, oil refineries, and transportation are major sources of SO_2 in the atmosphere, and SO_2 oxidation is often found to proceed at rates ranging from 0.1 percent to greater than 10 percent per hour under ambient conditions (Hidy et al. (ref. 76), and Calvert et al. (ref. 77)).

Compounding the problem has been a realization in recent years that sulfates are the end products of practically all sulfur-containing emissions into the atmosphere (Graedel (ref. 30)). Thus, sulfates are formed not only from SO_2 but also from hydrogen sulfide and organic mercaptans (RSH). Since hydrogen sulfide is emitted naturally for example from decomposing vegetation in marshy areas and from geothermal wells, ambient sulfates can also be produced from the oxidation of naturally occurring sulfur compounds. Indeed, Hitchcock (ref. 78) has estimated that in certain areas, a major part of the ambient concentration of sulfates can be ascribed to oxidation of naturally occurring sulfur compounds.

The problems created by SO_2 emissions into the atmosphere have been exacerbated recently by the increased sulfur content of fuels used as a result of the energy crisis (U.S. House of Representatives (ref. 74)). Consequently, there has been a large upsurge in attempts to formulate chemical mechanisms which faithfully describe the conversion of SO_2 to sulfate under ambient conditions by homogeneous and heterogeneous processes. This means that direct processes (involving SO_2 by itself), or indirect processes (resulting from other photo-oxidation processes and radical production) have to be considered in model development. Thus, a number of workers have formulated models to describe SO_2 oxidation (chiefly by homogeneous routes) in real or simulated atmospheres (Durbin et al. (ref. 79), Calvert (ref. 80), Calvert and McQuigg (ref. 18), Graedel (ref. 34), and Miller (ref. 81)). Most recently, Calvert et al. (ref. 77) and Sander and Seinfeld (ref. 82) have summarized the major processes occurring in the homogeneous atmospheric oxidation of SO_2 . In view of the extensive summary of Calvert et al. (ref. 77), only the selected points will be discussed in detail here. More details on the sulfate model development are given elsewhere (ref. 31) and consequently will be discussed briefly here.

Atmospheric Chemistry of SO_2

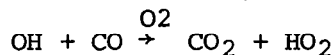
A discussion of the atmospheric chemistry of SO_2 should include both homogeneous and heterogeneous oxidation processes. Homogeneous processes are generally assumed to be gas-phase homogeneous paths, whereas, heterogeneous processes usually include those involving aerosols, surfaces, and water vapor, although by definition, both categories encompass a much broader spectrum of reactions. A crucial question in the atmospheric oxidation of SO_2 is the relative importance of homogeneous gas-phase chemistry compared with the heterogeneous routes (Hidy and Burton (ref. 75) and Calvert (ref. 80)). Heterogeneous reactions are assumed to be most important in areas of high relative humidity

and/or aerosol loading and also in pollutant plumes which may contain catalysts such as iron or manganese. Homogeneous processes are generally understood to be significant in areas of high photochemical activity with elevated levels of ozone and other oxidants. The following discussion considers homogeneous gas-phase processes only.

Sulfur dioxide does absorb ultraviolet radiation (Calvert and Pitts (ref. 21)), but unlike nitrogen dioxide it does not dissociate to produce an oxygen atom until about 2180 Å, far shorter wavelengths than found in the lower atmosphere. However, the role played by excited $\text{SO}_2(^3\text{B}_1)$, formed in the atmosphere by absorption of the available radiation, is insignificant, and Calvert et al. (ref. 77) estimate that the maximum rate of oxidation of SO_2 by direct photoabsorption is less than 0.02 percent per hour. In view of the fact that atmospheric oxidation rates ranging anywhere from 0.1 percent to greater than 10 percent per hour have been observed, it is apparent that the direct photoabsorption reaction will be of very minor significance. Thus, other processes make the major contribution toward the atmospheric oxidation of SO_2 . These processes have been listed previously by other workers (e.g., Calvert (ref. 80) and Hidy and Burton (ref. 75)) and involve inorganic radical intermediates such as O atoms, OH, HO_2 , and NO_3 radicals, and organic radical intermediates such as RO, RO_2 , and RCO_3 . The importance and occurrence of these species as contributors to SO_2 oxidation are discussed separately in the following section.

On the basis of this survey of the data, a number of reactions which the author believes to be important in the conversion of SO_2 to sulfate in the presence of hydrocarbons and NO_x have been postulated; these 10 reactions, shown in table IV, have been added to the previous list of 46 reactions in table I used to model the hydrocarbon/ NO_x system. The importance of various reactions are discussed initially, while subsequent discussions describe the ability of this reaction scheme to reproduce the results of selected chamber studies.

$\text{OH} + \text{SO}_2 \xrightarrow{\text{M}} \text{HSO}_3^-$ - It is generally recognized (Calvert and McQuigg (ref. 18), Sander and Seinfeld (ref. 82), and Calvert et al. (ref. 77)) that this is the most important single reaction consuming SO_2 in the atmosphere. The rate constant for this reaction has been studied by many workers but a reliable value applicable to atmospheric conditions is less easy to obtain since the reaction is in the pressure-dependent region for pressures normally studied under laboratory conditions. In addition, several workers (Davis et al. (ref. 56), Payne et al. (ref. 83), Cox (ref. 84), Wood et al. (ref. 85), Castleman et al. (ref. 86), and Castleman and Tang (ref. 87)) studied this reaction in competition with the reaction,



which is shown as reaction (9) in table I. Recently this reaction has been shown to exhibit a pressure dependence at the low pressures often used in laboratory studies (Sie et al. (ref. 88), Cox et al. (ref. 89), and Chan et al. (ref. 90)). Consequently, the rate constants obtained for $\text{OH} + \text{SO}_2$ from the competitive rate studies must be increased by approximately a factor of 2 to bring them in line with the new measurements of the rate constant k_9 for reaction (9).

In addition to these competitive rate studies, several results have been obtained by using the flash photolysis resonance fluorescence technique. These results include studies by Davis and Schiff (unpublished, 1974), Harris and Wayne (ref. 91), and Atkinson et al. (ref. 92). The last workers obtained a high-pressure limit of $5.0 \times 10^5 \text{ m}^3\text{-mol}^{-1}\text{-sec}^{-1}$ by extrapolation of their data to the high pressure. The study of Gordon and Mulac (ref. 93) was carried out at 1-atm total pressure and 435 K, and they obtained a value of $1.08 \times 10^6 \text{ m}^3\text{-mol}^{-1}\text{-sec}^{-1}$.

The value of $7.18 \times 10^5 \text{ m}^3\text{-mol}^{-1}\text{-sec}^{-1}$ has been chosen (using a corrected value for k_9) in the model calculations. This is equivalent to $1.76 \times 10^3 \text{ ppm}^{-1}\text{-min}^{-1}$. This value is about the same as that obtained by Calvert et al. by taking an average of the results of the most comprehensive data sets at atmospheric pressure.

For modeling purposes, it is important to know the subsequent fate of HSO_3 . Together with other workers, the present author has assumed that molecular oxygen will add to this intermediate to produce HSO_5 under atmospheric conditions. This is then assumed to oxidize NO to NO_2 or combine with NO_2 or even disproportionate with HO_2 . The HSO_4 species is then assumed to react similarly to the OH radical either by disproportionation or by hydrogen abstraction to give sulfuric acid (H_2SO_4). This follows the suggestion of Calvert and McQuigg (ref. 18). The specific reactions are shown in table IV.

$\text{HO}_2 + \text{SO}_2 \rightarrow \text{SO}_3 + \text{OH}$. - It is evident from this reaction that OH radicals are produced in the oxidation of SO_2 by HO_2 . The only reported determination of the rate constant for this reaction is that by Payne et al. (ref. 83). They obtained a rate constant for this reaction relative to the reaction, $\text{HO}_2 + \text{HO}_2 \rightarrow \text{H}_2\text{O}_2 + \text{O}_2$, and obtained a value of $5.2 \times 10^2 \text{ m}^3\text{-mol}^{-1}\text{-sec}^{-1}$. However, if the value for $k(\text{HO}_2 + \text{HO}_2)$ recommended by Hampson and Garvin (ref. 25) is used, a value of $8.9 \times 10^2 \text{ m}^3\text{-mol}^{-1}\text{-sec}^{-1}$ ($2.2 \text{ ppm}^{-1}\text{-min}^{-1}$) is obtained. This is the value which has been used in the calculations. However, since the formulation of this model, recent studies have shown that the rate constant for this reaction is a factor of 100 to 1000 less than that used here. Thus, HO_2 is likely to be relatively unimportant in gas-phase SO_2 photooxidation.

In photooxidation systems, such as those encountered in polluted urban atmospheres, the concentration of hydroperoxyl radicals is often a factor of 100 to 1000 greater than the OH steady-state concentration (Demerjian et al. (ref. 14)). Thus, although the rate constant for $\text{HO}_2 + \text{SO}_2$ is about a factor of 1000 less than that for $\text{OH} + \text{SO}_2$, the overall rates contributed by both intermediates are approximately equal.

It has been suggested that the product of this reaction could be one of addition, that is, HO_2SO_2 , but evidence for this is slim. Thus, Calvert et al. (ref. 77) estimate that this reaction would make only a very minor contribution to the overall measured rate for $\text{HO}_2 + \text{SO}_2$.

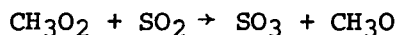
$\text{O} + \text{SO}_2 + \text{M} \rightarrow \text{SO}_3 + \text{M}$. - The reaction of ground-state oxygen atoms with SO_2 is generally regarded to be of little significance in the atmospheric oxidation of SO_2 . This is because most of the oxygen atoms produced from the photolysis of ambient NO_2 react with oxygen molecules to produce ozone.

The rate constant for this reaction has been measured by a number of people and these determinations have been summarized and/or evaluated by Schofield (ref. 94), Hampson and Garvin (ref. 25), and Westenberg and DeHaas (ref. 95). The recent experimental work of Westenberg and DeHaas indicates that the earlier measurements were a factor of 2 too high. The measurements of Westenberg and DeHaas give a value of $2.8 \times 10^4 \text{ m}^3\text{-mol}^{-1}\text{-sec}^{-1}$ for an atmosphere of nitrogen. Calvert et al. (ref. 77) using data for nitrogen and oxygen as third bodies, obtained a value of $3.4 \times 10^4 \text{ m}^3\text{-mol}^{-1}\text{-sec}^{-1}$ applicable to atmospheric conditions. The latter value has been used in the present calculations. But whichever value is used, the contribution of this reaction to atmospheric SO_2 oxidation is negligible, although in theory its importance in SO_2 oxidation in stack gas plumes may be more significant.

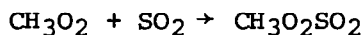
$\text{NO}_3 + \text{SO}_2 \rightarrow \text{SO}_3 + \text{NO}_2$. - The oxidation of SO_2 by NO_3 radicals, formed largely by the reaction of NO_2 with O_3 , has been invoked in some modeling studies, for example, Durbin et al. (ref. 79), as contributing in a major way to SO_2 oxidation; this would be particularly true in the later stages of photo-oxidation of hydrocarbon/ NO_x / SO_x mixtures where the NO_3 concentration increases significantly. However, studies by Daubendiek and Calvert (ref. 96) and Davis and Klauber (ref. 97) find that the rate constant for this reaction has a value of around $6.0 \times 10^{-4} \text{ m}^3\text{-mol}^{-1}\text{-sec}^{-1}$. Thus, this reaction is unlikely to be of any significance during the daytime oxidation of NO_2 , although it is possible that if the NO_3 concentration increases significantly during nighttime hours (as a result of the reaction of O_3 with NO_2), then this reaction could assume more importance in the oxidation of SO_2 .

Reactions of organic radicals with SO_2 . - The reactions which may be considered to be of importance for SO_2 oxidation by organic radicals include the alkyl peroxy radicals, acyl peroxy radicals, and the Criegee intermediates formed in the reaction of ozone with olefins.

Previous modeling studies (Calvert (ref. 80) and Calvert and McQuigg (ref. 18)) have shown that alkyl peroxy radicals could play a significant role in terms of SO_2 oxidation. However, it is only recently that an estimate has been obtained for the rate constant for the reaction,

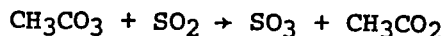


This has been obtained by Whitbeck et al. (ref. 98) who observed the kinetics of the decay of methyl peroxy radicals spectroscopically following its generation in the flash photolysis of a mixture of azomethane and oxygen and azomethane, oxygen, and SO_2 . A rate constant of $3.18 \times 10^3 \text{ m}^3\text{-mol}^{-1}\text{-sec}^{-1}$ was obtained for a combination of this reaction and the alternative pathway,

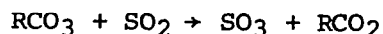


However, Calvert et al. (ref. 77) estimate that the latter pathway will make only a minor contribution to the overall rate constant. Thus, this rate constant is sufficiently large to make the reaction of alkyl peroxy radicals contribute about the same amount to SO_2 oxidation as that contributed by HO_2 .

The reaction of acyl peroxy radicals with SO₂ has not been studied directly and the contribution which it makes to SO₂ oxidation is subject to some uncertainty. However, it now appears that the reaction,



makes a negligible contribution to SO₂ oxidation under ambient conditions. This conclusion is based largely on the studies of Pate et al. (ref. 99) who showed that the introduction of SO₂ into a PAN mixture had no effect on the kinetics observed for PAN decomposition. In addition, it has been shown that SO₂ introduction into a synthetic photochemical smog mixture has a negligible effect upon the PAN yields. If the reaction,



was important, then it would compete with the reaction $\text{RCO}_3 + \text{NO}_2$ to produce PAN. Thus, a change in PAN concentration should be noted upon the introduction of SO₂ if indeed the reaction of RCO₃ with SO₂ were important. Since this is not the case, the results give the same conclusion as that obtained by Pate et al., and this reaction has not been included in the present simulations.

Reaction of SO₂ with the products of ozone-olefin reactions.- It is well known that the direct reaction of SO₂ with O₃ is slow. But Cox and Penkett (refs. 100 and 101) found that the addition of an olefin to a mixture of SO₂ and ozone led to a rapid increase in the SO₂ oxidation rate. This has been interpreted as being due to the oxidation of SO₂ by products of the ozone-olefin reactions, such as the Criegee intermediate (RCHO₂). However, later studies (Calvert and McQuigg (ref. 18) and Calvert et al. (ref. 77)) suggest that most of this increased oxidation is due to other products of the ozone-olefin reaction such as hydroxyl radicals and hydroperoxyl radicals. The contribution of the Criegee intermediate to SO₂ oxidation is likely to be slow but probably not negligible. Thus in the present model the same rate constant has been assigned to the oxidation of SO₂ by the Criegee intermediate as for the reaction of RO₂ with SO₂; that is, 7.8 ppm⁻¹-min⁻¹ (3.18 × 10³ m³-mol⁻¹-sec⁻¹).

Testing of HC/NO_x/SO_x System

Table IV shows the additional chemical reactions which have been utilized to predict the conversion of SO₂ to sulfates in the presence of hydrocarbon/NO_x mixtures. It was assumed that all the SO₃ formed would eventually produce sulfates and this supposition is apparently a reasonable one to make (Calvert et al. (ref. 77)). It can be seen that the species chosen for the oxidation process are O, OH, HO₂, RO₂ (including AO₂ formed from the addition of OH to an olefin in the presence of oxygen), and the Criegee intermediates. The basis for the choice of rate constants has been detailed in the previous section and those for AO₂ and the Criegee intermediate have been chosen to be the same as that for RO₂ + SO₂ in view of the lack of any experimental measurements.

The data base initially used to test the reaction mechanism was that obtained from the Battelle Columbus Laboratory chamber simulations and supplied by B. Dimitriades of the U.S. Environmental Protection Agency. These

results were obtained in a 17.8 m³ smog chamber. SO₂ concentrations were measured using a Beckman Instruments, Inc., model 906 analyzer, while SO₃ concentrations were obtained from aerosol size distributions measured with a Thermo-Systems, Inc., electrical aerosol analyzer, by assuming that equilibrium existed between sulfuric acid aerosol in the condensed and vapor phases. Independent chemical measurements of SO₃ apparently showed that this method was very accurate. The measured sulfate concentration-time profiles proved to be very difficult to reproduce with the model in spite of numerous changes in the mechanism and rate constants to try to obtain a good fit with the SO₃ experimental data. Unfortunately, there appears to be a paucity of reliable and comprehensive smog chamber data for systems including SO₂, and thus the task of obtaining a reliable chemical mechanism, tested in detail against an extensive smog chamber data base, can only be initiated at this time. Currently, studies are underway which will help to correct this situation (Miller (ref. 81)) and hopefully these studies will contain well-defined multihydrocarbon mixtures typical of ambient atmospheres, in addition to the single hydrocarbon systems often employed previously (e.g., Battelle).

The effect of adding SO₂ to the propylene/NO_x mixture in air was modeled by including the SO₂ reactions in the chemical mechanism and testing the predictions against Battelle data such as run 114; the result is shown in figure 7. This plot is typical of those obtained. The major conclusion from these calculations is that it proved impossible to get a reasonable fit simultaneously for NO, NO₂, and O₃ in addition to that for SO₂ and SO₃. Model refinement is being continued by using more comprehensive smog chamber data.

In parallel with this continued effort, the other approach used by Calvert and co-workers (Calvert et al. (refs. 18 and 77)), namely to use the most reliable rate constants and mechanisms to make sensitivity studies and predictions based on that mechanism, is being attempted. Thus, a number of calculations have been carried out following this approach and the results are given elsewhere (ref. 31).

CURRENT MEASUREMENT NEEDS IN AIR POLLUTION MODELING

The final section defines some of the areas in which measurement needs are urgently required to refine the chemical aspects of air quality modeling. These needs may be divided into three general areas, which are discussed separately:

- (1) Basic kinetic and mechanistic data
- (2) Role of heterogeneous reactions in simulated atmospheric experiments
- (3) Atmospheric data

Basic Kinetic and Mechanistic Data Needs

The following general areas should be pursued in order to improve the understanding of the chemical processes in mixtures of hydrocarbons, NO_x, and air in both the presence and the absence of sulfur oxides:

(1) Quantum yields for radical production during the photolysis of both aldehydes and ketones should be accurately determined in the presence of O_2 .

(2) Kinetic and mechanistic data should be acquired for the reactions of alkyl peroxy radicals with NO , NO_2 , and other reactive species present in photochemical smog mixtures.

(3) The major reaction paths for ozone-olefin reactions in the presence of O_2 and NO_x under atmospheric conditions still need much elucidation in spite of significant progress in recent studies (Niki et al. (ref. 51) and Herron and Huie (ref. 20)).

(4) The kinetic and mechanistic behavior of various types of peroxy nitrates and other nitrogen-containing compounds should be determined under atmospheric conditions and as a function of temperature.

(5) The kinetics of the reaction of SO_2 with intermediates such as $RCHO_2$ and the product formed by the addition of OH with olefins in the presence of O_2 are not known and require direct study. The reaction of HO_2 with SO_2 should be reexamined, preferably by using a direct technique such as laser magnetic resonance.

(6) Work should continue on nitrogen loss processes for mixtures of hydrocarbons and NO_x in air. The formation of, for example, nitrates, which involves chain-terminating reactions, plays an important role in computer model predictions.

(7) Product data for systems containing mixtures of hydrocarbons, nitrogen oxides, SO_2 , and air are practically nonexistent. A detailed search should be made for organic sulfur compounds and organic sulfur-nitrogen compounds.

(8) Smog chamber data for the hydrocarbon/ NO_x / SO_2 system are much less extensive than those available for the hydrocarbon/ NO_x system. Thus, more smog chamber studies are required which contain a variety of mixed hydrocarbons as well as single hydrocarbons in the presence of NO_x and SO_2 . Such studies should include a variation in the proportions of hydrocarbons, NO_x , and SO_2 in the mix and also within a particular mix. For example, the concentration of total hydrocarbons should be kept constant, but the percentage, for example, of olefins, paraffins, and aromatics should be varied within that mixture.

(9) While significant progress is being made (Niki et al. (ref. 62) and Hendry et al. (ref. 28)), substantial work is still required on the kinetic and mechanistic data for the oxidation of aromatic hydrocarbons under atmospheric conditions.

Fortunately, with the advent of Fourier transform infrared spectroscopy, which is capable of in situ studies, significant progress is being made in some of these areas by, for example, Calvert and co-workers at Ohio University, Hanst and co-workers at the U.S. Environmental Protection Agency in North Carolina, Niki and co-workers at the Ford Research Laboratories in Detroit, and Pitts, Winer, and co-workers at the University of California, Riverside.

Heterogeneous Interactions Occurring in Experiments Simulating

Atmospheric Conditions

Smog chamber studies continue to be the basis upon which to test chemical mechanisms proposed to describe the oxidation of hydrocarbons and SO₂ under atmospheric conditions. In recent years, it has been increasingly recognized that certain phenomena are occurring in these studies, which lead to increased reactivity compared with what one might expect on the basis of the best available kinetic and mechanistic data (Wu et al. (ref. 42)). This is accounted for in computer model development in various ways: by including an initial nitrous acid concentration which gives an immediate release of hydroxyl radicals under irradiation (e.g., Whitten and Hogo (ref. 33)), by the inclusion of a steady hydroxyl radical flux coming from the walls, or by assuming that impurities such as propylene bleed off the wall to give oxidized hydrocarbon radicals (e.g., Dodge (ref. 37)). Clearly, the role of wall reactions and of heterogeneous chemistry in general should be studied so that this major area of uncertainty can be clarified and a further degree of freedom eliminated from the model formulation.

Atmospheric Data Needs

With the increase in detailed data from smog chamber studies, it is now possible to formulate reasonably detailed models which include a variety of hydrocarbons of the same or different classes and to obtain reasonable agreement of the predicted results with smog chamber data for these mixtures. However, it is becoming apparent that, not surprisingly, the atmospheric air quality data measurements have not kept pace with the data obtained under simulated atmospheric conditions. Thus, it is of little use to develop a sophisticated chemical model to be applied to ambient conditions when, in fact, some of the key parameters needed as input for the detailed mechanism are not available. For example, in applying the model described earlier, in which the hydrocarbons are broken down into five classes, including two classes of aldehydes, the atmospheric data are not available for aldehydes and it is rarely that such data bases as LARPP are available which contain detailed hydrocarbon profiles over large periods of the day. In many cases, all one has available are total hydrocarbon (THC) measurements; not only is there the difficulty of obtaining the concentrations of nonmethane hydrocarbons, but there is the additional difficulty of partitioning the THC among the olefins, paraffins, and aromatics. Thus, there is a great need to measure detailed hydrocarbon concentrations in many locations for as long a period as possible to obtain the diurnal variation. This applies also to gas-phase nitric acid, pernitric acid, nitrous acid, aldehydes, ketones, acids, and any other nitrogen-containing organic compounds, such as organic nitrates, and any sulfur-containing compounds.

One of the major parameters affecting photochemical smog formation and its prediction is ultraviolet light available to photolyze such species as nitrogen dioxide, nitrous acid, aldehydes, and so forth. Thus, good measurements of this parameter are needed in many locations and the effect of cloud cover and aerosol loading on k_1 values (the NO₂ photodissociation rate) should be studied.

The role of gas-to-particle conversion processes is the subject of much investigation, but these processes are complex and require continuing study. For example, the roles of heterogeneous and homogeneous processes in the conversion of SO₂ to sulfates remain largely unknown.

In addition to these chemical requirements, other parameters such as meteorological data and emissions inventory data are critical inputs necessary to develop predictive and useful air quality models. Improved measurements in these areas are needed if the maximum benefit is to be obtained from improved chemical measurements. It is only when progress on all these fronts is maintained in a fully coordinated program that significant improvement will be achieved in the reliability and utility of air quality models. Clearly, the areas which have been listed form the framework of a very extensive and long-lasting research program.

It should be emphasized that model development is a continuing activity which must reflect the constant supply of new experimental data. Thus, certain parts of the chemical mechanism described in this paper (e.g., ozone-olefin reaction and aromatic hydrocarbon photooxidation) have been changed since the preparation of this paper. This work is being carried out under continued funding from the CRC.

REFERENCES

1. Haagen-Smit, A. J.: Chemistry and Physiology of Los Angeles Smog. *Ind. & Eng. Chem.*, vol. 44, no. 6, June 1952, pp. 1342-1346.
2. Middleton, John T.; Kendrick, J. B., Jr.; and Schwalm, H. W.: Smog in the South Coastal Area. *California Agric.*, Nov. 1950, pp. 7-10.
3. Haagen-Smit, A. J.; and Fox, M. M.: Ozone Formation in Photochemical Oxidation of Organic Substances. *Ind. & Eng. Chem.*, vol. 48, no. 9, Sept. 1956, pp. 1484-1487.
4. Stephens, Edgar R.; Hanst, Philip L.; Doerr, Robert C.; and Scott, William E.: Reactions of Nitrogen Dioxide and Organic Compounds in Air. *Ind. & Eng. Chem.*, vol. 48, no. 9, Sept. 1956, pp. 1498-1504.
5. Stephens, Edgar R.: The Formation, Reactions, and Properties of Peroxyacyl Nitrates (PANs) in Photochemical Air Pollution. *Advances in Environmental Science and Technology*, Volume 1, James N. Pitts and Robert L. Metcalf, eds., John Wiley & Sons, c.1969, pp. 119-146.
6. Chass, Robert L.; and Feldman, Edward S.: Tears for John Doe. *Southern California Law Rev.*, vol. 27, 1954, pp. 349-372.
7. Leighton, Philip A.: *Photochemistry of Air Pollution*. Academic Press, Inc., 1961.
8. Jones, I. T. N.; and Bayes, Kyle D.: Photolysis of Nitrogen Dioxide. *J. Chem. Phys.*, vol. 59, no. 9, Nov. 1, 1973, pp. 4836-4844.
9. Darley, Ellis F.; Stephens, Edgar R.; Middleton, John T.; and Hanst, Philip L.: Oxidant Plant Damage From Ozone-Olefin Reactions. *Int. J. Air Pollut.*, vol. 1, no. 3, 1959, pp. 155-162.
10. Niki, H.; Daby, E. E.; and Weinstock, B.: Mechanisms of Smog Reactions. *Adv. Chem. Ser. No. 113*, 1972, pp. 16-57.
11. Greiner, N. R.: Hydroxyl-Radical Kinetics by Kinetic Spectroscopy. II. Reactions With C_2H_6 , C_3H_8 , and Iso- C_4H_{10} at $300^\circ K$. *J. Chem. Phys.*, vol. 46, no. 9, May 1, 1967, pp. 3389-3392.
12. Lewis, Bernard; and Von Elbe, Guenther: *Combustion, Flames and Explosions of Gases*. Academic Press, Inc., 1951.
13. Altshuller, Aubrey P.; and Bufalini, Joseph J.: Photochemical Aspects of Air Pollution: A Review. *Environmental Science & Technology*, Inc., vol. 5, no. 1, Jan. 1971, pp. 39-64.
14. Demerjian, Kenneth L.; Kerr, J. Alistair; and Calvert, Jack G.: The Mechanism of Photochemical Smog Formation. *Advances in Environmental Science and Technology*, Volume 4, James N. Pitts, Jr., and Robert L. Metcalf, eds., John Wiley & Sons, c.1974, pp. 1-262.

15. Pitts, J. N., Jr.; Lloyd, A. C.; and Sprung, J. L.: Ecology, Energy and Economics. Chem. Britain, vol. 11, no. 7, July 1975, pp. 247-256.
16. Finlayson-Pitts, Barbara J.; and Pitts, James N., Jr.: The Chemical Basis of Air Quality: Kinetics and Mechanisms of Photochemical Air Pollution and Application to Control Strategies. Advances in Environmental Science and Technology, Volume 7, James N. Pitts, Jr., and Robert L. Metcalf, eds., John Wiley & Sons, c.1977, pp. 75-162.
17. Pitts, J. N., Jr.; Winer, A. M.; Darnall, K. R.; Lloyd, A. C.; and Doyle, G. J.: Hydrocarbon Reactivity and the Role of Hydrocarbons, Oxides of Nitrogen, and Aged Smog in the Production of Photochemical Oxidants. International Conference on Photochemical Oxidant Pollution and Its Control - Proceedings: Volume II, EPA-600/3-77-001b, U.S. Environ. Prot. Agency, Jan. 1977, pp. 687-704. (Available from NTIS as PB 264 233.)
18. Calvert, Jack G.; and McQuigg, Robert D.: The Computer Simulation of the Rates and Mechanisms of Photochemical Smog Formation. Chemical Kinetics Data for the Upper and Lower Atmosphere, Int. J. Chem. Kinet., Symp. No. 1, 1975, pp. 113-154.
19. Finlayson, Barbara J.; and Pitts, James N., Jr.: Photochemistry of the Polluted Troposphere. Science, vol. 192, no. 4235, Apr. 9, 1976, pp. 111-119.
20. Herron, John T.; and Huie, Robert E.: Stopped-Flow Studies of the Mechanisms of Ozone-Alkene Reactions in the Gas Phase. Ethylene. J. American Chem. Soc., vol. 99, no. 16, Aug. 3, 1977, pp. 5430-5435.
21. Calvert, J. G.; and Pitts, J. N.: Photochemistry. John Wiley & Sons, Inc., 1966.
22. Weaver, James; Meagher, James; and Hecklen, Julian: Photo-Oxidation of CH_3CHO Vapor at 3130 Å. J. Photochem., vol. 6, no. 2, Dec. 1976, pp. 111-126.
23. Dodge, M. C.; and Hecht, T. A.: Rate Constant Measurements Needed To Improve a General Kinetic Mechanism for Photochemical Smog. Chemical Kinetics Data for the Upper and Lower Atmosphere, Int. J. Chem. Kinet., Symp. No. 1, 1975, pp. 155-163.
24. Simonaitis, R.; and Hecklen, Julian: Reaction of HO_2 With NO and NO_2 . J. Phys. Chem., vol. 78, no. 7, Mar. 28, 1974, pp. 653-657.
25. Hampson, Robert F., Jr.; and Garvin, David, eds.: Chemical Kinetic and Photochemical Data for Modelling Atmospheric Chemistry. NBS Tech. Note 866, U.S. Dep. Commer., June 1975.
26. Schuck, E. A.; Pitts, J. N., Jr.; and Wan, J. K. S.: Relationships Between Certain Meteorological Factors and Photochemical Smog. Air & Water Pollut., vol. 10, no. 10, Oct. 1966, pp. 689-711.

27. Stephens, Edgar R.: Summary Report: Hydrocarbons in Polluted Air. CRC-APRAC-CAPA-5-68-1, Coordinating Research Council, Inc., June 1973. (Available from NTIS as PB 230 993.)
28. Hendry, Dale G.; and Kenley, Richard A.: Generation of Peroxy Radicals From Peroxy Nitrates (RO_2NO_2). Decomposition of Peroxyacyl Nitrates. J. American Chem. Soc., vol. 99, no. 9, Apr. 27, 1977, pp. 3198-3199.
29. Graham, Richard A.; Winer, Arthur M.; and Pitts, James N., Jr.: Temperature Dependence of the Unimolecular Decomposition of Pernitric Acid and Its Atmospheric Implications. Chem. Phys. Lett., vol. 51, no. 2, Oct. 15, 1977, pp. 215-220.
30. Graedel, T. E.; Farrow, L. A.; and Weber, T. A.: Kinetic Studies of the Photochemistry of the Urban Troposphere. Atmos. Environ., vol. 10, no. 12, 1976, pp. 1095-1116.
31. Development of an Atmospheric Model for Sulfate Formation. Document No. P-1534, Environmental Research & Technology, Inc., Sept. 1977.
32. Hecht, Thomas A.; Seinfeld, John H.; and Dodge, Marcia C.: Further Development of Generalized Kinetic Mechanism for Photochemical Smog. Environ. Sci. & Technol., vol. 8, no. 4, Apr. 1974, pp. 327-339.
33. Whitten, G. Z.; and Hogo, H.: Mathematical Modeling of Simulated Photochemical Smog - Final Report. EPA-600/3-77-011, U.S. Environ. Prot. Agency, June 1975/June 1976. (Available from NTIS as PB 263 348.)
34. Graedel, T. E.: Sulfur Dioxide, Sulfate Aerosol, and Urban Ozone. Geophys. Res. Lett., vol. 3, no. 3, Mar. 1976, pp. 181-184.
35. Graedel, T. E.; Farrow, L. A.; and Weber, T. A.: Kinetic Studies of the Photochemistry of the Urban Troposphere. Atmos. Environ., vol. 10, no. 12, 1976, pp. 1095-1116.
36. Wayne, Lowell; Danchick, Roy; Weisburd, Mel; Kokin, Allan; and Stein, Arnold: Modeling Photochemical Smog on a Computer for Decision-Making. J. Air Pollut. Control Assoc., vol. 21, no. 6, June 1971, pp. 334-340.
37. Dodge, M. C.: Combined Use of Modeling Techniques and Smog Chamber Data To Derive Ozone-Precursor Relationships. International Conference on Photochemical Oxidant Pollution and Its Control - Proceedings: Volume II, EPA-600/3-77-001b, U.S. Environ. Prot. Agency, Jan. 1977, pp. 881-889. (Available from NTIS as PB 264 233.)
38. Chan, Walter H.; Nordstrom, Robert J.; Calvert, Jack G.; and Shaw, John H.: Kinetic Study of HONO Formation and Decay Reactions in Gaseous Mixtures of HONO, NO, NO_2 , H_2O , and N_2 . Environ. Sci. & Technol., vol. 10, no. 7, July 1976, pp. 674-682.

39. Chan, Walter H.; Nordstrom, Robert J.; Calvert, Jack G.; and Shaw, John H.: An IRFTS Spectroscopic Study of the Kinetics and the Mechanism of the Reactions in the Gaseous System, HONO, NO, NO₂, H₂O. Chem. Phys. Lett., vol. 37, no. 3, Feb. 1, 1976, pp. 441-446.
40. Cox, R. A.: The Photolysis of Gaseous Nitrous Acid - A Technique for Obtaining Kinetic Data on Atmospheric Photooxidation Reactions. Chemical Kinetics Data for the Upper and Lower Atmosphere, Int. J. Chem. Kinet., Symp. No. 1, 1975, pp. 379-398.
41. Cox, R. A.; and Derwent, R. G.: The Ultraviolet Absorption Spectrum of Gaseous Nitrous Acid. J. Photochem., vol. 6, no. 1, 1977, p. 23.
42. Wu, C. H.; Japar, S. M.; and Niki, H.: Relative Reactivities of HO-Hydrocarbon Reactions From Smog Reactor Studies. J. Environ. Sci. & Health - Environ. Sci. & Eng., vol. A11, no. 2, 1976, pp. 191-200.
43. Bufalini, J. J.; Kopczynski, S. L.; and Dodge, M. C.: Contaminated Smog Chambers in Air Pollution Research. Environ. Lett., vol. 3, no. 2, 1972, pp. 101-109.
44. Jeffries, H.; Fox, D.; and Kamens, R.: Outdoor Smog Chamber Studies. Effect of Hydrocarbon Reduction on Nitrogen Dioxide. EPA-650/3-75011, U.S. Environ. Prot. Agency, June 1975. (Available from NTIS as PB 245 829.)
45. Howard, Carleton J.: Kinetics of the Reaction of HO₂ With NO₂. J. Chem. Phys., vol. 67, no. 11, Dec. 1, 1977, pp. 5258-5263.
46. Niki, H.; Maker, P.; Savage, C.; and Breitenbach, L.: IR Fourier-Transform Spectroscopic Studies of Atmospheric Reactions. The 12th Informal Conference on Photochemistry - Extended Abstracts, Natl. Bur. Stand., U.S. Dep. Commer., June-July 1976, pp. N2-1 - N2-4.
47. Levine, Stuart Z.; Uselman, William M.; Chan, Walter H.; Calvert, Jack G.; and Shaw, John H.: The Kinetics and Mechanism of the HO₂-NO₂ Reactions; the Significance of Peroxynitric Acid Formation in Photochemical Smog. Chem. Phys. Lett., vol. 48, no. 3, June 15, 1977, pp. 528-535.
48. Simonaitis, R.; and Heicklen, Julian: Reactions of HO₂ With NO and NO₂ and of OH With NO. J. Phys. Chem., vol. 80, no. 1, Jan. 1, 1976, pp. 1-7.
49. Cox, R. A.; and Derwent, R. G.: Kinetics of the Reaction of Hydroperoxy With Nitric Oxide and Nitrogen Dioxide. J. Photochem., vol. 4, nos. 1-2, 1975, pp. 139-153.
50. Niki, H.; Maker, P. D.; Savage, C. M.; and Breitenbach, L. P.: Fourier Transform IR Spectroscopic Observation of Pernitric Acid Formed Via HOO + NO₂ → HOONO₂. Chem. Phys. Lett., vol. 45, no. 3, Feb. 1, 1977, pp. 564-566.

51. Niki, H.; Maker, P. D.; Savage, C. M.; and Breitenbach, L. P.: Fourier Transform IR Spectroscopic Observation of Propylene Ozonide in the Gas Phase Reaction of Ozone—Cis-2-Butene—Formaldehyde. *Chem. Phys. Lett.*, vol. 46, no. 2, Mar. 1, 1977, pp. 327-330.
52. Walter, Theodore A.; Bufalini, Joseph J.; and Gay, Bruce W., Jr.: Mechanism for Olefin - Ozone Reactions. *Environ. Sci. & Technol.*, vol. 11, no. 4, Apr. 1977, pp. 382-386.
53. Hanst, Philip L.; Stephens, Edgar R.; Scott, William E.; and Doerr, Robert C.: Atmospheric O₃-Olefin Reactions. *American Chem. Soc., Div. Pet. Chem., Preprints*, vol. 4, no. 4, 1959, pp. A7-A16.
54. Carter, William P. L.; Darnall, Karen R.; Lloyd, Alan C.; Winer, Arthur M.; and Pitts, James N., Jr.: Evidence for Alkoxy Radical Isomerization in Photooxidations of C₄-C₆ Alkanes Under Simulated Atmospheric Conditions. *Chem. Phys. Lett.*, vol. 42, no. 1, Aug. 15, 1976, pp. 22-27.
55. Darnall, Karen R.; Carter, William P. L.; Winer, Arthur M.; Lloyd, Alan C.; and Pitts, James N., Jr.: Importance of RO₂ + NO in Alkyl Nitrate Formation From C₄-C₆ Alkane Photooxidations Under Simulated Atmospheric Conditions. *J. Phys. Chem.*, vol. 80, no. 17, Aug. 12, 1976, pp. 1948-1950.
56. Davis, D. D.; Bollinger, W.; and Fischer, S.: A Kinetics Study of the Reaction of the OH Free Radical With Aromatic Compounds. I. Absolute Rate Constants for Reaction With Benzene and Toluene at 300° K. *J. Phys. Chem.*, vol. 79, no. 3, Jan. 1975, pp. 293-294.
57. Hansen, D. A.; Atkinson, R.; and Pitts, J. N., Jr.: Rate Constants for the Reaction of OH Radicals With a Series of Aromatic Hydrocarbons. *J. Phys. Chem.*, vol. 79, no. 17, Aug. 14, 1975, pp. 1763-1766.
58. Doyle, George J.; Lloyd, Alan C.; Darnall, K. R.; Winer, Arthur M.; and Pitts, James N., Jr.: Gas Phase Kinetic Study of Relative Rates of Reaction of Selected Aromatic Compounds With Hydroxyl Radicals in an Environmental Chamber. *Environ. Sci. & Technol.*, vol. 9, no. 3, Mar. 1975, pp. 237-241.
59. Lloyd, Alan C.; Darnall, Karen R.; Winer, Arthur M.; and Pitts, James N., Jr.: Relative Rate Constants for Reaction of the Hydroxyl Radical With a Series of Alkanes, Alkenes, and Aromatic Hydrocarbons. *J. Phys. Chem.*, vol. 80, no. 8, Apr. 8, 1976, pp. 789-794.
60. Perry, R. A.; Atkinson, R.; and Pitts, J. N., Jr.: Kinetics and Mechanism of the Gas Phase Reaction of OH Radicals With Aromatic Hydrocarbons Over the Temperature Range 296-473 K. *J. Phys. Chem.*, vol. 81, no. 4, Feb. 24, 1977, pp. 296-304.
61. Pitts, James N., Jr.: Measurements, Mechanisms, and Models: Application to Air Pollution Control. *International Conference on Environmental Sensing and Assessment - Volume 2*, Inst. Electr. & Electron. Eng., Inc., c.1976, paper 24-1.

62. Niki, H.; Maker, P. D.; Savage, C. M.; and Breitenbach, L. P.: Relative Rate Constants for the Reaction of Hydroxyl Radical With Aldehydes. *J. Phys. Chem.*, vol. 82, no. 2, Jan. 26, 1978, pp. 132-134.
63. Pitts, James N., Jr.; Winer, Arthur M.; Darnall, Karen R.; Doyle, George J.; and McAfee, John M.: Chemical Consequences of Air Quality Standards and of Control Implementation Programs: Roles of Hydrocarbons, Oxides of Nitrogen and Aged Smog in the Production of Photochemical Oxidant. ARB Contract No. 4-214, Univ. of California, May 1976.
64. Dodge, Marcia C.; and Whitten, Gary Z.: Aldehydes and Photochemical Smog. Paper presented before the Division of Environmental Chemistry, American Chemical Society (New York, New York), Apr. 1976.
65. Lee, Edward K. C.; Lewis, Roger S.; and Miller, Richard G.: Photochemistry of Formaldehydes: Past and Present. The 12th Informal Conference on Photochemistry - Extended Abstracts, Natl. Bur. Stand., U.S. Dep. Commer., June-July 1976, p. C2-1.
66. Lloyd, Alan C.: Tropospheric Chemistry of Aldehydes. Environmental Research & Technology, Inc., paper presented at Chemical Kinetic Data Needs for Modeling the Lower Troposphere (Reston, Virginia), May 1978.
67. Pitts, James N., Jr.; Winer, Arthur M.; Darnall, Karen R.; Doyle, George J.; and McAfee, John M.: Chemical Consequences of Air Quality Standards and of Control Implementation Programs: Roles of Hydrocarbons, Oxides of Nitrogen and Aged Smog in the Production of Photochemical Oxidant. ARB-R-3-017-75-52, Air Resources Board, State of California, July 1975. (Available from NTIS as PB 269 376.)
68. Pitts, James N., Jr.; Darnall, Karen R.; Winer, Arthur M.; and McAfee, John M.: Mechanisms of Photochemical Reactions in Urban Air - Volume II. Chamber Studies. EPA-600/3-77-014b, U.S. Environ. Prot. Agency, Feb. 1977. (Available from NTIS as PB 265 593.)
69. Beauchene, J. H.; Bekowies, P. J.; McAfee, J. M.; Winer, A. M.; Zafonte, L.; and Pitts, J. N., Jr.: A Novel 20 KW Solar Simulator Designed for Air Pollution Research. Space Simulation, NASA SP-336, 1973, pp. 811-825.
70. Gear, C. W.: Algorithm 407 - DIFSUB for Solution of Ordinary Differential Equations. *Commun. ACM*, vol. 14, no. 3, Mar. 1971, pp. 185-190.
71. Air Quality Criteria for Sulfur Oxides. NAPCA Publ. No. AP-50, U.S. Dep. Health, Educ., & Welfare, Jan. 1969. (Available from NTIS as PB 190 252.)
72. Health Consequences of Sulfur Oxides: A Report from CHESS, 1970-1971. EPA-650/1-74-004, U.S. Environ. Prot. Agency, May 1974.
73. California Air Resources Board Bulletin. Vol. 7, no. 3, Mar. 1976.

74. Research and Development Related to Sulphates in the Atmosphere. Hearings Before the Subcommittee on the Environment and the Atmosphere of the Committee on Science and Technology, U.S. House of Representatives, Ninety-Fourth Congress, First Session, No. 39, July 8-14, 1975.
75. Hidy, G. M.; and Burton, C. S.: Atmospheric Aerosol Formation by Chemical Reactions. Chemical Kinetics Data for the Upper and Lower Atmosphere, Int. J. Chem. Kinet., Symp. No. 1, 1975, pp. 509-541.
76. Hidy, G. M.; Rice, Harbert; and Nochumson, David: Perspective on the Current Airborne Sulfate Problem - A survey of Current Knowledge. Document No. P-5057, Environmental Research & Technology, Inc., Oct. 1977.
77. Calvert, Jack G.; Su, Fu; Bottenheim, Jan W.; and Strausz, Otto P.: Mechanism of the Homogeneous Oxidation of Sulfur Dioxide in the Troposphere. Atmos. Environ., vol. 12, no. 1-3, 1978, pp. 197-226.
78. Hitchcock, Dian R.: Atmospheric Sulfates From Biological Sources. J. Air Pollut. Control Assoc., vol. 26, no. 3, Mar. 1976, pp. 210-215.
79. Durbin, P. A.; Hecht, T. A.; and Whitten, G. Z.: Mathematical Modeling of Simulated Photochemical Smog - Final Report, June 1974-June 1975. EPA-650/4-75-026, U.S. Environ. Prot. Agency, June 1975. (Available from NTIS as PB 246 122.)
80. Calvert, Jack G.: Modes of Formation of the Salts of Sulfur and Nitrogen in an NO_x - SO_2 -Hydrocarbon Polluted Atmosphere. Conference on Health Effects of Atmospheric Salts and Gases of Sulfur and Nitrogen in Association With Photochemical Oxidant. Volume II - Reference Documents, T. Timothy Crocker, ed., ARB Contract No. 3-197, Univ. of California, Jan. 1974, pp. VIII-1 - VIII-16. (Available from NTIS as PB 251 233.)
81. Miller, D. F.: Precursor Effects on SO_2 Oxidation. Atmos. Environ., vol. 12, no. 1-3, 1978, pp. 273-280.
82. Sander, Stanley P.; and Seinfeld, John H.: Chemical Kinetics of Homogeneous Atmospheric Oxidation of Sulfur Dioxide. Environ. Sci. & Technol., vol. 10, no. 12, Nov. 1976, pp. 1114-1123.
83. Payne, W. A.; Stief, L. J.; and Davis, D. D.: A Kinetics Study of the Reaction of HO_2 With SO_2 and NO . J. American Chem. Soc., vol. 95, no. 23, Nov. 14, 1973, pp. 7614-7619.
84. Cox, R. A.: Photolysis of Nitrous Acid in the Presence of Carbon Monoxide and Sulfur Dioxide. J. Photochem., vol. 3, no. 4, 1974, pp. 291-304.
85. Wood, W. P.; Castleman, A. W., Jr.; and Tang, I. N.: Mechanisms of Aerosol Formation From SO_2 . J. Aerosol. Sci., vol. 6, no. 5, Sept. 1975, pp. 367-374.

86. Castleman, A. W., Jr.; Davis, Richard E.; Munkelwitz, H. R.; Tang, I. N.; and Wood, William P.: Kinetics of Association Reactions Pertaining to H₂SO₄ Aerosol Formation. Chemical Kinetics of Association Reactions Pertaining to H₂SO₄ Aerosol Formation. Chemical Kinetics Data for the Upper and Lower Atmosphere, Int. J. Chem. Kinet., Symp. No. 1, 1975, pp. 629-640.
87. Castleman, A. W., Jr.; and Tang, I. N.: Kinetics of the Association Reaction of Sulfur Dioxide With the Hydroxyl Radical. J. Photochem., vol. 6, no. 5, 1977, pp. 349-354.
88. Sie, B. K. T.; Simonaitis, R.; and Heicklen, J.: The Reaction of OH With CO. Int. J. Chem. Kinet., vol. 8, no. 1, 1976, pp. 85-98.
89. Cox, Richard A.; Derwent, Richard G.; and Holt, Pauline M.: Relative Rate Constants for the Reactions of OH Radicals With H₂, CH₄, CO, NO, and HONO at Atmospheric Pressure and 296 K. J. Chem. Soc., Faraday Trans. I, vol. 72, pt. 9, 1976, pp. 2031-2043.
90. Chan, Walter H.; Uselman, William M.; Calvert, Jack G.; and Shaw, John H.: The Pressure Dependence of the Rate Constant for the Reaction: HO + CO → H + CO₂. Chem. Phys. Lett., vol. 45, no. 2, Jan. 15, 1977, pp. 240-243.
91. Harris, G. W.; and Wayne, R. P.: Reaction of Hydroxyl Radicals With NO, NO₂, and SO₂. J. Chem. Soc., Faraday Trans. I, vol. 71, pt. 3, 1975, pp. 610-617.
92. Atkinson, R.; Perry, R. A.; and Pitts, J. N., Jr.: Rate Constants for the Reactions of the OH Radical With NO₂ (M = Ar and N₂) and SO₂ (M = Ar). J. Chem. Phys., vol. 65, no. 1, July 1, 1976, pp. 306-310.
93. Gordon, Sheffield; and Mulac, William A.: Reaction of the OH(X²II) Radical Produced by the Pulse Radiolysis of Water Vapor. Chemical Kinetics Data for the Upper and Lower Atmosphere, Int. J. Chem. Kinet., Symp. No. 1, 1975, pp. 289-299.
94. Schofield, Keith: Evaluated Chemical Kinetic Rate Constants for Various Gas Phase Reactions. J. Phys. & Chem. Ref. Data, vol. 2, no. 1, 1973, pp. 25-84.
95. Westenberg, A. A.; and DeHaas, N.: Rate of the Reaction O + SO₂ + M → SO₃ + M. J. Chem. Phys., vol. 63, no. 12, Dec. 15, 1975, pp. 5411-5415.
96. Daubendiek, Richard L.; and Calvert, Jack G.: A Study of the N₂O₅-SO₂-O₃ Reaction System. Environ. Lett., vol. 8, no. 2, 1975, pp. 103-116.
97. Davis, D. D.; and Klauber, Gary: Atmospheric Gas Phase Oxidation Mechanisms for the Molecule SO₂. Chemical Kinetics Data for the Upper and Lower Atmosphere, Int. J. Chem. Kinet., Symp. No. 1, 1975, pp. 543-556.

98. Whitbeck, Michael R.; Bottenheim, Jan W.; Levine, Stuart Z.; and Calvert, Jack G.: A Kinetic Study of CH_3O_2 and $(\text{CH}_3)_3\text{CO}_2$ Radical Reactions by Kinetic Flash Spectroscopy. The 12th Informal Conference on Photochemistry - Extended Abstracts, Natl. Bur. Stand., U.S. Dep. Commer., June-July 1976, p. K1-1.
99. Pate, C. T.; Atkinson, R.; and Pitts, J. N., Jr.: Rate Constants for the Gas Phase Reaction of Peroxyacetyl Nitrate With Selected Atmospheric Constituents. J. Environ. Sci. & Health, Part A, vol. A11, no. 1, 1976, pp. 19-31.
100. Cox, R. A.; and Penkett, S. A.: Photo-Oxidation of Atmospheric SO_2 . Nature, vol. 229, no. 5285, Feb. 12, 1971, pp. 486-488.
101. Cox, R. A.; and Penkett, S. A.: Oxidation of Atmospheric SO_2 by Products of the Ozone-Olefin Reaction. Nature, vol. 230, Review Suppl., Apr. 2, 1971, pp. 321-322.

TABLE I.- GENERALIZED REACTION MECHANISM

In addition to the normal chemical symbols used for elemental species, the designations given at the end of the table are used

Reaction	Rate constants	
	ppm ⁻¹ -min ⁻¹ (a)	m ³ -mol ⁻¹ -sec ⁻¹ (a)
(1) NO ₂ + hν → O + NO	3.20 × 10 ⁻¹	5.33 × 10 ⁻³
(2) O + O ₂ ^M → O ₃	4.12 × 10 ⁶	1.68 × 10 ⁹
(3) O ₃ + NO → NO ₂ + O ₂	2.50 × 10	1.02 × 10 ⁴
(4) NO + NO ₂ + H ₂ O → 2HONO	2.20 × 10 ⁻⁹	8.97 × 10 ⁻⁷
(5) HONO + HONO → NO + NO ₂ + H ₂ O	1.40 × 10 ⁻³	5.71 × 10 ⁻¹
(6) HONO + hν → OH + NO	8.96 × 10 ⁻²	1.49 × 10 ⁻³
(7) OH + NO ^M → HONO	1.50 × 10 ⁴	6.11 × 10 ⁶
(8) OH + NO ₂ ^M → HNO ₃	1.50 × 10 ⁴	6.11 × 10 ⁶
(9) OH + CO ^{O₂} → CO ₂ + HO ₂	4.40 × 10 ²	1.80 × 10 ⁵
(10) HO ₂ + NO → NO ₂ + OH	1.20 × 10 ⁴	4.80 × 10 ⁶
(11) HO ₂ + NO ₂ → 0.1 HONO + 0.9 HO ₂ NO ₂ + 0.1 O ₂	1.20 × 10 ³	4.90 × 10 ⁵
(12) HO ₂ NO ₂ → HO ₂ + NO ₂	4.00	6.67 × 10 ⁻²
(13) HO ₂ + HO ₂ → H ₂ O ₂ + O ₂	8.40 × 10 ³	3.43 × 10 ⁶
(14) NO ₂ + O ₃ → NO ₃ + O ₂	5.00 × 10 ⁻²	2.04 × 10
(15) NO ₃ + NO → 2NO ₂	1.30 × 10 ⁴	5.30 × 10 ⁶
(16) NO ₃ + NO ₂ → N ₂ O ₅	5.60 × 10 ³	2.28 × 10 ⁶
(17) N ₂ O ₅ + H ₂ O → 2HNO ₃	5.00 × 10 ⁻⁶	2.04 × 10 ⁻³
(18) N ₂ O ₅ → NO ₃ + NO ₂	2.40 × 10	9.80 × 10 ³
(19) OH + OLEF ^{O₂} → AO ₂	4.00 × 10 ⁴	1.63 × 10 ⁷
(20) AO ₂ + NO → NO ₂ + AO	2.90 × 10 ⁴	1.18 × 10 ⁷
(21) AO + O ₂ → RCHO + HCHO + HO ₂	4.10 × 10 ⁵	6.83 × 10 ³
(22) O ₃ + OLEF ^{O₂} → 0.5 HCHO + 0.5 RCHO + 0.25 HO ₂ + 0.25 RCO ₃ + 0.5 OH + 0.5 RCHO ₂	2.00 × 10 ⁻¹	8.15 × 10
(23) RCHO ₂ + NO ₂ → NO ₃ + 0.5 HCHO + 0.5 RCHO	2.30 × 10 ⁴	9.38 × 10 ⁶
(24) RCHO ₂ + NO → NO ₂ + 0.5 HCHO + 0.5 RCHO	2.90 × 10 ⁴	1.18 × 10 ⁷
(25) O + OLEF ^{O₂} → 0.3 EPOX + 0.3 RCHO + 0.4 HO ₂ + 0.4 RO ₂	2.30 × 10 ⁴	9.38 × 10 ⁶
(26) OH + PA ^{O₂} → H ₂ O + PAO ₂	3.80 × 10 ³	1.55 × 10 ⁶
(27) PAO ₂ + NO → NO ₂ + 0.85 PAO + 0.15 RO ₂	2.90 × 10 ⁴	1.18 × 10 ⁷
(28) PAO ₂ + NO → NTRA	2.60 × 10 ³	1.06 × 10 ⁶

^aThe units given are for second-order rate constants; the units for first-order rate constants are min⁻¹ and sec⁻¹.

TABLE I.- Concluded

Reaction	Rate constants	
	ppm ⁻¹ -min ⁻¹ (a)	m ³ -mol ⁻¹ -sec ⁻¹ (a)
(29) PAO → RO ₂ + 0.5 HCHO + 0.5 RCHO	1.40 × 10 ⁵	2.33 × 10 ³
(30) PAO + O ₂ → 0.5 KET + 0.5 RCHO + HO ₂	6.70 × 10 ⁴	1.12 × 10 ³
(31) PAO + NO ₂ → 0.85 NTRA + 0.15 RCHO + 0.15 HONO	2.30 × 10 ⁴	9.38 × 10 ⁶
(32) RO ₂ + NO → NO ₂ + PAO	2.90 × 10 ⁴	1.18 × 10 ⁷
(33) OH + RCHO + O ₂ → RCO ₃ + H ₂ O	2.20 × 10 ⁴	8.97 × 10 ⁶
(34) RCHO + hν + O ₂ → RO ₂ + HO ₂ + CO	1.40 × 10 ⁻⁴	2.33 × 10 ⁻⁶
(35) RCO ₃ + NO → CO ₂ + NO ₂ + RO ₂	2.90 × 10 ⁴	1.18 × 10 ⁷
(36) RCO ₃ + NO ₂ → PAN	1.70 × 10 ⁴	6.93 × 10 ⁶
(37) PAN → RCO ₃ + NO ₂	6.60 × 10 ⁻²	1.10 × 10 ⁻³
(38) HCHO + hν + O ₂ → 2 HO ₂ + CO	2.30 × 10 ⁻⁴	3.83 × 10 ⁻⁶
(39) HCHO + OH + O ₂ → H ₂ O + HO ₂ + CO	2.10 × 10 ⁴	8.56 × 10 ⁶
(40) RO ₂ + HO ₂ → RO ₂ H + O ₂	4.20 × 10 ³	1.71 × 10 ⁶
(41) O ₃ + WALL → LOSS OF O ₃	3.12 × 10 ⁻⁴	5.2 × 10 ⁻⁶
(42) AR + OH + O ₂ → AROH + HO ₂	2.24 × 10 ⁴	9.13 × 10 ⁶
(43) AROH + OH → ARCO	5.02 × 10 ⁴	2.05 × 10 ⁷
(44) ARCO + NO → NO ₂ + RCHO	2.90 × 10 ⁴	1.18 × 10 ⁷
(45) AR + OH → H ₂ O + ARO	5.60 × 10 ³	2.28 × 10 ⁶
(46) ARO + NO + O ₂ → NO ₂ + HO ₂ + AR'CHO	2.90 × 10 ⁴	1.18 × 10 ⁷

^aThe units given are for second-order rate constants; the units for first-order rate constants are min⁻¹ and sec⁻¹.

AR aromatic hydrocarbons
 AROH cresols
 ARCO product of addition of OH and O₂ to a cresol
 ARO product of H abstraction from side chain alkyl group on benzene ring followed by addition of O₂ to radical formed
 AR'CHO aromatic aldehyde
 AO₂ product of OH addition to olefin in the presence of O₂
 AO alkoxy radical equivalent of AO₂
 EPOX epoxide formed from O atom addition to olefin
 OLEF alkenes
 PA alkanes
 PAO₂ alkyl peroxy radical from the O₂ addition to the radical formed by H abstraction from a paraffinic hydrocarbon
 PAO alkoxy radical formed from PA
 NITRA organic nitrate
 KET ketones

TABLE II.- DETAILED COMPOSITION OF HYDROCARBON SURROGATE MIXTURE

[Modified from Pitts et al. (ref. 67)]

Compound class	Compound	Compound concentration, ppb of carbon
Alkanes	Ethane	160
	Propane	40
	n-butane	785
	2,3-dimethyl butane	615
Olefins	Ethene	84
	Propene	35
	Cis-2-butene	60
	2-methyl-2-butene	70
Aromatics	Toluene	115
	m-xylene	325
Aldehydes	Formaldehyde	54
	Acetaldehyde	5
Miscellaneous	Acetylene	101
	Acetone	6
	Methane	2800
	Carbon monoxide	7000

TABLE III.- CONTRIBUTION OF O, OH, AND O₃ TO TOTAL RATE OF OLEFIN OXIDATION

Time after irradiation, min	Percent contribution to olefin oxidation rate of -		
	O	OH	O ₃
15	2.3	84.8	12.9
180	2.2	11.2	86.6
360	.9	2.2	96.9

TABLE IV.- ADDITIONAL REACTIONS USED FOR HYDROCARBON/NO_x/SO_x

HOMOGENEOUS REACTION MECHANISM

[SO₃ is defined as being any species which will eventually form a sulfate; as such it may also contain nitrogen, for example combination of HSO₅ and NO₂. AO₂ is the product of the addition of OH to an olefin in the presence of O₂]

Reaction	Rate constant	
	ppm ⁻¹ -min ⁻¹ (a)	m ³ -mol ⁻¹ -sec ⁻¹ (a)
O + SO ₂ + M → SO ₃ + M	8.40 × 10	3.43 × 10 ⁴
OH + SO ₂ → HSO ₅	1.76 × 10 ³	7.18 × 10 ⁵
HSO ₅ + NO → HSO ₄ + NO ₂	2.90 × 10 ⁴	1.18 × 10 ⁷
HSO ₅ + NO ₂ → SO ₃	1.00 × 10 ³	4.08 × 10 ⁵
HO ₂ + SO ₂ → OH + SO ₃	2.2	8.97 × 10 ²
HO ₂ + HSO ₄ → SO ₃ + O ₂ + H ₂ O	4.2 × 10 ³	1.71 × 10 ⁶
RCHO ₂ + SO ₂ → SO ₃ + RCHO	7.8	3.18 × 10 ³
RO ₂ + SO ₂ → RO + SO ₃	7.8	3.18 × 10 ³
AO ₂ + SO ₂ → AO + SO ₃	7.8	3.18 × 10 ³
SO ₃ + Wall → Loss of SO ₃	3.12 × 10 ⁻⁵	5.20 × 10 ⁻⁷

^aThe units given are for second-order rate constants; the units for first-order rate constants are min⁻¹ and sec⁻¹.

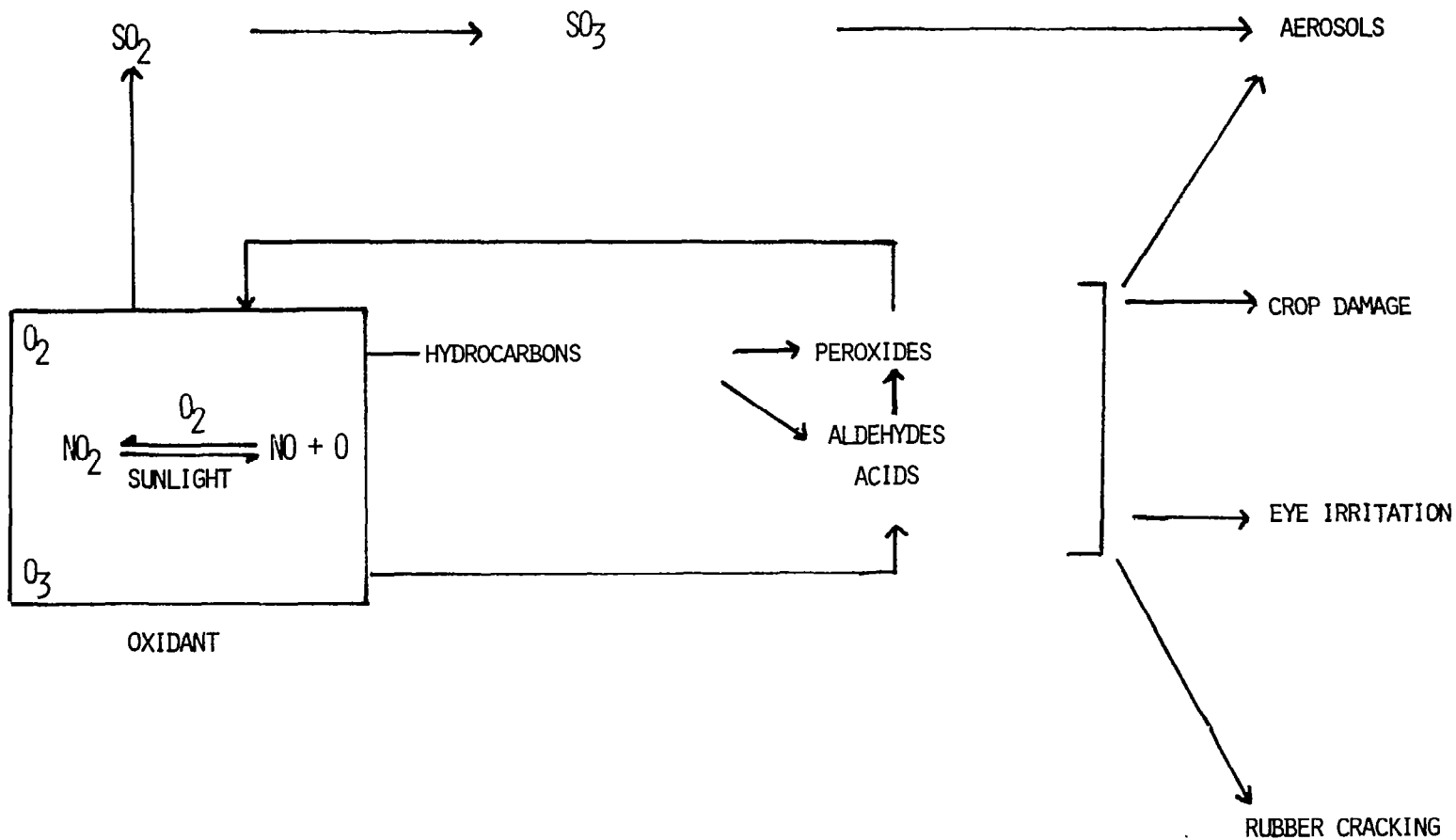
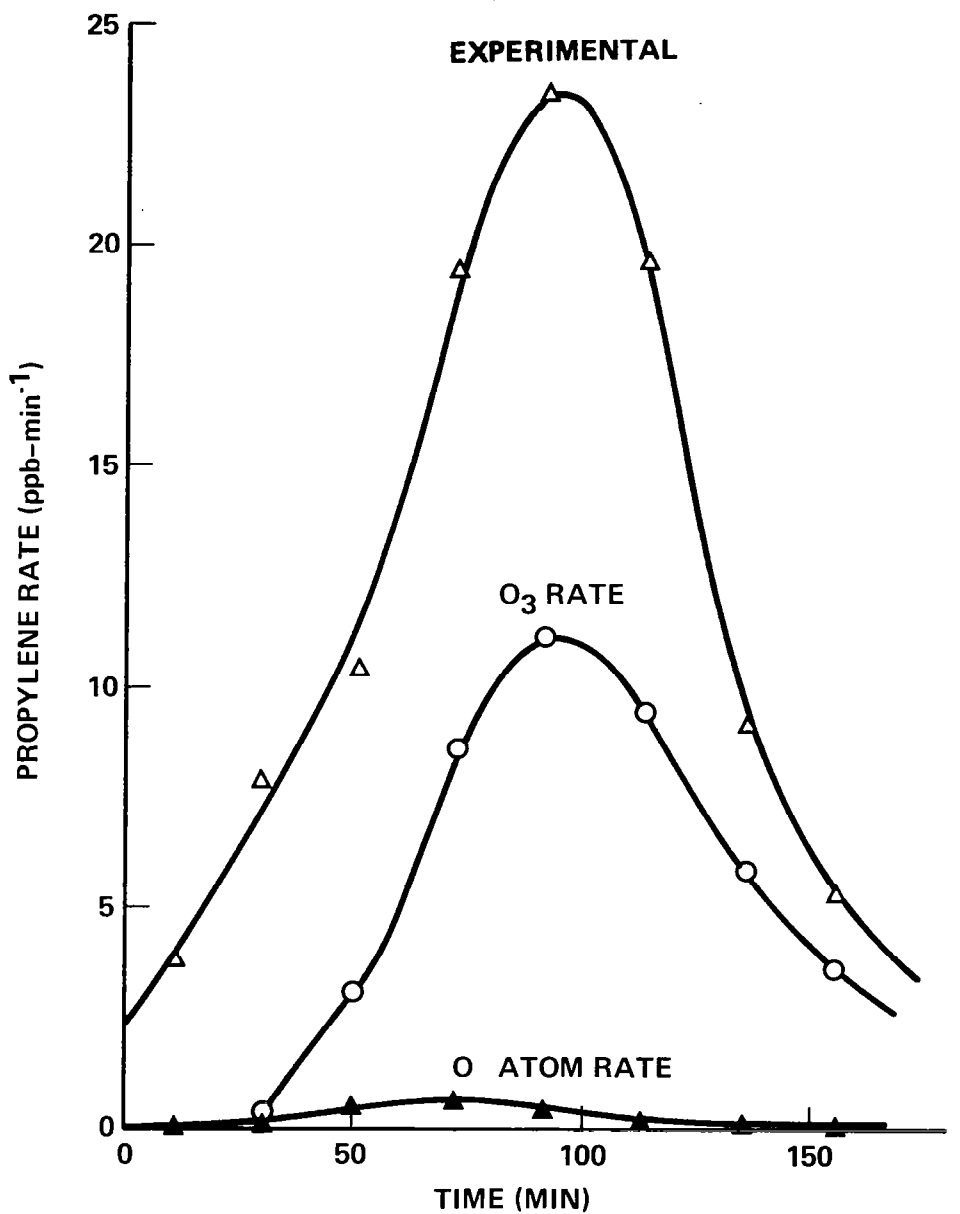


Figure 1.- Schematic representation of reactions in air leading to smog symptoms.
 (Reprinted with permission from Haagen-Smit (ref. 1); copyright by American
 Chemical Society.)



Mechanisms of Smog Reactions

Figure 2.- Comparison of experimentally observed rates of C_3H_6 consumption with calculated rates of C_3H_6 reaction with O atom and O_3 . (From Niki et al. (ref. 10) with permission.)

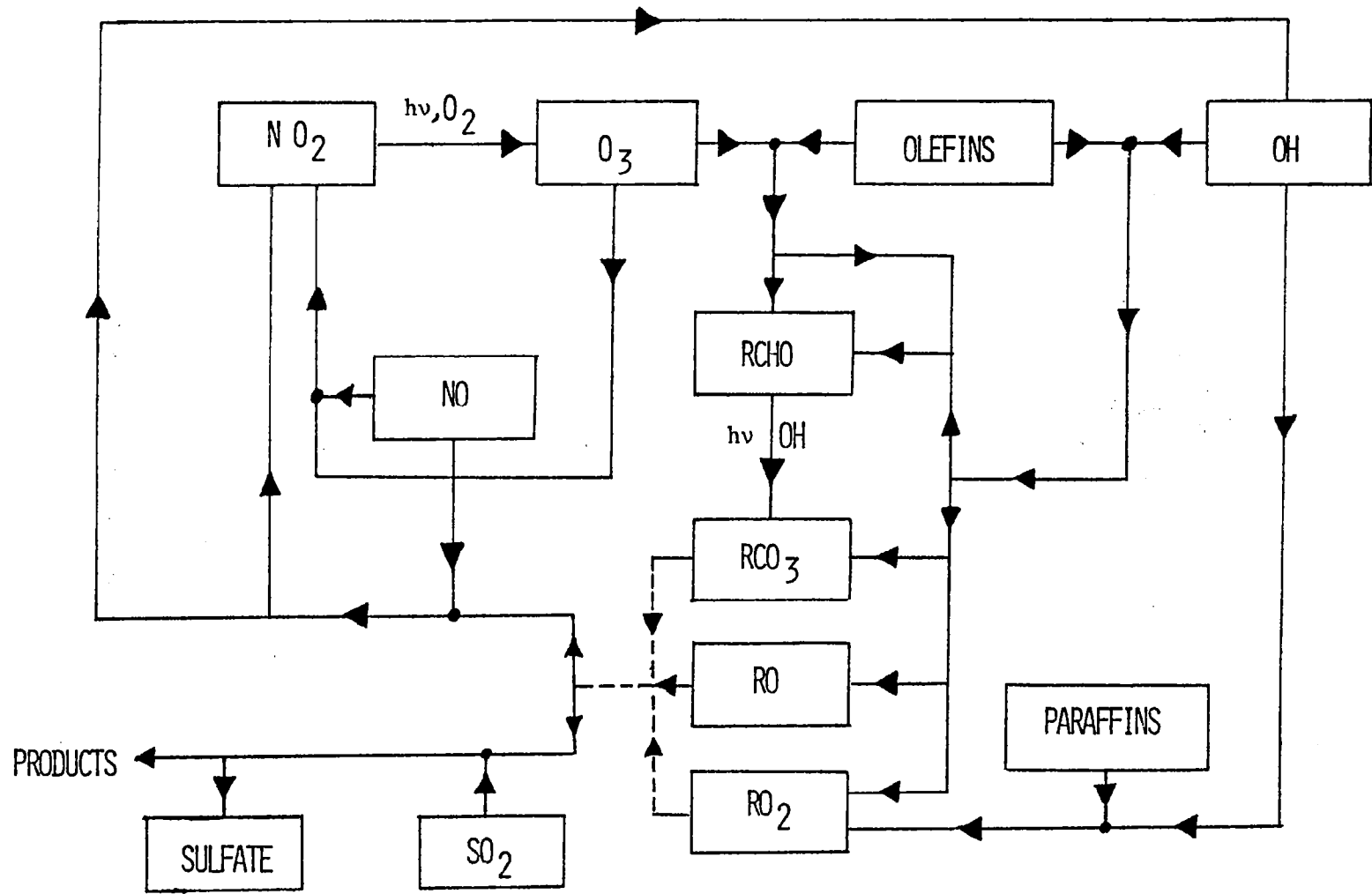
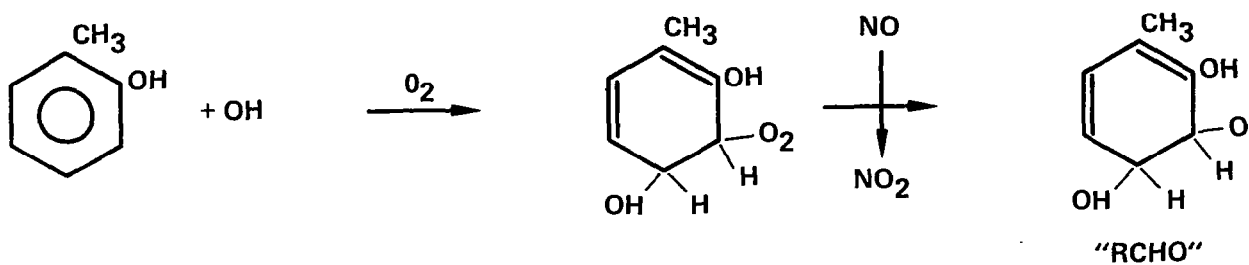
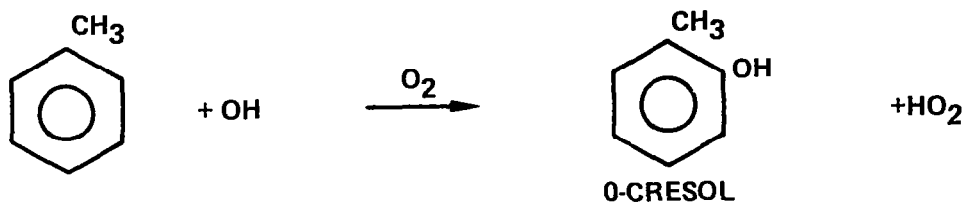


Figure 3.- Schematic representation of current knowledge of overall features of gas-phase photochemical smog formation.

ADDITION OF OH



ABSTRACTION BY OH

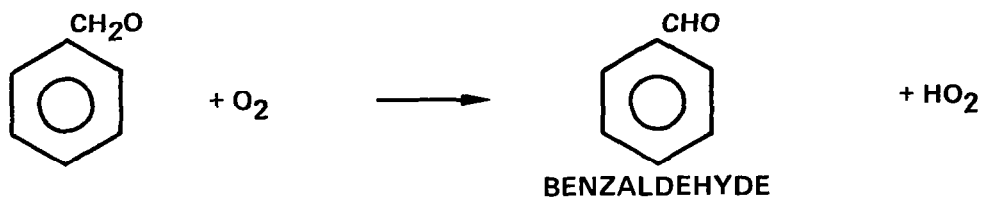
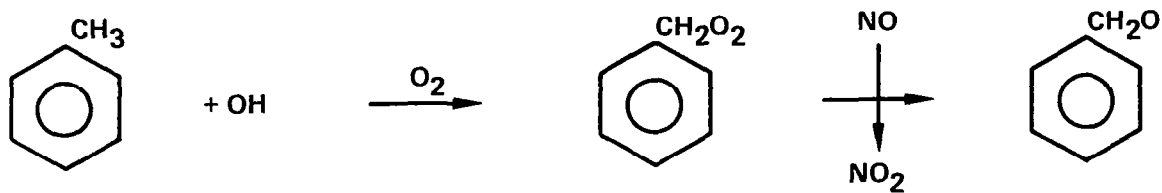
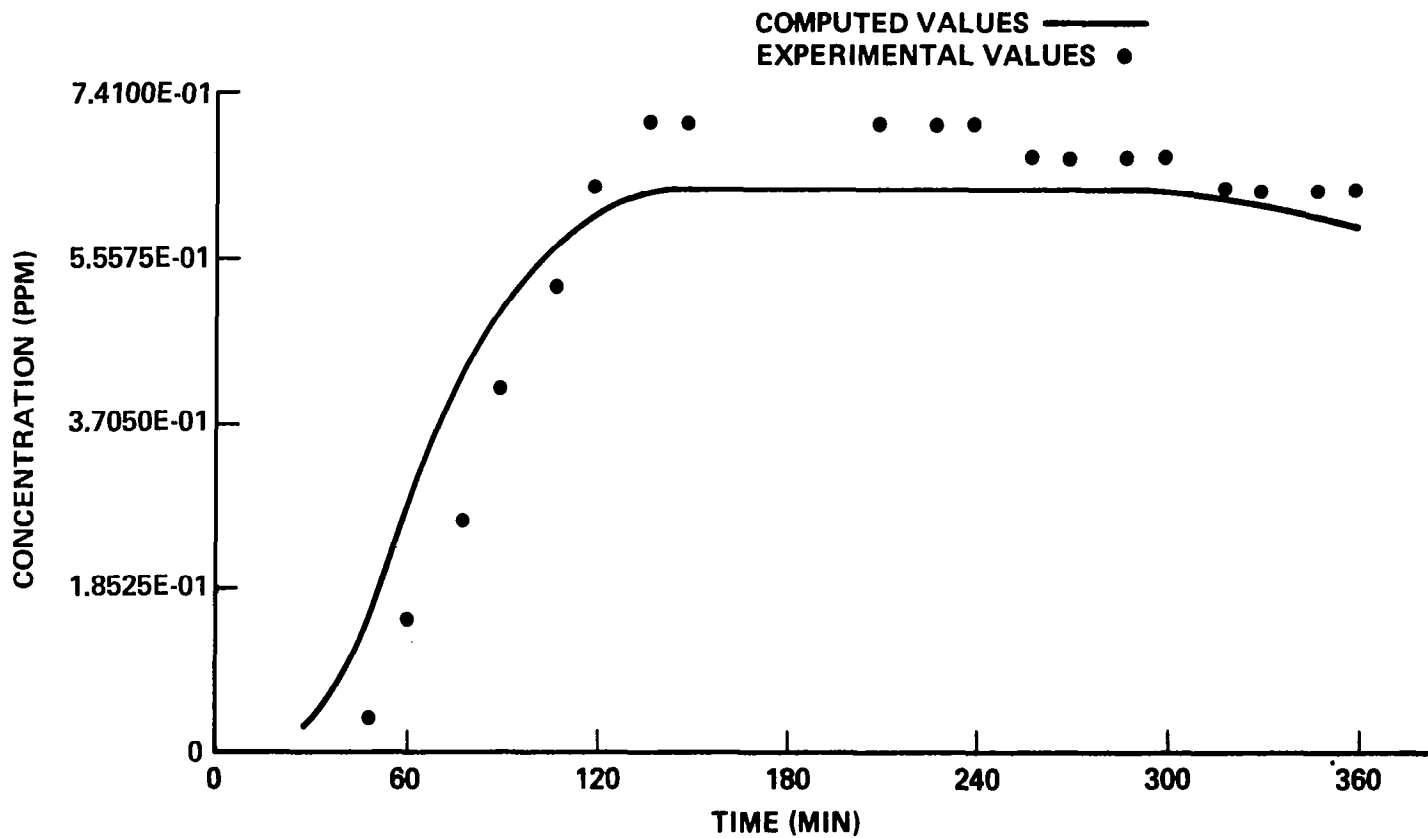
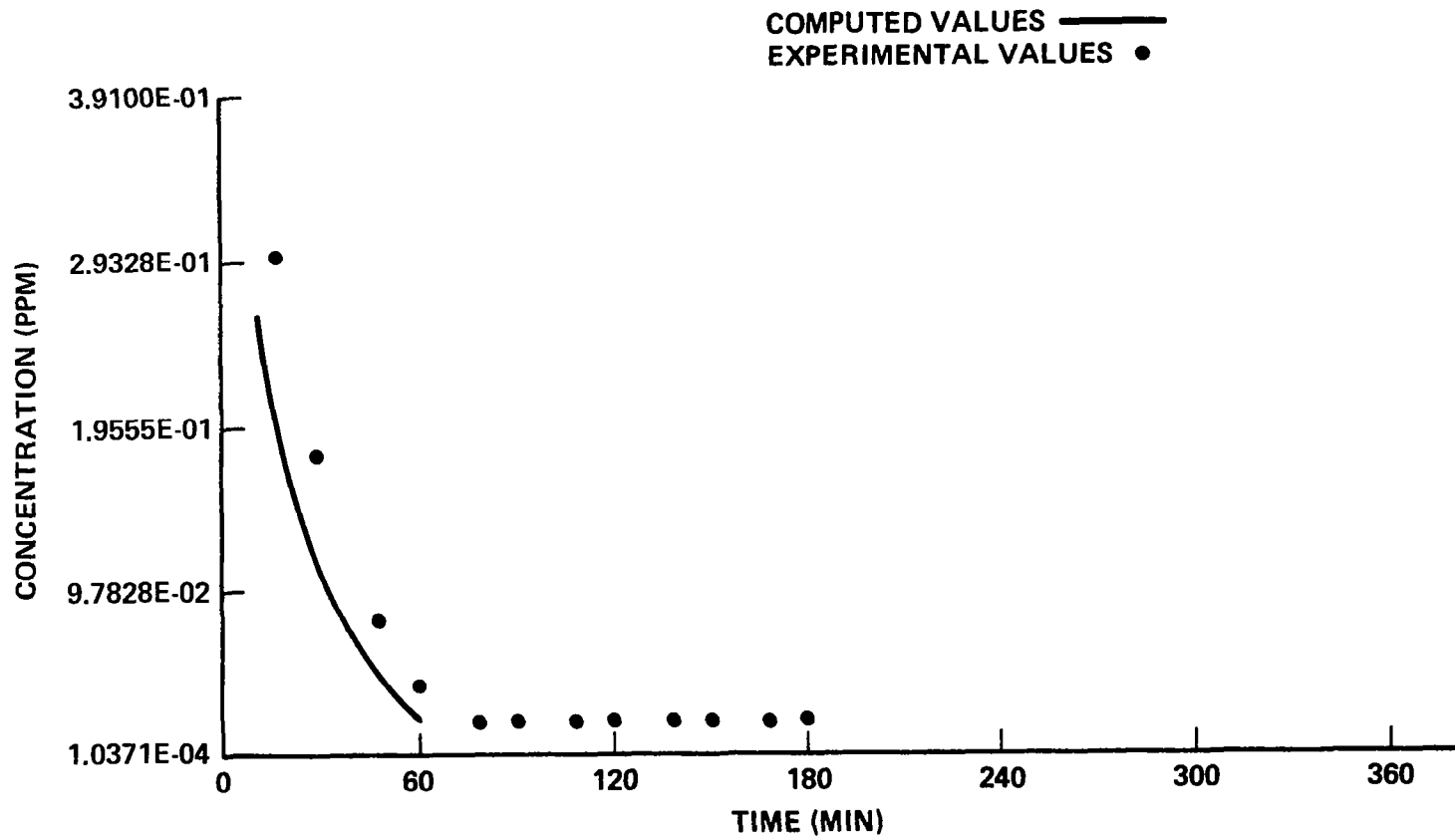


Figure 4.- Mechanism used to model oxidation of aromatic hydrocarbons using toluene as an example.



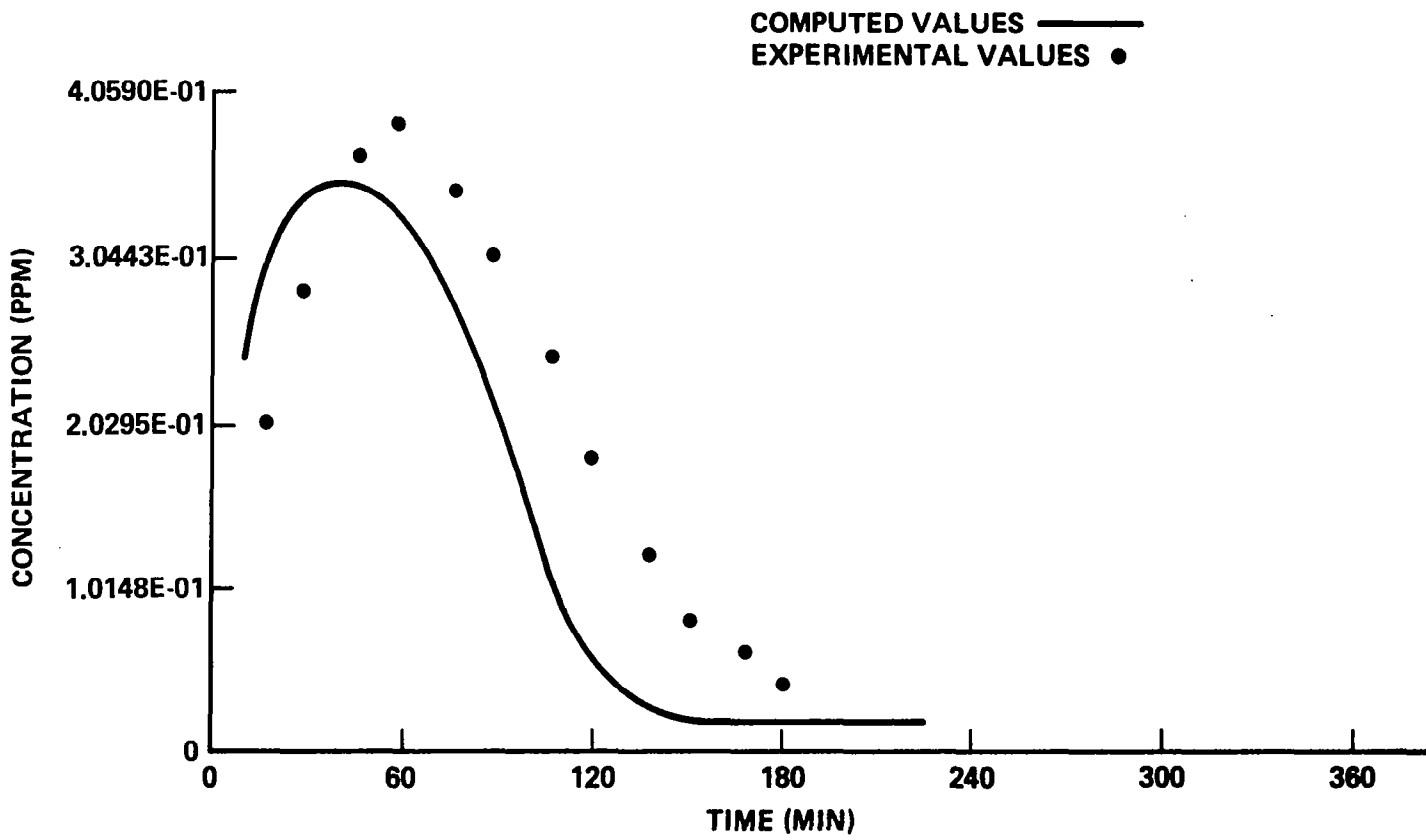
(a) O₃ concentration.

Figure 5.- Comparison of experimental data with computer model predictions for propylene/n-butane/NO_x mixture in air.



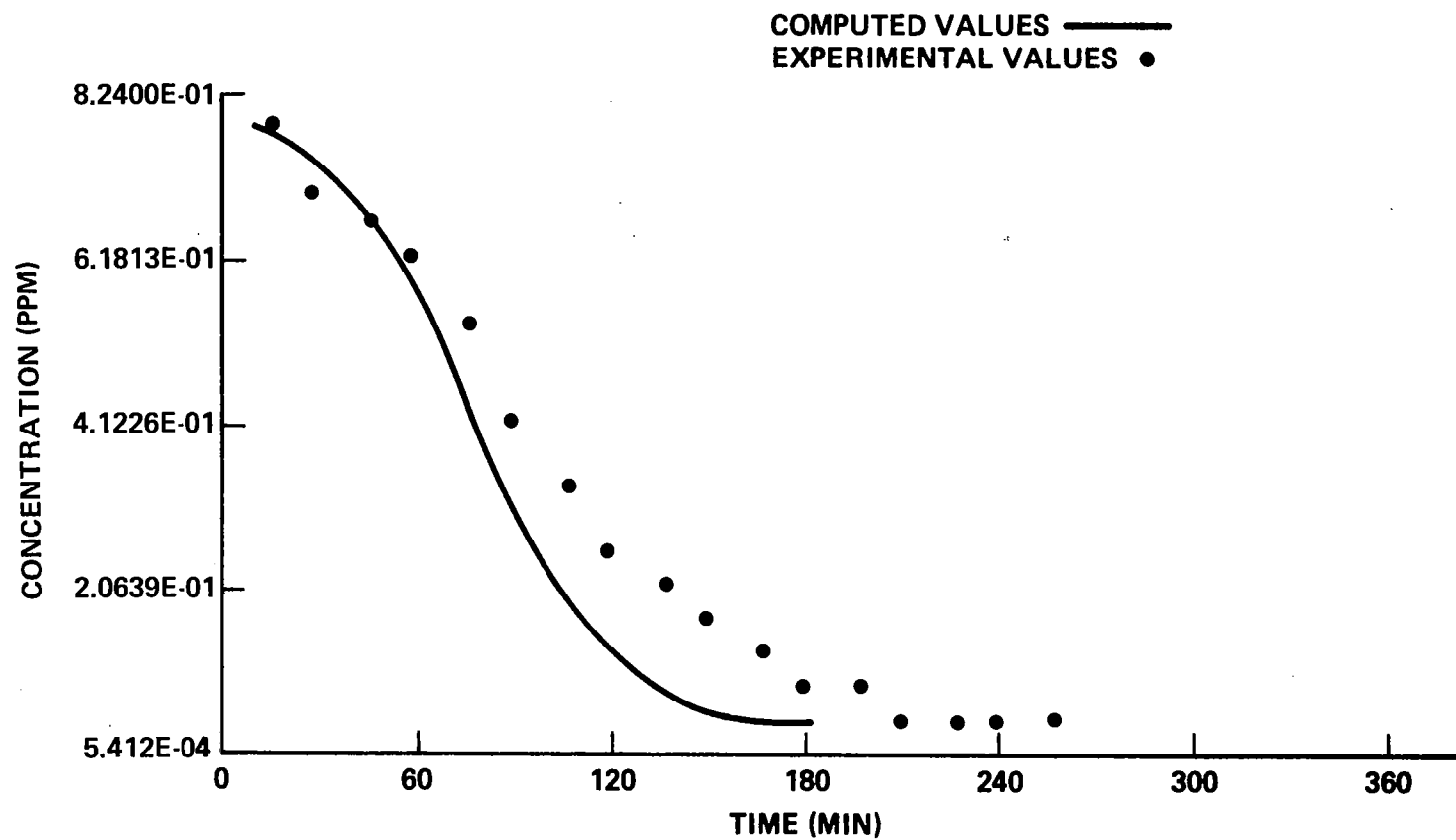
(b) NO concentration.

Figure 5.- Continued.



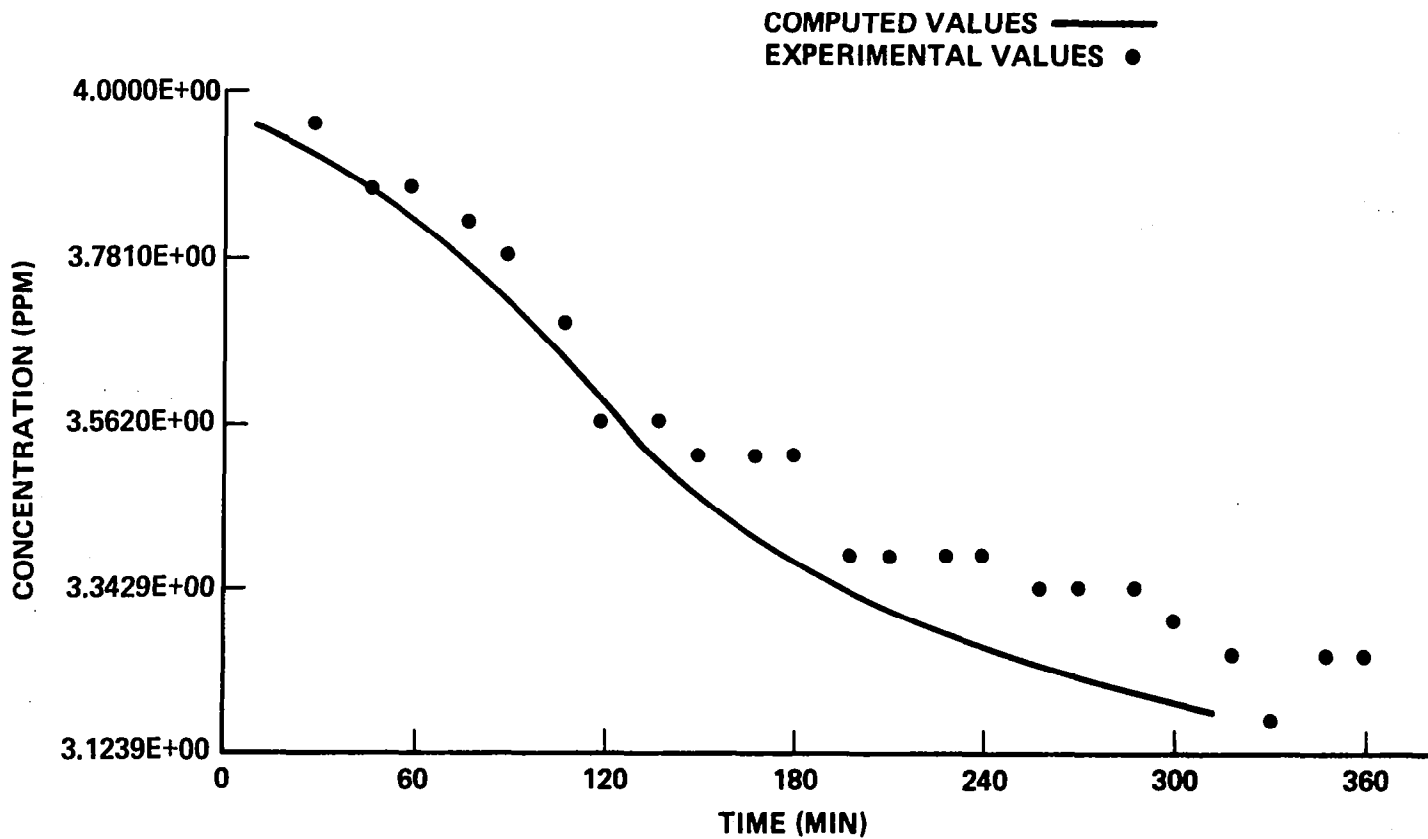
(c) NO₂ concentration.

Figure 5.- Continued.



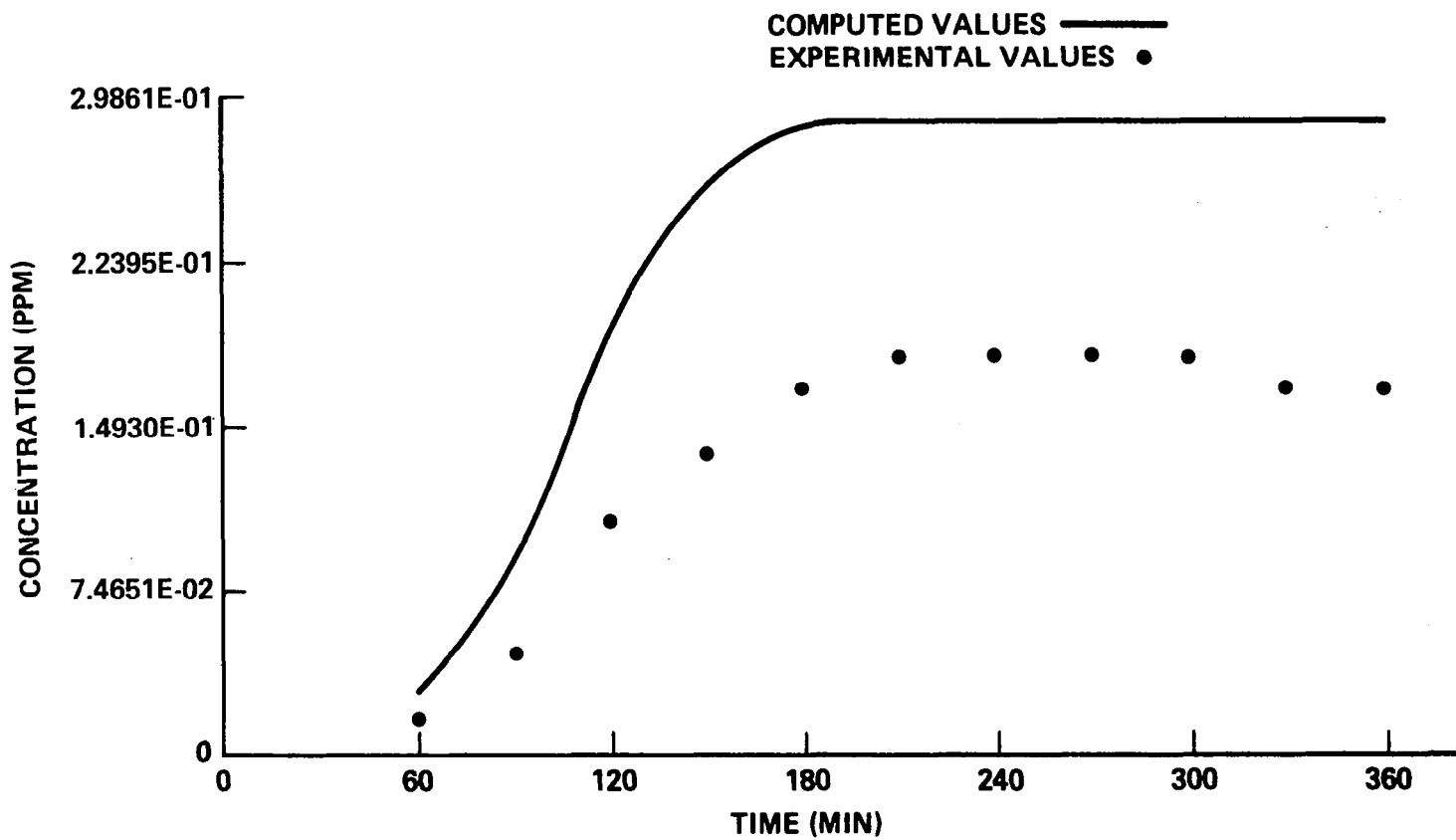
(d) Olefin concentration.

Figure 5.- Continued.



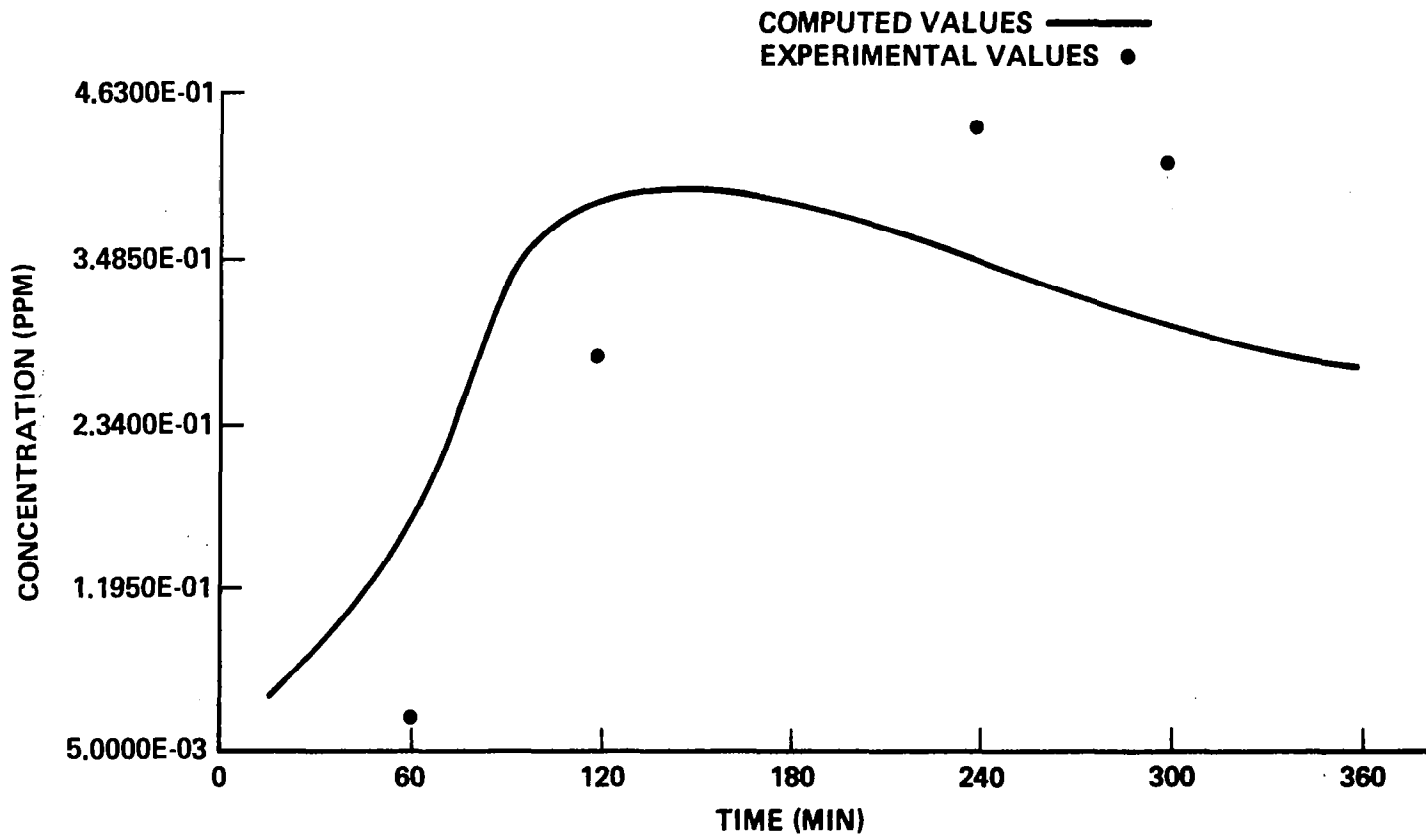
(e) Alkane concentration.

Figure 5.- Continued.



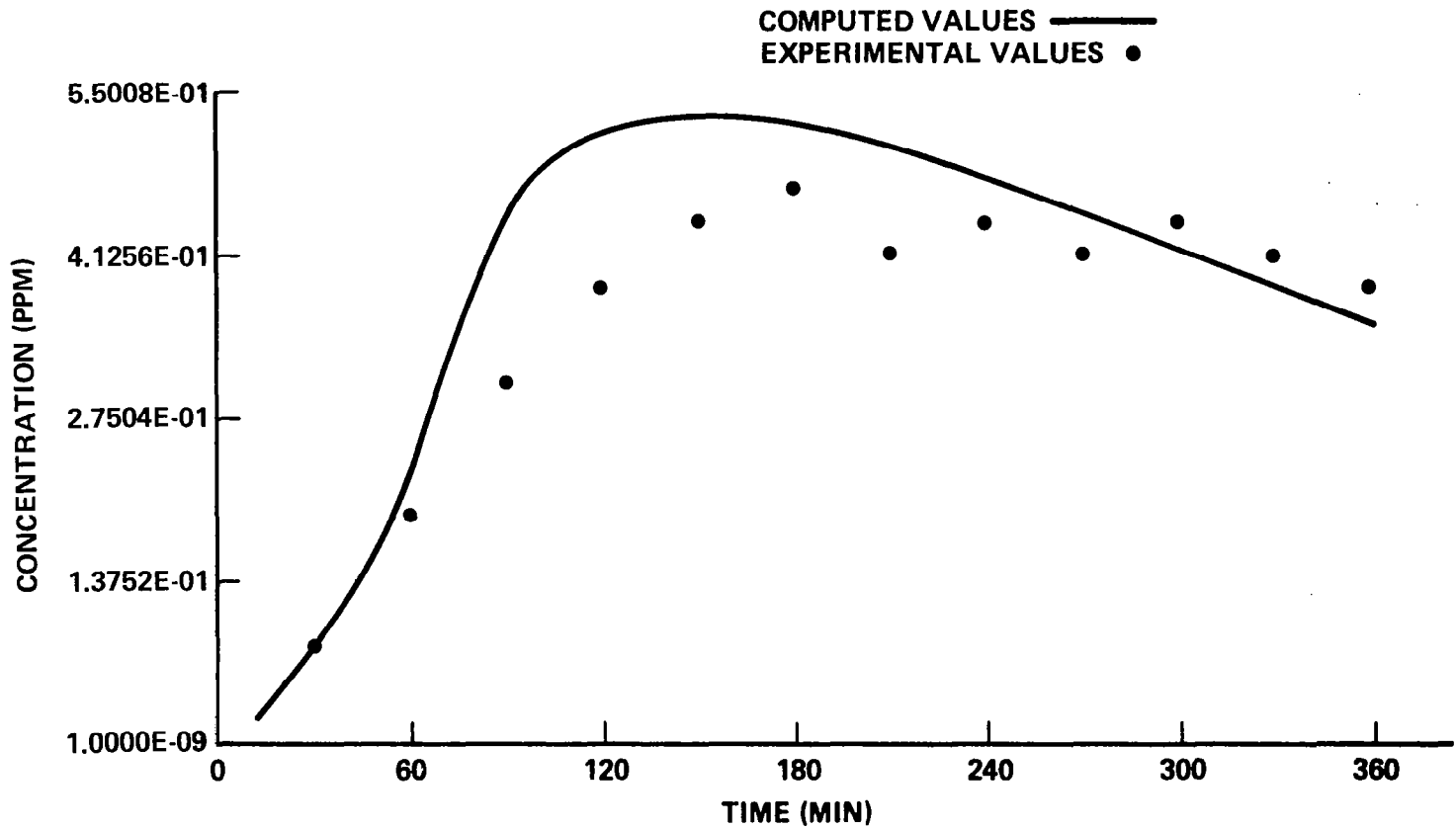
(f) PAN concentration.

Figure 5.- Continued.



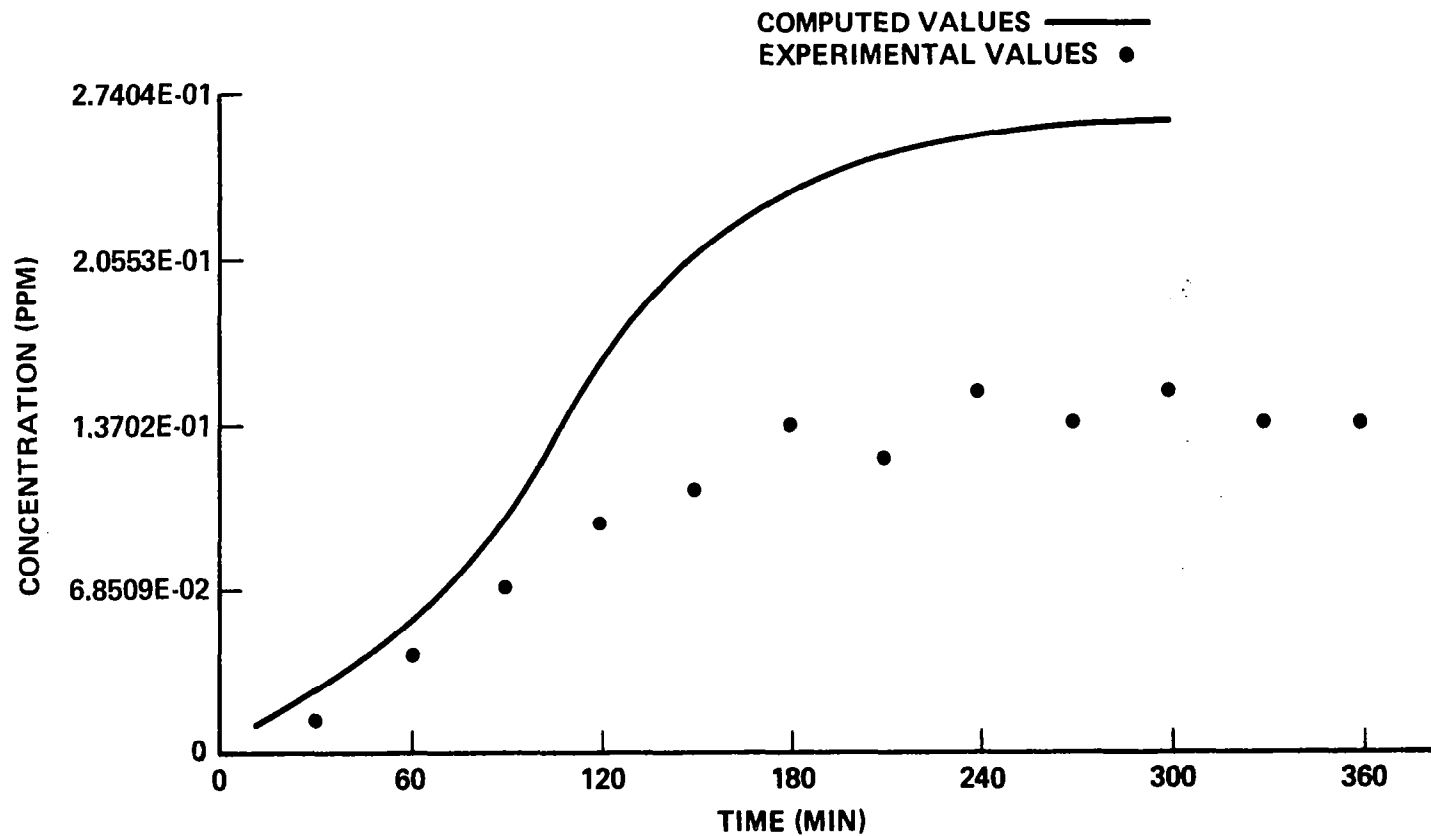
(g) HCHO concentration.

Figure 5.- Continued.



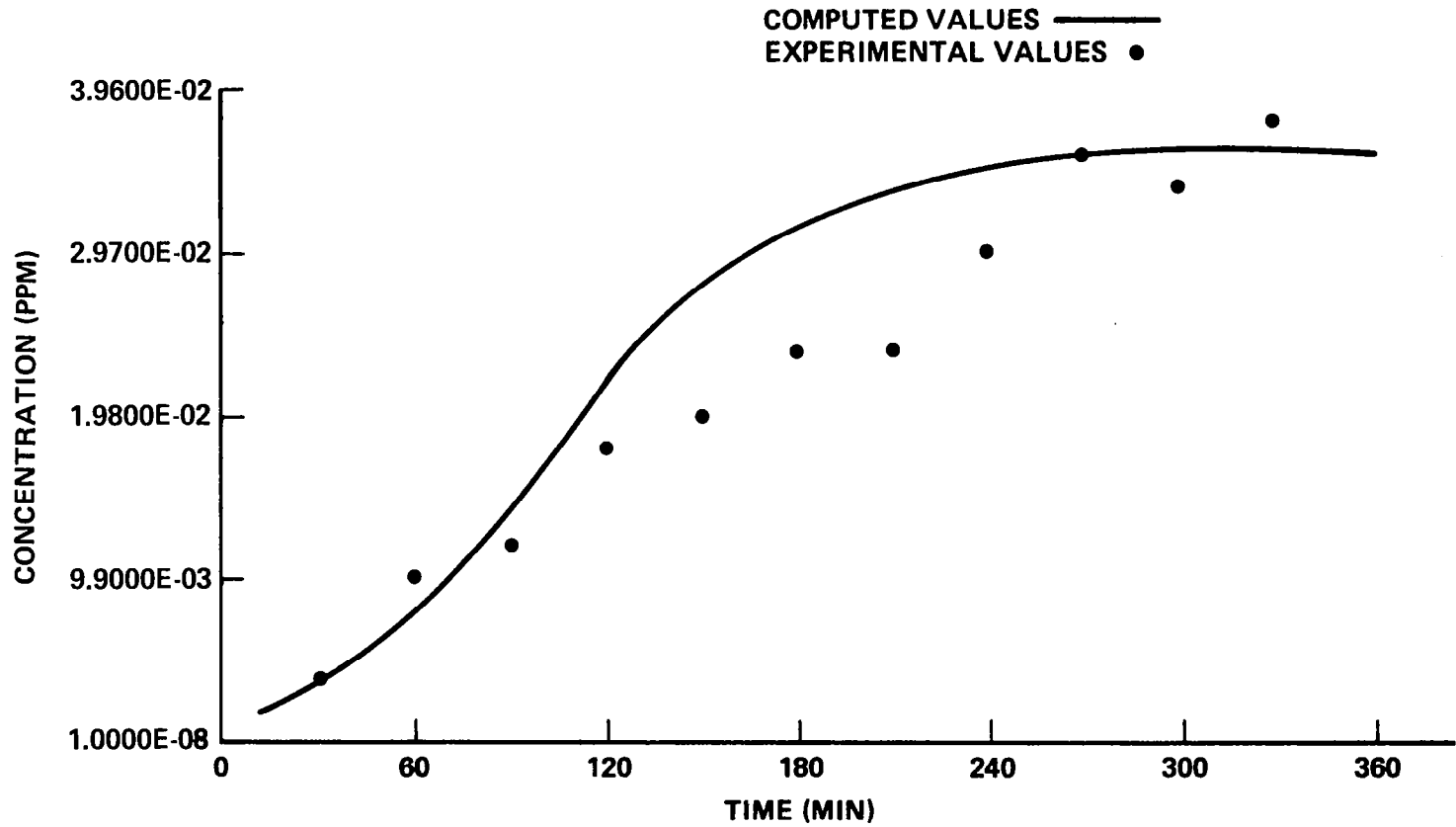
(h) RCHO concentration.

Figure 5.- Continued.



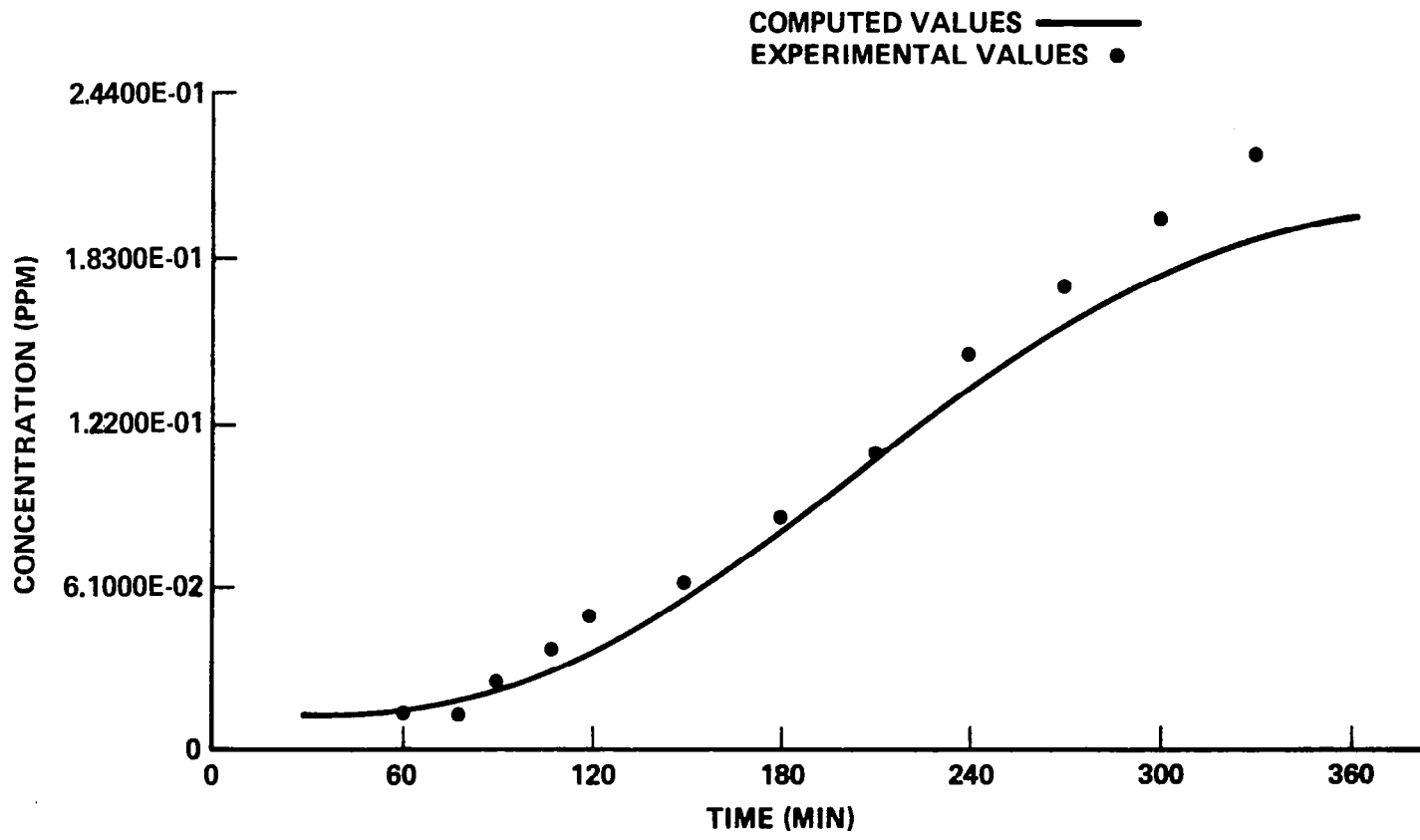
(i) Ketone concentration.

Figure 5.- Continued.



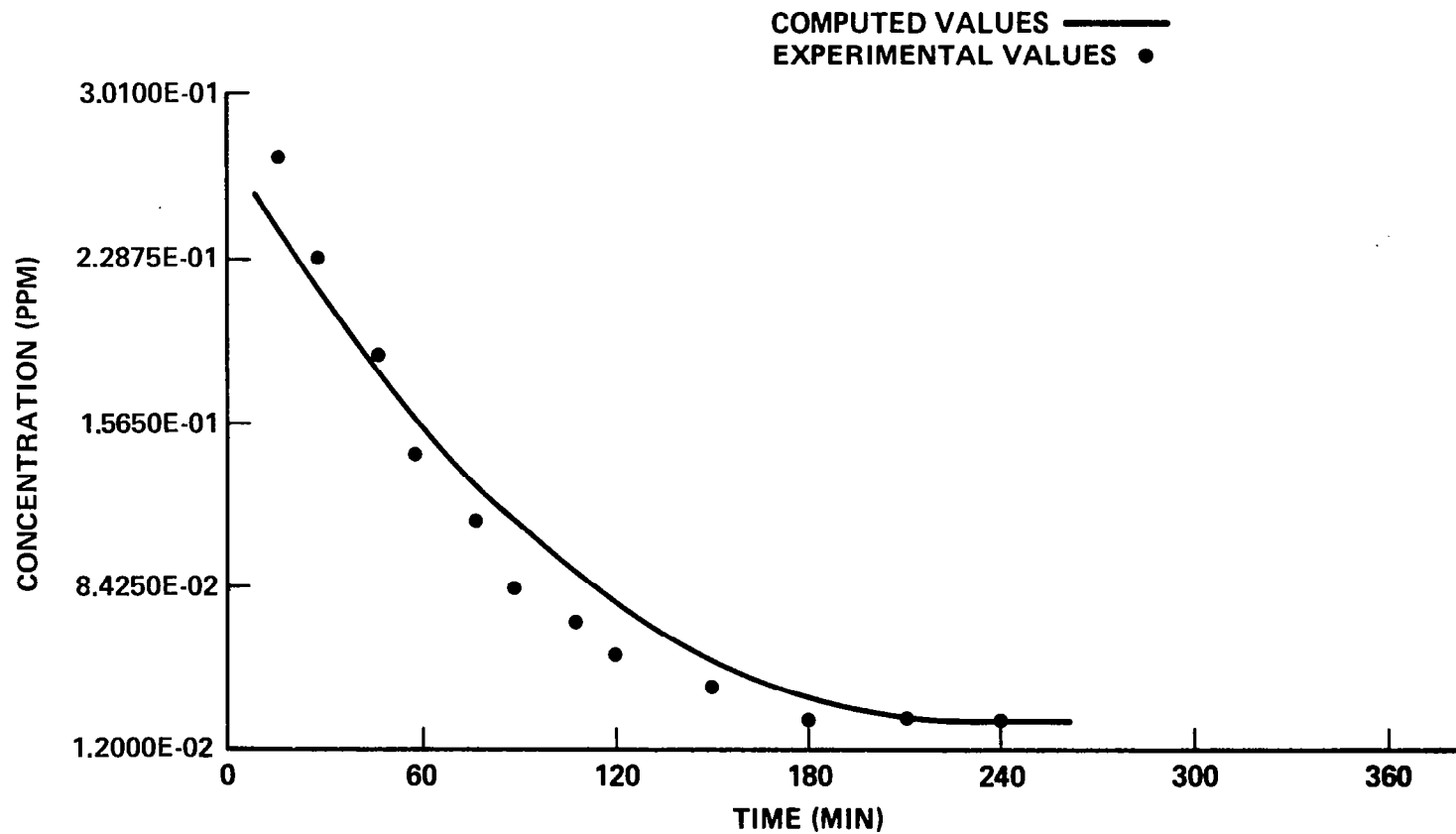
(j) Nitrate concentration.

Figure 5.- Concluded.



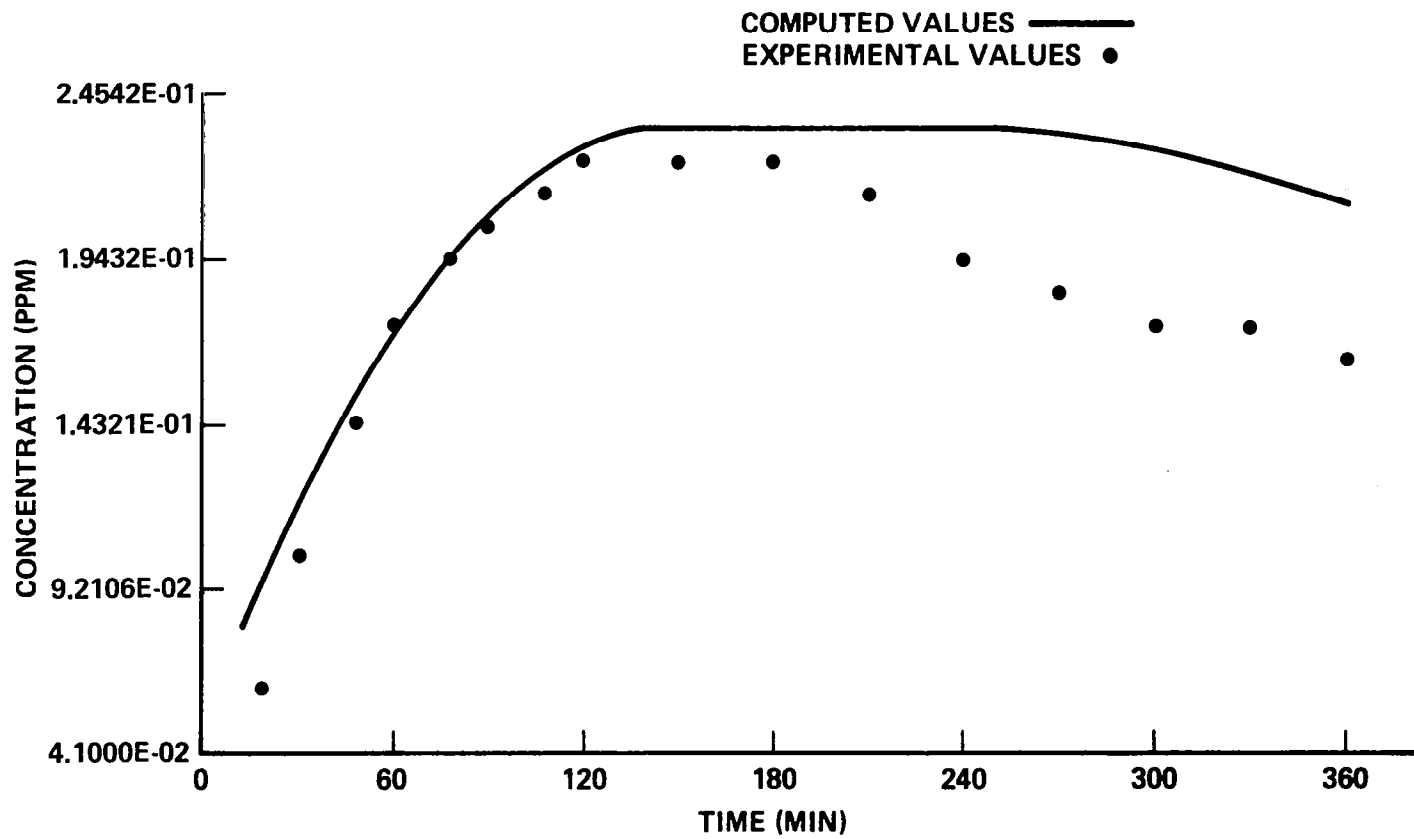
(a) O₃ concentration.

Figure 6.- Comparison of experimental data with computer model predictions for surrogate hydrocarbon/NO_x mixture in air.



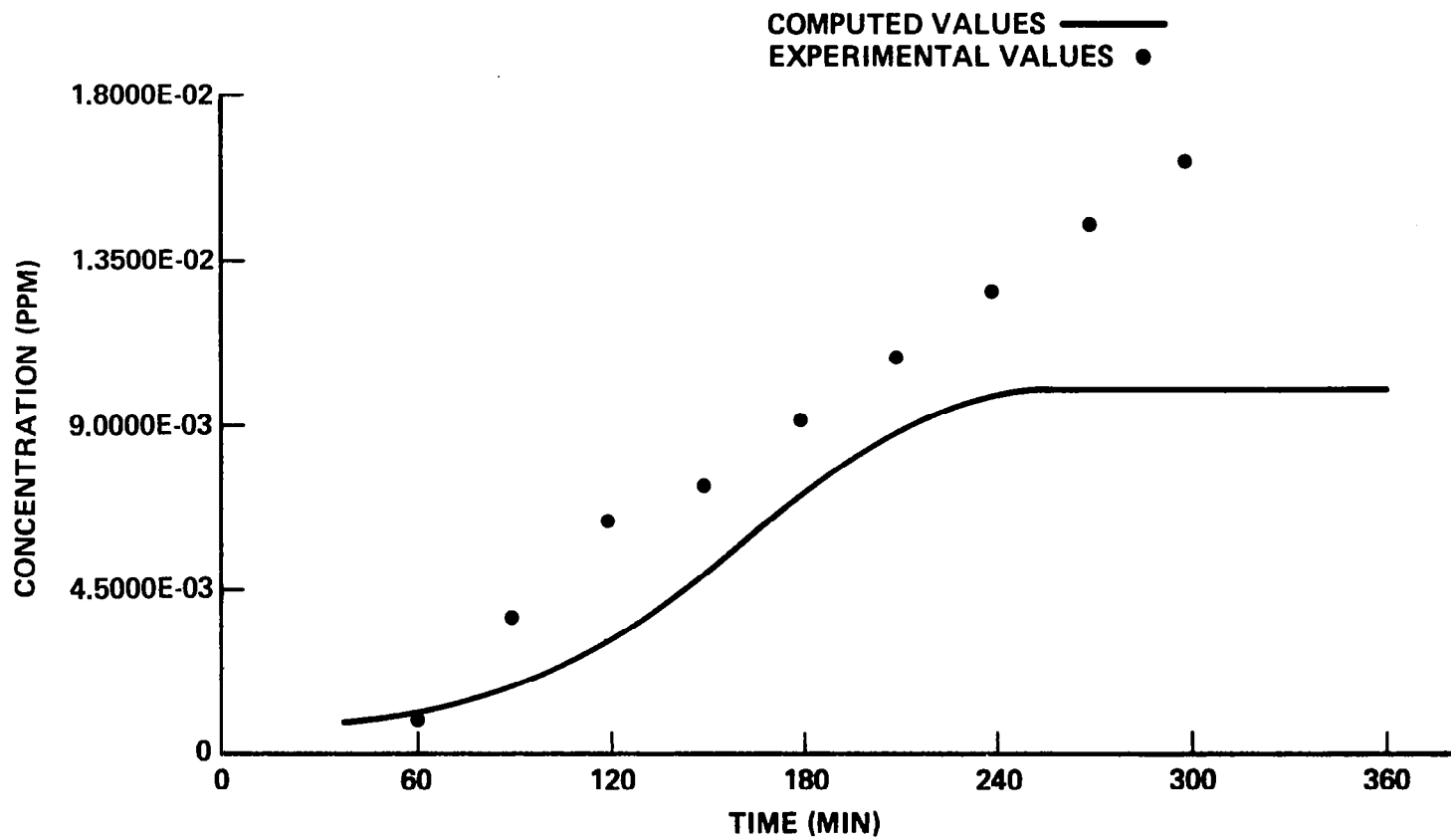
(b) NO concentration.

Figure 6.- Continued.



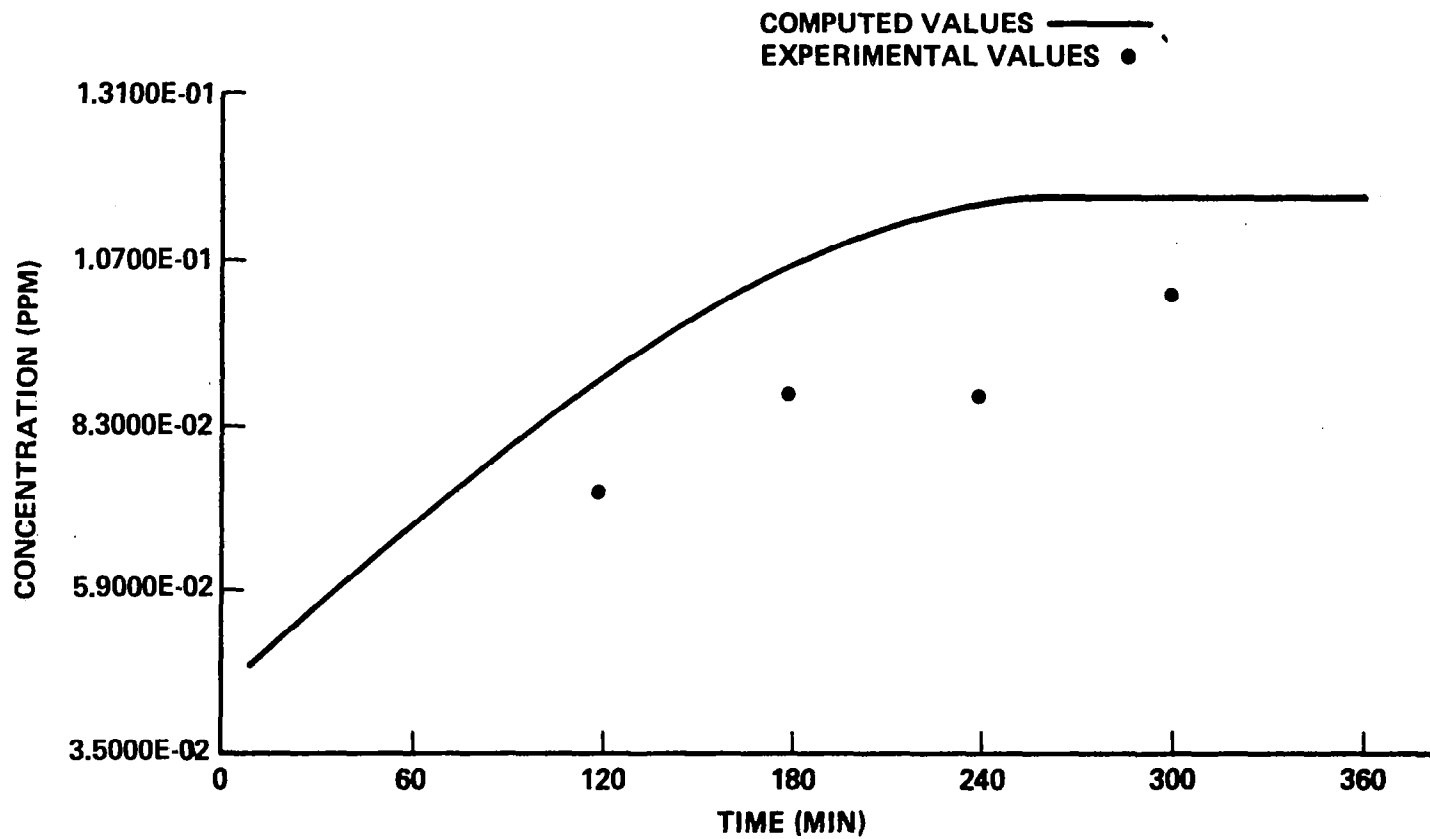
(c) NO₂ concentration.

Figure 6.- Continued.



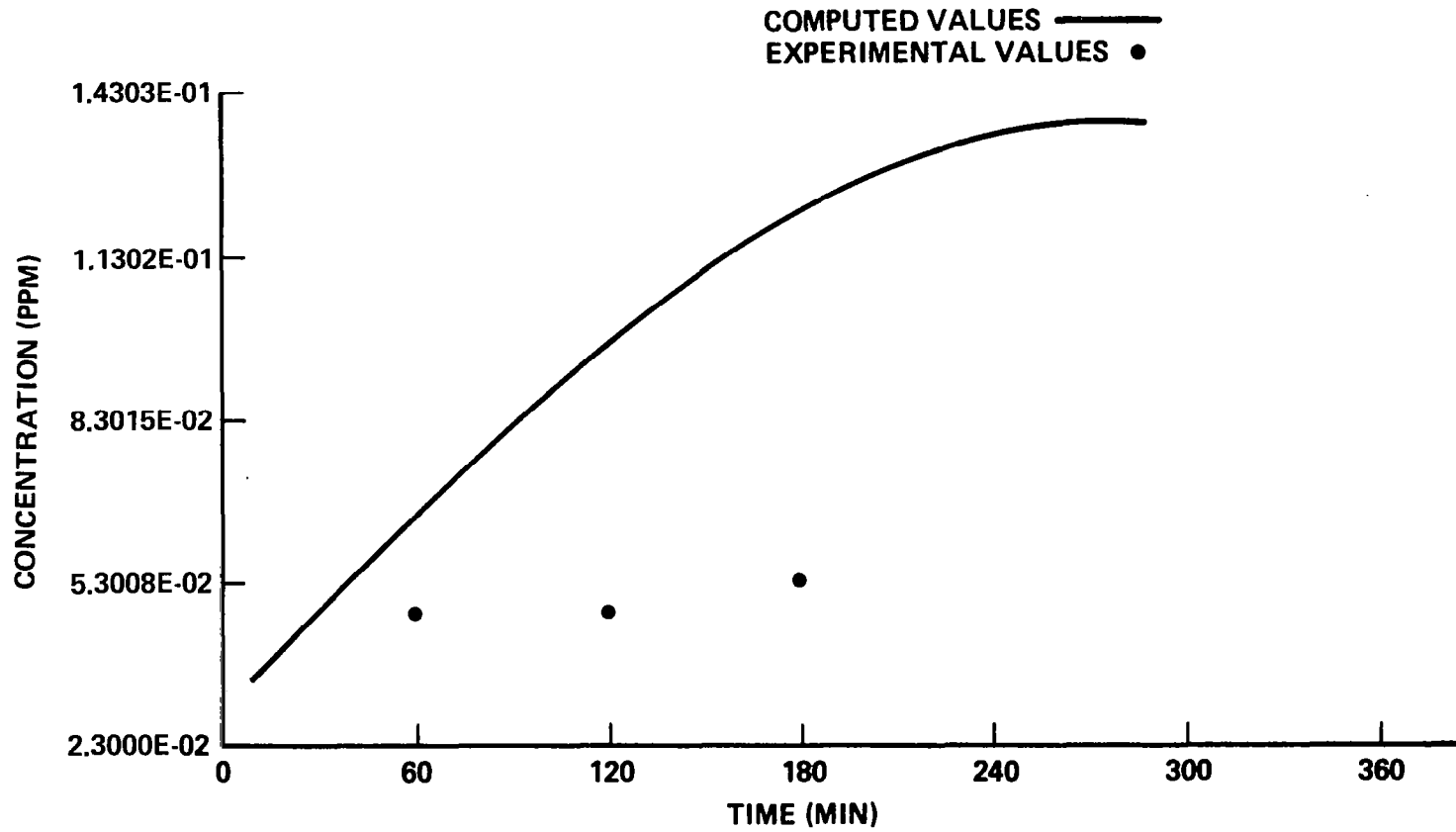
(d) PAN concentration.

Figure 6.- Continued.



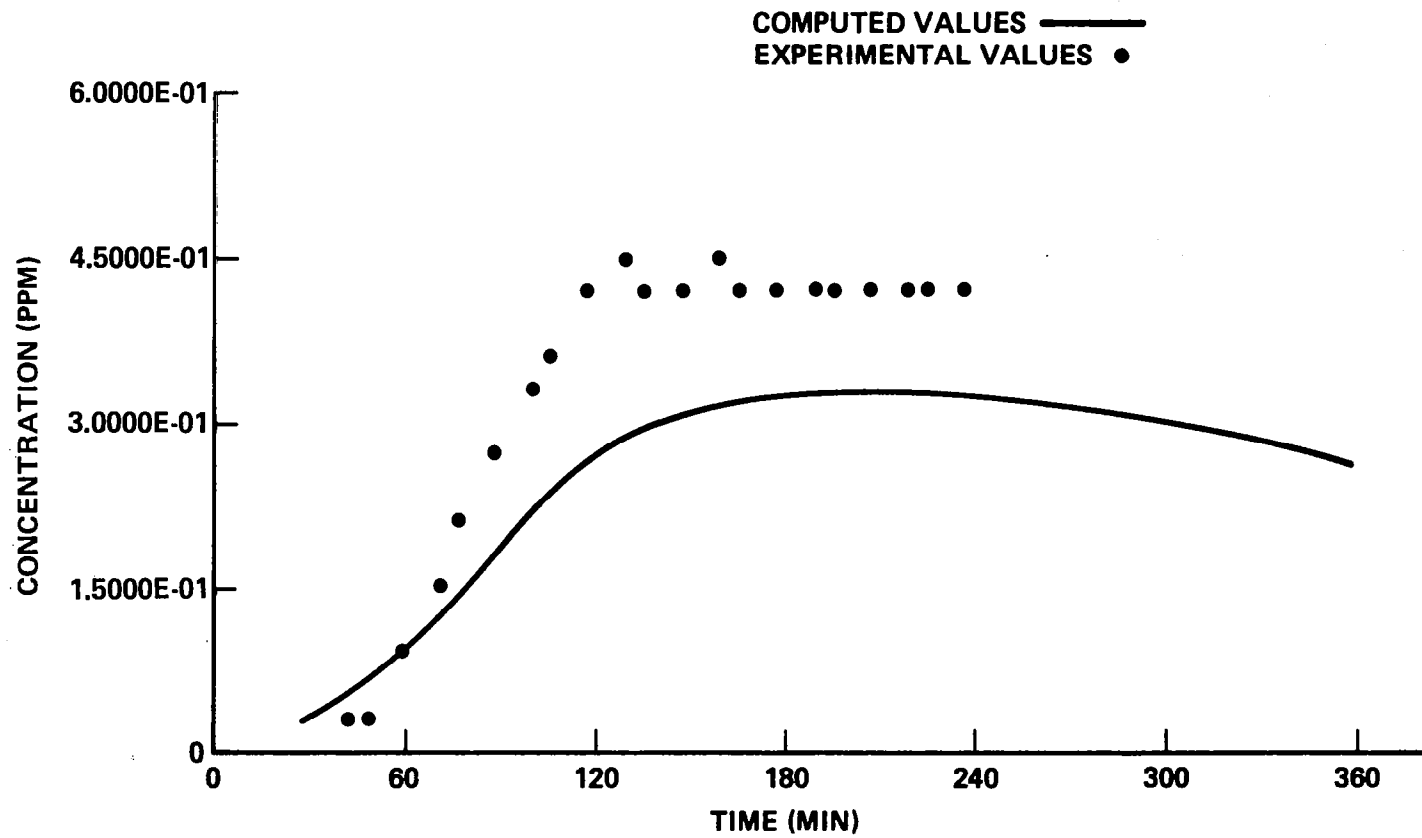
(e) HCHO concentration.

Figure 6.- Continued.



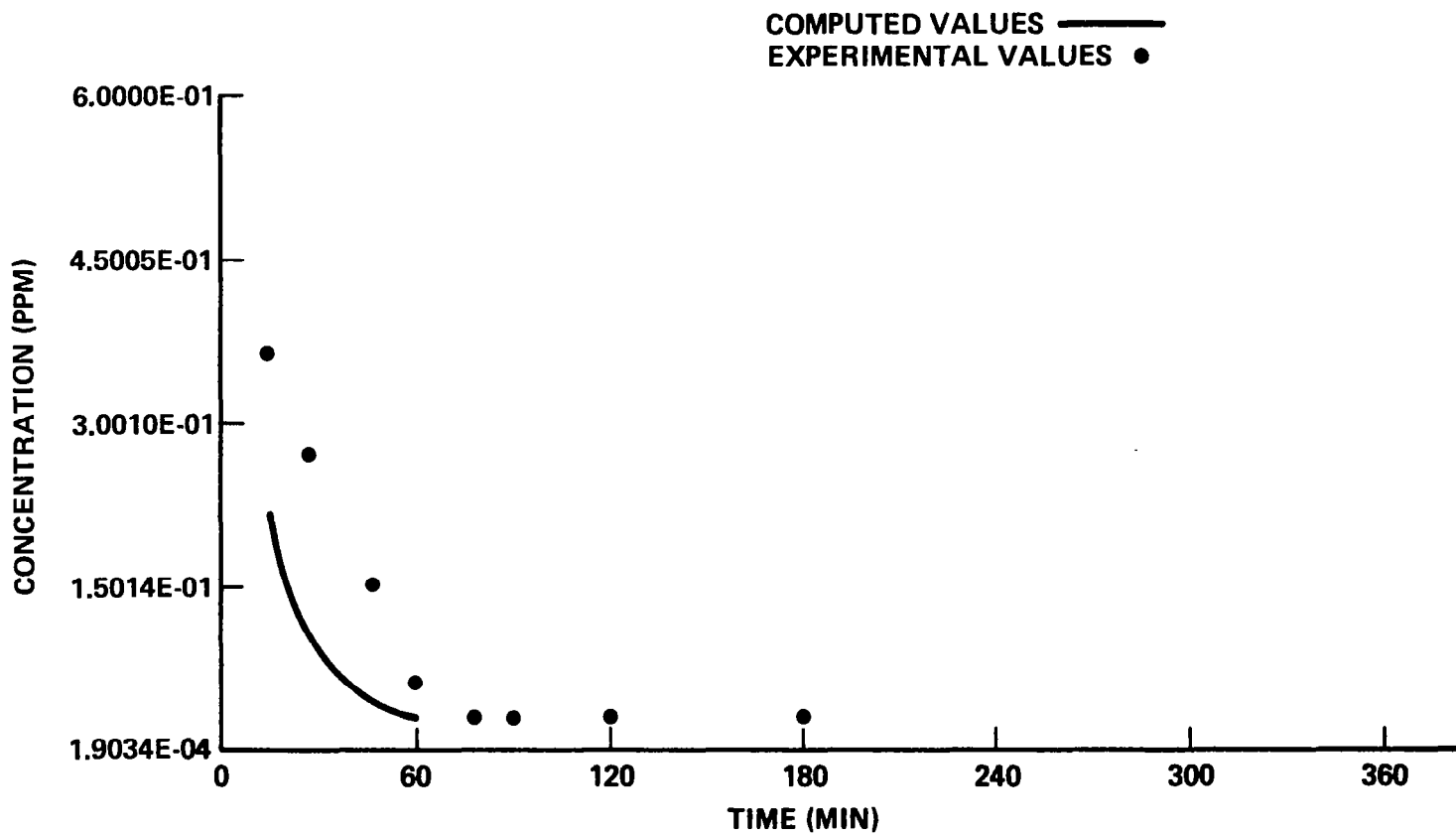
(f) RCHO concentration.

Figure 6.- Concluded.



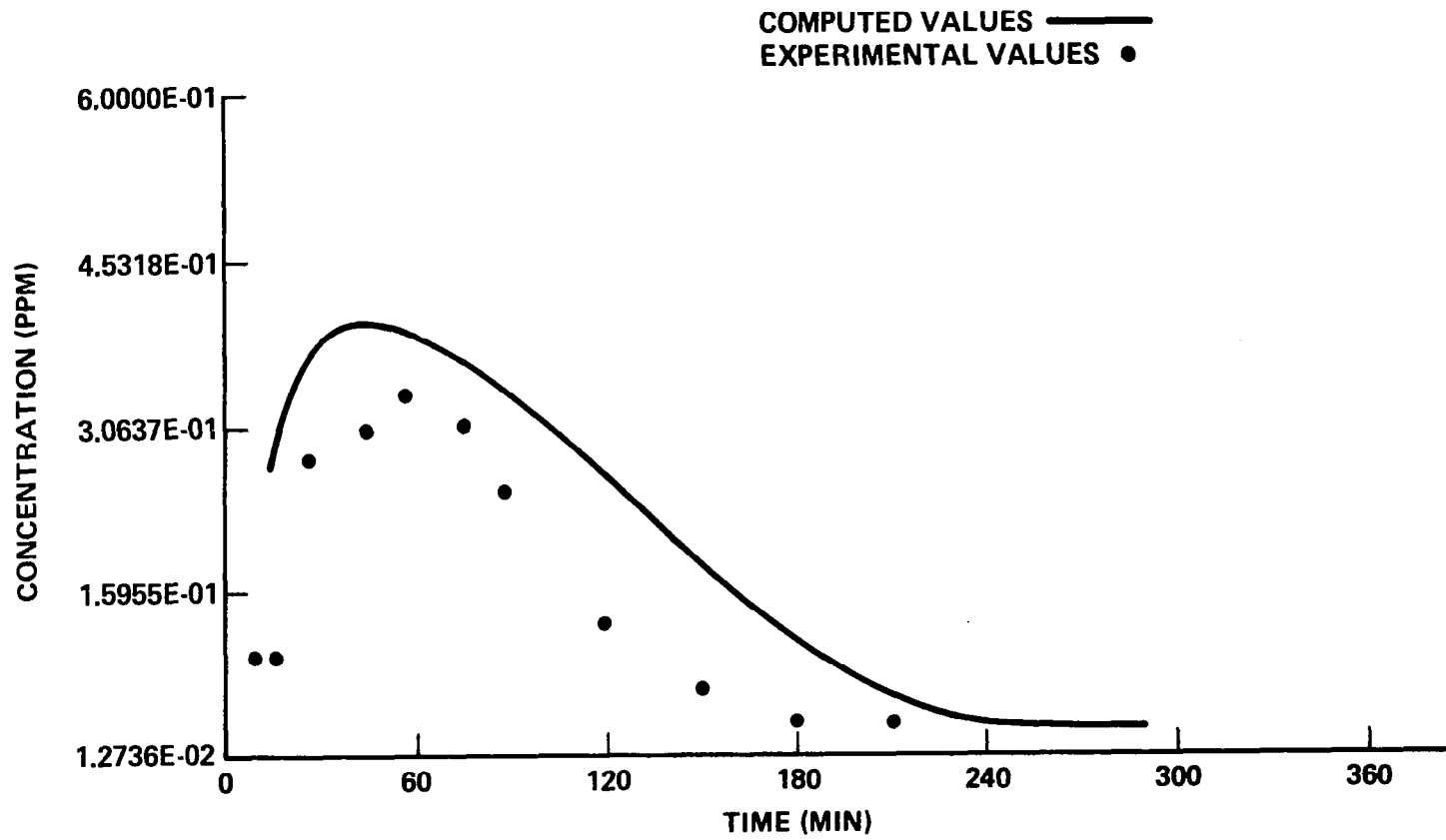
(a) O₃ concentration.

Figure 7.- Comparison of experimental data with computer model predictions for propylene/NO_x/SO_x mixture in air.



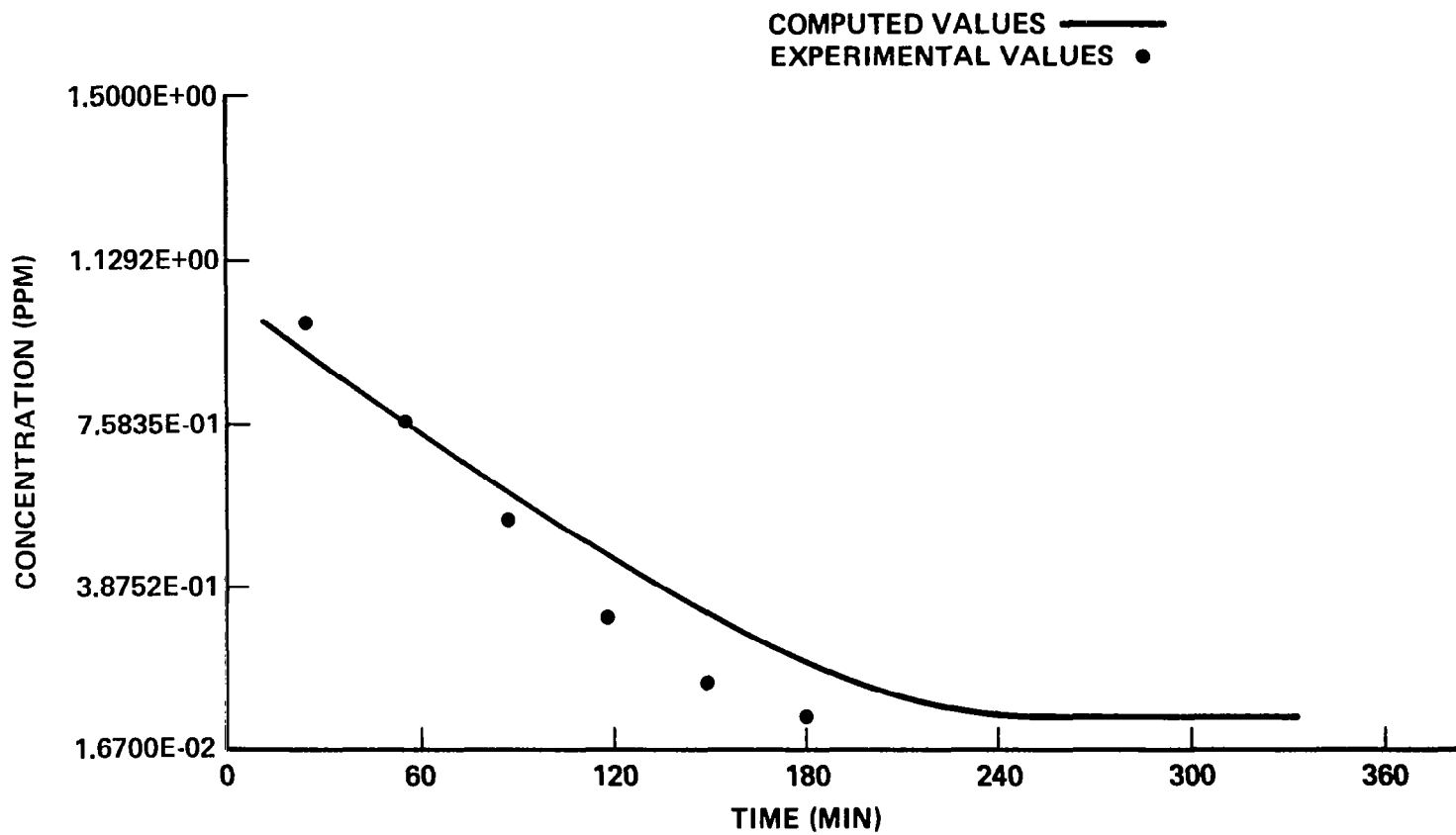
(b) NO concentration.

Figure 7.- Continued.



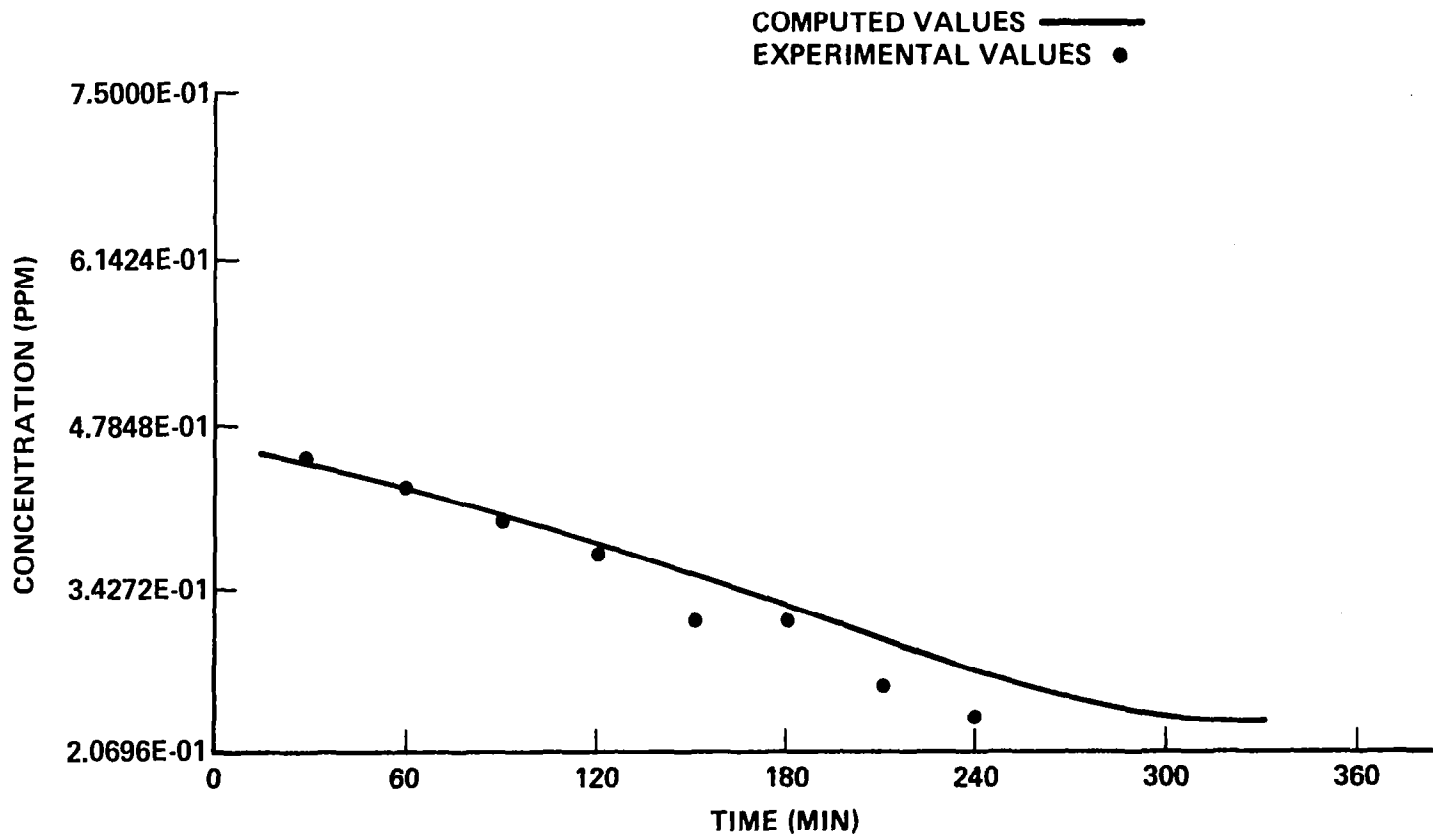
(c) NO₂ concentration.

Figure 7.- Continued.



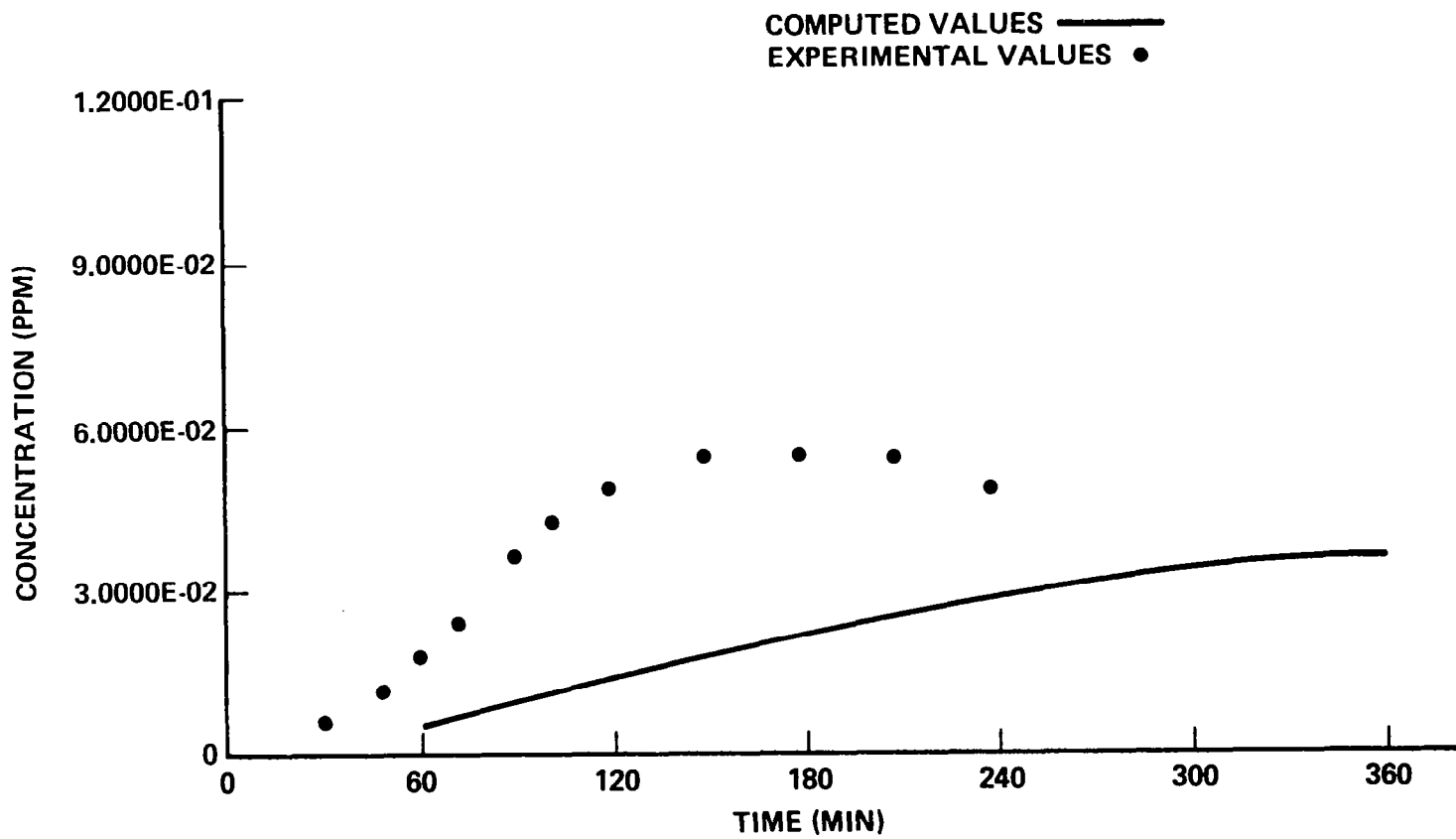
(d) Olefin concentration.

Figure 7.- Continued.



(e) SO₂ concentration.

Figure 7.- Continued.



(f) SO₃ concentration.

Figure 7.- Concluded.

ATMOSPHERIC SULFUR BEHAVIOR IN POWER PLANT AND REGIONAL PLUMES*

Rudolf B. Husar
Air Pollution Research Laboratory
St. Louis, Missouri

INTRODUCTION

A key question in the current energy debate concerns the economic and environmental costs of increased coal usage as a replacement for gas and oil. The environmental constraints are due to mining, transportation, and the release of combustion products (SO_x , NO_x , CO_2 , and fly ash). Sulfur oxide emissions and their effect on the environment have been under intense study during the past 25 years, first because of the acute air pollution episodes that occurred in populated areas (e.g., the 1952 and 1962 London episodes) and more recently because of the chronic effects on the ecosystem (e.g., acidification of lakes in southern Scandinavia and the Northeastern United States).

The past years of monitoring and research have contributed appreciably to the understanding of atmospheric sulfur behavior. The key findings are summarized in the following sections.¹

Sources

The emission rate of sulfur dioxide (SO_2) in the United States from man-made sources was 32×10^6 metric tons/year in 1973 (U.S. Environmental Protection Agency (ref. 1)), or about 0.5 kg of SO_2 per person per day. Fuel combustion accounted for 80.1 percent, while industrial processes (metal, petroleum, and chemical manufacturing) contributed 17.9 percent and transportation 2 percent to the national SO_2 emissions (fig. 1). Of the fuels used by utility and industry, coal contributed 65 percent and oil 13 percent. About 75 percent of the SO_2 is emitted east of the Mississippi River with the highest emission density in the area of the Ohio River Valley (fig. 2). Within this region, fuels accounted for 92 percent of the total SO_2 emissions. West of the Mississippi River (25 percent of the national SO_2 emissions), 62 percent of SO_2 was due to mining and industrial processes and 38 percent to fuels.

Sulfur compounds are also emitted from natural sources, for example, sea spray and decomposition of organic materials. Globally, natural emissions are

*This research was supported in part by the Federal Interagency Energy/Environment Research and Development Program through U.S. Environmental Protection Agency Grant No. R803896.

¹Much of the work discussed is also based on intense efforts over the past years by the author's colleagues, D. E. Patterson, N. V. Gillani, and J. D. Husar. The technical support of William E. Wilson, Jr., of the U.S. Environmental Protection Agency is also acknowledged.

estimated to be comparable with man-made sulfur emissions (Granat et al. (ref. 2)), but over regional scales (e.g., northern Europe), it is concluded that man-made sources dominate the sulfur budget (Rodhe (ref. 3) and International Symposium on Sulfur in the Atmosphere (ISSA) Workshop (ref. 4)).

SO₂ and Sulfate Concentrations

Currently, a solid historical data base exists for the SO₂ levels in urbanized areas of the United States and shows a decline from an annual average of 38 µg/m³ in 1970 to 26 µg/m³ in 1974. The annual mean sulfur dioxide standard of 80 µg/m³ was only exceeded in 1974 at 31 out of 1030 stations (3 percent). The 24-hour SO₂ standard was exceeded at 5 percent of the reporting stations. In the 1960's, high SO₂ concentrations were recorded within large urbanized areas and those show the strongest reduction of SO₂ concentrations. In smaller cities, the concentrations have remained essentially constant for about the past 5 years, at about 18 µg/m³ (U.S. Environmental Protection Agency (ref. 1)).

The historical data base for sulfate (SO₄²⁻) concentrations is less satisfactory. Inspection of the existing data (Frank and Possiel (ref. 5)) reveals decline of sulfate in large metropolitan areas and an upward trend over the past 10 years in rural and small urban areas. Over 90 percent of the National Air Surveillance Network (NASN) monitoring sites are located in urbanized areas, while the emissions have been shifting away from central city locations and are now emitted from taller stacks. Thus, the overall strong decline of SO₂ concentrations and the more or less constant sulfate levels are most likely due to the redistribution of source location and emission height. This speculative argument is currently under study by both governmental and industrial research teams.

Transformations

The primary pollutant, SO₂, is subject to chemical reactions in the atmosphere which lead to a change in the oxidation state, most commonly to SO₄²⁻. The reactions are accompanied by gas-particle conversion having as the end product particulate sulfur which is a secondary pollutant.

Evidence is accumulating that the effects of sulfur oxides (e.g., on terrestrial and aquatic ecosystems, health, visibility, weather and climate modification, material damage) are associated with the reaction products rather than with SO₂ itself. For this reason, an appreciable fraction of current sulfur research is focused on the SO₂ transformations. The questions of main concern pertain to (1) the mechanism and rate of conversion, (2) the fraction of SO₂ transformed to sulfate, and (3) the chemical and physical properties of the particulate sulfur.

It is the current understanding that the oxidation of SO₂ without the presence of interfering compounds is slow compared with the observed or inferred atmospheric conversion rates. Hence, the current challenge of atmospheric

chemistry is to determine which substances and environmental or emission parameters promote or inhibit SO₂ oxidation in the atmosphere.

From the point of view of effective controls, the specific questions are

(1) Is the aerosol formation rate linearly proportional to SO₂ concentration? If so, "linear rollback" control strategies will work as expected; a cutback in SO₂ emissions will lead to a proportional reduction of sulfates. It is conceivable, however, that the conversion rate is dominated by external parameters and is only weakly dependent on SO₂. In that case, large reductions of SO₂ would yield only marginal improvement in sulfate levels.

(2) Are the oxidizing agents of SO₂ man-made and can they be controlled? If SO₂ oxidation is promoted by man-made oxidizing agents (as it is now suspected), then the specific role of those substances (e.g., the HO radical) should be established and the means of their control should be explored.

(3) Do natural (e.g., meteorological) parameters influence the SO₂ conversion? Temperature, humidity, solar radiation, or any other natural parameter may influence the conversion rate and offer a possibility of supplemental controls.

(4) What is the chemical composition of the particulate sulfur? Acidic aerosol is believed to be environmentally more harmful than neutral aerosol. The conditions that favor acid aerosol formation should be established.

In order to answer these questions, an understanding of the SO₂ conversion mechanisms is necessary. Following is a brief account of the current understanding of the subject. There are four mechanisms which are believed to be of significance for atmospheric SO₂ conversion.

Indirect photooxidation is a major route for SO₂-to-sulfate conversion in the troposphere. The SO₂ is oxidized following gas-phase collision with strong oxidizing radicals such as HO[•], HO₂[•], and CH₃O₂[•]. The sources of these radicals in the polluted troposphere are hydrocarbon-NO_x emissions, which in the process of daytime photooxidation produce oxidizing radicals as intermediate products. The SO₂ oxidation step is therefore indirectly linked to photochemistry. The chemical kinetics of this mechanism has been formulated in models using measured rate constants (Calvert et al. (ref. 6)). The modeling results were consistent with laboratory tests of SO₂ conversion in the presence of photochemically reacting hydrocarbon-NO_x mixtures (Miller (ref. 7)). An unambiguous confirmation of the homogeneous conversion mechanism would require the direct observation of the reactive intermediates (HO[•], HO₂[•], CH₃O₂[•], etc.) under a variety of atmospheric conditions. Currently, such data are not available.

Numerical simulations of chemical kinetics for typical urban mixtures (fig. 3) indicate 2 to 4 percent/hour for sunny summer days (Calvert et al. (ref. 6)). Eggleton and Cox (ref. 8), in a summary of European results, conclude that in the western European summer, SO₂ oxidation rates due to gas-phase radical reactions in sunlight are expected to be between 0.5 and 5 percent/hour, depending on the degree of pollution of the atmosphere. The

lower figure refers to a cleaner troposphere. In the winter, because of the reduced sunlight intensity and duration, the conversion rates are expected to be slower by at least a factor of 2 to 5.

Smog chamber measurements occasionally show higher conversion rates (Miller (ref. 7)). It is likely that the homogeneous conversion rate will depend on the absolute concentration as well as on the initial ratio of hydrocarbons to NO_x .

The specific roles of temperature, dew point, solar radiation, solar intensity, and so forth in the indirect photooxidation require systematic future studies. The current understanding is sufficient, however, to incorporate gas-phase chemistry into large-scale reactive plume models.

Catalytic SO_2 oxidation in droplets has been studied extensively, but the results regarding its role in the atmosphere are less conclusive. The consensus at the International Symposium on Sulfur in the Atmosphere in Dubrovnik, Yugoslavia, was as follows (ref. 4):

"The catalyzed oxidation of SO_2 in solution by transition metals (e.g., Fe, Mn) is believed to be important in situations in which relatively high ($>10^{-5}$ M) concentrations of catalyst are present in the droplet and in which the total atmospheric concentrations of catalytic elements are also high. Such conditions can exist in urban and stack plumes and perhaps in urban fogs. In cleaner rural air this reaction would occur only in clouds. However, unless the pH and metal concentrations in cloud water are substantially different from those in rain water, this process is unlikely to be of significance. Both laboratory and field studies of such reactions are necessary."

Oxidation in the liquid phase by strong oxidants has recently been receiving increasing attention (Eggleton and Cox (ref. 8) and Beilke and Gravenhorst (ref. 9)). Ozone and H_2O_2 absorbed in liquid droplets can promote the oxidation rate to be comparable with or exceed the indirect photooxidation rate. However, the current oxidation rate data vary by 2 orders of magnitude which prohibits an assessment of its importance in the atmosphere. The ozone and H_2O_2 in polluted atmosphere also originate from the gas-phase photooxidation of hydrocarbon- NO_x mixtures. Within clouds or fogs, such gases are absorbed into the water droplets within seconds. Measurements of H_2O_2 in polluted and clean atmosphere are necessary as well as chamber studies to resolve the discrepancy of existing laboratory data.

Surface catalyzed oxidation of SO_2 upon collision with solid particles has been demonstrated in the laboratory. Elemental carbon (soot) appears to be particularly effective in this regard (Novakov et al. (ref. 10)). However, since the existing data refer to SO_2 oxidation on filters containing soot, the importance of this mechanism for suspended aerosol formation cannot be assessed quantitatively.

Common features of the major SO_2 conversion mechanisms discussed are that (1) the rate-controlling species can be identified, (2) they may, in principle, be controlled independently from SO_2 , and (3) their source is not necessarily

that of the SO_2 . It is regrettable that currently only the indirect photo-oxidation mechanism can yield SO_2 oxidation rates, and therefore one cannot evaluate the relative importance of each mechanism. A major difficulty with the interpretation of laboratory liquid-phase reaction results is that in the atmosphere that reaction probably occurs in events (clouds) rather than continuously.

Removal

The residence time and the transport distance of sulfur are essentially determined by the overall removal rate of sulfur compounds from the atmosphere. The overall removal has four major components: dry removal of SO_2 , wet removal of SO_2 , dry removal of SO_4^{2-} , and wet removal of SO_4^{2-} . Dry removal of SO_2 and wet removal of SO_4^{2-} appear to be the two major components.

Dry removal is a mass transfer process whereby SO_2 is first transported to surfaces by turbulent and molecular diffusion and then removed by adsorption or absorption at the surface. The overall mass transfer rate can be characterized by a mass transfer coefficient (v_d) and the difference between the bulk and surface concentrations. Since the units of v_d are length per time, it is called "deposition velocity." Conceptually, it is also convenient to utilize the overall resistance to mass transfer $r = 1/v_d$, which is the sum of several, largely independent resistances.

The ranges of deposition velocities were summarized at ISSA in Dubrovnik, and are given in table I.

The surface resistance (r_s) incorporates adsorption and absorption. In case of vegetation, r_s is believed to be dominated by the size of the stomatal openings. The aerodynamic resistance (r_a) is due to turbulent diffusion in the atmospheric surface layer and controls the dry deposition rate during stable (inversion) conditions.

Wet removal of sulfur compounds proceeds through the collection of material into cloud droplets and the subsequent deposition in rain. The wet removal rate, therefore, can be estimated from the sulfur content and the rate of rainfall. Table II summarizes the current estimates of wet and dry deposition rates.

Wet and dry removal rates are evidently of comparable magnitude, dry deposition dominating the SO_2 removal (about 60 percent of the total) and wet deposition dominating the SO_4^{2-} removal (40 percent). Both removal processes limit the lifetime of sulfur compounds to 2 to 3 days (Workshop (ref. 4)).

The residence time of the sulfur dioxide is determined by the competing rates of transformations to sulfate and of removal of SO_2 and SO_4^{2-} . Taking a conversion rate of 1 to 2 percent/hour and an overall removal rate of 2 to 5 percent/hour leads to a characteristic residence time of 14 to 33 hours or about 1 day for SO_2 .

The residence time of sulfate is the sum of the formation and removal times. According to the current estimates (Workshop (ref. 4)), the sulfate residence time is between 3 and 5 days.

Sulfur Transport

The concentrations and the fate of atmospheric sulfur are influenced by meteorology through the horizontal and vertical transport mechanisms. Horizontal transport characterized by the wind speed field provides dilution and "long-range transport"; the turbulent eddy exchange in the vertical direction disperses the matter within the mixing layer and delivers the pollutants to the surfaces for the dry deposition. The mixing of plume material with the potentially reactive background air is facilitated by both horizontal and vertical dispersion.

The characteristic residence time is on the order of 1 day for SO₂ and about 1 week for sulfate. A typical transport speed in the planetary boundary layer (1 km) is about 500 km/day; hence, the transport distances are on the order of 500 km for SO₂ and 3000 km for sulfate. The meteorological framework in which sulfur transport needs to be considered is therefore over the synoptic scale. The recognition of this fact leads to the strong current interest in the long-range transport (OECD (ref. 11) and Ottar (ref. 12)), specifically to the question of sulfur transport across national boundaries.

FIELD OBSERVATIONS OF SULFUR BEHAVIOR

Laboratory studies of sulfur transformations (smog chamber and bucket experiments) and of dry and wet removal generally are designed for a systematic parameter by parameter examination of these processes. The utility of these studies is that they may elucidate the possible atmospheric mechanism and rates. The burden of establishing the actual mechanism and rates falls upon the field experiment.

Field observations may be conducted over the mesoscale range (about 100 km) or on the regional scale (about 1000 km). Both the experimental approach and the obtained results are quite different for mesoscale and regional studies.

Regional-Scale Monitoring and Modeling

In this approach, an emission inventory over a region and meteorological transport parameters are used as inputs to regional-scale (order of 1000 km) transport models. The models also incorporate the rates of SO₂ conversion and removal. The actual rate constants are unknowns but they can be extracted from a best fit comparison between calculated and observed values. In the OECD study of Long-Range Transport of Air Pollutants (ref. 11), the trajectory models were tuned to monitoring data obtained daily at about 70 (European) stations. The measured daily concentration data for SO₂, SO₄⁻, and SO₄⁻ in precipitation were compared with calculations, and the rate constants for transformations and

dry and wet removal were adjusted until a best fit was obtained. The key model parameters for the OECD study are listed in table III.

The year-round average conversion rate of 1 to 2 percent/hour and the overall average dry removal rate of about 3 to 4 percent/hour are key new results of the OECD study. Studies similar in scope and objectives to the OECD study are being conducted in the United States. The Sulfate Regional Experiment (SURE) (Perhac (ref. 13)) by the Electric Power Research Institute, the Multistate Atmospheric Power Production Pollutant Study (MAP3S) (MacCracken (ref. 14)) by the Department of Energy, and the Sulfur Transport and Transformations in the Environment (STATE) (Robinson (ref. 15)) by the Environmental Protection Agency are examples of projects.

The main utility of the regional approach is that the obtained rate constants are inherently averages over all sources and spatial-temporal scales of interest. It is recognized, however, that the rate constants for removal and transformations are actually variables which may depend on source configuration, meteorological parameters, and external (non-sulfur) species present.

A pictorial illustration of long-range transport is given in figure 4 (Husar et al. (ref. 16)). Contour maps of noon visibility outline the spatial extent and temporal changes of a hazy air mass over the eastern half of the United States. Inspection of the sequence of contour maps reveals that during the 2-week period, multistate regions were covered with the haze layer in which the noon visibility was less than 9.6 km. Long-range trajectory calculations and evaluation of surface wind data from the weather stations indicate that the hazy air mass located south of the Great Lakes (June 25 to 27) entered the continental United States in Louisiana and moved northward somewhat east of St. Louis. The air movement directions were also checked by surface wind directions obtained at the weather stations.

During June 28 to 30, the "blob" drifted slowly westward under easterly winds, passing over St. Louis, Missouri, on June 28 and 29 and then continuing across Missouri, Kansas, Iowa, and Minnesota for the next 2 days (July 1 and 2). Starting on July 3, the hazy air mass was transported to the southeast corner of the continental United States by a southward-moving Canadian front. By July 5, the hazy air mass caused visibility deterioration of less than 6.4 km over Atlanta, Georgia, Birmingham, Alabama, and Tallahassee, Florida.

The daily weather charts for the period from June 29 to July 4, 1975, are shown in figure 5 (Husar et al. (ref. 16)). A major feature of the weather system during that period was the tropical storm Amy, located off the northeast coast. By its presence, the tropical storm provided a barrier against large-scale eastward motion. From the northwest, a front was approaching the Great Lakes. With the advance of the Canadian front toward the southwest, the high-pressure zone located between the front and the tropical storm Amy drifted slowly to the southwest, passing over Missouri on July 2 and 3. By July 4, the front itself reached Missouri.

The two passages of the blob over St. Louis, Missouri, are confirmed by the two peaks (June 27 to 29 and July 2 to 4) of the light scattering coefficients (b_{scat}) measured locally with integrating nephelometers (fig. 6(a)). A

similar temporal pattern may be observed (fig. 6(b)) for the extinction coefficients (b_{ext}), based on visibility observations in St. Louis, Missouri, and in Springfield, Illinois. The similarity of b_{scat} and b_{ext} patterns at distant monitoring points confirms that the major changes in the light scattering and extinction coefficients during this case study have spatial scales substantially larger than the St. Louis metropolitan area. Also, these observations confirm that the light scattering aerosol is the result of external inflow, rather than the result of local source contributions. The correlation between b_{scat} and b_{ext} shown in figure 6 demonstrates the utility of visibility observations as a qualitative surrogate for measurements of the light scattering aerosol concentration.

The daily average sulfate concentrations using high-volume filters were measured before, during, and after the passage of the hazy air mass over St. Louis, Missouri. High-volume filter samples, collected every 6 days by the St. Louis County Department of Health, were analyzed for particulate sulfur by using the flash volatilization-flame photometric detection method (Husar et al. (ref. 17)). An increase from $9.2 \mu\text{g}/\text{m}^3$ on June 23 to $32.7 \mu\text{g}/\text{m}^3$ on June 29 is shown in figure 6. The sulfate content then dropped to $8.0 \mu\text{g}/\text{m}^3$ on July 5 after the passage of the Canadian front. Sulfate accounted for 19 percent of total aerosol mass before, 34 percent during, and 15 percent after the passage of the hazy air mass. The daily average sulfate concentrations were compared with daily average b_{ext} (uncorrected for relative humidity effects) for the entire summer (June, July, and August 1975). The correlation coefficient was found to be $r = 0.7$ and the regression equation for 16 points was $b_{\text{ext}}(10^{-4}\text{m}^{-1}) = 3.24 + 0.11[\text{SO}_4^{2-}](\mu\text{g}/\text{m}^3)$. These results tend to suggest that a substantial fraction of the haze aerosol, particularly during the passage of blobs, is associated with sulfates.

This brief analysis of national visibility data, local air pollution data, and synoptic air parcel trajectories points toward two intriguing phenomena. First, multistate-scale haziness may be caused by long-range transport from sources 1000 km or more away, and secondly, the haze aerosol ($<1 \mu\text{m}$ in diameter) in such air masses is largely composed of sulfates.

By inspection of visibility contour maps for June, July, and August 1975, the author has identified six blobs with an average residence time of 8 days over various multistate regions of the midwestern and eastern United States. In the St. Louis metropolitan area, the hazy air masses were accompanied by high midday ozone concentrations, generally exceeding the ambient air quality standard of 0.08 ppm.

Establishing the spatial distribution and the movement of hazy air masses is only the first step toward the understanding of their characteristics and their impact on human health and welfare, on weather and climate, and on other aspects of the ecosystem. The remaining major questions pertain to the sources of hazy air masses (both anthropogenic and natural), to gaseous precursors of haze particles, to the environmental conditions which promote their development, and to the fate of such hazy air masses.

Mesoscale Plume Studies

The average rate constants for transformation and removal may be obtained from the regional monitoring and modeling efforts. However, the specific dependence of the rates on the underlying chemical and physical processes has to be studied on a smaller scale. The gap between regional-scale (1000 km) and laboratory simulation can be bridged by mesoscale studies of sulfur transport, transformations, and removal (transmission). These are generally referred to as plume studies. Inherently, quantitative single plume studies are limited to a spatial scale of less than 500 km and a plume age below 12 hours.

The results of a 4-year plume mapping study (Midwest Interstate Sulfur Transformation and Transport (MISTT): Wilson (ref. 18)) conducted in St. Louis, Missouri, on the Labadie power plant (2400 MW, 6 kg/sec sulfur output, and 218 m stack height) show that the transport, transformations, and removal processes in power plant plumes all have diurnal cycles (fig. 7).

Transformations.- The daytime conversion rate was observed to be quite variable, between 1 and 4 percent/hour, while the nighttime values were consistently below 0.5 percent/hour (Husar et al. (ref. 19)). Hence, in the midwestern United States, during summer, the conversion-rate-controlling parameter was associated with the time of day. The data were insufficient to conclude which mechanism controlled the daytime conversion because the observed variation was consistent with indirect photooxidation as well as with liquid-phase oxidation in clouds. Observations of aerosol size spectrum dynamics in plumes (Whitby et al. (ref. 20)) have shown, however, that homogeneous nucleation occurred consistently. Gillani et al. (ref. 21) noted that the aerosol formation in the same plumes is frequently accompanied by ozone formation within the plume. Both of these observations would support homogeneous indirect photooxidation. However, in summer in the St. Louis region, the plume material is transferred through clouds at least once on most days. Hence, the estimation of the relative contributions of homogeneous and heterogeneous chemistry is not possible at this time.

Horizontal transport.- The speed at which plume material is transported over a given location is a function of both height and time. For the St. Louis region, the Regional Air Pollution Study (RAPS) provides an extensive data base for the time-height dependence of wind speed and direction as well as temperature and dew point (Myers and Reagan (ref. 22)). The average vertical profiles of wind speed and their standard deviation from July 1976, are shown in figure 8(a). Vertical velocity soundings at 1300 CDT show on the average a uniform speed of 4 to 5 m/sec up to about 1000 m. Hence, the noon wind speed within the planetary boundary layer is less than the geostrophic wind speed (6 m/sec) above, because of the drag of buoyant thermals. At 1900 CDT, there is evidence of an increase in speed between 300 and 600 m which becomes more pronounced at 0100 CDT. The peak average speed of 12 m/sec is recorded at 450 m, with a strong vertical shear near the ground and a weaker shear layer between 450 and 1200 m. The high wind speed at 450 m is called a low-level jet, and it is illustrated in more detail by Smith et al. (ref. 23). By 0700 CDT, the vertical profile has become more homogeneous at reduced speeds, with the exception of the lowest 200 m, which is already subject to drag from the nascent mixing layer. The diurnal pattern of the wind speed obtained from

hourly averages at seven heights is shown in figure 8(b). The ground-level (10 m) wind speed is obtained from RAPS surface measurements. The figure illustrates that within the diurnal cycle in the St. Louis region, nighttime plume transport is greater than at midday by a factor of nearly 2. Nocturnal plumes emitted from tall stacks are affected by 10 to 20 m/sec low-level jets in two ways: their effective stack height is reduced because of the crosswind, and the distance traveled overnight is increased to as much as 500 km. Since such plumes are subject to minimal vertical mixing, aircraft sampling is feasible up to several hundred kilometers.

In addition to the longitudinal and vertical transport, plume dispersion also occurs by "veer," that is, wind directional change with height. The vertical profiles of veer for a given hour were obtained by taking the absolute value of the directional change per 100 m. Of the four profiles shown in figure 8(c), the 1400 CDT readings showed the least average veer. Evidently, the vigorous daytime mixing inhibits the development of such lateral dispersion. Soundings at 0400 CDT exhibited the strongest veer effects near the surface, supporting the notion that the low-level nocturnal jet is decoupled from the surface stable layer.

Therefore, while transformation has been shown to be a daytime mechanism, the long-range transport in the midwestern United States is primarily a nocturnal phenomenon.

Vertical transport.- Pollutants are delivered by turbulent mass transfer from the plume height to the roughness height of the canopy level, where dry deposition takes place. During the daytime, the lower levels of the atmosphere are heated by the warmer surface causing convective mixing between the surface and an inversion layer, sometimes referred to as the lid of the mixed layer. The height of the mixed layer has a characteristic diurnal pattern. For the St. Louis region, this pattern is illustrated in figure 7(a), which shows that the mixed layer height rapidly increases from near ground level in the morning to 1000 m at noon and then levels off at about 1200 m by midafternoon. At night, the convective mixing tends to die out because of the development of a cold stable air layer near the ground. The former mixed layer becomes thermally stratified and pollutants tend to remain in the strata into which they were introduced.

In the afternoon, the low wind speed and slight instability of the mixed layer permit thermally buoyant plumes to rise without appreciable transport or dilution up to the inversion layer, which usually persists at 1000 to 1500 m. The large effective stack height of afternoon buoyant plumes has important consequences regarding sulfur transformations and removal, that is, the sulfur budget.

The rise of thermals above cities, industrial areas, and power plants is well documented in the "heat island" literature. In St. Louis, development of thermals has been frequently observed over the Wood River refinery complex, causing industrial cumulus formation sometimes penetrating the inversion layer (e.g., Auer (ref. 24)). Similar cumulus formation has also been noted over the 2400-MW Labadie power plant. It is recognized that such cloud formation is

only possible under light wind conditions. The average wind speed in the mixed layer during the convective hours is between 4 and 5 m/sec (fig. 8(b)). When there is an appreciable wind, the rising buoyant plume is bent in the direction of the wind flow and reaches the top of the mixed layer without penetrating it. The dilution of such a plume is minimal, and it persists overnight as "convective debris" (Edinger (ref. 25)) at 1000 to 1500 m. Hence, the plume center line is just below the upper inversion lid. Such a plume will remain in an elevated stratified layer until the next day when the rising mixing layer reaches the plume.

There are two consequential phenomena of the diurnal vertical plume transport pattern worth emphasizing: (1) the decoupling of the daytime mixed layer from the underlying surface via the nocturnal inversion, and (2) the lifting of late afternoon plumes which remain in high strata at least until the following noon when they may or may not be entrained in the mixing layer.

Dry removal.- Unlike the field measurement of sulfur transformation which has a measurable product in the form of particulate sulfur, the estimation of removal rates is inherently more difficult. Removal rate is obtained from the difference between total sulfur (S_T) at two heights (gradient method) or at two plume ages (plume budget method). The difficulties which appear in practice in such estimates arise from taking the difference of two values of comparable magnitudes, each with uncertainties comparable with the difference. This is particularly true for elevated plumes emitted from tall stacks, where removal is often not appreciable for the first several hours of plume age. This necessitates the combined use of deposition velocity estimates, ground-level concentration data in the vicinity of power plants, and sulfur budget data from plume mapping experiments, as described by Husar et al. (ref. 19).

TWO-BOX MODEL OF THE SULFUR BUDGET IN LARGE PLUMES

The essence of the previous considerations of dispersion is that the plume has two distinctly different regimes during the diurnal cycle. The first regime develops when the plume is decoupled from the underlying surfaces by radiation inversion or by other stable strata. In this regime, material is lost by entrainment into a second mixing-deposition regime. In the second regime, the plume is dispersed rapidly within the mixed layer, loses material at the surface, and gains material by entrainment from above. Conversion of gaseous sulfur to particulate sulfur occurs in each regime. During its lifetime, the plume sequentially passes through these two regimes every day, as illustrated schematically in figure 9.

For estimating the sulfur budget in a plume passing through the diurnal cycle, it is instructive to describe the system in terms of a "two-box model." The sulfur budget at any given time can then be obtained by carrying out the mass balance in each of the boxes. Box I shall be the quiescent "aging reservoir," decoupled from the surface. The mass balance equation for gaseous sulfur S_g and for particulate sulfur S_p in box I can be written as follows:

$$\frac{d}{dt} S_g^I = - \frac{1}{H'} \frac{dH}{dt} S_g^I - k_t S_g^I$$

$$\frac{d}{dt} S_p^I = - \frac{1}{H'} \frac{dH}{dt} S_p^I + k_t S_p^I$$

where t is time, H is the mixing layer height, H' is the difference between the maximum mixing layer height and H , and k_t is the transformation rate constant. The first terms on the right-hand sides of the equations signify the transfer of material from box I to box II due to the rising mixed layer height. The second terms are the conversion terms.

The material balance for the mixing-transformation-removal box II can be written as follows:

$$\frac{d}{dt} S_g^{II} = \frac{1}{H'} \frac{dH}{dt} S_g^I - k_t S_g^{II} - d_g S_g^{II}$$

$$\frac{d}{dt} S_p^{II} = \frac{1}{H'} \frac{dH}{dt} S_p^I + k_t S_p^{II} - d_p S_p^{II}$$

The terms involving the dry removal rate constants d_g and d_p are the dry removal terms for gaseous and particulate sulfur, respectively (Husar et al. (ref. 19)).

During the nighttime, elevated plumes are emitted into the reservoir box and reside there until entrainment into the next day's mixed layer. Daytime emissions are also held in the reservoir box for a characteristic "mixing time," following which perfect mixing is assumed. All plume material is then transferred into the mixing-transformation-removal box (fig. 9). At 1800, the collapse of the mixing height, followed by the decoupling of the surface layer from the former mixed layer, is interpreted as a "catastrophe." The consequence of this abrupt transition is to transfer the bulk (90 percent) of the plume material back into the reservoir box. A token amount (10 percent) of the material is retained in the mixing-transformation-removal box of the nocturnal mixing layer and is subject to dry deposition. By morning, the stable layer near the ground is nearly depleted of SO_2 , while the mass in the reservoir is conserved. At 0600, the rising mixed layer starts to entrain material from box I to box II and subjects an increasing amount of matter to dry removal. By late afternoon, practically all material has been transferred to the mixing box II, followed by a repeat of the catastrophic transfer from box II to box I at 1800.

The gaseous and particulate sulfur contents of the two boxes are displayed in figure 9 for a 4-day period following emission. The foregoing kinetic process may be envisioned in terms of a "two-bucket analogy," in which the reservoir bucket, box I, is connected to a mixing-transformation-removal bucket, box II, through a pipe regulated by a valve which represents entrainment. Bucket II has a porous bottom, reflecting dry removal at the surface. The contents of the reservoir bucket are slowly transferred to bucket II which through its porous bottom loses about 40 percent of its contents during the first day. At 1800, the remaining contents are poured back into the reservoir and the process repeats itself.

The plume sulfur budget is obtained by combining the gaseous and particulate sulfur content of both boxes to get the total amount converted to S_p and that remaining as S_g . Such sulfur budgets are shown in figure 10 for four release times. In the budget figures, the dotted upper portion represents the cumulative percent of aerosol formed. The lower hatched area stands for the cumulative fraction of removal by dry deposition. The open area in between is the gaseous sulfur remaining in the atmosphere. For each of the four emission types, both aerosol formation and dry removal occur in daily waves with peak effects during the daylight hours. Overall, however, the SO_2 decay resembles that of an exponential function.

It is recognized, of course, that the model results can be no better than their input. Nevertheless, the consequences of the previously derived diurnal pattern of plume dispersion, transformation, and removal upon the calculated sulfur budget will be examined next. The most intriguing is the afternoon emission at 1600 CDT. The plume leaving the stack rises to nearly 1000 m and undergoes some transformation (10 percent) without removal overnight. It is not until noon the next day that the plume is entrained into the mixed layer, and by that time about 16 percent of the original sulfur mass has already converted to S_p form. Following entrainment in the mixed layer, the S_g decay is roughly exponential; about half of the decay is due to transformation and half to removal.

The 2200 CDT emission is also emitted into a stable, but lower, stratus and is therefore mixed earlier the next morning, about 1000 CDT. In this case, as well as for the 0400 CDT emission, the transformation and removal processes have their first major impact almost simultaneously. The morning emission at 1000 CDT is injected within the mixed layer and therefore is exposed to the ground within less than 1 hour. Here again, SO_2 depletion by transformation and removal starts simultaneously.

Figure 11(a) shows the fraction of total gaseous sulfur which is converted to sulfate aerosol at plume ages of 6 hours up to 8 days. The total fraction converted ranges between 30 and 45 percent, which is attained within 8 days. For the average daily emission, about half of the ultimate particulate sulfur is formed within 24 hours after emission. The highest fraction converted (45 percent) belongs to the afternoon emissions, because of their head start in conversion. This exercise points to the late afternoon releases as most conducive to sulfate formation and provokes the thought that any reduction in the afternoon emissions would yield a most efficient sulfate reduction.

The formation time for particulate sulfur, expressed in terms of the time required to form 50 and 66 percent of the ultimate S_p (fig. 11(b)), has a characteristic value between 25 and 40 hours. There is a significant variation of the 1/e decay time of S_g ranging between 26 hours for the 1000 CDT emission to 46 hours for the 1600 CDT emission (fig. 11(c)). The SO_2 half-life exhibits even more variability, varying from 10 hours for the 0800 CDT emission to 38 hours for the 1600 CDT emission.

The characteristic transport distances associated with different plume ages are estimated as follows: (1) a plume height or range of heights was assigned to each hourly emission throughout its mixing history; (2) the horizontal wind speed $\bar{u}(t)$ was obtained from the RAPS data of figure 8. The travel distance is therefore a numerical integral of $\bar{u}(t) \Delta t$ from the emission time. The transport distance (\bar{x}) obtained is the range to which the plume would travel if the wind direction and wind speed were invariant in space; this being unlikely, the characteristic distance may at best approximate the distance traveled along a curved synoptic-scale trajectory. The calculated distances for 6, 12, and 24 hours and for 1/e decay time are shown in figure 11(d). The low \bar{x} of 200 km at 12 hours age for 0600 CDT emissions arises from the low daytime transport velocity within the mixing layer. The plume emitted at 2000 CDT travels to $\bar{x} = 410$ km within the first 12 hours. After 24 hours of plume age, \bar{x} is 600 km irrespective of emission time. From the point of view of plume impact, it is also worth estimating the distance the plume travels when SO_2 has decayed to a fraction 1/e of its initial value (fig. 11(d)). Because of the low 1/e decay time, the impact distance is about 700 km for the 0600 to 1200 CDT emissions; the distance then rises rapidly to over 1000 km for the 1400 to 2400 CDT emissions. Hence, not only does the afternoon plume appear to have higher sulfate formation, but it seems that its SO_2 impact is further away from the plant.

CONCLUSIONS OF INTERNATIONAL SYMPOSIUM ON SULFUR

IN THE ATMOSPHERE

It seems appropriate to state here the conclusions of the International Symposium on Sulfur in the Atmosphere (ISSA) as perceived by this author.

(1) Global sulfur budget: The revision of the global natural sulfur emission rate from about 100 to 30 Tg/year (Granat et al. (ref. 2)) has not been disputed at ISSA. Hence, it is the current thinking that man contributes about 60 percent of the global sulfur emissions, most of it over northwestern Europe and the industrialized part of North America (≈ 5 percent of the Earth's surface).

(2) Regional budgets: (a) Recent data show that the concentration of natural sulfur compounds over continental Europe is low compared with man-made sulfur (Georgii (ref. 26)); (b) there is a close resemblance of the airborne sulfur concentration and the man-made sulfur emission field over northwestern Europe (Ottar (ref. 12)); (c) high sulfur concentrations in rain over "remote" European stations are now largely attributed to long-range transport of man-made sulfur rather than to natural sources (Granat et al. (ref. 2)). It

follows that the natural source strength is small (<10 percent) compared with man-made emissions over northwestern Europe (Rodhe (ref. 3)). By inference, this also holds for northeastern United States and southeastern Canada.

(3) Removal: Dry and wet removal rates are of comparable magnitude and the overall average removal rate is about 2 to 3 percent/hour. Dry removal rate is controlled both by the stomatal resistance of the vegetation and by the atmospheric resistance to mixing (Garland (ref. 27) and Hales (ref. 28)).

(4) Transformations: The average oxidation rate over the lifetime of SO_2 is about 1 to 2 percent/hour as obtained by fitting the rate constants in regional-scale models to European monitoring data (Eliassen (ref. 29)). In plumes of a midwestern United States power plant, the daytime conversion rate was measured to be 1 to 4 percent/hour and <0.5 percent/hour at night (Husar et al. (ref. 19)). Laboratory simulations of gas-phase-controlled SO_2 conversion in the presence of oxidizing radicals (Calvert et al. (ref. 6) and Eggleton and Cox (ref. 8)) come "embarrassingly close" (Friedlander (ref. 30)) to the 1 to 2 percent/hour daily average conversion rate. The contribution of liquid-phase oxidation is not well established, but it is thought to be significant (Beilke and Gravenhorst (ref. 9), Hegg and Hobbs (ref. 31), and Workshop (ref. 4)).

(5) Aerosol: About 20 to 50 percent of the SO_2 converts in the atmosphere to aerosol, and the product has been positively identified to be SO_4^- ion (Stevens et al. (ref. 32)). The main cations are NH_4^+ or H^+ depending on the air mass history (Brosset (ref. 33) and Charlson et al. (ref. 34)). The sulfate (except in marine aerosol) is in the submicrometer size range (Whitby et al. (ref. 20), Jaenicke (ref. 35), Newman (ref. 36), and Stevens et al. (ref. 32)). For gas-phase-controlled conversion, the aerosol growth kinetics is qualitatively understood (Friedlander (ref. 30), Whitby et al. (ref. 20), and Workshop (ref. 4)).

(6) Residence times: The turnover (average residence) times are about 1 day for SO_2 ; 3 to 5 days for SO_4^- , and about 2 to 3 days for sulfur (Rodhe (ref. 3) and Workshop (ref. 4)). The corresponding transport distances may be estimated by taking a speed of about 500 km/day.

(7) Large projects: Large-scale monitoring networks (Ottar (ref. 12), Perhac (ref. 13), Whelpdale (ref. 37), and MacCracken (ref. 14)) in conjunction with long-range transport models (Eliassen (ref. 29) and Fisher (ref. 38)) are useful tools for the estimation of regional-scale (order of 1000 km) distribution and budgets. On the other hand, mesoscale or plume studies (Wilson (ref. 18)) elucidate the diurnal pattern and other details of transport, transformation, and removal processes. A continuous exchange of findings and some coordination of these projects is desirable.

REFERENCES

1. Monitoring and Air Quality Trends Report, 1974. EPA-450/1-76-001, U.S. Environ. Prot. Agency, Feb. 1976. (Available from NTIS as PB 252 269.)
2. Granat, L.; Rodhe, H.; and Hallberg, R. O.: The Global Sulphur Cycle. *Ecol. Bull.*, vol. 22, 1976, pp. 89-134.
3. Rodhe, Henning: Budgets and Turn-Over Times of Atmospheric Sulfur Compounds. *Atmos. Environ.*, vol. 12, no. 1-3, 1978, pp. 671-680.
4. [ISSA] Workshop. *Atmos. Environ.*, vol. 12, no. 1-3, 1978, pp. 7-23.
5. Frank, Neil H.; and Possiel, Norman C.: Seasonality and Regional Trends in Atmospheric Sulfates. Paper presented before Div. Environ. Chem., American Chem. Soc. (San Francisco, California), Aug.-Sept. 1976.
6. Calvert, Jack G.; Su, Fu; Bottenheim, Jan W.; and Strausz, Otto P.: Mechanism of the Homogeneous Oxidation of Sulfur Dioxide in the Troposphere. *Atmos. Environ.*, vol. 12, no. 1-3, 1978, pp. 197-226.
7. Miller, D. F.: Precursor Effects on SO₂ Oxidation. *Atmos. Environ.*, vol. 12, no. 1-3, 1978, pp. 273-280.
8. Eggleton, A. E. J.; and Cox, R. A.: Homogeneous Oxidation of Sulphur Compounds in the Atmosphere. *Atmos. Environ.*, vol. 12, no. 1-3, 1978, pp. 227-230.
9. Beilke, S.; and Gravenhorst, G.: Heterogeneous SO₂-Oxidation in the Droplet Phase. *Atmos. Environ.*, vol. 12, no. 1-3, 1978, pp. 231-239.
10. Novakov, T.; Chang, S. G.; and Harker, A. B.: Sulfates as Pollution Particulates: Catalytic Formation on Carbon (Soot) Particles. *Science*, vol. 186, no. 4160, Oct. 18, 1974, pp. 259-261.
11. The OECD Programme on Long Range Transport of Air Pollutants - Measurements and Findings. *Organ. Econ. Coop. & Dev.*, 1977.
12. Ottar, B.: An Assessment of the OECD Study on Long Range Transport of Air Pollutants (LRTAP). *Atmos. Environ.*, vol. 12, no. 1-3, 1978, pp. 445-454.
13. Perhac, Ralph M.: Sulfate Regional Experiment in Northeastern United States: The 'Sure' Program. *Atmos. Environ.*, vol. 12, no. 1-3, 1978, pp. 641-647.
14. MacCracken, Michael C.: MAP3S: An Investigation of Atmospheric, Energy Related Pollutants in the Northeastern United States. *Atmos. Environ.*, vol. 12, no. 1-3, 1978, pp. 649-659.
15. Robinson, G. D.: Inadvertent Weather Modification Workshop. CEM Rep. 4215-604 (NSF Grant No. ENV-77-10186), Center Environ. & Man, Inc., Sept. 1977.

16. Husar, R. B.; Gillani, N. V.; Husar, J. D.; Paley, C. C.; and Turcu, P. N.: Long Range Transport of Pollutants Observed Through Visibility Contour Maps, Weather Maps and Trajectory Analysis. Washington Univ. paper presented at Third Symposium on Atmospheric Turbulence, Diffusion and Air Quality (Raleigh, North Carolina), Oct. 1976.
17. Husar, Janja D.; Husar, Rudolf B.; and Stubits, Pamela K.: Determination of Submicrogram Amounts of Atmospheric Particulate Sulfur. *Anal. Chem.*, vol. 47, no. 12, Oct. 1975, pp. 2060-2065.
18. Wilson, William E.: Sulfates in the Atmosphere: A Progress Report on Project MISTT. *Atmos. Environ.*, vol. 12, no. 1-3, 1978, pp. 537-547.
19. Husar, R. B.; Patterson, D. E.; Husar, J. D.; Gillani, N. V.; and Wilson, W. E., Jr.: Sulfur Budget of a Power Plant Plume. *Atmos. Environ.*, vol. 12, no. 1-3, 1978, pp. 549-568.
20. Whitby, K. T.; Cantrell, B. K.; and Kittelson, D. B.: Nuclei Formation Rates in a Coal-Fired Power Plant Plume. *Atmos. Environ.*, vol. 12, no. 1-3, 1978, pp. 313-321.
21. Gillani, N. V.; Husar, R. B.; Husar, J. D.; Patterson, D. E.; and Wilson, W. E., Jr.: Project MISTT: Kinetics of Particulate Sulfur Formation in a Power Plant Plume Out to 300 km. *Atmos. Environ.*, vol. 12, no. 1-3, 1978, pp. 589-598.
22. Myers, R. Lee; and Reagan, James A.: The Regional Air Monitoring System. St. Louis, Missouri U.S.A. International Conference on Environmental Sensing and Assessment, Volume 1, Sept. 1975, [paper] 8-6.
23. Smith, T. B.; Blumenthal, D. L.; Anderson, J. A.; and Vanderpol, A. H.: Transport of SO₂ in Power Plant Plumes: Day and Night. *Atmos. Environ.*, vol. 12, no. 1-3, 1978, pp. 605-611.
24. Auer, August H., Jr.: Observations of an Industrial Cumulus. *J. Appl. Meteorol.*, vol. 15, no. 4, Apr. 1976, pp. 406-413.
25. Edinger, James G.: Vertical Distribution of Photochemical Smog in Los Angeles Basin. *Environ. Sci. & Technol.*, vol. 7, no. 3, Mar. 1973, pp. 247-252.
26. Georgii, H.-W.: Large Scale Spatial and Temporal Distribution of Sulfur Compounds. *Atmos. Environ.*, vol. 12, no. 1-3, 1978, pp. 681-690.
27. Garland, J. A.: Dry and Wet Removal of Sulphur From the Atmosphere. *Atmos. Environ.*, vol. 12, no. 1-3, 1978, pp. 349-362.
28. Hales, J. M.: Wet Removal of Sulfur Compounds From the Atmosphere. *Atmos. Environ.*, vol. 12, no. 1-3, 1978, pp. 389-399.

29. Eliassen, Anton: The OECD Study of Long Range Transport of Air Pollutants: Long Range Transport Modelling. Atmos. Environ., vol. 12, no. 1-3, 1978, pp. 479-487.
30. Friedlander, S. K.: A Review of the Dynamics of Sulfate Containing Aerosols. Atmos. Environ., vol. 12, no. 1-3, 1978, pp. 187-195.
31. Hegg, Dean A.; and Hobbs, Peter V.: Oxidation of Sulfur Oxide in Aqueous Systems With Particular Reference to the Atmosphere. Atmos. Environ., vol. 12, no. 1-3, 1978, pp. 241-253.
32. Stevens, Robert K.; Dzubay, Thomas G.; Russwurm, George; and Rickel, Dwight: Sampling and Analysis of Atmospheric Sulfates and Related Species. Atmos. Environ., vol. 12, no. 1-3, 1978, pp. 55-68.
33. Brosset, Cyrill: Water-Soluble Sulphur Compounds in Aerosols. Atmos. Environ., vol. 12, no. 1-3, 1978, pp. 25-38.
34. Charlson, Robert J.; Covert, David S.; Larson, Timothy V.; and Waggoner, Alan P.: Chemical Properties of Tropospheric Sulfur Aerosols. Atmos. Environ., vol. 12, no. 1-3, 1978, pp. 39-53.
35. Jaenicke, R.: Physical Properties of Atmospheric Particulate Sulfur Compounds. Atmos. Environ., vol. 12, no. 1-3, 1978, pp. 161-169.
36. Newman, L.: Techniques for Determining the Chemical Composition of Aerosol Sulfur Compounds. Atmos. Environ., vol. 12, no. 1-3, 1978, pp. 113-125.
37. Whelpdale, D. M.: Large-Scale Atmospheric Sulfur Studies in Canada. Atmos. Environ., vol. 12, no. 1-3, 1978, pp. 661-670.
38. Fisher, B. E. A.: The Calculation of Long Term Sulphur Deposition in Europe. Atmos. Environ., vol. 12, no. 1-3, 1978, pp. 489-501.

TABLE I.- DEPOSITION VELOCITIES

[From Workshop (ref. 4)]

(a) Over vegetation

Vegetation		Height, m	Range of deposition velocity, cm/sec	Typical deposition velocity, cm/sec (a)
Height	Example			
Short	Grass	0.1	0.1 to 0.8	0.5
Medium	Crops	1.0	0.2 to 1.5	.7
Tall	Forest	10.0	0.2 to 2.0	Uncertain

^aThese values were obtained in a humid climate. Much smaller values are likely in arid climates.

(b) Over soil^b

Soil type	pH	State	Range of deposition velocity, cm/sec	Typical deposition velocity, cm/sec
Calcareous	≥7	Dry	0.3 to 1.0	0.8
Calcareous	≥7	Wet	0.3 to 1.0	.8
Acid	≈4	Dry	0.1 to 0.5	.4
Acid	≈4	Wet	0.1 to 0.8	.6

^bAs yet no information is available to assess deposition velocity on desert sand or lateritic soils.

TABLE II.- REPRESENTATIVE ANNUAL AVERAGE WET AND DRY DEPOSITION RATES

[Workshop (ref. 4)]

Location		Excess precipitation sulfate concentration, mg S/liter	Wet deposition rate, g S/m ² -yr	Dry deposition rate, g S/m ² -yr
Heavily industrialized areas	North America	3 to ?	^a 0.1 to 3	?
	Europe	3 to 20	2 to 4	3 to 15
Rural	North America	0.5 to 2	0.1 to 2	0.2 to 2.6
	Europe	0.5 to 3	0.2 to 2	0.5 to 5.0
Remote	North Atlantic Ocean	0.2 to 0.6	1 to 3	0.04 to 0.4
	Other Oceans	0.04	^a 0.01 to 0.2	<0.1
	Continents	0.1	^a 0.01 to 0.5	0.4

^aLow deposition rates result from low precipitation.

TABLE III.- PARAMETER VALUES APPLIED IN CALCULATIONS WITH THE
LAGRANGIAN DISPERSION MODEL

[The same values have also been applied in the calculations
with the trajectory model (OECD (ref. 11))]

Parameter	Definition	Value
α	Part of sulphur emission deposited locally	0.15
β	Part of sulphur emission transformed directly to sulphate	0.05
k	Decay rate SO_2 $\left\{ \begin{array}{l} \text{Rain} \\ \text{Dry} \end{array} \right.$	$4 \times 10^{-5} \text{ sec}^{-1}$ $1 \times 10^{-5} \text{ sec}^{-1}$
k_t	Transformation rate $SO_2 \rightarrow SO_4$	$3.5 \times 10^{-6} \text{ sec}^{-1}$
κ	Loss rate SO_4	$4 \times 10^{-6} \text{ sec}^{-1}$
h	Mixing height	1000 m

1973 U.S. SO_x EMISSIONS

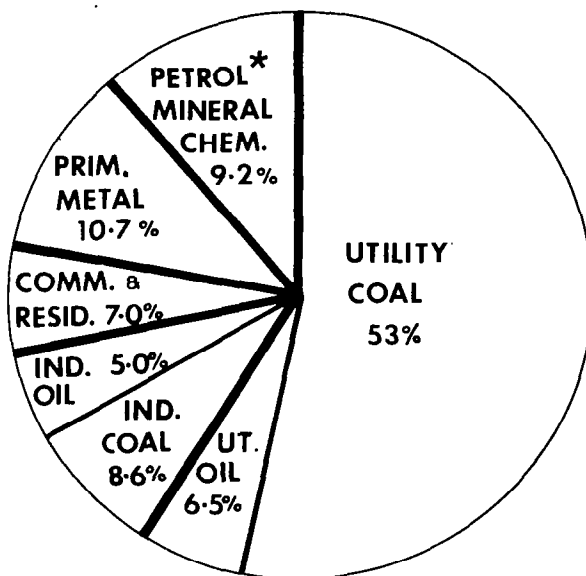


Figure 1.- Sources of SO₂ in the United States, 1973. Petrol mineral chem. section includes 2 percent attributed to transportation. (U.S. Environmental Protection Agency (ref. 1).)

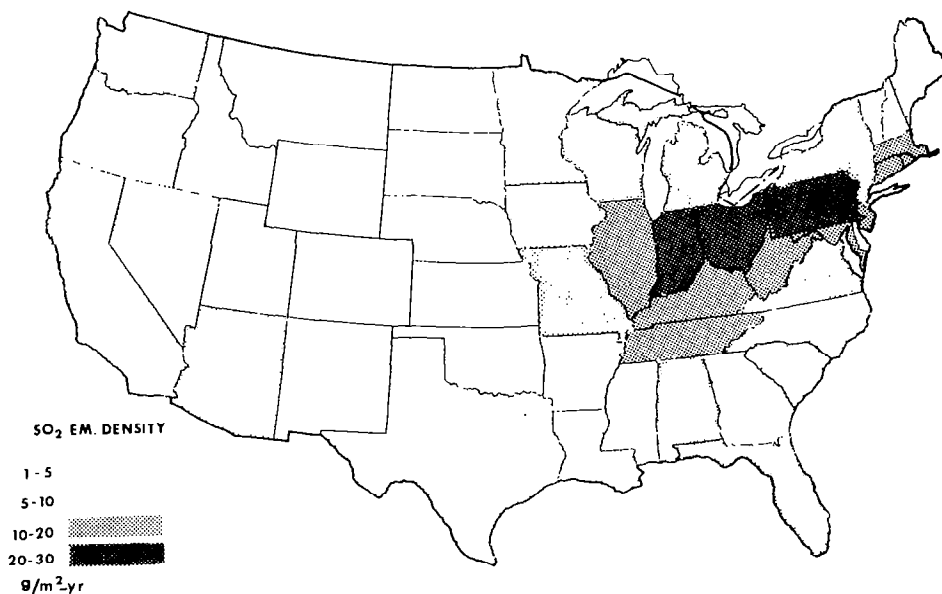


Figure 2.- SO₂ emission density by state. (U.S. Environmental Protection Agency (ref. 1).)

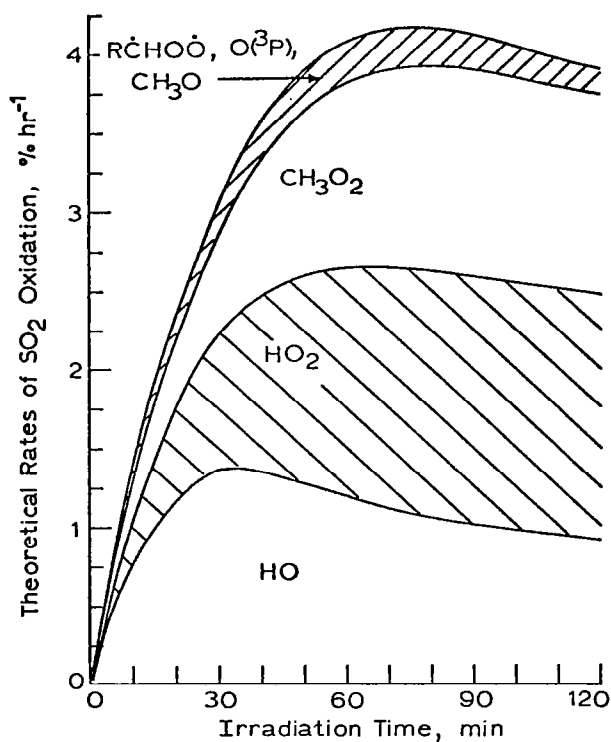


Figure 3.- Theoretical rate of attack of various free radical species on SO₂ for a simulated sunlight-irradiated (solar zenith angle = 40°) polluted atmosphere. Initial concentrations (ppm): [SO₂] = 0.05, [NO] = 0.15, [NO₂] = 0.05, [CO] = 10, [CH₄] = 1.5, [CH₂O] = 0, [CH₃CHO] = 0; relative humidity, 50 percent (25° C). (From Calvert et al. (ref. 6) with permission from Pergamon Press, Ltd.)

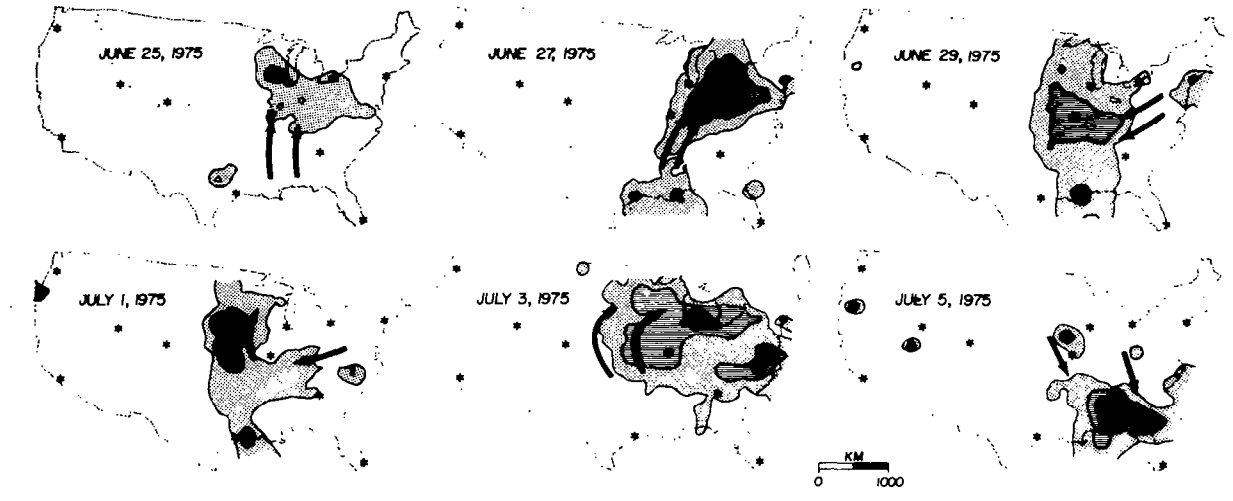


Figure 4.- Maps of noon visibility over the continental United States between June 25 and July 5, 1975. Contours are plotted for extinction coefficients of 4×10^{-4} , 6×10^{-4} , and $8 \times 10^{-4} \text{ m}^{-1}$, corresponding to visual ranges of 10 to 6 km (light shade), 6 km (medium shade), and 5 km (black shade). (From Husar et al. (ref. 16).)

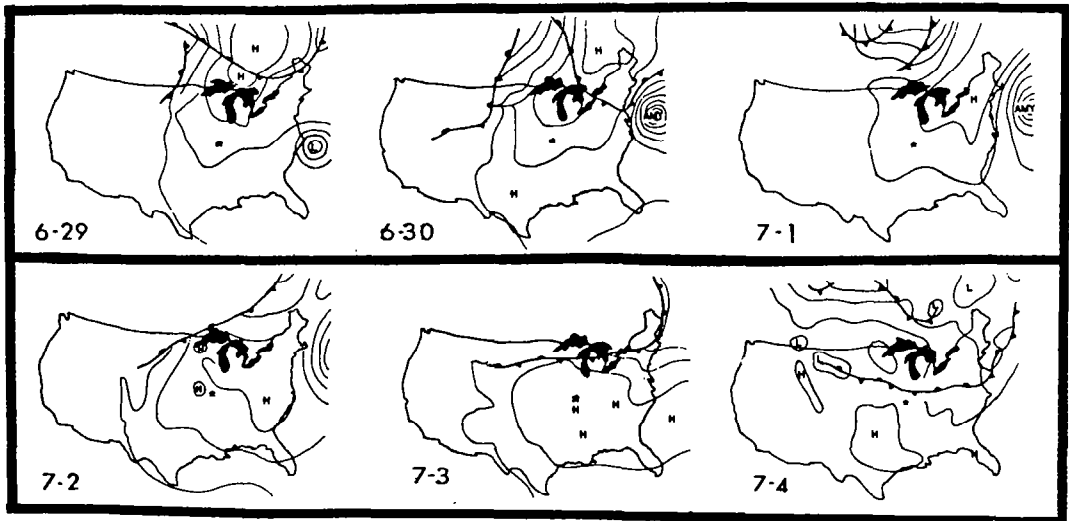
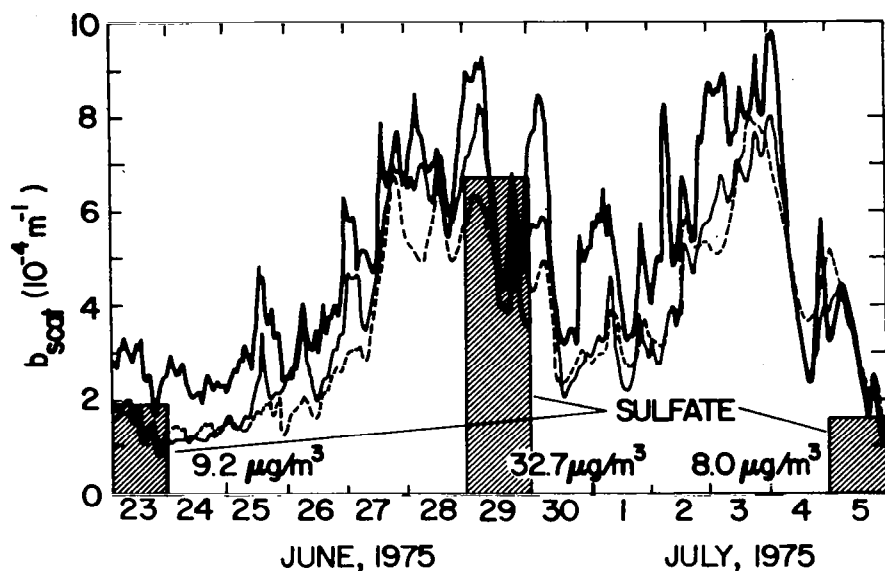
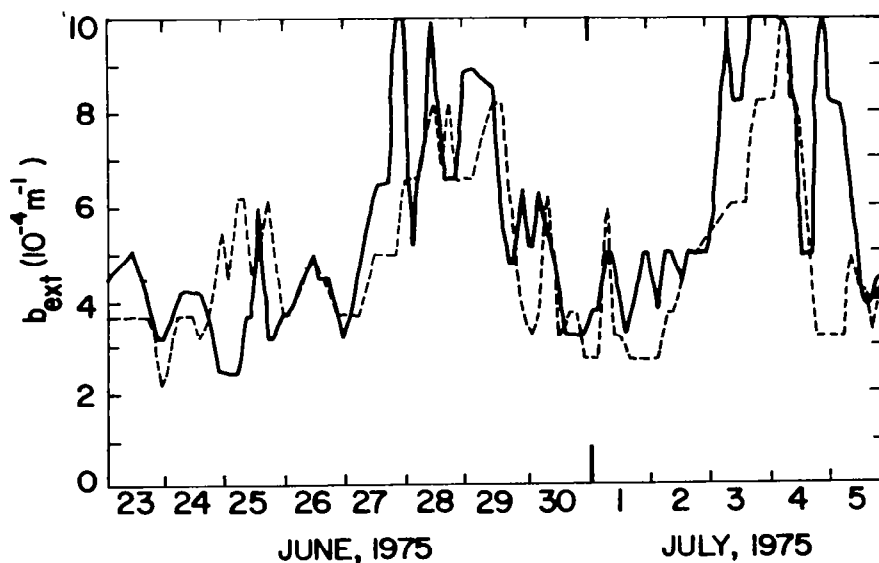


Figure 5.- Daily weather maps for June 29 to July 4, 1975. (From Husar et al. (ref. 16).)

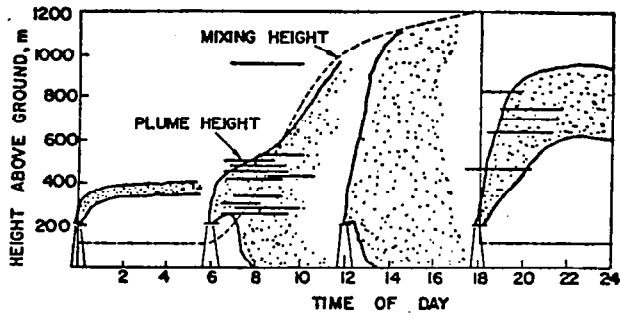


(a) Light scattering coefficient (b_{scat}) recorded by St. Louis County Department of Health near downtown (— station 4), near the western city limits (— station 9), and at background location (--- station 6, 38 km west of city). Nephelometers located north and south of the city show similar b_{scat} patterns (not shown).

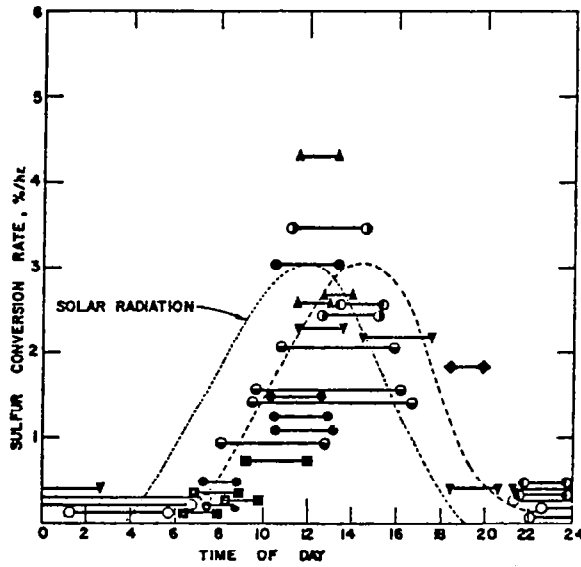


(b) Extinction coefficients (b_{ext}) calculated by $b_{\text{ext}} = 3.92/V$ from observations of visible range V at St. Louis Lambert Airport (—) and at Springfield, Illinois, airport (---) located 150 km northeast of St. Louis.

Figure 6.— Visibility observations near St. Louis for June 29 to July 4, 1975. (From Husar et al. (ref. 16).)

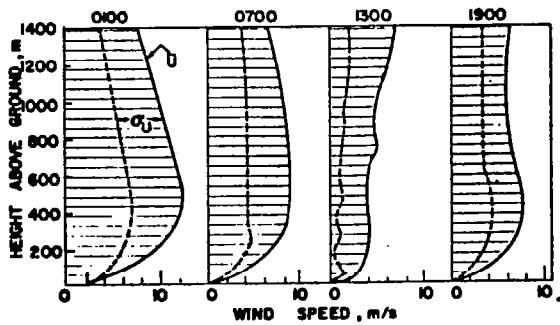


(a) Diurnal pattern of plume dispersion.

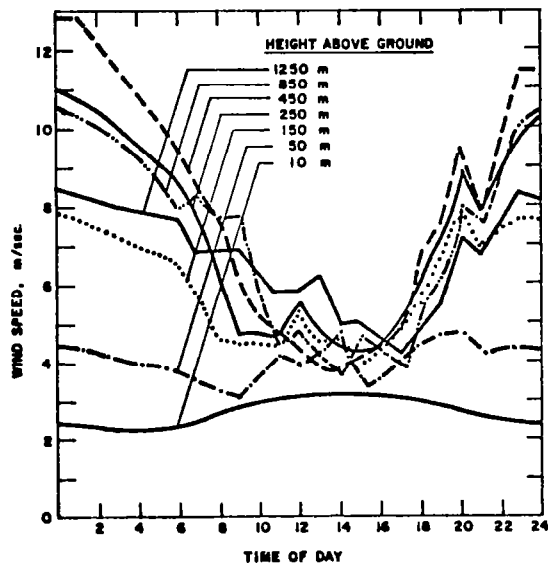


(b) Conversion rate.

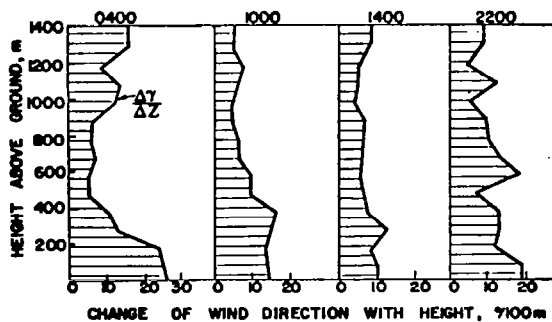
Figure 7.- Diurnal pattern of plume behavior.
(From Husar et al. (ref. 19).)



(a) Vertical profiles of velocity for 0100, 0700, 1300, and 1900 CDT releases. Note appearance of nocturnal jet at about 500 m and uniform low wind speed at midday.



(b) Diurnal pattern of wind speed at seven different heights.



(c) Change of wind direction with height. Evidently, nocturnal jet has little "veer," less than $8^\circ/100$ m on the average.

Figure 8.- Wind data obtained from hourly releases by RAPS balloon sounding network, averaged for July 1976. (From Husar et al. (ref. 19).)

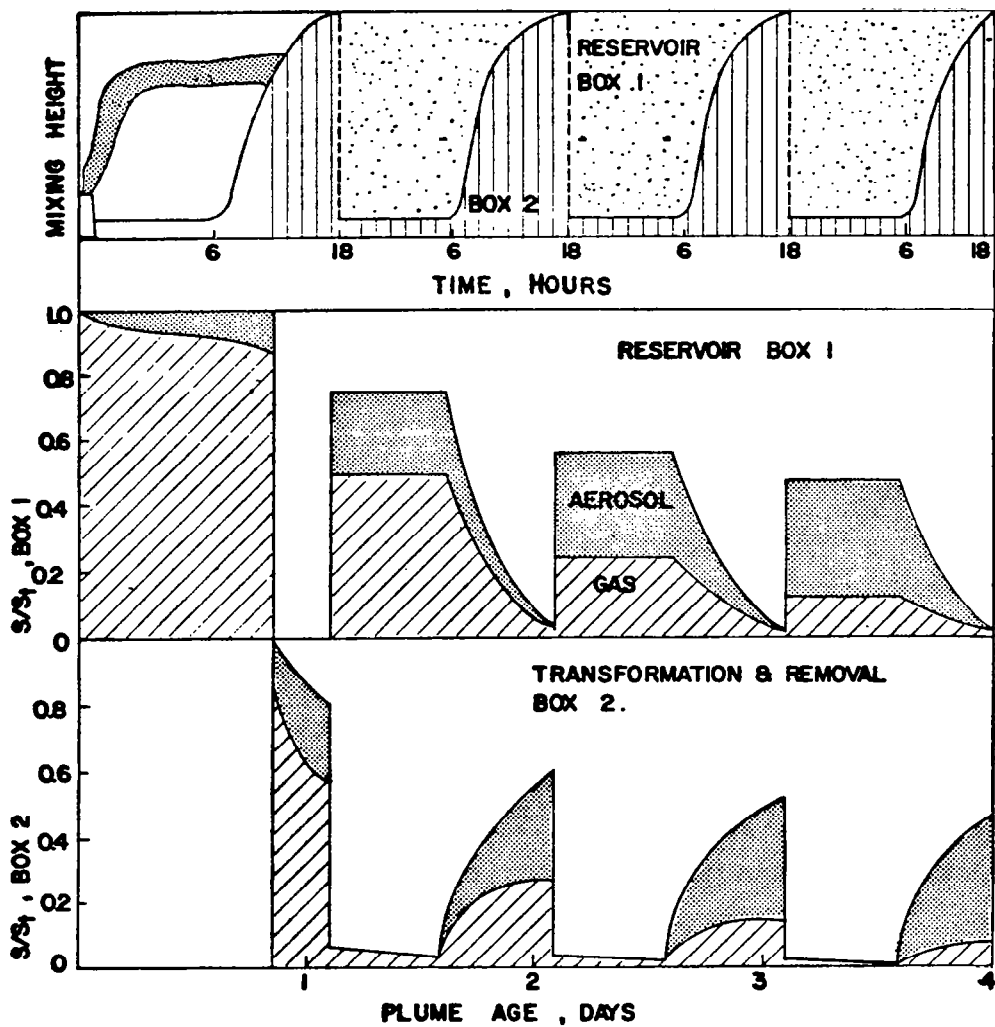


Figure 9.- Schematics of plume transition from the quiescent reservoir to mixing, transformation, and removal regime (top), gaseous and particulate sulfur in the reservoir box (center), and removal regime (bottom).

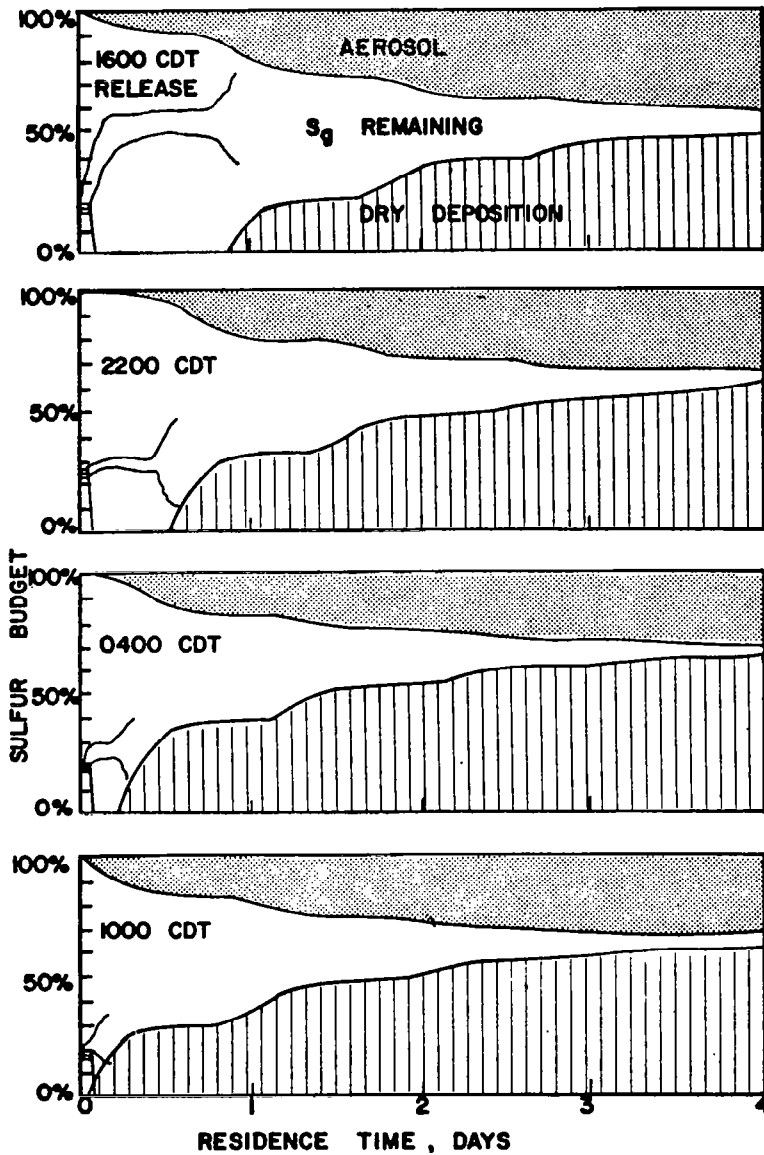
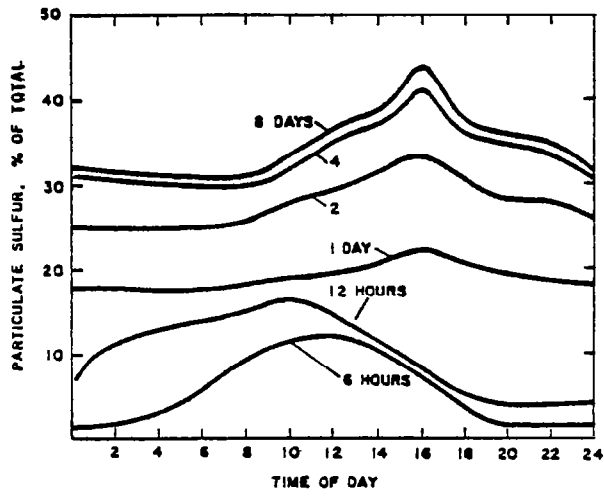
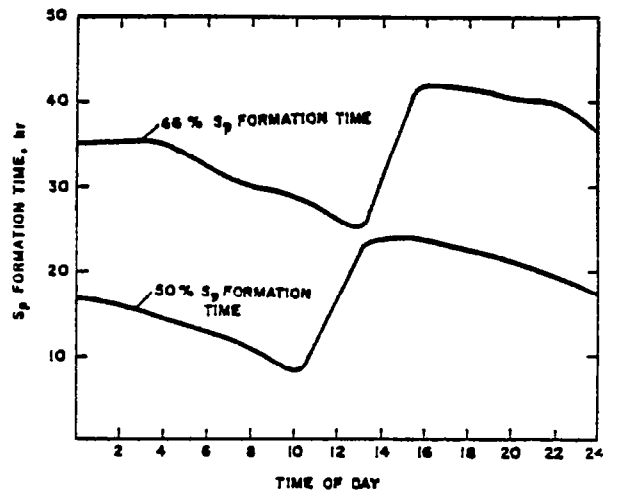


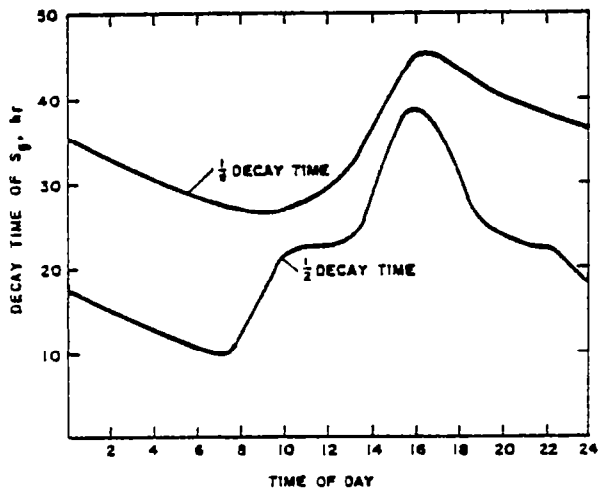
Figure 10.- Sulfur budget over 4 days for power plant emission obtained from two-box model, for four emission times.



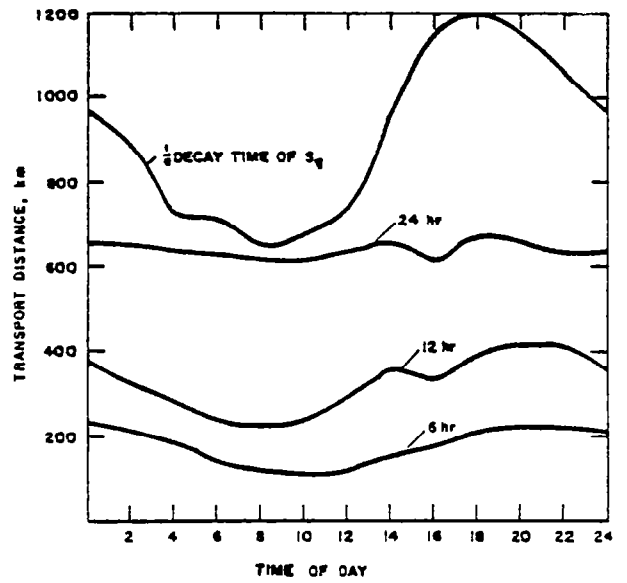
(a) Particulate sulfur fraction for different plume ages.



(b) Particulate sulfur formation time.



(c) S_g decay time.



(d) Transport distance.

Figure 11.- Results of model calculations to explore role of emission time.

SOOT-CATALYZED OXIDATION OF SULFUR DIOXIDE*

S. G. Chang and T. Novakov
Lawrence Berkeley Laboratory
Berkeley, California

SUMMARY

Experimental results are reviewed which demonstrate that combustion-generated soot particles can oxidize SO_2 in both the absence ("dry" mechanism) and the presence ("wet" mechanism) of liquid water. The wet mechanism is much more efficient than the dry one and is applicable to situations where the aerosol particles are covered with a liquid water layer. Calculations are presented which suggest that the soot-catalyzed oxidation of SO_2 can be the dominant mechanism under realistic atmospheric conditions.

INTRODUCTION

Over the past 4 to 5 years, the principal objective of the Lawrence Berkeley Laboratory Atmospheric Aerosol Research Group has been to assess the contribution of primary carbonaceous particles to the ambient particulate burden and to evaluate the role of these primary particles in the formation of suspended sulfates.

During the early days of environmental awareness, primary particulate emissions were easily visible, and smoke or soot was the first air pollutant to be recognized and controlled. In more recent times, improvements in combustion technology and use of better grade fuels have led to a substantial reduction of visible smoke emissions. Consequently, the importance of soot as a pollutant became less obvious, and the emphasis of air pollution control moved away from primary emissions toward controlling gaseous emissions, especially those considered to be precursors for the production of secondary particles - sulfur dioxide for sulfate, hydrocarbons for organic particulates, and so forth.

Nevertheless, there is considerable evidence that primary soot particles are still very important contributors to atmospheric pollution in California and elsewhere. The difference between the concepts of soot and visible smoke is largely confined to the size of the particles. Smoke consists of large particles that are responsible for the opacity of plumes. Soot is any carbonaceous particulate material emitted from sources, even if these do not produce visible plumes or smoke. In most cases, soot particles are very small when emitted, having diameters of the order of 100 \AA , and are therefore invisible to the naked eye. Soot can also be described as a chemically complex carbonaceous material which consists of a "graphitic" component and an organic component. There are

*Work supported by the National Science Foundation - Research Applied to National Needs and the U.S. Department of Energy.

significant differences in the overall properties of the two components. For example, the graphitic component is nonvolatile, insoluble in organic solvents, and strongly light absorbing. In contrast, the organic component of soot is volatile, soluble in solvents, and does not appreciably absorb light. Novakov et al. previously found that as much as 80 percent of the ambient particulate carbon collected in different parts of California is in the form of soot (refs. 1 and 2).

More recently, Rosen et al. (refs. 3 and 4) have employed Raman spectroscopy and an optical attenuation technique to identify the graphitic component of ambient carbonaceous particles and used this component as a tracer for primary emissions. The graphitic soot tracer technique suggests that a major and possibly dominant fraction of the ambient carbonaceous aerosol burden is due to primary emissions. The results also indicate that if there are significant concentrations of secondary species, their production does not seem to depend on the photochemical activity as manifested by the ozone concentration.

Soot particles, in addition to being a major constituent of ambient particles, are a catalytically and surface chemically active material. For example, Novakov et al. (ref. 1) have shown that SO_2 oxidation to sulfate can be catalyzed by combustion-generated soot particles. They propose that the soot-catalyzed SO_2 oxidation plays a major role in atmospheres characterized by high concentrations of primary particulate carbon. Chang et al. (ref. 5) have recently extended research on the role of soot particles as catalysts for SO_2 oxidation by studying the effect of liquid water on the soot-catalyzed reaction. The effects of liquid water are important because, in plumes, liquid water may condense on the soot particles, and soot particles may encounter liquid water in their passage through fogs and clouds. Also, hygroscopic and deliquescent materials associated with soot particles may hold significant amounts of liquid water, even at a relatively low relative humidity. This "wet" mechanism is much more efficient for SO_2 oxidation than the corresponding "dry" mechanism that was suggested previously.

This paper reviews laboratory results on heterogeneous oxidation of SO_2 on soot particles in air and presents results of simple numerical calculations which suggest that soot-catalyzed oxidation can be the dominant heterogeneous mechanism for sulfate formation under realistic atmospheric conditions.

EXPERIMENTAL STUDIES OF CATALYTIC SO_2 OXIDATION ON SOOT PARTICLES

Novakov et al. (refs. 1 and 6) used photoelectron spectroscopy (ESCA) to study the oxidation of SO_2 on soot particles produced by a propane flame. The investigators found that under some conditions, a significant amount of sulfate can be produced by the catalytic action of soot particles.

Photoelectron spectra representing the sulfur (2p) and carbon (1s) regions of propane soot particles produced by a Bunsen burner are shown in figure 1(a). The S(2p) photoelectron peak at a binding energy of 169 eV corresponds to sulfate. The C(1s) peak appears essentially as a single component line and corresponds to a substantially neutral charge state consistent with the soot structure. It is of interest to note that even the combustion of very low-

sulfur-content fuels (0.005 percent by weight) results in the formation of an easily detectable sulfate emission.

The specific role of soot particles as a catalyst for the oxidation of SO_2 is demonstrated with the aid of figure 1(b). Shown here are the S(2p) and C(1s) photoelectron peaks of soot particles generated in an analogous manner, but with SO_2 added to the laboratory-confined "plume." A marked increase in the sulfate peak intensity relative to carbon is evident. The atomic ratios of sulfur to carbon in figures 1(a) and 1(b) are about 0.15 and 0.50, respectively.

The sulfate associated with soot particles was water soluble and contributed to the acidification of the solution. The hydrolysis product of this sulfate behaves chemically as sulfuric acid because it forms ammonium sulfate easily in reaction with gaseous ammonia.

Experiments like those just described have been found difficult to reproduce quantitatively because it is difficult to control important parameters such as soot concentration, temperature, and relative humidity. Although these early experiments were qualitative, it was nevertheless possible to conclude the following:

- (1) Soot-catalyzed oxidation of SO_2 is more efficient at a higher humidity.
- (2) The oxygen in air plays an important role in SO_2 oxidation.
- (3) Soot-catalyzed oxidation exhibits a saturation effect.
- (4) The saturation level of sulfate produced is probably related to properties of carbon particles, such as size, active surface area, and adsorbed surface oxygen.
- (5) SO_2 can be oxidized on other types of graphitic carbonaceous particles, such as ground graphite particles and activated carbon.

Results from the experiments with combustion-produced soot particles are essentially similar to those obtained for activated carbon by Davtyan and Tkach (ref. 7) and Siedlewski (ref. 8).

The experiments just described provide a hint about the importance of water in the catalytic oxidation of SO_2 on carbonaceous particles. For example, the oxidation was apparently more efficient when prehumidified, rather than dry, air was used to dilute the SO_2 . However, the role of water, and specifically of liquid water, was not made clear in these experiments. An understanding of the effect that liquid water may have on this type of SO_2 oxidation is imperative because of the ubiquitous presence of liquid water in the atmosphere.

Chang et al. (ref. 5) recently investigated the kinetics of SO_2 in an aqueous suspension of soot particles. The reaction was studied in systems containing various concentrations of sulfurous acid and suspended carbonaceous particles. The range of carbon concentrations used in the suspensions was from 0.005 percent to 0.32 percent by weight, and that of sulfurous acid was between 1.5×10^{-4} M and 10^{-3} M. The concentration of sulfurous acid was monitored by

using iodometric titration during the course of the reaction. Also, in some selected runs, the concentration of sulfuric acid was monitored by the turbidimetric method. Soots that were produced by the combustion of acetylene and natural gas, as well as by a diesel engine, and collected by impinging the effluent into water, were used in this study and found to be good catalysts.

Figure 2 shows the typical reaction curves of the oxidation of H_2SO_3 by dissolved oxygen in aqueous suspensions of soot particles collected from acetylene and natural gas flames. The reaction occurs in two steps. The rate of the initial disappearance of H_2SO_3 is so fast that it could not be followed by the analytical technique used. The second process is characterized by a much slower linear reduction in the concentration of H_2SO_3 . The results obtained with these combustion-produced soots are essentially reproduced (fig. 3) by suspensions of similar concentrations of activated carbon (Nuchar¹). Figure 3 shows that there is a mass balance between the sulfurous acid consumed and the sulfuric acid produced. Since it is difficult to reproducibly prepare soot suspensions, suspensions of activated carbon were used as a model system.

In order to investigate the reaction rate and mechanism, a series of experiments were done with activated carbon as a model catalyst. The effects of the concentrations of carbon, sulfurous acid, and dissolved oxygen on the rate of oxidation of sulfurous acid were studied (figs. 4, 5, and 6). The amount of sulfurous acid oxidized, at a constant temperature, by the rapid first step process is linearly proportional to the concentration of the carbon particles (fig. 7). It was found that there was a linear relationship between the half-life of the second process and the reciprocal of the carbon concentration and also a linear relationship between the half-life of the second process and the initial sulfurous acid concentration. This behavior suggests a first-order reaction with respect to the carbon catalyst concentration and zeroth order with respect to the sulfurous acid concentration under the conditions of this experiment (activated carbon, between 0.005 percent and 0.32 percent by weight; sulfurous acid, between 1.5×10^{-4} M and 10^{-3} M; pH, between 1.5 and 7.5). The rate of reaction with respect to the concentration of dissolved oxygen was found to be a fractional order (0.7) in figure 8, which was plotted by using data given in figure 6.

In order to assess the dependence of the SO_2 oxidation reaction on pH, a known volume of H_2SO_4 or NH_4OH was mixed into the sulfurous acid solution before adding activated carbon. In a separate run at a high pH, an Na_2SO_3 solution was used for the experiment. The pH of the solution decreases during the course of the reaction. The change in pH varies from 0.05 to 1.0 pH unit, depending on the pH of the solution. The larger the pH, the larger the change. The results, represented in figure 9, demonstrate that the reaction rate essentially does not depend on the pH of the aqueous suspension under the conditions of this investigation. The pH of these experiments ranged from 1.45 to 7.5, which should cover the entire range of interest at atmospheric conditions. This preceding observation is very striking, as it differs from other heterogeneous reactions involving liquid water in not being dependent on the pH of the liquid water.

¹Nuchar: Trademark of West Virginia Pulp & Paper Co.

In summary, the reaction occurs in two steps: an initial rapid oxidation followed by a much slower one. The rate of the first process is too fast to follow. The reaction of the second process has the following characteristics:

(1) The reaction rate is first order, zeroth order, and a fractional order (0.7) with respect to the concentration of carbon, sulfurous acid, and dissolved oxygen, respectively.

(2) The reaction rate is pH independent.

(3) There is a mass balance between the consumption of sulfurous acid and the production of sulfuric acid.

DISCUSSION

It is obvious from the foregoing review of experimental results that soot particles can oxidize SO₂ in both the absence and the presence of liquid water. In this discussion, these two situations will be referred to as the "dry" and the "wet" mechanisms, respectively. The wet mechanism is much more efficient than the dry one and is applicable to the situations in plumes and in the ambient atmosphere when the aerosol particles are covered with a liquid water layer. The dry mechanism is expected to operate in stacks or under conditions of low relative humidity.

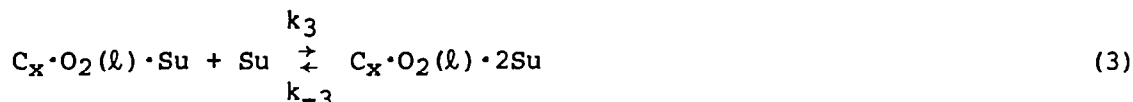
To the authors' knowledge, a reaction rate study involving dry combustion-produced soot particles has not been conducted. However, Yamamoto et al. (refs. 9 and 10) did study the reaction kinetics on dry activated carbon in the presence of O₂ and H₂O vapor. The rate of reaction was found to be first order with respect to SO₂, provided that the concentration of SO₂ was less than 0.01 percent, and depended on the square root of the concentration of O₂ and H₂O vapor. The activation energy was found to vary from -4 to -7 kcal/mole between 70° C and 150° C, depending on the origin of the activated carbon. The effect of the physical properties of activated carbon, such as surface area and micropore and macropore volumes, on the rate of oxidation of SO₂ was also investigated by Yamamoto et al. (refs. 9 and 10). Initially the reaction occurs on the surface of both micropores and macropores, and the rate is constant for a given activated carbon until the amount of accumulated H₂SO₄ reaches about 10 percent by weight of the carbon. Beyond that amount, the rate gradually decreases with the reaction time until the micropore volume is filled up by H₂SO₄. The reaction continues only on the macropores at a constant, but much slower, rate.

According to the results given by Yamamoto et al. (refs. 9 and 10), a rate expression until the amount of H₂SO₄ formed reaches 10 percent by weight of the carbon can be written as follows:

$$\frac{d[\text{H}_2\text{SO}_4]}{dt} = - \frac{98}{64} \frac{d[\text{SO}_2]}{dt} = [\text{C}_x][\text{SO}_2][\text{O}_2]^{0.5}[\text{H}_2\text{O}]^{0.5}(k_{\text{micro}} + k_{\text{macro}})e^{-E_a/RT}$$

where t is time, $[C_x]$ is the concentration of carbon, k_{micro} and k_{macro} are the rate constants on the surface of the micropores and macropores, E_a is the activation energy, R is the universal gas constant, and T is absolute temperature. The rate of oxidation of SO_2 depends on the origin of carbon.

On the basis of their experimental observations, Chang et al. (ref. 5) proposed the following reaction mechanism:



where Su represents sulfite species and SuO represents sulfate species. Equation (1) indicates that dissolved oxygen is adsorbed on the soot particle surface to form an activated complex. This adsorbed oxygen complex then oxidizes the sulfurous acid to form sulfuric acid according to equations (2) to (4). If one assumes that the reaction follows the condition of Langmuir adsorption equilibrium, the rate of acid formation is

$$\begin{aligned} \frac{d[\text{SuO}]}{dt} &= 2k_4[C_x \cdot O_2(l) \cdot 2\text{Su}] \\ &= 2k_4[C_x] \left(\frac{K_1[O_2(l)]}{1 + K_1[O_2(l)] + K_W[H_2O] + K_S[\text{Su}]} \right) \left(\frac{K_2[\text{Su}]}{1 + K_2[\text{Su}]} \right) \left(\frac{K_3[\text{Su}]}{1 + K_3[\text{Su}]} \right) \end{aligned}$$

where K_i ($i = 1$ to 3) are the equilibrium constants for equations (1) to (3), K_W is the equilibrium constant for the adsorption of water molecules on carbon particles, and K_S is the equilibrium constant for the adsorption of sulfite species on carbon particles. If $k_2[\text{Su}] \gg k_{-2}$ and $k_3[\text{Su}] \gg k_{-3}$, the rate law simplifies to

$$\frac{d[\text{SuO}]}{dt} = 2k_4[\text{C}_x] \left(\frac{K_1[\text{O}_2(\ell)]}{1 + K_1[\text{O}_2(\ell)] + K_W[\text{H}_2\text{O}] + K_S[\text{Su}]} \right)$$

If the power rate form (Freundlich isotherm) instead of the Langmuir form is used, the rate law becomes

$$\frac{d[\text{SuO}]}{dt} = k[\text{C}_x][\text{O}_2(\ell)]^n$$

which corresponds to the experimental results where $n = 0.7$. The value of k at 20°C was taken to be 1.8×10^{-4} liter/sec-g which represents the average of the rate constant determined from natural gas and acetylene soot (fig. 2).

Chang et al. (ref. 5) have also carried out a simple box-type calculation to compare the relative importance of wet soot-particle-catalyzed reactions with other reactions involving liquid water. The systems which were considered are $\text{SO}_2\text{-H}_2\text{O}(\ell)\text{-air}$, $\text{NH}_3\text{-SO}_2\text{-H}_2\text{O}(\ell)\text{-air}$, $\text{O}_3\text{-SO}_2\text{-H}_2\text{O}(\ell)\text{-air}$, $\text{NH}_3\text{-O}_3\text{-SO}_2\text{-H}_2\text{O}(\ell)\text{-air}$, $\text{Fe}^{+3}\text{-SO}_2\text{-H}_2\text{O}(\ell)\text{-air}$, $\text{NH}_3\text{-Fe}^{+3}\text{-SO}_2\text{-H}_2\text{O}(\ell)\text{-air}$, $\text{Mn}^{+2}\text{-SO}_2\text{-H}_2\text{O}(\ell)\text{-air}$, and soot- $\text{SO}_2\text{-H}_2\text{O}(\ell)\text{-air}$. The kinetics of each of these processes, other than the soot-catalyzed reactions, have been studied by many investigators. The results of Beilke et al. (ref. 11), Erickson et al. (ref. 12), Freiberg (ref. 13), and Matteson et al. (ref. 14) for oxygen, ozone, iron, and manganese systems, respectively, were used in this calculation. The following initial conditions were used in the calculation: liquid water, 0.05 g/m^3 ; SO_2 , 0.01 ppm ; O_3 , 0.05 ppm ; and CO_2 , 0.000311 atm . For NH_3 , a concentration of 5 ppb was used, which is higher than the highest equilibrium partial pressure of NH_3 over the United States as calculated by Lau and Charlson (ref. 15). Concentrations of particulate Fe and Mn of 250 ng/m^3 and 20 ng/m^3 , respectively, were assumed. However, only 0.13 percent of the total iron and 0.25 percent of the manganese are water soluble, according to Gordon et al. (ref. 16). A soot particle concentration of $10 \text{ } \mu\text{g/m}^3$ was assumed.

The following assumptions were made in the calculations:

(1) The size of liquid water drops suspended inside the box is so small that the absorption rate of gaseous species (SO_2 and NH_3) is governed by chemical reactions.

(2) There is no mass transfer of any species across the box during the reaction. Therefore, the SO_2 (and NH_3) in each box is depleted with time. The mass balances of the sulfur and ammonia (i.e., $\Delta[\text{SO}_2(\text{g})] = \Delta[\text{SO}_2 \cdot \text{H}_2\text{O}] + \Delta[\text{HSO}_3^-] + \Delta[\text{SO}_3^-] + \Delta[\text{HSO}_4^-] + \Delta[\text{SO}_4^-]$, and $\Delta[\text{NH}_3(\text{g})] = \Delta[\text{NH}_3 \cdot \text{H}_2\text{O}] + \Delta[\text{NH}_4^+]$) are always maintained.

(3) The growth of liquid water droplets due to the vapor pressure lowering effect of the sulfuric acid formed in the droplets is neglected.

The amount of sulfate formed as a function of time was calculated according to the following procedure:

(1) Initially, the droplets achieve chemical equilibrium with CO_2 , SO_2 , and NH_3 at the partial pressures adopted. The concentrations $[\text{H}^+]$, $[\text{SO}_2 \cdot \text{H}_2\text{O}]$, $[\text{HSO}_3^-]$, $[\text{SO}_3^-]$, $[\text{NH}_3 \cdot \text{H}_2\text{O}]$, and $[\text{NH}_4^+]$ are calculated when $[\text{HSO}_4^-]$ and $[\text{SO}_4^-]$ are equal to zero.

(2) Assuming a time step Δt , $[\text{HSO}_4^-]$ and $[\text{SO}_4^-]$ are calculated with the aid of the corresponding reaction rate law for each process.

(3) The gaseous SO_2 and NH_3 are depleted. The remaining concentrations $[\text{SO}_2]$ and $[\text{NH}_3]$ are calculated from the mass balance equation.

(4) Then $[\text{H}^+]$, $[\text{SO}_2 \cdot \text{H}_2\text{O}]$, $[\text{HSO}_3^-]$, $[\text{SO}_3^-]$, $[\text{NH}_3 \cdot \text{H}_2\text{O}]$, and $[\text{NH}_4^+]$ are again calculated and the process is repeated until a 24-hour period is completed.

The result of this calculation is given in table I and in figure 10. From this calculation, one can conclude that the soot-catalyzed oxidation of SO_2 can be the dominant mechanism under realistic atmospheric conditions.

REFERENCES

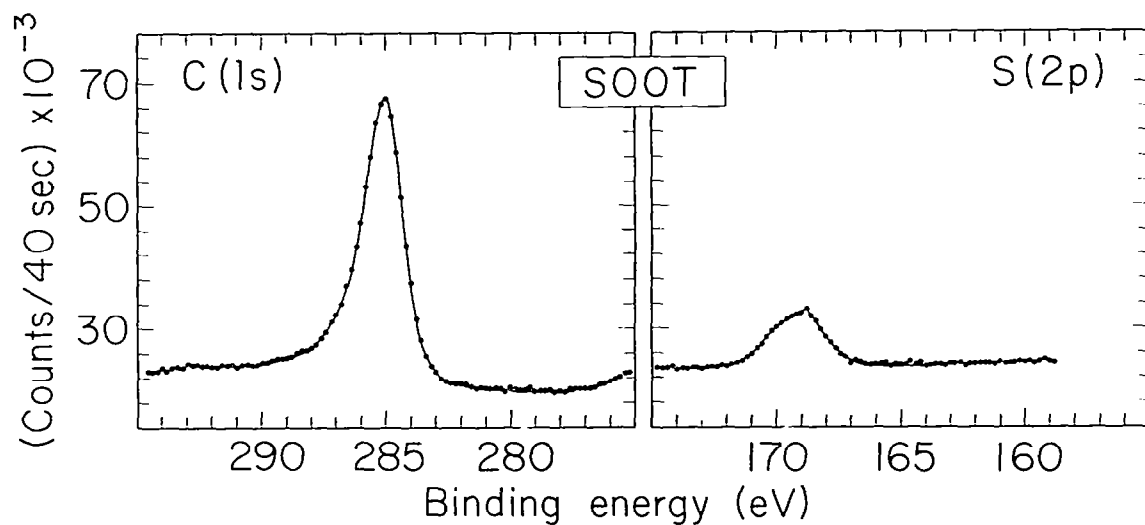
1. Novakov, T.; Chang, S. G.; and Harker, A. B.: Sulfates as Pollution Particulates: Catalytic Formation on Carbon (Soot) Particles. *Science*, vol. 186, no. 4160, Oct. 18, 1974, pp. 259-261.
2. Chang, S. G.; and Novakov, T.: Formation of Pollution Particulate Nitrogen Compounds by NO-Soot and NH₃-Soot Gas-Particle Surface Reactions. *Atmos. Environ.*, vol. 9, no. 5, May 1975, pp. 495-504.
3. Rosen, H.; Hansen, A. D. A.; Gundel, L.; and Novakov, T.: Identification of the Graphitic Carbon Component of Source and Ambient Particulates by Raman Spectroscopy and an Optical Attenuation Technique. Lawrence Berkeley Laboratory paper presented at Conference on Carbonaceous Particles in the Atmosphere (Berkeley, California), Mar. 1978.
4. Hansen, A. D. A.; Rosen, H.; Dod, R. L.; and Novakov, T.: Optical Attenuation as a Tracer for the Primary Component of the Carbonaceous Aerosol. Lawrence Berkeley Laboratory paper presented at Conference on Carbonaceous Particles in the Atmosphere (Berkeley, California), Mar. 1978.
5. Chang, S.-G.; Brodzinsky, R.; Toossi, R.; Markowitz, S. S.; and Novakov, T.: Catalytic Oxidation of SO₂ on Carbon in Aqueous Suspensions. Lawrence Berkeley Laboratory paper presented at Conference on Carbonaceous Particles in the Atmosphere (Berkeley, California), Mar. 1978.
6. Novakov, T.; Chang, S. G.; and Dod, R. L.: Application of ESCA to the Analysis of Atmospheric Particulates. *Contemporary Topics in Analytical and Clinical Chemistry - Volume I*, David M. Hercules, Gary M. Hieftje, Lloyd R. Snyder, and Merle A. Evenson, eds., Plenum Press, Inc., c.1977, pp. 249-286.
7. Davtyan, O. K.; and Tkach, Yu. A.: The Mechanism of Oxidation, Hydrogenation, and Electrochemical Oxidation on Solid Catalysts. II. The Catalytic Activity of Surface "Oxides" on Carbon. *Russian J. Phys. Chem.*, vol. 35, pt. 1, no. 5, May 1961, pp. 486-489.
8. Siedlewski, J.: The Mechanism of Catalytic Oxidation on Activated Carbon. The Influence of Free Carbon Radicals on the Adsorption of SO₂. *Int. Chem. Eng.*, vol. 5, no. 2, Apr. 1965, pp. 297-301.
9. Yamamoto, Kyoko; Seki, Michiharu; and Kawazoe, Kunitaro: Absorption of Sulfur Dioxide on Activated Carbon in the Flue Gas Desulfurization Process. III. Rate of Oxidation of Sulfur Dioxide on Activated Carbon Surfaces. *Nippon Kagaku Kaishi*, vol. 6, 1972, pp. 1046-1052.
10. Sugiyama, Iseko; Kawazoe, Kunitaro; Yamamoto, Kyoko; and Seki, Michiharu: Absorption of Sulfur Dioxide on Activated Carbon in the Flue Gas Desulfurization Process. IV. Effect of Particle Size of the Activated Carbon Pellets on the Rate of Sulfur Dioxide Oxidation. *Nippon Kagaku Kaishi*, vol. 6, 1972, pp. 1052-1058.

11. Beilke, S.; Lamb, D.; and Müller, J.: On the Uncatalyzed Oxidation of Atmospheric SO₂ by Oxygen in Aqueous Systems. *Atmos. Environ.*, vol. 9, no. 12, 1975, pp. 1083-1090.
12. Erickson, Ronald E.; Yates, Leland M.; Clark, Robert L.; and McEwen, David: The Reaction of Sulfur Dioxide With Ozone in Water and Its Possible Atmospheric Significance. *Atmos. Environ.*, vol. 11, no. 9, 1977, pp. 813-817.
13. Freiberg, Johnny: The Mechanism of Iron Catalyzed Oxidation of SO₂ in Oxygenated Solutions. *Atmos. Environ.*, vol. 9, no. 6/7, June/July 1975, pp. 661-672.
14. Matteson, Michael J.; Stöber, Werner; and Luther, Horst: Kinetics of the Oxidation of Sulfur Dioxide by Aerosols of Manganese Sulfate. *Ind. & Eng. Chem. Fundam.*, vol. 8, no. 4, Nov. 1969, pp. 677-687.
15. Lau, Ngar-Cheung; and Charlson, Robert J.: On the Discrepancy Between Background Atmospheric Ammonia Gas Measurements and the Existence of Acid Sulfates as a Dominant Atmospheric Aerosol. *Atmos. Environ.*, vol. 11, pp. 475-478.
16. Gordon, G. E.; Davis, D. D.; Israel, G. W.; Landsberg, H. E.; and O'Haver, T. C.: Atmospheric Impact of Major Sources and Consumers of Energy. NSF/RA/E-75/189 (Grant NSF-ESR75-02667 to Univ. of Maryland), 1975. (Available from NTIS as PB 262 574.)

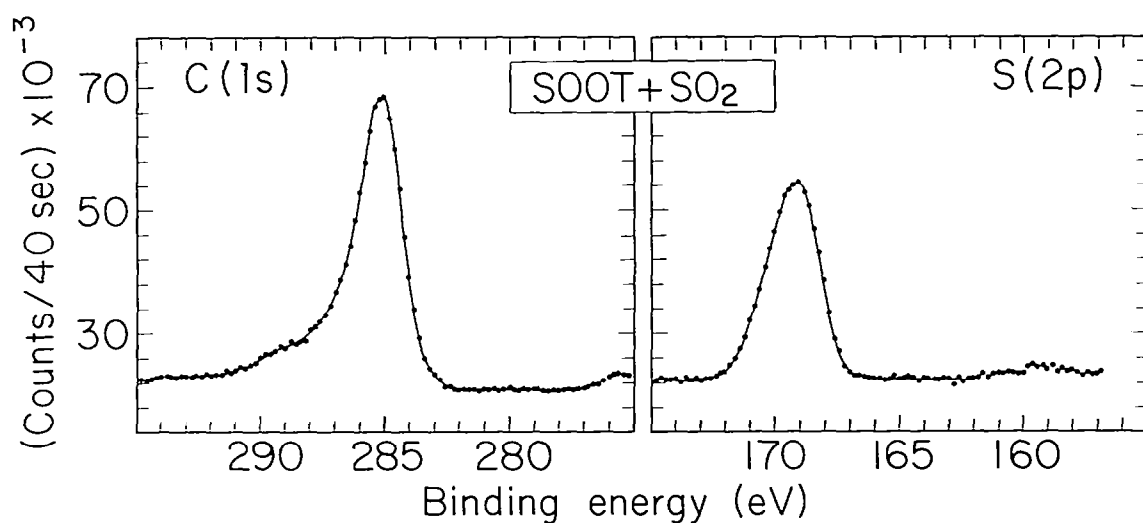
TABLE I.- COMPARISON OF RELATIVE SIGNIFICANCE OF VARIOUS SO₂ CONVERSION PROCESSES
IN AQUEOUS DROPLETS

[Initial conditions of experiment: [H₂O(l)], 0.05 g/m³; [SO₂], 0.01 ppm (10⁻⁸ atm);
[NH₃], 5 ppb (5 × 10⁻⁹ atm); [O₃], 0.05 ppm (5 × 10⁻⁸ atm); [Mn⁺²], 20 ng/m³ × 0.25%;
[Fe⁺³], 250 ng/m³ × 0.13%; soot, 10 μg/m³; temperature, 10° C

Mechanism	1 hr		6 hr		12 hr		24 hr	
	[SO ₄ ⁼], μg/m ³	Percent conversion	[SO ₄ ⁼], μg/m ³	Percent conversion	[SO ₄ ⁼], μg/m ³	Percent conversion	[SO ₄ ⁼], μg/m ³	Percent conversion
Mn ⁺²	2.55 × 10 ⁻⁵	6.2 × 10 ⁻⁵	1.6 × 10 ⁻⁴	3.9 × 10 ⁻⁴	3.1 × 10 ⁻⁴	7.5 × 10 ⁻⁴	6 × 10 ⁻⁴	1.45 × 10 ⁻³
O ₂	1.8 × 10 ⁻³	4.3 × 10 ⁻³	9.6 × 10 ⁻³	2.3 × 10 ⁻³	1.8 × 10 ⁻²	4.4 × 10 ⁻²	3.4 × 10 ⁻²	8.2 × 10 ⁻²
Fe ⁺³	4.7 × 10 ⁻³	1.1 × 10 ⁻²	2.1 × 10 ⁻²	5 × 10 ⁻²	3.3 × 10 ⁻²	8.0 × 10 ⁻²	4.8 × 10 ⁻²	0.12
O ₃	0.13	0.33	0.27	0.66	0.35	0.85	0.47	1.13
O ₂ -NH ₃	.52	1.26	1.54	3.7	2.02	4.89	2.50	6.1
Fe ⁺³ -NH ₃	2.3	5.6	3.2	7.76	3.6	8.73	3.9	9.45
O ₃ -NH ₃	4.51	10.94	5.14	12.5	5.28	12.8	5.28	12.8
C _x	1.8	4.4	10.8	26.4	21.6	52.4	41.25	100



(a) Soot particles produced by combustion of propane saturated with benzene vapor (sulfur content of this fuel, 0.005 percent by weight).



(b) Soot particles generated in a manner analogous to (a) but exposed to additional SO_2 in humid air.

Figure 1.- Carbon(1s) and sulfur(2p) photoelectron spectra.

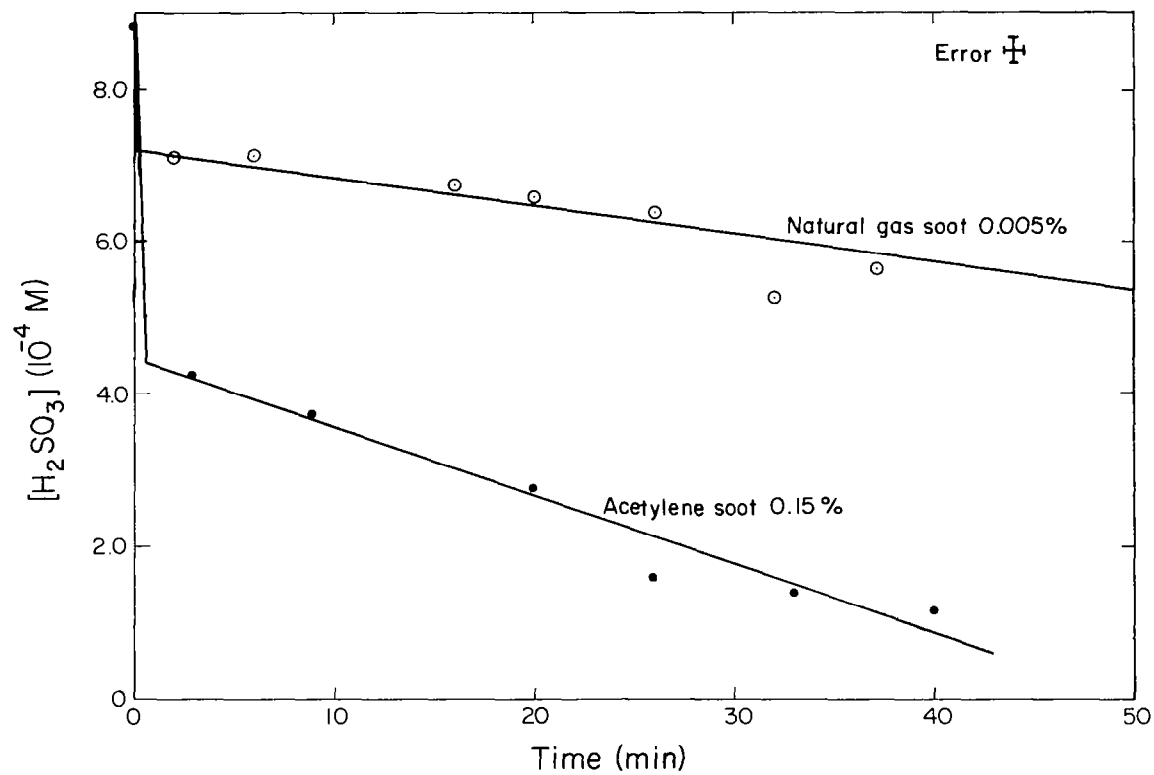


Figure 2.- H_2SO_3 concentration as a function of time for acetylene and natural gas soot suspensions.

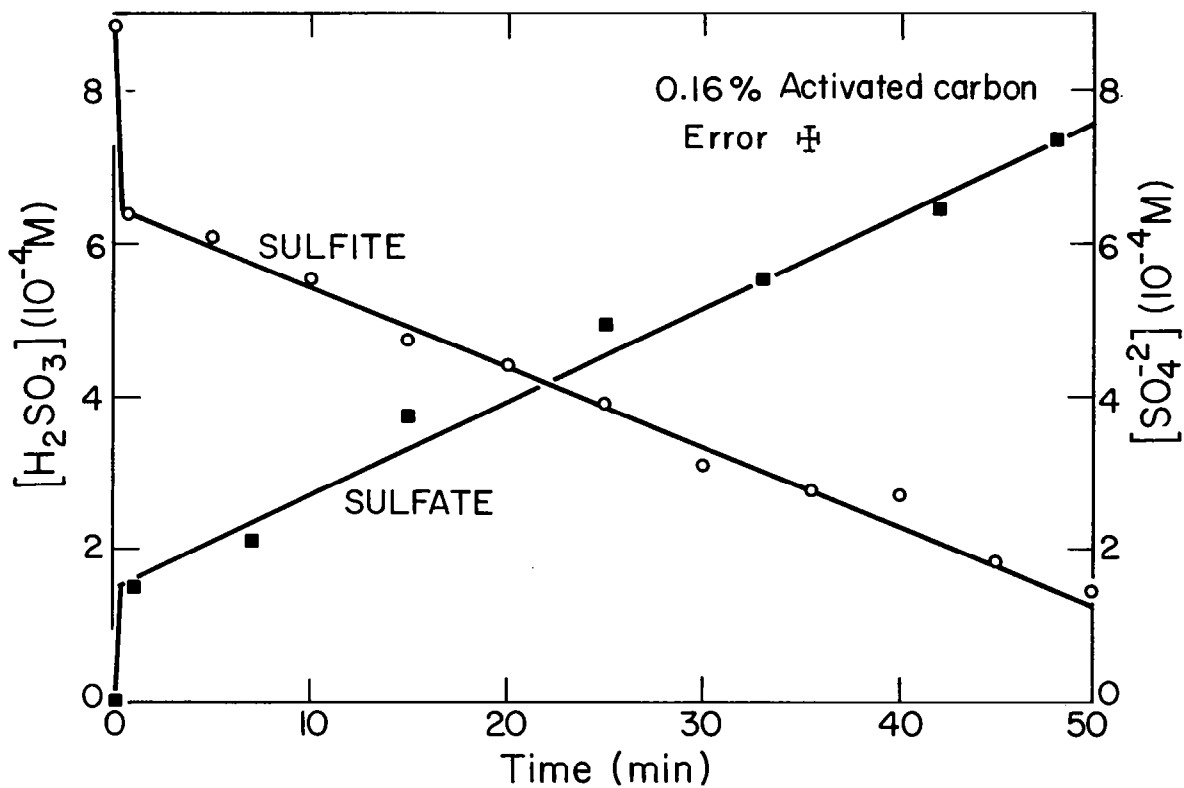


Figure 3.- H₂SO₃ and H₂SO₄ concentrations as a function of time for activated carbon suspensions.

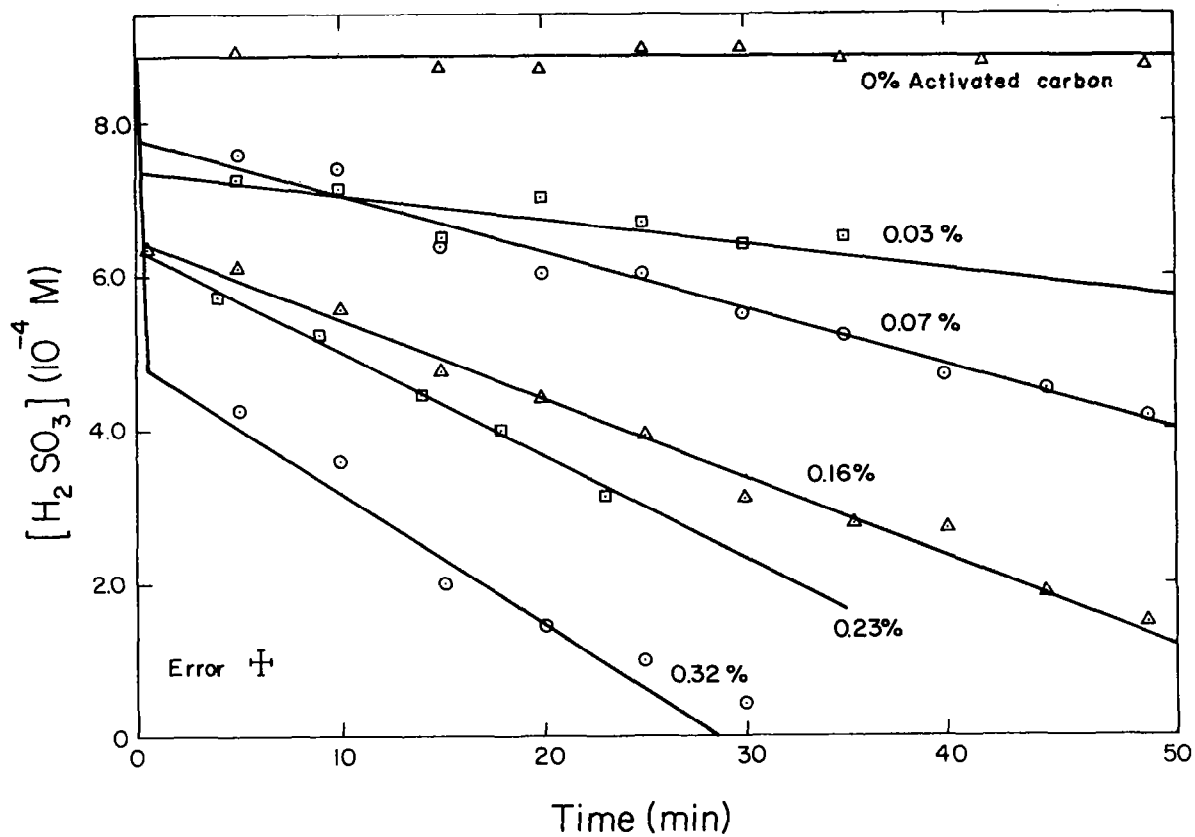


Figure 4.- H_2SO_3 concentration as a function of time for various activated carbon concentrations. Initial H_2SO_3 concentration was $8.85 \times 10^{-4} \text{ M}$.

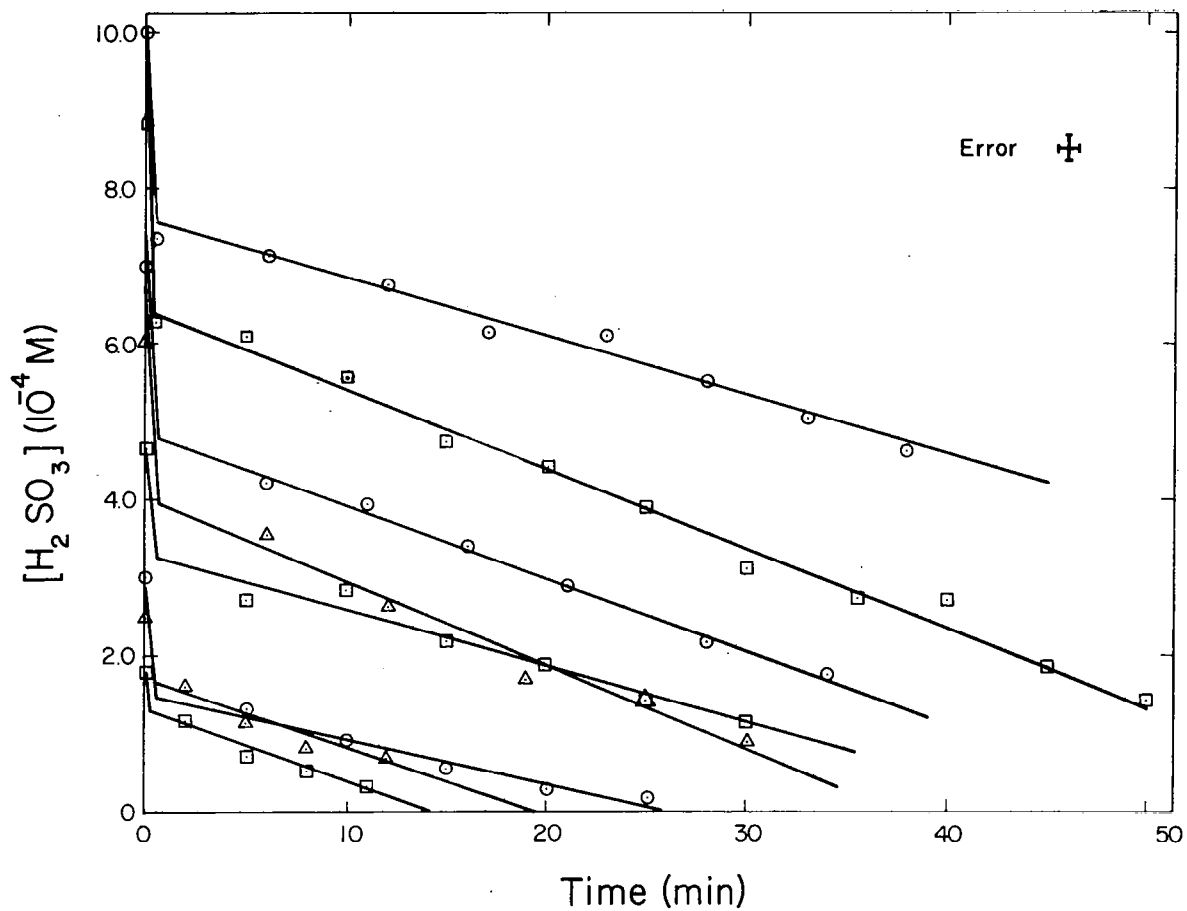


Figure 5.- H_2SO_3 concentration as a function of time for various initial concentrations of H_2SO_3 at a fixed activated carbon concentration of 0.16 percent by weight.

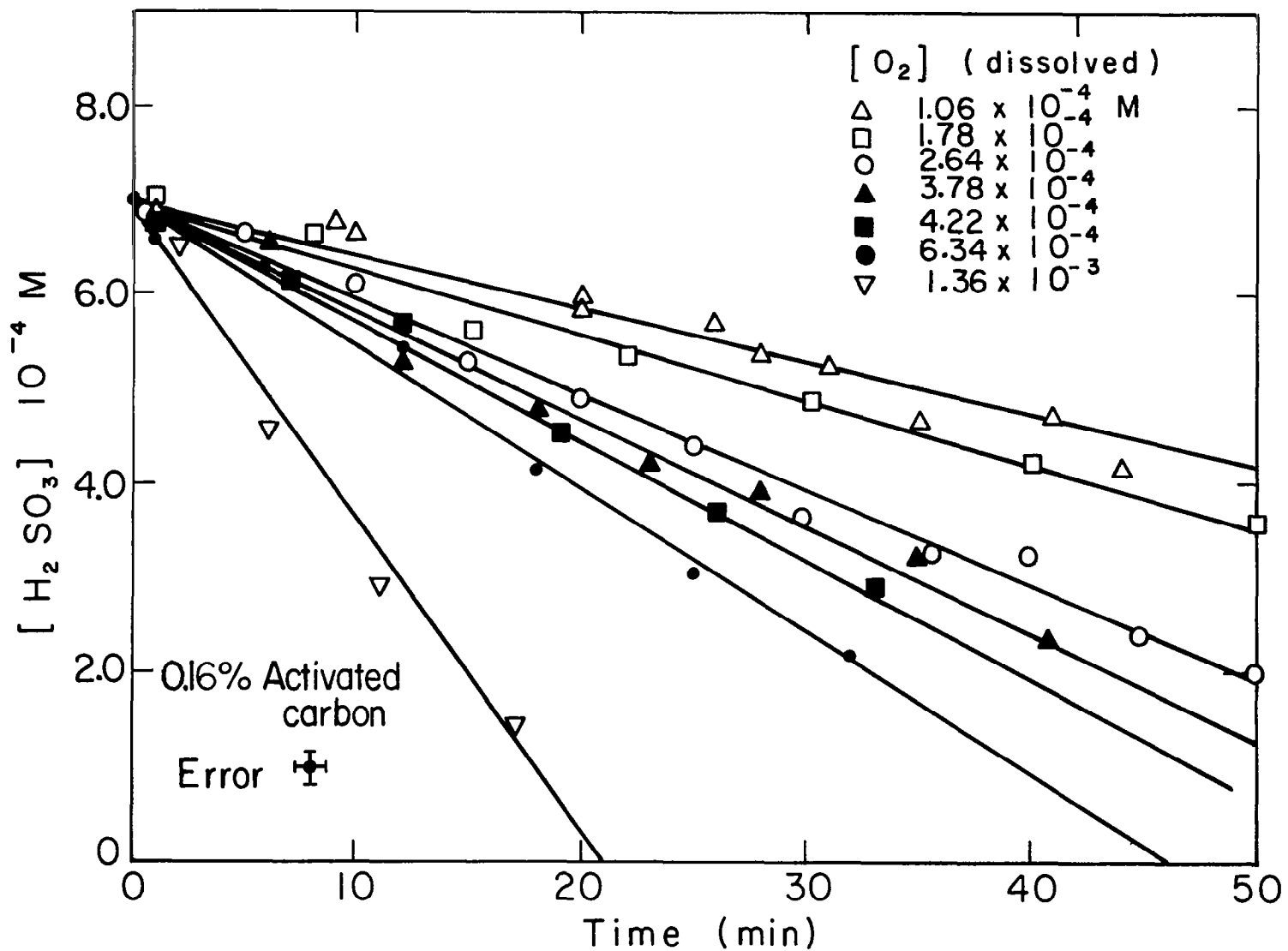


Figure 6.- H_2SO_3 concentration as a function of time for various concentrations of dissolved oxygen at a fixed activated carbon concentration of 0.16 percent by weight.

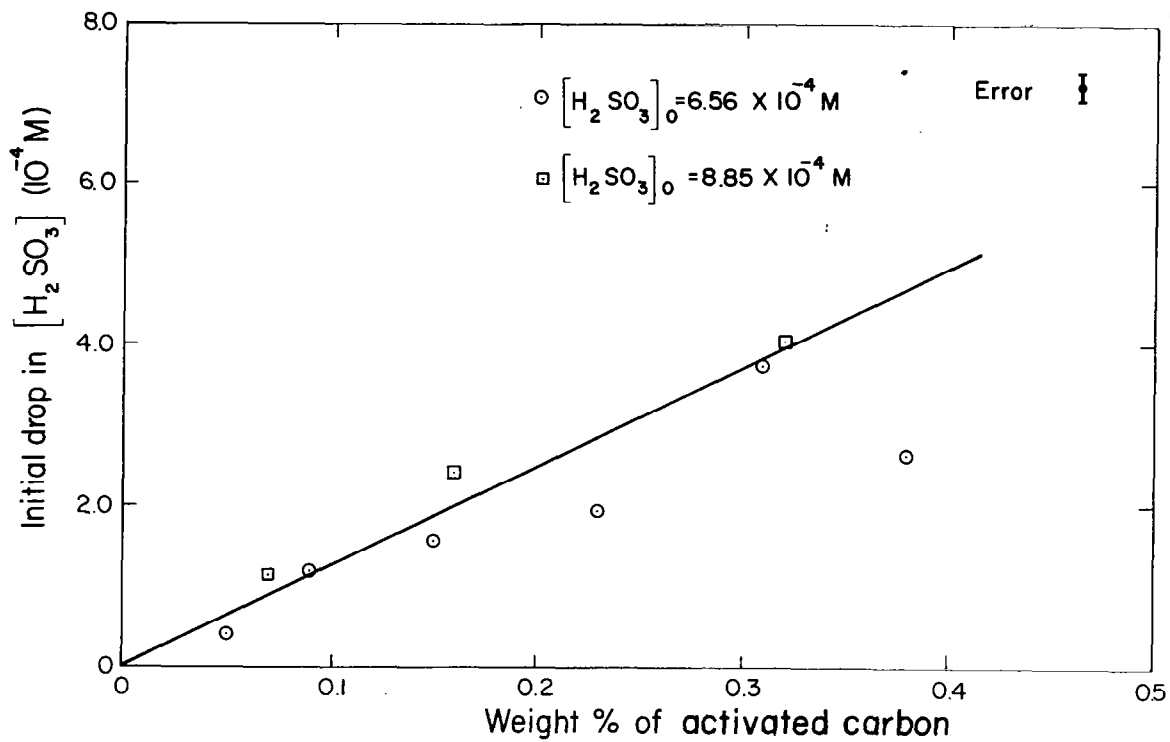


Figure 7.- The amount of H_2SO_3 oxidized by first rapid process for various concentrations of activated carbon.

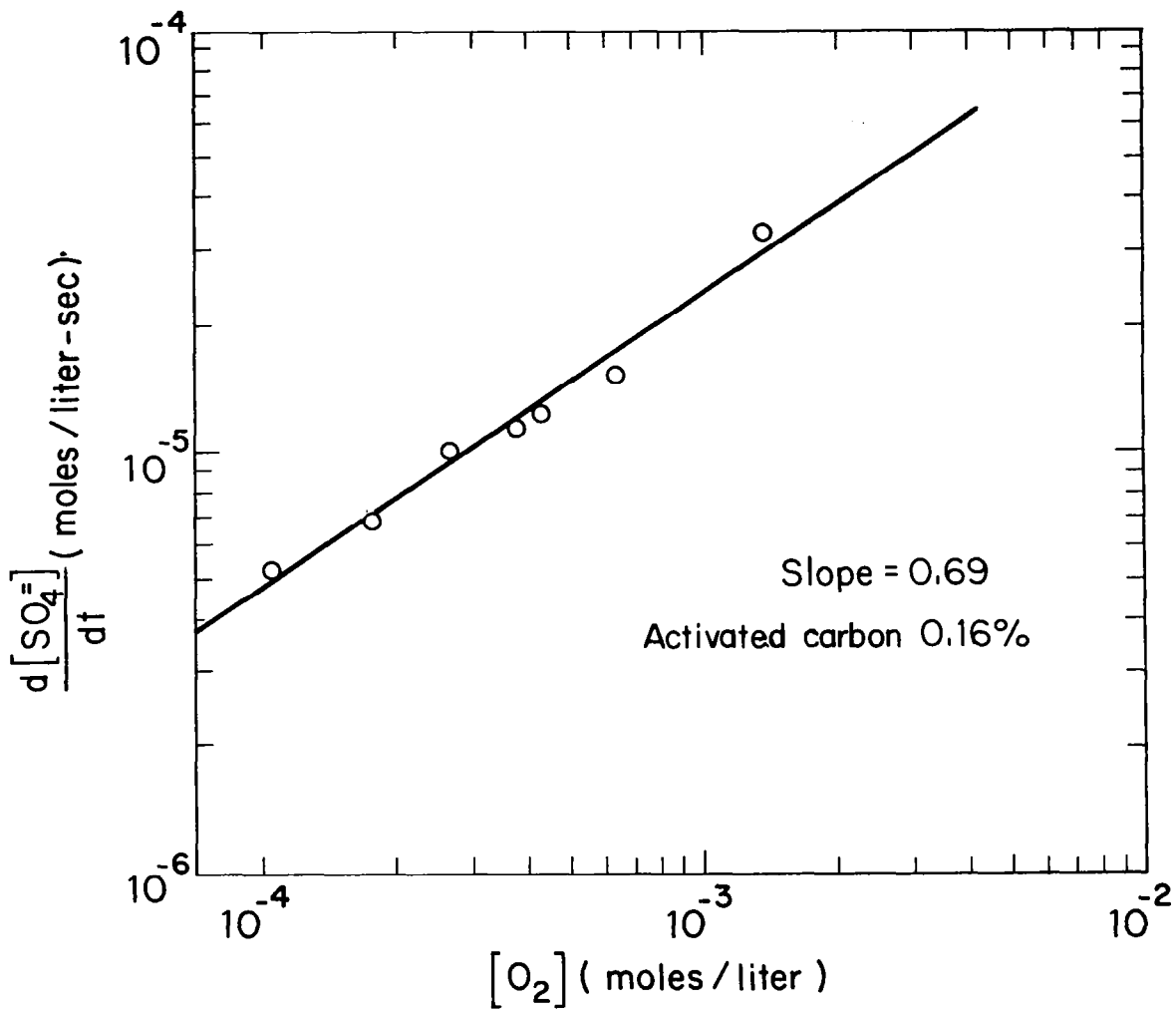


Figure 8.- The rate of formation of sulfuric acid for various concentrations of dissolved oxygen at a fixed activated carbon concentration of 0.16 percent by weight.

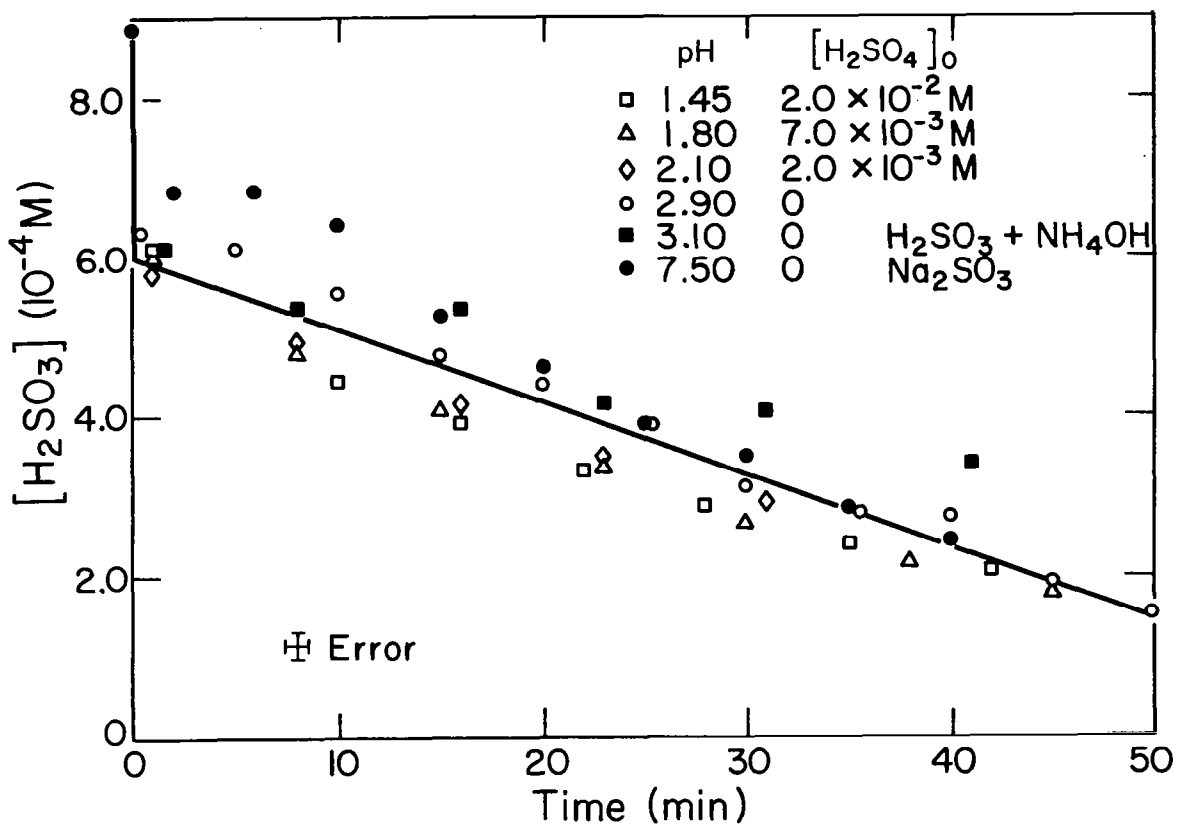


Figure 9.- H_2SO_3 concentration as a function of time at an activated carbon concentration of 0.16 percent by weight at various pH values. Initial H_2SO_3 concentration was $8.85 \times 10^{-4} M$.

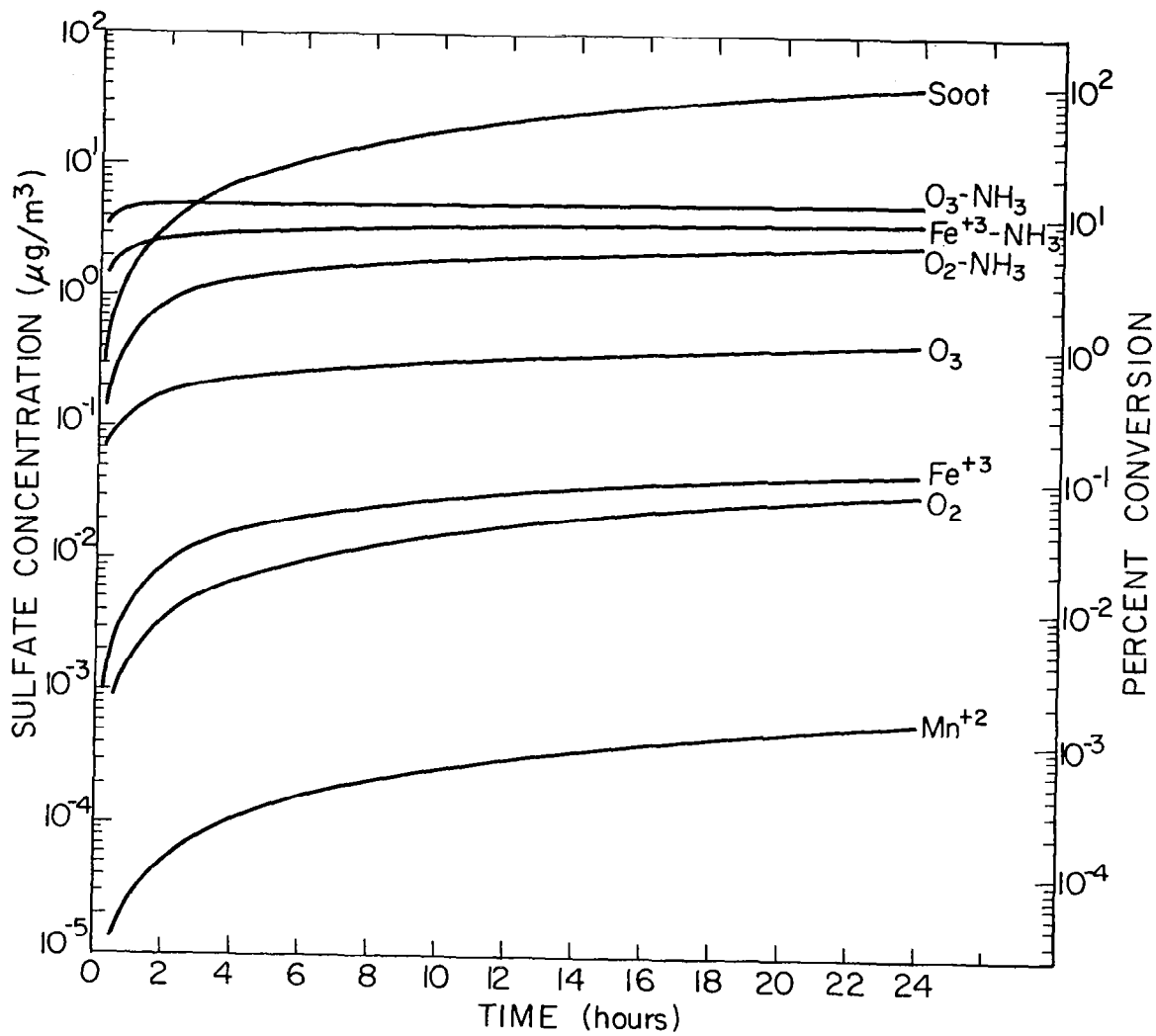


Figure 10.- Comparison of relative significance of various SO_2 conversion processes in aqueous droplets.



CONTRIBUTORS

- *W. L. Chameides
Department of Physics and Astronomy
University of Florida
Gainesville, FL 32611
- S. G. Chang
Energy and Environment Division
Lawrence Berkeley Laboratory
University of California, Berkeley
Berkeley, CA 94720
- Phillip D. Falconer
Atmospheric Sciences Research Center
State University of New York at Albany
Albany, NY 12222
- *T. E. Graedel
Bell Laboratories
Murray Hill, NJ 07974
- Sultan Hameed
Laboratory for Planetary Atmospheres Research
Department of Mechanical Engineering
State University of New York at Stony Brook
Stony Brook, NY 11794
- *Rudolf B. Husar
Air Pollution Research Laboratory
Department of Mechanical Engineering
Washington University
St. Louis, MO 63130
- *Shaw C. Liu
National Center for Atmospheric Research
Boulder, CO 80307
- *Alan C. Lloyd
Environmental Research & Technology, Inc.
2030 Alameda Padre Serra
Santa Barbara, CA 93103
- *Volker A. Mohnen
Atmospheric Sciences Research Center
State University of New York at Albany
Albany, NY 12222
- *T. Novakov
Energy and Environment Division
Lawrence Berkeley Laboratory
University of California, Berkeley
Berkeley, CA 94720
- Joseph Pinto
Laboratory for Planetary Atmospheres Research
Department of Mechanical Engineering
State University of New York at Stony Brook
Stony Brook, NY 11794

*Delivered lecture on which paper is based.

*James N. Pitts, Jr. Statewide Air Pollution Research Center
and Department of Chemistry
University of California, Riverside
Riverside, CA 92521

Robert Pratt Atmospheric Sciences Research Center
State University of New York at Albany
Albany, NY 12222

*John H. Seinfeld Department of Chemical Engineering
California Institute of Technology
Pasadena, CA 91125

*Richard W. Stewart NASA Goddard Space Flight Center
Greenbelt, MD 20771

*Delivered lecture on which paper is based.

1. Report No. NASA RP-1022	2. Government Accession No.	3. Recipient's Catalog No.	
4. Title and Subtitle MAN'S IMPACT ON THE TROPOSPHERE. LECTURES IN TROPOSPHERIC CHEMISTRY		5. Report Date September 1978	6. Performing Organization Code
		8. Performing Organization Report No.	
7. Author(s) Joel S. Levine and David R. Schryer, editors		10. Work Unit No. 176-20-33-01	11. Contract or Grant No.
9. Performing Organization Name and Address NASA Langley Research Center Hampton, VA 23665		13. Type of Report and Period Covered Reference Publication	
		14. Sponsoring Agency Code	
12. Sponsoring Agency Name and Address			
15. Supplementary Notes			
16. Abstract The chemistry of the natural and polluted troposphere is discussed in a series of 10 invited papers originally presented at the Langley Research Center during the summer of 1977. These papers consider the modeling and measurement of tropospheric species on the spatial scales of local photochemical smog, regional urban plumes, the global troposphere, and tropospheric-stratospheric interchange. The papers discuss the sources and sinks of tropospheric species, the global budgets that control species concentrations, and man's impact on the composition of the troposphere.			
17. Key Words (Suggested by Author(s)) Natural and polluted troposphere Atmospheric photochemistry and chemistry Air pollution Ozone Tropospheric nitrogen, carbon, hydrogen, and sulfur species		18. Distribution Statement Unclassified - Unlimited Subject Category 46	
19. Security Classif. (of this report) Unclassified	20. Security Classif. (of this page) Unclassified	21. No. of Pages 376	22. Price* \$13.00

* For sale by the National Technical Information Service, Springfield, Virginia 22161

NASA-Langley, 1978

National Aeronautics and
Space Administration

Washington, D.C.
20546

Official Business

Penalty for Private Use, \$300

SPECIAL FOURTH CLASS MAIL
BOOK

Postage and Fees Paid
National Aeronautics and
Space Administration
NASA-451



10 1 1U,E,RP, 090178 S00903DS 74073
DEPT OF THE AIR FORCE
AF WEAPONS LABORATORY
ATTN: TECHNICAL LIBRARY (SUL)
KIRTLAND AFB NM 87117

NASA

POSTMASTER: If Undeliverable (Section 158
Postal Manual) Do Not Return
